

Seismic Performance of Steel Girder Bridge Superstructures with Ductile End Cross Frames and Seismic Isolators

by
Lyle P. Carden, Ahmad M. Itani and Ian G. Buckle



Technical Report MCEER-08-0002

January 7, 2008

NOTICE

This report was prepared by the University of Nevada, Reno as a result of research sponsored by MCEER through a contract from the Federal Highway Administration. Neither MCEER, associates of MCEER, its sponsors, the University of Nevada, Reno, nor any person acting on their behalf:

- a. makes any warranty, express or implied, with respect to the use of any information, apparatus, method, or process disclosed in this report or that such use may not infringe upon privately owned rights; or
- b. assumes any liabilities of whatsoever kind with respect to the use of, or the damage resulting from the use of, any information, apparatus, method, or process disclosed in this report.

Any opinions, findings, and conclusions or recommendations expressed in this publication are those of the author(s) and do not necessarily reflect the views of MCEER or the Federal Highway Administration.

Seismic Performance of Steel Girder Bridge Superstructures with Ductile End Cross Frames and Seismic Isolators

by

Lyle P. Carden,¹ Ahmad M. Itani² and Ian G. Buckle³

Publication Date: January 7, 2008

Submittal Date: October 17, 2005

Technical Report MCEER-08-0002

Task Number 094-C-3.2

FHWA Contract Number DTFH61-98-C-00094

- 1 Design Engineer, Martin & Chock, Inc.; Former Graduate Assistant, Department of Civil and Environmental Engineering, University of Nevada, Reno
- 2 Associate Professor, Department of Civil and Environmental Engineering, University of Nevada, Reno
- 3 Professor, Department of Civil and Environmental Engineering, University of Nevada, Reno

MCEER

University at Buffalo, The State University of New York

Red Jacket Quadrangle, Buffalo, NY 14261

Phone: (716) 645-3391; Fax (716) 645-3399

E-mail: mceer@buffalo.edu; WWW Site: <http://mceer.buffalo.edu>

NTIS DISCLAIMER



This document has been reproduced from the best copy furnished by the sponsoring agency.

Preface

The Multidisciplinary Center for Earthquake Engineering Research (MCEER) is a national center of excellence in advanced technology applications that is dedicated to the reduction of earthquake losses nationwide. Headquartered at the University at Buffalo, State University of New York, the Center was originally established by the National Science Foundation in 1986, as the National Center for Earthquake Engineering Research (NCEER).

Comprising a consortium of researchers from numerous disciplines and institutions throughout the United States, the Center's mission is to reduce earthquake losses through research and the application of advanced technologies that improve engineering, pre-earthquake planning and post-earthquake recovery strategies. Toward this end, the Center coordinates a nationwide program of multidisciplinary team research, education and outreach activities.

MCEER's research is conducted under the sponsorship of two major federal agencies, the National Science Foundation (NSF) and the Federal Highway Administration (FHWA), and the State of New York. Significant support is also derived from the Federal Emergency Management Agency (FEMA), other state governments, academic institutions, foreign governments and private industry.

The Center's Highway Project develops improved seismic design, evaluation, and retrofit methodologies and strategies for new and existing bridges and other highway structures, and for assessing the seismic performance of highway systems. The FHWA has sponsored three major contracts with MCEER under the Highway Project, two of which were initiated in 1992 and the third in 1998.

Of the two 1992 studies, one performed a series of tasks intended to improve seismic design practices for new highway bridges, tunnels, and retaining structures (MCEER Project 112). The other study focused on methodologies and approaches for assessing and improving the seismic performance of existing "typical" highway bridges and other highway system components including tunnels, retaining structures, slopes, culverts, and pavements (MCEER Project 106). These studies were conducted to:

- assess the seismic vulnerability of highway systems, structures, and components;
- develop concepts for retrofitting vulnerable highway structures and components;
- develop improved design and analysis methodologies for bridges, tunnels, and retaining structures, which include consideration of soil-structure interaction mechanisms and their influence on structural response; and
- develop, update, and recommend improved seismic design and performance criteria for new highway systems and structures.

The 1998 study, “Seismic Vulnerability of the Highway System” (FHWA Contract DTFH61-98-C-00094; known as MCEER Project 094), was initiated with the objective of performing studies to improve the seismic performance of bridge types not covered under Projects 106 or 112, and to provide extensions to system performance assessments for highway systems. Specific subjects covered under Project 094 include:

- development of formal loss estimation technologies and methodologies for highway systems;
- analysis, design, detailing, and retrofitting technologies for special bridges, including those with flexible superstructures (e.g., trusses), those supported by steel tower substructures, and cable-supported bridges (e.g., suspension and cable-stayed bridges);
- seismic response modification device technologies (e.g., hysteretic dampers, isolation bearings); and
- soil behavior, foundation behavior, and ground motion studies for large bridges.

In addition, Project 094 includes a series of special studies, addressing topics that range from non-destructive assessment of retrofitted bridge components to supporting studies intended to assist in educating the bridge engineering profession on the implementation of new seismic design and retrofitting strategies.

The end cross frames of steel plate girder bridges are critical elements in the transverse seismic load path of the superstructure. It has been suggested that if these cross frames were to yield in a ductile manner, the elastic base shear in the bridge would be substantially reduced. This report describes experimental and analytical studies on a two girder bridge superstructure to investigate the validity of this proposition. Two types of end cross frames are studied, one comprising ductile single angle braces, and the other buckling restrained braces. The results show a reduced base shear that is about 40% of the elastic base shear. The buckling restrained braces resulted in 20% to 30% smaller drifts in the superstructure than with the X-braces at the same level of base shear, a result that is attributed to better energy dissipation. Removing some shear studs near the supports of the girders, and allowing the transverse shear to be transferred into the end cross frames using the top chord, allows the girders to “rock,” enabling considerable transverse drifts in the girders without distress to the slab-girder connection. The maximum drift measured in the girders during the experiments was 7% of the girder height, with no damage observed in the girders or bearings, and minimal distress to the deck slab. Lead-rubber isolation bearings were also used to reduce the seismic base shear, and shown to give a greater reduction in the base shear than was possible with the ductile end cross frames. However, the capacity of the bearings was limited by their stability, with the critical limit state being observed in the bearings during large ground motions.

ABSTRACT

The end cross frames of steel plate girder bridges are critical elements in the transverse seismic load path of the superstructure. It has been suggested that if these cross frames were to yield in a ductile manner, the elastic base shear in the bridge would be substantially reduced. This report describes experimental and analytical studies on a two girder bridge superstructure to investigate the validity of this proposition. End cross frames comprising of ductile single angle braces and later buckling restrained braces are studied and the results presented which show reduced base shear of the order of 40% of the elastic base shear. The buckling restrained braces resulted in 20% to 30% smaller drifts in the superstructure than with the X-braces at the same level of base shear, a result that is attributed to better energy dissipation, although the displacement capacity of the X-braces was greater. Removing some shear studs near the supports of the girders, and allowing the transverse shear to be transferred into the end cross frames using the top chord, allows the girders to “rock” enabling considerable transverse drifts in the girders without distress to the slab-girder connection. The maximum drift measured in the girders during experiments was 7% of the girder height, with no damage observed in the girders, bearings and minimal distress to the deck slab. Lead rubber isolation bearings were also used to reduce the seismic base shear, with a greater reduction in the elastic base shear possible using the isolators than possible with the ductile end cross frames. The capacity of the bearings was limited by their stability, with the critical limit observed in the bearings with large ground motions.

ACKNOWLEDGEMENTS

This project was funded by the Federal Highway Administration through the Highway Project at the Multidisciplinary Center for Earthquake Engineering, University of Buffalo under contract DTFH61-98-C-00094. Additional funding was provided by the California Department of Transportation under contract 59Y564. Grateful acknowledgement is made of both agencies for their generous support.

The authors would also like to acknowledge the contribution of Nippon Steel Corporation for providing the buckling restrained braces used in this study with the assistance of Dr. Ian Aiken. In addition they would like to thank Dynamic Isolation Systems for providing the lead rubber isolation bearings. Francisco Garcia-Alvarez is acknowledged for his enormous effort in the construction of the bridge and early experimentation. Thanks is also extended to the laboratory manager, Patrick Laplace, and development technician, Paul Lucas for their efforts.

This report was prepared by the first author and as part of this authors' doctoral dissertation and supervised by the second and third authors. Opinions expressed in this report are those of the authors and do not necessarily reflect the views of the funding organisations.

TABLE OF CONTENTS

SECTION	TITLE	PAGE
1	INTRODUCTION	1
1.1	Overview	1
1.2	Transverse Seismic Design using Ductile Elements in the Superstructure	1
1.2.1	General Principles	1
1.2.2	Previous Research on Ductile End Cross Frames or Diaphragms in Bridges	6
1.2.3	Other Potential Ductile Systems	8
1.2.4	Seismic Isolation	10
1.3	Superstructure Flexibility	10
1.4	Objectives and Scope	10
2	ANALYSIS AND DESIGN OF THE BRIDGE MODEL	13
2.1	Introduction	13
2.2	General Design of Bridge Model	13
2.3	Design of Critical Components in the Ductile Transverse Response of the Bridge	16
2.3.1	Overview	16
2.3.2	Analysis Procedures	17
2.3.2.1	Response Modification Factor Design	17
2.3.2.2	Displacement Based Design Approach using a Capacity Spectrum Analysis	20
2.3.3	Ductile Columns - Elastic X-Braces	22
2.3.4	Ductile End Cross Frames using Light Single Angle X-Braces – Elastic Substructure	25
2.3.5	Ductile End Cross Frames using Unbonded Braces - Elastic Substructure	29
2.3.6	Seismic Isolation using Lead Rubber Bearings	31
2.4	Simulation of Earthquake Loading	32
2.4.1	Reversed Static Transverse Loading	32
2.4.2	Shake Table Earthquake Simulation	33
2.5	Instrumentation	39
2.5.1	Overview	39
2.5.2	Load Cells	45
2.5.3	Displacement Transducers	45
2.5.4	Accelerometers	45
2.5.5	Strain Gages	48
3	CYCLIC BEHAVIOR OF INELASTIC COMPONENTS IN THE BRIDGE MODEL	55
3.1	Introduction	55
3.2	Single Angle X-Brace Diagonals	55
3.2.1	Coupon Tests	55
3.2.2	Axial Component Experiments	55
3.2.2.1	Background	55
3.2.2.2	Experimental Assembly	56
3.2.2.3	Hysteretic Properties	60
3.2.2.4	Yield Tensile Strength	60

TABLE OF CONTENTS (CONT'D)

SECTION	TITLE	PAGE
3.2.2.5	Buckling Capacity	73
3.2.2.6	Ultimate Displacement Capacity	75
3.2.2.7	Energy Dissipation in the Single Angles	77
3.2.3	Analytical Model of Single Angle Members	77
3.3	Unbonded Braces	82
3.3.1	Overview	82
3.3.2	Coupon Tests	82
3.3.3	Axial Component Experiments	83
3.3.3.1	Experimental Setup	83
3.3.3.2	Hysteretic Properties	90
3.3.3.3	Axial Forces	94
3.3.3.4	Ultimate and Cumulative Displacement Capacity	94
3.3.3.5	Energy Dissipation in the Unbonded Braces	97
3.3.3.6	Strain Gage Readings	99
3.3.4	Analytical Model	99
3.4	Lead Rubber Bearings	106
3.4.1	Overview	106
3.4.2	Experimental Setup	106
3.4.3	Hysteretic Properties	106
3.4.4	Energy Dissipation	109
3.4.5	Analytical Model	109
4	PERFORMANCE OF THE BRIDGE SUPERSTRUCTURE WITH ELASTIC AND DUCTILE END CROSS FRAMES	111
4.1	Introduction	111
4.2	Deformation of Ends of Bridge Model	111
4.3	Results from Reversed Static Experiments	113
4.3.1	Background	113
4.3.2	Experiment RSHXB1 - Elastic Heavy Single Angle X-Braces -Preliminary	113
4.3.3	Experiment RSHXB2 -Essentially Elastic Heavy Single Angle X-Braces	115
4.3.3.1	Hysteretic Behavior	115
4.3.4	Experiment RSLXB -Light Single Angle X-Braces	115
4.3.4.1	Overview	115
4.3.4.2	Yield Forces	120
4.3.4.3	Post-Yield Forces	121
4.3.4.4	Maximum Displacements	121
4.4	Results from Shake Table Experiments	124
4.4.1	Experiment STHXB - Elastic Heavy Single Angle X-Braces	124
4.4.1.1	Response to El Centro	124
4.4.1.2	Response to Sylmar and Kobe	124
4.4.2	Experiment STLXB - Inelastic Light Single Angle X-Braces	128
4.4.2.1	Overall Response	128
4.4.2.2	Yield Forces	128

TABLE OF CONTENTS (CONT'D)

SECTION	TITLE	PAGE
4.4.2.3	Post-Yield Forces	133
4.4.2.4	Maximum Displacements	133
4.4.2.5	Permanent Drift in the Cross Frames	134
4.4.3	Experiment STPUB -Unbonded Braces with Pin Ended Connections	135
4.4.3.1	Effect of Removing Shear Studs at Ends of Bridge Model	135
4.4.3.2	Hysteretic Response	136
4.4.3.3	Yield Forces	136
4.4.3.4	Post-Yield Force	140
4.4.3.5	Maximum Displacements	140
4.4.3.6	Permanent Drift in the Cross Frames	142
4.4.4	Experiment STFUB -Unbonded Braces with Fixed End Connections	143
4.4.4.1	Hysteretic Response	143
4.4.4.2	Maximum Forces	147
4.4.4.3	Maximum Displacements	148
4.4.4.4	Response to Sylmar and Kobe.	148
4.4.5	Experiment STFUB2S - Response of Two Span Bridge with Ductile End Cross Frames	148
4.5	Comparisons and Design Parameters for Ductile End Cross Frames	148
4.5.1	Post-Earthquake Evaluation	150
5	PERFORMANCE OF THE BRIDGE SUPERSTRUCTURE WITH SEISMIC ISOLATORS	153
5.1	Introduction	153
5.2	Transverse Response of the Simply Supported Bridge Model	153
5.2.1	Hysteretic Response	153
5.2.2	Initial Stiffness	153
5.2.3	Characteristic Strength	155
5.2.4	Post-yield Stiffness	158
5.2.5	Maximum Displacement and Critical Load	159
5.2.6	Longevity of Isolation Bearings	162
5.3	Biaxial Response of Simply Supported Bridge Model	162
5.4	Differential Support Excitation	167
5.5	Response of the Two Span Bridge Model	168
5.6	Comparisons with Ductile End Cross Frames and Design Parameters for Seismic Isolation Bearings	171
6	PARAMETRIC STUDIES AND COMPARISONS OF THE NON-LINEAR TRANSVERSE RESPONSE OF THE BRIDGE MODEL WITH DUCTILE END CROSS FRAMES AND SEISMIC ISOLATORS	173
6.1	Introduction	173
6.2	Non-Linear Modeling of the Bridge Model	173
6.2.1	Modeling of the Ductile X-braces, Unbonded Braces and Lead Rubber Bearings	173
6.2.2	Response during Reversed Static Experiments	176

TABLE OF CONTENTS (CONT'D)

SECTION	TITLE	PAGE
6.2.3	Response during Shake Table Experiments	182
6.2.4	Summary and Comparison of Maximum Response for Ductile Systems	197
6.3	Cumulative Plastic Strain Demand	197
6.4	Parametric Studies	199
6.4.1	Ductile End Cross Frames and Seismic Isolation Systems of Different Strengths	199
6.4.2	Response to Artificial Design Level Earthquakes	199
6.4.3	Parametric Studies on Superstructure Stiffness	202
6.4.4	Parametric Studies on Substructure Stiffness	206
7	CONCLUSIONS AND RECOMMENDATIONS	207
7.1	Summary	207
7.2	Conclusions	209
7.3	Recommendations	210
8	REFERENCES	213
	APPENDIX A. PROPERTIES OF LEAD RUBBER BEARINGS	219

LIST OF FIGURES

FIGURE	TITLE	PAGE
1-1	Damage to bearing assembly of Santa-Clara River bridge during 1994 Northridge earthquake (Astaneh-Asl, 1994)	2
1-2	End cross frame gusset plate fracture in Pico-Lyons Overcrossing during 1994 Northridge earthquake (Astaneh-Asl, 1994)	2
1-3	Bearing stiffener damage in Pico-Lyons Overcrossing during 1994 Northridge earthquake (Astaneh-Asl, 1994)	3
1-4	Damage to girders of Hanshin Expressway during 1995 Hyogen-Nanbu earthquake	3
1-5	Damage to girders and bracing of Hanshin Expressway during 1995 Hyogen-Nanbu (Kobe) earthquake	4
1-6	Fractured lateral bracing and buckled cross frame in Capitol Arch bridge during 2001 Nisqually earthquake (WSDOT, 2001)	4
1-7	Damaged web stiffener in Capitol Arch bridge during 2001 Nisqually earthquake (WSDOT, 2001)	5
1-8	Ductile end cross frame using curved single angle members (Astaneh-Asl, 1996)	5
1-9	Ductile end diaphragms using: a) shear panel system (SPS); b) eccentric braced frame (EBF), and; c) triangular-plate added damping and stiffness device (TADAS) (Zahrai, 1998b)	7
1-10	Typical X-brace cross frame shown at intermediate cross frame location	8
1-11	Typical configuration of buckling restrained (unbonded) brace	9
2-1	Slab-on-girder bridge superstructure model	13
2-2	Steel plate girder bridge model - girder and deck slab dimensions	14
2-3	Bridge model deck slab reinforcing	14
2-4	Typical intermediate cross frame in bridge model	15
2-5	Laminated elastomeric bearing	16
2-6	Lead rubber bearing with transverse restraints	16
2-7	Shape function for transverse deformation of simply supported bridge	17
2-8	Terms for definition of bi-linear model	21
2-9	“Heavy” end cross frames at the north end in the bridge model	24
2-10	“Heavy” end cross frames at the south end in the bridge model	25
2-11	“Heavy” end cross frames in the bridge model with welded connections	26
2-12	“Light” end cross frames in the bridge model	27
2-13	Unbonded brace in the bridge model	28
2-14	Deformed end region of two girder bridge with trimmed bearing stiffeners	30
2-15	Deformed end region of two girder bridge with “rocking” girders	30
2-16	Lead rubber bearing	32
2-17	Actuator connected to bridge model at 1/3 points along length of bridge	33
2-18	Actuator displacements vs time for RSHXB1	35
2-19	Actuator forces vs time for RSHXB1	35
2-20	Actuator forces vs time for RSHXB2	36
2-21	Actuator forces vs time for RSLXB	36
2-22	Bridge Model attached to three 50 ton shake tables	37

LIST OF FIGURES (CONT'D)

FIGURE	TITLE	PAGE
2-23	Acceleration time histories for a) 180 component and b) 270 component of El Centro	40
2-24	Acceleration time histories for a) 360 component and b) 90 component of Sylmar	41
2-25	Acceleration time histories for a) 00 component and b) 90 component of Kobe	42
2-26	Acceleration time histories for El Centro 180 component through soil layer	43
2-27	Theoretical earthquake response spectra (5% damping)	43
2-28	Earthquake response spectrum for 2.0 El Centro (5% damping)	44
2-29	Multi-axial Load Cell	44
2-30	Instrumentation -load cells	46
2-31	Instrumentation -Displacement Transducers	47
2-32	Instrumentation - Typical displacement transducers for end X-braces	48
2-33	Instrumentation - Displacement transducers for unbonded braces	49
2-34	Instrumentation -Accelerometers	50
2-35	Instrumentation - Strain gages on end cross frames	51
2-36	Instrumentation - Strain gages on typical intermediate cross frame	52
2-37	Instrumentation -Additional strain gages on end stiffener	52
2-38	Instrumentation - Strain gages on east girder	53
2-39	Instrumentation - Strain gages on west girder	54
3-1	Single angle component experiment specimens	57
3-2	Single angle with unreinforced bolted connection to gusset plate	58
3-3	Single angle with reinforced bolted connection to gusset plate	59
3-4	Single angle with balanced welded connection to gusset plate	59
3-5	Experimental setup for axial loading of single angle specimens	61
3-6	Failure of single angle with unreinforced bolted connection	62
3-7	Failure of single angle with reinforced bolted connection	62
3-8	Failure of single angle with welded connection	63
3-9	Hysteresis loop of single angle specimen A	63
3-10	Hysteresis loop of single angle specimen B	64
3-11	Hysteresis loop of single angle specimen C	64
3-12	Hysteresis loop of single angle specimen D	65
3-13	Hysteresis loop of single angle specimen E	65
3-14	Hysteresis loop of single angle specimen F	66
3-15	Hysteresis loop of single angle specimen G	66
3-16	Hysteresis loop of single angle specimen H	67
3-17	Hysteresis loop of single angle specimen I	67
3-18	Hysteresis loop of single angle specimen J	68
3-19	Hysteresis loop of single angle specimen K	68
3-20	Hysteresis loop of single angle specimen L	69
3-21	Hysteresis loop of single angle specimen M	69
3-22	Hysteresis loop of single angle specimen N	70
3-23	Hysteresis loop of single angle specimen O	70

LIST OF FIGURES (CONT'D)

FIGURE	TITLE	PAGE
3-24	Hysteresis loop of single angle specimen P	71
3-25	Hysteresis loop of single angle specimen Q	71
3-26	Illustration of ratio of enclosed hysteretic area to rectangular area bounded by maximum force and displacement for given cycle of loading	78
3-27	Energy dissipated per cycle for long, heavy single angle specimens	78
3-28	Energy dissipated per cycle for short, heavy single angle specimens	79
3-29	Energy dissipated per cycle for long, light single angle specimens	79
3-30	Energy dissipated per cycle for short, light single angle specimens	80
3-31	Hysteresis loops for single angle analytical model for loading history equivalent to loading history for single angle specimen P	81
3-32	Hysteresis loops for single angle analytical model for loading history equivalent to loading history for single angle specimen Q	81
3-33	Energy dissipated per cycle for analytical models of Specimens P and Q	82
3-34	Experimental setup for testing of unbonded braces	84
3-35	Pin ended connection in unbonded brace component experiment	85
3-36	Fixed ended connection in unbonded brace component experiment	85
3-37	Displacement history for unbonded brace A	86
3-38	Displacement history for unbonded brace B	87
3-39	Displacement history for unbonded brace C	87
3-40	Displacement history for unbonded brace D	88
3-41	Displacement history for unbonded brace E	88
3-42	Displacement history for unbonded brace F	89
3-43	Displacement history for unbonded brace G	89
3-44	Hysteresis loop for unbonded brace A	90
3-45	Hysteresis loop for unbonded brace B	91
3-46	Hysteresis loop for unbonded brace C	91
3-47	Hysteresis loop for unbonded brace D	92
3-48	Hysteresis loop for unbonded brace E	92
3-49	Hysteresis loop for unbonded brace F	93
3-50	Hysteresis loop for unbonded brace G	93
3-51	Comparison of response for dynamic and static loading histories for unbonded braces C and D	96
3-52	Comparison of response for dynamic and static loading histories for unbonded braces C and E	96
3-53	Energy dissipated per cycle for different unbonded braces based on displacements across the core length	98
3-54	Energy dissipated per cycle for unbonded brace A considering hysteretic behavior across the core length and across the total length	98
3-55	Strain gage 1 on unbonded brace B	100
3-56	Strain gage 2 on unbonded brace B	100
3-57	Strain gage 3 on unbonded brace B	101
3-58	Strain gage 4 on unbonded brace B	101

LIST OF FIGURES (CONT'D)

FIGURE	TITLE	PAGE
3-59	Measured axial forces vs axial forces computed using measured strains for unbonded brace A while responding elastically	102
3-60	Hysteresis loops for analytical model of unbonded brace A	103
3-61	Hysteresis loops for analytical model of unbonded brace B	103
3-62	Hysteresis loops for analytical model of unbonded brace C	104
3-63	Hysteresis loops for analytical model of unbonded brace D	104
3-64	Hysteresis loops for analytical model of unbonded brace D with yield strength increased by 15% to allow for dynamic loading	105
3-65	Energy dissipated per cycle for bi-linear models of different unbonded braces	105
3-66	Hysteresis loops for lead rubber bearings A & B	107
3-67	Hysteresis loops for lead rubber bearings C & D	107
3-68	Hysteresis loops for lead rubber bearings E & F	108
3-69	Energy dissipated per cycle for lead rubber bearings	108
4-1	Deformed end region for bridge model due to lateral shear with rotation of the girders about their vertical longitudinal axes	112
4-2	Deformed end region for bridge model due to lateral shear assuming rotation of the entire section with axial deformations in bearings	112
4-3	Deformed end region for bridge model resulting in distortion of section with axial deformations in bearings	113
4-4	RSHXB1 - Hysteresis loop for diagonals of north end cross frames (all cycles)	114
4-5	RSHXB1 - Hysteresis loop for diagonals of south end cross frames (all cycles)	114
4-6	RSHXB2 - Hysteresis loops for actuators	116
4-7	RSHXB2 -Load cell end shear force vs horizontal displacement measured at deck slab level for each end	116
4-8	RSHXB2 -Load cell end shear force vs horizontal displacement measured using the diagonal displ.transducer between the top and bottom girder flanges at each end	117
4-9	RSHXB2 -Load cell end shear force vs displacement in end cross frame diagonals at north end	117
4-10	RSHXB2 -Load cell end shear force vs displacement in end cross frame diagonals at south end	118
4-11	RSLXB - Actuator hysteresis loops	118
4-12	RSLXB -Load cell end shear force vs horizontal deck slab displacement at both ends	119
4-13	RSLXB -Load cell end shear force vs horizontal displacement measured between the top and bottom flanges of the girders at both ends	119
4-14	RSLXB - Hysteresis loop for diagonal angles of north end cross frames	122
4-15	RSLXB - Hysteresis loop for diagonal angles of south end cross frames	123
4-16	RSLXB - Midspan displacement	123
4-17	STHXB - North end shear vs end horizontal displacement at deck slab in response to 2.0 El Centro	125
4-18	STHXB - South end shear vs end horizontal displacement at deck slab in response to 2.0 El Centro	125

LIST OF FIGURES (CONT'D)

FIGURE	TITLE	PAGE
4-19	STHXB - North end shear vs end horizontal displacement of deck slab relative to average bearing displacement in response to 2.0 El Centro	126
4-20	STHXB - South end shear vs end horizontal displacement of deck slab relative to average bearing displacement in response to 2.0 El Centro	126
4-21	STHXB -North end shear vs end horizontal displacement between top and bottom flanges in response to 2.0 El Centro	127
4-22	STHXB -South end shear vs end horizontal displacement between top and bottom flanges in response to 2.0 El Centro	127
4-23	STLXB - North end shear vs end deck slab displacement relative to average bearing displacement in response to increasing amplitude El Centro ground motions	129
4-24	STLXB - South end shear vs end deck slab displacement relative to average bearing displacement in response to increasing amplitude El Centro ground motions	129
4-25	STLXB - Envelopes for hysteresis loops at north and south ends	130
4-26	STLXB - North end shear vs end deck slab displacement relative to average bearing displacement in response to 2.0 El Centro ground motion	130
4-27	STLXB - South end shear vs end deck slab displacement relative to average bearing displacement in response to 2.0 El Centro ground motion	131
4-28	STLXB - North end shear vs horizontal displacement measured at deck slab level in response to increasing amplitude El Centro ground motions	131
4-29	STLXB - South end shear vs horizontal displacement measured at deck slab level in response to increasing amplitude El Centro ground motions	132
4-30	STLXB - North end shear vs horizontal displacement measured between top and bottom flanges of girders in response to increasing amplitude El Centro	132
4-31	STLXB - South end shear vs horizontal displacement measured between top and bottom flanges of girders in response to increasing amplitude El Centro	133
4-32	STLXB - Total base shear vs horizontal midspan deck slab displacement measured in response to increasing amplitude El Centro ground motions	134
4-33	STLXB -Horizontal displacement time histories for ends of bridge model measured at the deck slab relative to the average bearing displacement in response to increasing amplitude excitation up to 2.0 El Centro	135
4-34	STPUB - North end shear vs end deck slab displacement relative to the bearing displacement in response to increasing amplitude excitation up to 2.0 El Centro	137
4-35	STPUB - South end shear vs end deck slab displacement relative to the bearing displacement in response to increasing amplitude excitation up to 2.0 El Centro	137
4-36	STPUB - North end shear vs horizontal displacement measured between the top and bottom flange of the girders in response to increasing amplitude excitation up to 2.0 El Centro	138
4-37	STPUB - South end shear vs horizontal displacement measured between the top and bottom flange of the girders in response to increasing amplitude excitation up to 2.0 El Centro	138

LIST OF FIGURES (CONT'D)

FIGURE	TITLE	PAGE
4-38	STPUB - North end shear vs end deck slab displacement relative to the bearing displacement in response to 2.25 El Centro	139
4-39	STPUB - South end shear vs end deck slab displacement relative to the bearing displacement in response to 2.25 El Centro	139
4-40	STPUB - End shear vs axial displacement for braces with pinned connections in response ramped up to 2.0 El Centro	141
4-41	STPUB - End shear vs axial displacement for braces with pinned connections in response to 2.25 El Centro	141
4-42	Deformed unbonded brace mechanism showing end displacement relative to axial displacement of brace	142
4-43	Alternative configuration for unbonded brace with increased core length	143
4-44	STPUB -Horizontal displacement time histories for ends of bridge model measured between top and bottom flange of girders in response to increasing amplitude excitation up to 2.0 El Centro	144
4-45	STFUB - North end shear vs end deck slab displacement relative to the bearing displacement in response to 2.0 El Centro	144
4-46	STFUB - South end shear vs end deck slab displacement relative to the bearing displacement in response to 2.0 El Centro	145
4-47	STFUB - North end shear vs end deck slab displacement relative to the bearing displacement in response to 2.25 El Centro	145
4-48	STFUB - South end shear vs end deck slab displacement relative to the bearing displacement in response to 2.25 El Centro	146
4-49	STFUB - End shear vs axial displacement for braces with fixed connections in response to 2.25 El Centro	146
4-50	STFUB - North end shear vs end deck slab displacement relative to the bearing displacement in response to 1.0 Kobe	147
4-51	Haunch of deck slab and girder at midspan after maximum excitation at midspan resulting in 7% drift in the girders	149
5-1	STLRB - Relative deck slab displacement in response to 2.0 El Centro	154
5-2	STLRB - Deck and bearing displacements at north end in response to 2.0 El Centro	154
5-3	STLRB - Deck and bearing displacements at south end in response to 2.0 El Centro	155
5-4	STLRB -Hysteretic response of bearings at north end for 0.25 - 2.0 El Centro compared to backbone and design curves	156
5-5	STLRB - Hysteretic response of bearings at south end for 0.25 - 2.0 El Centro compared to backbone and design curves	156
5-6	STLRB - Hysteresis loop at north end in response to 0.25 El Centro compared with calculated initial slope	157
5-7	STLRB - Hysteresis loop at north end in response to 1.5 El Centro Soil	157
5-8	STLRB -Hysteresis loop at south end in response to 1.5 El Centro Soil	158

LIST OF FIGURES (CONT'D)

FIGURE	TITLE	PAGE
5-9	STLRB -Longitudinal bearing response at each end for 1.5 El Centro with rock excitation at north end and soil excitation at south end	160
5-10	STLRB - Average longitudinal bearing displacement vs total base shear in response to 1.5 El Centro with rock excitation at north end and soil excitation at south end	160
5-11	STLRB -Longitudinal bearing response at each end for 2.0 El Centro with rock excitation at north end and soil excitation at south end	161
5-12	STLRB - Average longitudinal bearing displacement vs total base shear in response to 2.0 El Centro with rock excitation at north end and soil excitation at south end	161
5-13	STLRB, STLRBS2 - Hysteretic response of north end in response to 2.0 El Centro during two different series of shake table experiments	163
5-14	STLRB, STLRBS2 - Hysteretic response of south end in response to 2.0 El Centro during two different series of shake table experiments	163
5-15	STLRB - Longitudinal shake table displacements in response to 1.5 El Centro with rock excitation at north end and soil excitation at south end	169
5-16	STLRB - Longitudinal bearing response to 1.5 El Centro with rock excitation at both ends	169
5-17	STLRB - Longitudinal bearing response to 1.5 El Centro with soil excitation at both ends	170
5-18	STLRB2S -Bearing displacements in response to 2.0 El Centro	170
5-19	STLRB - Envelopes for horizontal bearing displacements and corresponding maximum and minimum design bi-linear models	171
6-1	Illustration of simplified non-linear analytical model of bridge	174
6-2	End region of analytical model with heavy X-braces	174
6-3	End region of analytical model with light X-braces	175
6-4	End region of analytical model with buckling restrained brace	175
6-5	RSNECF -End shear vs end displacement at north end of analytical model compared to experimental data	177
6-6	RSNECF -End shear vs end displacement at south end of analytical model compared to experimental data	177
6-7	RSNECF -Total applied force vs midspan deck slab displacement of analytical model compared to experimental data	178
6-8	RSPC -End shear vs end displacement at north end of analytical model compared to experimental data	179
6-9	RSPC -End shear vs end displacement at south end of analytical model compared to experimental data	179
6-10	RSPC -Total applied force vs midspan displacement of analytical model compared to experimental data	180
6-11	RSHXB2 -End shear vs end displacement at north end of analytical model compared to experimental data	180

LIST OF FIGURES (CONT'D)

FIGURE	TITLE	PAGE
6-12	RSHXB2 -End shear vs end displacement at south end of analytical model compared to experimental data	181
6-13	RSHXB2 - Total applied force vs midspan displacement of analytical model compared to experimental data	181
6-14	RSLXB -End shear vs end displacement at north end of analytical model compared to experimental data	183
6-15	RSLXB -End shear vs end displacement at south end of analytical model compared to experimental data	183
6-16	RSLXB - Total applied force vs midspan displacement of analytical model compared to experimental data	184
6-17	STNECF -End shear vs end displacement at north end of analytical model compared to experimental data in response to 1.0 El Centro	184
6-18	STNECF -End shear vs end displacement at south end of analytical model compared to experimental data in response to 1.0 El Centro	185
6-19	STNECF - Total shear vs midspan displacement of analytical model compared to experimental data in response to 1.0 El Centro	185
6-20	STHXB - End shear vs displacement at north end of analytical model compared to experimental data in response to 2.0 El Centro	186
6-21	STHXB - End shear vs displacement at south end of analytical model compared to experimental data in response to 2.0 El Centro	186
6-22	STHXB -Total shear vs midspan displacement of analytical model compared to experimental data in response to 1.0 El Centro	187
6-23	STLXB -End shear vs displacement at north end of analytical model compared to experimental data in response to 1.5 El Centro	188
6-24	STLXB -End shear vs displacement at south end of analytical model compared to experimental data in response to 1.5 El Centro	188
6-25	STLXB -End shear vs displacement at north end of analytical model compared to experimental data in response to 2.0 El Centro after previous excitation	189
6-26	STLXB -End shear vs displacement at south end of analytical model compared to experimental data in response to 2.0 El Centro after previous excitation	189
6-27	STLXB - Total shear vs midspan displacement of analytical model compared to experimental data in response to 2.0 El Centro	191
6-28	STLXB -End shear vs displacement at north end of analytical model compared to experimental data in response to 2.0 El Centro assuming no prior loading	191
6-29	STLXB -End shear vs displacement at south end of analytical model compared to experimental data in response to 2.0 El Centro assuming no prior loading	192
6-30	STFUB -End shear vs displacement at north end of analytical model compared to experimental data in response to 2.0 El Centro	192
6-31	STFUB -End shear vs displacement at south end of analytical model compared to experimental data in response to 2.0 El Centro	193
6-32	STFUB - Total shear vs midspan displacement of analytical model compared to experimental data in response to 2.0 El Centro	193

LIST OF FIGURES (CONT'D)

FIGURE	TITLE	PAGE
6-33	STPUB -End shear vs displacement at north end of analytical model compared to experimental data in response to 2.0 El Centro neglecting slippage	194
6-34	STPUB -End shear vs displacement at south end of analytical model compared to experimental data in response to 2.0 El Centro neglecting slippage	194
6-35	STPUB - Total shear vs midspan displacement of analytical model compared to experimental data in response to 2.0 El Centro neglecting slippage	195
6-36	STLRB - End shear vs bearing displacement at north end of analytical model compared to experimental data in response to 2.0 El Centro	195
6-37	STLRB - End shear vs bearing displacement at north end of analytical model compared to experimental data in response to 2.0 El Centro	196
6-38	STLRB - End shear vs bearing displacement at north end of analytical model compared to experimental data in response to 2.0 El Centro	196
6-39	Acceleration response spectrum for simulated earthquake to match the time scaled AASHTO isolation design spectrum, site II.	200
6-40	Acceleration time history for simulated earthquake using RSCTH (SUNY, 2002) to match the time scaled AASHTO isolation design spectrum, site II.	200
6-41	Acceleration time history for first simulated earthquake using SIMQKE (Gasparini, 1976) to match the time scaled AASHTO isolation design spectrum, site II.	201
6-42	Acceleration time history for second simulated earthquake using SIMQKE (Gasparini, 1976) to match the time scaled AASHTO isolation design spectrum, site II.	201
6-43	Maximum total base shear versus maximum north end drift in response to artificial design level earthquake	203
6-44	Maximum base shear for bridge model with different superstructure stiffnesses in response to artificial design level earthquakes	204
6-45	Maximum end drift for bridge model with different superstructure stiffnesses in response to artificial design level earthquakes	204
6-46	Maximum base shear for bridge model with different substructure stiffnesses in response to artificial design level earthquakes	205
6-47	Maximum end drift for bridge model with different substructure stiffnesses in response to artificial design level earthquakes	205

LIST OF TABLES

TABLE	TITLE	PAGE
2-1	Damping Coefficient, B	22
2-2	Reversed Static Experiments	34
2-3	Shake Table Experiments	38
2-4	Earthquake Data for Shake Table Experiments	39
3-1	Coupon Test Results for Single Angle Members from ASTM A36 Steel	55
3-2	Details of Component Experiments on Single Angle Members	56
3-3	Measured and calculated tensile forces in the single angle specimens	72
3-4	Measured Buckling Force and Calculated Effective Length Factor for Single Angle Specimens	74
3-5	Ultimate Axial Strain and Cumulative Plastic Strains in Single Angle Specimens	75
3-6	Coupon Test Results for Unbonded Braces from LYP-225 Steel	83
3-7	Yield and Maximum Forces for Unbonded Braces	95
3-8	Maximum Strains, Cumulative Plastic Strains and Cumulative Plastic Ductilities in Unbonded Braces during Bridge and Component Experiments	95
3-9	Design Bi-Linear Properties for Lead Rubber Bearings at 100% Shear Strain	106
4-1	Maximum Axial Brace Displacements at End and Midspan of 2 Span Bridge Model with Unbonded Braces in Response to Different Earthquake Excitations	150
4-2	Comparisons of Bridge Model Response with X-braces and Unbonded Braces	151
5-1	Combined Maximum Displacements from Uniaxial Excitation of the Bridge Model	165
5-2	Measured and Calculated Maximum Displacements from Biaxial Excitation of the Bridge Model	166
6-1	Comparisons of Bridge Model to Analytical Model Response with X-braces, Unbonded Braces and Lead Rubber Bearings at 2.0 El Centro	197
6-2	Cumulative Plastic Strains and Ductilities in Analytical Model with Single Angle X-Braces for Different Earthquakes Subjected Braces to 3.0% Strain	198
6-3	Cumulative Plastic Strains and Ductilities in Analytical Model with Unbonded Braces for Different Earthquakes Subjected Braces to 3.0% Strain	198

LIST OF SYMBOLS

a_g	Ground acceleration
A	Acceleration coefficient
A_b	Bonded rubber area
A_c	Area of lead core
A_g	Gross cross sectional area of member
A_i	Total bearing rubber area less area of the core
A_n	Net cross sectional area of member
A_r	Overlapping bonded rubber area at large displacements
A_{sc}	Cross sectional area of core plate for buckling restrained brace
A_t	Total bearing rubber area
B	Damping coefficient
B_c	Width (diameter) of lead core
B_b	Bonded bearing rubber width (diameter)
B_t	Total bearing width (diameter)
C^* (C')	Generalized viscous damping
C_s	Seismic coefficient
d	Displacement
d_1, d_2, d_3	Localized displacements
d_g	Horizontal component of diagonal displacement
d_{diag}	Diagonal displacement
d_{dk}	Horizontal deck slab displacement
d_i	Displacement of ductile end cross frame / isolation bearing
d_t	Total design displacement in bearing
d_{yi}	Yield displacement of individual ductile end cross frame /isolation bearing
E	Elastic modulus
E_b	Effective elastic modulus for rubber layer
f_b	Factor for bending stiffness of bearing
F	Force
F_d	Design force
F_y	Nominal yield stress
F_y	Yield force (isolation)

F_{ye}	Expected yield stress
g	Acceleration due to gravity
G	Shear modulus
G_l	Shear modulus of lead
h_{eff}	Effective height between bearings and center of mass (or actuator load)
H	Bearing height
I	Moment of inertia
I_b	Effective moment of inertia of bearing
k_d	Design (post-yield) stiffness of overall system
\bar{k} (k_{bar})	Rubber constant
k_{di}	Design (post-yield) stiffness of individual ductile end cross frame / isolation bearing
k_{eff}	Combined effective stiffness of ductile end cross frame / isolation system and substructure
k_{effi}	Effective (secant) stiffness of ductile end cross frame / isolation bearing
k_l	Shear stiffness of lead core
k_s	Shear stiffness of bearing
k_{sub}	Total substructure stiffness
k_t	Effective transverse stiffness of girder due to torsional stiffness
k_u	Initial stiffness
k_θ	Rotational stiffness
K	Effective length factor
K^* (K')	Generalized stiffness
l	Length of member
L	Length of bridge span
L_{eff}	Effective earthquake excitation factor
M	Total superstructure mass
M^* (M')	Generalized mass
m	Distributed mass per unit length
M_{eff}	Effective modal mass
n_r	Number of rubber layers in bearing
P^*_{eff}	Generalized effective load
P_b	Applied bearing axial load
P_{cro}	Critical buckling load for small displacements
P_{cr}	Critical buckling load for large displacements

P_e	Euler buckling load
P_b	Axial load on bearing
P_{nt}	Nominal tension yield force in member
P_{nc}	Nominal compression strength in member
Q_d	Characteristic strength of overall system
Q_{di}	Characteristic strength of individual ductile end cross frame / isolation bearing
r	Radius of gyration
r_i	Distance from the center of rotation to the center of shear stud
R	Response modification factor
R	Shear stiffness per unit height
s_g	Spacing between the girders
S	Site coefficient
S	Shape factor for rubber layers
t_c	Thickness of cover in bearing
t_i	Individual rubber layer thickness
t_p	Thickness of top and bottom plates
T_{eff}	Effective period
T_r	Total rubber thickness
T_s	Total shim thickness
W	Total weight of the structure
W_i	Weight per bearing
x	Distance along span
Z	Modal displacement
\dot{Z}	Modal velocity
\ddot{Z}	Modal acceleration
Z_x	Response quantity in x-direction
Z_y	Response quantity in y-direction
Z_r	Resultant response quantity from x and y components
α	Flexibility coefficient equal to the ratio of relative displacement at midspan to total displacement at midspan (Fig. 2-7)
α	Ratio of post-yield stiffness to initial stiffness
β_i	Equivalent viscous damping of end cross frame / isolation bearing
δ	Overlap factor

Δ_{ye}	Expected yield displacement
γ_c	Shear strain due to axial loads
γ_r	Shear strain due to rotation from service loads
$\gamma_{s,eq}$	Shear strain due to shear from seismic loads
λ	Slenderness parameter
τ_y	Shear yield stress of lead
Ψ	Shape function

SECTION 1

INTRODUCTION

1.1 Overview

For most bridges located in high seismic zones it is not practical to design them to remain elastic for moderate to large earthquakes. Therefore parts of the structure will respond inelastically during an extreme seismic event, either through design or as these parts happen to be the weakest links. In modern bridges, when ductile seismic design measures are employed, the substructure is typically designed to deform inelastically, therefore column bents and abutments are designed to be ductile with the expectation that the superstructure will remain elastic.

Steel plate girder bridge superstructures are constructed from a number of components, including: the deck slab, shear studs, girders, cross frames and bearings. In the past these components have not been typically designed for seismic loading, with the presumption that the strength of the substructure will limit forces transferred into the superstructure to levels below those which will cause the superstructure components to respond outside their elastic range. However, during recent earthquakes damage to the superstructure was observed in these types of bridges (Figs. 1-1 to 1-7) (Astaneh-Asl, 1994; Shinozuka, 1995; Bruneau, 1996; Chung, 1996). This damage showed that the assumption of all superstructure components remaining elastic during earthquakes is not necessary valid. Furthermore, this damage highlighted the potential to use some of these critical components as ductile elements in order to reduce the forces generated during an earthquake without relying entirely on ductile behavior in the substructure. This has advantages, from protecting the foundations of bridges where damage is difficult to identify and repair, to protecting the substructure for bridges, for example, when the substructure is partially submerged. Confining damage to purpose built ductile elements which can easily be replaced if necessary after an earthquake is a desirable characteristic of a bridge, and could reduce the need for a costly substructure repair and bridge closures. Better still, if devices which can undergo large inelastic deformations without the need for replacement are used then the need for bridge closures and repair costs can be further reduced.

A first report (Carden, 2005) identified the critical components in the transverse seismic load path of a steel girder bridge superstructure and discussed the various actions on these components. In this report elements of the superstructure, more specifically the end cross frames and bearings, are investigated as potentially ductile elements in order to reduce the transverse seismic demand in a steel plate girder bridge.

1.2 Transverse Seismic Design using Ductile Elements in the Superstructure

1.2.1 General Principles

In order to characterize different options for the seismic protection of bridges in the transverse direction it is useful to compare a typical bridge to a building. A typical uniform low-rise building has proportional mass and stiffness in each story resulting in relatively uniform deformations in each story when subjected to seismic loading. It is generally considered beneficial to design each story to yield at around the same time in order to prevent a concentration of deformations in one particular story and a potential “soft story” failure. In contrast a bridge has most of its weight concentrated at the top of the structure, therefore the shear in the structure is relatively constant



FIGURE 1-1 Damage to bearing assembly of Santa-Clara River bridge during 1994 Northridge earthquake (Astaneh-Asl, 1994)

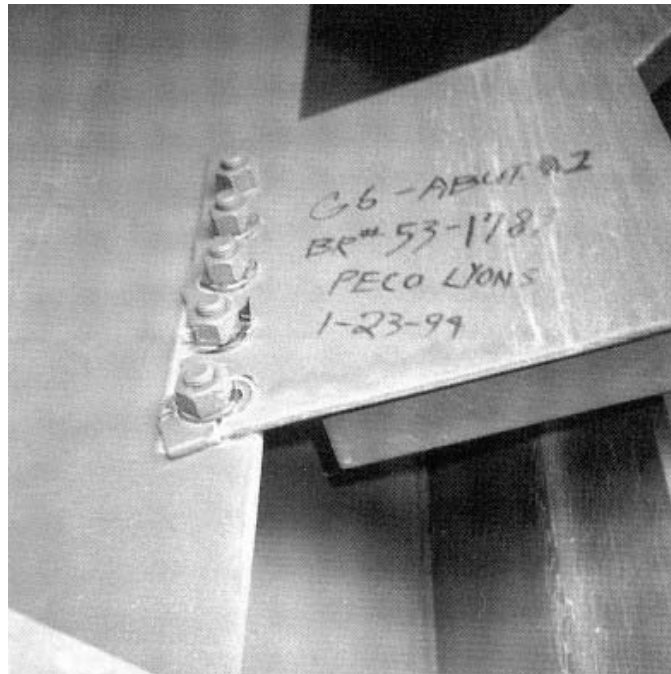


FIGURE 1-2 End cross frame gusset plate fracture in Pico-Lyons Overcrossing during 1994 Northridge earthquake (Astaneh-Asl, 1994)



FIGURE 1-3 Bearing stiffener damage in Pico-Lyons Overcrossing during 1994 Northridge earthquake (Astaneh-Asl, 1994)



FIGURE 1-4 Damage to girders of Hanshin Expressway during 1995 Hyogen-Nanbu earthquake



FIGURE 1-5 Damage to girders and bracing of Hanshin Expressway during 1995 Hyogen-Nanbu (Kobe) earthquake



FIGURE 1-6 Fractured lateral bracing and buckled cross frame in Capitol Arch bridge during 2001 Nisqually earthquake (WSDOT, 2001)



FIGURE 1-7 Damaged web stiffener in Capitol Arch bridge during 2001 Nisqually earthquake (WSDOT, 2001)

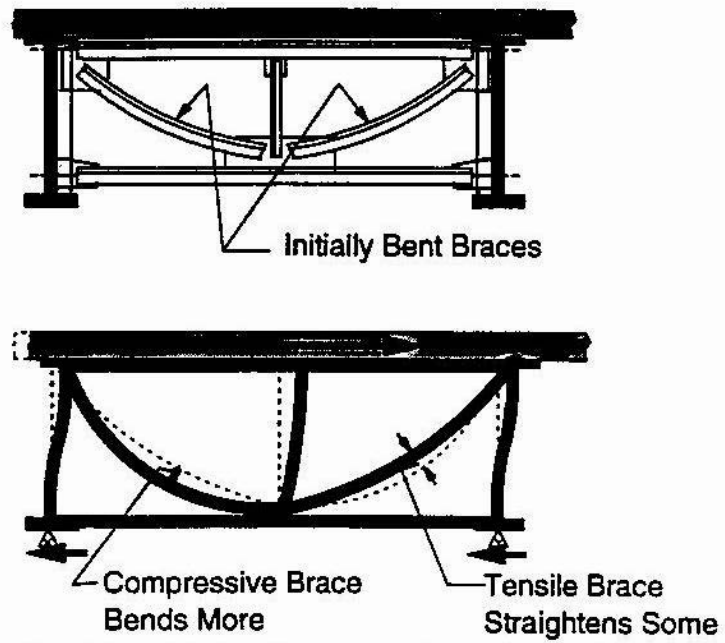


FIGURE 1-8 Ductile end cross frame using curved single angle members (Astaneh-Asl, 1996)

throughout the height of the structure. However, the stiffness is not typically evenly distributed throughout the height of the structure. For flexible substructures when subjected to transverse seismic loading, the deformations will typically be concentrated in the substructure. In contrast, with rigid substructures the deformation may be concentrated in the superstructure. Therefore it makes sense to design the more flexible layer to be ductile in order to reduce elastic seismic demand as deformations are already concentrated in this layer. In effect a “soft story” deformation is promoted in this type of bridge. This is similar to the basic concept of seismic isolation.

Designing the superstructure to remain elastic during an earthquake while being capacity protected by the substructure is one approach for the seismic design of steel plate girder bridges. Another proposed approach is to design the end cross frames to be ductile to reduce the transverse elastic forces in the bridge using these components (Zahrai, 1998b; 1999a). A third approach is to use a ductile device between the superstructure and the substructure in the form of seismic isolation bearings. It is necessary to determine which option will be the most effective for different bridges.

1.2.2 Previous Research on Ductile End Cross Frames or Diaphragms in Bridges

The use of ductile end cross frames to reduce the transverse seismic demand in a steel plate girder bridge was first proposed by Astaneh-Asl (1996). A configuration of cross frame was proposed used curved single angle members, as shown in Figure 1-8. The reason for using curved members is to reduce the initial strength of the cross frame prior to buckling and reduce strength degradation. Stiffness degradation in this system is still likely as the members elongate during tensile excursions.

Zahrai and Bruneau (1998a; 1998b; 1999a; 1999b) proposed and performed experiments on different configurations of ductile end diaphragms. They investigated the use of three types of diaphragms in which the inelastic components were principally subjected to flexural and shear deformations. The first was a shear panel system (SPS) which consisted of a steel panel orientated in a vertical plane designed to deform inelastically in shear (Fig 1-9a). The second system used an eccentric braced frame (EBF), similar to the SPS but with the inelastic member orientated in the horizontal direction (Fig. 1-9b). The third system studied was a triangular-plate added damping and stiffness device (TADAS) which consisted of triangular plates that yielded in flexure as ductile elements (Fig. 1-9c). These systems were shown in subassembly experiments to perform with ductile behavior up to drifts of around 3.0%, 3.0% (bolted) and 3.8% for the SPS, EBF and TADAS systems respectively compared to the girder height. In order to reduce the effect of the girders in the transverse load path, these experiments used trimmed web stiffeners which lowered the transverse flexural capacity of the stiffeners. Even with the trimmed stiffeners the transverse stiffness of these members resulted in considerable post yield stiffness. It was assumed that the girder sections in the subassembly had fixed top and bottom flanges, although, it was recognized that allowing rotation of the girder flanges about their longitudinal axes would result in reduced girder stiffness and reduced post yield stiffness in the system.

For the SPS and EBF systems at failure, based on the geometry of the systems, the average theoretical shear strains were approximately 23% and 17% respectively. For the TADAS system at failure the theoretical maximum direct strain due to flexure in the triangular plates was calculated at 11%. These calculations were only approximate as they assumed no slippage in the connections and deformations only in the deformable links. For example the actual measured distortions in the SPS specimen considered was around 12% (Zahrai, 1998b). Despite the

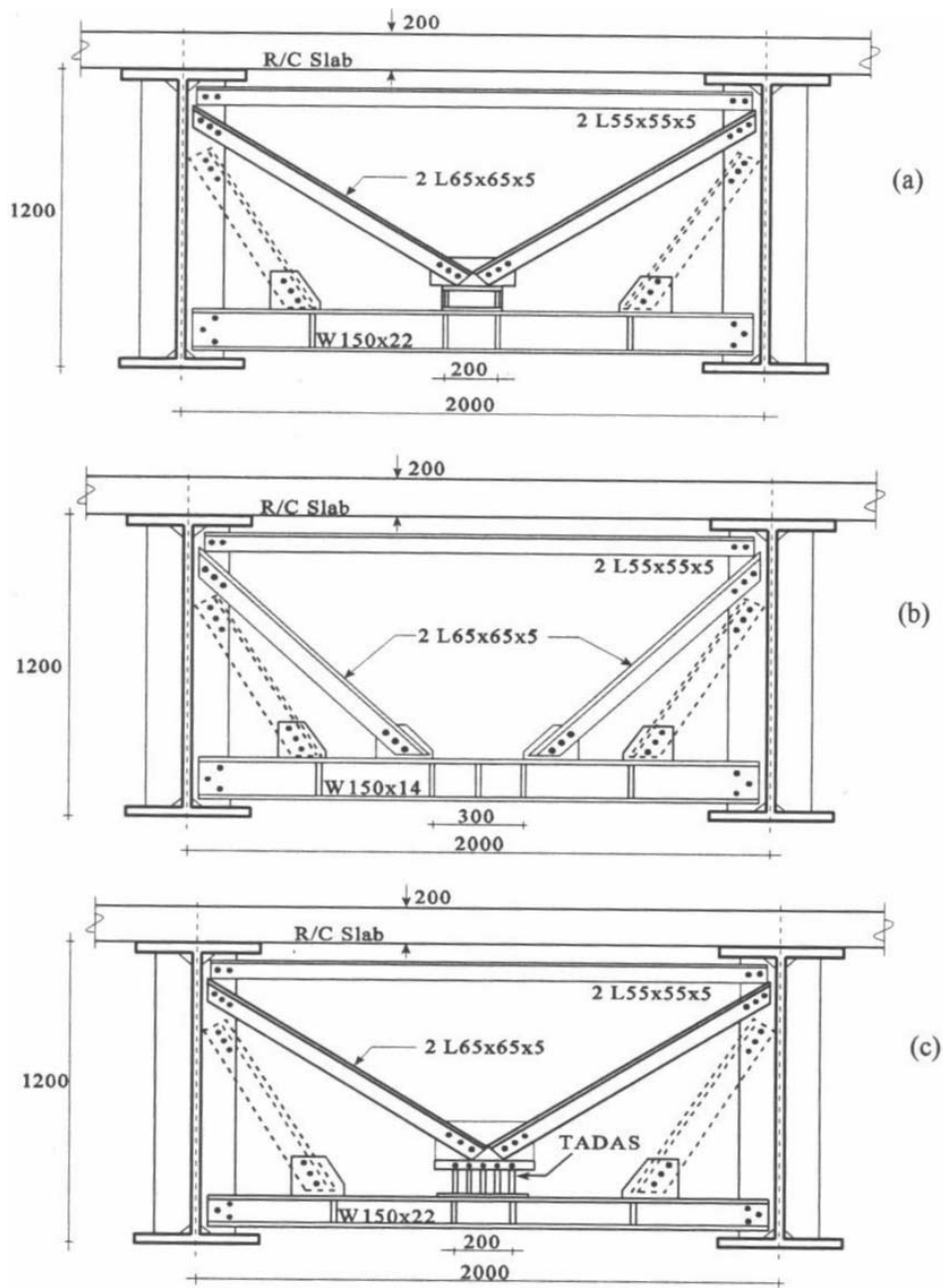


FIGURE 1-9 Ductile end diaphragms using: a) shear panel system (SPS); b) eccentric braced frame (EBF), and; c) triangular-plate added damping and stiffness device (TADAS) (Zahrai, 1998b)

approximations made, these numbers demonstrate that the localized strains in the ductile links were much larger than the girder drifts in each system. The implication of this is that the allowable deformation in these ductile end cross frames is limited. It was proposed in the ATC/MCEER - 49 guidelines (ATC/MCEER, 2003) that the drifts of ductile end cross frames should be limited to

2.0% of the girder height. Under these criteria it was shown that ductile cross frames are only practical when the girders are relatively tall, such as in retrofit of typically old two girder bridges (Zahrai, 1998b). This drift limitation is unlikely to be sufficient for effective ductile end cross frames in typical modern multi-girder bridges located in high seismic zones. However, if the ductile end cross frames and ends of the girders were able to accommodate a larger displacement capacity, then the number of bridges for which ductile end cross frames would become a viable design or retrofit strategy would broaden.

1.2.3 Other Potential Ductile Systems

As illustrated in Figure 1-10, single angle X-braces are often used in cross frames of steel plate girder bridges. Their inelastic response could therefore be studied to potentially design them as ductile elements. It is recognized from past research that concentric braces such as these have a tendency towards strength and stiffness degradation due to buckling of the compression members (Jain, 1978; Astaneh-Asl, 1982; Sabelli, 2001). This potentially results in increased displacements due to limited energy dissipation characteristics. In buildings this has been shown to have serious consequences as the strength degradation has a tendency to form weak stories, resulting in large deformations concentrated in these levels. In bridges the consequences of this are not as serious as “soft story” behavior is effectively being promoted. Therefore, as long as the girders and cross frames can accommodate the resulting seismic displacement demand, single angle X-braces are a potentially feasible system for ductile end cross frames. They could be used to seismically protect a structure in the transverse direction with no additional cost during bridge construction, except to ensure that the connection details are suitable to prevent brittle failure. Furthermore, the average axial strains in the end cross frames will be similar to the drift in the structure, i.e. a 1% axial strain in the diagonals will approximately correspond to a 1% or more drift in the structure, although the exact values depend on the geometry of the system. It is recognized that local strains around the plastic hinges formed during buckling, and the fact that axial strain capacities are generally less than shear capacities. However compared to the SPS, EBF and TADAS systems which have



FIGURE 1-10 Typical X-brace cross frame shown at intermediate cross frame location

strains in the deformable members many times larger than the girder drifts, smaller comparative strains in the cross frame members are likely to lead to larger drift capacities. Another potential advantage of this system is that strength degradation, although often considered unfavorable, is likely to result in maximum forces in the end cross frames close to the yield forces and as such it is possible to limit forces transferred into the superstructure and the substructure. Recognizing the problems with concentric braced frames in buildings, buckling restrained braced frames are becoming increasingly popular (Sabelli, 2001; Sabelli 2003b). Buckling and therefore strength and stiffness degradation is prevented by confining the axial members in these braces. One form of these braces is the “unbonded brace” constructed by Nippon Steel Corporation (Wada, 1989). Unbonded braces are constructed from a steel bar or cruciform core section which is surrounded by a mortar encasing and steel tube. An unbonding material covers the steel core section to allow it to slide longitudinally relative to the casing while all buckling, except very high mode buckling, is prevented by the casing when the core plate is put in compression. This results in similar properties when subjected to tensile and compressive loads (Black, 2002; SIE, 1999). A typical brace is illustrated in Figure 1-11. The design procedures for buckling restrained braced frames are evolving for implementation into buildings using similar procedures as for the design of any other system (Clark, 1999; Sabelli, 2003a; SEAoNC, 2003).

It was anticipated that using these braces as components in ductile end cross frames could result in the same benefits as for the single angles in terms of relatively large allowable drifts in the end cross frames to minimize base shear. However, with increased energy dissipation the same force levels could potentially be achieved with smaller drifts in the cross frames.

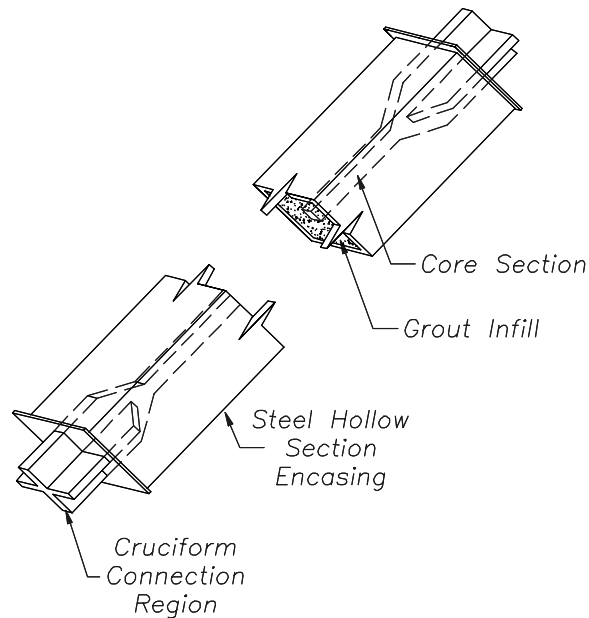


FIGURE 1-11 Typical configuration of buckling restrained (unbonded) brace

1.2.4 Seismic Isolation

As an alternative to a ductile substructure or ductile end cross frames remains the possibility of using seismic isolation between the superstructure and substructure. The basic principle of seismic isolation is to use a flexible layer to reduce the natural period of a structure in order to lower the seismic forces. However, the flexible layer must be designed to accommodate large displacements with additional damping generally added in order to limit displacement demand (Skinner, 1993). Ductile substructures or ductile end cross frames effectively perform in a similar manner as isolation systems by providing a flexible layer in a bridge, although the displacement capacity of these systems is not typically as high as that for an isolation system and consequently the reduction in elastic base shear is not as great. The correlation between seismic isolation and other ductile systems can be lost as completely different design methodologies are typically used.

Seismic isolation has been used quite extensively, perhaps due to the fact that thermal expansion bearings are often used in bridges, therefore replacing these bearings with isolation bearings results in little increase in cost and much better anticipated seismic performance. Despite this there is still relatively little strong motion verification of the concept in the field (Lee, 2001). Kunde and Jangid (2003) provide a thorough review of the application of seismic isolation in bridges. Isolation systems typically fall into two categories, elastomeric or sliding although there are other systems such as rocking systems (Robinson, 1993).

Seismic isolation can be used for new design and also retrofit of bridges where the substructure and foundation are found to have insufficient strength to resist large seismic loads (Buckle, 1990). Of particular interest in this study is the comparative performance of the seismic isolation systems and ductile end cross frames for modifying the transverse seismic response of a bridges in both retrofit and new design applications.

1.3 Superstructure Flexibility

While the flexibility of the substructure is known to control the response of a bridges and change the effectiveness of other ductile components such as seismic isolation systems (Saiidi, 1999), the flexibility of the superstructure is also likely to have an effect on the transverse response of a bridge. Maleki (2001) suggested and showed analytically that the superstructure of typical bridges are sufficiently rigid transversely that it does not significantly affect the response of a bridge. However for relatively narrow bridges and depending on the stiffness of the substructure this may not be valid. Alfawakhiri and Bruneau (2000) investigated the response of a bridge incorporating the relative stiffness of the superstructure and substructure. They showed that when using ductile end cross frames the displacement demand can be significantly affected by the flexibility of the superstructure (Alfawakhiri, 2001). This will also be true for the displacement demand of a ductile substructure in some instances. Therefore superstructure flexibility should be considered in the seismic analysis of a steel plate girder bridge.

1.4 Objectives and Scope

The objective of this report is to study the seismic response of straight steel plate girder bridges with ductile end cross frames and seismic isolation, using a single span scale model of a two girder bridge superstructure and corresponding finite element models. The main purpose of this study is to determine whether ductile cross frames and isolation, designed to reduce seismic demand in the

superstructure of this type of bridge, are effective, and if so, which systems are most effective. The ductile end cross frames investigated were designed using single angle X-braces and buckling restrained braces. The isolated bridge utilized lead rubber isolation bearings.

The study is limited to straight unskewed steel plate girder bridges constructed from steel built-up I-girders. The response of the bridge is generally limited to excitation in the transverse direction with limited investigation of longitudinal, and no consideration of vertical, excitation. This report focuses on the response of the bridge model and other models used in parametric studies. Preliminary design recommendations for ductile end cross frames and isolation systems for use in steel bridges are proposed.

SECTION 2 ANALYSIS AND DESIGN OF THE BRIDGE MODEL

2.1 Introduction

This chapter describes the preliminary analysis, design and construction of a twin girder, simply supported model of a slab-on-girder bridge superstructure, used in order to study the effects of earthquake loads on a typical straight steel plate girder bridge located in a high seismic zone. The bridge model was based on a prototype bridge, scaled by a factor of $2/5$, with further details described in a preceding report (Carden, 2005).

The design procedure for the various components presented in this chapter reflect the methodology used to design and analyze the bridge model before experiments were performed. After studying the response during many experiments on the bridge model, a more comprehensive design procedure is later developed, which will be presented in a future report.

2.2 General Design of Bridge Model

The steel plate girder bridge superstructure model used for experiments in this study is shown in Figure 2-1. Other aspects such as the deck slab reinforcing, cross frames, shear studs and bearings were designed specifically for the bridge model, based on forces scaled from the prototype bridge.



FIGURE 2-1 Slab-on-girder bridge superstructure model

The overall girder dimensions for the bridge model were scaled down from the two girder prototype. This resulted in 18.3 m long girders with cross sectional properties as shown in Figure 2-2. The webs and flanges were built-up from plates which were welded with 10 mm fillet welds along the length of the girders. Transverse stiffeners, 10 mm thick, were placed at 3.05 m centers on the exterior face of the girders and 1.52 m centers on the interior face. The web and flanges were constructed from ASTM A709 Gr50 steel, all other components were ASTM A36. The girders were generally simply supported, except during a few experiments where an intermediate support was added to the bridge resulting in two continuous spans.

The thickness of deck slab and haunch, spacing the girders, and length of overhang were scaled down from the prototype bridge resulting in cross sectional deck slab dimensions as shown in Figure 2-2. Two rows of 10 mm diameter Nelson Headed Anchor studs (TRW Nelson Division, 1977, TRW Nelson Division, 1988) were placed on each of the girders, as shown in Figure 2-3, spaced at 450 mm centers. These studs were not sufficient to provide full composite action to the bridge model for gravity loads and therefore provided a partial composite section (Carden, 2005).

The intermediate cross frames in the prototype bridge were spaced at 7.62 m based on the AASHTO Standard Specifications (1996). After scaling the intermediate cross frames in the bridge model were spaced 3.05 m apart. Typical intermediate cross frames for the bridge model are shown in Figure 2-4. These were constructed using the same angle sections as those used in the

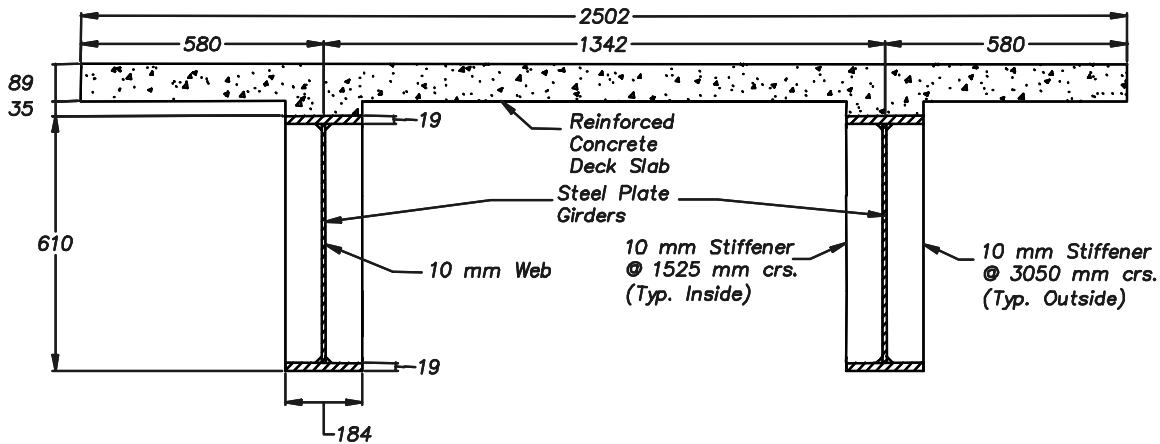


FIGURE 2-2 Steel plate girder bridge model - girder and deck slab dimensions

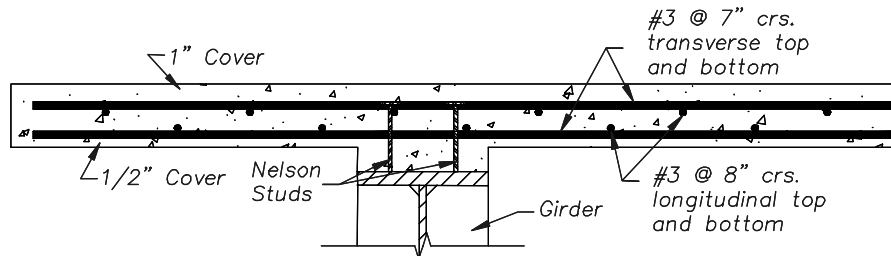


FIGURE 2-3 Bridge model deck slab reinforcing

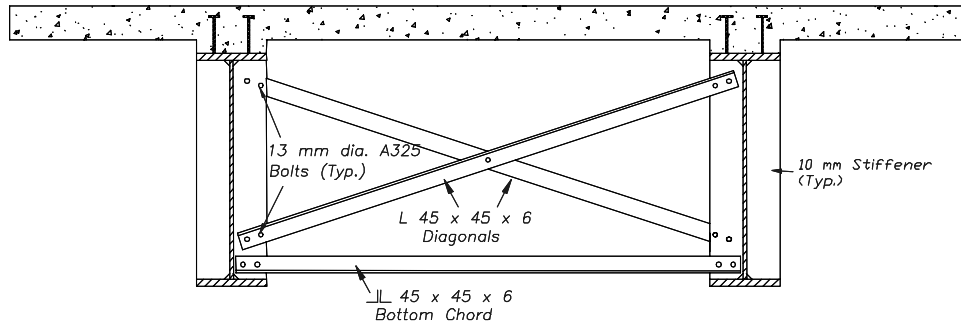


FIGURE 2-4 Typical intermediate cross frame in bridge model

“heavy” end cross frames described in Section 2.3.3. Compared with the end cross frames, the connection details for the intermediate cross frames were simplified, with connections directly to the stiffeners without the use of gusset plates, as strong connections to promote potential inelastic behavior were not necessary. There was a double angle bottom chord, but no top chord, as in the prototype.

For the reversed static experiments, which focused on the transverse load path and end cross frames, the bridge model was placed on four reinforced elastomeric bearings. These are typical of those used to accommodate temperature fluctuations in the longitudinal direction of a bridge superstructure. They are shown to be a relatively low maintenance, low cost option for bridge bearings, with good resilience for extreme loading conditions (AISI, 1996). The elastomeric bearings consisted of three layers of elastomer sandwiched between steel shims as shown in Figure 2-5. The bearings were constructed from a neoprene polymer with a shear modulus of 0.86 MPa. They were restrained in the transverse direction with stiffened angles as shown. Typically in this type of bridge there is some gap between the bearing and transverse restraint, however for the bridge model this gap was minimized using custom fitted shims in an attempt to simplify the transverse response. The bearings were able to allow rotation of the girder about a longitudinal axis, seen as advantageous with the use of ductile end cross frames which are described in the following section. Rotation about the vertical axis was partially restrained by the custom fitted shims, but is generally considered unrestrained.

Lead rubber seismic isolation bearings were used in the shake table experiments. The properties of these bearings are discussed in Section 2.3.6. They were used as isolation bearings, but were also restrained in order to study forces in the various end cross frame configurations. The transversely restrained lead rubber bearings are illustrated in Figure 2-6. These restraints were similar to those used for the elastomeric pads, with the angles orientated in the opposite direction for convenience of connection to the load cells. The restraints allowed rotation about the longitudinal axis of the bridge. As the tight-fitted shims were cut to a relatively short length of 3 in, and placed at the center of the bearing, they were able to allow effectively free rotations about the vertical axis of the bridge. The properties of the isolation bearings are given in Appendix 2.

The weight of the superstructure is critical for determining the dynamic response of the bridge. Assuming a density of reinforced concrete of 25 kN/m^3 and steel of 77 kN/m^3 the weight of the superstructure was calculated at 140 kN. The calculated weight of additional lead required for

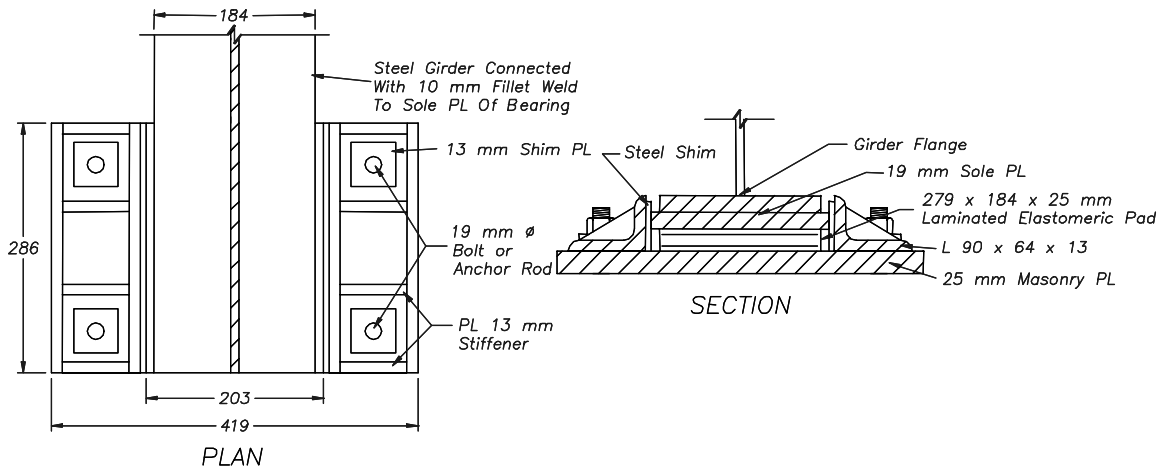


FIGURE 2-5 Laminated elastomeric bearing

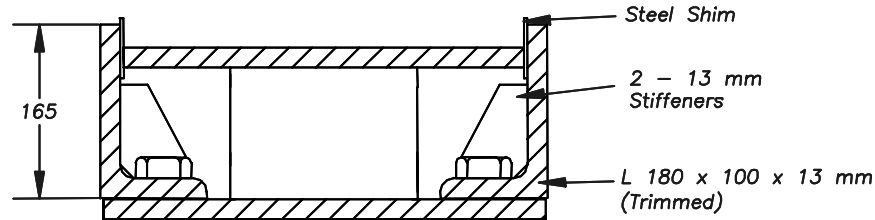


FIGURE 2-6 Lead rubber bearing with transverse restraints

similitude due to scaling was equal to 210 kN, 1.5 times the bridge weight. The resulting total calculated weight of the bridge was equal to 350 kN.

The measured weight of lead added to the bridge model was equal to 206 kN, equally distributed in six steel frames on the deck slab of the bridge model. The total weight of the bridge including lead, as measured from the load cells and checked using a crane scale at one end of the bridge, was 170 kN at the north end and 171 kN at the south end, summing to 341 kN. Therefore the weight of the bridge model alone was equal to 134 kN. The measured weight of the bridge model was within 6% of the expected weight. Dividing the weight equally between each of the bearings resulted in forces of 33.5 kip per bearing for the reversed static experiments, with no added lead. Similarly, the force during shake table experiments was equal to 85.4 kN per bearing. The load cells confirmed that the forces were evenly distributed between all the bearings as required for equilibrium.

2.3 Design of Critical Components in the Ductile Transverse Response of the Bridge

2.3.1 Overview

Three approaches were considered to allow ductile response of the steel girder bridge model subjected to transverse earthquake excitation. The ductile response was promoted using ductile end cross frames and seismic isolation bearings. In order to design these components an analysis

procedure for the bridge model is described below. This procedure does not reflect the final recommended analysis and design procedure for steel girder bridge superstructures, which will be described in more detail in a future report.

2.3.2 Analysis Procedures

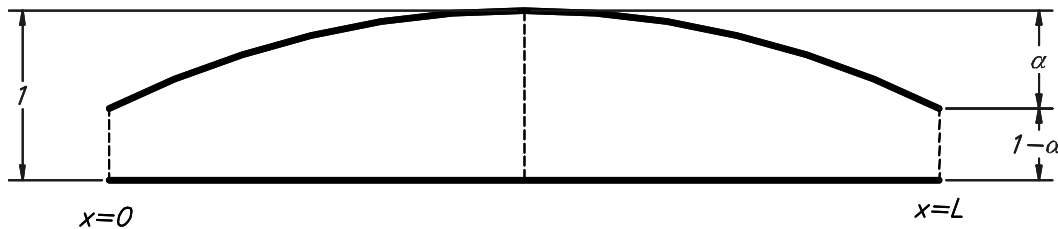
2.3.2.1 Response Modification Factor Design

The response modification factor (R-Factor) design approach is the approach specified in the majority of building and bridge codes for seismic design of structures, whereby the elastic response of the structure is calculated then elastic forces are divided by a response modification factor to calculate an inelastic demand. Critical elements in the system are then designed with a capacity equal to the inelastic force level and detailed to accommodate resulting inelastic displacement demand.

As the bridge model was simply supported an approximate closed form solution can be derived for the elastic transverse response of the bridge with a flexible superstructure and end springs to model the end cross frames and substructure. The formulation presented here is similar to that presented by Alfawakhiri and Bruneau (2000), although uses different notation. Assuming only the first mode contributes to the response of the bridge, the shape function for the deformed bridge is as shown in Figure 2-7. The equation for the shape function is:

$$\psi(x) = 1 + \alpha \left[\sin\left(\frac{\pi x}{L}\right) - 1 \right] \quad \dots 2.1$$

where: ψ is the shape function; α is the superstructure deformation ratio, ie. the ratio of the amplitude of the superstructure deformation at midspan to the maximum total deformation; x is the distance from the end of the bridge; and L is the length of the bridge. The α value is dependent on the stiffness of the superstructure compared to the stiffness of the ends of the bridge which include the end cross frames, bearings and substructure. It can be approximated by statically applying a uniform load to the bridge and calculating the relative deflection of the superstructure and ends of the bridge. Using this approximation and assuming a uniformly distributed transverse stiffness along the length of the superstructure, α is given by:



$$\psi(x) = 1 + \alpha \left[\sin\left(\frac{\pi x}{L}\right) - 1 \right]$$

FIGURE 2-7 Shape function for transverse deformation of simply supported bridge

$$\alpha = \frac{\frac{5 L^3}{384 EI}}{\frac{5 L^3}{384 EI} + \frac{1}{k_{\text{eff}}}} \quad \dots 2.2$$

where: EI is the distributed stiffness of the superstructure; L is the length of the bridge, and; k_{eff} is described by:

$$k_{\text{eff}} = \frac{k_{\text{sub}} k_{\text{effi}}}{k_{\text{sub}} + k_{\text{effi}}} \quad \dots 2.3$$

where: k_{effi} is the combined transverse stiffness of the end cross frames, and; k_{sub} is the stiffness of the substructure. It can be shown with Equation 2.3 that if the substructure is flexible compared to the end cross frames then it will dominate in the stiffness of the ends. The reverse is true for relatively flexible cross frames and rigid substructure. The stiffness of the end cross frames and substructure can be combined in this manner as they share the same shape factor and additional substructure mass is neglected.

The generalized single degree of freedom system can be described using the above modeshape. Therefore the response of the bridge can be found by solving the equation for the generalized system (Clough, 1993):

$$M^* \ddot{Z}(t) + C^* \dot{Z}(t) + K^* Z(t) = P^*_{\text{eff}}(t) \quad \dots 2.4$$

Where: M^* is the generalized mass; C^* is the generalized damping; K^* is the generalized stiffness; P^*_{eff} is the generalized effective load, and; $Z(t)$ is the generalized displacement. In this equation the generalized mass is defined by:

$$M^* = \int_0^L m(x) \psi(x)^2 dx = M \left[\left(\frac{3}{2} - \frac{4}{\pi} \right) \alpha^2 + \left(\frac{4}{\pi} - 2 \right) \alpha + 1 \right] \quad \dots 2.5$$

where: m is the mass per unit length; and M is the total mass of the superstructure. The stiffness matrix is given by:

$$K^* = \int_0^L EI(x) \frac{d^2 \psi}{dx^2} dx = \frac{\pi^4 EI}{2L^3} \alpha^2 + k_{\text{eff}} (1 - \alpha)^2 \quad \dots 2.6$$

and the generalized effective load is defined by:

$$P^*_{\text{eff}}(t) = -a_g(t) \int_0^L m(x) \psi(x) dx = -M \left[1 + \left(\frac{2}{\pi} - 1 \right) \alpha \right] a_g(t) \quad \dots 2.7$$

where: $a_g(t)$ is the ground acceleration as a function of time. The effective earthquake excitation factor, L_{eff} , is defined by:

$$L_{\text{eff}} = M \left[1 + \left(\frac{2}{\pi} - 1 \right) \alpha \right] \quad \dots 2.8$$

and the effective modal mass is given by:

$$M_{\text{eff}} = \frac{L_{\text{eff}}^2}{M^*} \quad \dots 2.9$$

The validity of a single degree of freedom model can be verified by comparing the effective modal mass with the generalized mass. The damping can also be defined by calculating a generalized damping, however for the purposes of design, 5% equivalent viscous damping was assumed for the system. Equation 2.4 can be solved using a response spectrum analysis for a given level of damping. The effective period of the generalized structure is given by:

$$T_{\text{eff}} = 2\pi \sqrt{\frac{M^*}{K^*}} \quad \dots 2.10$$

therefore the spectral acceleration coefficient, C_s , can be found from the AASHTO design spectrum and is defined as:

$$C_s = \frac{1.2AS}{T_{\text{eff}}^{2/3}} \leq 2.5A \quad \dots 2.11$$

where: A is the acceleration coefficient; and S is the site coefficient. The base shear of the bridge can then be calculated as:

$$F_d = M_{\text{eff}} C_s g \quad \dots 2.12$$

and the elastic displacement of the bridge is given by:

$$d(x) = \psi(x) \left(\frac{T_{\text{eff}}}{2\pi} \right)^2 \frac{L_{\text{eff}}}{M^*} C_s g \quad \dots 2.13$$

The elastic displacement can be calculated in the end cross frames, substructure and along the length of the bridge using this expression.

A series of simple span bridges were analyzed and compared to a finite element response spectrum analysis. The base shear calculated using this procedure was calculated to within 0.5% of that calculated using the finite element model. The displacements were with 2.5% of the finite element

model. The error is in the approximation of uniform loading in calculating the shape function but was shown to be negligible.

It can be assumed that the elastic base shear in the transverse direction is reduced by inelastic behavior in either the substructure, bearings or end cross frames. This reduction is given by the R-Factor. The R-Factor is defined by:

$$R = \frac{F_{\text{elastic}}}{F_{\text{inelastic}}} \quad \dots 2.14$$

where: $F_{\text{inelastic}}$ is defined by the capacity of the system. An R-factor can be selected for design of the ductile system using requirements in AASHTO (1998), from which the required capacity of the ductile system can be calculated based on the modified elastic response.

2.3.2.2 Displacement Based Design Approach using a Capacity Spectrum Analysis

The above R-factor design approach focuses on the reduction of elastic forces, however, selection of an R-factor needs to be appropriate to ensure that the inelastic displacement capacity of the ductile system is adequate. A capacity spectrum analysis (or capacity spectrum analysis) provides an estimate of the inelastic displacement of a ductile system. This is the approach generally used for the design of seismic isolation systems as these systems are designed specifically for large inelastic displacements and therefore determining the displacement response is critical. The displacement based procedure was used to design an isolation system for the bridge model based on the procedure outlined in the AASHTO Guide Specifications for Seismic Isolation Design (AASHTO, 1999). This procedure is outlined below.

The first step is to define the earthquake and site parameters in order to define the demand spectrum. For base isolated structures the acceleration coefficient is defined by:

$$C_s = \frac{AS}{T_{\text{eff}}B} \leq 2.5A \quad \dots 2.15$$

where: T_{eff} is the effective (secant) period of the isolated structure at the design displacement, and; B is a factor to account for damping in the isolation system. Note that this is different to the acceleration coefficient for non-seismically isolated structures as given in Equation 2.11 due to the addition of a damping component and the seismic coefficient being proportional to $1/T_{\text{eff}}$. The damping coefficient should only be applied to isolated modes, with other structural modes in a multi-mode analysis assumed to have a damping coefficient of 1.0.

The next step is to characterize the bi-linear properties of a proposed isolation system, which define the capacity curve. The bi-linear parameters are illustrated in Figure 2-8. As the isolation systems are typically able to be designed for much larger displacements than ductile substructures and cross frames then the design lateral shear force is comparatively less. Therefore this force is often governed by non-seismic lateral forces. These forces can be used to initially select an appropriate isolation system and initial dimensions.

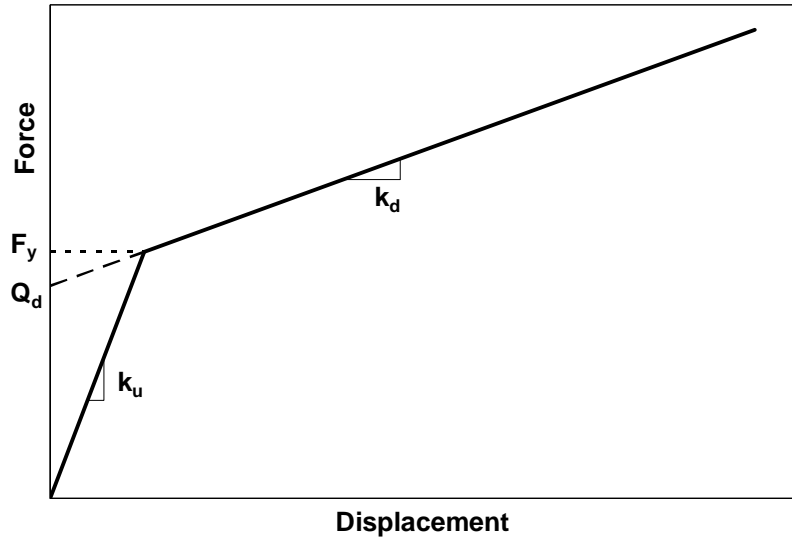


FIGURE 2-8 Terms for definition of bi-linear model

As the isolation system is typically flexible compared to the superstructure and substructure, α as defined in Equation 2.1 can be assumed to be equal to 1, therefore rigid body motion of the superstructure is assumed at the initial design stage. If accidental torsional effects are also neglected then each isolation bearing will have the same response. Having defined the demand and capacity spectra an iterative procedure can be used to find the design response of the system. This begins with an estimate of the design displacement, d_i , from which the design force, F_d , is equal to:

$$F_d = Q_d + k_d d_i \quad \dots 2.16$$

therefore the effective stiffness is equal to:

$$k_{effi} = \frac{F_d}{d_i} \quad \dots 2.17$$

and the effective period is given by:

$$T_{eff} = 2\pi \sqrt{\frac{W}{k_{effi} g}} \quad \dots 2.18$$

The equivalent viscous damping, β_i , for the hysteretic system at this displacement is given by:

$$\beta_i = \frac{2 Q_d}{\pi F_d} \left(\frac{d_i - d_{yi}}{d_i} \right) \quad \dots 2.19$$

where: d_{yi} is the yield displacement. The effective damping can be approximated by:

$$\beta_i \approx \frac{2 Q_d}{\pi F_d} \quad \dots 2.20$$

when the yield displacement is small compared to the estimated total displacement in the hysteretic system. This gives a modification factor for the acceleration demand due to damping, B , as given by Table 2-1.

Hence the design displacement (in inches) can be calculated as:

$$d_i = \frac{10 A S T_{eff}}{B} \quad \dots 2.21$$

TABLE 2-1 Damping Coefficient, B

Equivalent Viscous Damping (%)	2	5	10	20	30	40	50
B	0.8	1.0	1.2	1.5	1.7	1.9	2.0

The calculated design displacement can be compared to the estimated displacement and iterations performed until the response converges. The isolation system design can then be modified until the desired design response is achieved.

2.3.3 Ductile Columns - Elastic X-Braces

The first approach used in designing the cross frames in the bridge model was to assume an elastically responding superstructure and ductile substructure. An analysis of the two girder prototype was performed using the R-Factor methodology outlined in section 2.3.2.1. The design spectrum was taken from AASHTO (1998), assuming zone 4 ($A = 0.4$) and site category II ($S = 1.2$). The generalized weight for the structure was 2440 kN and generalized stiffness was 9.47 kN/mm, giving a calculated period of the structure, equal to 1.02 s. The resulting spectral acceleration coefficient was equal to 0.568 and resulting base shear was 1440 kN. This was assumed to be equal to the lateral force at the top of the column as half will come from each of the two adjacent spans.

In order to allow for inelastic behavior in the column, the lateral force was divided by an R-factor of 2. The resulting lateral force on the column was 729 kN and the corresponding bending moment, assuming a pin at the top and fixity at the base, was equal to 7540 kNm. From an analysis of the assumed cross section of the 1500 mm diameter column (using the "xSECTION" analysis program with results provided by CALTRANS), the yield moment was calculated to be

9680 kNm and the ultimate moment was 13300 kNm, corresponding to yield and ultimate shears of 987 kN and 1360 kN. As the yield strength was greater than the reduced seismic demand on the column the proposed properties were suitable.

Alfawakhiri (2001) showed that as the relative stiffness of the superstructure reduces compared to the substructure stiffness, the ductility demand on the ends increases and can be considerably greater than that calculated assuming a rigid superstructure. For this bridge the superstructure was relatively long and narrow compared to many bridges, therefore the relative stiffness of the superstructure was expected to be relatively low. However the α was only 0.059 indicating a relatively high superstructure stiffness compared to substructure stiffness. Consequently, the ductility demand on the column was not expected to be significantly larger than that calculated assuming a rigid superstructure. Using ductile column detailing adequate displacement capacity should be achieved.

The end shear for the design of the end cross frames was based on the ultimate moment in the column, using the capacity design principle, to order to ensure that the cross frames were stronger than the column. As half of the column shear was transferred into each of the adjacent spans, the shear in each of the cross frames was calculated from half the ultimate column shear. This resulted in a design shear for the end cross frames in the two girder prototype bridge of 680 kN.

For the bridge model the end shear force was scaled by the square of the scale factor ($^2/5$) resulting in a design shear of 109 kN. This shear was resisted by the diagonals of a single angle X-brace at the end of the bridge. Assuming only the tension diagonal contributed to the strength of the cross frame, a 45 x 45 x 6 mm single angle was used. This satisfied the b/t ratio and slenderness (Kl/r) ratio in accordance with AASHTO (1998). The design tension force for the angle member was 124 kN and the horizontal component of this force, based on an 18 degree angle to the horizontal for the diagonal member, was 117 kN. Hence these single angles were expected to be stronger than the capacity of the columns. The “heavy” end cross frames are shown in Figure 2-9.

The expected strength of the X-braces was considerably higher than the design strength. If the expected strength, calculated using an R_y of 1.5 based on AISC Seismic Provisions (1997) and the buckling strength of the angles was included, then the expected shear in the cross frames was equal to 340 kN. Hence the design was very conservative.

Top and bottom chords were designed to distribute earthquake forces evenly between the girders and bearings in the event that buckling of the diagonal members occurred and uneven forces resulted in the tension and compression diagonals. 45 x 45 x 6 mm double angles were used, as illustrated in Figure 2-9. In addition at the south end of the bridge the top chord was connected to the deck slab using a T-section, as illustrated in Figure 2-10. This detail was added at the north end of the bridge after the first experiment demonstrated its influence in the transverse seismic load path. This type of composite connection is used at abutments to minimize the effect of wheel loading where traffic travels onto a bridge. The T-section was connected to the deck slab using bolts grouted into holes cored in the deck slab to facilitate removal of the member when necessary when changing end cross frame configurations in the bridge model.

Two types of connection configurations were used at different stages of experiments on the bridge model. The first configuration, for which the above calculations apply, had bolted connections.

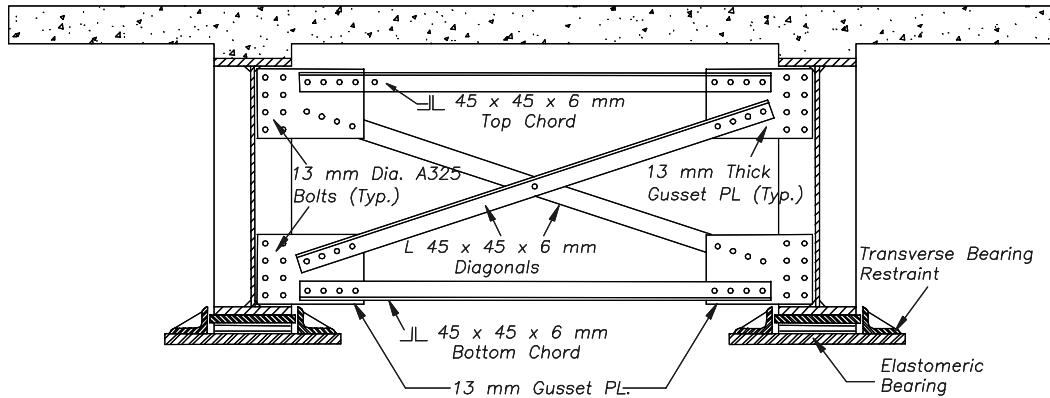


FIGURE 2-9 “Heavy” end cross frames at the north end in the bridge model

The diagonal, top and bottom chords of the end cross frames were connected to gusset plates which in turn were connected to the web stiffeners as shown in Figures 2-9 and 2-10. Gusset plates were used instead of connecting directly to the stiffeners in order to provide adequate connection strength and ensure any inelasticity would occur in the members and not result in failure of the connections. The second configuration used welded connections. For this configuration, as illustrated in Figure 2-11, no gusset plates were required as the angles were welded directly to the bearing stiffeners. This resulted in a longer unrestrained length in the compression diagonal which slightly lowered the buckling strength and therefore overall shear capacity of the end cross frames compared to the previous configuration. This was not considered to be important as forces in these cross frames never exceeded their yield force.

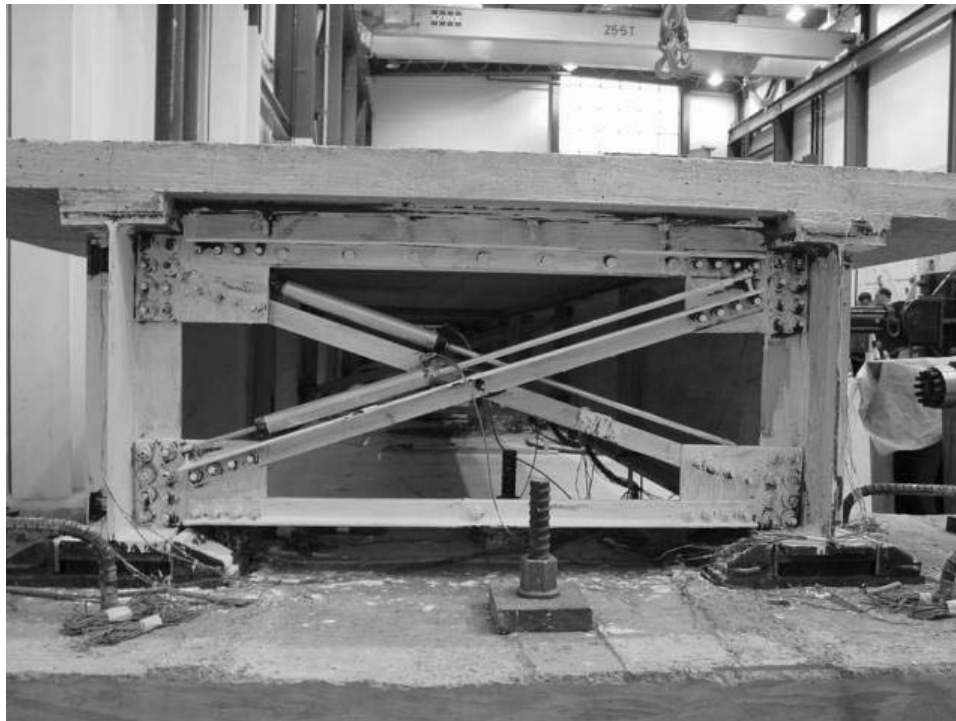
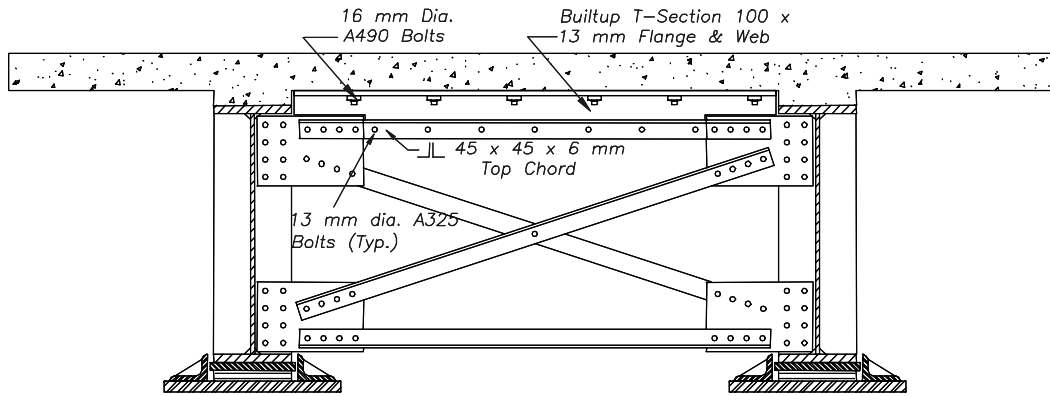


FIGURE 2-10 “Heavy” end cross frames at the south end in the bridge model

2.3.4 Ductile End Cross Frames using Light Single Angle X-Braces - Elastic Substructure

As an alternative to assuming the substructure will deform inelastically, in order to reduce the elastic seismic demand in the bridge model, the end cross frames were designed to respond inelastically. In considering ductile elements in the superstructure it was assumed that the substructure consisted of relatively rigid supports, such as abutments or relatively rigid piers founded on stiff soil, instead of the more flexible column bents previously assumed. Consequently the stiffness of the substructure was assumed to play little role in the response of the bridge. The strength of the substructure for this configuration was assumed to be the same as in the prototype bridge designed with ductile columns, assuming that yield strength was reached at a lateral force

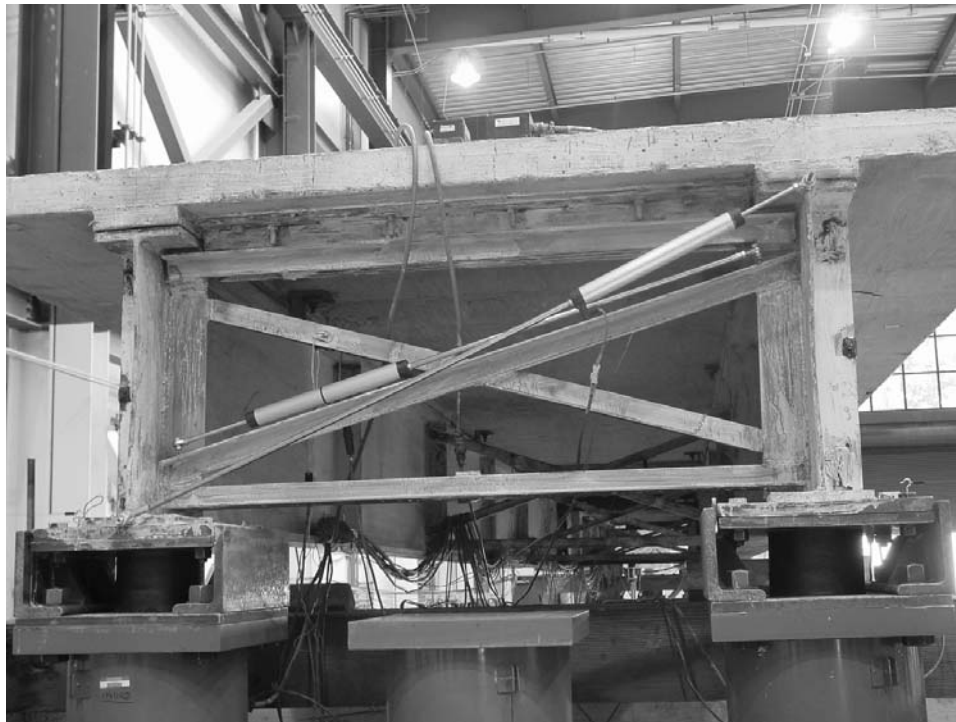
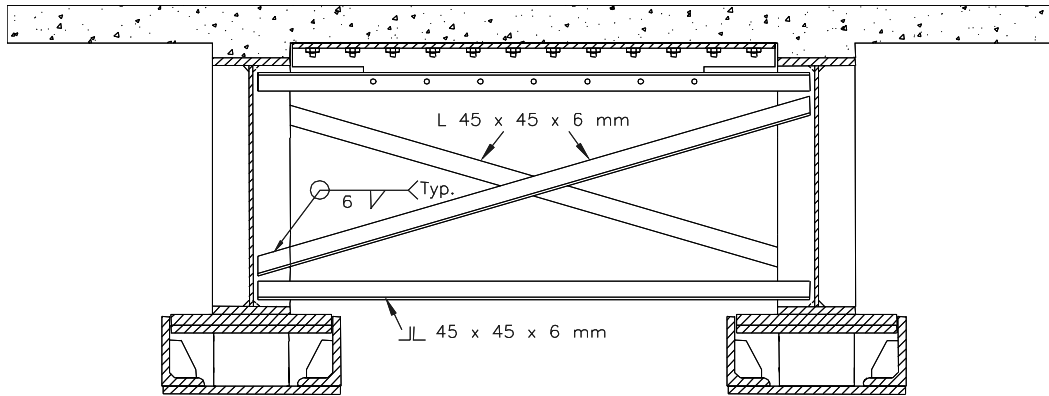


FIGURE 2-11 “Heavy” end cross frames in the bridge model with welded connections

of 987 kN. Therefore the force in each end cross frame, assuming there are two sets of cross frames at each support location from adjacent spans, needed to be less than 493 kN. For the scale model this is equivalent to 79 kN.

Single angles (25 x 25 x 5 mm) were selected for the cross frames designed to yield at around this level and are termed the “light” X-braces. These were the smallest available single angle members which satisfied the b/t and Kl/r ratios. The bridge model configuration with these X-braces is shown in Figure 2-12. They were welded directly to the bearing stiffeners, as shown, with welded connections designed to be stronger than the tensile capacity of the members to prevent premature failure and promote the best possible inelastic behavior.

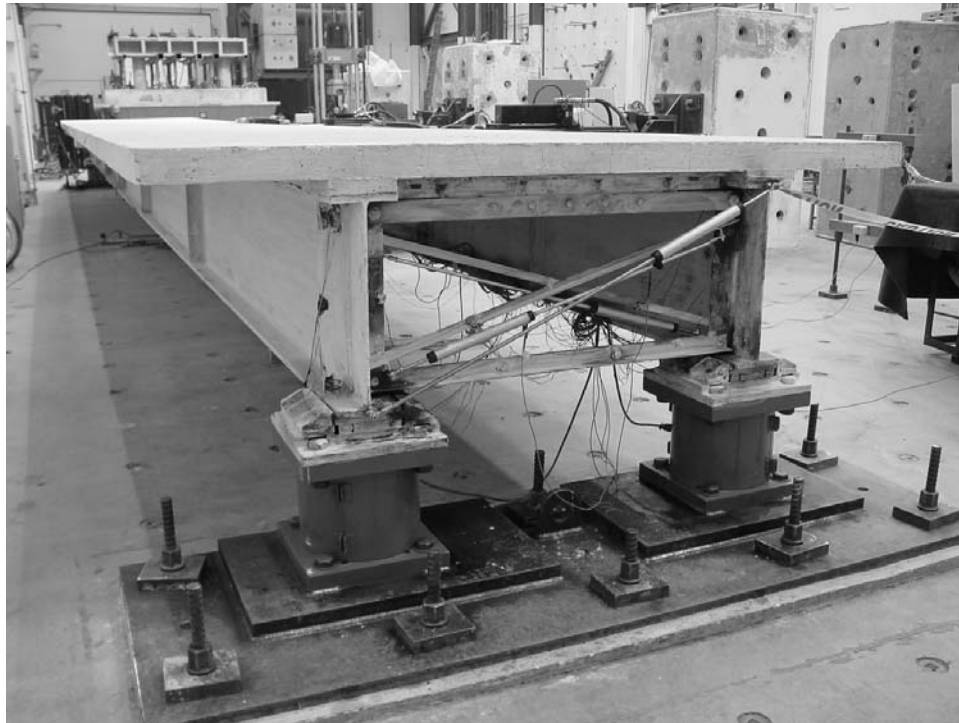
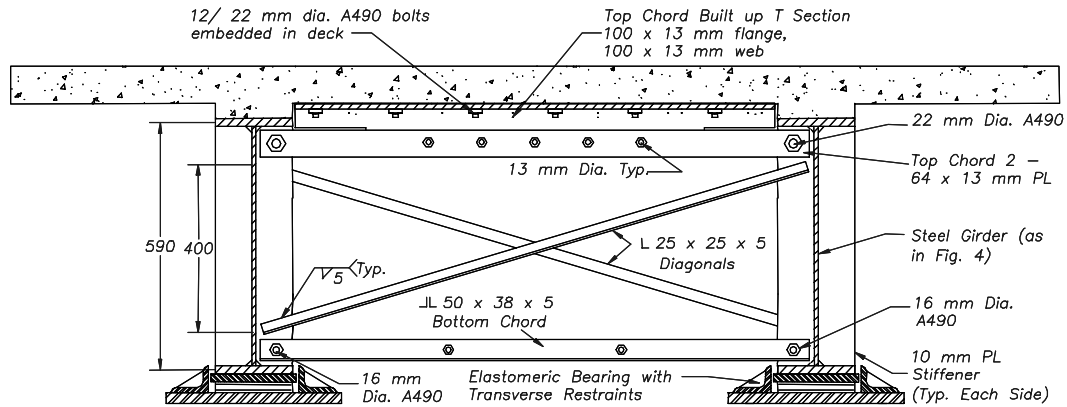


FIGURE 2-12 “Light” end cross frames in the bridge model

The design axial strength of the tension diagonal was equal to 52 kN. The design axial strength compression diagonal was equal to 32 kN. The compression diagonal was assumed to buckle with a strength defined by AASHTO (1998) assuming a length for buckling equal to half of the total diagonal length due to the connection at midspan, an effective length factor assumed to be 0.7, and r defined about the minor principle axis. This is similar to the assumptions used for design of the ductile members in special truss moment frames (Goel, 1994). The maximum tension and compression forces of the corresponding diagonals were not expected to be reached at the same time. The maximum tensile strength in the tension diagonal was expected to be reached after the buckling strength was reached in the compression diagonal. However, there was expected to be little degradation in the compression member when the tension member began to yield. Hence the design shear strength would be simply a combination of the two strengths multiplied by the cosine

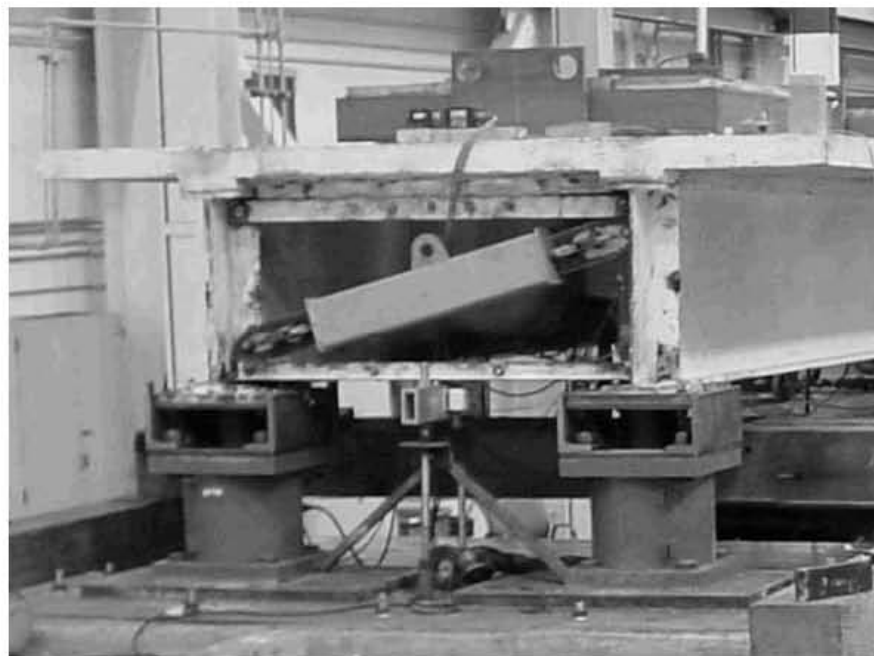


FIGURE 2-13 Unbonded brace in the bridge model

of the angle of inclination for the braces (18 degrees), which resulted in a calculated design strength of 79.2 kN. This was identical to the maximum force desired to prevent inelastic behavior in the substructure, however with the consideration of material overstrength, the strength in the cross frames was expected to be greater. Based on material yield strength from a coupon test the expected strength using direct combination of tension and compression strengths was equal to 109 kN. Based on this strength, the calculated strength was 38% larger than the ideal maximum strength of the cross frames, however this was unavoidable as it was the smallest available member size for the single angle diagonals.

Using a similar assumption as for the column design, it was assumed that the displacement capacity of the end cross frames would exceed the displacement demand. An objective of this experiment was to determine the validity of this assumption.

In order to maximize the shear force in the diagonal members and allow them to deform inelastically at the design shear, it was necessary to minimize the effect of other members at each end. Previous experiments (Zahrai, 1999b) showed that the web stiffeners had a considerable impact on the lateral stiffness and were likely to result in significant post-yield over-strength. In these past experiments the web stiffeners were trimmed in order to lower this lateral stiffness. The transverse deformation of the end region of a two girder bridge with trimmed web stiffeners is illustrated in Figure 2-14. For this particular bridge an alternative method for reducing the effect of the bearing stiffeners was employed, as illustrated in Figure 2-15. The top and bottom chords of the end cross frames in this configuration were specially designed to allow the end region to “rock”, with resistance primarily due to the diagonal members of the cross frames. Rotations were allowed at the base of the girders by elastomeric pads and lead rubber bearings respectively, both with relatively low rotational stiffness. Rotations were also facilitated between the deck slab and the girders by having few shear studs on top of the girders near the end regions. The top and bottom chords were then pinned in order to facilitate rocking. In the bridge model ideal pins were provided by single high strength bolts, however, in practice two bolt connections would be preferred. The members and connections of the top chord were designed to transfer the full shear from the deck slab into the web stiffeners. The members and connections of the bottom chord were designed to transfer the unbalanced force due to buckling of the cross frames evenly to the bearings. These were designed to ensure development of the full capacity of the diagonal members.

2.3.5 Ductile End Cross Frames using Unbonded Braces - Elastic Substructure

Buckling restrained braces have been shown to provide very reliable strength, good energy dissipation and reduce lateral storey drift in building applications compared to concentric braced framing systems (Black, 2002; Clark, 1999; Yamaguchi, 1998). These were considered to provide potential improvement in the response of steel plate girder bridges, compared to special X-braces, when used as ductile end cross frames. As the braces have similar properties in tension and compression a single brace was necessary. Buckling restrained braces constructed by Nippon Steel Corporation, called an unbonded braces, were installed in the bridge model, as illustrated in Figure 2-13.

The unbonded braces were designed to have a similar yield strength as the light X-braces in order to compare the two systems. The braces were designed with Japanese standard LYP-225 steel with a specified expected yield strength of 225 MPa. A cross section of 16 x 25 mm was assumed

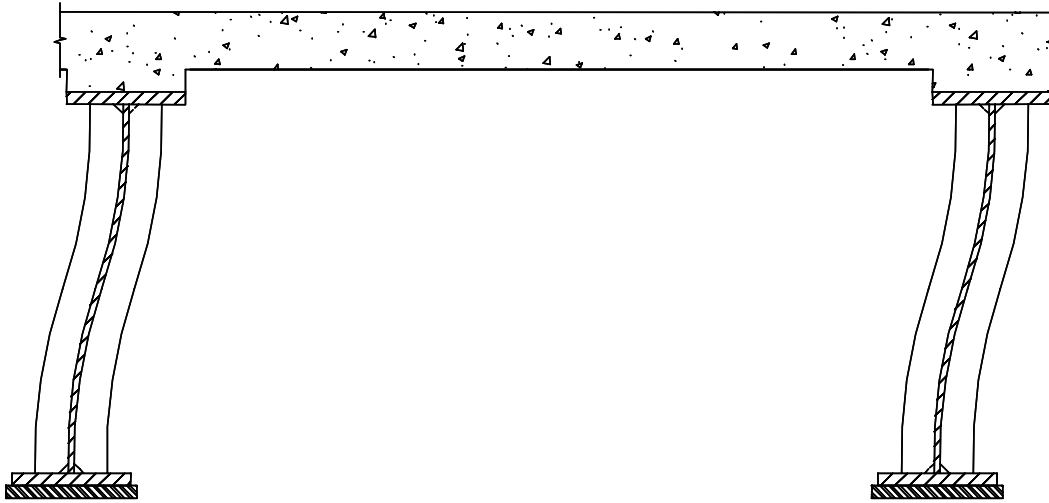


FIGURE 2-14 Deformed end region of two girder bridge with trimmed bearing stiffeners

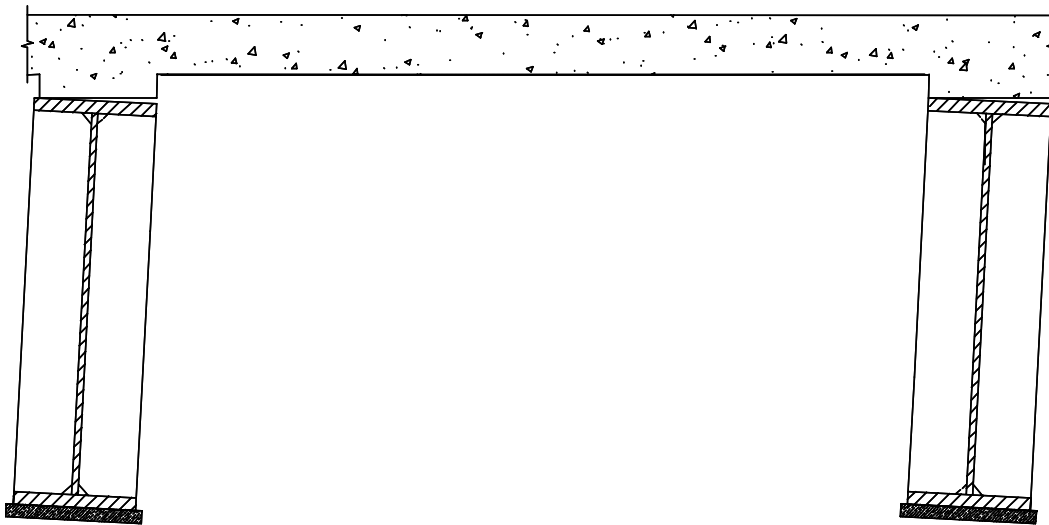


FIGURE 2-15 Deformed end region of two girder bridge with "rocking" girders

in the core region of the unbonded braces, as experiments have been previously performed on braces with this cross section by Nippon Steel Corporation. This gives an expected strength for the unbonded brace of 90.7 kN. Based on the average of two coupon experiments the expected strength was slightly higher at 92.5 kN. As the brace was placed at an angle of 15 degrees to the horizontal then the design end shear was 89.4 kN. This was 18% less than the expected strength of the X-braces and was similar enough to provide reasonable comparisons between the two systems.

Nippon Steel typically recommend design of unbonded braces with fixed end connections that are capable of carrying any moment generated in the brace. These connections are designed to be slip critical using the serviceability requirements of AISC (1998) for buildings. As the braces designed for the bridge model were relatively short, there was a concern that the bending generated in the braces due to the deformed geometry would be large with fixed end connections, which could have an impact on the seismic performance of the brace. The alternative was to use pinned connections

to prevent bending moments being induced in the brace, however the impact of this is a connection which is not slip critical and a higher chance of buckling in the braces as the effective length was increased. In order to allow testing of both configurations, the braces were designed with pinned end connections which were later welded in order to create fixed end connections. The top and bottom chords used for the unbonded braces were the same as those used for the ductile X-braces.

2.3.6 Seismic Isolation using Lead Rubber Bearings

The third approach for protecting the bridge model during earthquakes was to seismically isolate the superstructure using lead rubber bearings. A different design approach than that implemented in design of the ductile end cross frames was used for the design of the isolation system. Conventional seismic isolation design principles were implemented using a capacity spectrum analysis, as described in Section 2.3.2.2. As the isolators were able to undergo much larger deformations than comparable columns or ductile cross frames, it was possible to design them for a lower shear force. The isolation system was designed for a shear force of 0.2 time the weight of the superstructure at the same level of seismic demand as for the previous systems.

The resulting dimensions for the lead rubber bearings are illustrated in Figure 2-16. The calculated properties of the bearings and design response is given in Appendix 1. The bearings were constructed with 10 layers of rubber with a shear modulus of 0.43 MPa. The design displacement for these bearings was 53 mm at a base shear of 19.3 kN per bearing. At this displacement the equivalent viscous damping was 33% and effective period of the structure was 1.00 s. The design response was based on a time scaled ground motion, as described in following sections, therefore the equivalent full scale period would be 1.58 s and full scale design displacement would be 140 mm.

In achieving a low lateral stiffness, the bearings were relatively slender and consequently were susceptible to buckling (Buckle, 2002). The displacement at which buckling was expected to occur was calculated to be 82 mm, 1.55 times the design displacement. A normal application would ensure that shear buckling did not occur before at least 1.5 times the design displacement (AASHTO, 1999), therefore was barely satisfied. The axial load on the bearings was expected to vary due to the overturning moment, increasing the compression force in the bearings on one side of bridge but decreasing the force on the other bearings. This would decrease the buckling capacity of the bearing on one side but increase the capacity of the bearings on the other side. As both bearings are required to buckle simultaneously to create instability at each end, the overturning effects were expected to cancel out and therefore the average axial load was used in evaluation of the bearing buckling capacity. For excitation in the longitudinal direction there were no overturning effects.

As the combined shear force in the bearings at each end of the bridge was much lower than the yield strength of the end cross frames, with both light X-braces or unbonded braces, experiments were first performed on the lead rubber bearings with the light X-braces. Bearing restraints were later added in order to increase the transverse shear capacity of the bridge, allowing the X-braces and unbonded braces respectively to become the weakest links in the system.

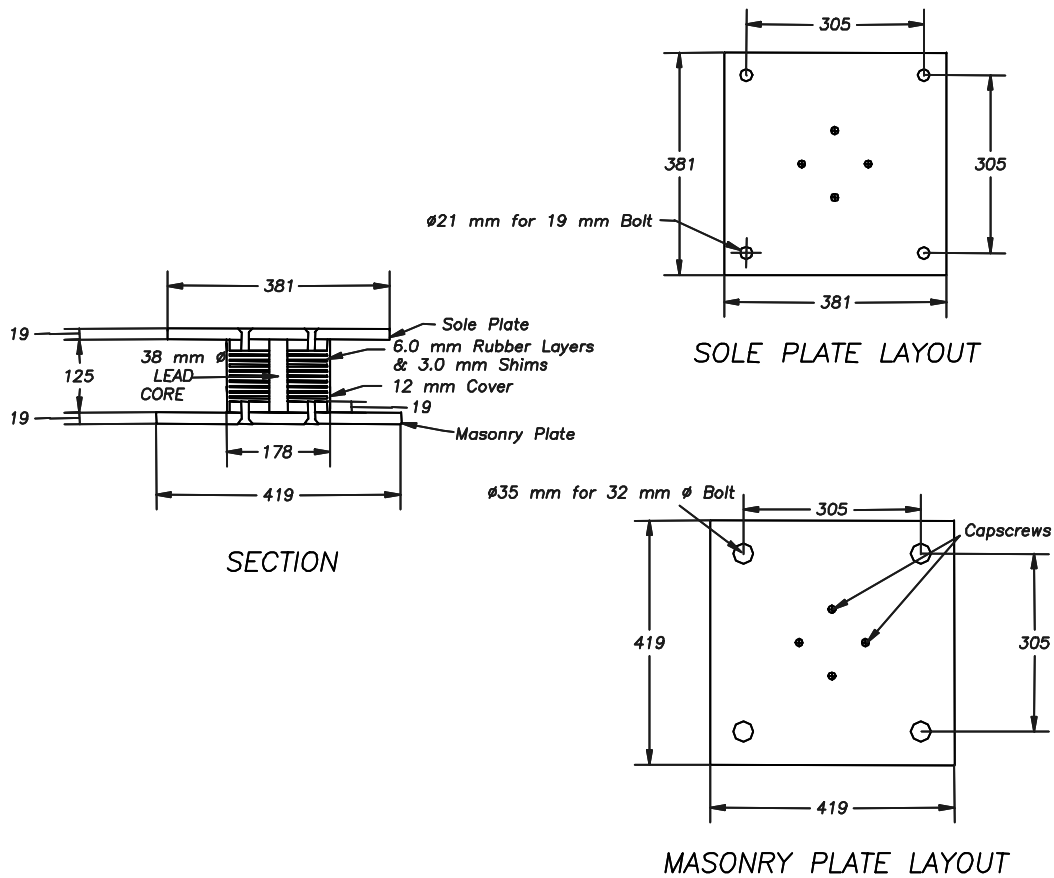


FIGURE 2-16 Lead rubber bearing

2.4 Simulation of Earthquake Loading

2.4.1 Reversed Static Transverse Loading

The first series of experiments on the bridge model simulated transverse earthquake loading in the model using actuators located at the one thirds points along the bridge as shown in the Figure 2-1. The center of mass of the bridge model was slightly below the centreline of the deck slab as 75% of the weight of the bridge model was concentrated in the deck slab. If barrier rails, wearing surface and some live load was included the proportion of weight at and above deck slab level would have increased further. Consequently, the actuator supports were designed to apply loads just (41 mm) below the centreline of the deck slab. A cross section of the bridge model at one support is illustrated in Figure 2-17. A hydraulic actuator support was used after the second experiment to minimize the effect of the actuator weight on the connected side of the bridge. The support was designed to move vertically with the bridge but apply a constant force equal and opposite to the weight of the actuator at the support point. A section of the deck slab around the actuator supports was removed to ensure that loads were transferred into the bridge without localized damage to the deck slab. A double angle strut was also added to resist forces induced by twisting of the bridge during transverse loading.

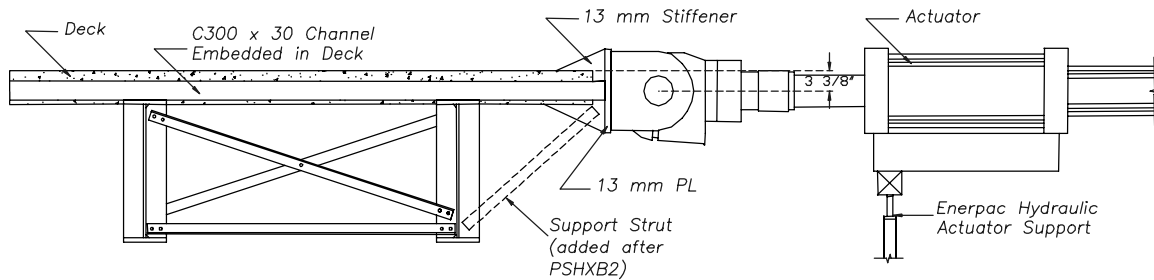


FIGURE 2-17 Actuator connected to bridge model at 1/3 points along length of bridge

The reversed static experiments investigated the effect of different end and intermediate cross frame configurations in the bridge model. Different configurations investigated included the influence of heavy diagonal X-braces; light X-braces; top chords, both with an without a direct connection to the deck slab; bottom chords and intermediate cross frames. Table 2-2 lists the 8 different reversed static experiments and the differences between them and further details are found in Carden et al. (2005). Focus in this report in on experiments RSHXB1 and RSHXB2 with heavy X-braces and RSLXB with ductile X-braces. Loading histories for these three experiments are given in Figures 2-18 to 2-21. While the first experiment was displacement controlled the remaining two were effectively force controlled with equal forces in the two actuators at all times.

2.4.2 Shake Table Earthquake Simulation

Following the series of reversed static experiments on the bridge model, a series of shake table experiments were performed. There were several advantages of shake table experiments over the reversed static experiments. One was a more realistic loading as the bridge was loaded directly by its own inertia, as in an earthquake. Another advantage was that the actual response of a bridge to a given level of excitation was found and not just the properties up to a specified displacement or force. This allows the elastic response to be compared to the inelastic response and also the design response. The trade-off is a more complex system to be analyzed. Therefore the reversed static and shake table experiments complemented each other.

Shake table experiments utilized three 50 tonne capacity shake tables. The bridge was attached as a simply supported span to Shake Tables 1 (north end) and 3 (south end), and also as a two span bridge to Shake Table 2 at the midspan (Fig. 2-22). The different series of experiments are listed in Table 2-3.. The bridge was first investigated as an isolated bridge with lead rubber bearings at the ends of the bridge (STLRB), with properties as described in Section 2.3.6. In the second experiment lead rubber bearings were added to the midspan of the bridge in order to achieve a two span bridge configuration (STLRB2S). Roller isolation bearings (STRB) were then placed in the bridge model in a simply supported configuration, although the results of these experiments are not discussed in this thesis. For the next series of experiments (STLXB) the lead rubber isolation bearings in the simply supported bridge model were restrained in the transverse direction and a series of experiments were performed in order to determine the inelastic behavior of the light diagonal X-braces. After considerable inelastic deformation in these braces they were replaced by unbonded braces at the ends of the bridge (STUB). An unbonded brace was also installed at the midspan of the bridge, although this had little effect on the response while the bridge was simply supported. However, for the next series of experiments (STUB2S) transversely restrained

TABLE 2-2 Reversed Static Experiments

No.	Abbrev. Name	Full Name	End Cross Frames					Intermediate Cross Frames
			Diagonals	Top Chord		Bottom Chord	Connections (Diag. / Chords)	
				Type	Composite			
1	RSHXB	Reversed Static "Heavy" X-Brace	Heavy Single L	Double L / T Section	South End Only	Double L	Bolted to Gusset Plates	Yes
2	RSHXB2	Reversed Static "Heavy" X-Brace 2	Heavy Single L	Double L / T Section	Both Ends	Double L	Bolted to Gusset Plates	Yes
3	RSNECF	Reversed Static No End Cross Frames	None	None	None	None	None	Yes
4	RSNBC	Reversed Static No Bottom Chord	None	Double L / T Section	Both Ends	None	Bolted to Gusset Plates	Yes
5	RSFC	Reversed Static Fixed Chords	None	Double L / T Section	Both Ends	Double L	Bolted to Gusset Plates	Yes
6	RSNCF	Reversed Static No Cross Frames	None	None	None	None	None	None
7	RSPC	Reversed Static Pinned Chords	None	Double PL / T Section	Both Ends	Double L	Welded / Single Bolt to Stiff.	Yes
8	RSLXB	Reversed Static "Light" X-Brace	Light Single L	Double PL / T Section	Both Ends	Double L	Welded / Single Bolt to Stiff.	Yes

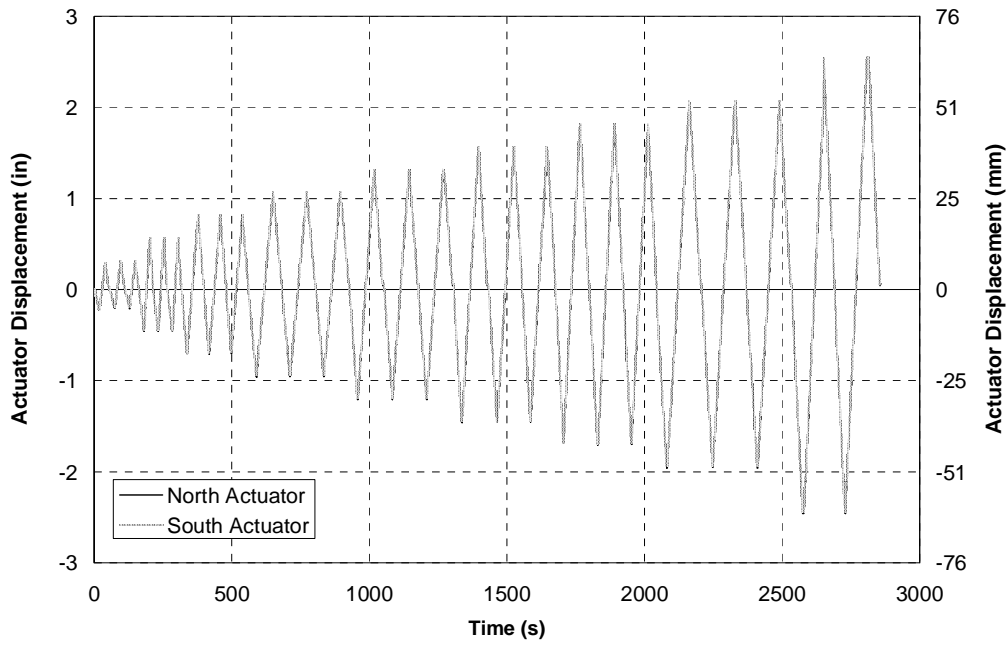


FIGURE 2-18 Actuator displacements vs time for RSHXB1

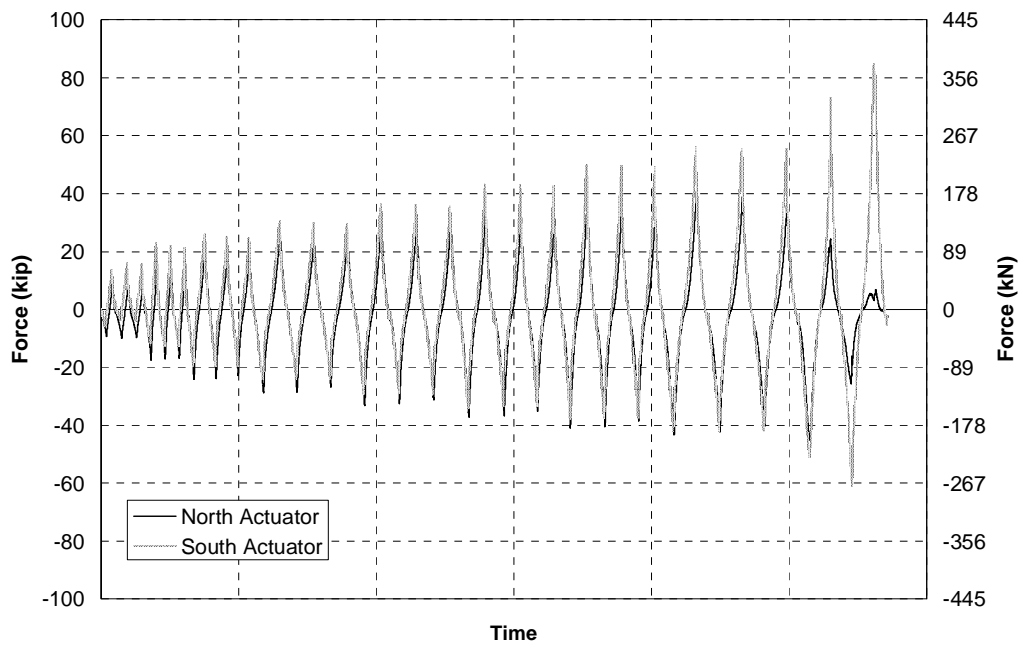


FIGURE 2-19 Actuator forces vs time for RSHXB1

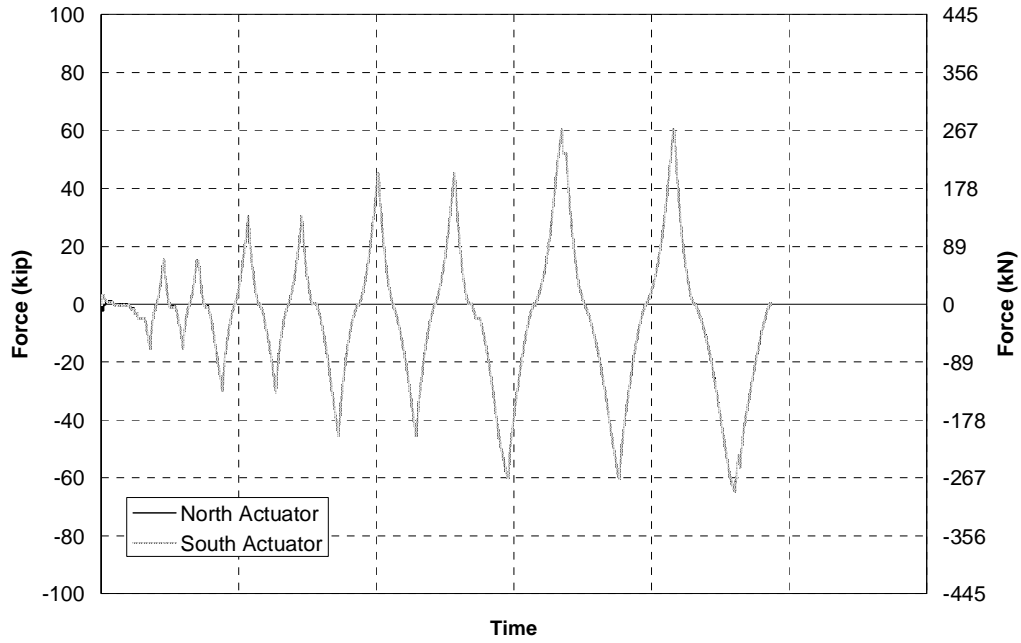


FIGURE 2-20 Actuator forces vs time for RSHXB2

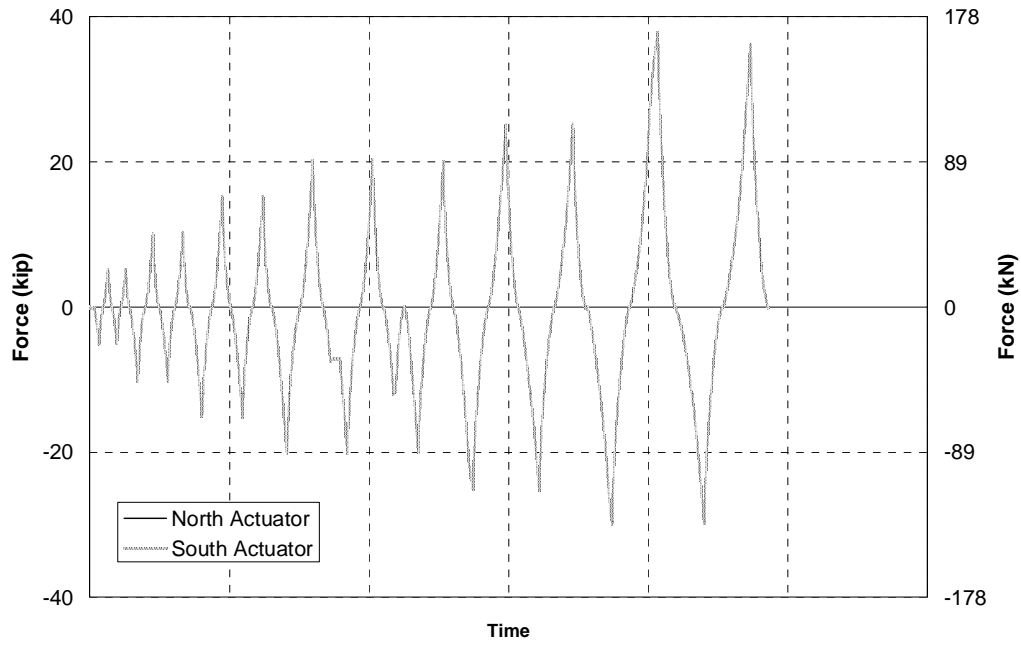


FIGURE 2-21 Actuator forces vs time for RSLXB



FIGURE 2-22 Bridge Model attached to three 50 ton shake tables

bearings were placed at the midspan of the bridge in order to determine its response with ductile unbonded braces in a two span configuration. The unbonded braces were then removed and earthquakes were simulated on the bridge model with no end cross frames (STNXF) in a simply supported configuration. Heavy single angle cross frames were then installed in the bridge in order to calculate the elastic response of the bridge to compare with the inelastic response of the ductile end cross frames. Following on, simulations on the isolated bridge model with the unrestrained lead rubber bearings were repeated to see if there was any change in response with the heavier cross frames (STLRB2), and to investigate potential degradation in the bearings. Finally, experiments were performed on the bridge model in a single span configuration with a ball bearing isolation system, although results are not discussed in this report.

For each series of experiments, a number of earthquakes were simulated in the bridge model. A complete list of earthquake simulations is given in Appendix 3. Three earthquakes were used for shake table experiments. The first was from the 1940 Imperial Valley earthquake recorded at the El Centro station. This was selected because of its extensive use in the past for analytical and shake table experiments. The second earthquake was from the 1994 Northridge earthquake recorded at the Sylmar hospital station. This was one of the largest recorded motions in the United States and has been used for past shake table experimentation. The third earthquake was from the 1995 Kobe earthquake in Japan recorded at the KJMA station. This has a particularly high peak ground acceleration and velocity, comparable to the Sylmar record. The details of each earthquake are listed in Table 2-4.

The earthquakes were obtained from the PEER strong motion database (PEER, 2002). Time histories for each earthquake are shown in Figures 2-23 to 2-25. Coincidentally, the dominant

TABLE 2-3 Shake Table Experiments

No.	Abbrev. Name	Full Name	Cross Frames		Top & Bottom Chords	Bearings		Spans
			Type	Connection		Type	Restrains	
1	STLRB	Shake Table Lead Rubber Bearings	Light X-Brace	Welded	Double PL & Double L - Pinned	LRBs	No	1
2	STLRB2S	Shake Table Lead Rubber Bearings 2 Span	Light X-Brace	Welded	Double PL & Double L - Pinned	LRBs	No	2
3 ¹	STRB	Shake Table Roller Bearings	Light X-Brace	Welded	Double PL & Double L - Pinned	Roller	No	1
4	STLXB	Shake Table "Light" X-Braces	Light X-Brace	Welded	Double PL & Double L - Pinned	LRBs	Yes	1
5	STPUB	Shake Table Pinned Unbonded Braces	Unbonded brace	Bolted / Pin	Double PL & Double L - Pinned	LRBs	Yes	1
6	STFUB	Shake Table Fixed Unbonded Braces	Unbonded brace	Welded	Double PL & Double L - Pinned	LRBs	Yes	1
7	STFUB2S	Shake Table Fixed Unbonded Braces 2 Span	Unbonded brace	Welded	Double PL & Double L - Pinned	LRBs	Yes	2
8	STNECF	Shake Table No End Cross Frames	None	-	None	LRBs	Yes	1
9	STHXB	Shake Table "Heavy" X-Braces	Heavy X-Brace	Welded	Double PL & Double L - Pinned	LRBs	Yes	1
10	STLRB2	Shake Table Lead Rubbers Bearing series 2	Heavy X-Brace	Welded	Double PL & Double L - Pinned	LRBs	No	1
11 ¹	STSB	Shake Table Seismic Ball Bearings	Heavy X-Brace	Welded	Double PL & Double L - Pinned	Ball Bearings / LRBs	No	1

Notes: 1. These experiments are not discussed in this dissertation.

TABLE 2-4 Earthquake Data for Shake Table Experiments

Name	Comp.	Year	Earthquake	Station	Direction	PGA (g)	PGV (m/s)
El Centro	NS	1940	Imperial Valley	El Centro Array #9	180	0.313	0.46
	EW				270	0.215	0.47
Sylmar	NS	1994	Northridge	Sylmar Hospital	360	0.843	2.01
	EW				090	0.604	1.21
Kobe	NS	1995	Kobe	KJMA	000	0.821	1.26
	EW				090	0.599	1.15

component for each earthquake, ie. the component with largest peak acceleration, were the north-south (0 or 180 degree) components. Therefore when considering only one component, unless specifically stated otherwise, the north-south component was used. The response spectrum for 2.0 x El Centro, as shown in Figure 2-28, compares reasonable to with the design spectrum. This level of excitation is used for much of the analysis of the bridge model.

In addition the north-south component of El Centro was passed through a simulated soil layer using EduShake (EduPro, 1999). This motion assumed a 75 ft layer of sand with a shear wave velocity of 900 ft/s and density of 120 pcf corresponding to medium-stiff material for soil type III in AASHTO (1998). Average Seed and Idriss models were used for the modulus and damping curves. The resulting output time history at the top of the soil layer is shown in Figure 2-26. This motion was used to investigate the effect of differential ground motion at the different supports of the bridge.

The earthquakes were scaled in the time domain to account for scaling of the bridge model. The scale factor for time was equal to $\sqrt{0.4} = 0.632$. Response spectra for each of the time scaled earthquakes at 5% damping are shown in Figure 2-27. The El Centro spectra are below both the AASHTO LRFD (1998) and AASHTO Isolation (1999) design spectra at all periods. In contrast, the dominant components of the Sylmar and Kobe records exceed the design spectra up to periods in excess of 1 s. The soft soil El Centro record exhibits an amplified response of up to 3 times at around 0.55 s compared to the original El Centro 180 record.

2.5 Instrumentation

2.5.1 Overview

A number of instruments were placed on the bridge model in order to measure the deformations, forces, strains and accelerations in the bridge during reversed static and shake table experiments. A complete inventory of instruments is shown graphically, with names for reference purposes given in the following sections. A convention for naming the instruments was used in order to describe the type of instrument, location of instrument and direction of measurement. For example, label DK15AccVE refers to an instrument on the deck slab of the bridge model, 4570 mm (15 ft) from the north end, measuring accelerations in the vertical direction on the eastern side of the bridge model. Not all the instruments shown were on the bridge model for every experiment, however reference is made to them as appropriate during analysis throughout the following chapters.

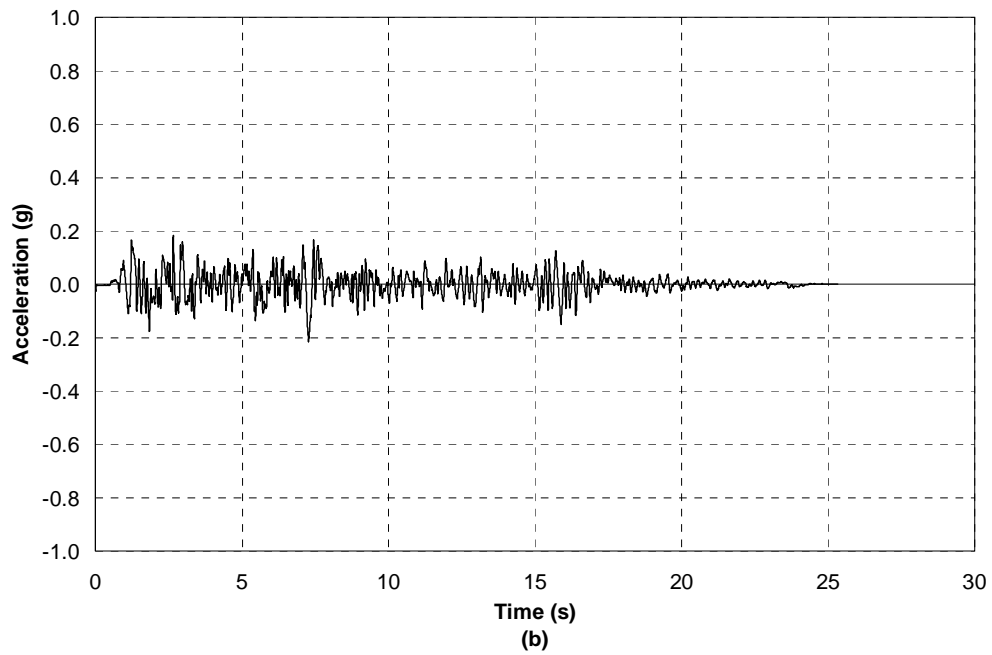
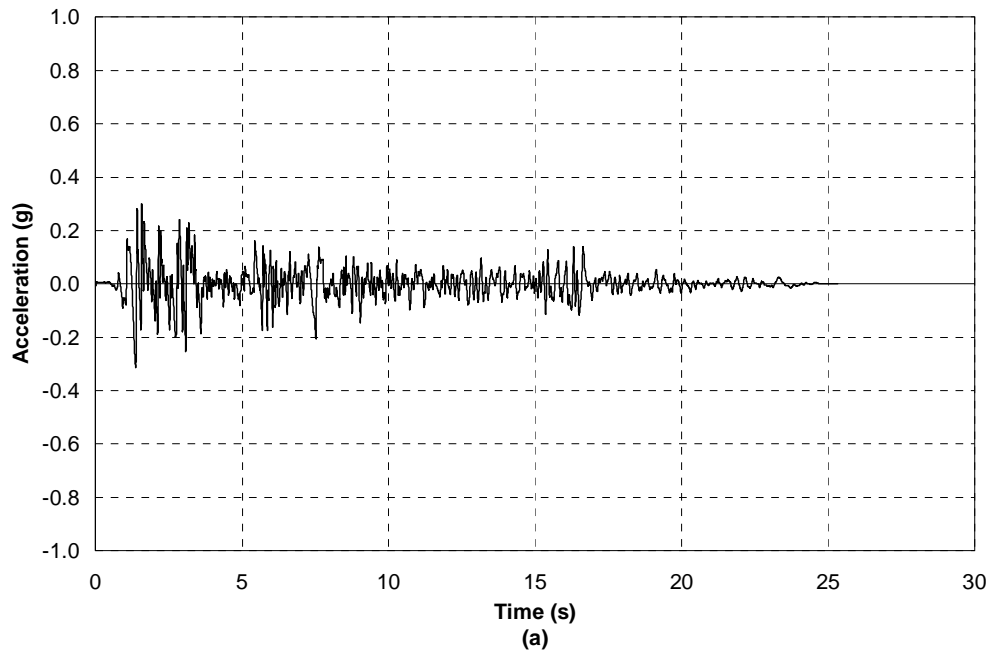


FIGURE 2-23 Acceleration time histories for a) 180 component and b) 270 component of El Centro

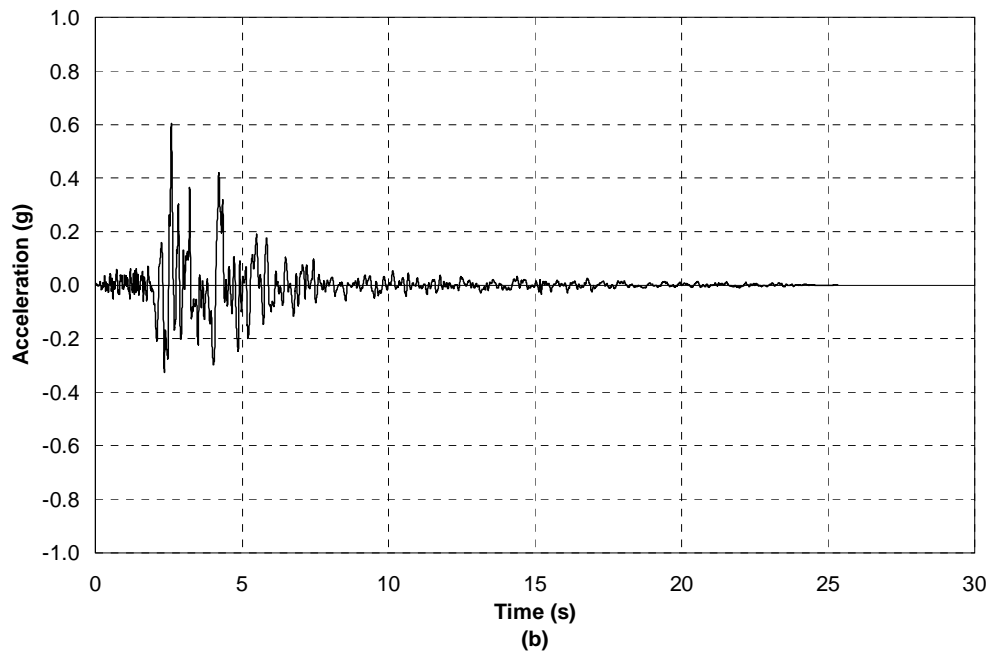
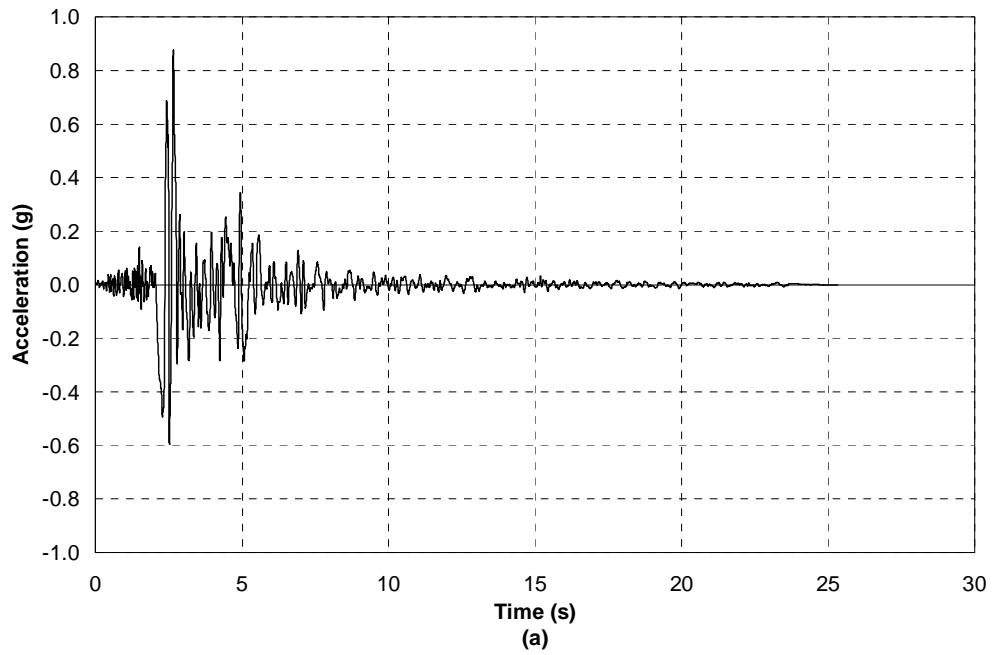


FIGURE 2-24 Acceleration time histories for a) 360 component and b) 90 component of Sylmar

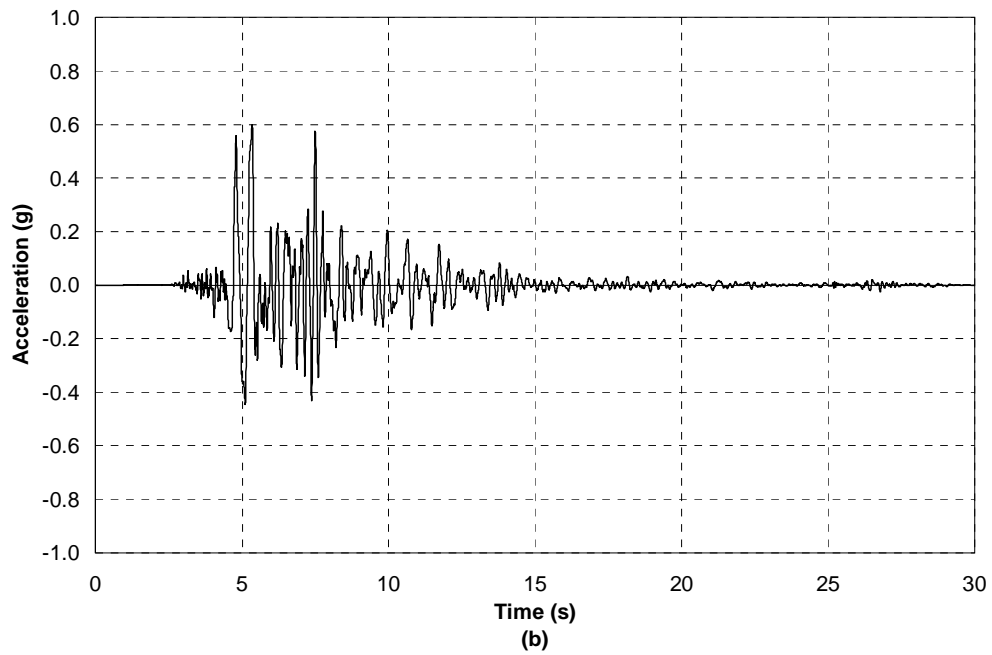
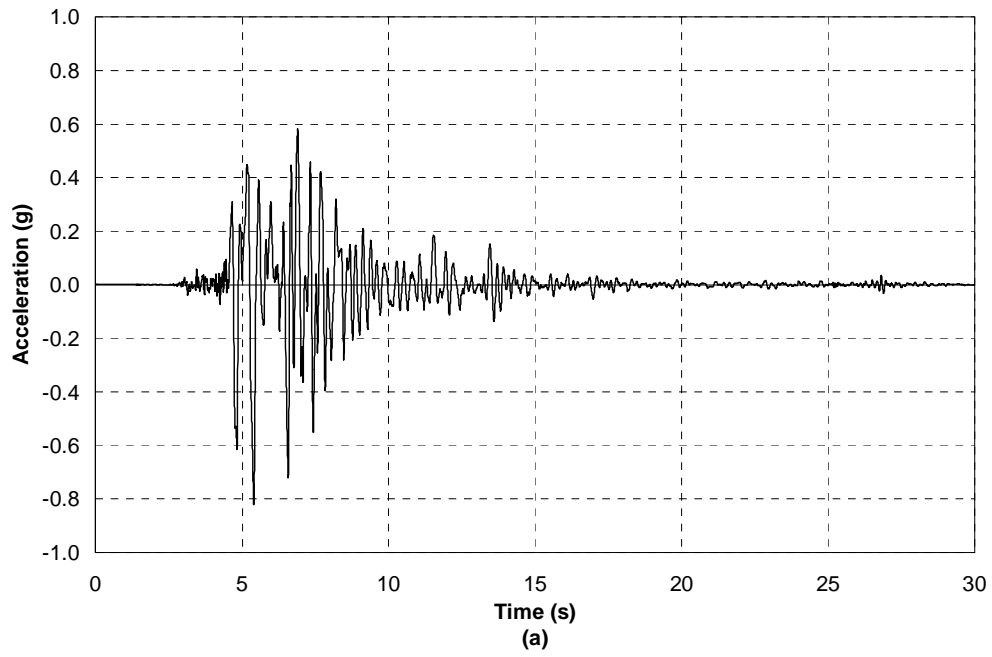


FIGURE 2-25 Acceleration time histories for a) 00 component and b) 90 component of Kobe

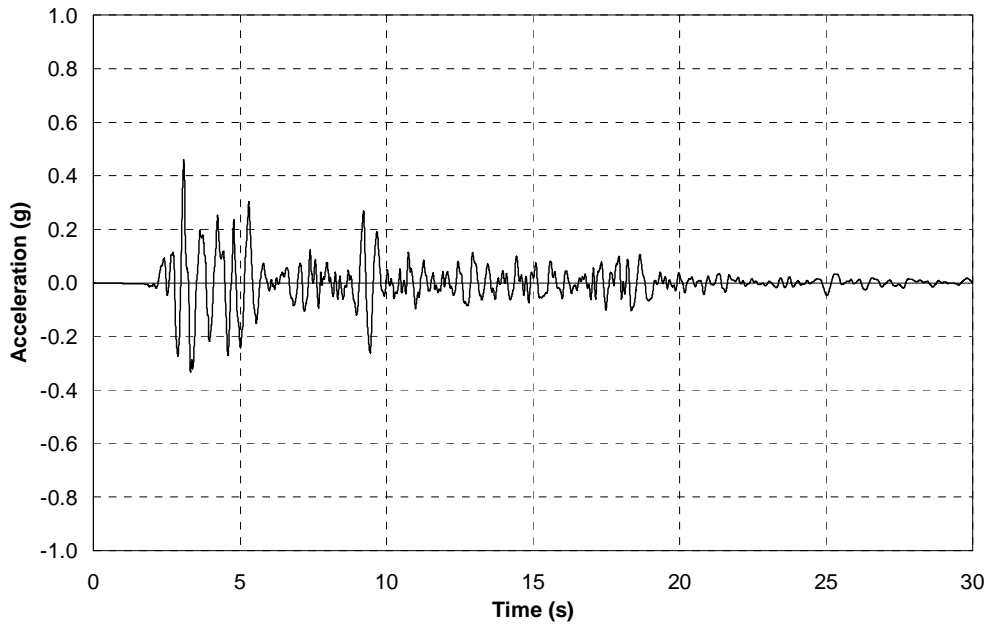


FIGURE 2-26 Acceleration time histories for El Centro 180 component through soil layer

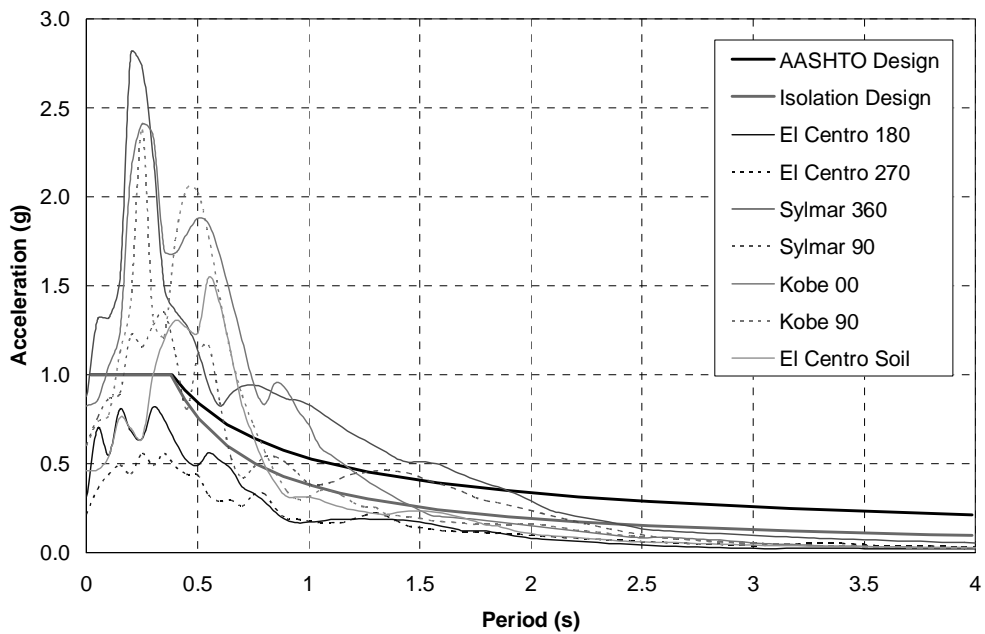


FIGURE 2-27 Theoretical earthquake response spectra (5% damping)

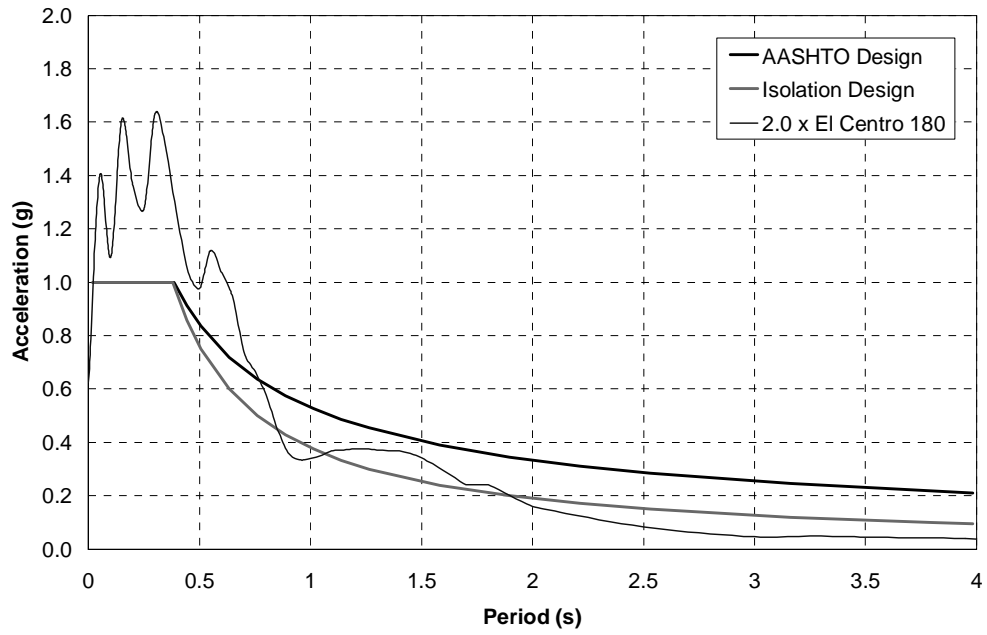


FIGURE 2-28 Earthquake response spectrum for 2.0 El Centro (5% damping)

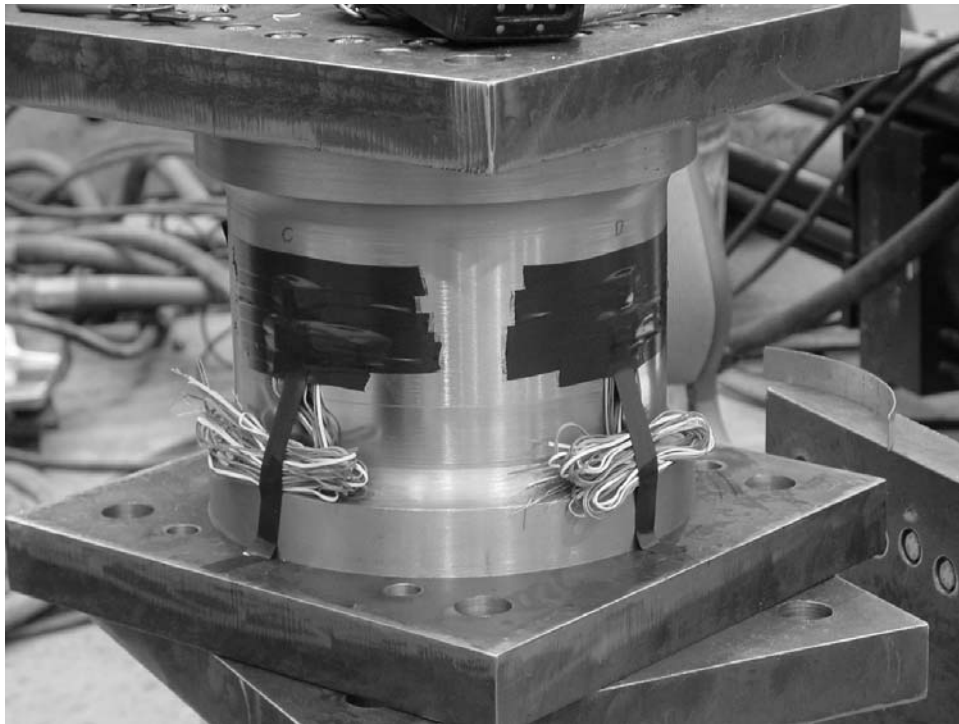


FIGURE 2-29 Multi-axial Load Cell

2.5.2 Load Cells

Six multi-axial load cells were designed and constructed in order to measure the forces beneath the bearings in the bridge model. The load cells were designed using a series of strain gage circuits (Fig. 2-29) which were able to measure all six components of force, based on a design by Reinhorn et al. (2001).

The load cells were calibrated in the axial and two components of shear in order to convert the strain gage circuit output to forces. Further details for the calibration are given in the preceding report (Carden, 2005). The load cells were placed under the bearings at the ends of the bridge model and at midspan as illustrated, for example, in Figure 2-12. The load cells were numbered as shown in Figure 2-30. The axes with positive orientations are shown.

2.5.3 Displacement Transducers

Deformations in the bridge model were measured using displacement transducers attached to the bridge at different locations. Some transducers were attached to the bridge model and a fixed point in the laboratory, such as those attached to the deck slab, therefore measured absolute displacements. Others were attached to the bridge model and fixed points relative to the shake tables therefore measured relative displacements. The majority of displacement transducers used were Celesco PT100 series cable-extension transducers including the displacement transducers along the length of the superstructure, as shown in Figure 2-31. Celescocs were also used for the displacement transducers at the bearings, the length of the cables connecting the transducers to the bridge model were relatively short, therefore for bi-directional motion the longitudinal and transverse components were coupled, and corrections were made where necessary to the raw data to allow for this coupling.

At the end cross frames Novotechnik linear potentiometers were used to measure displacements in the end regions. The positions of these transducers are shown in Figures 2-32 and 2-33 respectively. Diagonally placed transducers were used to measure the lateral deformation between the top and bottom flanges of the girders as shown in these figures. Additional transducers were used to measure displacements across the yielding portions of the X-braces and unbonded braces respectively.

2.5.4 Accelerometers

Accelerometers were situated throughout the bridge model for system identification, measurement of modeshapes and natural frequencies, and for comparison between shake table and bridge response. Accelerometers were placed on the deck slab, bottom flange and on top of bearings as shown in Figure 2-34. Horizontal accelerometers on the deck slab were Kinematic $\pm 2g$ accelerometers. Horizontal accelerometers on the bottom flange and bearings were $\pm 4g$ accelerometers. Vertical accelerometers were also $\pm 4g$ accelerometers and were attached to the edges of the deck slab in order to measure vertical and rotational modes of deformation.

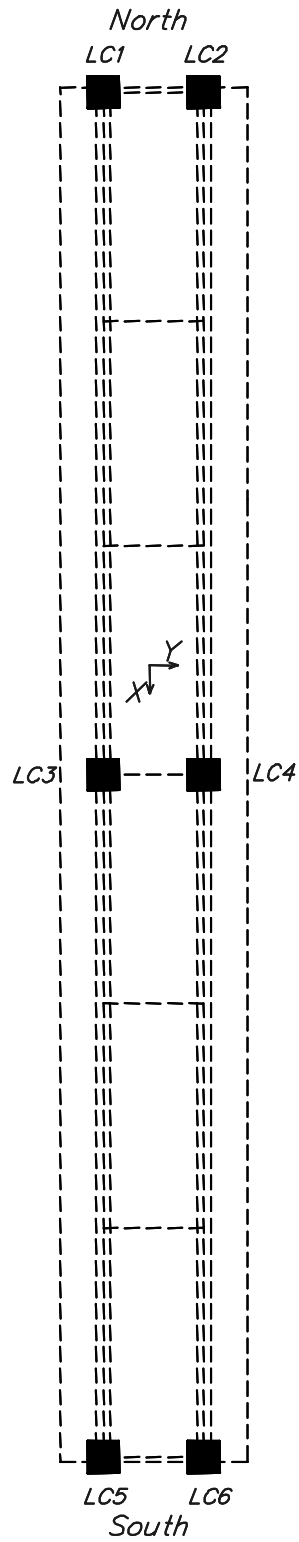


FIGURE 2-30 Instrumentation - load cells

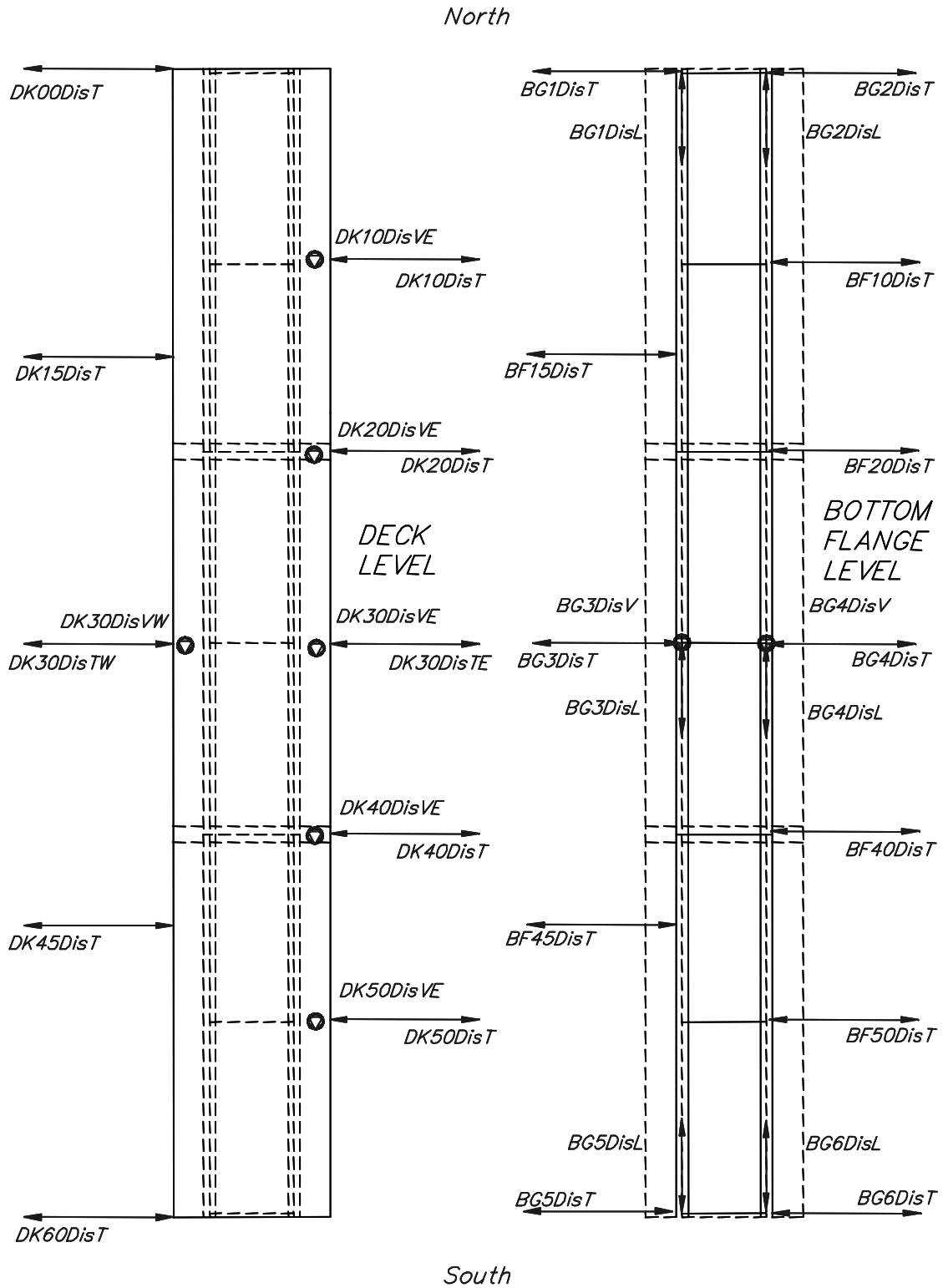


FIGURE 2-31 Instrumentation - Displacement Transducers

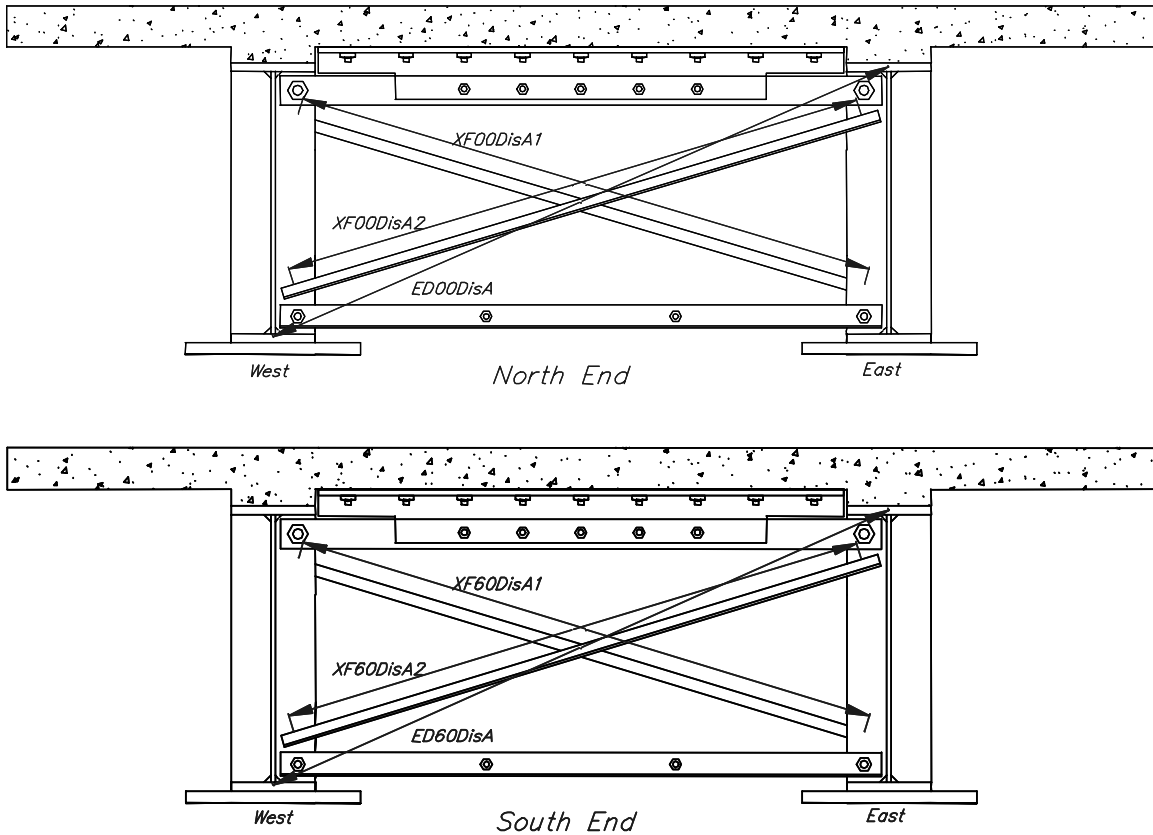


FIGURE 2-32 Instrumentation - Typical displacement transducers for end X-braces

2.5.5 Strain Gages

Strain gages were placed throughout the bridge model in order to measure localized strains at critical locations on the plate girders and in the deck slab. They were also situated on the cross frames in an attempt to correlate strains to forces in the cross frames. To avoid clutter, dimensions for every strain gage are not shown however where necessary their locations can be scaled off the drawings.

Eight strain gages were typically placed on the end cross frames as shown on Figure 2-35. It was shown from the end cross frames that the measured strains on the inside and outside of the angle members were similar. Therefore, the intermediate cross frames typically have four strain gages on each set as shown in Figure 2-36.

There were a number of strain gages placed on the stiffeners at the ends of the bridge model. Eight strain gages at each end are shown in Figure 2-35. In addition for another set of strain gages was placed on the bearing stiffener of the west girder, at the north end of the bridge at the edges of the stiffeners, in order to get a better understanding of the distribution of bending strains in the stiffener (Fig. 2-37).

A series of strain gages were also placed on the girders in order to measure the distribution of strains along the length of the girders. The strain gages on the east girder were distributed as

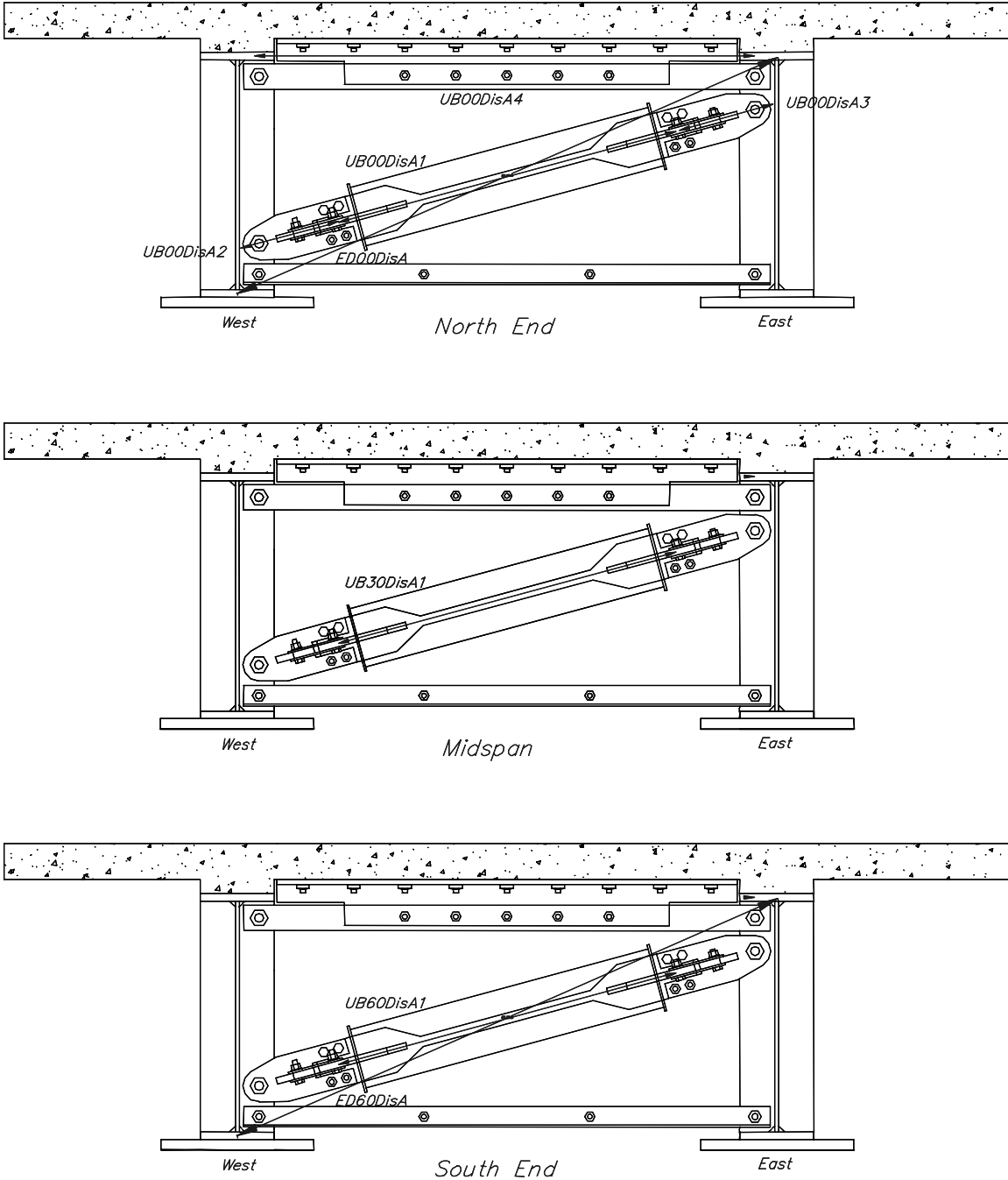


FIGURE 2-33 Instrumentation - Displacement transducers for unbonded braces

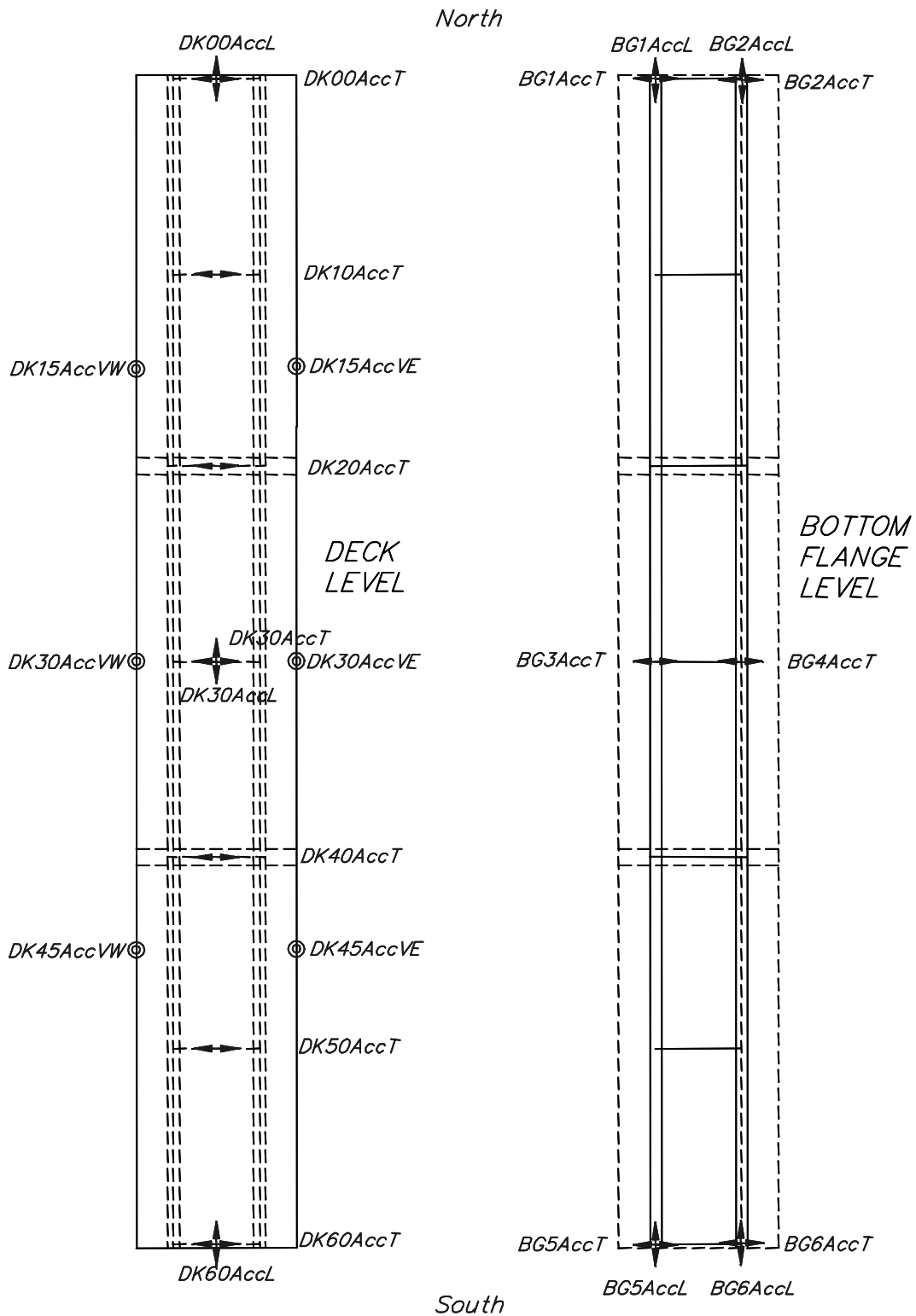


FIGURE 2-34 Instrumentation - Accelerometers

shown in Figure 2-38. On the west girder strain gages were placed on the outside edges of the top and bottom flanges concentrated at the north end of the bridge model (Fig. 2-39) in order to get more detailed measurements of strain distributions at the end of a girder when there were large transverse deformations in the girders.

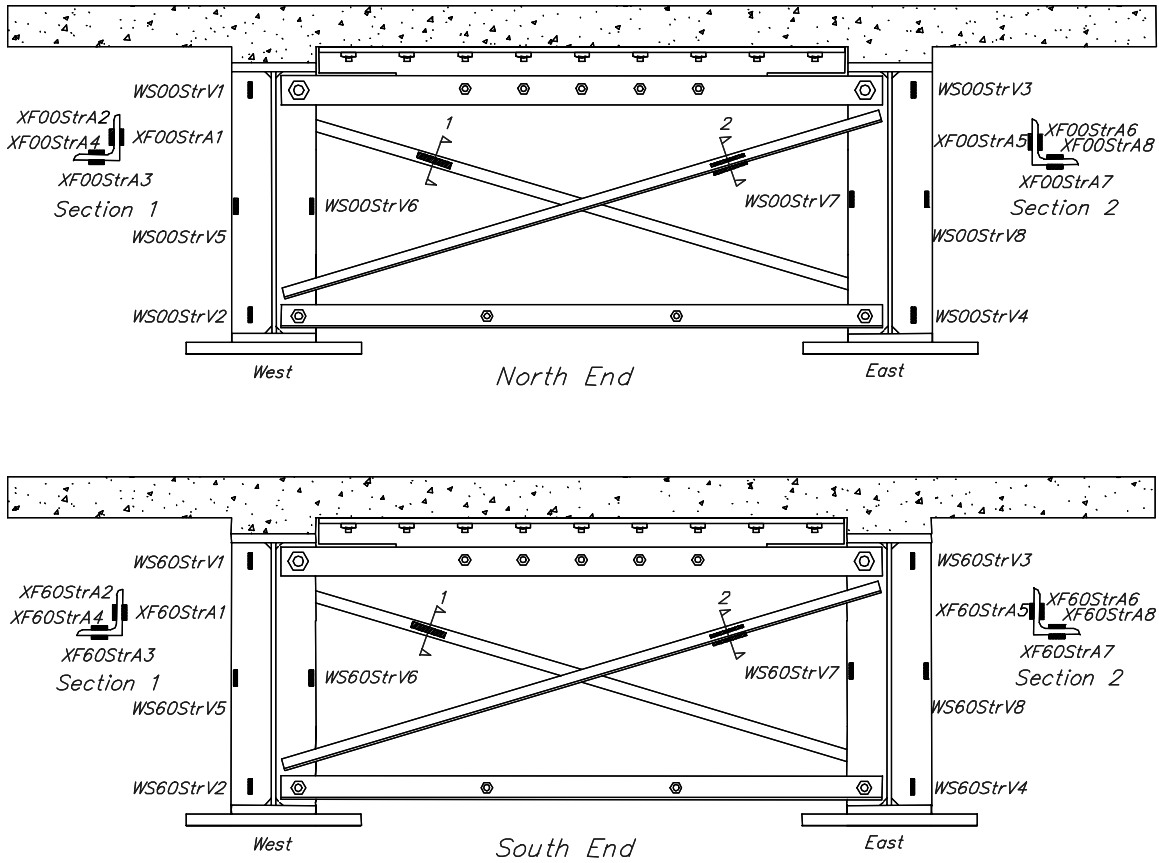


FIGURE 2-35 Instrumentation - Strain gages on end cross frames

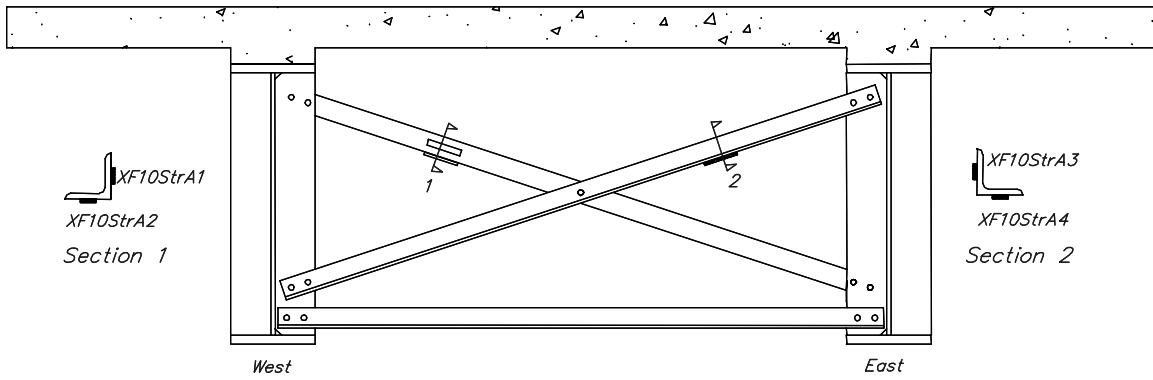


FIGURE 2-36 Instrumentation - Strain gages on typical intermediate cross frame

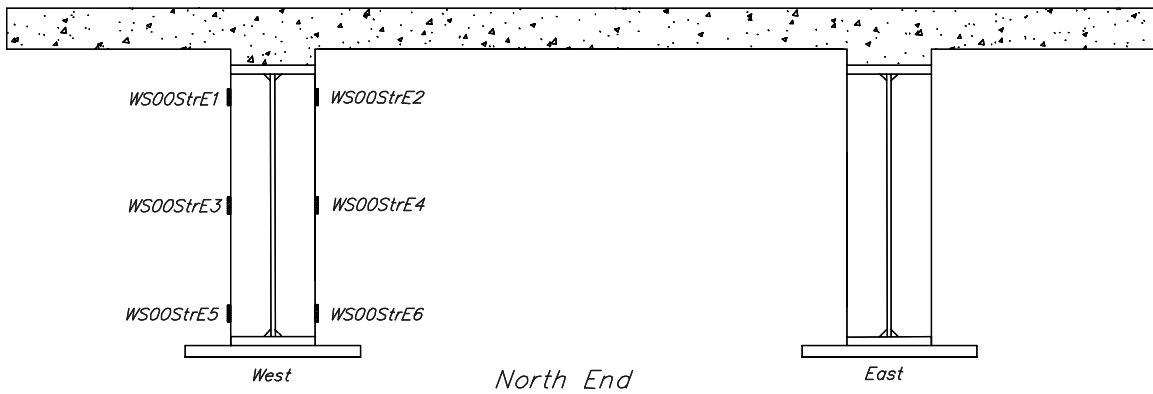


FIGURE 2-37 Instrumentation - Additional strain gages on end stiffener

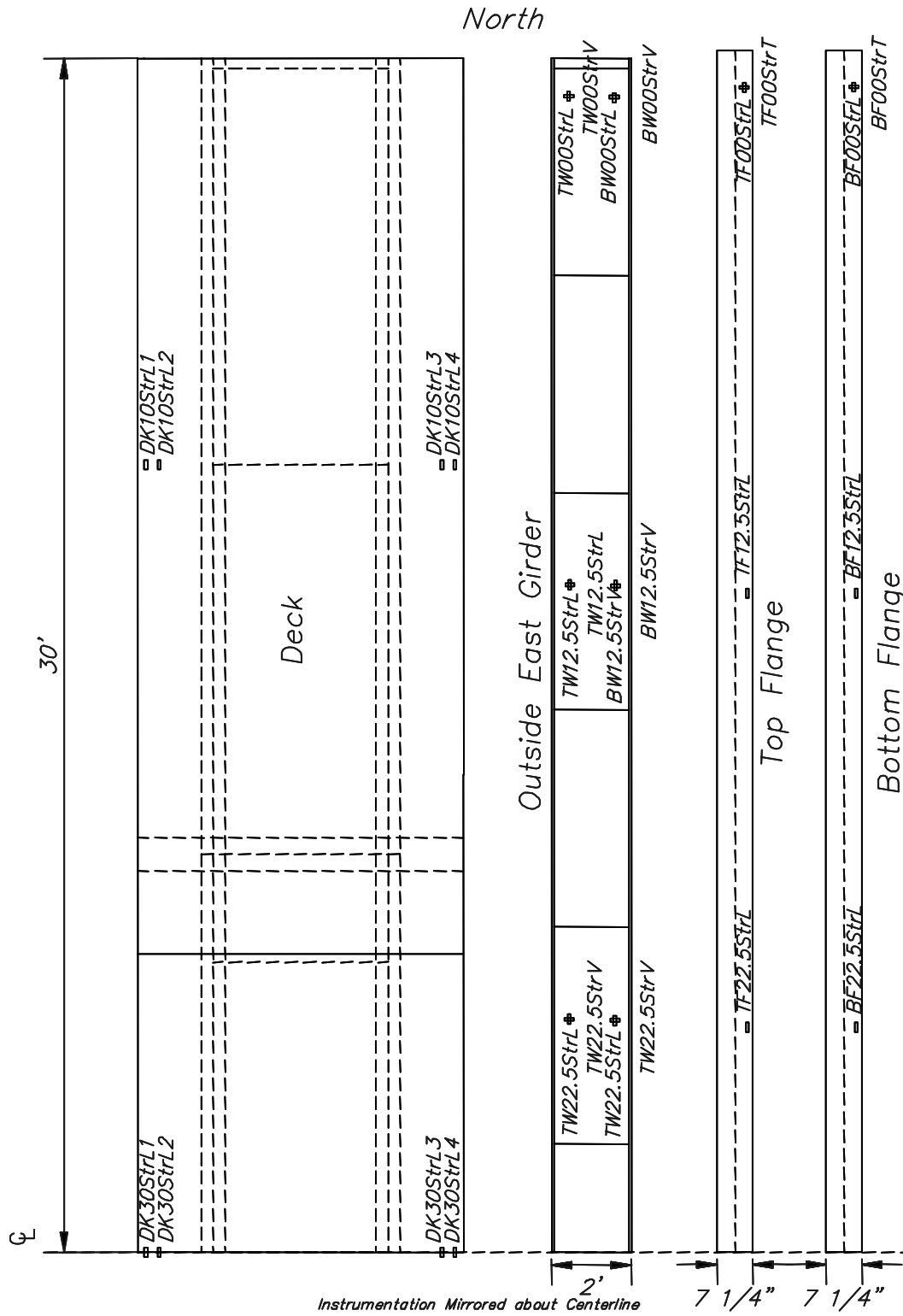


FIGURE 2-38 Instrumentation - Strain gages on east girder

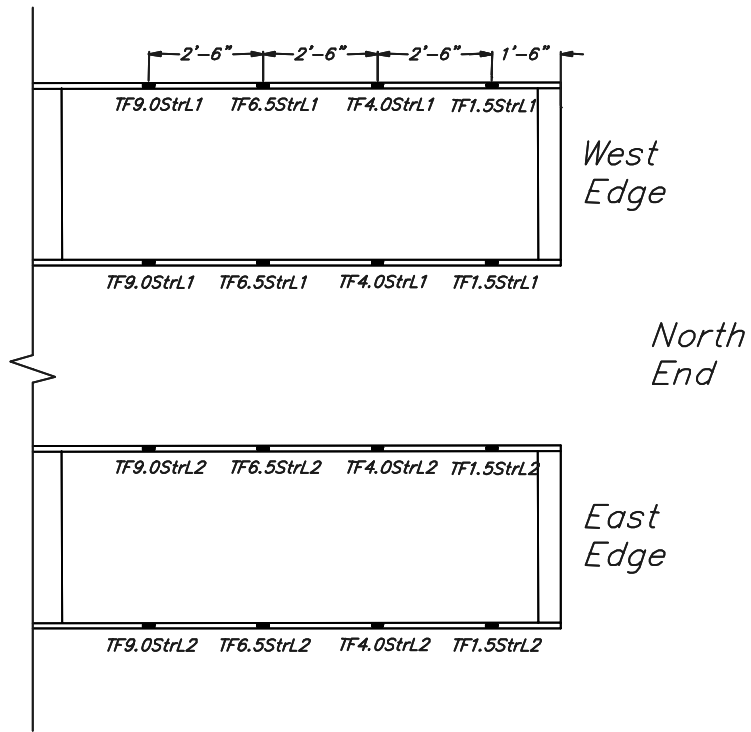


FIGURE 2-39 Instrumentation - Strain gages on west girder

SECTION 3 CYCLIC BEHAVIOR OF INELASTIC COMPONENTS IN THE BRIDGE MODEL

3.1 Introduction

This chapter investigates the properties of the inelastic members in the ductile end cross frames and isolation bearings used in the bridge model based on a series of component experiments. The inelastic properties of single angles were studied as the critical diagonal components in the X-braces. Buckling restrained braces (BRBs) were also studied as a another component of ductile end cross frames used in the bridge model. Component experiments for the lead rubber bearings, used to seismically isolate the bridge model, are also described.

3.2 Single Angle X-Brace Diagonals

3.2.1 Coupon Tests

Tests were performed on coupons taken from single angle members of the same heat numbers as the members used in the bridge model in accordance with ASTM A370 standard coupon test for flat bars. The coupon test results are summarized in Table 3-1. Test 1 was for the heavy single angles with bolted connections, Test 2 was for the heavy single angles with welded connections and Test 3 was for the light single angles. Each set of angles came from a different heat number. The yield strengths from the three tests were 55%, 27% and 36% larger respectively than the minimum specified strength of 250 MPa for the ASTM A36 steel members. The ultimate strength was 50-52% larger than the measured yield stress for each specimen and the elongation at fracture was between 30-35% for each specimen.

TABLE 3-1 Coupon Test Results for Single Angle Members from ASTM A36 Steel

Coupon Test #	Test 1	Test 2	Test 3
Width (mm)	14	13	13
Coupon Dimensions			
Thickness (mm)	6	6	5
Length (mm)	51	51	51
Yield Stress (MPa)	386	316	338
Ultimate Stress (MPa)	578	475	514
Ultimate Elongation (%)	35	30	31 ¹
Modulus of Elasticity (GPa)	206	220	218

Notes: 1. Displacement measurement failed at 26% elongation. Ultimate elongation estimated based on loading rate.

3.2.2 Axial Component Experiments

3.2.2.1 Background

Axial component experiments were performed on 17 members in order to characterize the properties of the single angle components used in the bridge model. The strength, stiffness,

potential for overstrength, energy dissipation and ultimate displacement capacity of the single angles were studied. The components studied include a series of single angles with bolted and welded connections.

3.2.2.2 Experimental Assembly

Details of the single angles and connections for each experiment are listed in Table 3-2 while the different specimens are illustrated in Figure 3-1. Two sizes of single angles were used in experiments that were the same as those used in the heavy and light cross frames of the bridge model. The angles came from three different batches of steel corresponding to the three coupon tests. Different lengths were used to represent the full and half lengths of the diagonal members in the cross frames. Full and half lengths were used because, while forces were distributed through the entire length of a tension member, biased buckling was expected to occur over half the length of a compression member due to the restraint at midspan (El-Tayem, 1986; Beaulie, 1989; Kanada, 1996).

TABLE 3-2 Details of Component Experiments on Single Angle Members

Spec.	Section	Coupon Test	Effective Length (in)	Gusset Thickness (in)	Connection (Reinforced Plate Thickness (mm))	First Cycle	A_r/A_g	b/t ¹	KL/r ²
A	45x45x6	1	1030	13	Bolted	Compression	0.81	7	119
B	45x45x6	1	1030	25	Bolted	Compression	0.81	7	83
C	45x45x6	1	1030	25	Bolted	Tension	0.81	7	83
D	45x45x6	1	1030	25	Bolted (5)	Tension	0.93	7	83
E	45x45x6	1	1030	25	Bolted (8)	Compression	1.00	7	83
F	45x45x6	1	570	25	Bolted	Compression	0.81	7	46
G	45x45x6	1	570	25	Bolted	Compression	0.81	7	46
H	45x45x6	1	570	25	Bolted (5)	Tension	0.93	7	46
I	45x45x6	1	570	25	Bolted (8)	Compression	1.00	7	46
J	45x45x6	2	1030	25	Welded	Compression	1.00	7	83
K	45x45x6	2	1030	25	Welded	Tension	1.00	7	83
L	45x45x6	2	570	25	Welded	Compression	1.00	7	46
M	45x45x6	2	570	25	Welded	Tension	1.00	7	46
N	25x25x5	3	1280	25	Welded	Compression	1.00	5.33	181
O	25x25x5	3	1280	25	Welded	Tension	1.00	5.33	181
P	25x25x5	3	640	25	Welded	Compression	1.00	5.33	91
Q	25x25x5	3	640	25	Welded	Tension	1.00	5.33	91

- Notes: 1. Limiting b/t for special concentric braced frames in accordance with AISC Seismic Provisions (2002) is 8.5 and for AASHTO (1998) is 12.8, therefore are satisfied by all members.
2. Limiting KL/r for special concentric braced frames based on AISC Seismic Provisions (2002) is 167 and for AASHTO (1998) is 120 for main members, therefore are satisfied by all members except Specimens N & O. $K = 1.0$ for Specimen A, $K = 0.7$ for remaining specimens.

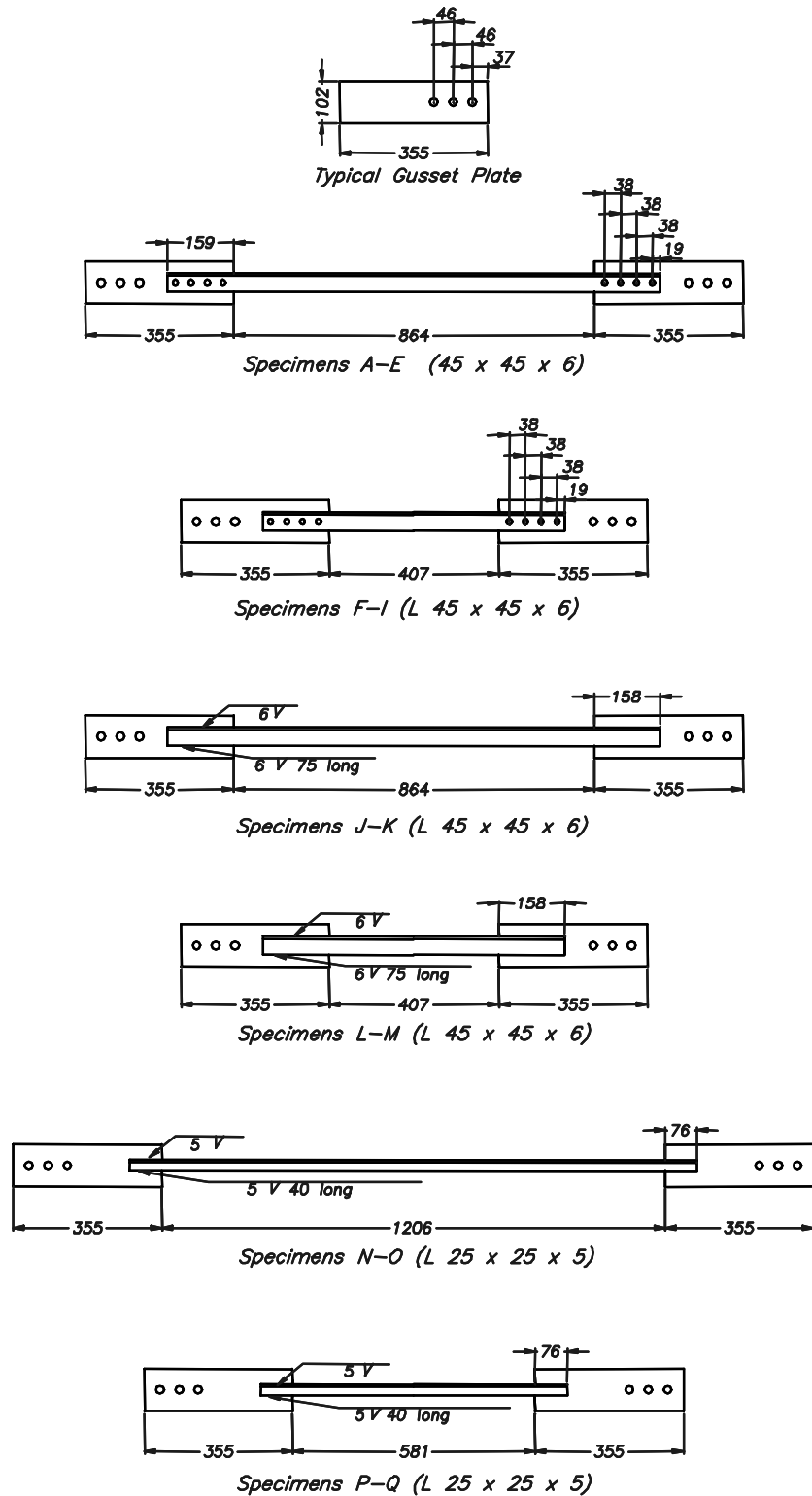


FIGURE 3-1 Single angle component experiment specimens

Gusset plates, 13 mm thick, were used in the first experiment, resulting in bending of the gusset plates at each end. It was apparent that the gusset plates were more flexible than those in the bridge model which were at least partially restrained from bending by the top and bottom chords. Therefore 25 mm thick gusset plates were used for subsequent experiments to promote formation of plastic hinges in the angles during buckling rather than in the gusset plates. This was expected to more accurately represent the behavior in the bridge model.

Some specimens were bolted using connections with three different A_n/A_g ratios. The first was based on the ratio for a member that was bolted to a gusset plate with the bolt holes resulting in an A_n/A_g ratio of 0.81, as shown in Figure 3-2. The other two ratios were increased by reinforcing the connection regions with a plate welded to the connected leg of the single angles, as shown in Figure 3-3. The members were then bolted through the reinforced section to a gusset plate with resulting A_n/A_g ratios of 0.90 for members reinforced with 5mm plates and 1.0 for members reinforced with 6 mm plates. Other specimens were welded using balanced welds in order to minimize bending in the member about an axis perpendicular to the connected leg when axial loads were applied to the member. The balanced welds meant that the edge at the outstanding leg of the angle was connected with a full length weld while the other edge was welded along approximately half the length in contact with the gusset plate, as shown in Figure 3-4. The results presented in the following section show that this connection detail had a large influence on the inelastic performance of these members.

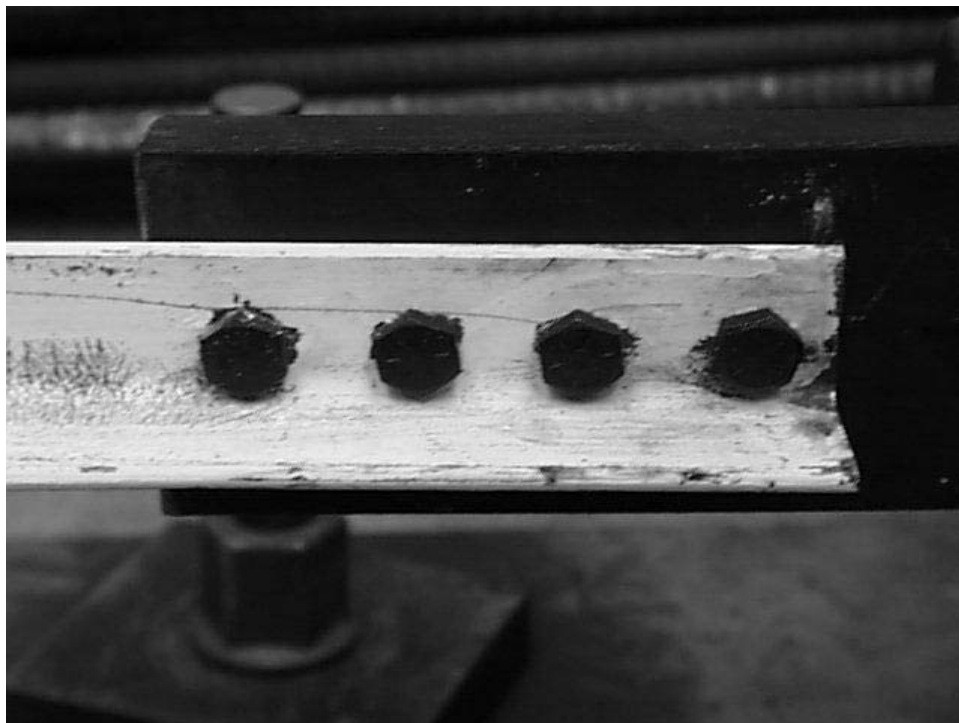


FIGURE 3-2 Single angle with unreinforced bolted connection to gusset plate



FIGURE 3-3 Single angle with reinforced bolted connection to gusset plate

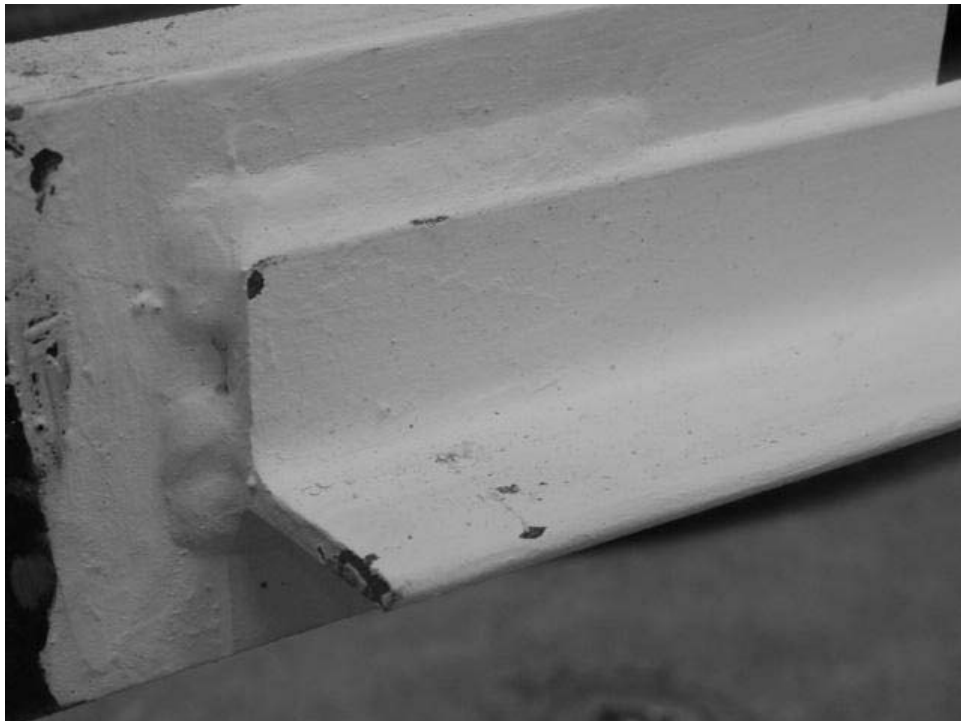


FIGURE 3-4 Single angle with balanced welded connection to gusset plate

Each specimen was subjected to cycles of alternating tension and compression with amplitudes increasing in 13 mm increments of displacement. For some of the specimens the initial displacement cycle was larger than 13 mm, as necessary to observe buckling or yielding of the member. Some of the members were started in tension while others were started in compression as given in Table 3-2.

The assembly used for the single angle experiments is shown in Figure 3-5. Axial forces were applied to the members using an actuator which was attached to slider to ensure only axial loads. The variation in force due to friction in the a slider was measured at less than 1 kip and was, therefore, ignored in the analysis. Loading was applied in displacement control. Displacements and forces were monitored for all specimens and strain gages were using to measure strains in selected specimens.

3.2.2.3 *Hysteretic Properties*

The force-displacement traces for each component are shown in Figures 3-9 to 3-25. The shape of the observed hysteresis loops is typical for single angles (Jain, 1978; El-Tayem, 1986). The failure mode of the members depended largely on the type of connection. The bolted specimens with unreinforced connections fractured in the region between the edge and the first bolt hole in the connected leg, as illustrated in Figure 3-6. Failure was typically observed much earlier in members with this type of connection than in the other members. With the reinforced bolted connections, which had an increased A_n/A_g ratio, the failure was moved to outside the connection region. Failure in these members occurred in the plastic hinge formed during buckling at either end of the member (Fig. 3-7) with a crack propagating from the edge of the connected leg. The welded connections resulted in an even further improvement in the performance of the angles. These members failed in the plastic hinges formed either at the end of the angle or at midspan as shown in Figure 3-8. The balanced weld appeared to delay the initiation of cracking at the edge of the connected leg due to an apparently lower stress concentration in this region compared to the bolted connections.

3.2.2.4 *Yield Tensile Strength*

The tensile yield point for the single angle specimens is defined as the point where the entire member yields. For a concentrically loaded member subject to a monotonic axial loads, this point can be clearly identified using such limits as the force at 0.2% offset strain. However, for the single angle members subjected to cyclic loads it was more difficult to identify the yield point. This is firstly because there was an eccentricity in the connection between the single angles and the gusset plates with the resulting moment causing part of the member to yield before the entire member yielded. Secondly, there was slippage in the bolted connections that resulted in additional axial displacement, effectively reducing the stiffness in the member prior to yielding. In addition, some of the members buckled in compression before being subjected to tension, hence the properties of these members were modified by the formation of a plastic hinge due to buckling. These factors made it impossible to use a consistent method to identify the yield point. The yield point was subsequently identified by inspection at the point where the yield plateau was observed, indicating that the entire member had yielded. The yield force was relatively insensitive to variation in selection of the yield point and prior loading history. The estimated yield forces for each experiment are summarized in Table 3-3.

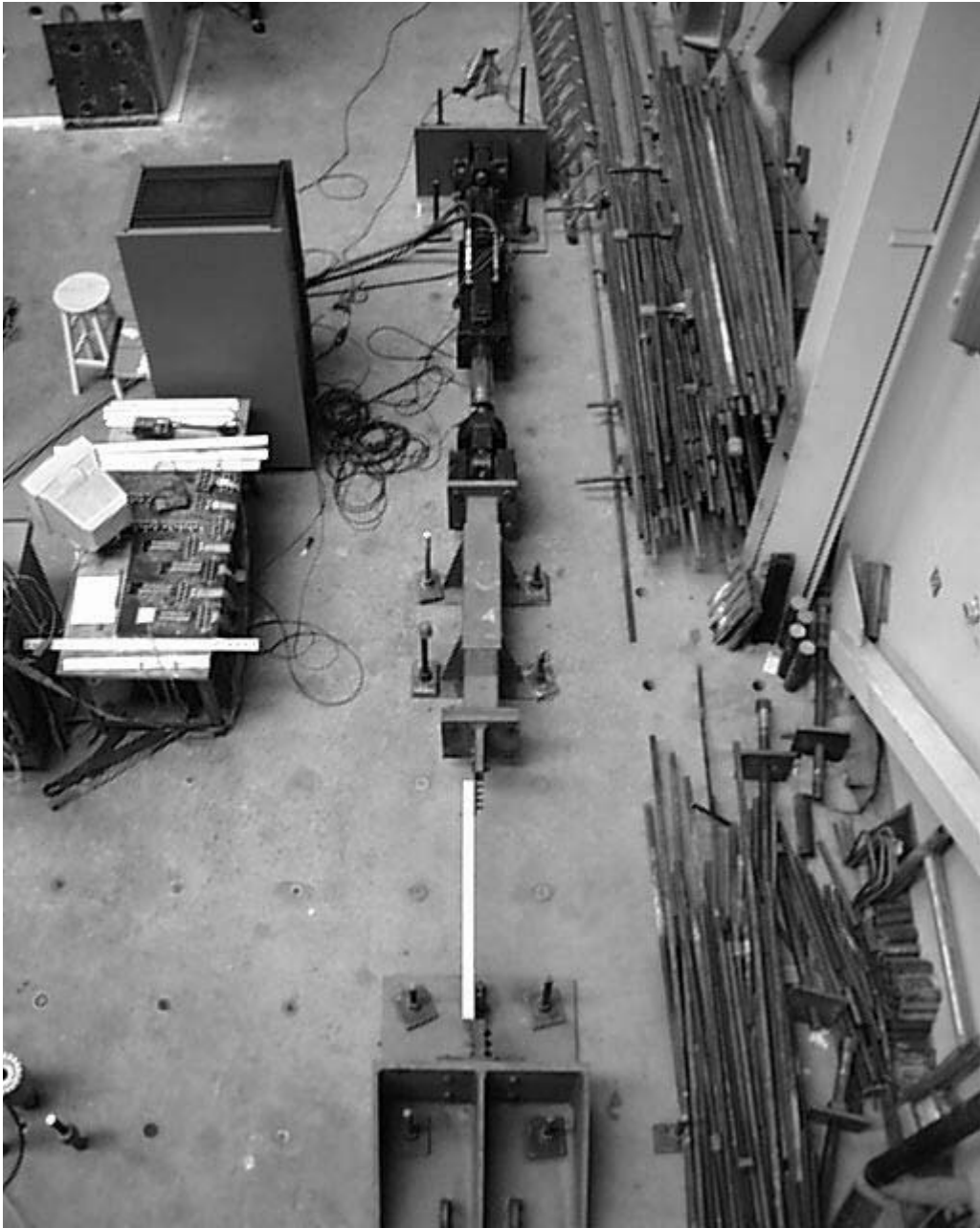


FIGURE 3-5 Experimental setup for axial loading of single angle specimens

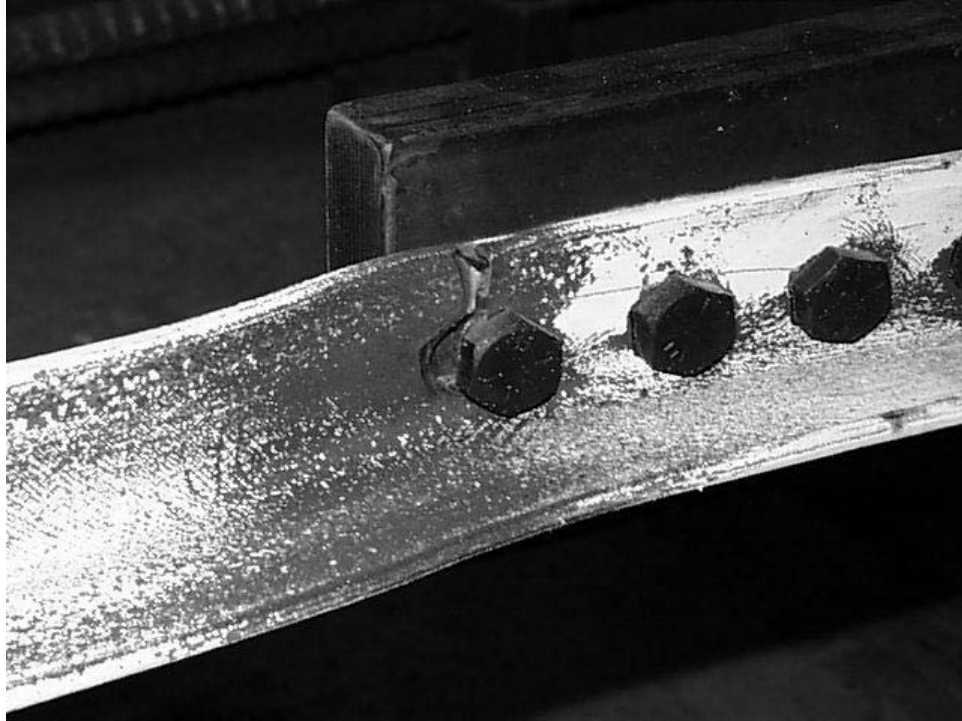


FIGURE 3-6 Failure of single angle with unreinforced bolted connection



FIGURE 3-7 Failure of single angle with reinforced bolted connection



FIGURE 3-8 Failure of single angle with welded connection

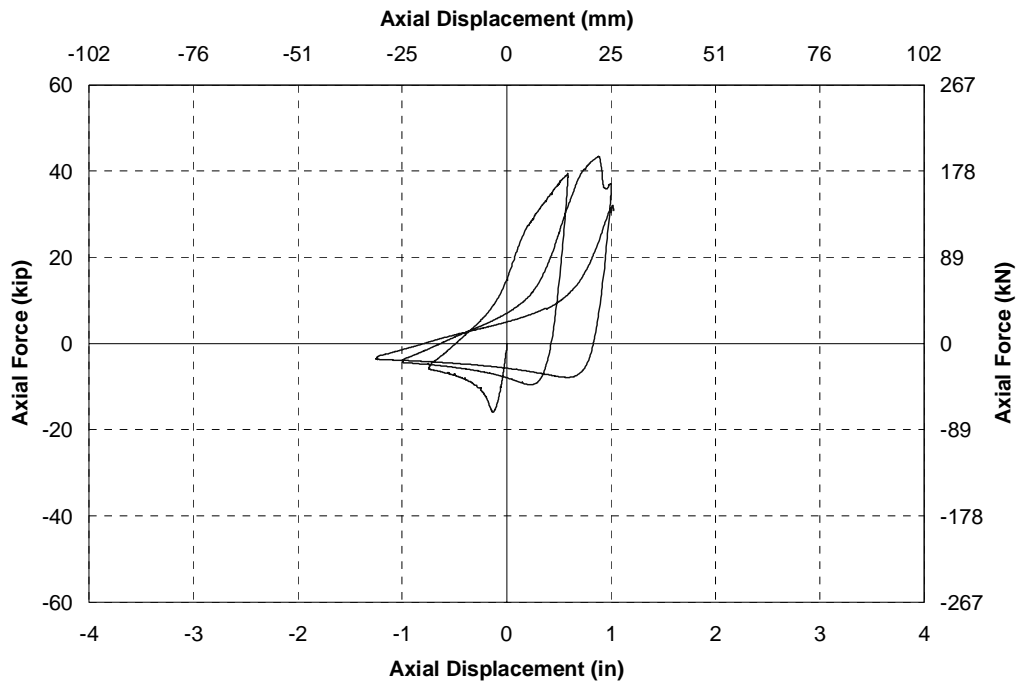


FIGURE 3-9 Hysteresis loop of single angle specimen A

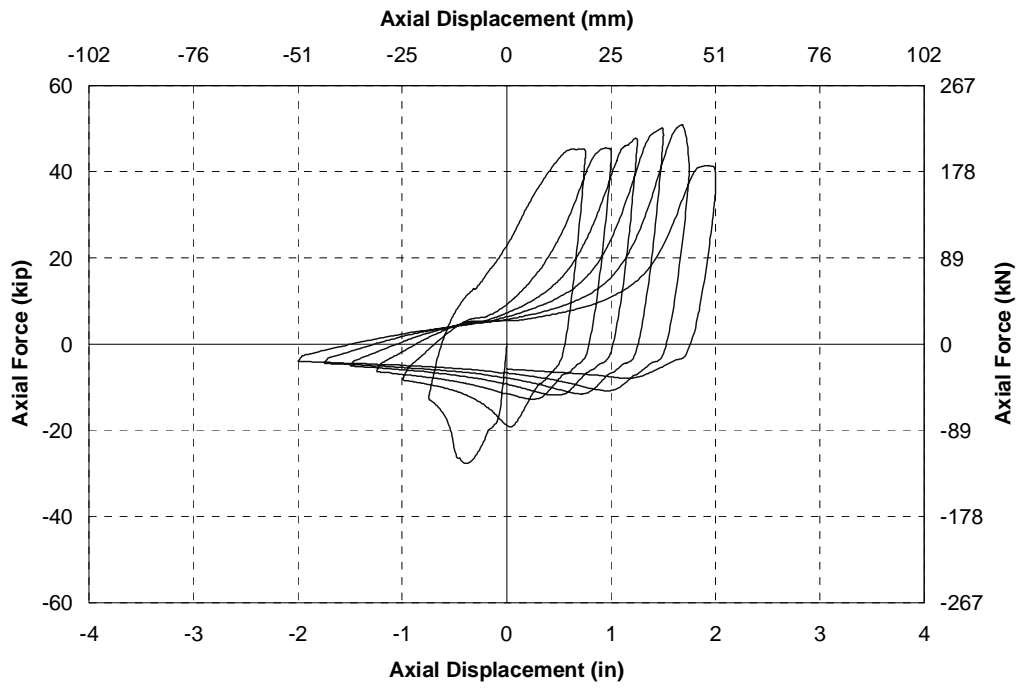


FIGURE 3-10 Hysteresis loop of single angle specimen B

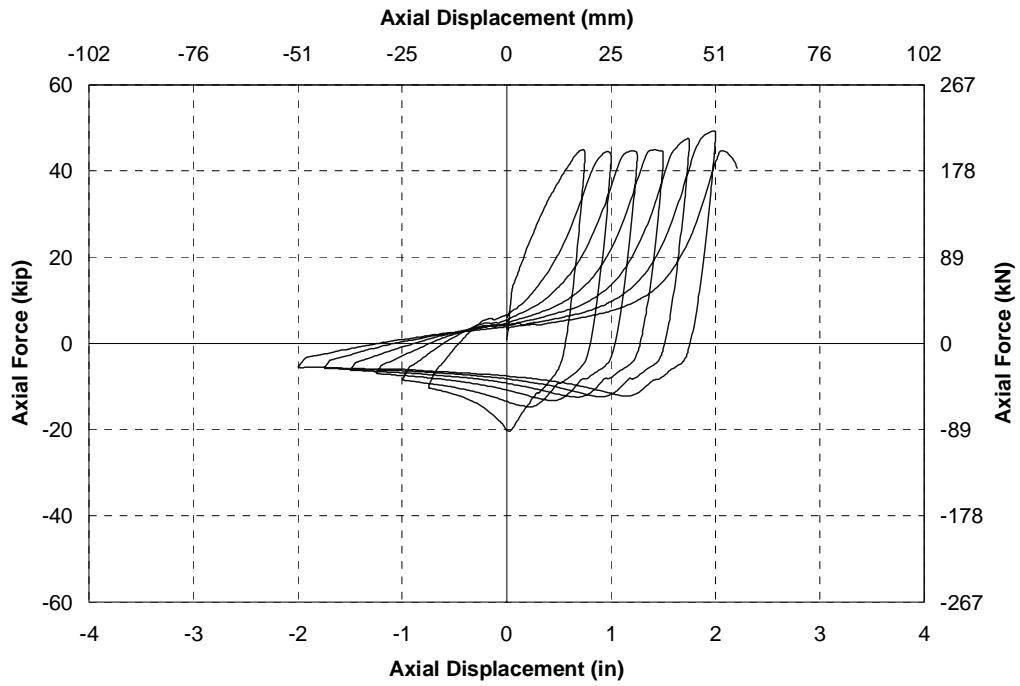


FIGURE 3-11 Hysteresis loop of single angle specimen C

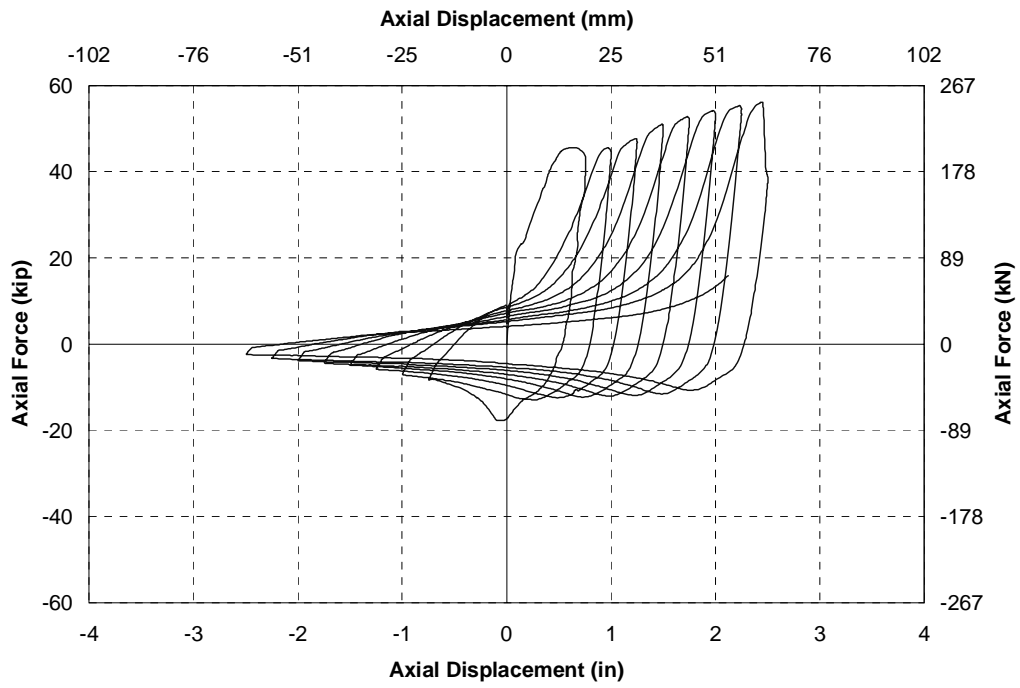


FIGURE 3-12 Hysteresis loop of single angle specimen D

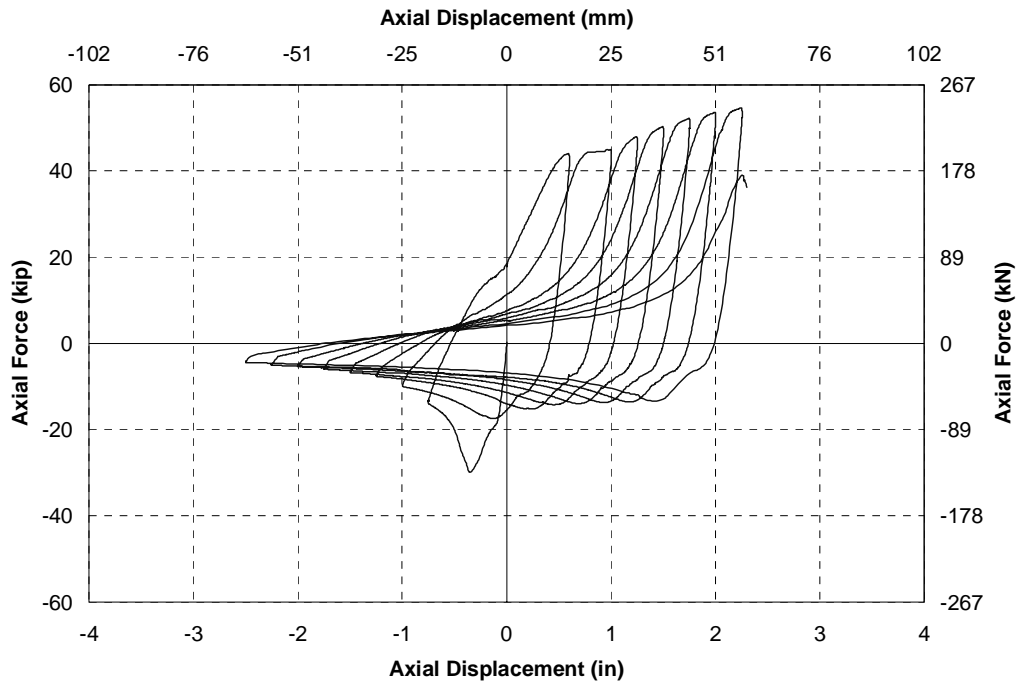


FIGURE 3-13 Hysteresis loop of single angle specimen E

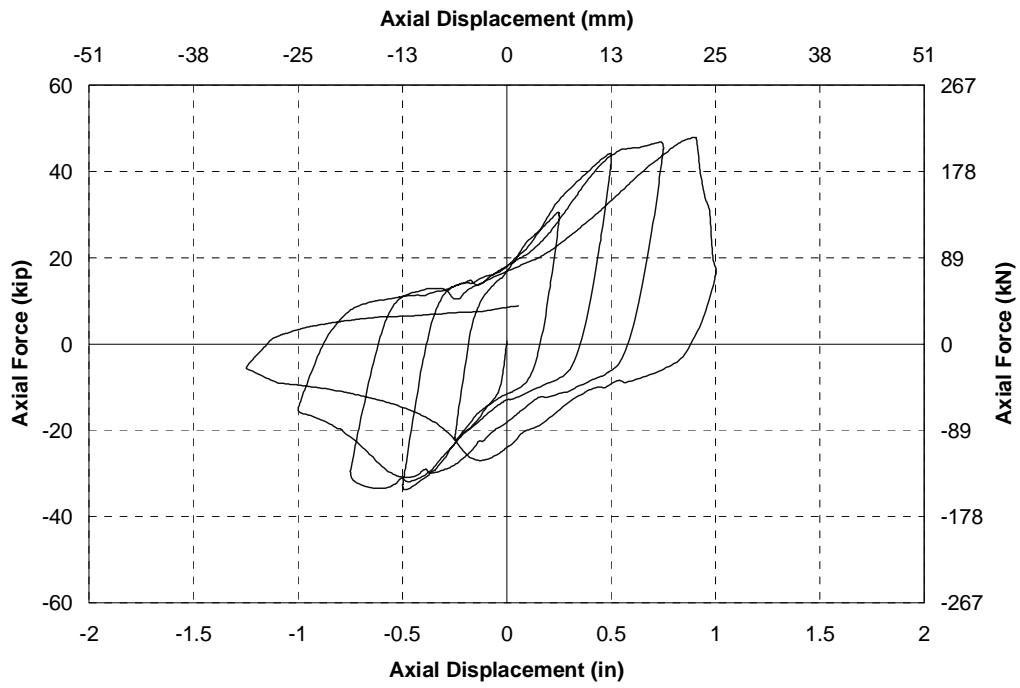


FIGURE 3-14 Hysteresis loop of single angle specimen F

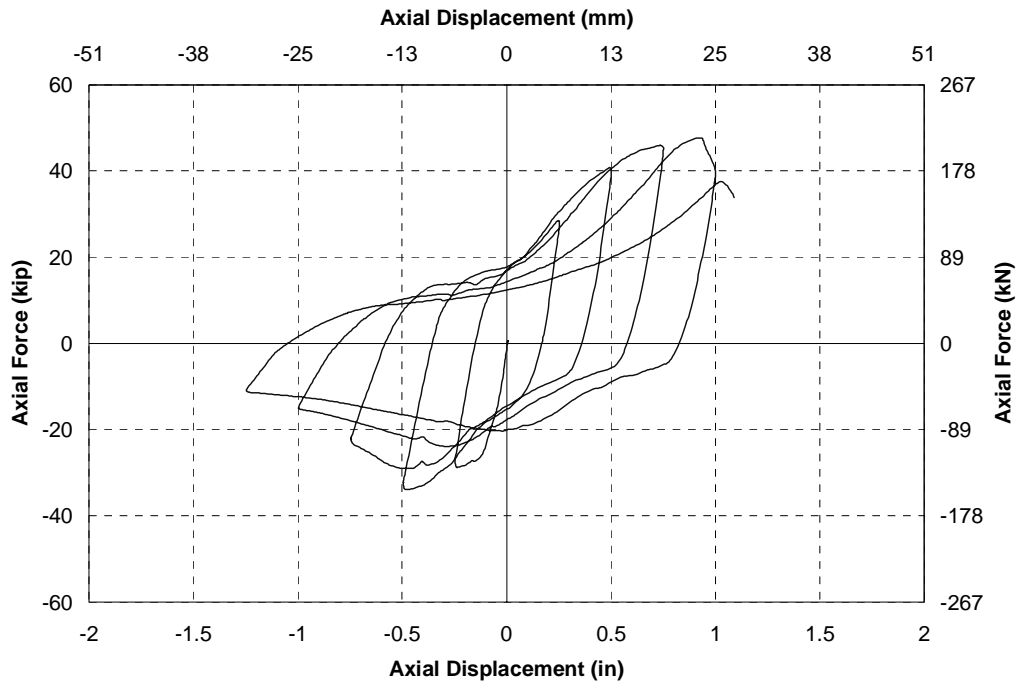


FIGURE 3-15 Hysteresis loop of single angle specimen G

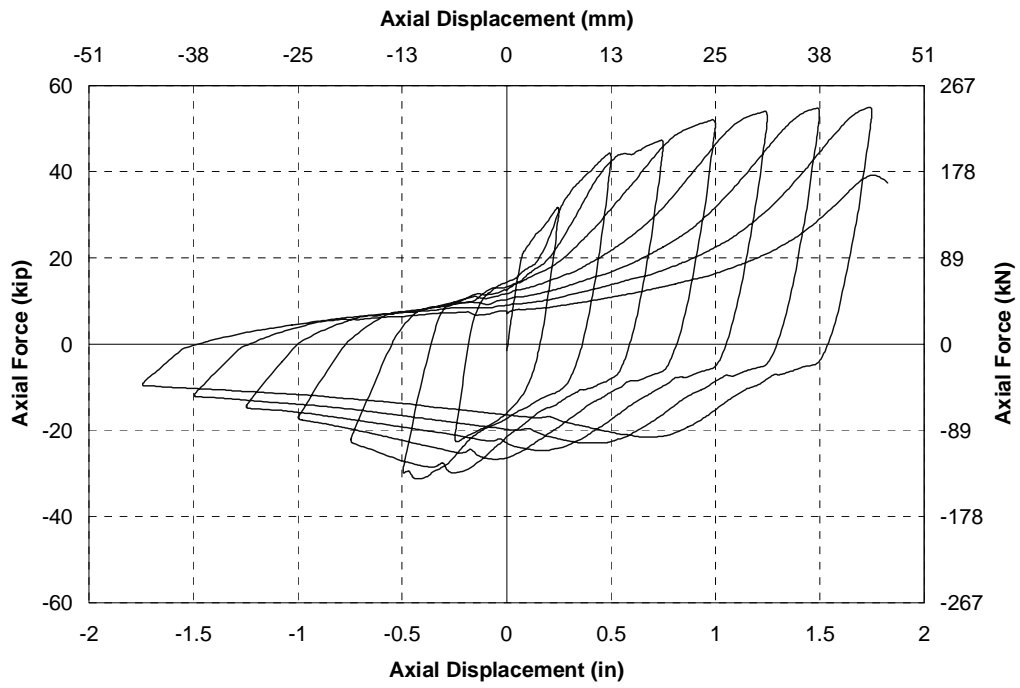


FIGURE 3-16 Hysteresis loop of single angle specimen H

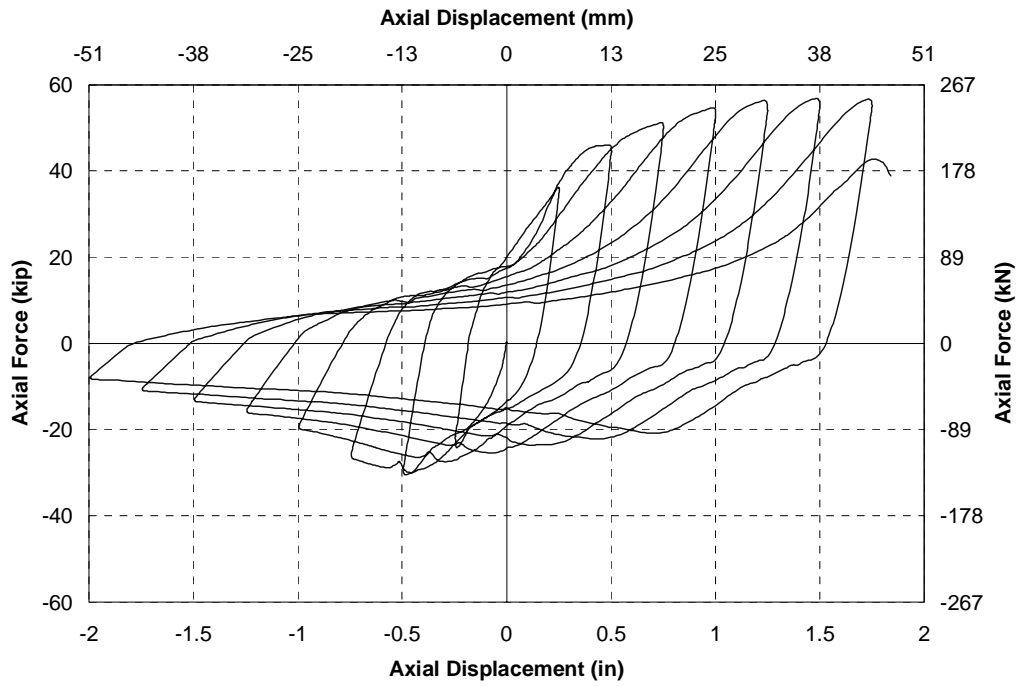


FIGURE 3-17 Hysteresis loop of single angle specimen I

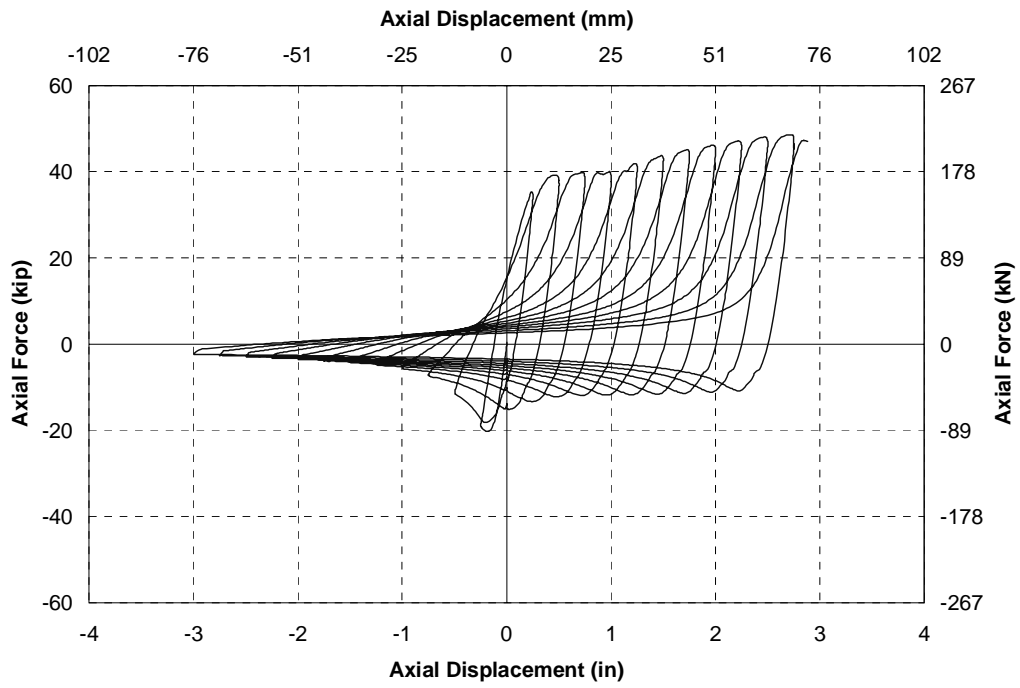


FIGURE 3-18 Hysteresis loop of single angle specimen J

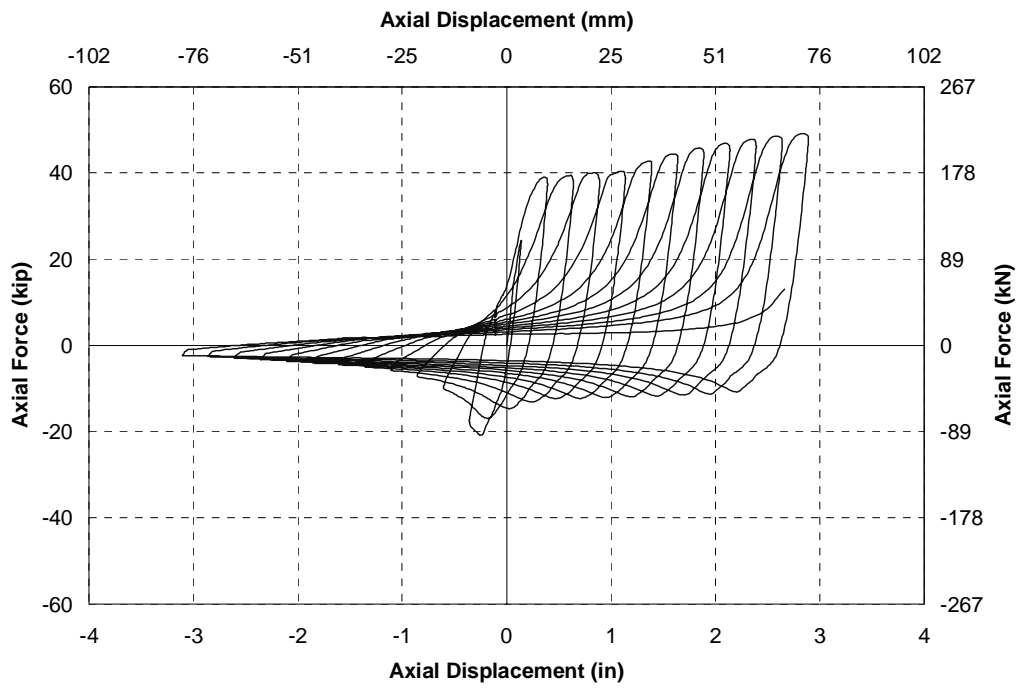


FIGURE 3-19 Hysteresis loop of single angle specimen K

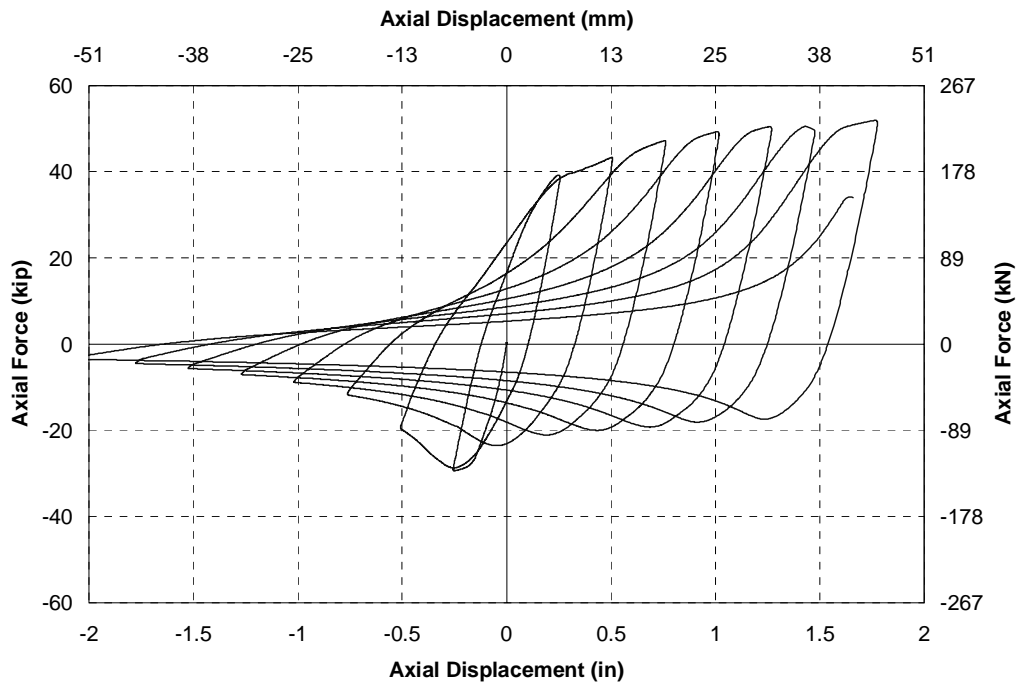


FIGURE 3-20 Hysteresis loop of single angle specimen L

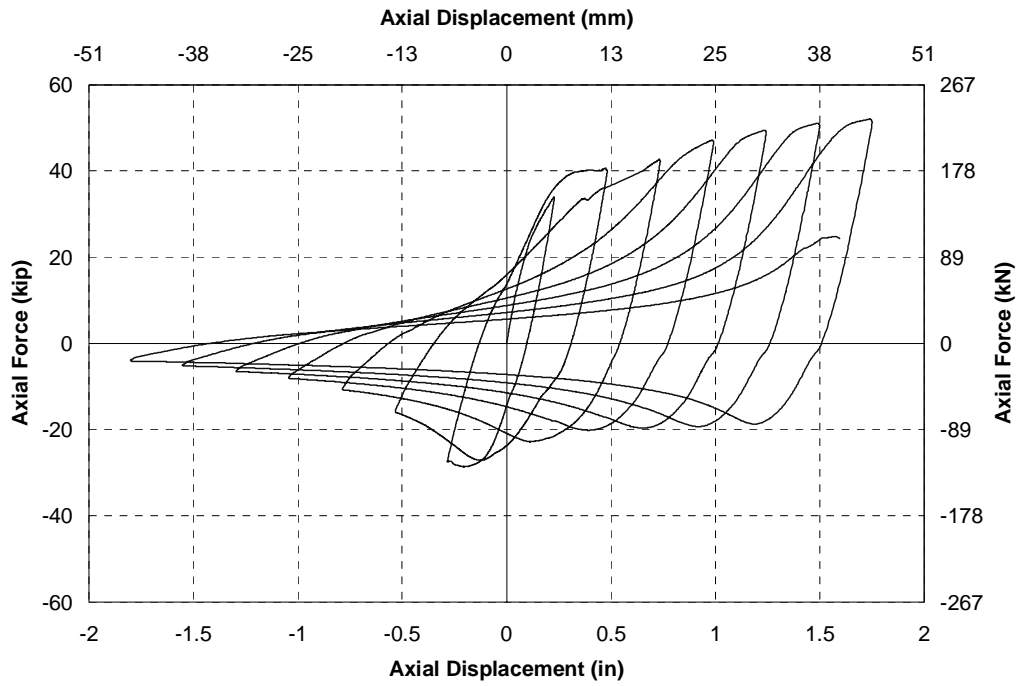


FIGURE 3-21 Hysteresis loop of single angle specimen M

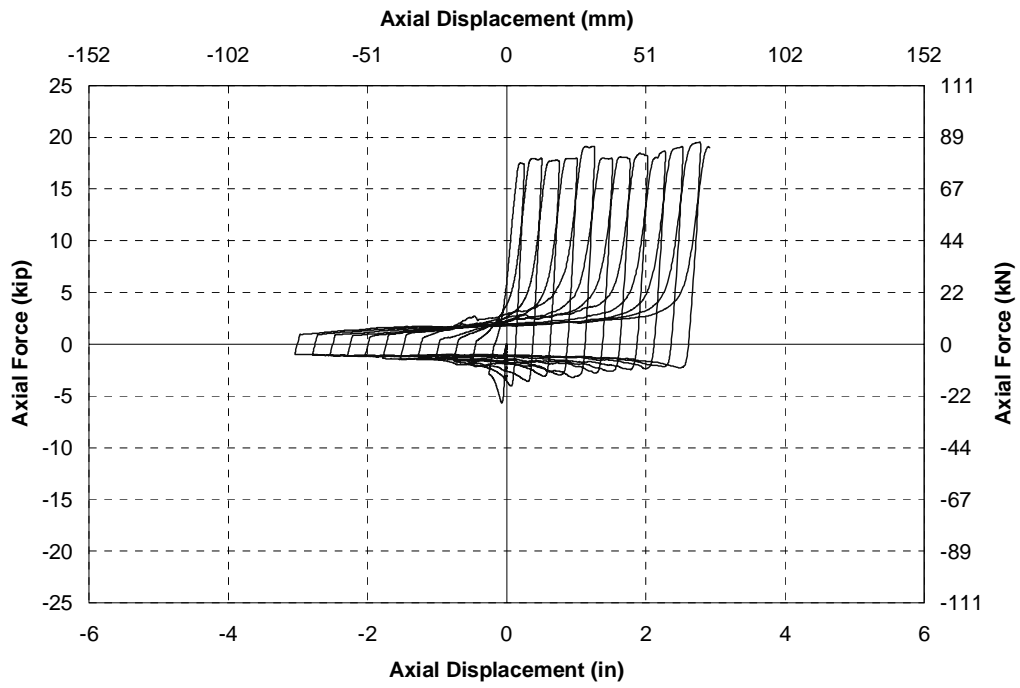


FIGURE 3-22 Hysteresis loop of single angle specimen N

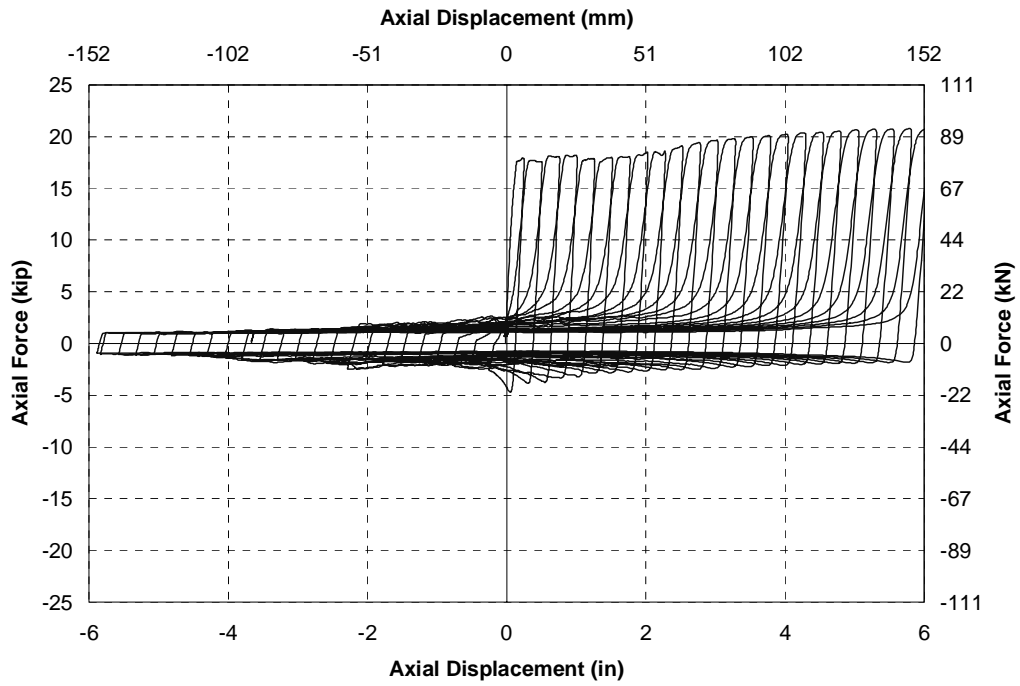


FIGURE 3-23 Hysteresis loop of single angle specimen O

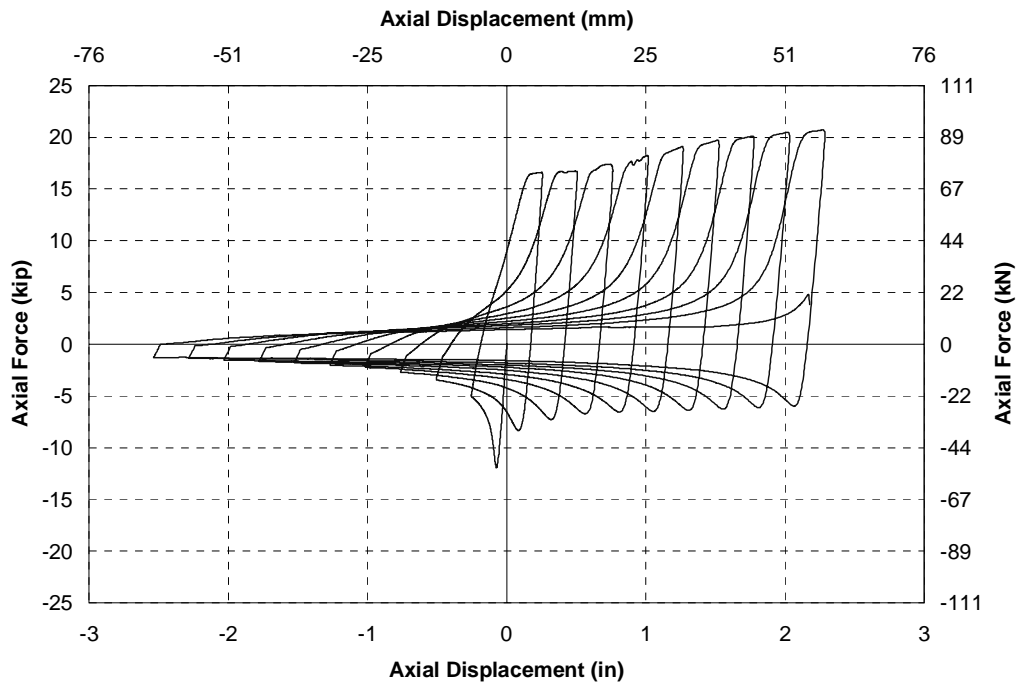


FIGURE 3-24 Hysteresis loop of single angle specimen P

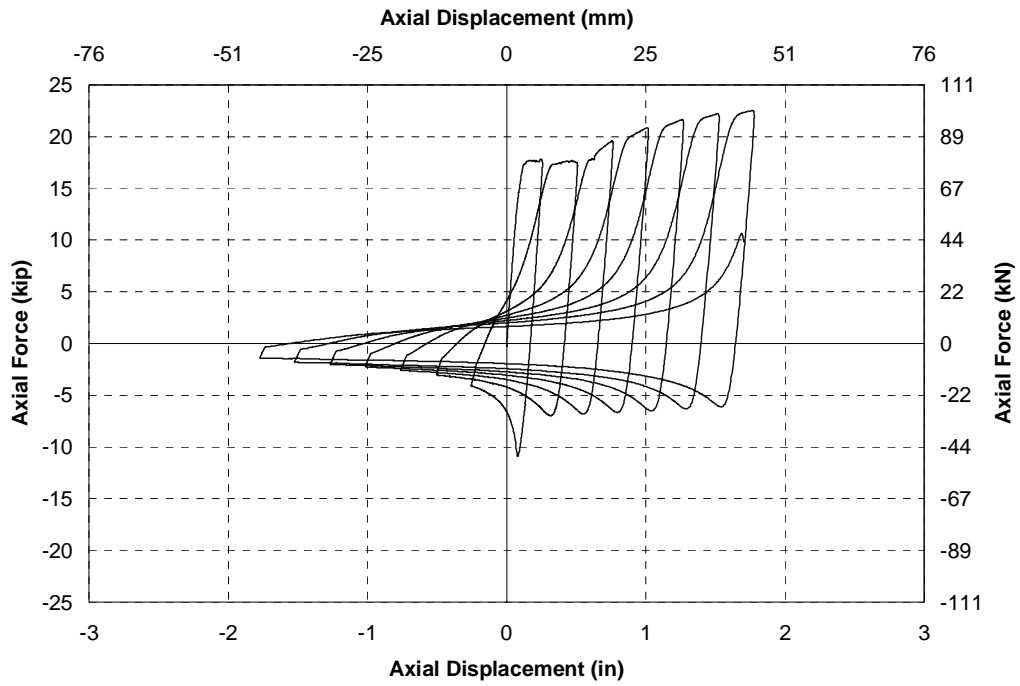


FIGURE 3-25 Hysteresis loop of single angle specimen Q

TABLE 3-3 Measured and calculated tensile forces in the single angle specimens

Spec.	Measured Yield Force (kN)	Measured Ultimate Force (kN)	Design Yield Force (kN)	Nominal Yield Force (kN)	Yield Force - Coupons (kN)	Expected Yield Force (kN)
A	1	193	124	130	202	195
B	200	226	124	130	202	195
C	198	219	124	130	202	195
D	199	249	124	130	202	195
E	195	243	124	130	202	195
F	201	213	124	130	202	195
G	201	212	124	130	202	195
H	200	244	124	130	202	195
I	199	253	124	130	202	195
J	171	216	124	130	166	195
K	172	219	124	130	166	195
L	178	231	124	130	166	195
M	179	231	124	130	166	195
N	73	83	52	54	74	82
O	77	92	52	54	74	82
P	74	92	52	54	74	82
Q	78	100	52	54	74	82

Notes: 1. Yield force not clearly identified.

In order to compare the measured yield and ultimate forces with predicted values the design and nominal yield forces, force based on the strength from coupon tests, and the expected yield force, were each calculated. These quantities were generally based on AASHTO (1998). The nominal tensile strength is given by:

$$P_{nt} = F_y A_g \quad \dots 3.1$$

where: P_{ny} is the nominal yield force; F_y is the minimum specified yield stress of the material, and; A_g is the gross area of the section. The design yield force was calculated by multiplying the quantity in Equation 3.1 by the strength reduction factor of 0.95 (AASHTO, 1998). The coupon yield force was calculated by using the actual yield strength of the material from the coupon tests instead of the minimum specified strength in Equation 3.1. The expected force, P_{ye} , was calculated by multiplying the nominal force by an R_y factor of 1.5 as specified in the AISC Seismic Provisions (2002) for A36 steel.

Each of these predicted values are given in Table 3-3. This table shows that the coupon and expected yield strengths were very similar and that they were both typically within 5% of the measured yield strength. Therefore the expected yield force gave a good estimate of the yield strength for these members. In the worst case, the expected strength was 14% larger than the

measured strength. In all cases the strength of the members was above their minimum specified values

The ultimate force is defined as the maximum force measured in each specimen. For each member the ultimate strength was on average 21% larger than their measured yield strength, with the maximum difference being 28% (Table 3-3).

3.2.2.5 Buckling Capacity

The buckling capacity of each specimen is listed in Table 3-4. The buckling capacity was dependent on the material and cross sectional properties of the members as well as the effective length of the members. It was also shown to be dependent on the loading history as members subjected to prior tensile yielding had a reduced buckling capacity. The buckling capacity was predicted using AASHTO (1998) where:

$$\lambda = \left(\frac{KI}{r\pi} \right)^2 \frac{F_y}{E} \quad \dots 3.2$$

and for the slenderness parameter, $\lambda < 2.25$:

$$P_{nc} = 0.66^\lambda F_y A_g \quad \dots 3.3$$

By comparing the measured buckling force with a calculated force, the effective length factor for each member was calculated based on the material properties from the coupon tests, the appropriate cross sectional properties and the length between the centre of the connections, as given in Table 3-4. This table shows a wide variation in the effective length factors. This is, in part, due to the variability in the specimens, out-of-straightness of members and other factors. It is also due to the flexural stiffness of the gusset plate connections relative to the flexural stiffness of the members. Specimen A with the 13 mm gusset plates had a high member stiffness relative to the gusset stiffness and resulted in an effective length close to 1.0, effectively pinned ends. At the other extreme, Specimen N was a long, lightweight angle attached to a 1 in. thick gusset plate providing effectively full fixity to the ends that resulted in an effective length factor of 0.5.

In the past attempts have been made to quantify the effective length factor based on the relative stiffness of gusset plate components (El-Tayem, 1986; Astaneh-Asl, 1982). El-Tayem suggested an effective length factor of 0.85, with the length defined by the full length of the angles, is appropriate for typical single angle X-brace members with simple gusset plate connections. In the aforementioned study the plastic hinges at the ends of the members, formed during buckling, occurred in the gusset plates. However when the diagonals of typical X-braces were connected in such a way that the plastic hinges form in the angles rather than the gusset plates then the effective length is decreased. This occurs when the diagonals are connected to gusset plates along with a top or bottom chord in the cross frames, and consequently the top and bottom chords prevent plastic hinges from forming in the gusset plates. Similarly, when the diagonals are connected directly to a web-stiffener, the connection of the stiffener to the flange and the web provides a comparatively rigid connection and the plastic hinge was again expected in the angle rather than in the stiffener. Different effective length factors should be considered depending on whether the

TABLE 3-4 Measured Buckling Force and Calculated Effective Length Factor for Single Angle Specimens

Spec.	Measured Buckling Force (kip)	Effective Length Factor, K	Calculated Buckling Force, K = 0.70 (kip)
A	71	0.95	64
B	123	0.68	115
C	91	1	115
D	79	1	115
E	133	0.60	115
F	150	1	170
G	151	1	170
H	139	1	170
I	136	1	170
J	90	0.80	104
K	93	0.79	104
L	127	0.96	143
M	128	1	143
N	28	0.50	12
O	20	1	12
P	53	0.52	41
Q	48	1	41

Notes: 1. Experiments with tension yielding prior to buckling which affects calculation of reliable K value

plastic hinge is expected to form in the gusset plate or in the angles. When it is apparent that the plastic hinge due to buckling will occur in the gusset plate, an effective length factor of 1.0 is appropriate when the length is defined between the center of the connections. Alternatively, when the gusset plates are restrained from bending out-of-plane, or there are no gusset plates and the plastic hinges are expected in the angles, then an effective length factor of 0.7 can be shown to be more suitable.

For the single angle experiments an effective length factor of 0.7 was assumed for all but the first specimen, which had an assumed effective length of 1.0. The resulting calculated buckling capacity is given in Table 3-4. For specimens not affected by prior tension yielding, the measured buckling strengths were within approximately 20% of the calculated strengths. As the buckling force was a relatively small part of the overall strength of the system a 20% error in buckling force correlated to typically a 5% to 10% error in the overall X-brace strength. Prior tensile loading typically reduced the buckling capacity of the members by up to 25%, therefore this would contribute to a similar change in the strength of cross frames by 5% to 10%. Specimen N was the one member, first subjected to compression, that had a measured strength which differed from the calculated strength by more than 20%. This was also one of the most slender members with a Kl/r ratio of 129. All other members have a Kl/r ratio of less than 120. For members that are slender, the buckling capacity is more sensitive to the effective length factor, however, for non-slender

members the capacity is relatively insensitive. Therefore, it is recommended that these members should be treated as primary members for seismic loading in which case AASHTO limits the Kl/r ratio to less than 120. This will prohibit slender members such as specimen N from being used. The b/t ratios defined by AISC Seismic Provisions (2002) for special concentric braced frames should also be satisfied to prevent local buckling.

TABLE 3-5 Ultimate Axial Strain and Cumulative Plastic Strains in Single Angle Specimens

Spec.	Failure Mode	Measured Ultimate Axial Strain (%)	Theoretical Yield Displacement (mm)	Cumulative Eff. Plastic Strain (%)	Cumulative Plastic Ductility
A	At bolt hole	3.1%	1.92	23%	124
B	At bolt hole	4.9%	1.92	77%	412
C	At bolt hole	5.4%	1.92	82%	442
D	At end plastic hinge	6.2%	1.92	127%	685
E	At end plastic hinge	6.2%	1.92	115%	620
F	At bolt hole	5.6%	1.06	52%	281
G	At bolt hole	5.6%	1.06	57%	305
H	At end plastic hinge	8.1%	1.06	127%	682
I	At end plastic hinge	8.9%	1.06	144%	775
J	At midspan plastic hinge	7.4%	1.92	176%	946
K	At midspan plastic hinge	7.7%	1.92	190%	1021
L	At end plastic hinge	9.1%	1.06	146%	783
M	At end plastic hinge	8.0%	1.06	128%	688
N	At end plastic hinge	6.0%	2.38	142%	761
O	At midspan plastic hinge	12.2%	2.38	596%	3199
P	At end plastic hinge	10.1%	1.19	201%	1081
Q	At midspan plastic hinge	7.1%	1.19	113%	609

3.2.2.6 Ultimate Displacement Capacity

The ultimate average axial strain is used to describe the ultimate displacement of each specimen. This is independent of the yield displacement which was shown to be difficult to determine. The ultimate strain can be converted to an ultimate drift in X-brace assemblies.

Table 3-5 gives the maximum average axial strain for each specimen, calculated from the maximum measured displacement divided by the length between the centroid of the connection regions at the two ends of the specimen. The values ranged from 3% to 12%, indicating a large variation in the displacement capacity of the members. Even between theoretically identical members there was up to a 100% difference in their ultimate strains. While there was much variability, distinct factors had an effect on the ultimate displacement capacity. An increased A_n/A_g correlated to an increase in the ultimate displacement due to prevention of premature failure around the bolt holes. For the welded members and reinforced bolted members the minimum ultimate strain was 6%, while for all unreinforced bolted members it was below 6%. There was

also a correlation between Kl/r and the ultimate strain, with a larger slenderness ratio resulting in reduced ultimate displacements. This was most noticeable when comparing Specimens A and B where the sole difference was in the thickness of the gusset plate which modified the effective length. Specimen A had the lowest ultimate strain at 3.1% which was attributed to both the longest effective length and lowest A_n/A_g ratio.

The cumulative plastic displacement of each member was calculated in terms of cumulative plastic strain (CPS) and cumulative plastic ductility (CPD), a measure defined in the Draft Provisions for Design of Buckling Restrained Braces (SEAONC, 2003). CPS is defined as the absolute sum of the average plastic axial strains in excess of the yield strain for each cycle of deformation in the braces. CPD is defined as the absolute sum of the axial displacements in excess of the yield displacement divided by the yield displacement for each cycle of deformation in the braces. These measures are therefore very similar, with CPS preferred in this study as it is consistent with the ultimate displacement capacity of the members described in terms of strains. However, CPD is given for comparison to past research. In order to define the CPS or CPD the yield displacement had to be determined. As the yield displacement was sensitive to factors such as slippage and prior loading history, it was not possible to obtain a consistent measured yield displacement for the single angle specimens. For the welded members where no slippage was observed, the observed yield displacement was close to the theoretical expected yield displacement. Hence the yield ductility was defined in terms of the theoretical expected yield displacement, Δ_{ye} , which is given by:

$$\Delta_{ye} = \frac{F_{ye}l}{E} \quad \dots 3.4$$

Using the theoretical yield displacement allowed the plastic strains and ductilities to be defined in terms of a computable value. Where slippage occurred it was counted as additional ductility.

The CPS and CPD for each specimen are given in Table 3-5. Because of the increasing amplitude loading history there was a correlation between the maximum strains and the cumulative plastic ductility capacity of the specimens. All the welded members and reinforced bolted members had cumulative plastic ductilities in excess of 600 while the other members had values less than 450. Specimen O had an unusually high cumulative plastic ductility of 3200. This was unusual as it was theoretically identical to Specimen N, indicating the inherent variability in the cumulative displacement capacity. The average cumulative strain for welded and reinforced bolted specimens, neglecting Specimen O was 786%.

From this data it is proposed that these members should be designed for a maximum average axial design strain, calculated from the axial displacement divided by the length of the member, of 4%. This allows for a factor of safety of at least 1.5 for all members with connections which failed outside their connection regions. In practice this may require some reinforcement of the connected leg which is recommended to increase the A_n/A_g ratio to greater than 1.0 for these members. The 4% design value was exceeded even by the members with poor connection detailing, except specimen A. For 36 ksi steel this corresponds to a theoretical axial ductility of 32, and for 350 MPa steel an axial ductility of 23. Therefore these correspond to greater ductilities than traditionally employed but are justified with good estimates of the expected displacement response during design. For a system designed for a 4% maximum axial strain, when subjected to the

number of cycles observed in a typical earthquake, the expected cumulative plastic strain demand is less than the cumulative displacement capacity of the members as shown in Section 6.

3.2.2.7 Energy Dissipation in the Single Angles

The area enclosed by the hysteresis loop was calculated using a simple algorithm for each specimen. For each cycle the area enclosed by the hysteresis loop was divided by the rectangular area enclosed by the maximum force and displacement, as illustrated in Figure 3-26, to give the hysteretic area as a ratio of that for an “ideal” system. The energy dissipated per cycle is plotted against maximum axial strain amplitude for each specimen as shown in Figures 3-27 to 3-30. These figures show that the early cycles have hysteretic energy dissipation of typically around 40% of the “ideal” hysteretic area, while for subsequent cycles the equivalent energy dissipation reduced to typically 20% prior to failure.

The reduction in energy dissipation can be explained by considering the two primary sources of hysteretic behavior. The first is tensile plastic deformations with increasing amplitude positive displacements. This deformation is largely irrecoverable and essentially only contributes to the hysteretic behavior when a positive displacement amplitude exceeds previous amplitudes. This effect resulted in pinched hysteresis loops, and consequently, energy dissipation decreased with repeated cycles. This property results in the amount of energy dissipation for a given cycle being dependent on the loading history. For loading with large amplitude cycles at the beginning of the history the amount of energy dissipation at the maximum cycle is likely to be larger than for increasing amplitude reversed static loading histories. The second source of hysteretic energy dissipation in these types of members is plastic hinging caused by buckling of the members. The axial force resisted by plastic hinges is dependent on the displacement in the specimen, degrading as displacements increase in compression.

Comparing figures 3-27 to 3-30 shows that the members with larger slenderness (Kl/r) ratios have a larger reduction in energy dissipation than those with smaller values. This was expected as the displacement increments were constant for all specimens regardless of length, meaning that the shorter specimens had a larger increment in average axial strain than the larger specimens. This resulted in comparatively larger tensile plastic deformations per cycle and resulted in a greater relative hysteretic area than for the specimens with larger slenderness ratios, further justifying the proposed slenderness limit.

3.2.3 Analytical Model of Single Angle Members

To compare the single angle X-braces with other ductile systems an analytical model of the single angle components was developed. The special X-braces used in the bridge model had properties equivalent to single angle specimens P and Q. Therefore a model of these specimens was developed, using the kinematic NLLink elements of SAP2000 v8.30 (Computers and Structures, 2003), and was designed to capture the tension force envelope, compression force envelope, appropriate hysteretic energy per cycle and ability to model loading history dependent properties.

A model was developed using two NLLink elements in parallel. The first element captured the compression envelope, which was based directly on the envelope for specimen P (subjected to compression on the first cycle). The maximum buckling force was 53 kN. The first element had assumed elasto-plastic tension properties with a yield force equal to 10 kN. This constant tension

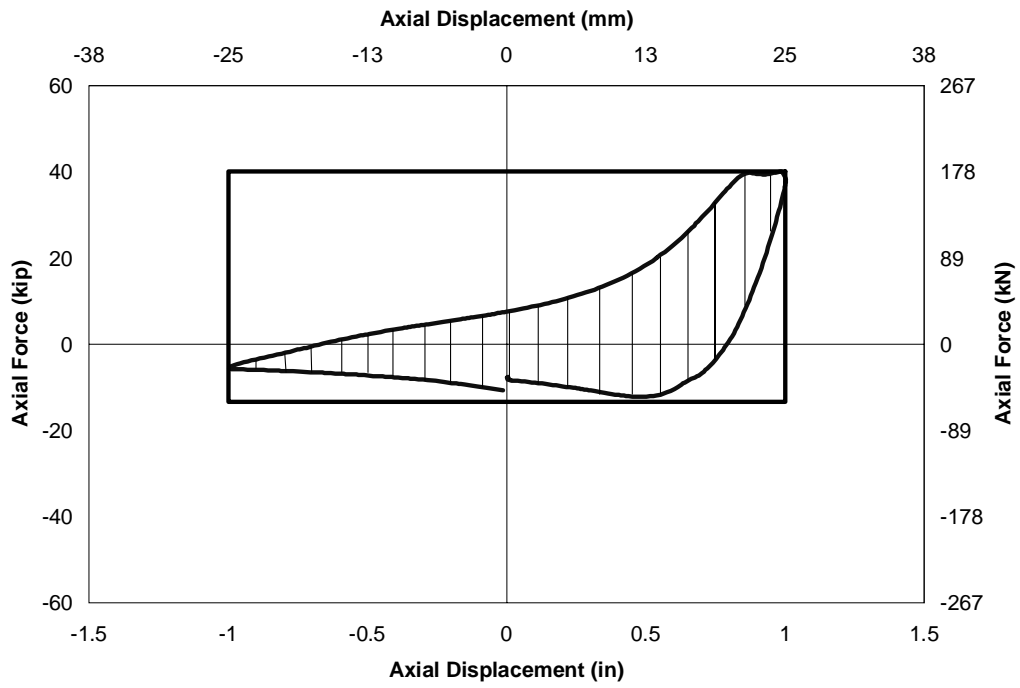


FIGURE 3-26 Illustration of ratio of enclosed hysteretic area to rectangular area bounded by maximum force and displacement for given cycle of loading

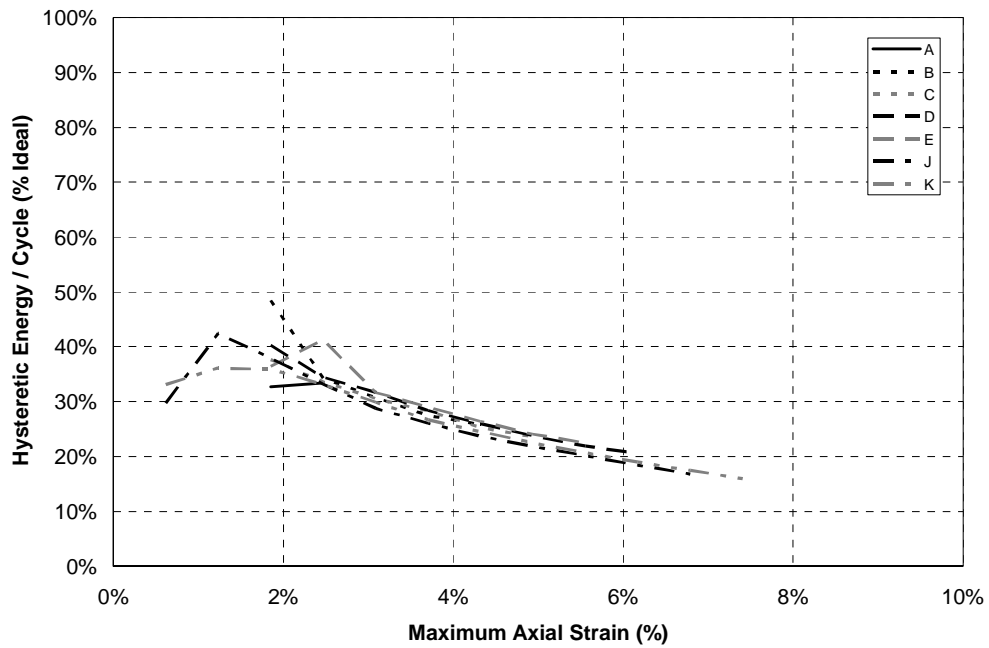


FIGURE 3-27 Energy dissipated per cycle for long, heavy single angle specimens

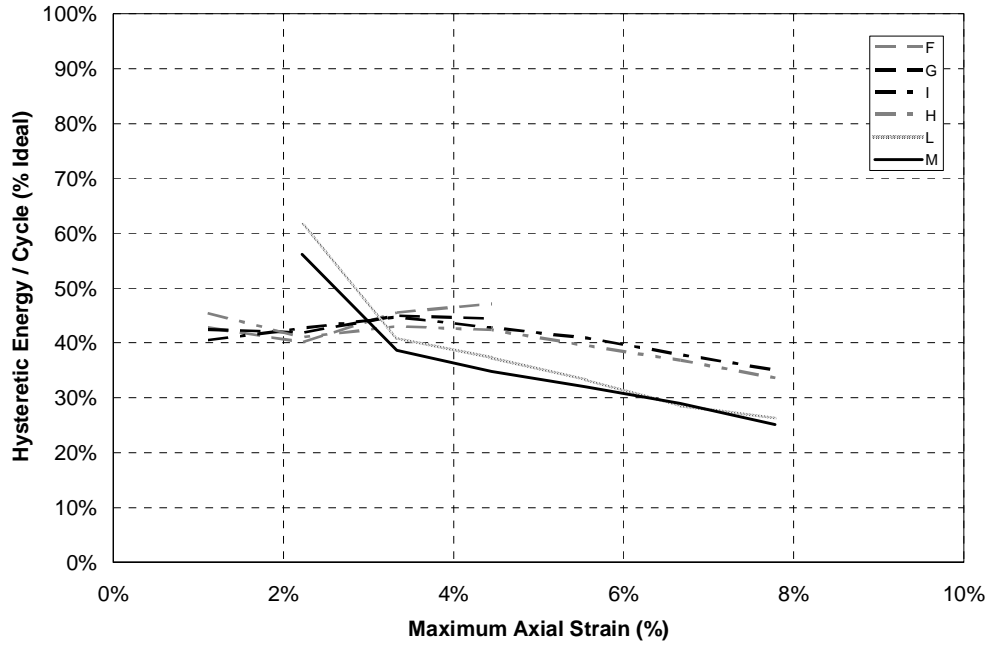


FIGURE 3-28 Energy dissipated per cycle for short, heavy single angle specimens

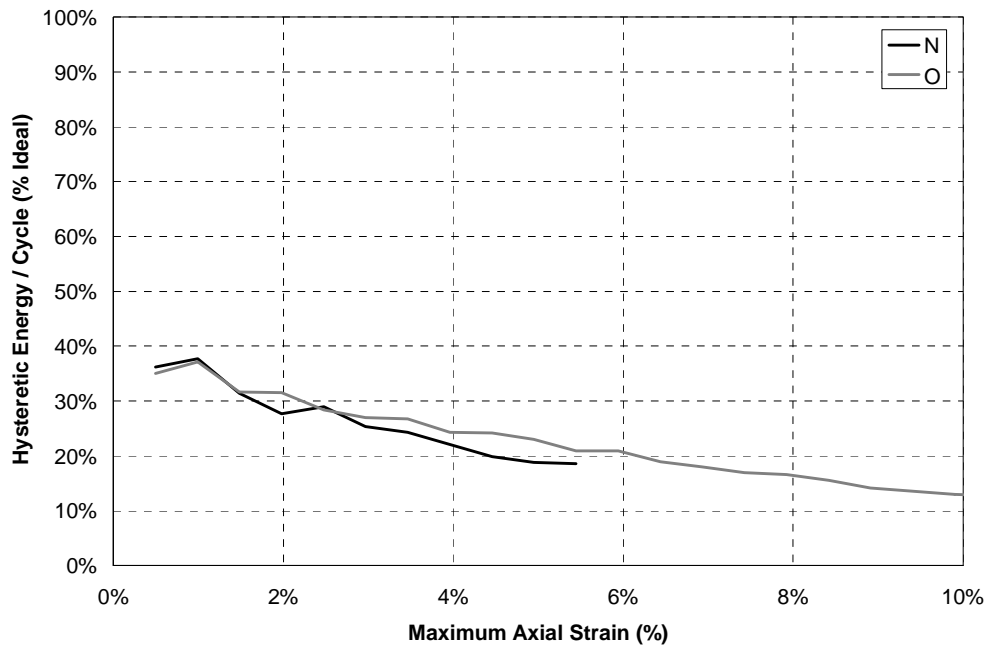


FIGURE 3-29 Energy dissipated per cycle for long, light single angle specimens

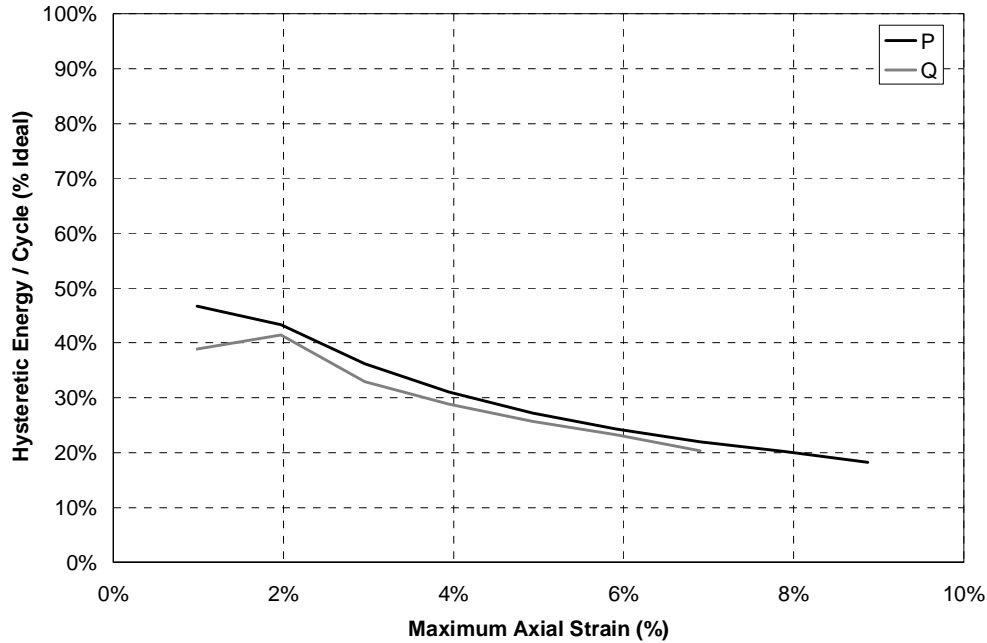


FIGURE 3-30 Energy dissipated per cycle for short, light single angle specimens

force was to allow for the residual force in the member as it straightens after a compression buckling excursion due to plastic hinging in the member. In reality this is not a constant force and is dependent on the out-of-plane displacement of the buckled member, however, a constant value of 10 kN resulted in an approximately equivalent hysteretic area. The second NLLink element captured the remaining tension properties allowing for pinching due to elongation of the member using the kinematic model. This acted so that the plastic tensile properties were activated once the tensile displacement exceeded that from previous cycles. This model assumed elasto-plastic behavior with a yield force determined by equating areas between the elasto-plastic model and average envelope between specimens P and Q. The overall yield force was equal to 85 kN which compared well to the expected values of 82 kN. The tension element was modeled assuming a nominally small elastic stiffness in compression.

Importing the loading histories into the analytical model from the experiments for specimens P and Q respectively, the hysteresis loops for the non-linear elements are shown in Figures 3-31 and 3-32. These figures show that the models fit the complex hysteretic shape of the single angles relatively well and the maximum tensile and compressive forces were captured. One area of inaccuracy in this model is at the start of a compression cycle. The model for the compression element assumes that the member will degrade in strength at an absolute compression displacement. Therefore any tensile deformation will be recovered assuming an elasto-plastic response until the compression displacement is reached at which degradation in strength starts to occur. This is noticeable after the first cycle in Figure 3-32. This inaccuracy could be overcome with the use of a hook element in series with the compression element, however the model becomes computationally much less efficient and it was not considered to result in significantly more accuracy.

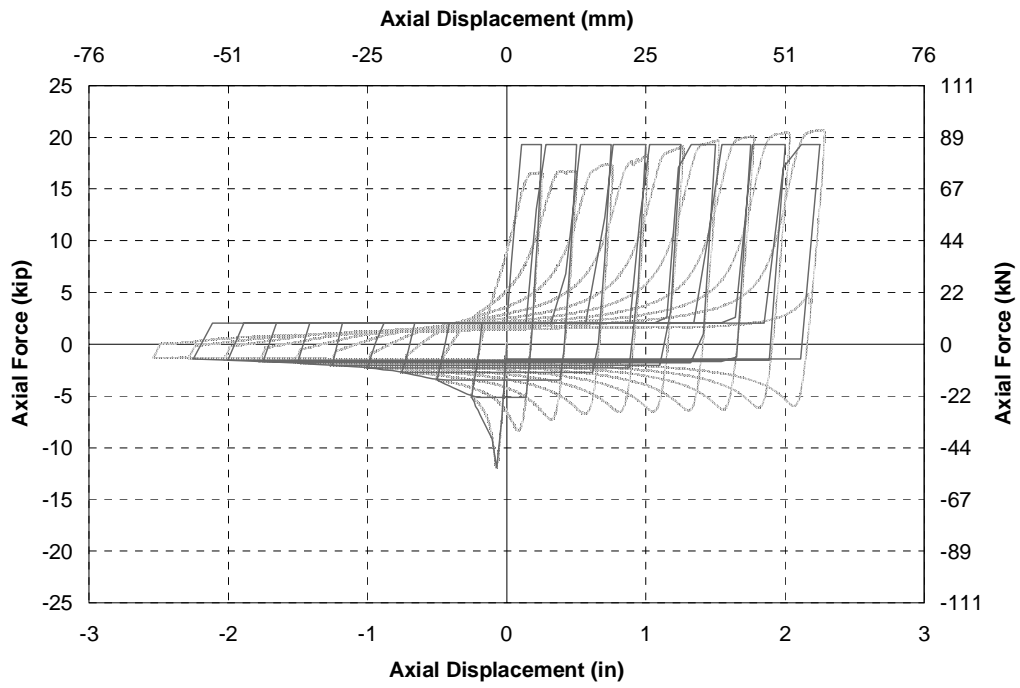


FIGURE 3-31 Hysteresis loops for single angle analytical model for loading history equivalent to loading history for single angle specimen P

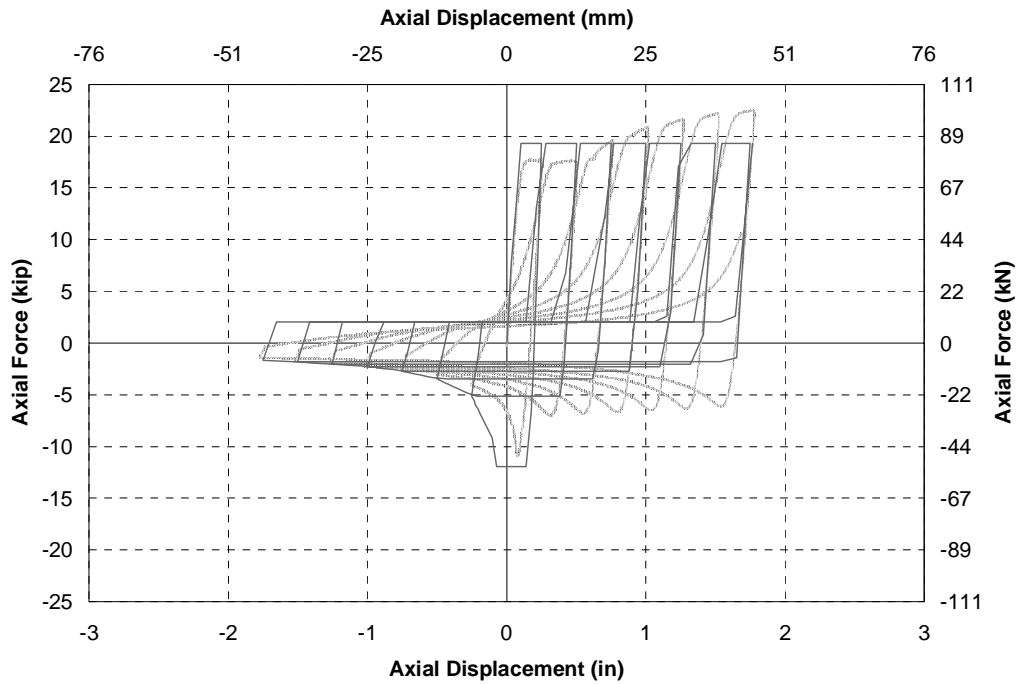


FIGURE 3-32 Hysteresis loops for single angle analytical model for loading history equivalent to loading history for single angle specimen Q

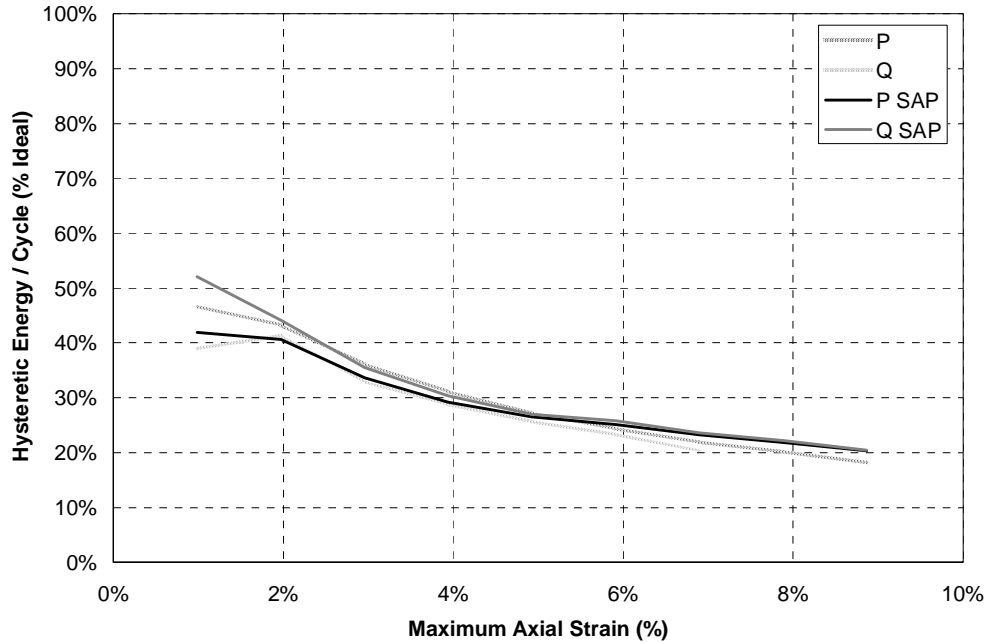


FIGURE 3-33 Energy dissipated per cycle for analytical models of Specimens P and Q

Figure 3-33 compares the energy dissipated per cycle between the analytical model and experimental results. Based on good correlations at the component level, the model was expected to result in good correlations between the measured and calculated hysteretic response for the ductile single angle X-braces the bridge model.

3.3 Unbonded Braces

3.3.1 Overview

Component experiments were performed on the buckling restrained braces, provided by Nippon Steel Corporation (unbonded braces) for experiments on the bridge model (Fig. 2-13). These were performed in order to characterize the properties of the braces and compare these to the design properties. Of seven available braces, four were used solely for component experiments, and the remaining three were used in bridge model experiments before being tested to failure using the component experiment assembly. Axial component experiments were performed to evaluate overall brace behavior, cumulative displacement capacity of the braces, effect of different loading histories and effect of dynamic loading.

3.3.2 Coupon Tests

Two coupon tests were performed on the LYP-225 steel used in the manufacturing of the unbonded braces, provided by Nippon Steel (2002). The resulting material properties for the two tests are given in Table 3-6. The yield strength was close to the nominal yield strength of 225 MPa. Unlike most US steels where the nominal strength is generally defined so that the majority

of specimens are stronger than the nominal strength, the nominal strength for the LYP-225 steel is defined in the middle of a relatively tight range (205 - 245 MPa) of acceptable yield strengths. Therefore the nominal strength of 225 MPa was taken as the expected strength for this material. The ultimate strength of the LYP-225 steel was around 35% higher than the yield strength, compared to 50% for the A36 steel from the single angle coupon tests., indicating that there was less strain hardening in the LYP-225 steel. The ultimate strain was much higher at around 65% for the LYP-225 steel compared to 30-35% for the A36 steel.

TABLE 3-6 Coupon Test Results for Unbonded Braces from LYP-225 Steel

Coupon Test #	Test 1	Test 2
Coupon Dimensions	N/A	N/A
Yield Stress (MPa)	223	235
Ultimate Stress (MPa)	302	302
Ultimate Elongation (%)	64	65
Modulus of Elasticity (GPa)	N/A	N/A

Notes: 1. N/A - not available

3.3.3 Axial Component Experiments

3.3.3.1 Experimental Setup

Axial loads were applied to the unbonded braces using an MTS load frame as illustrated in Figure 3-34. The length of the brace was equal to 968 mm including the connection regions on the cruciform section. The core length was considered to be 518 mm between the centers of the transition between the maximum cruciform and minimum core sections at either end of the brace. The core plate for the unbonded brace had cross sectional dimensions of 25 x 16 mm. The first brace was tested with a pinned connection connecting the gusset plates to grips in the load frame as shown in Figure 3-35, while the remaining braces were tested with moment resisting connections which were designed to be slip critical based on the serviceability criteria in the AISC LRFD provisions (1998) (Fig. 3-36). The force at which slippage was expected to occur was equal to 178 kN which was approximately two times the expected yield strength of the brace.

Three of the unbonded braces were instrumented with four strain gages to measure strains on each side of the plate at each end of the core length. The braces were also instrumented with two novatechniks on either side of the brace to measure displacements across the core length of the brace as shown in Figure 3-34. The displacement was also measured at the head of the actuator to give the displacement across the entire length including connection regions. The axial force was measured by the actuator load cell.

The loading history for each of the braces differed. Unbonded brace A was subjected to a modified ATC-24 (ATC, 1992) loading history. The loading history modifications involved subjecting the brace to two cycles at each excursion instead of three cycles as in ATC-24. The history was based on the expected force until yielding occurred then increased based on the



FIGURE 3-34 Experimental setup for testing of unbonded braces

displacement at yield. However as slippage in the pinned connection was considerable, the history was modified to achieve more uniform displacements in the core region. The loading rate was slow. The resulting displacement time history for brace A is given in Figure 3-37.

The loading history for the second brace was based on the loading history in the draft Recommended Provisions for Buckling-Restrained Brace Frames (BRBF) (SEAONC, 2003). This loading history is defined by a number of cycles at different levels of displacement ductilities. After the prescribed increasing amplitude cycles each specimen was cycled at a constant amplitude until failure at the maximum displacement amplitude. The displacements were controlled using the total displacement measured in the actuator. The yield displacement used to define the loading history was based on the estimated displacement calculated at a 0.2% offset strain, over the core length for brace A, which was equal to 1.63 mm. No slippage was observed before yielding therefore it did not affect the yield displacement. It is important to note that the displacement at 0.2% offset strain was considerably higher than would be estimated if a method such as the ATC-24 procedure (based on the slope at 75% of the yield force) was used. There was an even larger difference when compared to a theoretical yield displacement using a theoretical yield force and elastic modulus. As the BRBF guidelines (SEAONC, 2003) do not define the way in which the yield displacement is to be estimated, the method which resulted in the more severe displacements, that is at 0.2% offset strain was used. The other amplitudes were defined based on this



FIGURE 3-35 Pin ended connection in unbonded brace component experiment

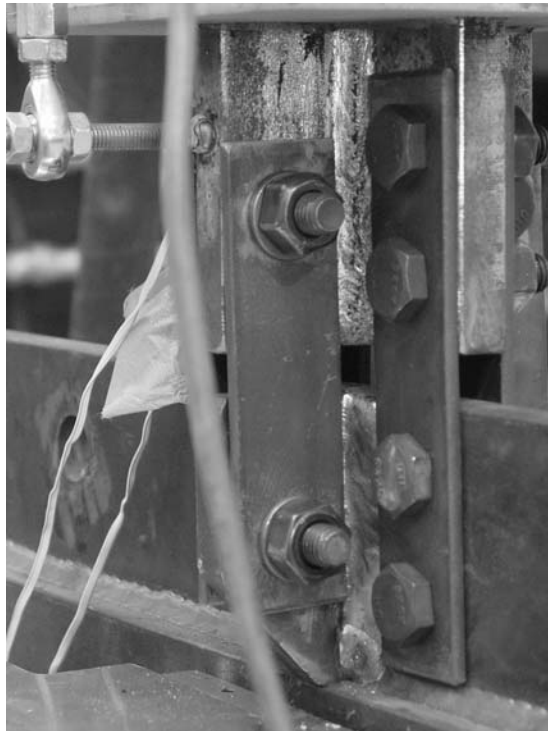


FIGURE 3-36 Fixed ended connection in unbonded brace component experiment

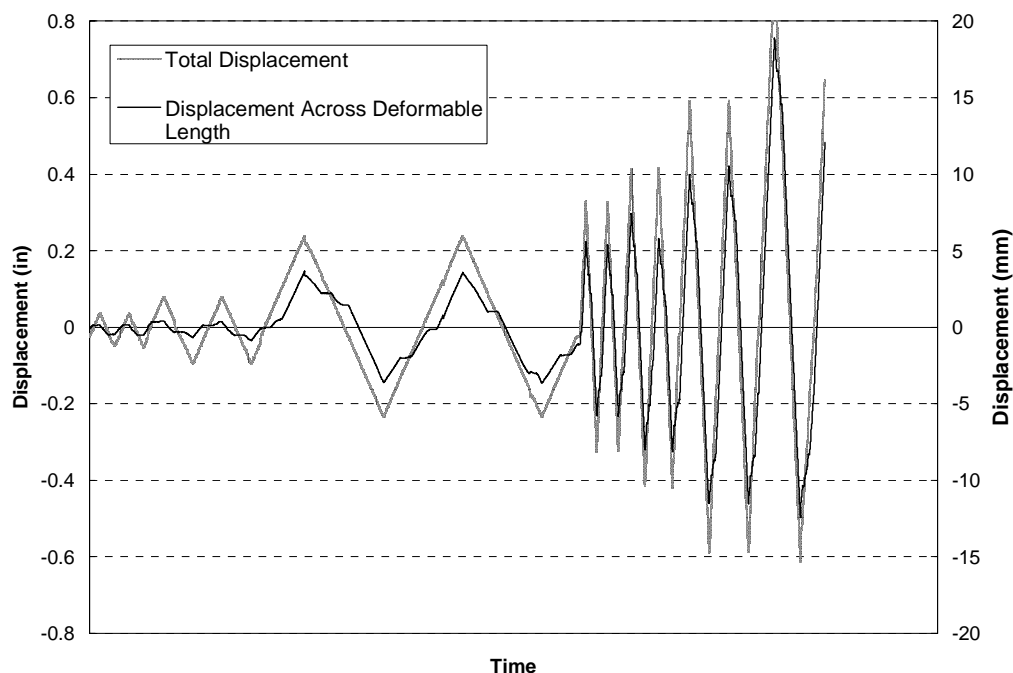


FIGURE 3-37 Displacement history for unbonded brace A

displacement at $\pm 2\Delta_y$, $\pm 4\Delta_y$ and $\pm 6\Delta_y$. The loading history for brace B is shown in Figure 3-38.

The loading history for unbonded brace C was the reverse of the history for B with some loading until failure. The resulting displacement time history was shown in Figure 3-39. The loading history for unbonded brace C was applied at a very slow rate. For unbonded brace D the same loading history (Fig. 3-40) was used but this time applied dynamically to the brace at a frequency of 2 Hz to simulate a bridge with a 0.5 s effective period. This was equivalent to a maximum strain rate of 25% /s.

Unbonded brace E was the brace first used in the north end of the bridge model and had already been subject to some inelastic deformation, although it had not failed. It was subjected to further inelastic behavior in a component experiment assembly. Initially one cycle of loading was slowly applied to simulate the maximum loading in the brace during bridge experiments, then the same loading history as that applied to unbonded brace D was applied at a dynamic rate of 2 Hz. Unbonded brace F was the brace used in the south end of the bridge model. It was subjected to a cycle of loading equal to the maximum cycle measured during the bridge experiments then cycled to failure at a constant amplitude of $\pm 3\Delta_y$ at a slow rate. The remaining brace, unbonded brace G, was the brace used at the midspan of the bridge model. It was subjected to one cycle as seen in the bridge model then $\pm 9\Delta_y$ until failure at a slow rate of loading. The displacement time histories for these braces, excluding the initial cycles, are shown in Figures 3-41 to 3-43.

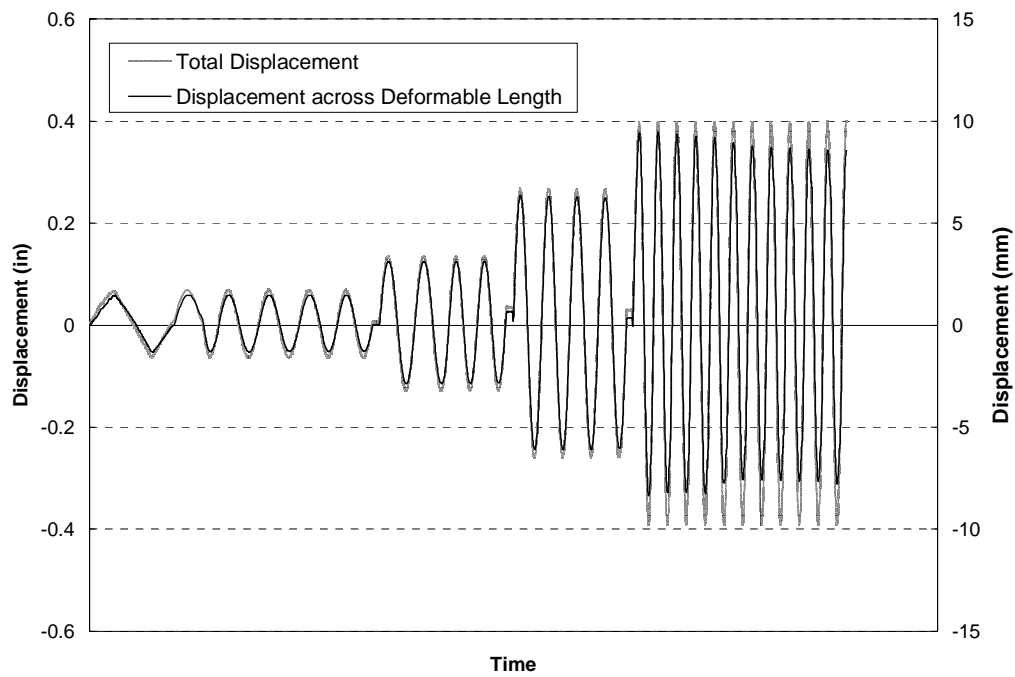


FIGURE 3-38 Displacement history for unbonded brace B

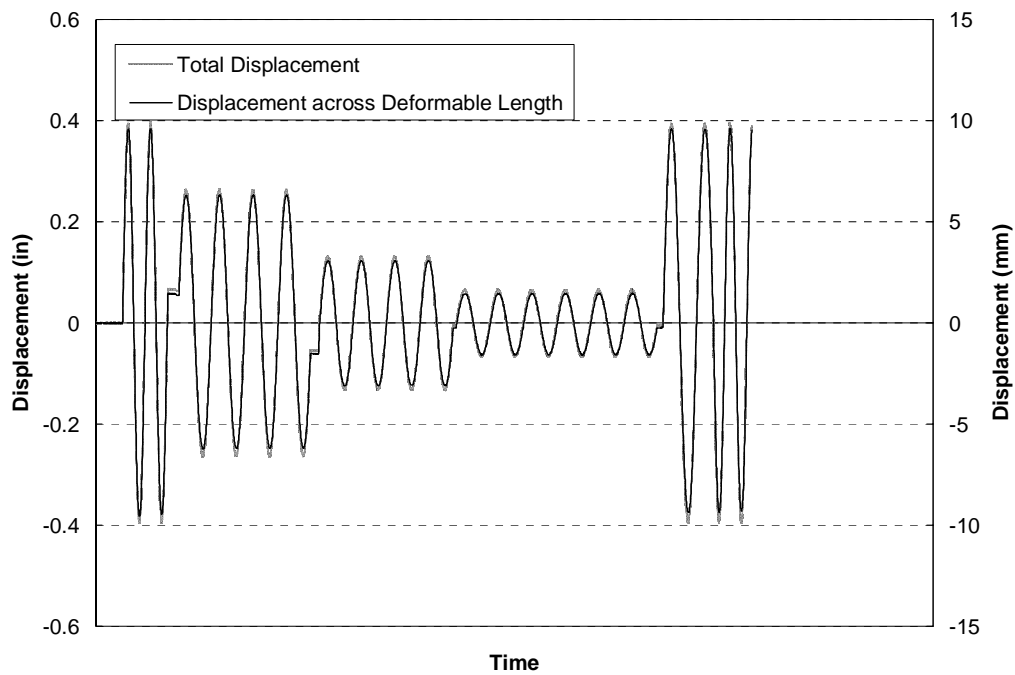


FIGURE 3-39 Displacement history for unbonded brace C

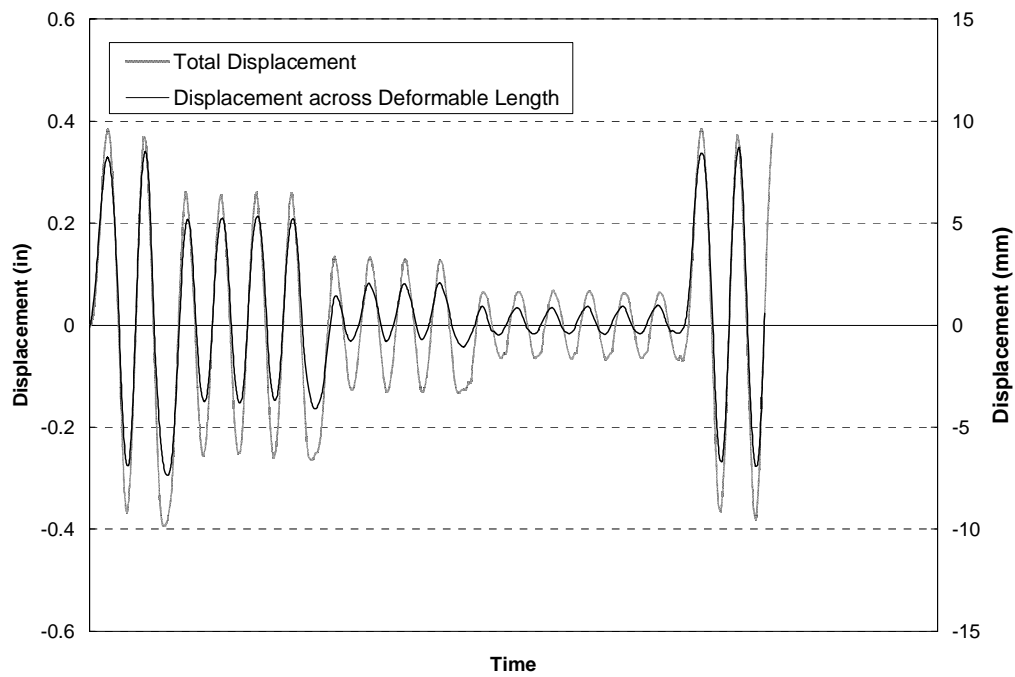


FIGURE 3-40 Displacement history for unbonded brace D

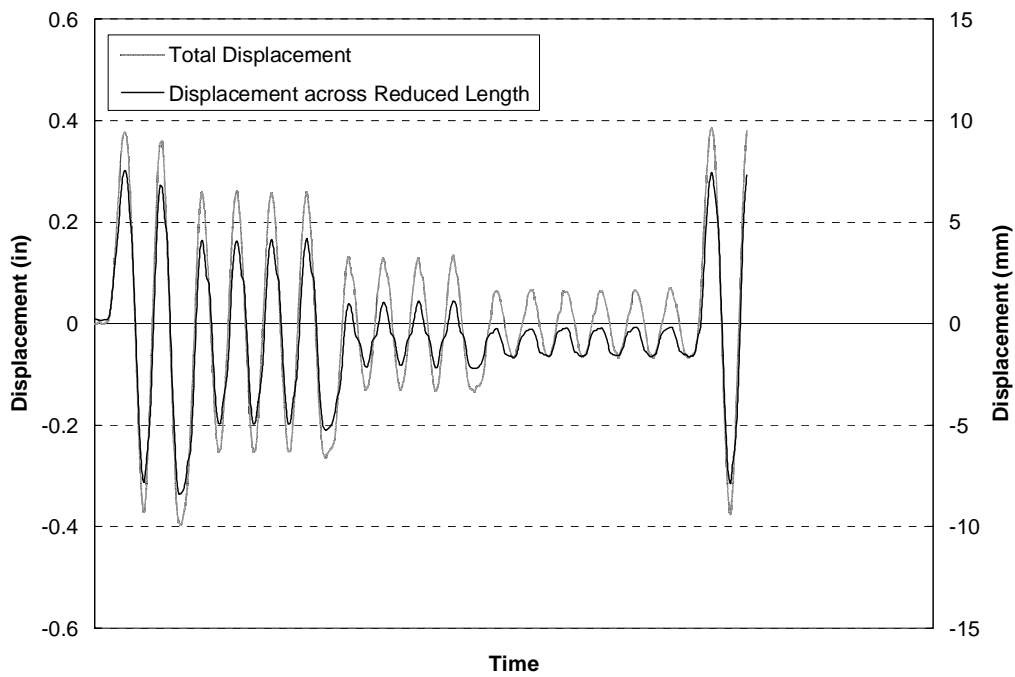


FIGURE 3-41 Displacement history for unbonded brace E

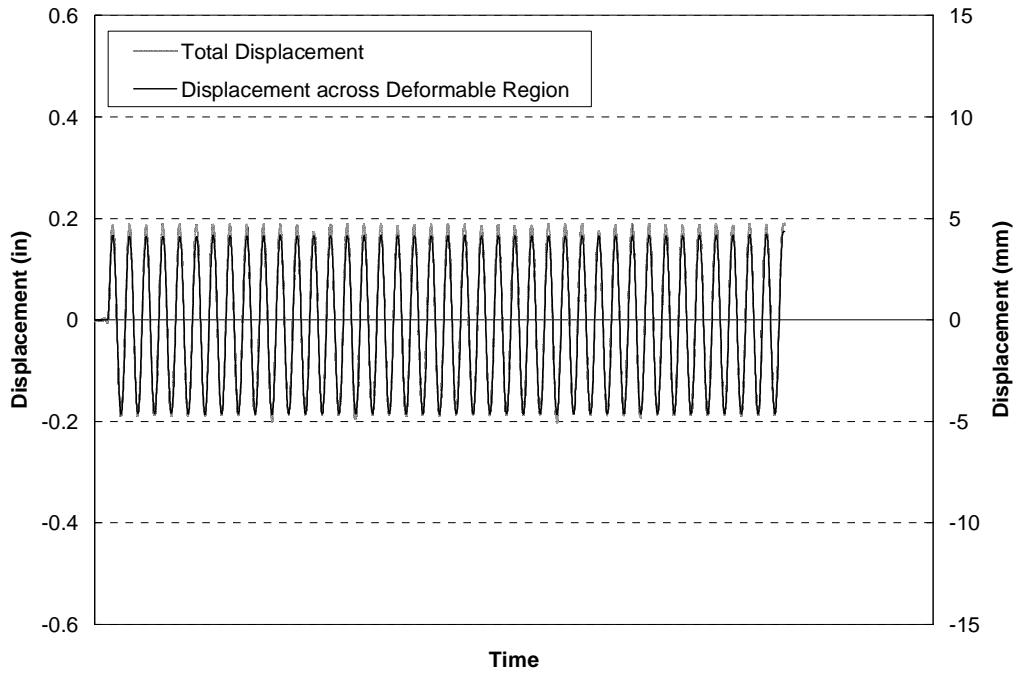


FIGURE 3-42 Displacement history for unbonded brace F

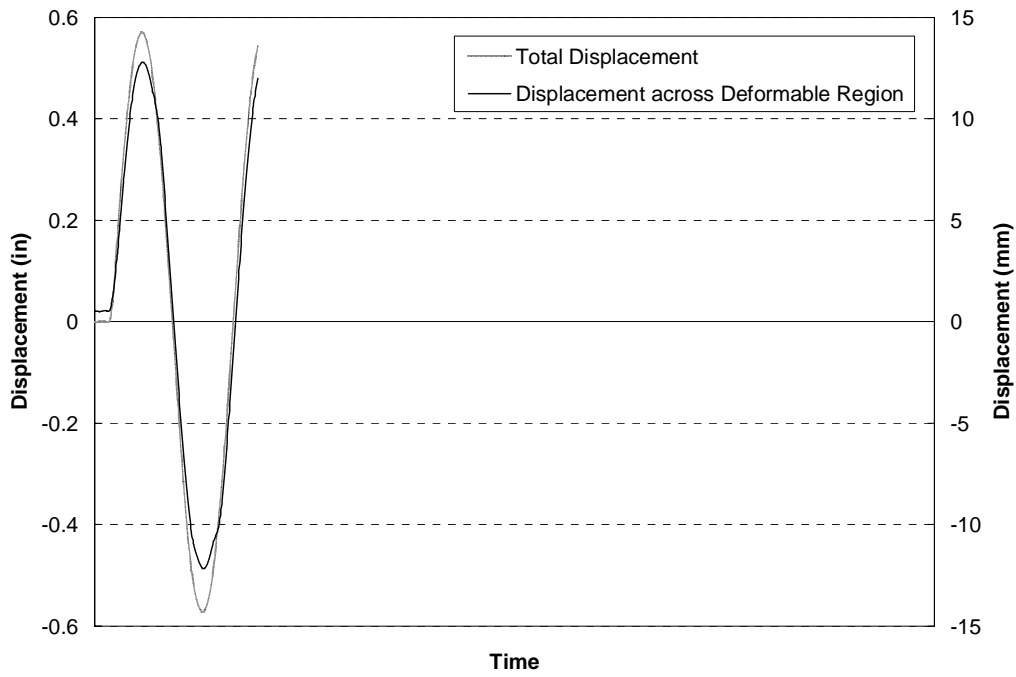


FIGURE 3-43 Displacement history for unbonded brace G

3.3.3.2 Hysteretic Properties

The force-displacement curves for each unbonded brace are shown in Figures 3-44 to 3-50. Overall the hysteresis loops exhibit good energy dissipation characteristics and repeatable behavior.

Figure 3-44 shows that there was a large difference between the displacement measured across the core length and the total displacement in unbonded brace A, due to slippage, as expected, in the pinned ended connection. The remaining braces were designed to have slip critical connections and Figure 3-45 shows that for brace B there was little difference between the displacement across the core length and total displacement at low amplitude cycles. The small difference can be attributed to elastic deformations in the connection region. At the maximum amplitude cycles the difference between the displacements did become larger indicating some slippage had occurred. For brace C no slippage was observed, however, more slippage was observed in the dynamic experiments with braces D and E and with the large amplitude displacements of brace G. The maximum force in the braces was less than the 178 kN force at which slippage was expected based on AISC serviceability criteria. Thus, despite the bolts being consistently tightened with a torque wrench, the force at which slippage was expected was unconservative.

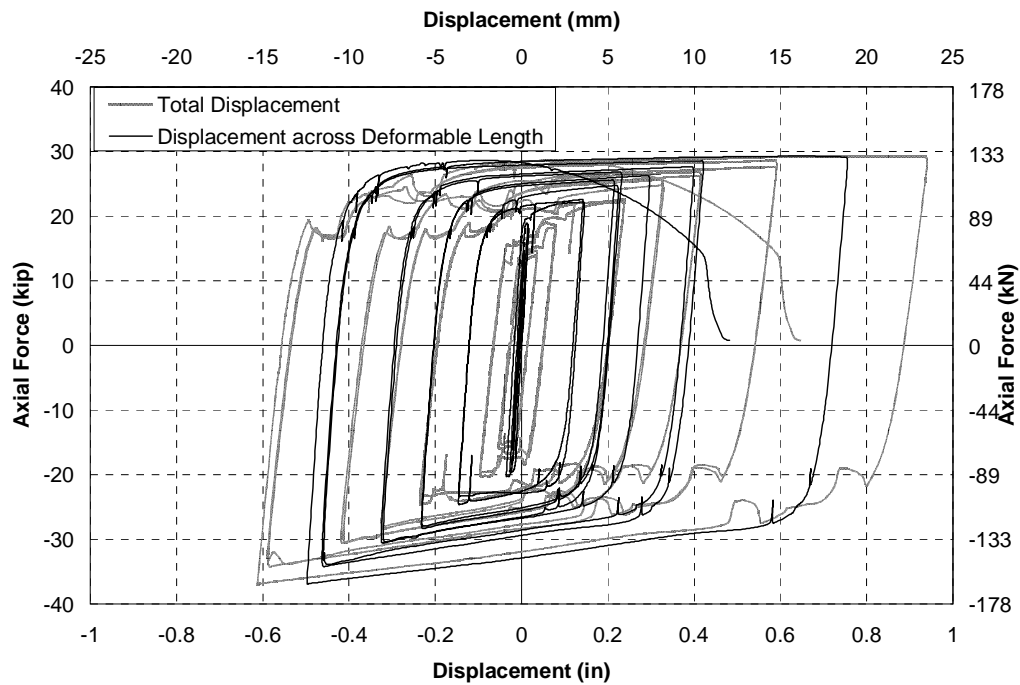


FIGURE 3-44 Hysteresis loop for unbonded brace A

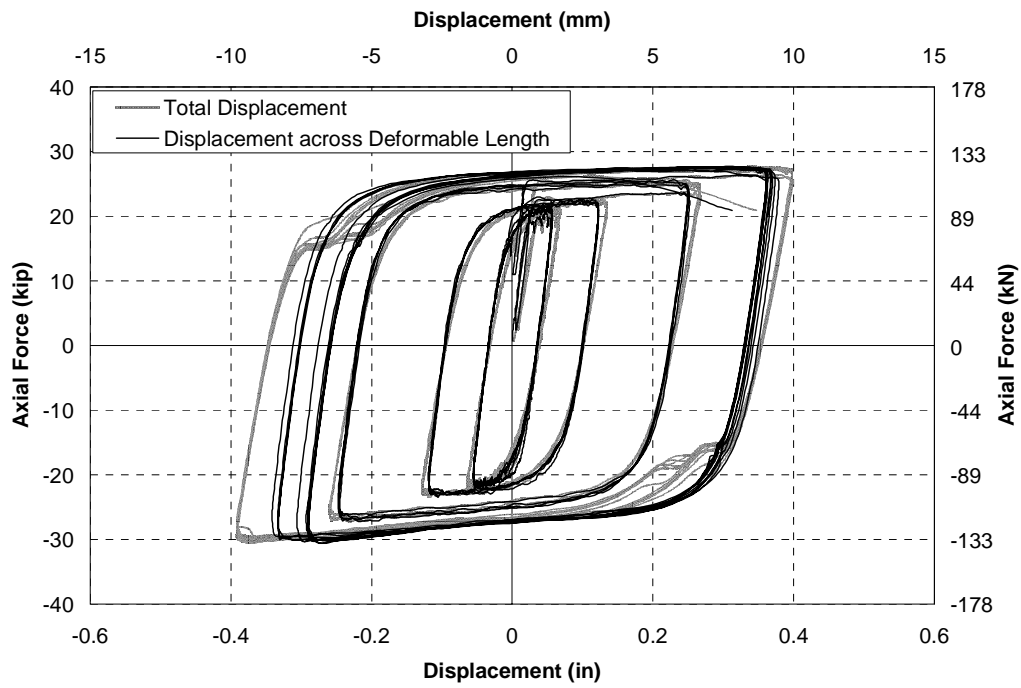


FIGURE 3-45 Hysteresis loop for unbonded brace B

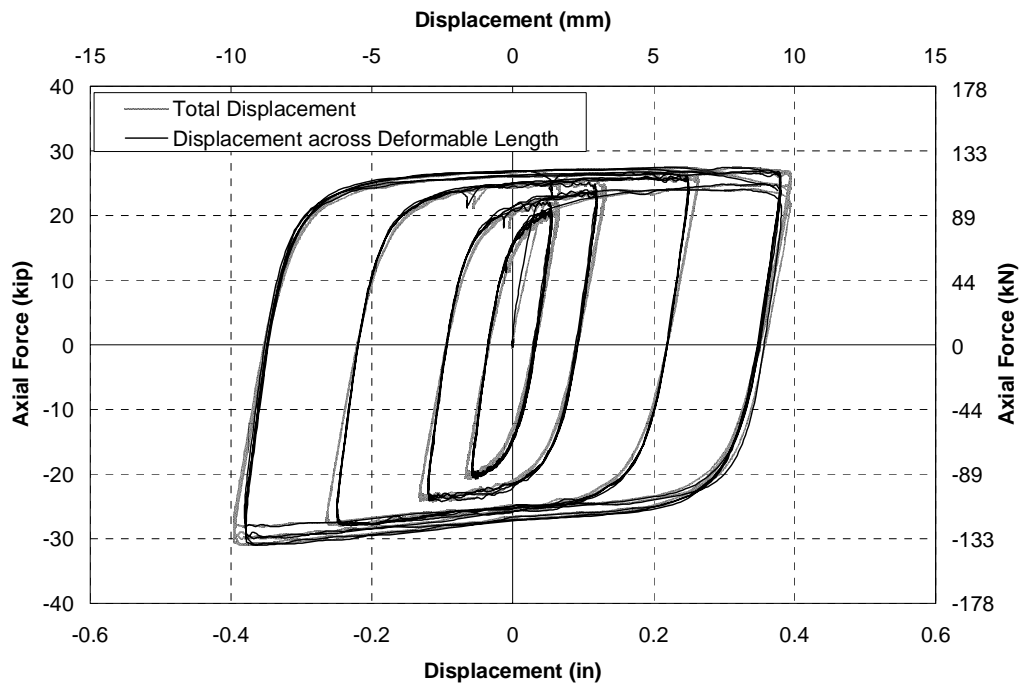


FIGURE 3-46 Hysteresis loop for unbonded brace C

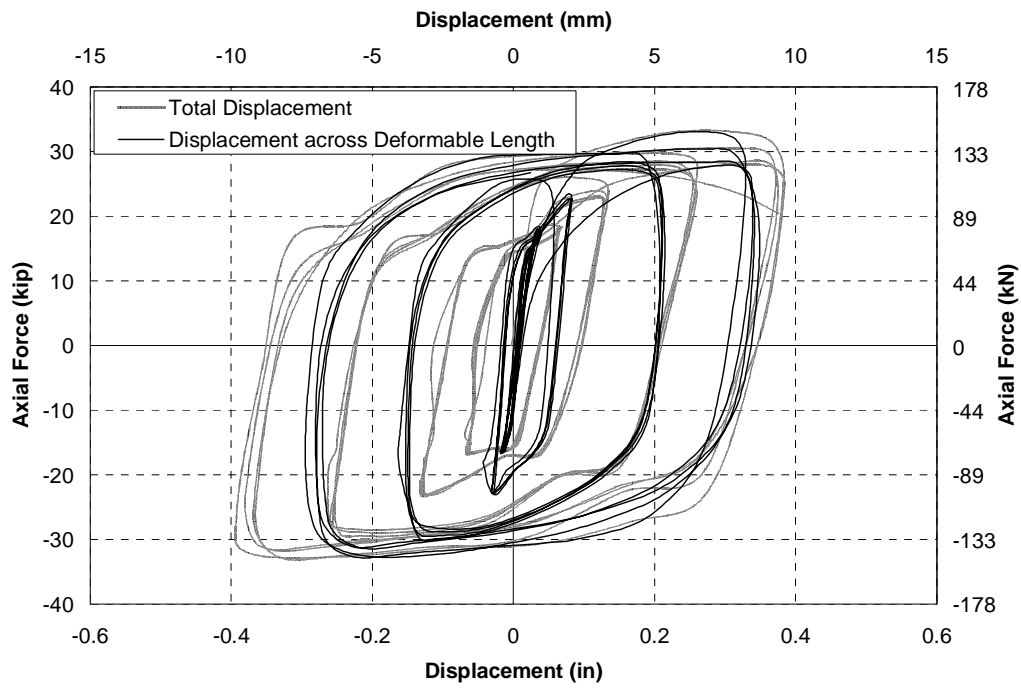


FIGURE 3-47 Hysteresis loop for unbonded brace D

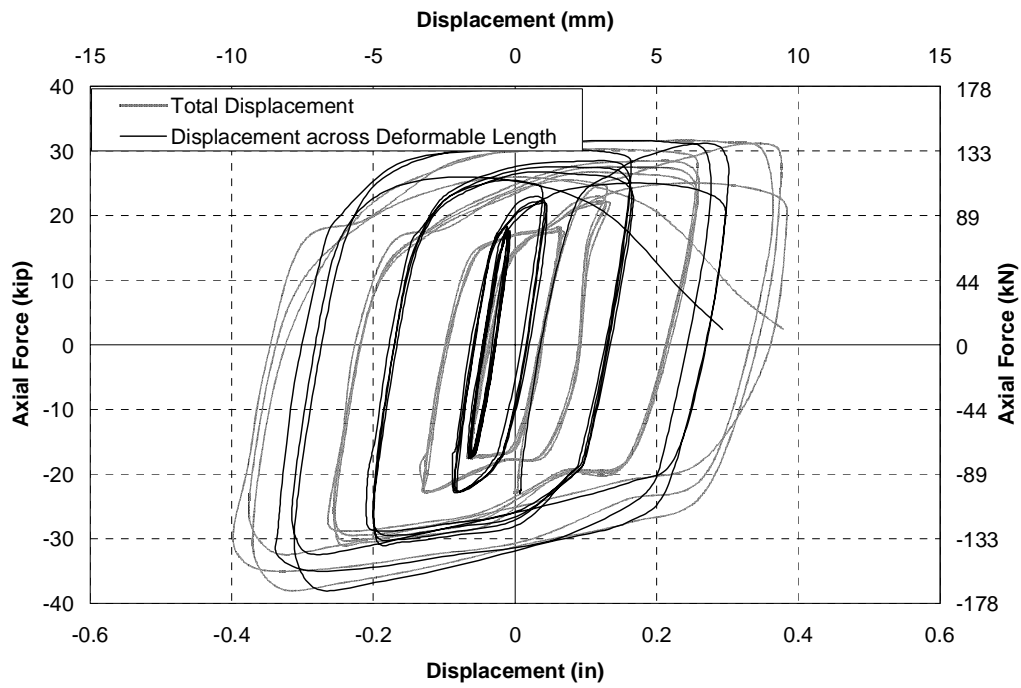


FIGURE 3-48 Hysteresis loop for unbonded brace E

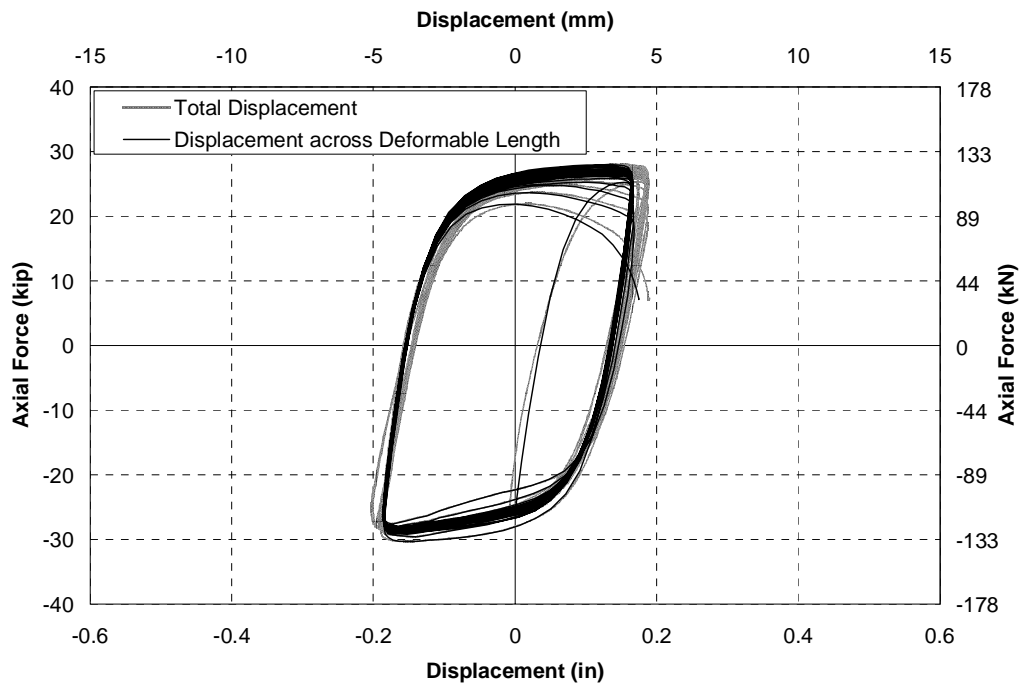


FIGURE 3-49 Hysteresis loop for unbonded brace F

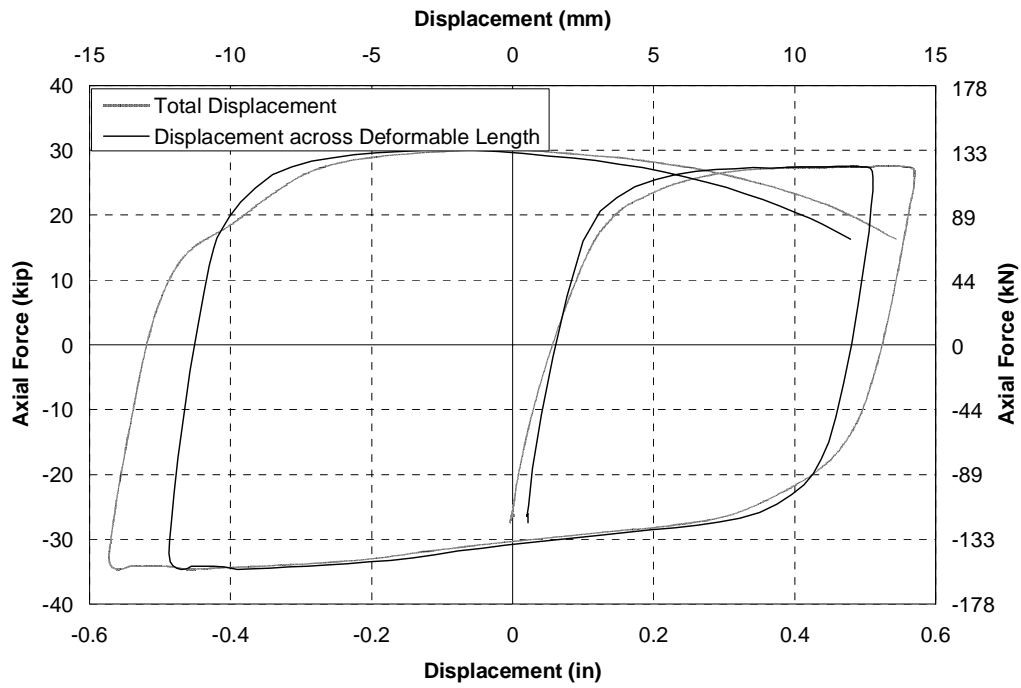


FIGURE 3-50 Hysteresis loop for unbonded brace G

3.3.3.3 Axial Forces

The expected yield force, P_{ye} , was defined as:

$$P_{ye} = F_{ye}A_{sc} \quad \dots 3.5$$

where: F_{ye} was equal to the expected yield stress, and; A_{sc} is the area of the steel core. For the unbonded braces the expected yield stress was equal to 225 MPa for the LYP-225 steel and the area of the steel core was equal to 400 mm², therefore the expected yield force was equal to 90 kN.

The yield force for each unbonded brace was estimated using the force at a 0.2% offset strain. The ultimate tensile force, F_{ut} , was equal to the maximum force measured for each brace while the brace was in tension. The factor, ω , describes the maximum force divided by the expected yield strength. The compression strength adjustment factor, β , was defined as the maximum compression force divided by the maximum tension force. The ω and β values are tabulated in Table 3-7 for each of the unbonded braces. This table shows that the measured yield forces were slightly larger than the expected yield forces but within 12% in all cases. The ω factor was generally around 1.35 but was also larger in some instances. Unbonded brace D had the largest overstrength factor which was attributed to strain rate effects which increased the force in the brace particularly during the first cycle of the loading. This can be observed in Figures 3-51 and 3-52 when comparing the response to the same loading history applied slowly for unbonded brace C and dynamically for braces D and E. The maximum force in the first cycle for brace D was 30% larger than for the first cycle of brace C, attributed to the different strain rates. The strain rate effect was more pronounced in the first virgin cycle of loading than in subsequent cycles, which stabilized to around a 15% difference when comparing braces C and D. Brace E had been previously loading in the bridge model and as a result maximum force in the first cycle of loading was not quite as high a that in brace D, although was still higher than for brace C. The braces with larger maximum strains across the core length, unbonded braces A and G, also exhibited larger ω factors.

The compression strength adjustment factor, β , was typically around 1.10 to 1.15. β was largest for the braces with the largest maximum strains in the brace increased as shown for braces A and G, while the reverse is true for smaller strains as in brace F. For brace D the maximum compression force was actually less than the maximum tension force due to the large observed tension force in the first reversal of the dynamically loaded specimen.

3.3.3.4 Ultimate and Cumulative Displacement Capacity

The maximum displacements, converted to equivalent strains across the core length of the unbonded braces during each of the component experiments, are given in Table 3-8. For the standard BRBF history the maximum strain was approximately 1.9% although slightly less in cases where slippage occurred. The maximum strain in brace A was 3.7%.

The cumulative displacement capacity was evaluated for the brace using CPS and CPD. These values for each specimen are given in Table 3-8. The yield displacement was assumed to be equal to the theoretical yield displacement over the core length using the expected yield stress for the

TABLE 3-7 Yield and Maximum Forces for Unbonded Braces

Brace	Loading History	Expected Yield Force (kN)	Measured Yield Force (kN)	Maximum Tension Force (kN)	Maximum Compres. Force (kN)	Tension Overstrength Factor	Maximum Compression to Tension Force Ratio
A	Modified ATC-24	90	96	130	164	1.44	1.26
B	BRBF Normal Static		94	123	136	1.36	1.11
C	BRBF Reversed Static		101	122	138	1.35	1.13
D	BRBF Reversed Dynamic		102	147	145	1.62	0.99
E	South Bridge and Reversed Dynamic		96	140	167	1.55	1.19
F	North Bridge and Constant Static		96	124	135	1.37	1.08
G	Midspan Bridge and Constant Static		98	134	154	1.47	1.15

TABLE 3-8 Maximum Strains, Cumulative Plastic Strains and Cumulative Plastic Ductilities in Unbonded Braces during Bridge and Component Experiments

Brace	Loading History	Max Strain ¹ (%)		Cumulative Plastic Strain (%)		Cumulative Plastic Ductility	
		Bridge	Axial	Bridge	Axial	Bridge	Axial
A	Modified ATC-24	-	3.71	-	54	-	479
B	BRBF Normal Static	-	1.86	-	98	-	875
C	BRBF Reversed Static	-	1.87	-	66	-	588
D	BRBF Reversed Dynamic	-	1.71	-	38	-	337
E	South Bridge and BRBF Reversed Dynamic	1.76	1.77	41	40	366	352
F	North Bridge and Constant Static	2.22	0.92	23	125	205	1109
G	Midspan Bridge and Constant Static	2.29	2.51	76	22	674	192

Notes: 1. Based on average strain resulting from axial displacement across the effective deformable length of 518 mm.

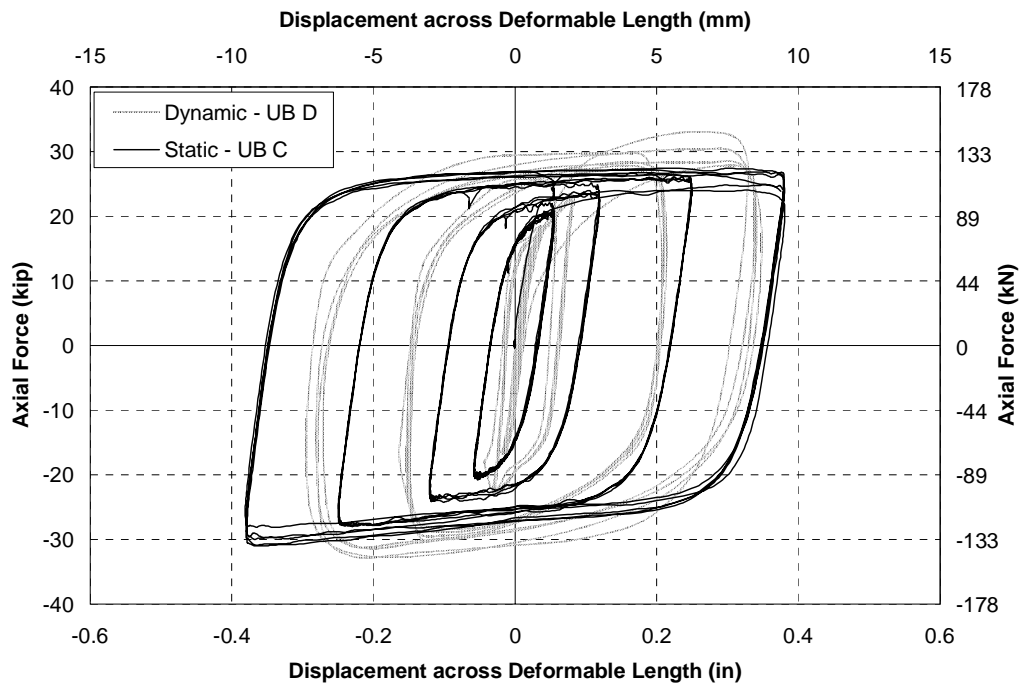


FIGURE 3-51 Comparison of response for dynamic and static loading histories for unbonded braces C and D

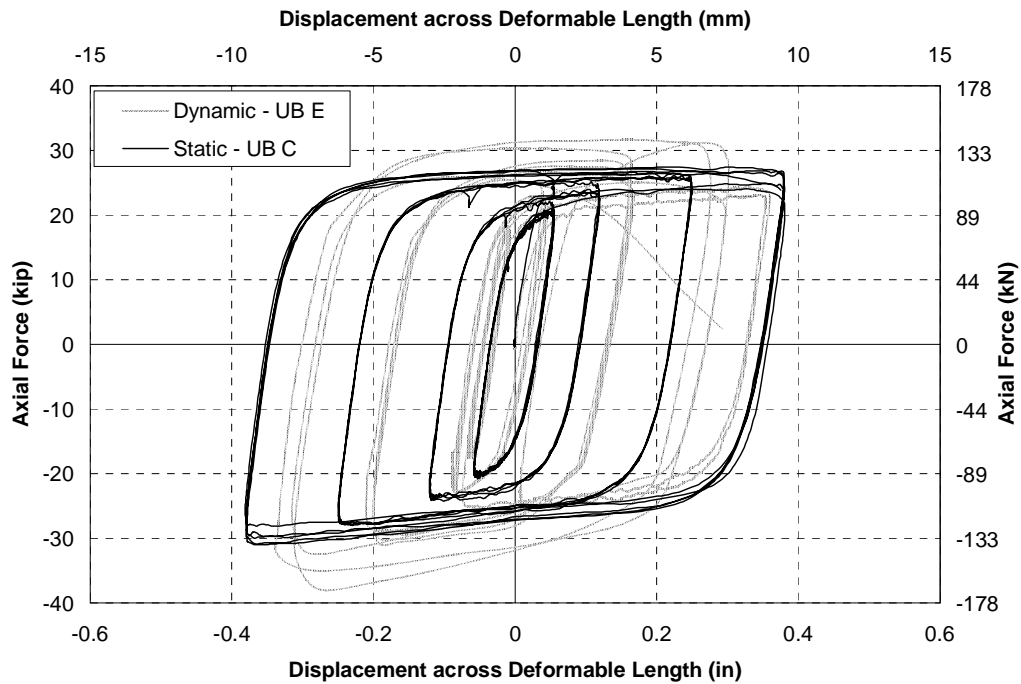


FIGURE 3-52 Comparison of response for dynamic and static loading histories for unbonded braces C and E

LYP-225 material and Equation 3.4. This resulted in a yield displacement of 0.582 mm. Note that this estimate of the yield displacement was around 29% less than the average yield displacement measured in the braces using the ATC-24 (1992) procedure. However this is only approximately 36% of the displacement calculated at the 0.2% offset strain used to define the loading history. This difference highlights the importance of clearly defining the method in which the yield displacement is calculated. The theoretical yield displacement is consistent and computable, and comparable to that for single angles.

Comparing the CPS, CPD and maximum strains in braces A and B, both with increasing amplitude statically applied loading, shows that a larger maximum strain reduced the cumulative displacement capacity of the braces. Therefore the CPS and CPD were not independent of the maximum strain. Comparing braces B and C, with the normal and reversed, slowly applied BRBF loading histories, showed that having the large amplitude cycles at the beginning of the history reduced the overall CPS in the brace, by 33% in this comparison. Furthermore, applying the loading history dynamically, as in brace D, further appeared to reduce the CPS. Although in contrast to this, brace E, which was subjected to deformations in the bridge model as well as in the load frame, had a similar total cumulative plastic ductility as brace C. It was difficult to draw definitive conclusions from those braces used in the bridge model as their loading histories were highly variable.

It is noted that the maximum strains observed in the unbonded braces were generally smaller than the comparative values for the single angle members. This can be largely explained by the irrecoverable elongation in the single angles resulting in smaller cumulative plastic strains over much of the length of the member than the overall displacements would suggest. In contrast, as buckling was largely prevented in the unbonded braces, the steel in the braces does more work as it undergoes cyclic tension and compression actions with better resulting energy dissipation characteristics as described below. There was also some slippage observed in the single angle members which was not subtracted from the overall deformations, although the amplitude of the slippage was thought to be small in these members compared to the overall deformations.

From these experiments it is recommended that ductile end cross frames using unbonded braces should be designed for a maximum deformation during an earthquake not exceeding 2.0% as this is easily less than the maximum strain, as measured in Brace A subjected to increasing amplitude loading to failure, divided by 1.5. Furthermore it is shown in Section 6 that at this level of strain the cumulative plastic strain demand from a series of maximum considered earthquake simulations on an analytical model is less than the minimum capacity measured in the braces.

3.3.3.5 Energy Dissipation in the Unbonded Braces

The area enclosed by the hysteresis loops was calculated for unbonded braces A to D at different cycles of loading during the component experiments. The displacement was based on the displacement measured across the core length. The hysteretic area was compared to the circumscribing rectangular area enclosed by the maximum force and displacement, as illustrated in Figure 3-26. The energy dissipated per cycle is plotted against maximum axial strain amplitude for each cycle in Figure 3-53. This figure demonstrates that once significant yielding has occurred the energy dissipation was typically around 80% of the rectangular area. Unlike the single angles the effective energy dissipation increased as the displacement amplitude increased. Hence the unbonded braces were much more efficient than the single angles for energy dissipation. This

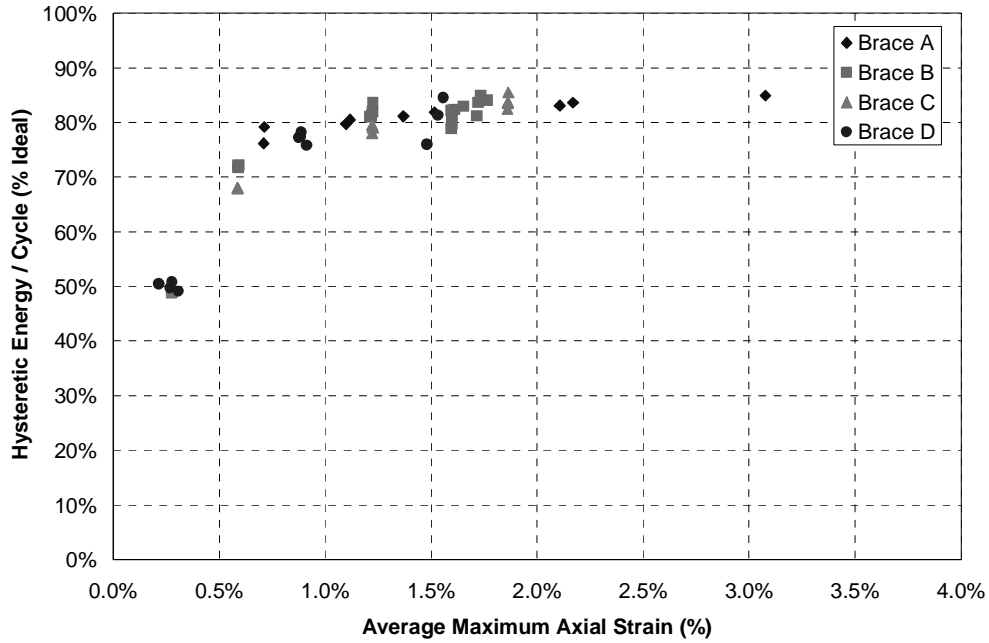


FIGURE 3-53 Energy dissipated per cycle for different unbonded braces based on displacements across the core length

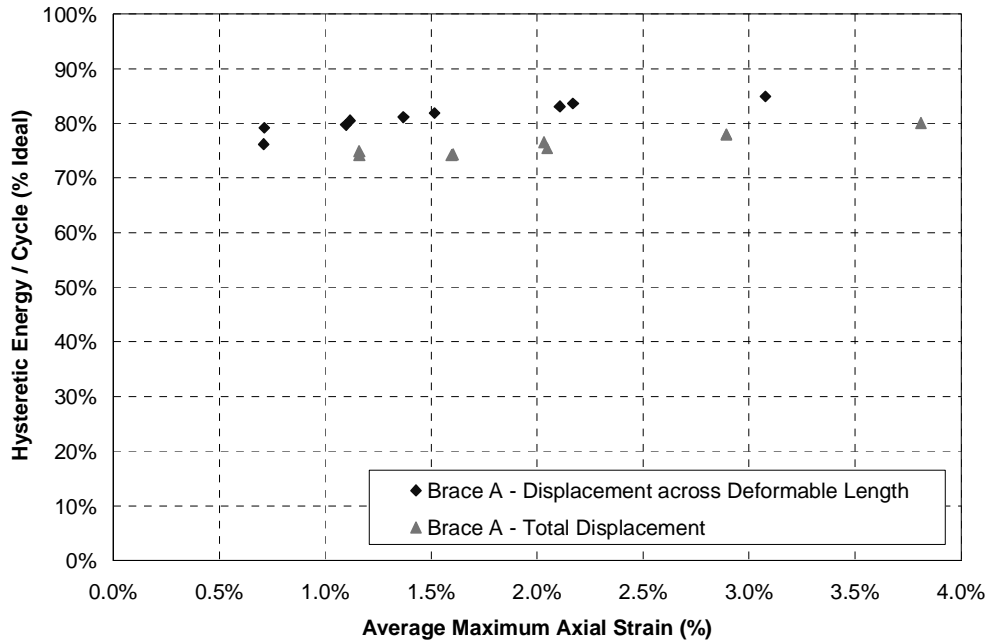


FIGURE 3-54 Energy dissipated per cycle for unbonded brace A considering hysteretic behavior across the core length and across the total length

implies that there should be smaller drifts in ductile end cross frames using unbonded braces compared to those using single angles for the same level of forces.

The hysteretic area for Figure 3-53 was based on the displacements across the core length. It was expected that slippage in the connections would reduce the effective energy dissipated. For brace A, the brace exhibiting the most slippage with the pin ended connections, the hysteretic energy dissipated per cycle was calculated based on the total displacements in the brace including the connections. Figure 3-54 shows that the energy dissipation, as a function of the ideal energy dissipation, was reduced by around 5% at any given level of strain. Therefore connection slippage had a relatively small effect on the overall energy dissipation in the brace. This was because the process of slippage had a tendency to provide its own hysteretic behavior. The effect of slippage on the hysteretic behavior of the other braces was even less than for brace A. Consequently there appeared to be no real advantage in providing slip critical connections in the unbonded braces for seismic loading, although the connections should be slip critical for service loading to minimize fatigue issues. One advantage of slippage during an earthquake is that it reduces the strains in the core length of the brace for a given total displacement.

3.3.3.6 Strain Gage Readings

Strain gages were placed on braces A and B, with gages on either side of the core plate near each end of the core length. The strain gages for brace B are plotted against axial forces in Figures 3-55 to 3-58. These plots show that there is hysteretic behavior with both tensile and compressive strains although there is some bias towards tensile strains, as demonstrated particularly well in Figure 3-58. This can be explained by the high mode buckling which is known to occur in the core section of buckling restrained braces. The magnitude of the maximum strains is higher, at 4.83%, compared to the maximum average computed strain from deformations in the brace of 1.86%. Brace A shows similar properties except that due to the larger deformation in the brace three of the gages reached their measurement limit at 5% strain.

While in the elastic range the strain gages were used to estimate the force in the unbonded brace using the elastic modulus, assumed to be equal to 200 GPa, and the area of the core plate. Figure 3-59 shows a good correlation between the measured and computed axial forces, where the difference between the two is less than 8%. The error could be reduced by increasing the elastic modulus. Therefore the strain gages can be used to accurately estimate the brace force while the brace remains elastic.

3.3.4 Analytical Model

Black (2002) has shown that the properties of an unbonded brace can be captured well with a Bouc-Wen model (Wen, 1976). However for use in capacity spectrum analysis it is more useful to characterize the behavior using a bi-linear model if possible. A bi-linear model can be shown to fit the experimental data reasonably well. The initial stiffness, K_i , was calculated based on the cross sectional properties of the core and the core length, giving an initial stiffness of 156 kN/mm. The post-yield stiffness ratio, α , was assumed to be equal to 0.025 in order to fit the backbone curve for the increasing amplitude cyclic displacements. The yield force was assumed to be equal to the expected yield of 90 kN.

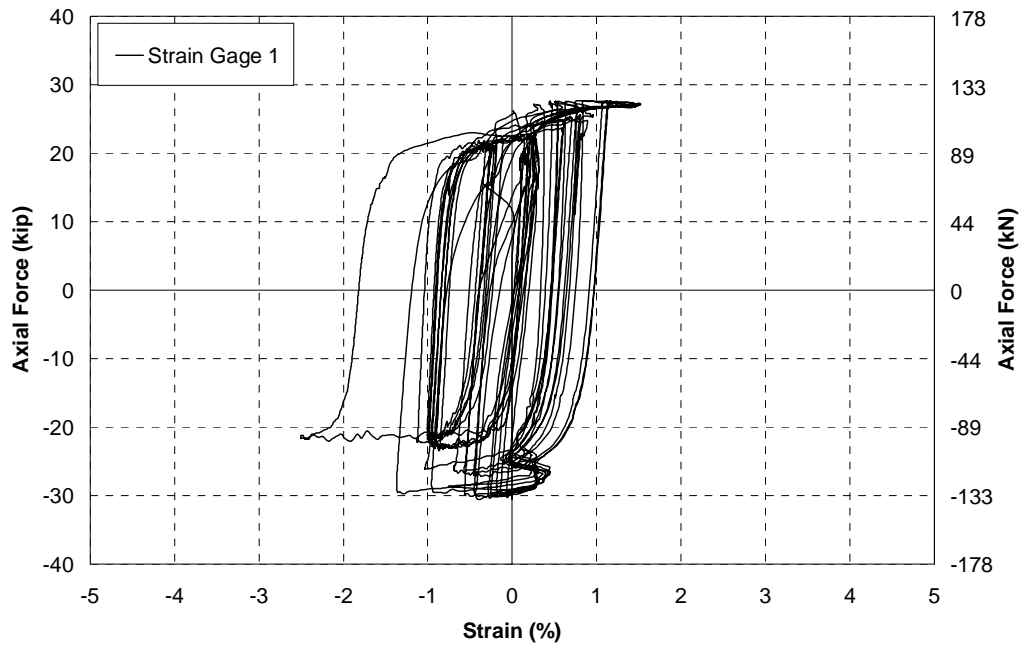


FIGURE 3-55 Strain gage 1 on unbonded brace B

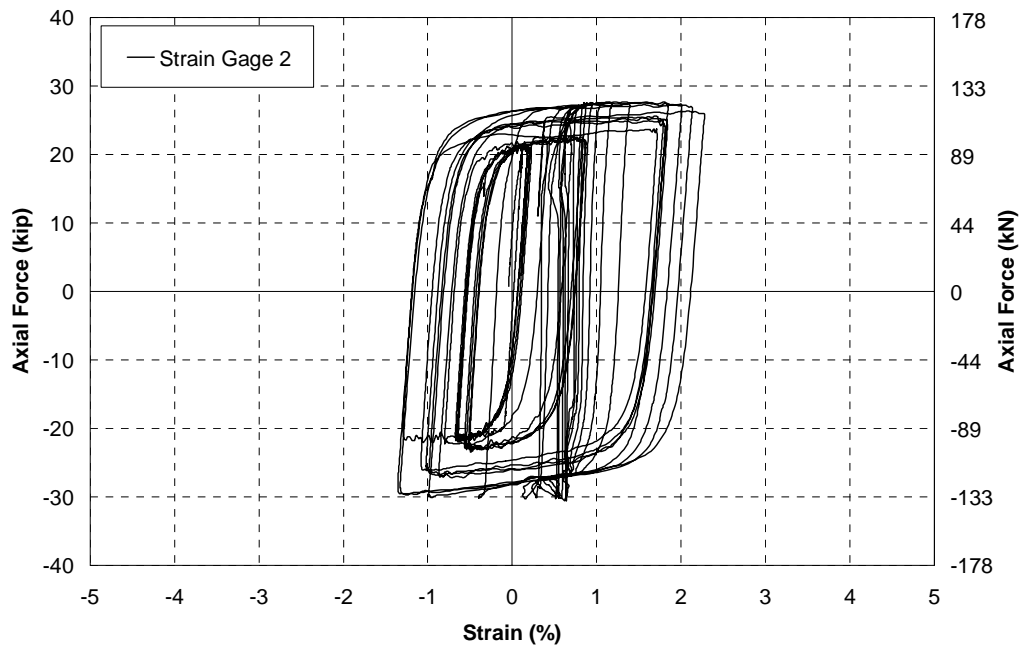


FIGURE 3-56 Strain gage 2 on unbonded brace B

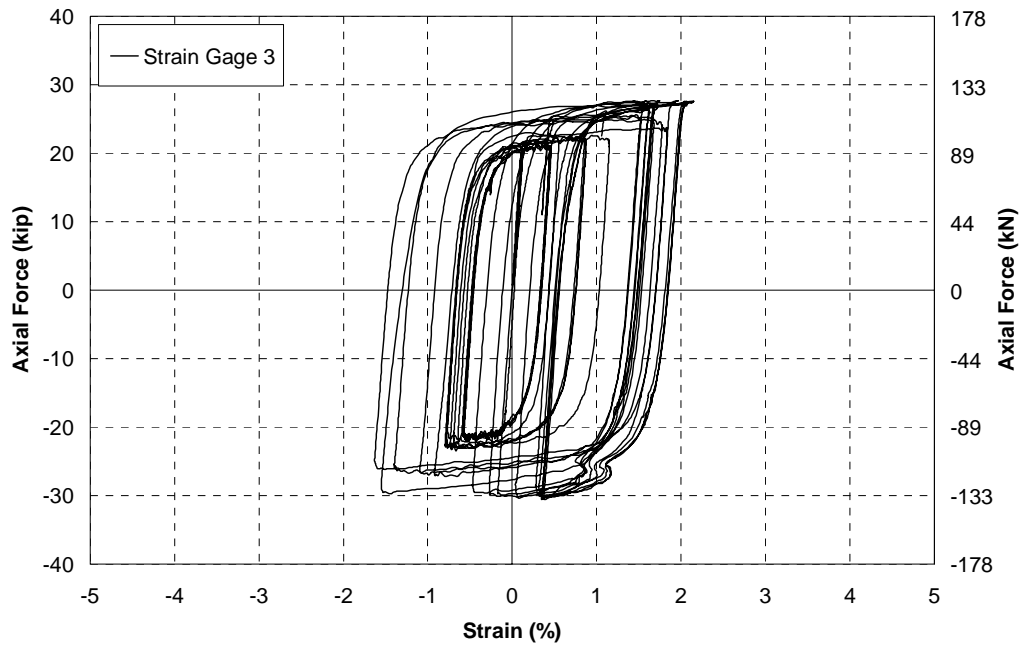


FIGURE 3-57 Strain gage 3 on unbonded brace B

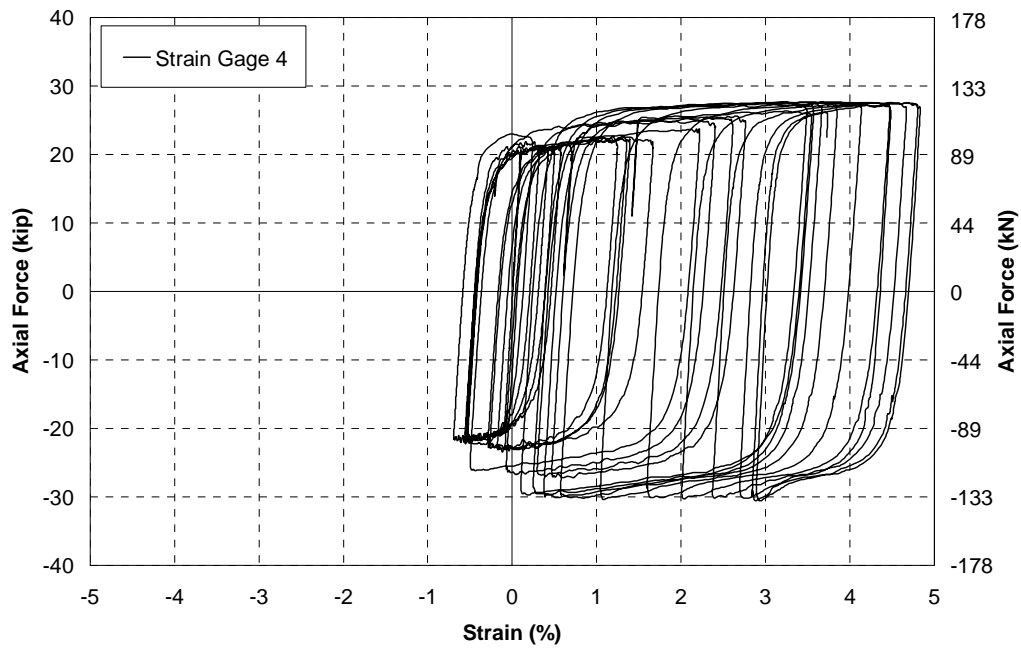


FIGURE 3-58 Strain gage 4 on unbonded brace B

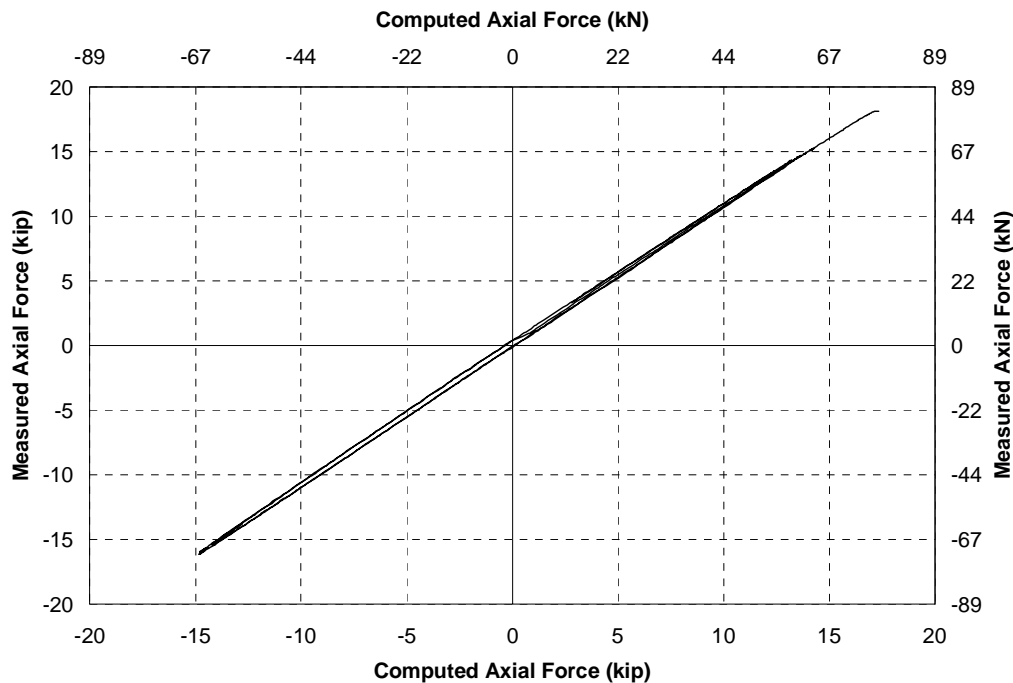


FIGURE 3-59 Measured axial forces vs axial forces computed using measured strains for unbonded brace A while responding elastically

The hysteresis loops for the analytical model using the loading history for brace A is shown in Figure 3-60. The bi-linear model is shown to fit the backbone curve for the experimental data well, although the force was overestimated for the last cycle of tensile loading and it was consistently conservative for the backbone curve in compression. This was unavoidable without a separate model for the tension and compression properties. The bi-linear model was shown to fit the experimental data better for the other experiments where maximum displacements were not quite as large. Figures 3-61 to 3-63 compare the analytical model with the experimental data for braces B to D. The analytical model characterizes the experimental data well for braces B and C. The dynamic strain rate effect is evident in brace D and as a result the analytical model generally underestimated the forces in the system. A factor to account for strain rate effects by which the forces in brace were increased by 15% was considered and is shown to improve the analytical model (Fig. 3-64).

While the bi-linear model captures the elastic unloading of the unbonded braces very accurately it loses some accuracy in modeling the initial reversal of loading in the braces, as observed in comparing the experimental and bi-linear hysteresis loops. The main effect of this is a difference in the area inside the hysteresis loops. A comparison of the hysteretic energy dissipated per cycle for the experimental data and the bi-linear model is shown Figure 3-65. This figure shows that the equivalent areas are similar at moderate strains with a notable difference only observed at larger amplitudes. This is not expected to greatly affect the modeling of the dynamic response of the bridge model with unbonded braces.

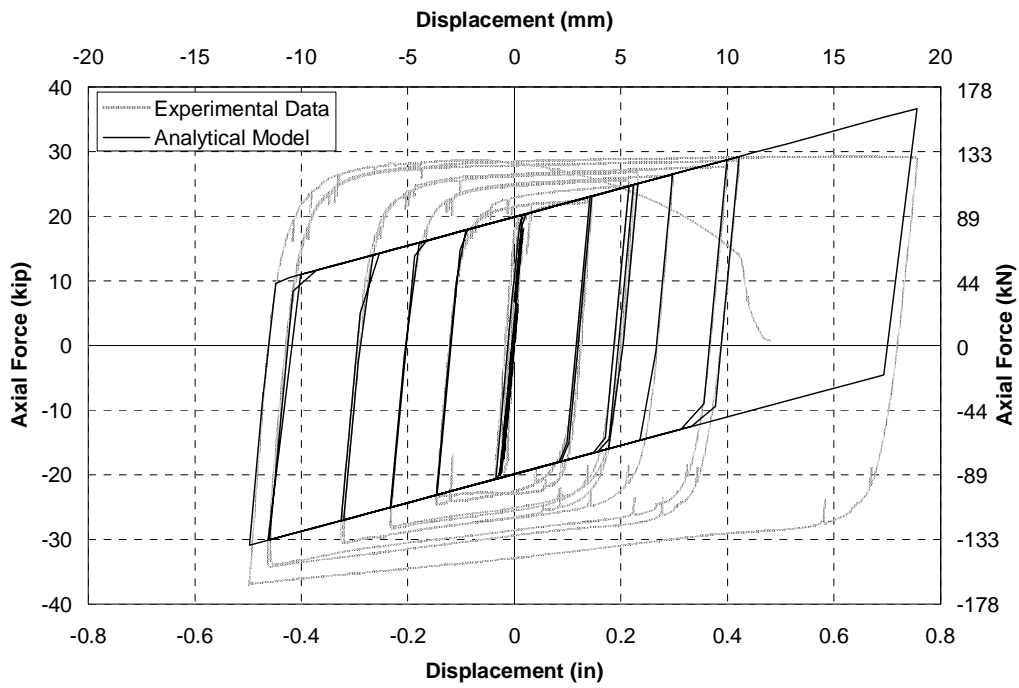


FIGURE 3-60 Hysteresis loops for analytical model of unbonded brace A

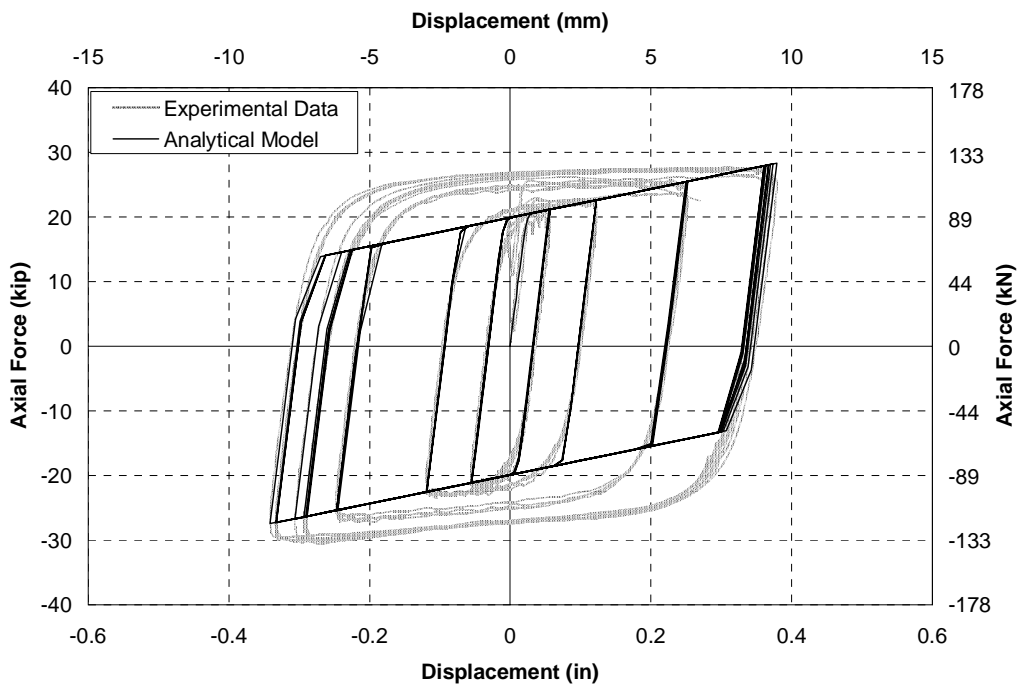


FIGURE 3-61 Hysteresis loops for analytical model of unbonded brace B

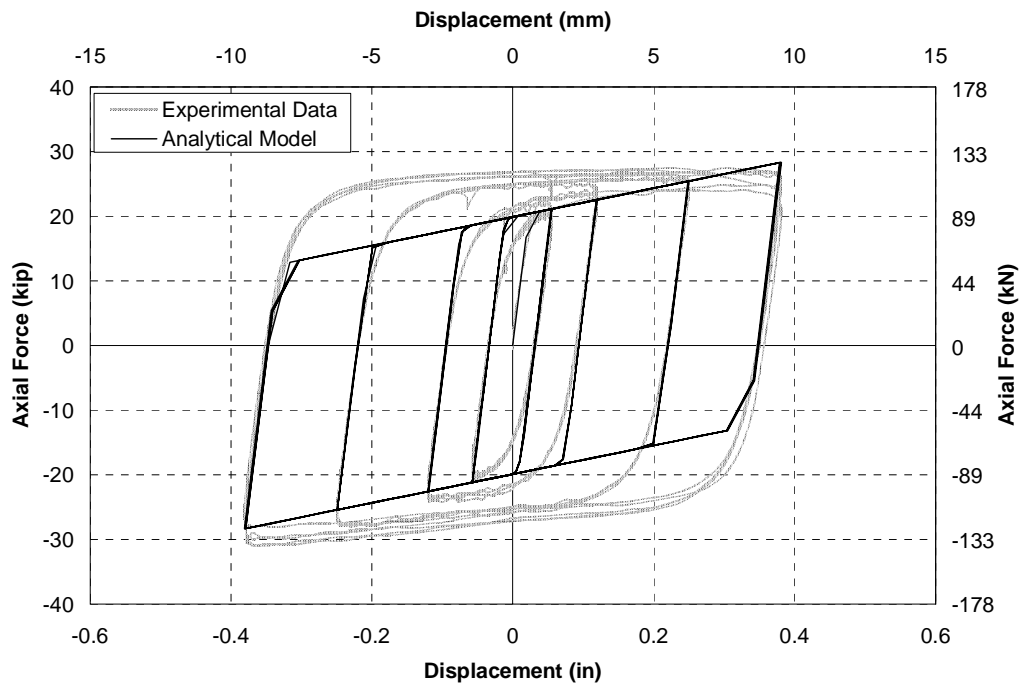


FIGURE 3-62 Hysteresis loops for analytical model of unbonded brace C

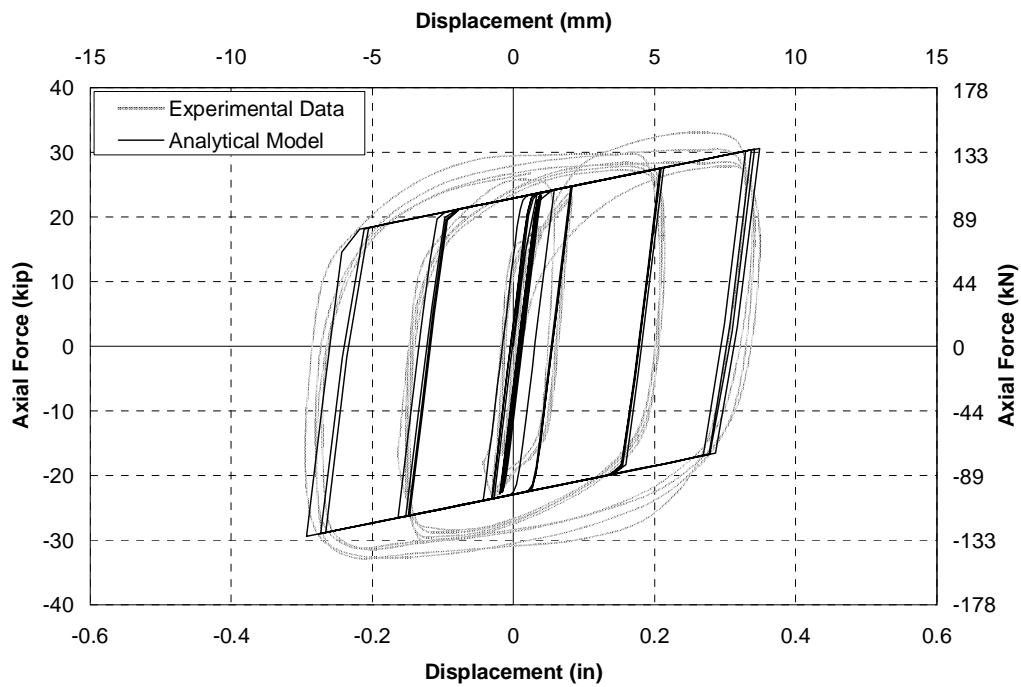


FIGURE 3-63 Hysteresis loops for analytical model of unbonded brace D

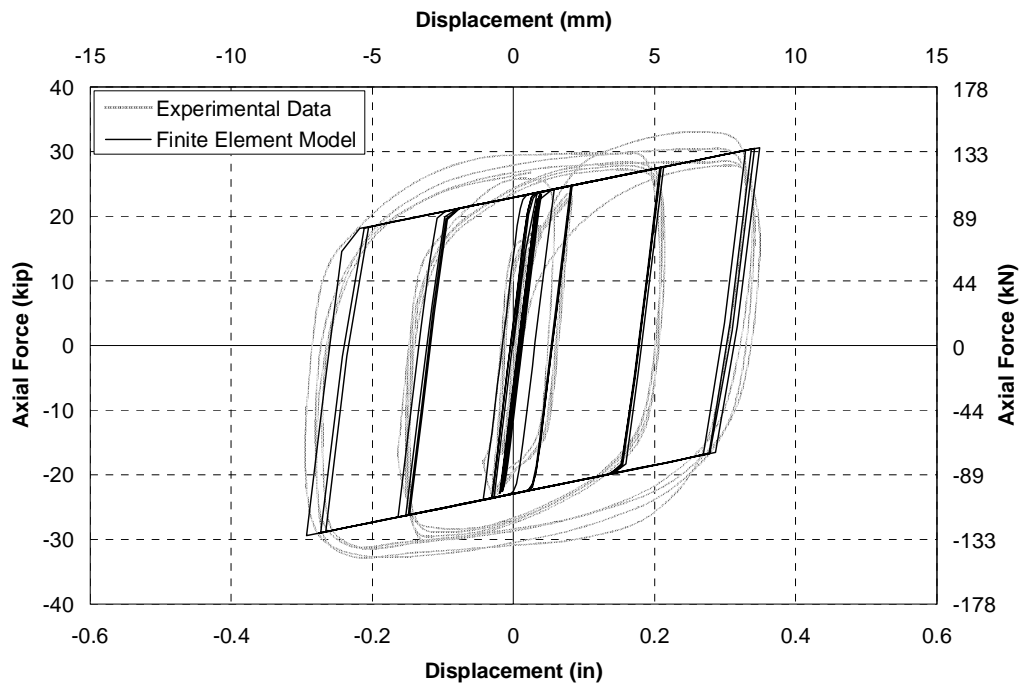


FIGURE 3-64 Hysteresis loops for analytical model of unbonded brace D with yield strength increased by 15% to allow for dynamic loading

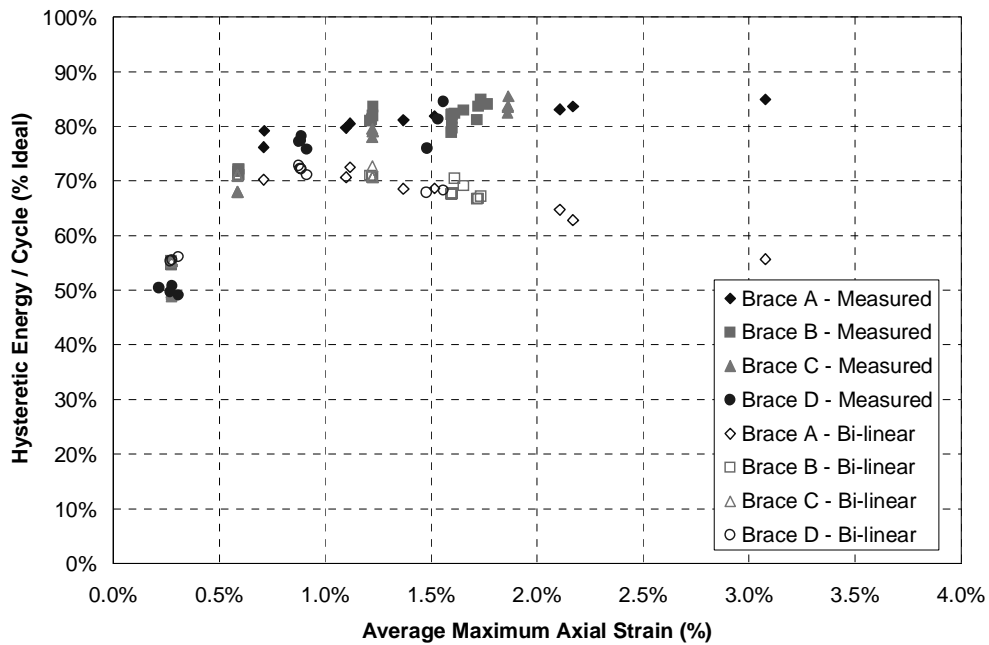


FIGURE 3-65 Energy dissipated per cycle for bi-linear models of different unbonded braces

3.4 Lead Rubber Bearings

3.4.1 Overview

This section investigates the non-linear properties of the lead rubber bearings used to seismically isolate the bridge model. Component experiments were performed by Dynamic Isolation Systems (DIS), the bearing manufacturers, in order to characterize the properties of the bearings and compare with the design properties.

3.4.2 Experimental Setup

Two lead rubber bearings at a time were tested and as a result measured properties are for an average of the two bearings in each pair. As the testing machine was calibrated for much larger bearings the accuracy of the measurements is not high, resulting in some noise, however the overall properties were identified. Each bearing was subjected to three cycles of $\pm 100\%$ shear strain in the rubber.

3.4.3 Hysteretic Properties

The hysteresis loops averaged for the two bearings in each experiment are shown in Figures 3-66 to 3-68. The figures show higher forces in the first cycle than for subsequent cycles as the bearing stiffness reduces. The difference between the second and third cycles shows stabilization of the properties which is typical for lead rubber bearings due to “scragging” of the rubber. On average scragging was attributed to a calculated 10% reduction in the characteristic strength and a 20% reduction in the design stiffness of the bearings between the first and third cycle of loading. These values are used in estimating the variability in the bearing properties as discussed in Chapter 7.

The design properties for the bearings at 100% shear strain are shown in Table 3-9. The bi-linear design hysteresis loop is compared to the measured hysteresis loops in Figures 3-66 to 3-68. These figures show that the third loop generally matches the design hysteretic properties well. The properties of bearings A & B and E & F compare particularly well with the design properties,

TABLE 3-9 Design Bi-Linear Properties for Lead Rubber Bearings at 100% Shear Strain

Quantity	Design Value at 100% shear strain
Maximum Displacement (mm)	62
Maximum Force (kN)	20.5
Effective (Secant) Stiffness (kN/mm)	0.33
Characteristic Strength (kN)	10.1
Equivalent Viscous Damping (%)	33.5
Design (post-yield) Stiffness (kN/mm)	0.17
Initial (unloading) Stiffness (kN/mm)	1.88
Yield Displacement (mm)	5.9
Yield Force (kN)	11.0

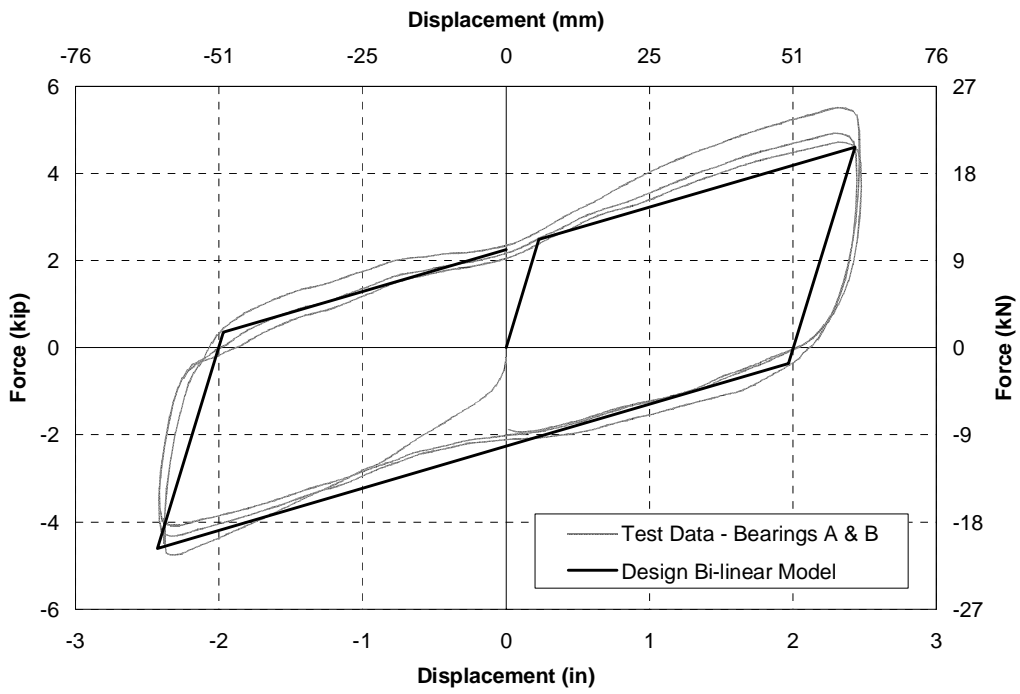


FIGURE 3-66 Hysteresis loops for lead rubber bearings A & B

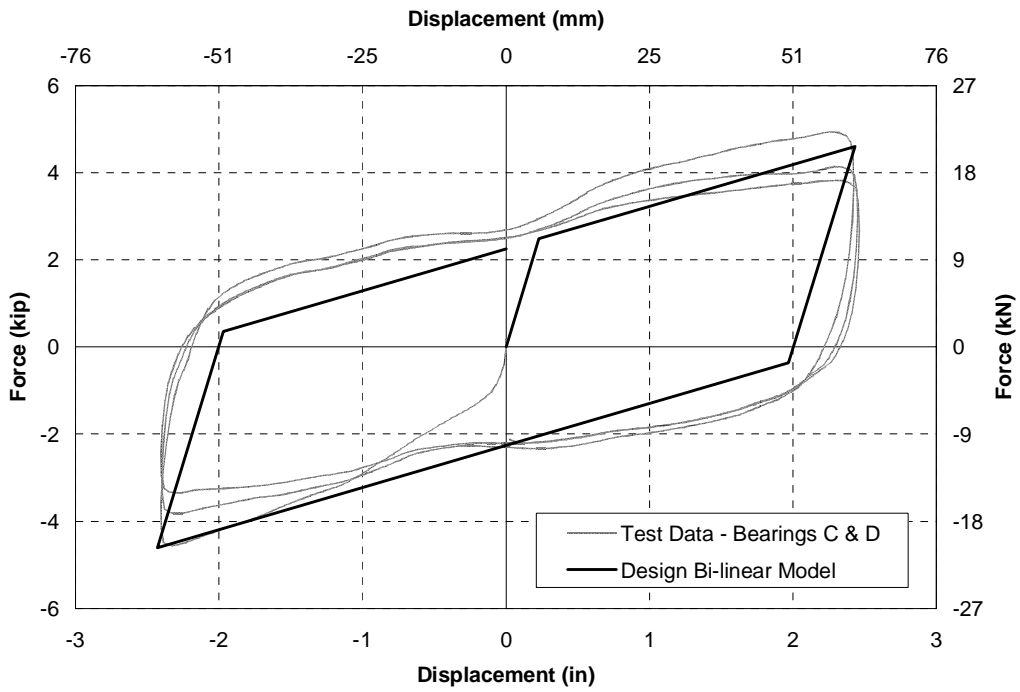


FIGURE 3-67 Hysteresis loops for lead rubber bearings C & D

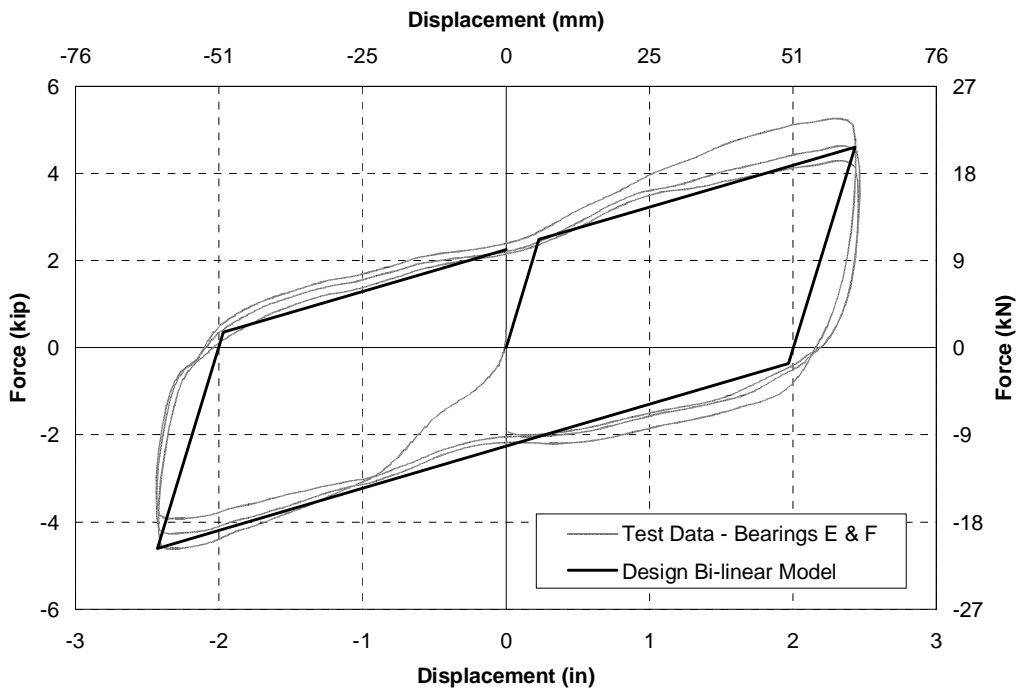


FIGURE 3-68 Hysteresis loops for lead rubber bearings E & F

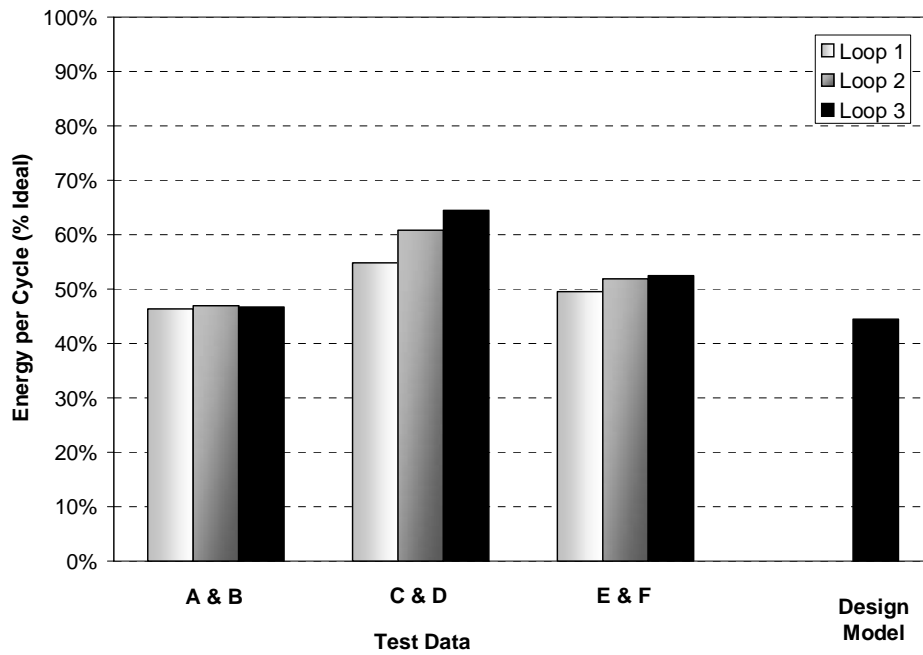


FIGURE 3-69 Energy dissipated per cycle for lead rubber bearings

although the design unloading stiffness is slightly lower than the measured value. Bearings C & D have a marginally lower post-yield stiffness corresponding to a lower rubber stiffness, however this is partially offset by a higher yield force.

3.4.4 Energy Dissipation

The energy dissipated per cycle for the lead rubber bearings is shown in Figure 3-69. It is plotted as a percentage of the rectangular area enclosed by the maximum and minimum forces and displacements for a given cycle. Figure 3-69 shows that from the test data the first cycle for each bearing had the lowest energy dissipation due to the elastic loading portion. The energy dissipated as a percentage of the rectangular area typically increased upon subsequent cycles as the maximum forces reduced and the hysteresis loops flattened out. The bi-linear model for each bearing shows similar amounts of energy dissipation compared to the third loop of the test data, although it is typically conservative by 10% in each case.

3.4.5 Analytical Model

The analytical model for the lead rubber bearings used a bi-linear model identical to the design bi-linear model shown in Figure 3-66. The properties of the analytical model were therefore identical to the design model.

SECTION 4

PERFORMANCE OF THE BRIDGE SUPERSTRUCTURE WITH ELASTIC AND DUCTILE END CROSS FRAMES

4.1 Introduction

The end cross frames in a steel plate girder bridge were determined to be critical in the transverse load path for seismic loading as described in the preceding report (Carden, 2005). Past earthquakes have resulted in damage to the end cross frames and it has become apparent that they need to be specifically designed for transverse earthquake loads. There are essentially two potential approaches to this design. The first is to design the cross frames to perform elastically, protected by capacity design of the substructure. The second approach is to design the cross frames to be ductile and use these ductile elements to protect other parts of the superstructure.

4.2 Deformation of Ends of Bridge Model

The transverse deformation at the ends of the bridge model consisted of displacements from a number of different sources. The deformed shape of the end region due to transverse loading is shown in Figure 4-1 which highlights a number of sources of deformation. The main source was due to twisting of the girders about their longitudinal axes along with bending of the bearing stiffeners which created a relative horizontal drift between the top and bottom flange of the girders. This drift was measured using the diagonal displacement (d_{diag}), which was converted to horizontal component (d_g) by multiplying the displacement by a factor of 1.09 based on the geometry of the end region. This assumes no vertical displacement in the girders. Deformation of the transverse bearing restraints provided an additional source of deformation in the girders. While the bearings were fitted with tight-fit shims between the restraints and sole plate, some deformation was inevitable. During shake table experiments the transverse bearing displacement was measured relative to the displacements in the shake tables, indicated in Figure 4-1 as d_1 and d_2 . It was possible that d_1 was different to d_2 due to differences in the transverse bearing restraints and slippage in the connection of the bottom chord allowing different relative girder translations. There was also inevitably some relative deformation between the top flange of the girders and the deck slab (d_3) due to slippage in the connections connecting the top chord to the deck slab and bearing stiffeners, and removal of shear studs. This deformation was not measured directly during experiments on the bridge model, but with standard hole sizes and allowing for some deformation in the hole, it could be expected to be around 3 mm. The overall displacement was measured at deck slab level (d_{dk}), given relative to the shake table displacement.

Other possible deformations which may have affected the measurement of the transverse end displacement in the bridge model were due to rotations and vertical distortion of the end region. If the superstructure had rotated as a rigid body due to axial deformations of the bearings, the displacement measured at the deck slab would be amplified even though there is no deformation in the girders and end cross frames, as illustrated in Figure 4-2. In contrast, if the end region had distorted due to relative vertical displacements of the ends of the girders, then the diagonal displacement measured would have been reduced indicating a smaller transverse displacement in the girders than actually observed (Fig. 4-3). These rigid body rotation and distortion modes were not expected to be significant and consequently were not measured in the bridge model.

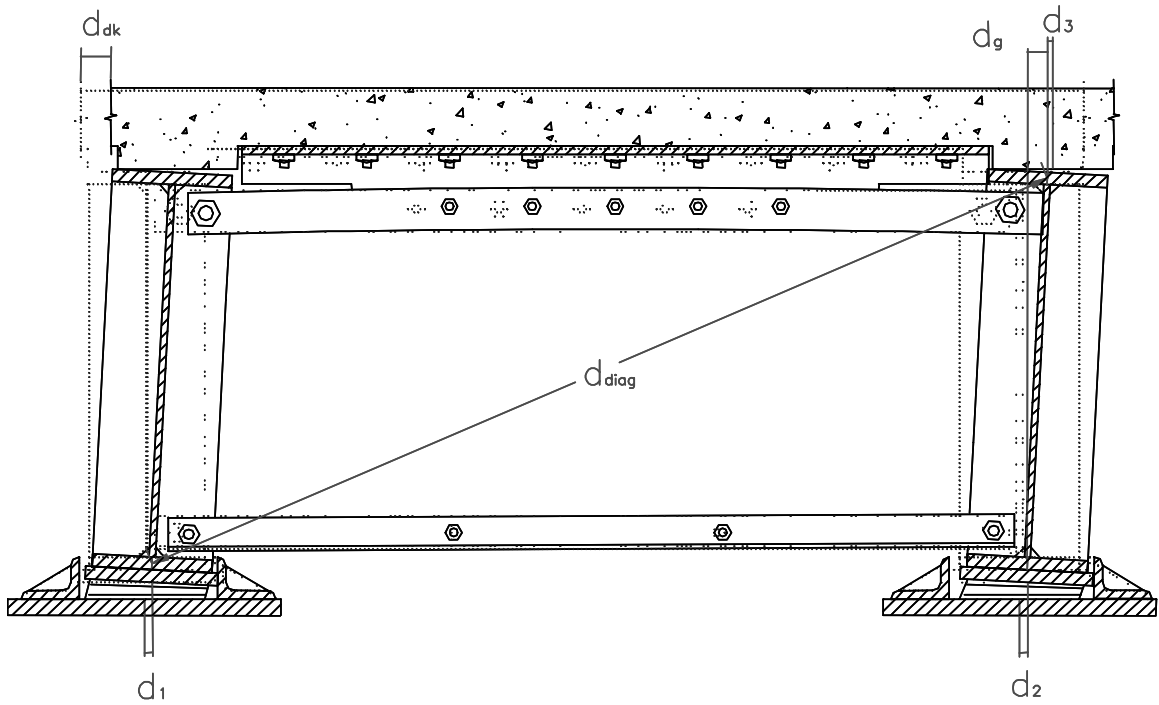


FIGURE 4-1 Deformed end region for bridge model due to lateral shear with rotation of the girders about their vertical longitudinal axes

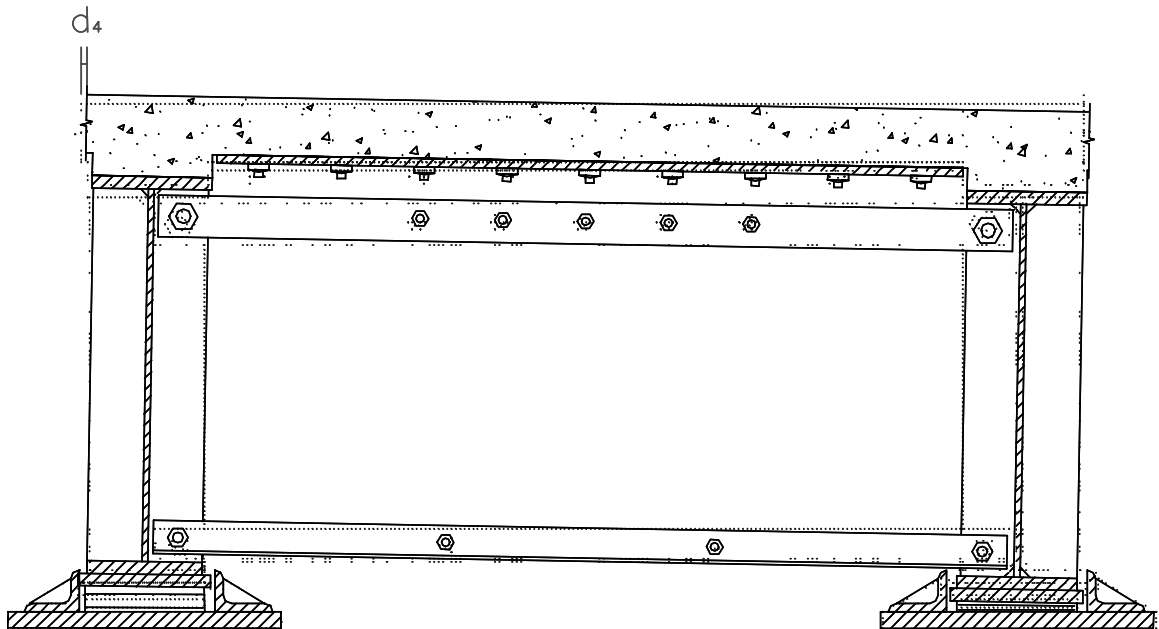


FIGURE 4-2 Deformed end region for bridge model due to lateral shear assuming rotation of the entire section with axial deformations in bearings

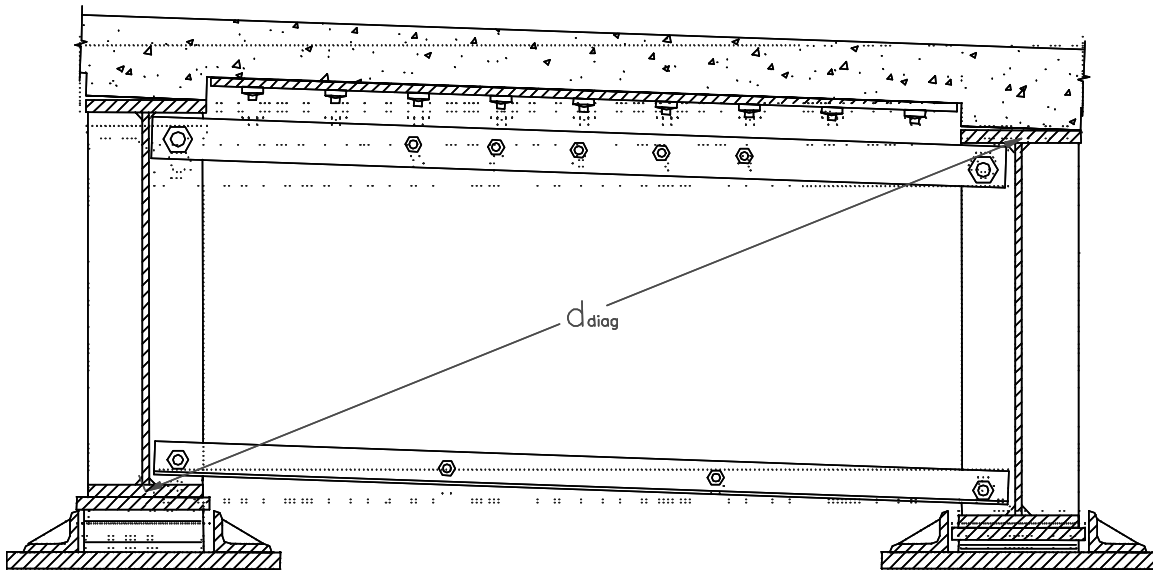


FIGURE 4-3 Deformed end region for bridge model resulting in distortion of section with axial deformations in bearings

Displacements were also measured in the ductile components of the end cross frames (Figs. 2-32 and 2-33). These were compared to the other displacements, depending on the geometry of the end regions.

4.3 Results from Reversed Static Experiments

4.3.1 Background

The heavy single angle end cross frames were expected to perform essentially elastically, as outlined in Chapter 2. The heavy X-braces are illustrated in Figures 2-9 and 2-10. In contrast the light X-braces (Fig 2-12) were designed to yield allowing a ductile response and limiting forces transferred into the substructure.

4.3.2 Experiment RSHXB1 - Elastic Heavy Single Angle X-Braces - Preliminary

The displacements in the diagonals of the end cross frames were shown to be very small, as illustrated in Figures 4-4 and 4-5, indicating that the end cross frames behaved essentially elastically. If any non-linearity had occurred in the cross frames it was due to slippage of the connections, however, there were no instruments in this first experiment to record the overall end cross frame deformations, hence any slippage was not measured. The end shear forces were also not measured during this experiment therefore displacements were plotted against total actuator force.

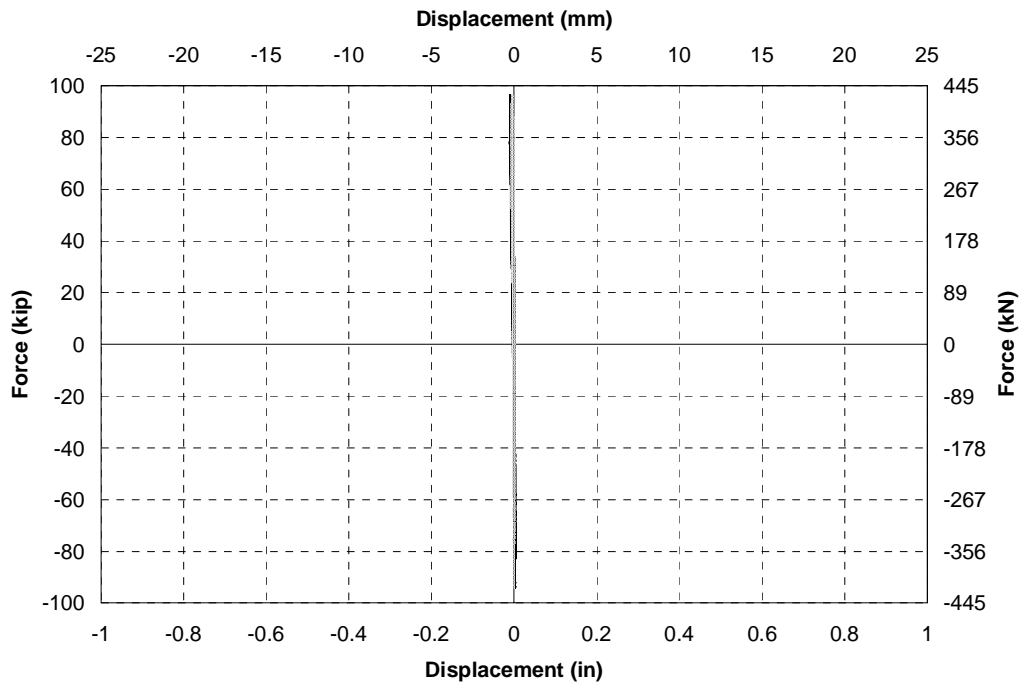


FIGURE 4-4 RSHXB1 - Hysteresis loop for diagonals of north end cross frames (all cycles)

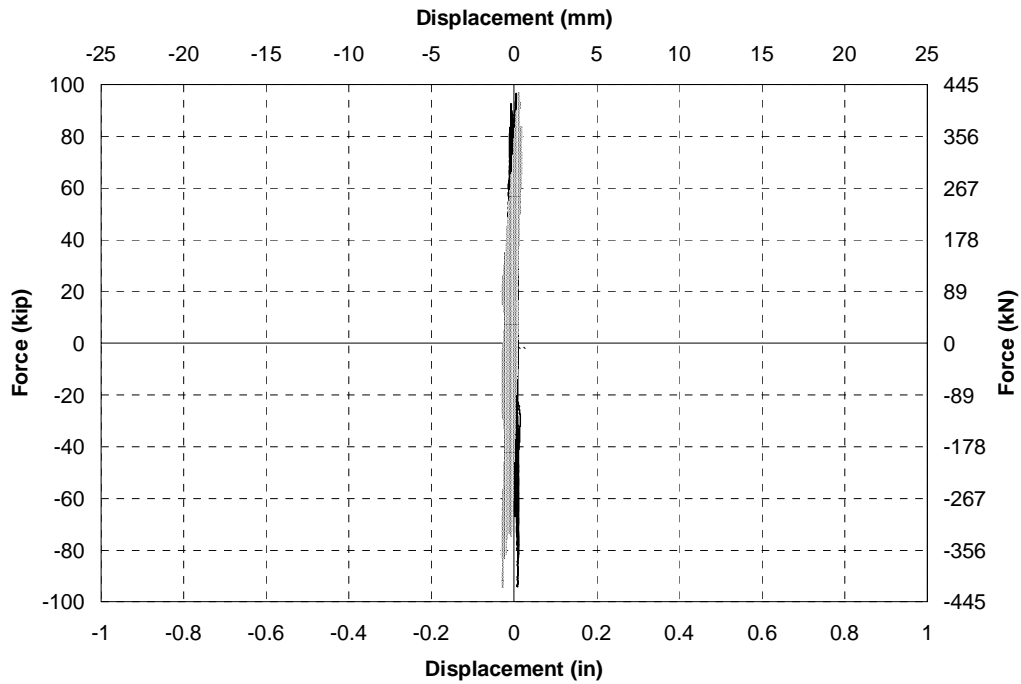


FIGURE 4-5 RSHXB1 - Hysteresis loop for diagonals of south end cross frames (all cycles)

4.3.3 Experiment RSHXB2 - Essentially Elastic Heavy Single Angle X-Braces

4.3.3.1 Hysteretic Behavior

RSHXB2 was essentially a continuation of the first experiment with some modifications. Load cells were placed under the bearings so that the forces at each end of the bridge could be monitored. A displacement transducer was added to measure the diagonal displacement in the end region as shown in Figures 2-12 and 4-1. The loading was also applied with equal forces in each actuator as described in Chapter 2. The shear studs that failed during RSHXB1 were replaced by removing concrete locally around the old studs, welding new studs to the girders, then grouting these into the deck slab.

The force-displacement traces for the actuators in RSHXB2 are shown in Figure 4-6. The force-displacement characteristics for each actuator are very similar and have better consistency between the shape of the hysteresis loops than observed in the RSHXB1. The loops exhibit some pinching particularly at higher levels of loading attributed to the behavior observed in the end cross frames. The horizontal transverse end displacements measured at the deck were plotted against the transverse shear forces measured in the load cells beneath the bearings in Figure 4-7. The pinched nature of the hysteresis in the cross frames is evident in this figure. This deformation can be attributed to slippage in the connections, slippage between the girders and deck slab, deformation in the bearings and the onset of buckling in the diagonal X-braces. The horizontal displacements measured between the top and bottom flange of the girders are shown in Figure 4-8. Compared to Figure 4-7 there is a 5 to 7 mm deformation, attributed to deformation between the girder and deck slab, and also the bearings. Figures 4-9 and 4-10 show the diagonal angle deformations versus end shears measured in the load cells at the north and south ends respectively. These indicate the onset of buckling in the north end cross frames at the completion of the experiment, although at the south end, the diagonal members were essentially elastic. Even at the north end, where buckling was observed, the deformations in the diagonals were only around 15% of the total deformation in the end region. Accordingly, it was apparent that the majority of deformation and hysteresis in the end region was due to slippage in the connections. Slippage was expected as the connections were not slip critical during transverse seismic loads.

4.3.4 Experiment RSLXB - Light Single Angle X-Braces

4.3.4.1 Overview

The transverse cyclic behavior of the light single angle X-braces was studied in RSLXB. These cross frames are illustrated in Figure 2-12. The single angle diagonals were welded directly to the bearing stiffeners which eliminated the slippage observed in RSHXB2. The cross frames also had pinned top and bottom chords in order to allow maximum load transfer and fully utilize inelastic behavior in the diagonal members, as described in Chapter 2.

The force-displacement trace for the actuators during this experiment is shown in Figure 4-11. This figure shows that the maximum actuator displacements were comparable to those in RSHXB2. The force-displacement traces for the two ends of the bridge, with displacements measured at deck slab level, are shown in Figure 4-12. In this experiment considerable inelastic behavior was observed in the end cross frames. The north end exhibited smaller forces and larger

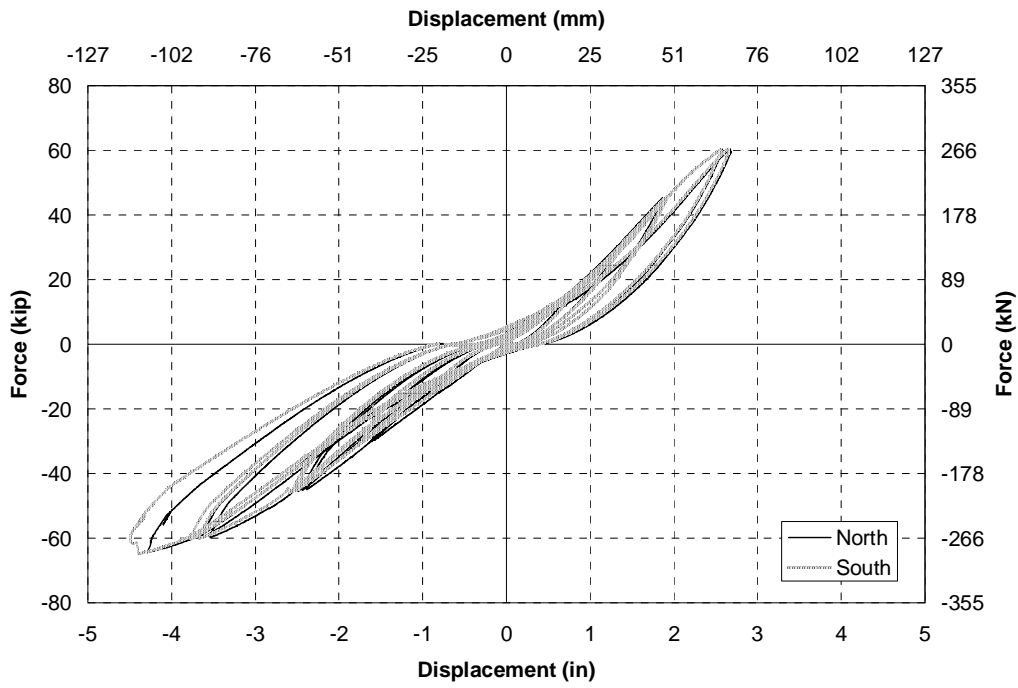


FIGURE 4-6 RSHXB2 - Hysteresis loops for actuators

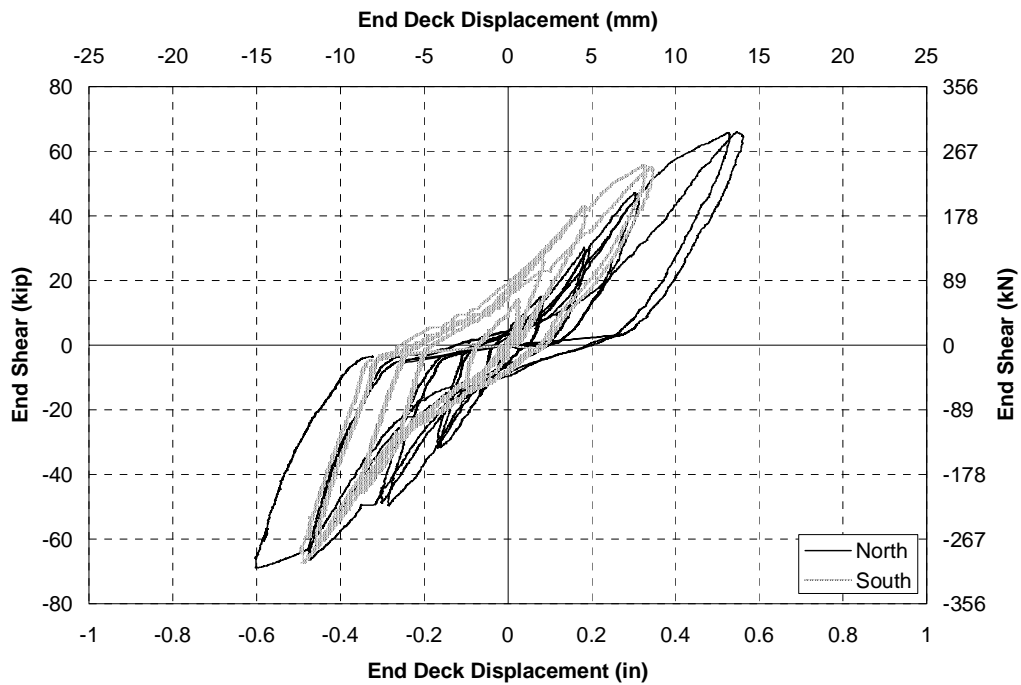


FIGURE 4-7 RSHXB2 - Load cell end shear force vs horizontal displacement measured at deck slab level for each end

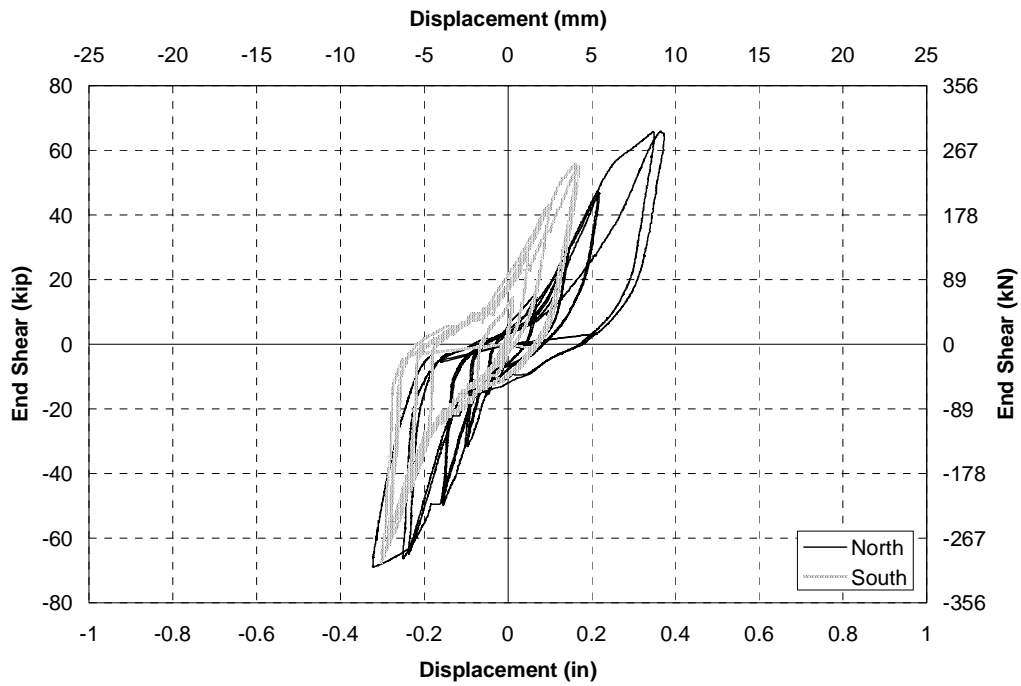


FIGURE 4-8 RSHXB2 - Load cell end shear force vs horizontal displacement measured using the diagonal displ.transducer between the top and bottom girder flanges at each end

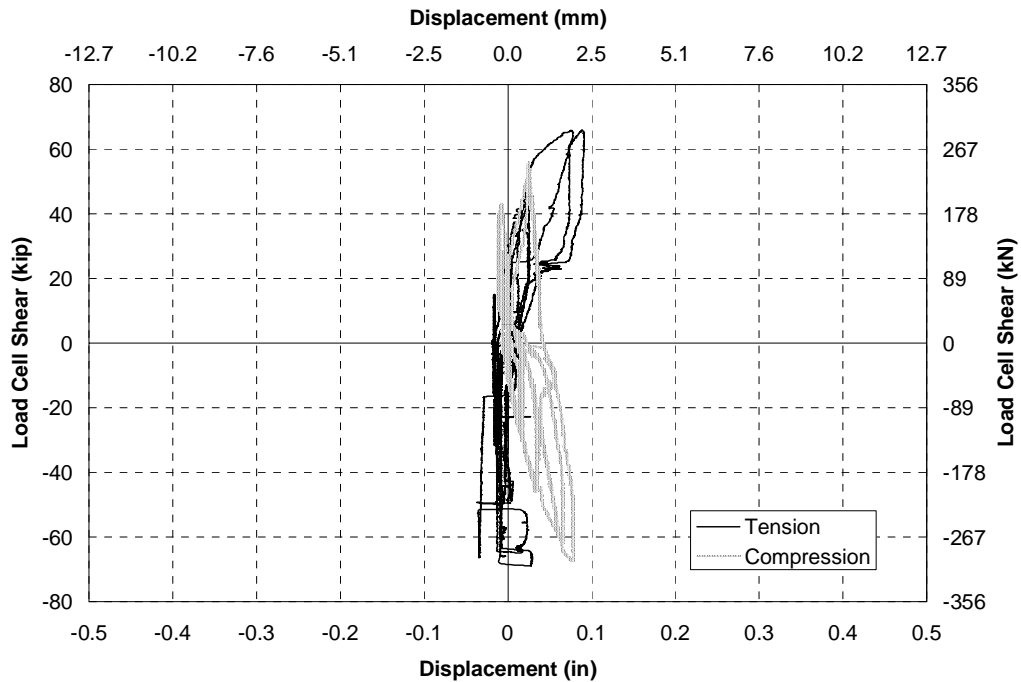


FIGURE 4-9 RSHXB2 - Load cell end shear force vs displacement in end cross frame diagonals at north end

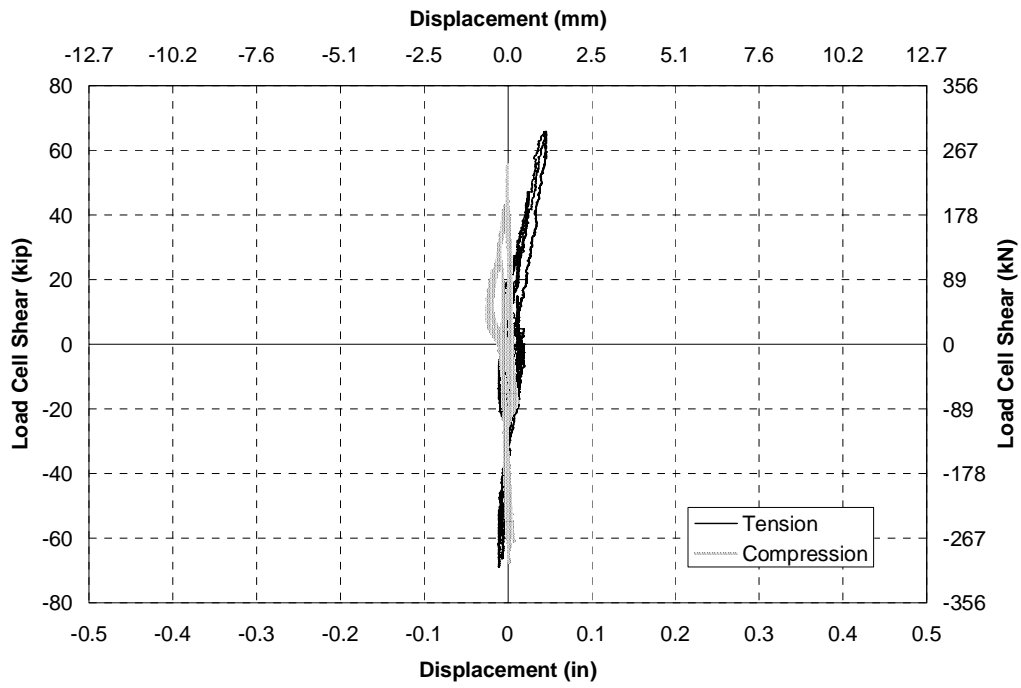


FIGURE 4-10 RSHXB2 - Load cell end shear force vs displacement in end cross frame diagonals at south end

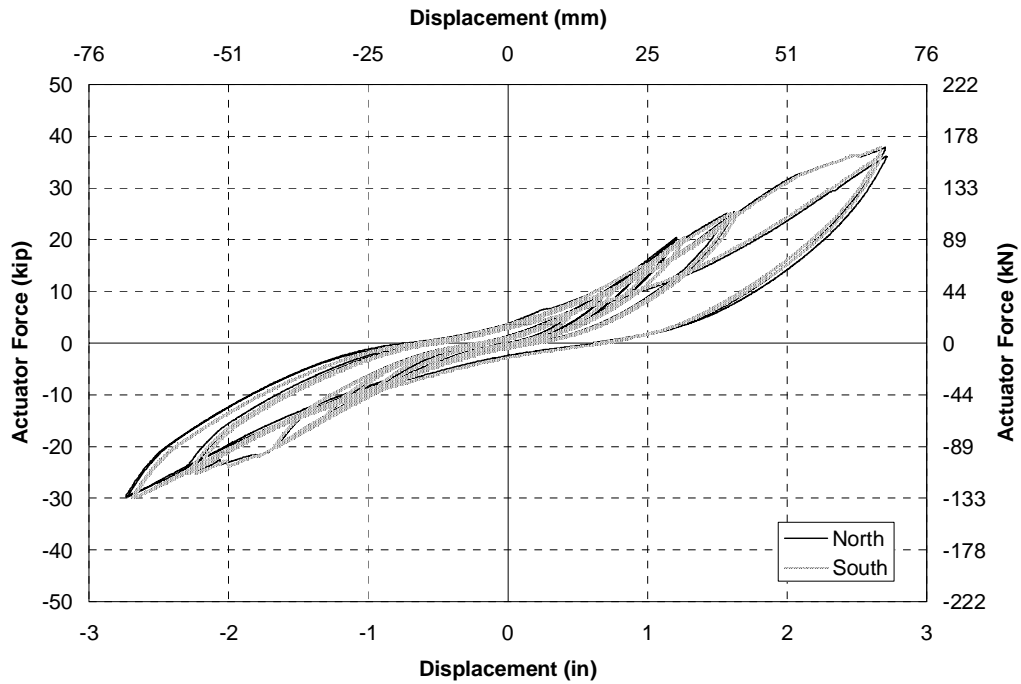


FIGURE 4-11 RSLXB - Actuator hysteresis loops

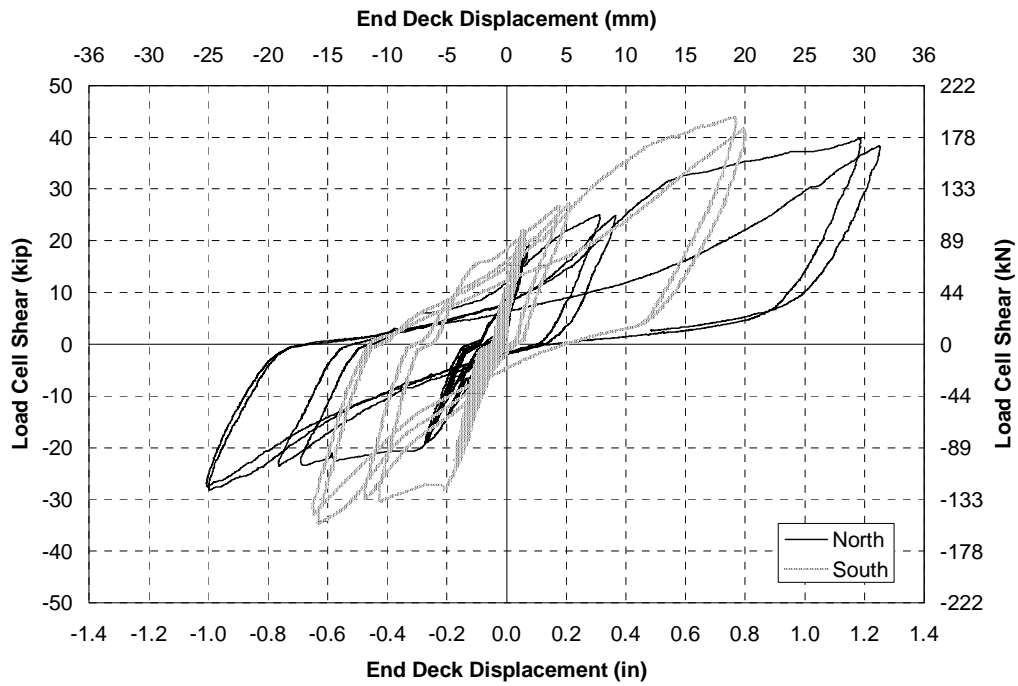


FIGURE 4-12 RSLXB - Load cell end shear force vs horizontal deck slab displacement at both ends

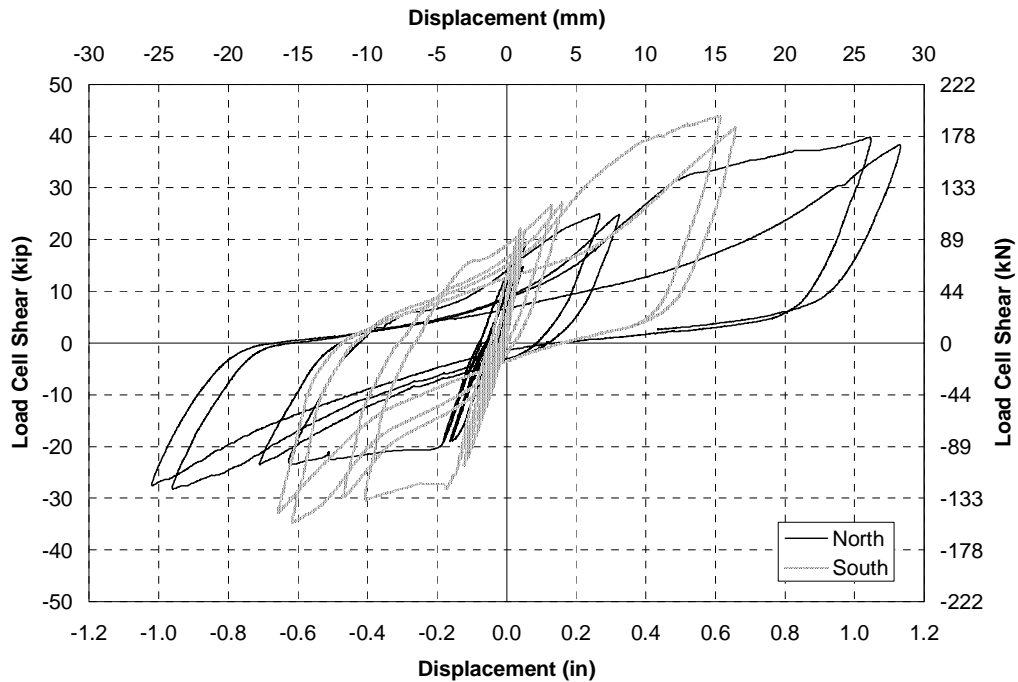


FIGURE 4-13 RSLXB - Load cell end shear force vs horizontal displacement measured between the top and bottom flanges of the girders at both ends

displacements than the south end, which is attributed to variability in the combination of tension and compression strengths, and also due to cracking around the shear studs allowing greater flexibility at this end.

Figure 4-12 demonstrates degradation in stiffness of the cross frames with consecutive cycles. At the end of these cycles pinching is observed in the hysteresis loops, which was caused by the buckled diagonal members from a previous compression cycle straightening as a result of tension. While they were straightening, their stiffness was comparatively low but once straightened their stiffness increased. The plastic tensile deformations were largely unrecoverable and thus the member elongated with successive cycles. This behavior was not ideal as the ability for the cross frame to dissipate energy is reduced, however; the X-braces are shown to have relatively “full” hysteresis loops in the first excursion up to a given displacement. During a typical earthquake, which has a maximum acceleration early in the loading history, the cross frames can be expected to perform well.

The transverse end deformations measured between the girders’ top and bottom flanges for each end of the bridge are shown in Figure 4-13. Compared to Figure 4-12 maximum end displacements measured at deck slab level are shown to be around 3 mm. larger than those measured between the top and bottom flanges. As with the heavy X-braces the difference was attributed to slippage between the deck slab and the girders and also deformations allowed by the lateral bearing restraints. For the light X-braces the difference between the deck slab end displacements and those measured between the top and bottom flanges was reduced and became small compared to the magnitude of the end cross frame displacements.

4.3.4.2 Yield Forces

Figure 4-13 shows that there was a large variability in the yield forces of the cross frames between the two ends of the bridge model. The yield force at the north end was 92 kN, much lower than at the south end, with a yield force of 121 kN. These were measured at the yield point in the first plastic cycle in the end cross frames. The difference in forces between the two ends was attributed to variation in the properties of the diagonal members, particularly the buckling strength. The buckling strength was likely to vary due to initial imperfections in the straightness of the members and angle properties, which could have been affected by prior cycles of loading. The difference between the two ends was also attributed to the combination of the buckling strength with the maximum tensile forces in the corresponding diagonals, with the combination of properties depended on how much degradation had occurred in the compression diagonal when the maximum tension force was reached. Different girder stiffness at the two ends also affected the yield force due to different levels of shear stud damage.

Based on the coupon tests to define the material strength, the original expected yield force for the X-braces was 113 kN, as described in Chapter 2. If the effect of girder stiffness, at an assumed yield displacement of 3.8 mm, and hysteresis in the top and bottom chords are considered (with effects as described in Chapter 4, with a transverse girder stiffness of 1.66 kN/mm and 2.17 kN/mm per girder at the north and south ends respectively and an additional yield force of 10 kN to allow for the hysteretic behavior of the top and bottom chords), then the expected yield strengths would be approximately 130 kN and 135 kN at the north and south ends respectively. These

calculated strengths are to be higher than the measured strengths at each end. Investigation of the end region using a frame analysis, showed that the eccentricity between line of action for the diagonals and the centers of the top and bottom flanges of the girder resulted in shear forces and bending moments in the stiffeners and forces in the diagonals. These diagonal forces were larger than those calculated based on the angle of the brace alone. Based on the frame analysis the end shear was 65% of the forces in the diagonals, compared to 95% assumed based on the angle of the braces in Chapter 2. This means that the yield strength shear strength of the end will be lower than that previously estimated and resulted in an expected shear strength in the diagonals, based on the measured coupon strength, of 75 kN. When the effects of girder stiffness and hysteresis in the top and bottom chords are added the strengths would be 97 kN and 100 kN respectively. These are closer to the measured strengths with some variation attributed to the aforementioned factors.

4.3.4.3 Post-Yield Forces

A concern with the use of concentric braced frames such as these single angle cross frames is their strength degradation due to buckling. Component experiments showed that after the single angles buckled the compression strength of members was reduced. However when the tension and compression members were combined in X-braces, the envelopes of Figure 4-12 show an increasing post elastic slope. This is because as the compression member lost strength, strain hardening in the tension member along with the forces resulting from the other components such as the girders, bearings and shear studs resulted in a positive post-yield slope.

At the north end of the bridge model the maximum force of 177 kN was 1.9 times higher than the yield force at this end. The maximum force at the south end of the bridge was 195 kN and was 1.6 times higher than the yield force. If the force from the calculated girder stiffness subtracted from the maximum force then for the single angle diagonals alone, the maximum estimated force at the north end was 99 kN, or 1.1 times larger than the yield force. At the south end the maximum estimated force in the diagonals was 129 kN, also 1.1 times the yield force. Therefore almost all of the post-yield strength increase is attributed to the girder stiffness. The result of interaction between the tension and compression diagonals was a comparatively low post yield stiffness compared to that expected from other systems yielding in shear or flexure. In this respect, single angle X-braces are an attractive system for use as ductile end cross frames as post-yield increase in force is minimized allowing the braces to act as effective shear force limiting “fuses” in the transverse response of a bridge.

4.3.4.4 Maximum Displacements

If fracture was to occur in the tension member of a cross frame, there would be considerable strength degradation and displacements would be likely to become unstable, therefore the connections should be designed and displacements limited so that fracture is avoided. The maximum transverse displacement in the end cross frames using the deck slab displacement was 32 mm. Based on a girder height of 591 mm. from the center of the top flange to the centre of the bottom flange, this corresponds to a drift of 5.3%. From the geometry of the system the displacement in the diagonal single angle members was equivalent to 65% of the horizontal displacement at the top flange. This transformation is based not only on the angle of the diagonal braces but also the difference between the height of the girders and the relative height of the lines of action for the X-brace diagonals. Based on this transformation, the equivalent maximum displacement in the cross frames would be 21 mm. The displacements in the individual diagonal

members were plotted against the end shear in Figures 4-14 and 4-15. The maximum measured diagonal displacement was 20mm and therefore was close to that expected based on the geometry of the system. This corresponds to a average axial strain of 1.6% which is around 40% of the proposed design limit of 4%, based on component experiments. At this level of displacements no fracture had occurred in the cross frames, as would be expected given that the strains were much lower than the design strains. If the allowable strains based on component experiments were reached in the cross frames, then the design drift in the end cross frames would be as high as 13%.

For the systems previously used including the SPS, EBF and TADAS systems (Zahrai, 1998a) the ultimate drifts were approximately 3.0%, 3.0% and 3.8% respectively. Therefore using a similar assumption as for the single angles where the design drift is 67% of the ultimate drift, the design drift for the three systems would be 2.0%, 2.0% and 2.5% respectively. Thus, the displacement capacity in the X-braces is significantly higher than for any of these other systems. The design displacement for the X-braces is likely to be governed by girder drift limits rather than limits in the braces themselves assuming the angles are designed with appropriate connections (Chapter 3). The bridge model was not subjected to larger displacements to prevent potential damage to the deck slab of the bridge model so that it could be used for later experiments.

As the displacements in the X-braces were much less than the design limit, the X-braces could have been designed for a lower shear to allow larger displacements, up to the drift limit of the girders. This was not possible in the bridge model as the section sizes were the smallest available, although, this could be achieved in a full scale bridge and is considered in Chapter 6.

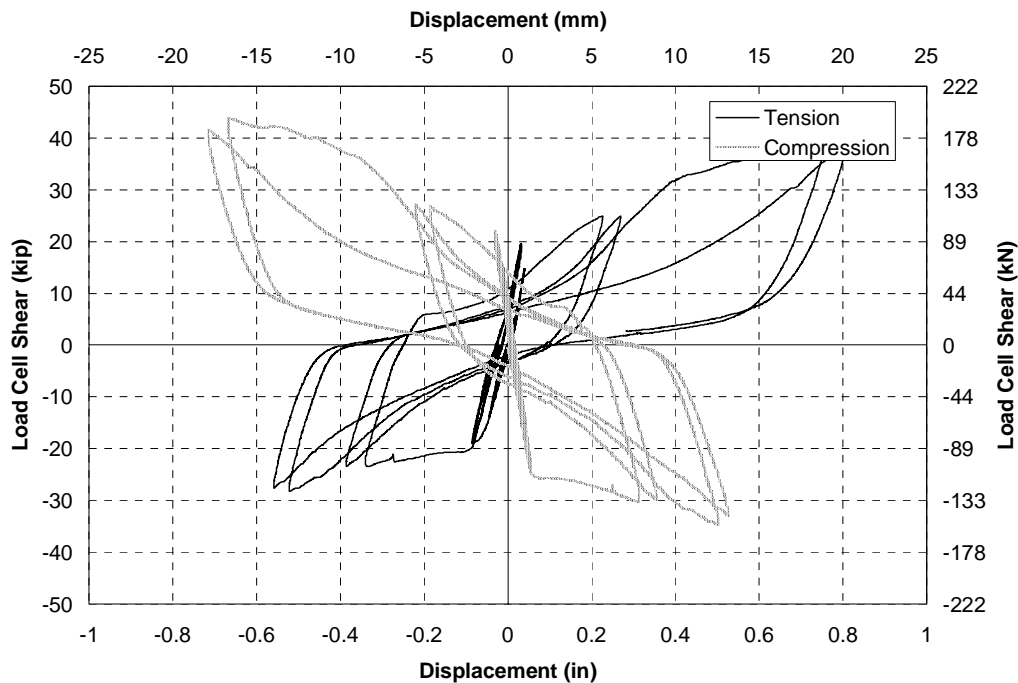


FIGURE 4-14 RSLXB - Hysteresis loop for diagonal angles of north end cross frames

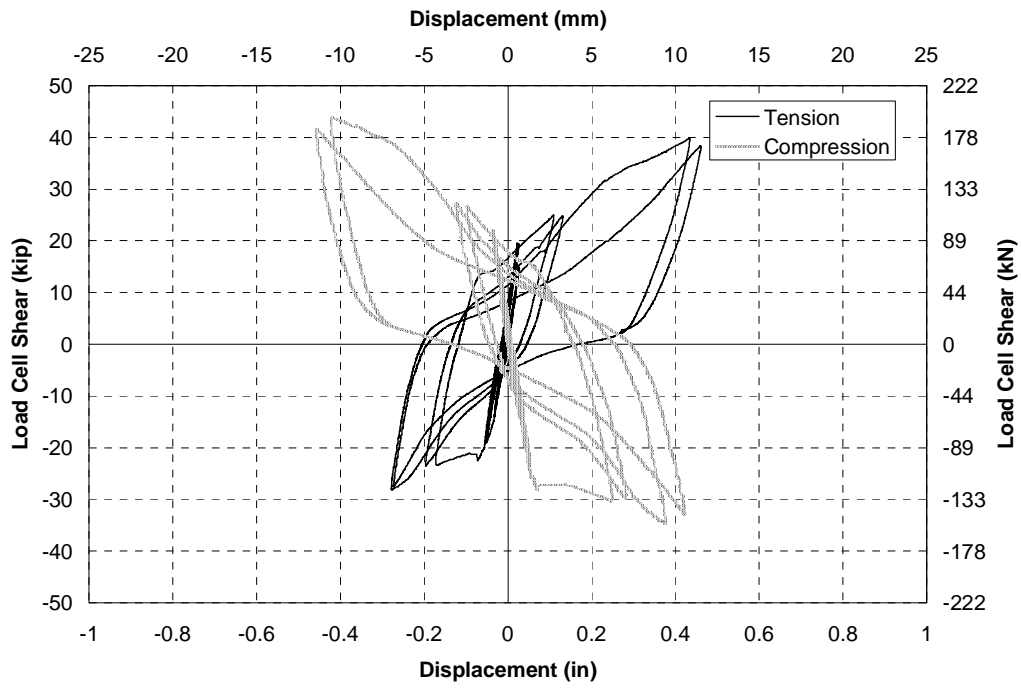


FIGURE 4-15 RSLXB - Hysteresis loop for diagonal angles of south end cross frames

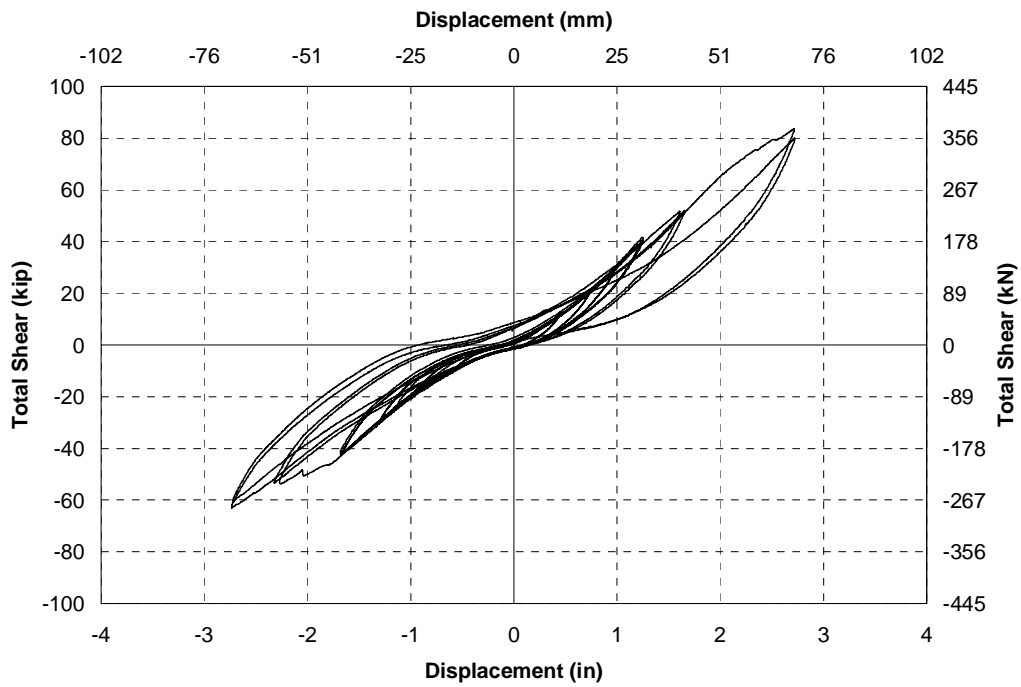


FIGURE 4-16 RSLXB - Midspan displacement

The midspan deck slab displacement was plotted against total base shear measured in the load cells as shown in Figure 4-16. The midspan displacements are shown to be much larger than the end displacements due to flexural torsional deformations in the superstructure. The hysteresis loops are also quite different to the shape of those for the ends of the bridge, indicating that energy dissipated at the ends has only limited effectiveness in the overall response of a bridge when the superstructure is flexible. This is not necessarily limited to ductile end cross frames and can also be expected with ductile columns. The effect of superstructure flexibility is investigated further in Chapter 6.

4.4 Results from Shake Table Experiments

4.4.1 Experiment STHXB - Elastic Heavy Single Angle X-Braces

4.4.1.1 Response to El Centro

Like for the reversed static experiments, the shake table experiments allowed the study of the backbone curve which describes the capacity of the different ductile end cross frames. However, shake table experiments went a step further as they also gave a measure of the force and displacement demand in response to different earthquake excitations.

The configuration of the bridge model with heavy cross frames used in shake table experiments is shown in Figure 2-11. The configuration of the cross frames was different to those in the static experiments in that they were welded directly to the web stiffener instead of the bolted gusset plate connections. The north-south component of El Centro was applied to the model with increasing amplitudes up to an amplitude of 2.0 times the recorded level. Figures 4-17 and 4-18 show that there were relatively small displacements at the ends of the bridge, measured at the level of the deck slab. The force-displacement relationship was not quite linear with some pinching observed, much of which can be attributed to deformations in the bearings, as observed when comparing Figures 4-17 and 4-18 with Figures 4-19 and 4-20. These latter figures show the deck slab displacement relative to the average measured bearing displacement. When the bearing displacement was removed the response is more linear. The horizontal component of the diagonal displacement measured between the top and bottom flanges of the girder is shown in Figures 4-21 and 4-22. This response is also essentially elastic, and the displacements appear to be very similar to those measured at the deck slab relative to the bearings. This indicates that the displacements due to slippage between the girders and the deck slab and other immeasurable types of deformation described earlier, appear to be small. The welded connections exhibited no slippage in the connections and a higher effective stiffness than with the bolted connections during reversed static experiments enabling good contrast between elastic cross frames and ductile cross frames.

The maximum end shear forces in response to 2.0 x El Centro were 232 kN and 199 kN at the north and south ends respectively. This corresponds to a 14% difference between the two ends. The effective stiffnesses at the two ends were similar.

4.4.1.2 Response to Sylmar and Kobe

Experiments were performed to measure the transverse responses to 1.0 x Sylmar and 0.75 x Kobe. The force-displacement relationship at the ends of the bridge in response to these earthquakes was again essentially elastic. The maximum force at the ends in response to 1.0 x

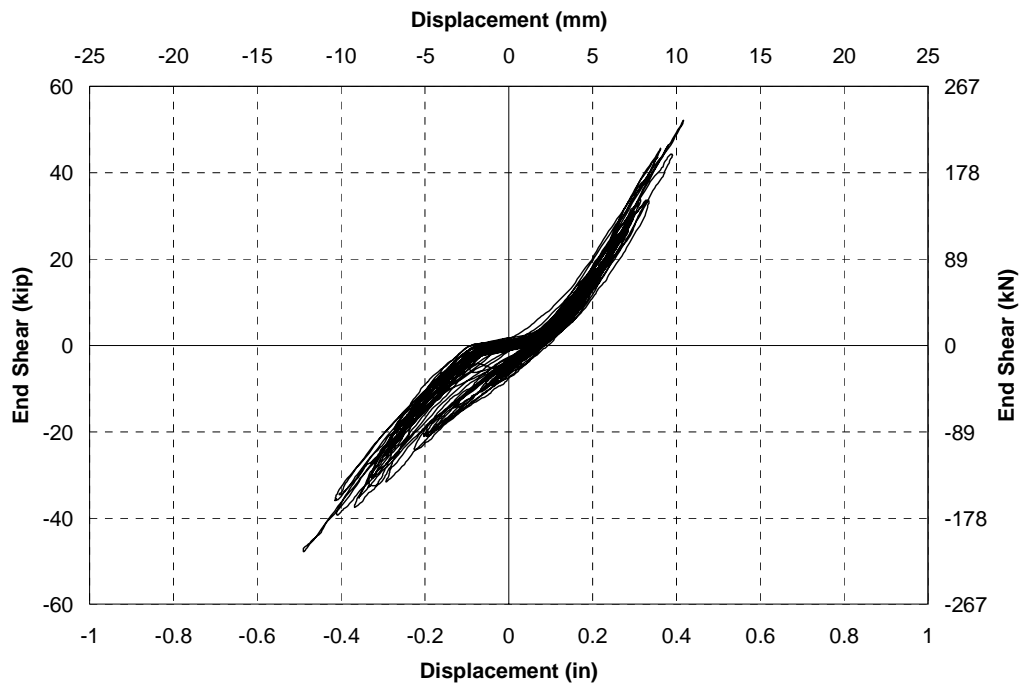


FIGURE 4-17 STHXB - North end shear vs end horizontal displacement at deck slab in response to 2.0 El Centro

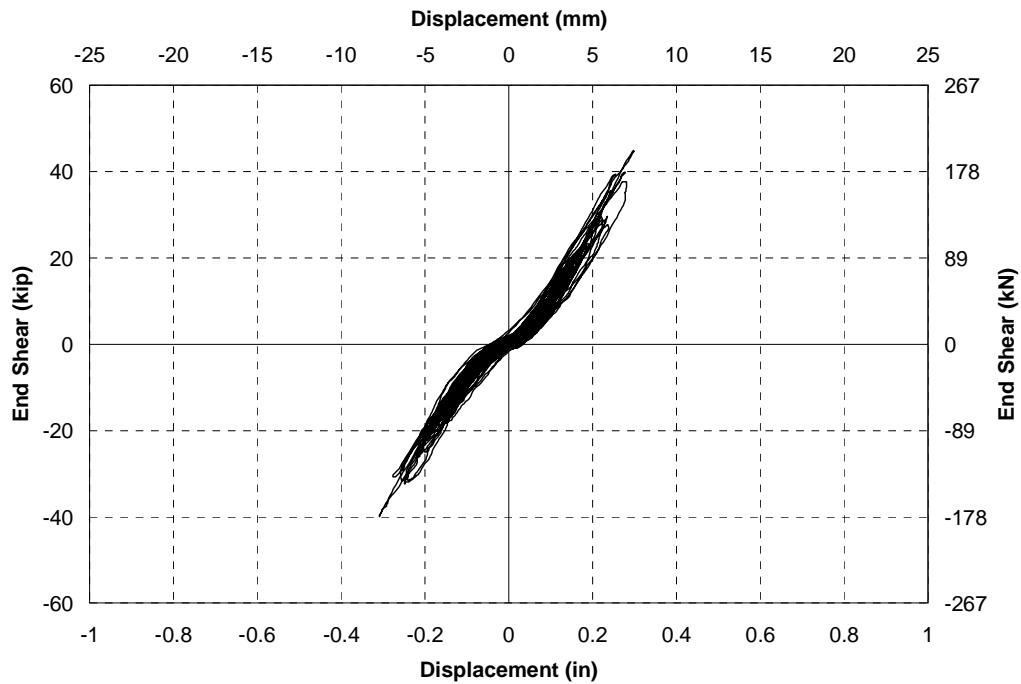


FIGURE 4-18 STHXB - South end shear vs end horizontal displacement at deck slab in response to 2.0 El Centro

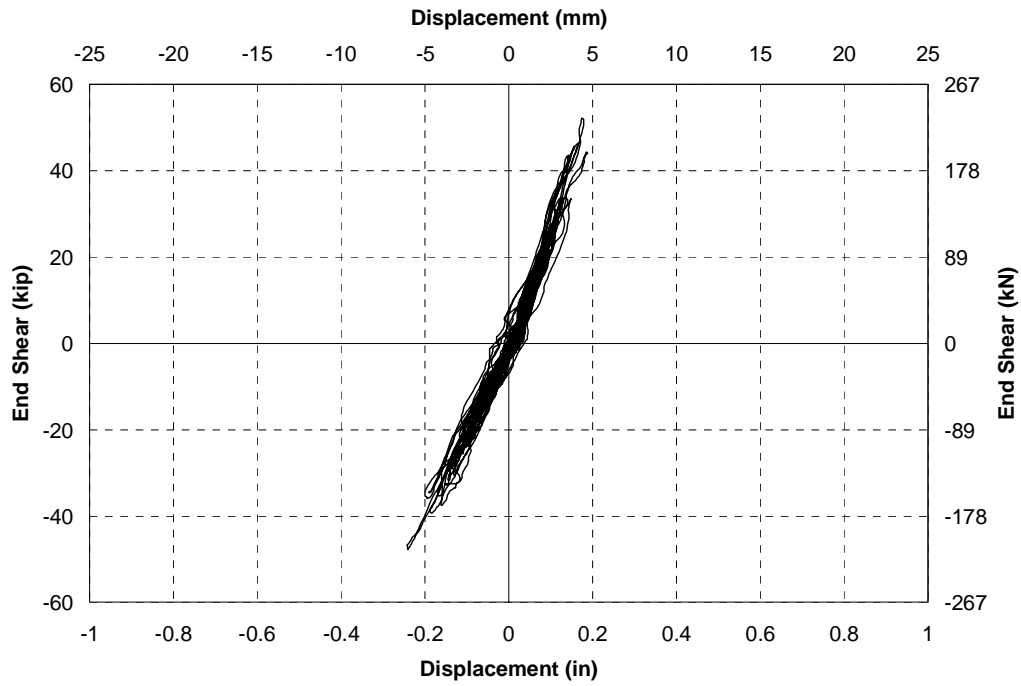


FIGURE 4-19 STHXB - North end shear vs end horizontal displacement of deck slab relative to average bearing displacement in response to 2.0 El Centro

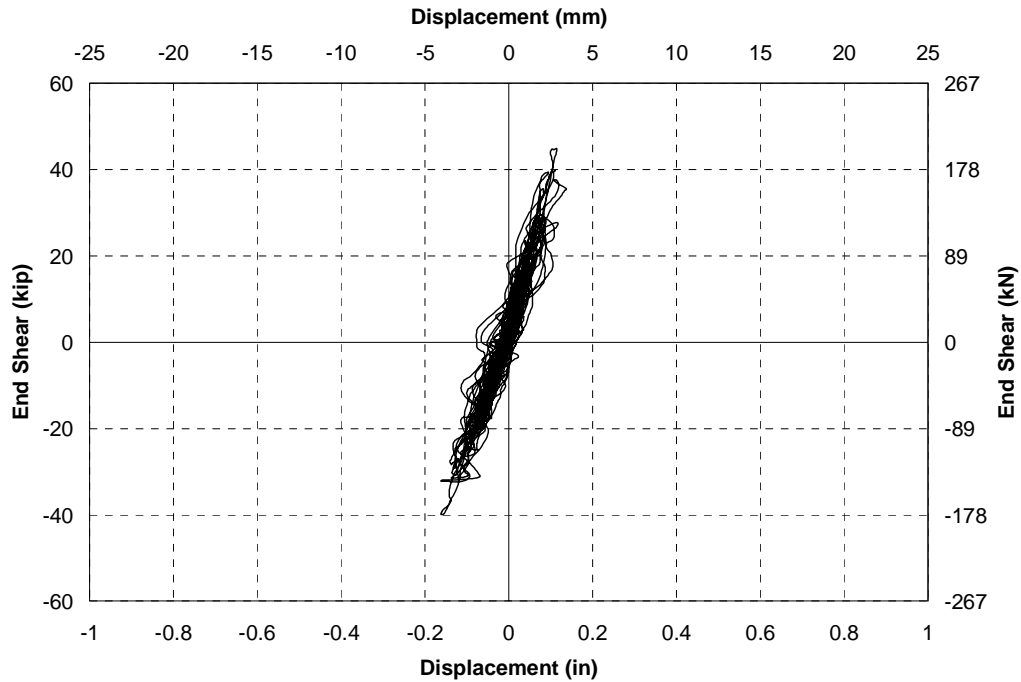


FIGURE 4-20 STHXB - South end shear vs end horizontal displacement of deck slab relative to average bearing displacement in response to 2.0 El Centro

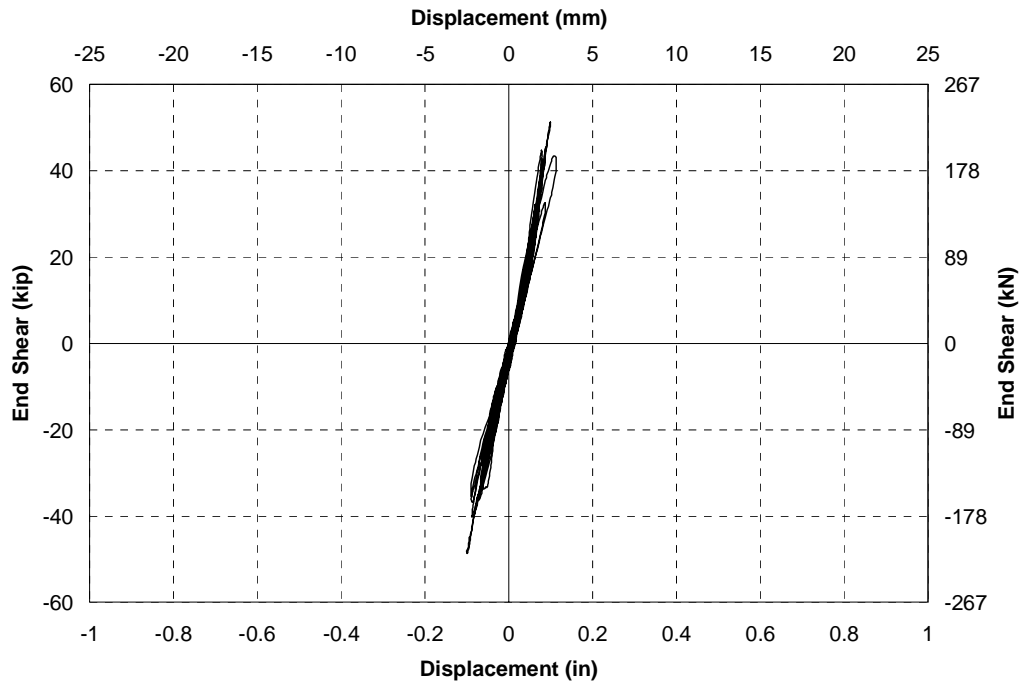


FIGURE 4-21 STHXB - North end shear vs end horizontal displacement between top and bottom flanges in response to 2.0 El Centro

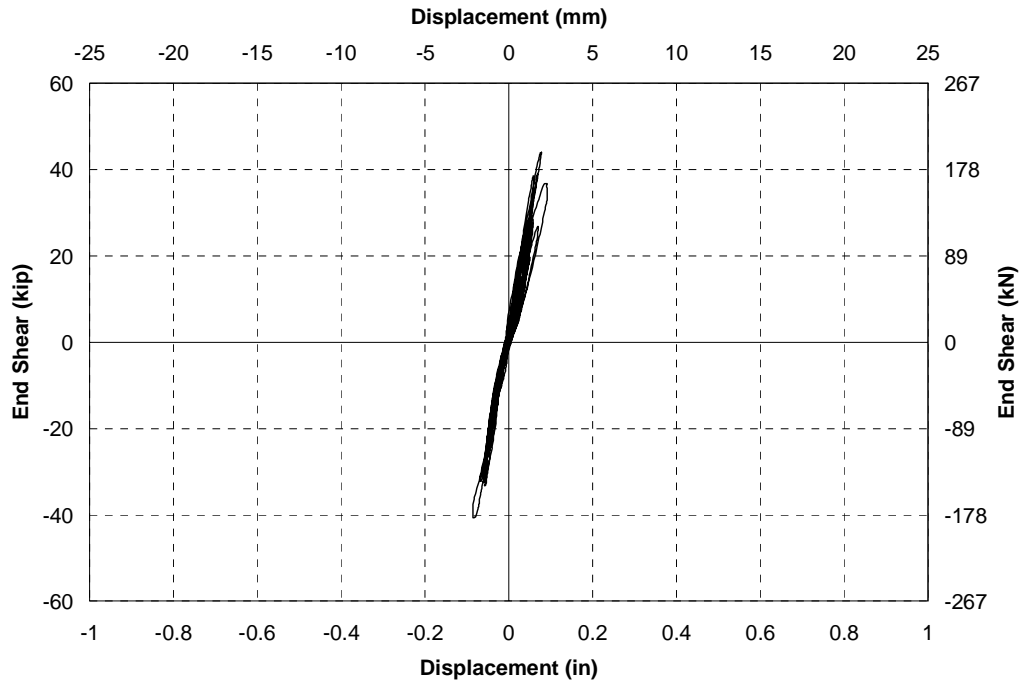


FIGURE 4-22 STHXB - South end shear vs end horizontal displacement between top and bottom flanges in response to 2.0 El Centro

Sylmar was equal to 241 and 225 kN at the north and south end respectively. In response to 0.75 x Kobe the maximum shear force at each end was 234 and 224 kN respectively. Assuming a linear amplification of response, which was reasonable for this elastic system, the maximum forces in response to 1.0 x Kobe would have been 313 and 298 kN respectively. Because these forces were in excess of the design capacity of the cross frames, 1.0 x Kobe was not simulated.

4.4.2 Experiment STLXB - Inelastic Light Single Angle X-Braces

4.4.2.1 Overall Response

A series of experiments was performed with the bridge model in a simply supported configuration with light single angle X-braces as illustrated in Figure 2-12. The north-south component of El Centro was applied to the model with increasing amplitude up to an amplitude of 2.0 times the recorded level.

The transverse shear forces measured at each end of the bridge are plotted against the horizontal component of the end deck slab displacements relative to the average bearing displacement, as shown in Figures 4-23 and 4-24. These figures show that the envelopes for the hysteretic behavior at the ends were almost ideally elasto-plastic, as shown in Figure 4-25. There was less post-yield stiffness observed in these envelopes than those from the reversed static experiments as the lead rubber bearings had a lower rotational stiffness than the elastomeric pads used in the reversed static experiments.

Figures 4-26 and 4-27 show the hysteretic response for 2.0 x El Centro only. When compared to Figures 4-23 and 4-24, the ends show some degradation in stiffness due to previous excitations of the bridge model. This degradation can be considered a trade-off for the essentially elasto-plastic envelope.

The displacements measured at the deck slab level, including bearing deformations, were around 3 to 5 mm larger than those measured between the top and bottom flanges of the girders (Figs. 4-28 and 4-29). This level of bearing displacement was consistent with previous experiments. The horizontal component of displacement measured between the top and bottom flange of the girders is shown for each end in Figures 4-30 and 4-31. The resulting displacements were similar to those measured using the deck slab displacement relative to the average bearing displacement (Figs. 4-23 and 4-24). Therefore for the light X-braces the difference between the overall end deck slab displacements and measured girder displacements can largely be attributed to bearing deformations.

4.4.2.2 Yield Forces

The measured yield forces were 124 and 111 kN at the north and south ends respectively. Based on the frame analysis described for the reversed static experiments the expected transverse strength of the X-braces alone was 75 kN. With the stiffness and strength of the girders, chords and bearings added to the strength of the diagonals the yield force at each end was expected to be 98 and 99 kN respectively. Therefore the expected yield force was conservatively estimated in the cross frames by 10-25%.

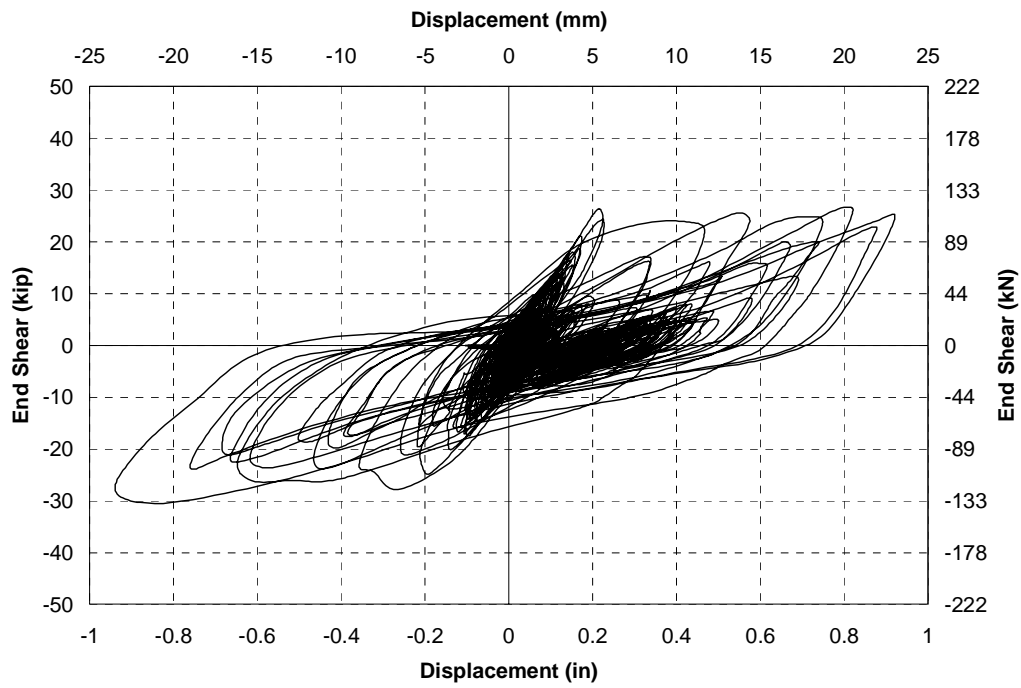


FIGURE 4-23 STLXB - North end shear vs end deck slab displacement relative to average bearing displacement in response to increasing amplitude El Centro ground motions

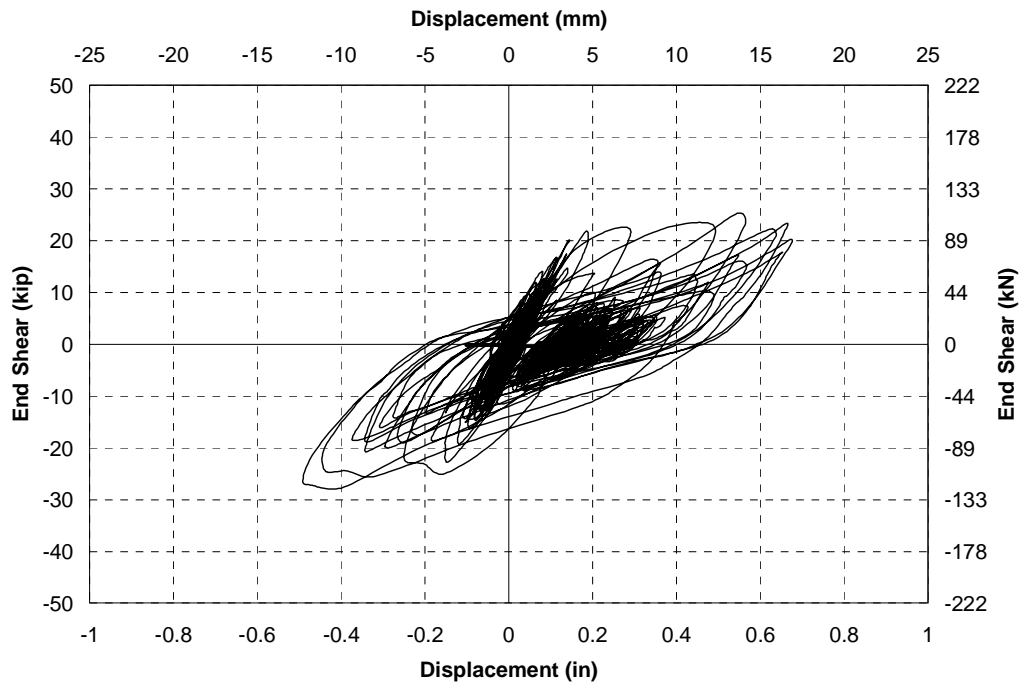


FIGURE 4-24 STLXB - South end shear vs end deck slab displacement relative to average bearing displacement in response to increasing amplitude El Centro ground motions

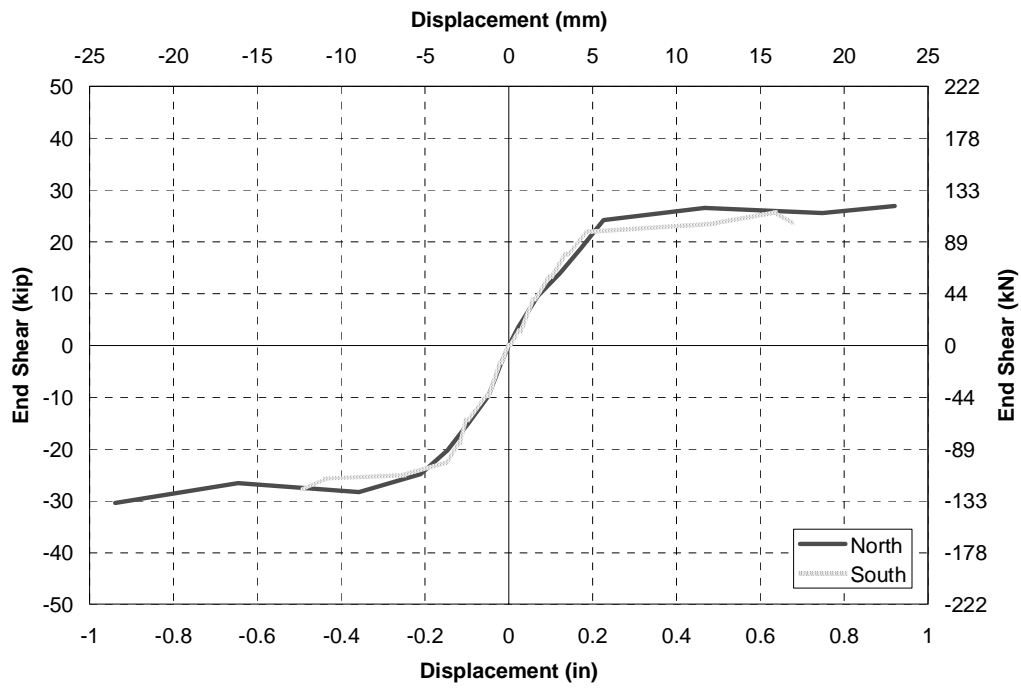


FIGURE 4-25 STLXB - Envelopes for hysteresis loops at north and south ends

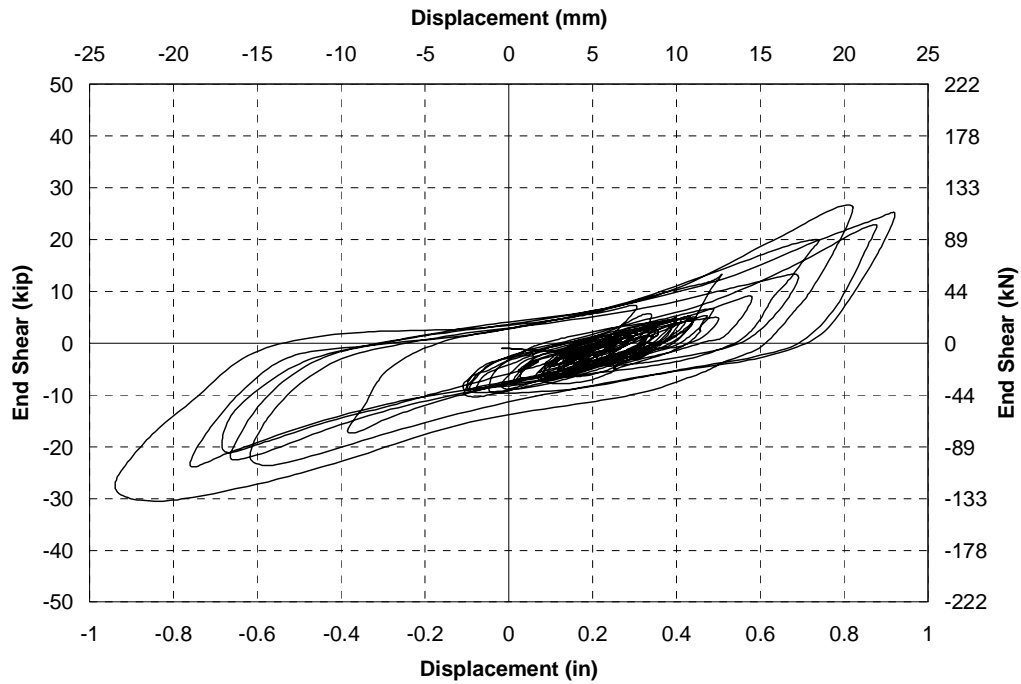


FIGURE 4-26 STLXB - North end shear vs end deck slab displacement relative to average bearing displacement in response to 2.0 El Centro ground motion

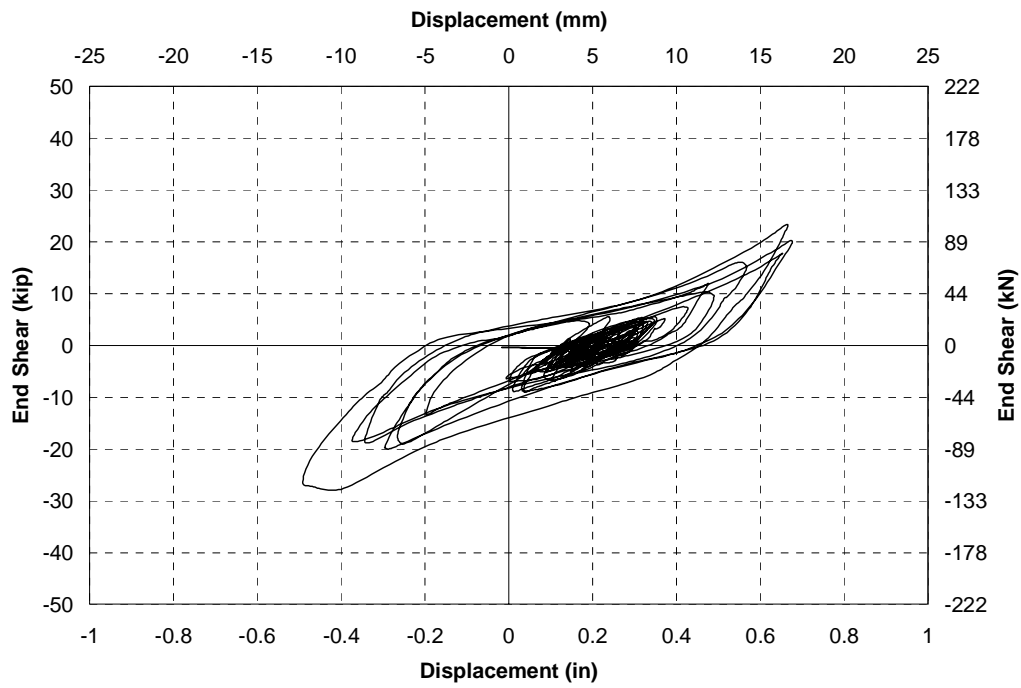


FIGURE 4-27 STLXB - South end shear vs end deck slab displacement relative to average bearing displacement in response to 2.0 El Centro ground motion

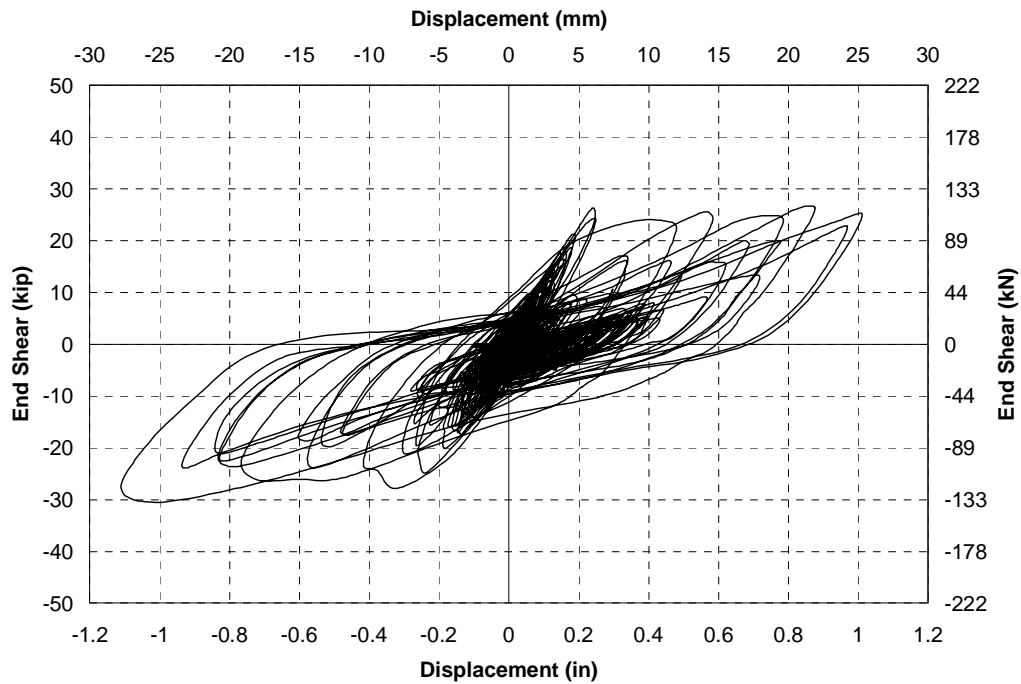


FIGURE 4-28 STLXB - North end shear vs horizontal displacement measured at deck slab level in response to increasing amplitude El Centro ground motions

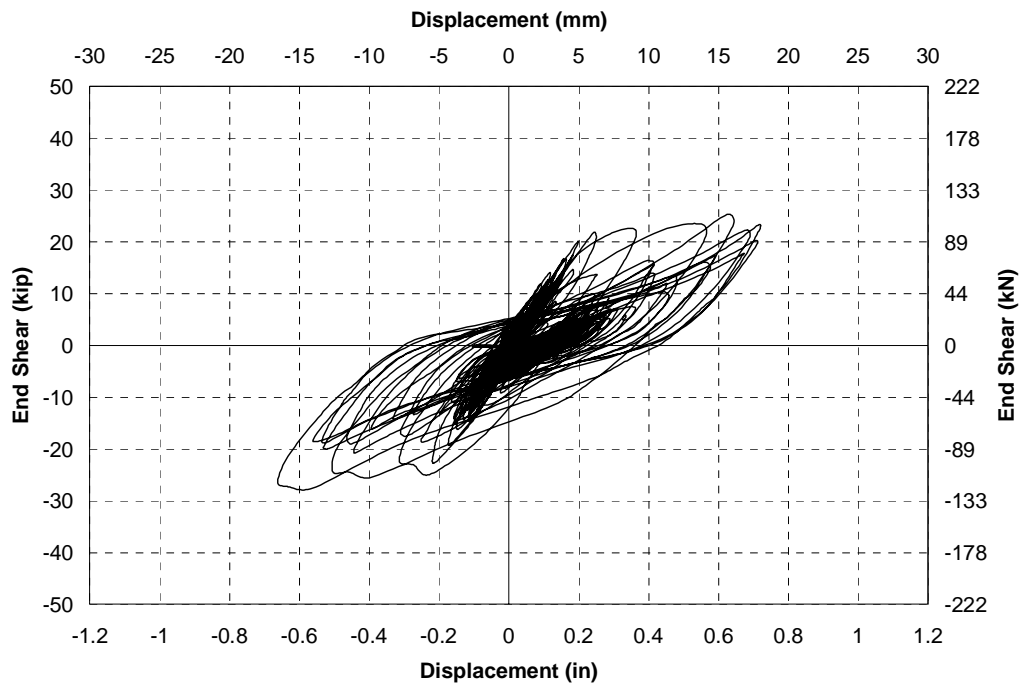


FIGURE 4-29 STLXB - South end shear vs horizontal displacement measured at deck slab level in response to increasing amplitude El Centro ground motions

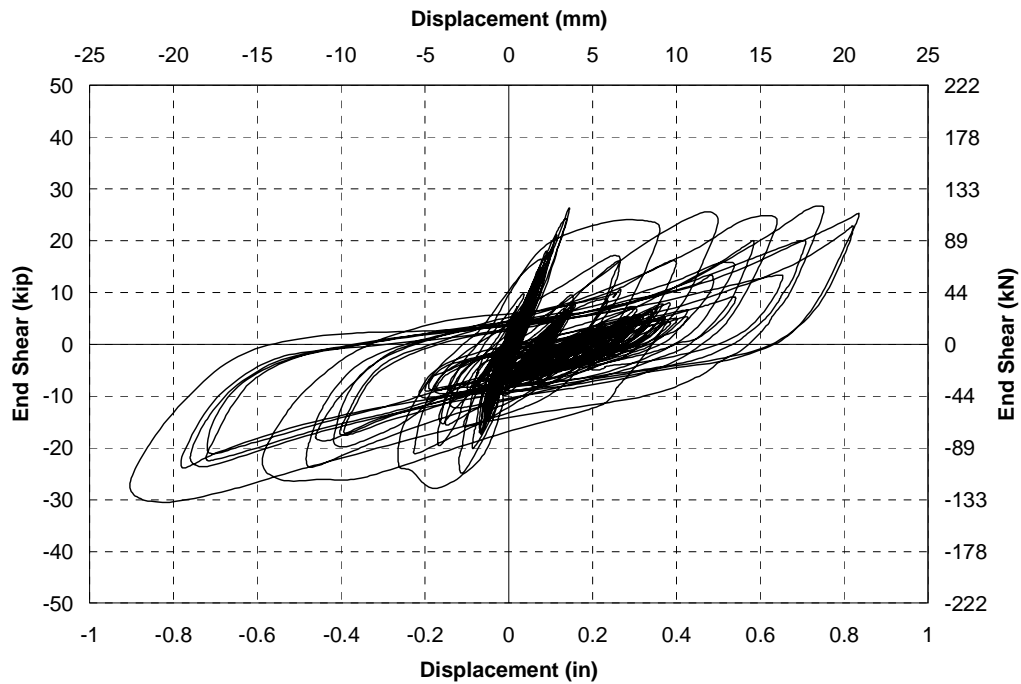


FIGURE 4-30 STLXB - North end shear vs horizontal displacement measured between top and bottom flanges of girders in response to increasing amplitude El Centro

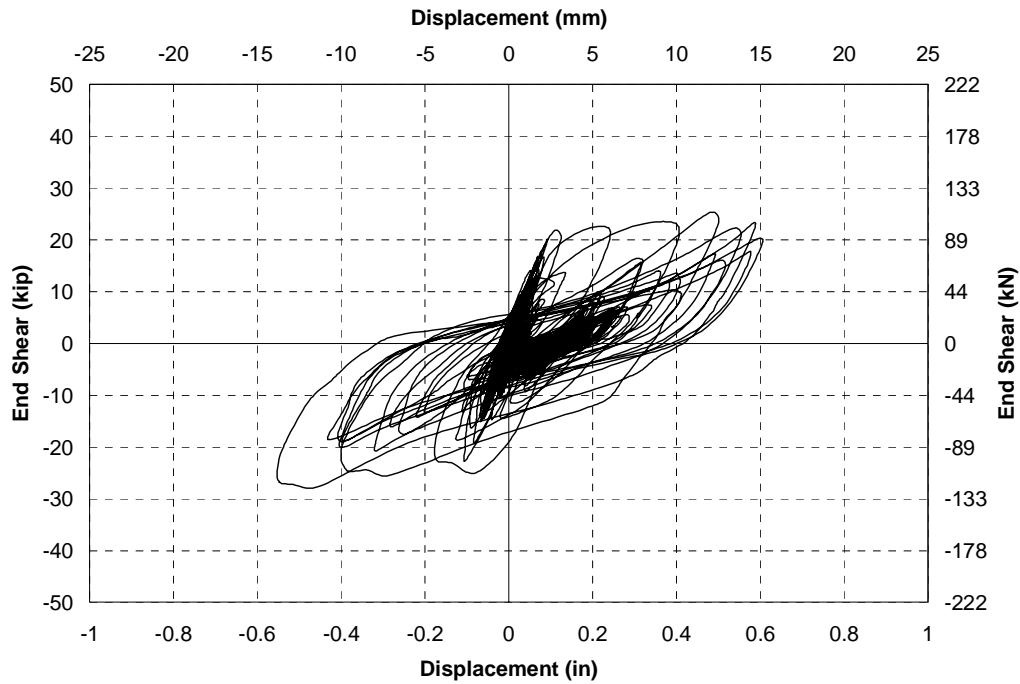


FIGURE 4-31 STLXB - South end shear vs horizontal displacement measured between top and bottom flanges of girders in response to increasing amplitude El Centro

4.4.2.3 Post-Yield Forces

As in the reversed static experiments, while there was likely to be some stiffness degradation observed in the diagonal members, with the contribution of girder stiffness the overall post yield stiffness was close to zero and minimal overall degradation or post-yield increase in strength was observed. The maximum force at the north end was 135 kN, 1.1 times the yield force. At the south end the maximum force was 124 kN, also 1.1 times the yield force, thus the post-yield overstrength was minimal. Removing the effects of the girders and assuming a linear girder stiffness resulted in an estimated maximum force of 121 and 108 kN at the two ends. Therefore the maximum forces were almost exactly equal to the measured yield forces indicating no increase in strength after yielding. Post-yield stiffness can therefore be attributed to the stiffness of the girders.

4.4.2.4 Maximum Displacements

Comparing Figures 4-23 and 4-24 shows that, although the end shears were comparable, the displacement at the north end was considerably larger than that at the south end. This is similar to the response observed in the reversed static experiments. This demonstrates the sensitivity of the X-brace displacements to a relatively small difference in forces. The maximum displacement at the north end of the girders was 24 mm, was equivalent to a drift of 4.0%. The maximum axial displacement in the diagonal was 15 mm corresponding to a strain of 1.2%. Based on a strain limit of 4%, and corresponding cross frame drift limit of 13% proposed from component experiments,

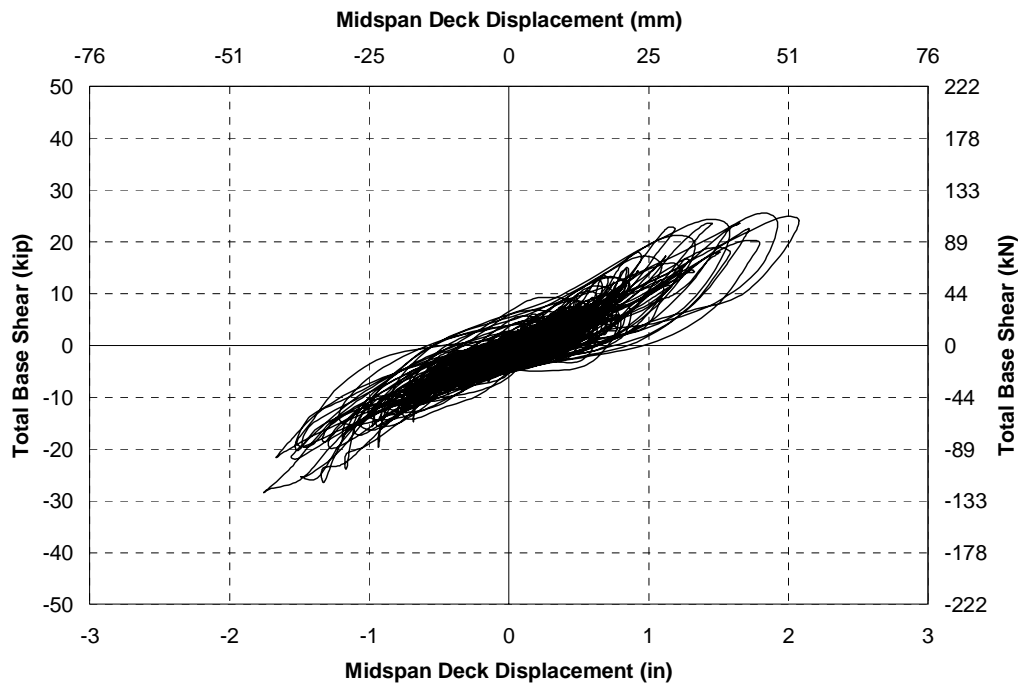


FIGURE 4-32 STLXB - Total base shear vs horizontal midspan deck slab displacement measured in response to increasing amplitude El Centro ground motions

the cross frames were capable of much larger displacements, although these were not applied to prevent potential damage to the girders for future experiments.

The maximum displacement was around 5 times the maximum displacement of the end with elastic cross frames. This was significantly higher than the level of force reduction, with forces reduced by a factor of 1.6. This was largely attributed to the flexible superstructure which has been shown analytically to result in increased end displacements according to a study by Alfawakhiri and Bruneau (2001). The transverse midspan displacement at deck slab level in the bridge model in response to increasing amplitude excitations up to 2.0 x El Centro is shown in Figure 4-32. The maximum displacement of 53 mm is considerably larger than the displacement at the ends of the bridge. As with the reversed static experiments, the hysteretic area is also much smaller than at the ends of the bridge showing that the effectiveness of energy dissipation at the ends is limited with a flexible superstructure.

4.4.2.5 Permanent Drift in the Cross Frames

The time histories for the horizontal end deck slab displacements relative to the bearings are shown in response to increasing amplitude excitations up to 2.0 x El Centro in Figure 4-33. This figure shows a permanent offset was observed in the ends of the bridge model when the X-braces first buckled at an amplitude of 1.5 El Centro. This permanent offset is expected in most concentric braced framing systems due to biased buckling in which the system first buckles during loading in one direction becoming weaker in that direction and consequently, the system tends to drift in that direction. This was observed in the X-braces after successive earthquakes applied to

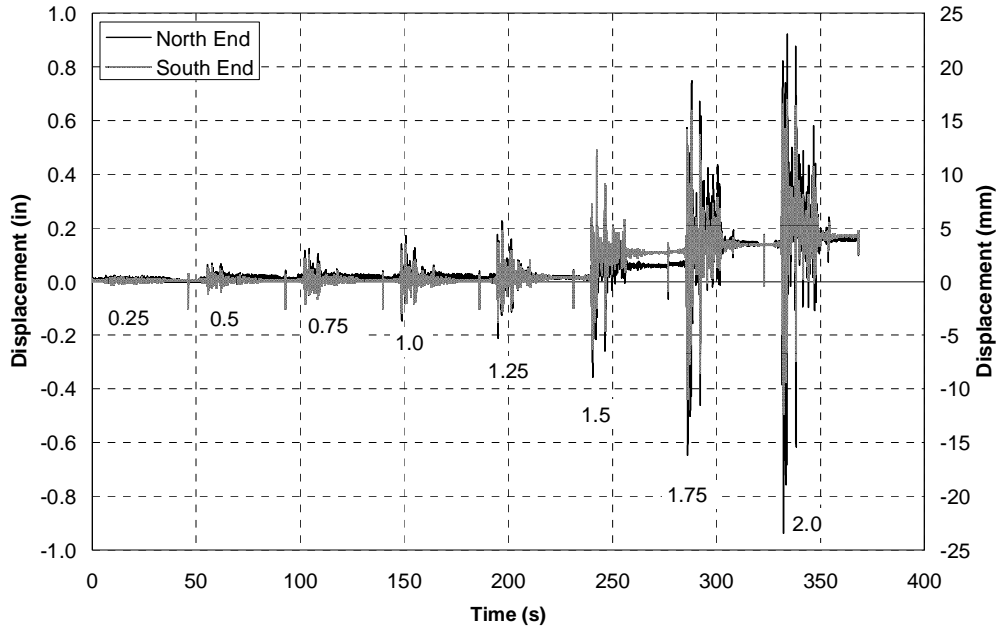


FIGURE 4-33 STLXB - Horizontal displacement time histories for ends of bridge model measured at the deck slab relative to the average bearing displacement in response to increasing amplitude excitation up to 2.0 El Centro

the bridge model with the permanent displacement remaining a positive value and increasing slightly after each earthquake. The permanent offsets of 2 mm and 3 mm at the north and south ends respectively after 1.5 x El Centro were 13% and 22% of the maximum displacements observed during this excitation. After 2.0 x El Centro the permanent displacements were 4 mm, 17% and 25% of the maximum displacements respectively at the two ends.

4.4.3 Experiment STPUB - Unbonded Braces with Pin Ended Connections

4.4.3.1 Effect of Removing Shear Studs at Ends of Bridge Model

Ductile cross frames using unbonded braces were placed in the bridge model to replace the X-braces. A small amplitude motion of 0.5 x El Centro was applied to the bridge model with unbonded braces at each end and with the deck slab and shear studs in the same state as at the conclusion of the experiments with the light X-braces, that is considerable cracking in the deck slab around the shear stud locations near the north end, but only minor cracking at the south end. The effect of two rows of shear studs at end of the bridge were removed by coring around them. The same ground motion was then applied to the bridge in order to determine the change in properties of the end region. The measured effective linear stiffness at the north end before and after coring was 50.6 kN/mm and 51.3 kN/mm respectively. At the south end the effective stiffness was 44.8 kN/mm and 45.5 kN/mm before and after coring respectively. Therefore at both ends there was little change in stiffness, with any effect of coring immeasurable during these

experiments owing to the fact that the studs were already ineffective in the transverse load path due to distress from prior experiments.

4.4.3.2 Hysteretic Response

The force-displacement curves for the north and south ends of the bridge, as a result of El Centro ramped up to 2.0 x the original acceleration levels, are shown in Figures 4-34 and 4-35, with displacements measured at the level of the deck slab relative to the bearing displacements. Instead of using an average bearing displacement as for the X-braces, the displacement for the bearing adjacent to the lower connection of the unbonded brace was used as this was considered the critical bearing in this asymmetric configuration. For these experiments the unbonded braces were connected with pin ended connections to the bearing stiffeners. The hysteresis curves show that there was greater apparent post yield stiffness in the ends with the unbonded braces compared to the ductile X-braces, with decreased overall displacements. There is some observed pinching in the hysteresis loops due to slippage in the connections, although there is no degradation of stiffness with successive cycles as observed in with the X-braces. The horizontal components of the diagonal end displacements measured between the top and bottom girder flanges are shown in Figures 4-36 and 4-37. These figures show reduced displacements compared to the deck slab displacement relative to that of the bearings, as expected due to slippage between the deck slab and the girders. The difference is between 3 to 5 mm at each end which is similar to that observed with the X-braces, although as the displacements with the unbonded braces were notably less than with the X-braces, this difference is more apparent.

The end responses for the bridge model in response to 2.25 x El Centro are shown in Figures 4-38 and 4-39. This was the largest excitation in the unbonded braces with pin ended connections. In these figures the slippage in the connections was apparent with pinching observed in the hysteresis loops. This slippage was attributed not only to the connections between the unbonded braces and the bearing stiffeners, which were connected with tight fit pins, but also due to the connections of the top and bottom chords to the bearing stiffeners. Slippage in these connections allowed the girders to move apart and rotate relative to each other which can account for additional deformation in the end region not measured in the braces.

4.4.3.3 Yield Forces

From the hysteresis loops at the ends it was difficult to identify the yield force in the braces as significant yielding did not occur in any one excitation but became gradually apparent over several increasing excitations. It was also difficult to separate the effects of slippage from yielding in the unbonded braces. Investigation of the backbone curves for the end shear plotted against axial displacement in the braces indicated that yielding occurred at end shear forces of around 90 kN. From a frame analysis using an analytical model, shown in Figure 6-4, the actual end shear was 60% of the axial force in the braces. Adding the forces from the hysteretic behavior of the bearings and top and bottom chords, as well as due to stiffness from the girders, bearings and shear studs, resulted in an estimated yield force in each end of around 74 kN. This was conservative by around 20% compared to the approximate yield force measured in the braces.

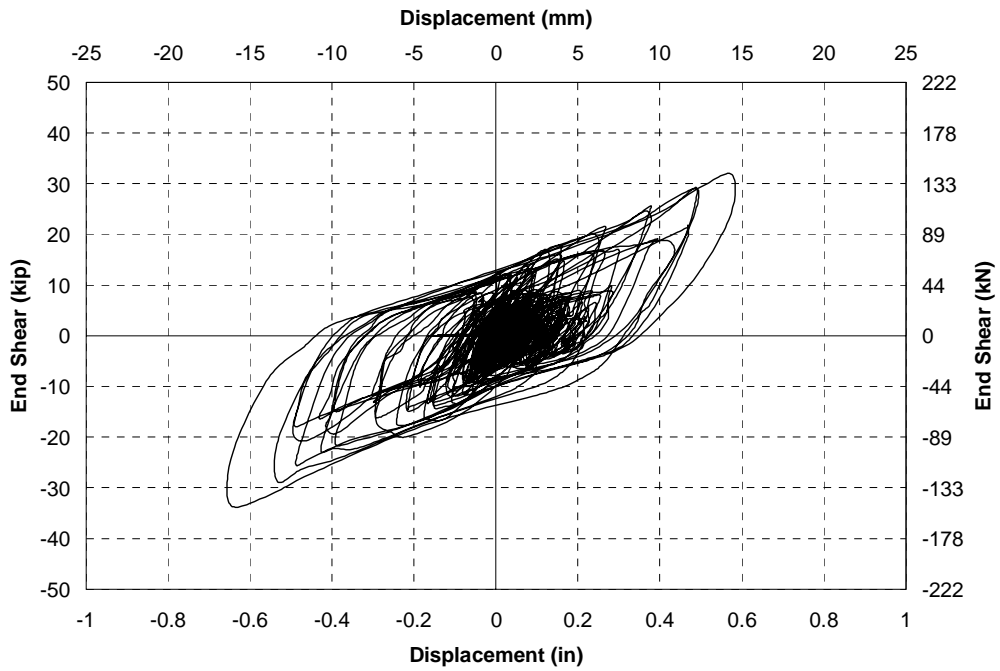


FIGURE 4-34 STPUB - North end shear vs end deck slab displacement relative to the bearing displacement in response to increasing amplitude excitation up to 2.0 El Centro

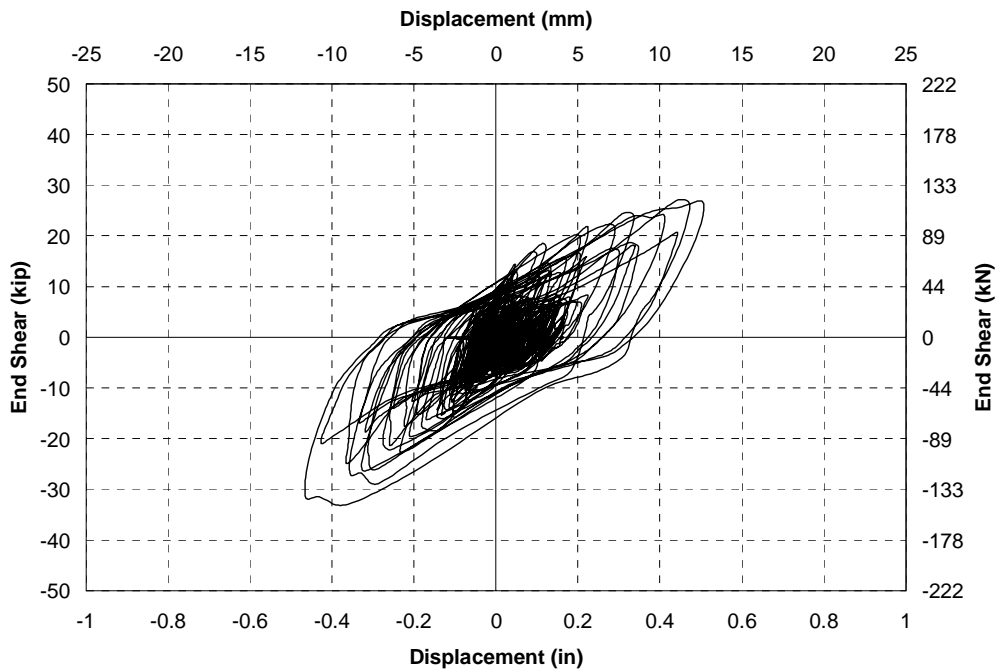


FIGURE 4-35 STPUB - South end shear vs end deck slab displacement relative to the bearing displacement in response to increasing amplitude excitation up to 2.0 El Centro

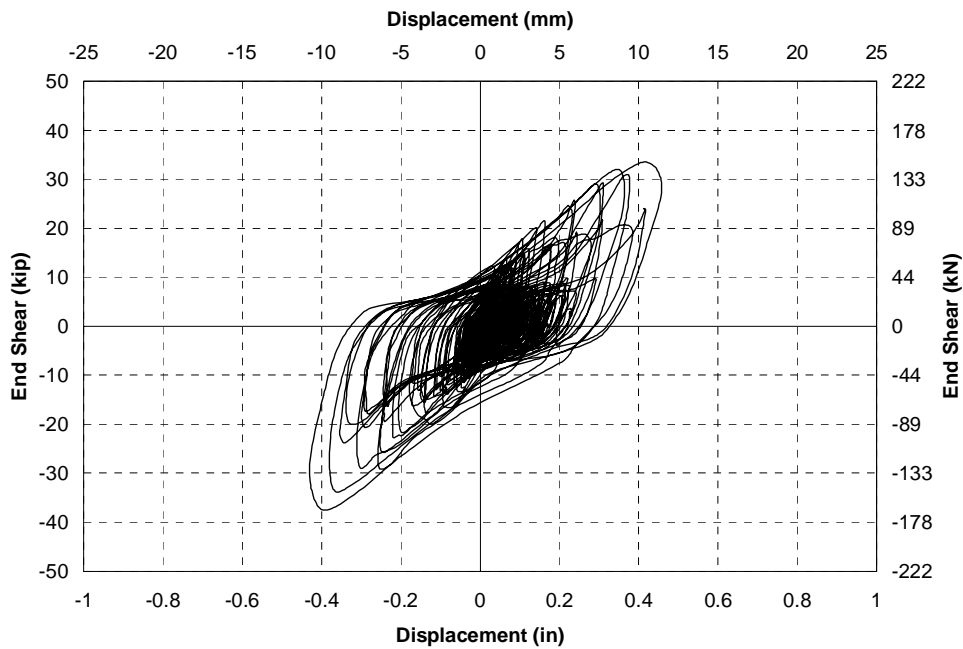


FIGURE 4-36 STPUB - North end shear vs horizontal displacement measured between the top and bottom flange of the girders in response to increasing amplitude excitation up to 2.0 El Centro

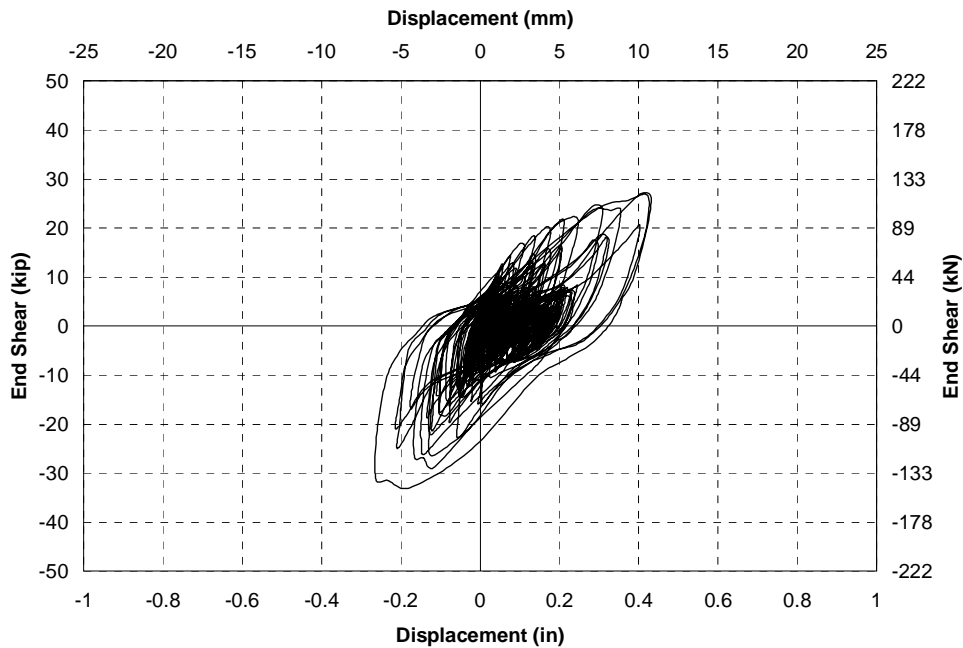


FIGURE 4-37 STPUB - South end shear vs horizontal displacement measured between the top and bottom flange of the girders in response to increasing amplitude excitation up to 2.0 El Centro

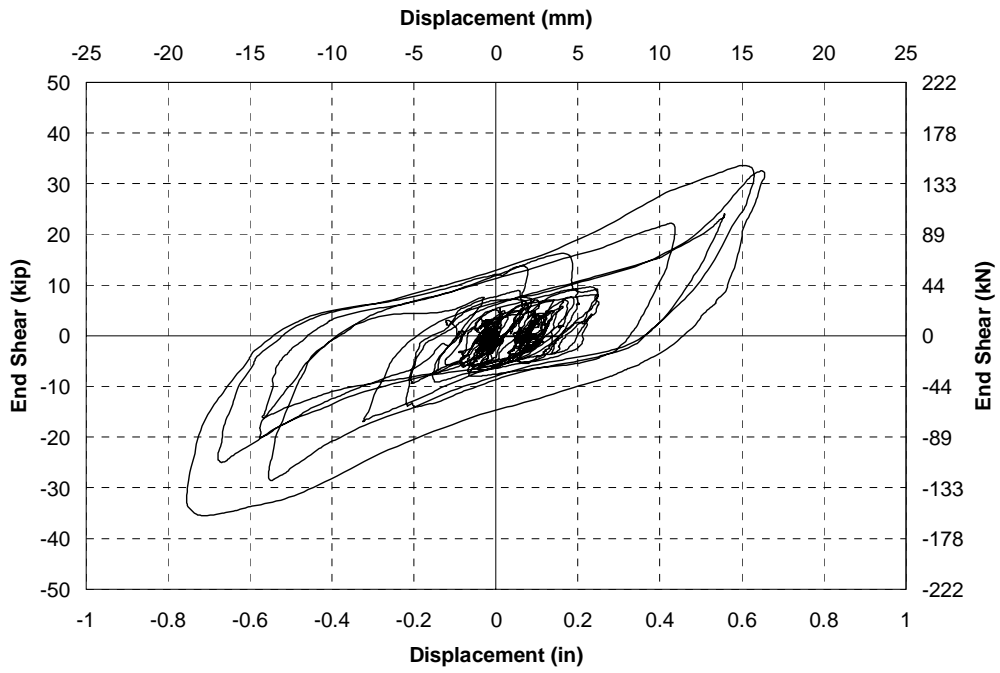


FIGURE 4-38 STPUB - North end shear vs end deck slab displacement relative to the bearing displacement in response to 2.25 El Centro

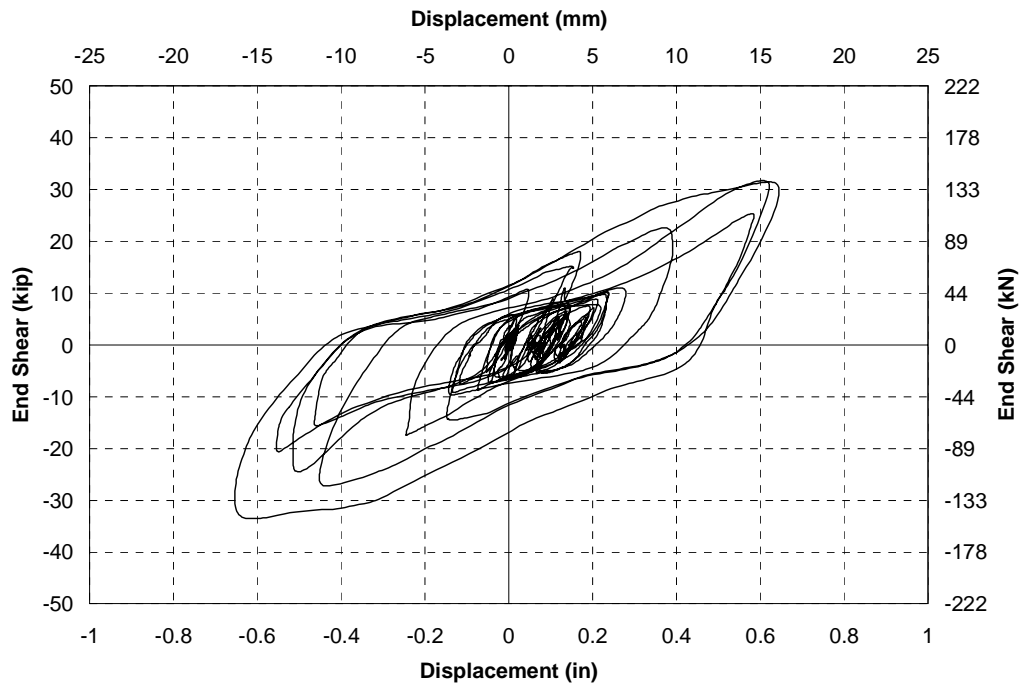


FIGURE 4-39 STPUB - South end shear vs end deck slab displacement relative to the bearing displacement in response to 2.25 El Centro

4.4.3.4 *Post-Yield Force*

The maximum shear forces at the ends of the bridge model in response to 2.0 x El Centro were equal to 148 and 147 kN at the north and south ends respectively. These were notably higher than the yield forces indicating considerable overstrength in the braces. The component experiments showed that the backbone curve for the response of the unbonded braces could be modeled with a post-yield to initial stiffness ratio of 0.025. The ratio found to be more appropriate for modeling the braces in the ends of the bridge model was closer to 0.05 even when considering the effects of girder, bearing and shear stud stiffnesses separately as is demonstrated later with analytical models. The reasons for this increase in the post-yield stiffness are likely to be due to such factors as flexural resistance, even with the pin ended connections, or eccentricities and misalignments between the two girders.

4.4.3.5 *Maximum Displacements*

The end shear forces plotted against the measured axial displacements in the core region of the braces for 2.0 x El Centro is shown in Figure 4-40, and for 2.25 x El Centro, in Figure 4-41. The maximum displacements in response to 2.0 x El Centro based on the deck slab displacement relative to the bearing displacement were 17 and 13 mm respectively at the north and south ends. For 2.25 x El Centro the maximum displacements were 18 and 15 mm. From geometry of the end region it was calculated that without slippage in the connections the deformation in the braces should be 60% of the horizontal deformation in the end regions, as illustrated in Figure 4-42. This would correspond to a maximum axial brace displacement of 11 mm and 9 mm at the two ends. Figure 4-41 shows that the axial deformations were considerably smaller than these levels as a result of slippage in the brace connections, with maximum displacements of 3 and 5 mm respectively. Axial displacements in the core length of the braces only accounted for 30 to 50% of the total deformation in the end region. Hence it was proposed to weld the connections at the ends of the unbonded braces to provide fully fixed connections in order to increase their efficiency.

The maximum calculated axial strains in the braces based on the measured axial displacements were around 0.86%, much lower than the maximum recommended design level strain of 2.0%. Therefore, failure would not be expected and indeed was not observed in any of the braces. At a maximum design brace strain of 2.0% the design drift calculated for the girders would be 3.0%. This is 20% to 50% greater than the corresponding design drift in the SPS, EBF and TADAS systems (Zahrai, 1998b). However this is just 25% of the theoretical allowable drift in the X-braces. There are two reasons for the large difference in displacement capacities. The first is that the unbonded brace does more work per cycle than the single angles, with largely recoverable yielding in both tension and compression, and as a result the allowable design strain in the brace was calculated to be less at 2.0% compared to 4.0% in the single angles, based on component experiments. The second reason is that the core length for the unbonded brace is much less than the effective length of the single angles, therefore at a given average axial strain the displacement in the angles is greater.

It can be shown that if the braces could be designed for a larger displacement, then a larger reduction in base shear may be possible. It would be possible to increase the displacement capacity of a buckling restrained braces if the core length in the brace was increased. This could be achieved by using more efficient connection details, which connect the brace directly to the stiffener without the use of gusset plates. Such a configuration is demonstrated in Figure 4-43. In

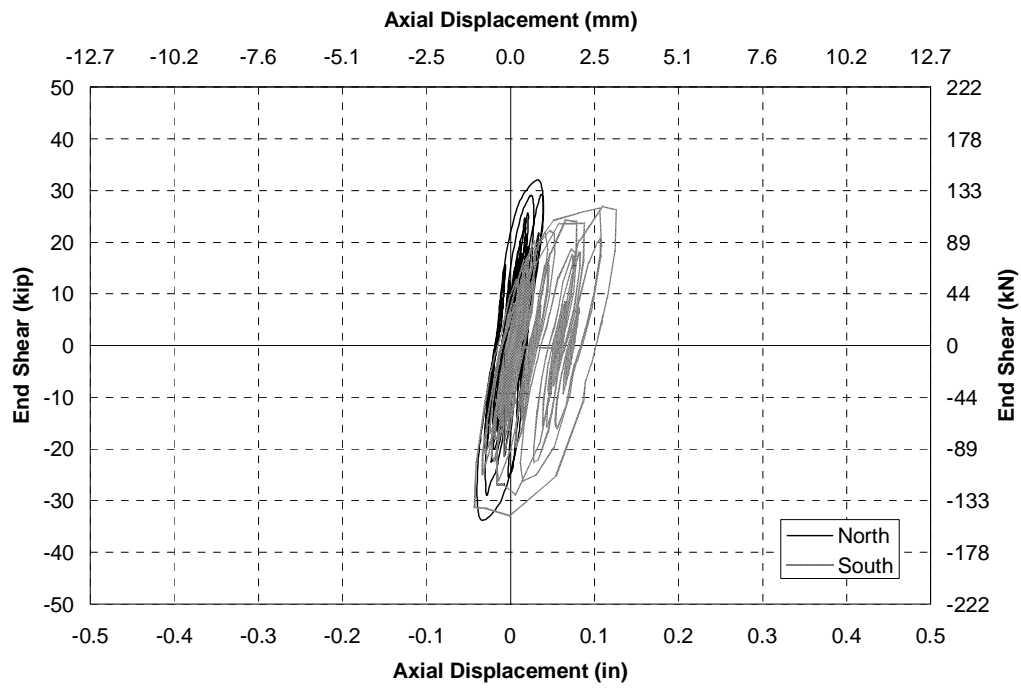


FIGURE 4-40 STPUB - End shear vs axial displacement for braces with pinned connections in response ramped up to 2.0 El Centro

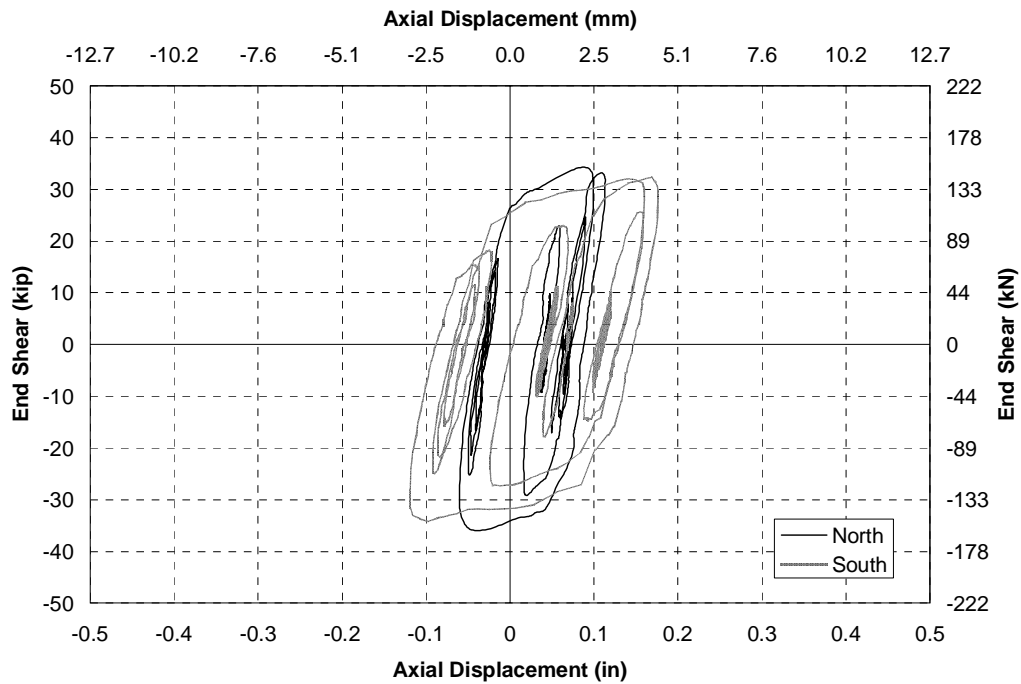


FIGURE 4-41 STPUB - End shear vs axial displacement for braces with pinned connections in response to 2.25 El Centro

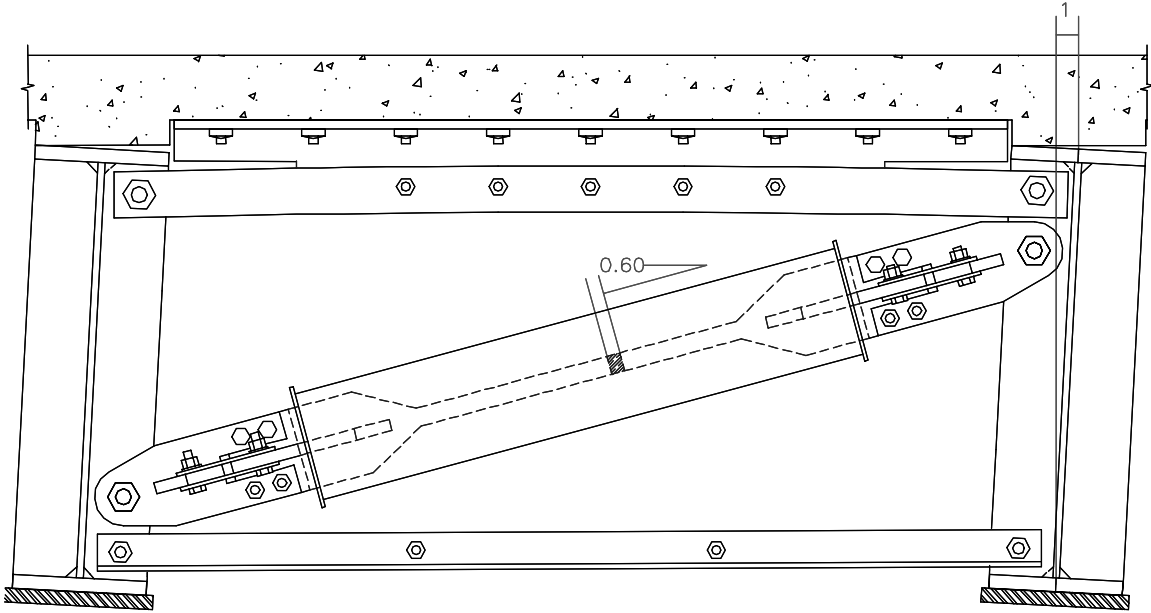


FIGURE 4-42 Deformed unbonded brace mechanism showing end displacement relative to axial displacement of brace

this configuration the effective core length was increased by 52%. Therefore the maximum drift in the girder at a corresponding brace strain of 2.0% was around 27 mm (4.6%). This design drift is now significantly greater than the design drifts for other systems such as the SPS, EBF and TADAS diaphragms, although still not as great as the design drift for the X-braces. A single row of bolts at each interface, that were not designed to be slip critical under extreme earthquake loads, was assumed to result in an effectively pinned connection. Further study would be beneficial in examining different connection configurations for the buckling restrained braces in this type of bridge application.

4.4.3.6 Permanent Drift in the Cross Frames

The horizontal transverse displacement time histories at the two ends of the bridge are shown in Figure 4-44 up to an amplitude to 2.0 x El Centro. A permanent offset was also observed with the unbonded brace cross frames. The permanent displacement was shown to increase gradually with each successive excitation with displacement after 1.5 x El Centro equal to 1 and 2 mm at the north and south ends respectively. These corresponded to displacements of 5% and 20% of the maximum displacements at the two ends respectively. These were similar to the levels observed with the ductile X-braces. After 2.0 x El Centro the permanent displacements were 1 and 3 mm at the north and south ends respectively. These were less than the permanent displacements measured in the X-braces and as a ratio of the maximum displacement measured in the cross frames, were equal to 7% and 17%. These permanent drifts were sufficiently small that one would not expect closure of a bridge to be necessary.

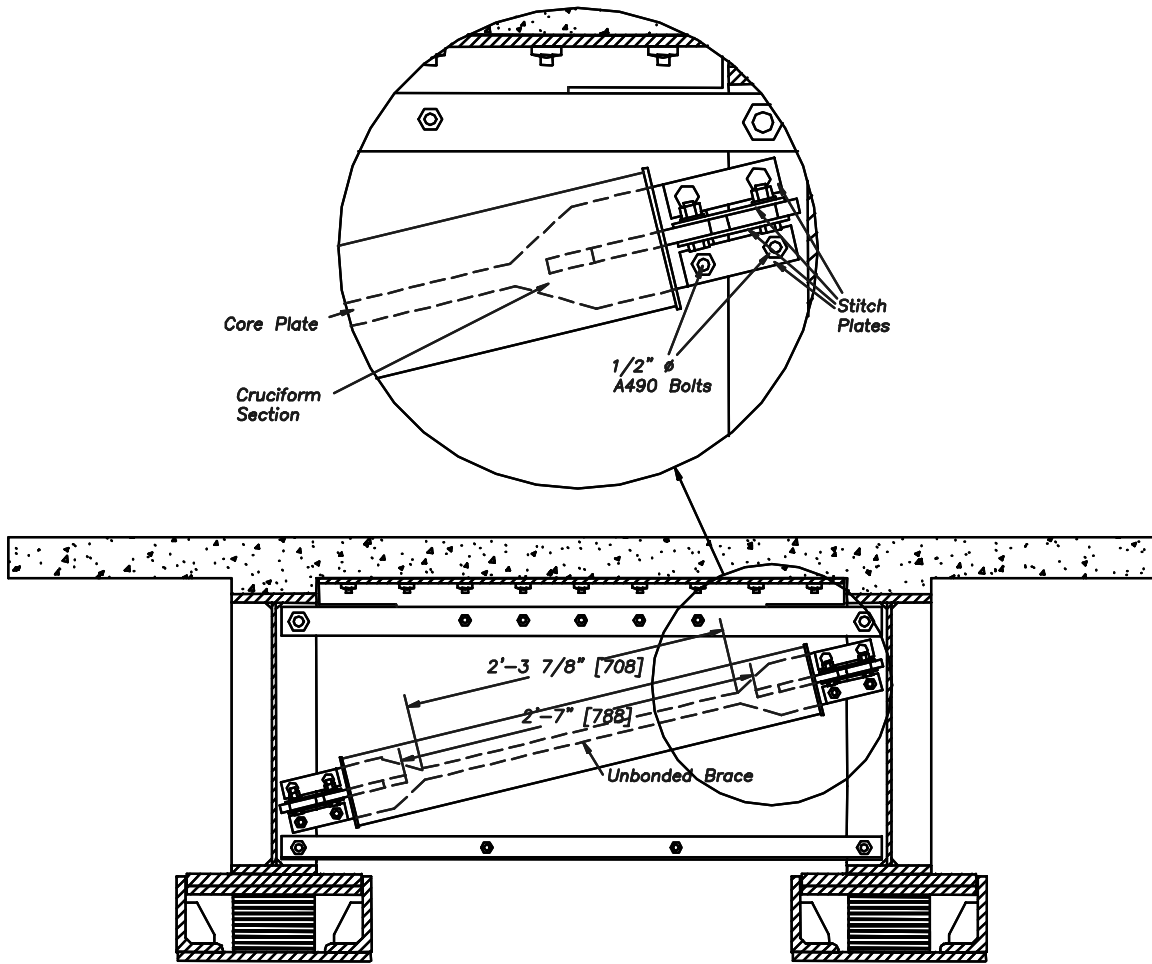


FIGURE 4-43 Alternative configuration for unbonded brace with increased core length

4.4.4 Experiment STFUB - Unbonded Braces with Fixed End Connections

4.4.4.1 Hysteretic Response

As a result of the slippage discussed in the previous section, the pin ended connections of unbonded the braces to the bearing stiffeners were welded. This provided a fixed moment resisting connection effectively like that typically used for unbonded braces in building applications. The 2.0 x El Centro response at each end with the welded braces is shown in Figures 4-45 and 4-46, which can be compared to that for the pinned braces in Figures 4-34 and 4-35. The end shear versus measured axial displacement across the reduced section of the brace is shown in Figure 4-35. The 2.25 x El Centro responses for the welded braces are shown in Figures 4-47 and 4-48, which can be compared to the pin ended braces in Figures 4-38 and 4-39. The estimated axial force plotted against the measured axial displacement for this motion is shown in Figure 4-49. The figures show that compared to the braces with pin ended connections the maximum force at the ends of the bridge increased while the overall displacements at the ends remained at similar levels. Therefore there was no great benefit in having fully fixed connections in the braces.

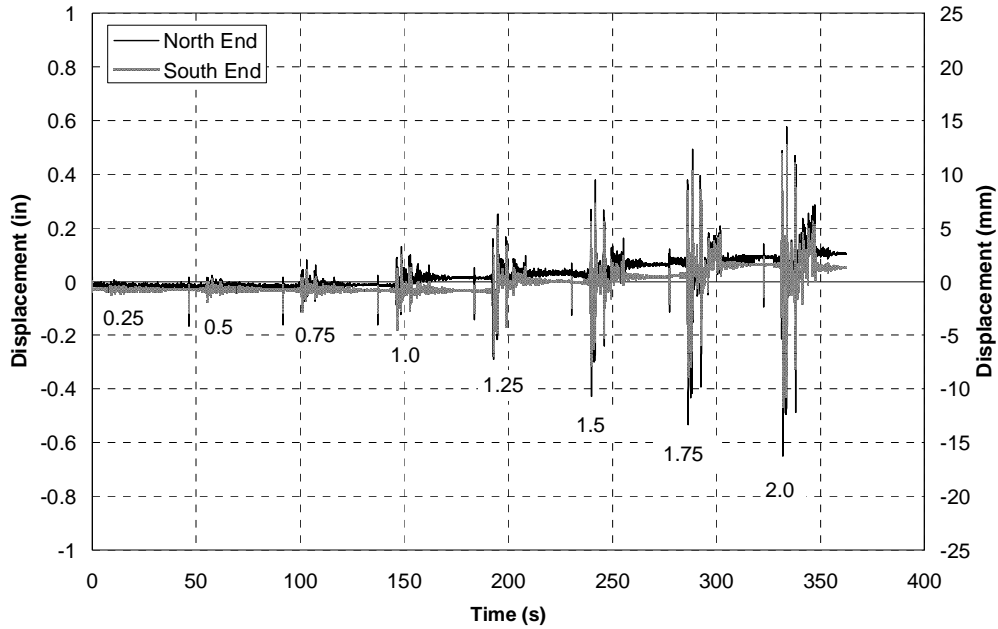


FIGURE 4-44 STPUB - Horizontal displacement time histories for ends of bridge model measured between top and bottom flange of girders in response to increasing amplitude excitation up to 2.0 El Centro

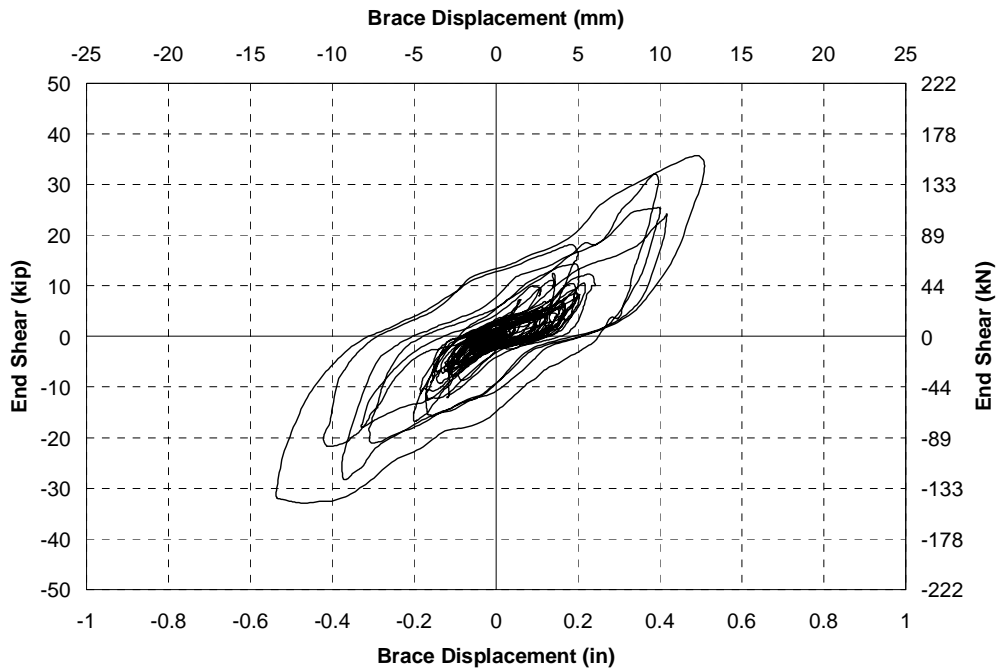


FIGURE 4-45 STFUB - North end shear vs end deck slab displacement relative to the bearing displacement in response to 2.0 El Centro

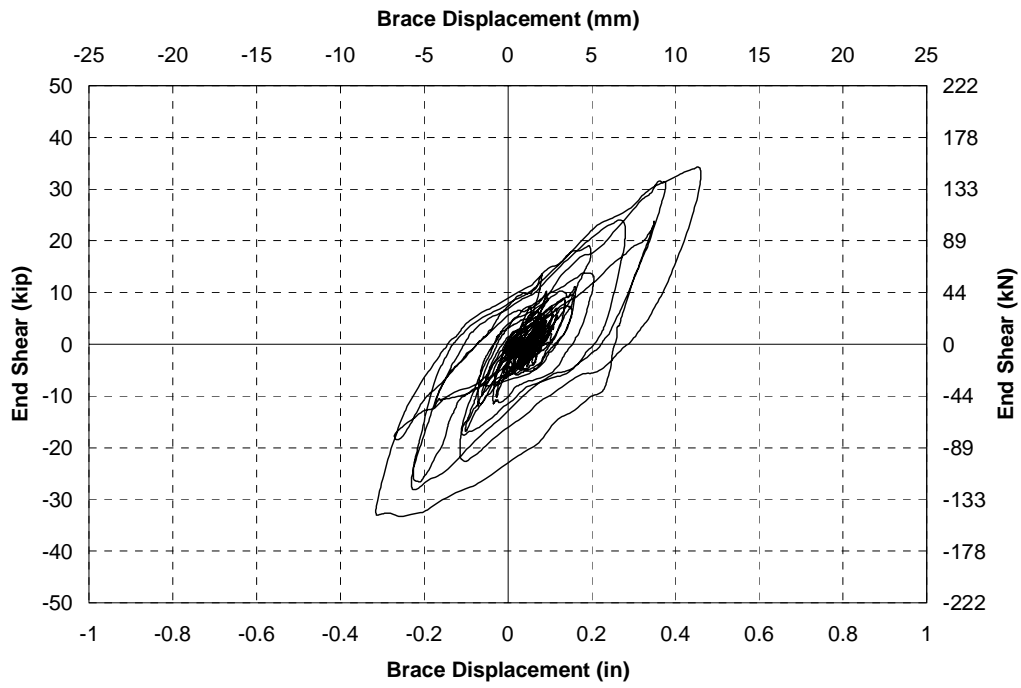


FIGURE 4-46 STFUB - South end shear vs end deck slab displacement relative to the bearing displacement in response to 2.0 El Centro

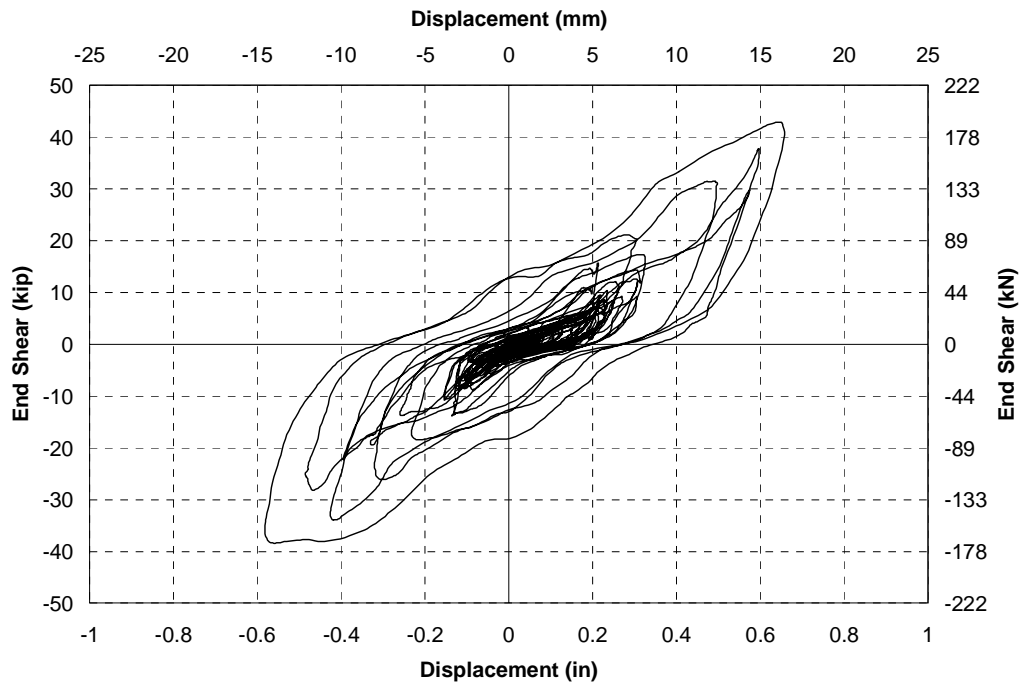


FIGURE 4-47 STFUB - North end shear vs end deck slab displacement relative to the bearing displacement in response to 2.25 El Centro

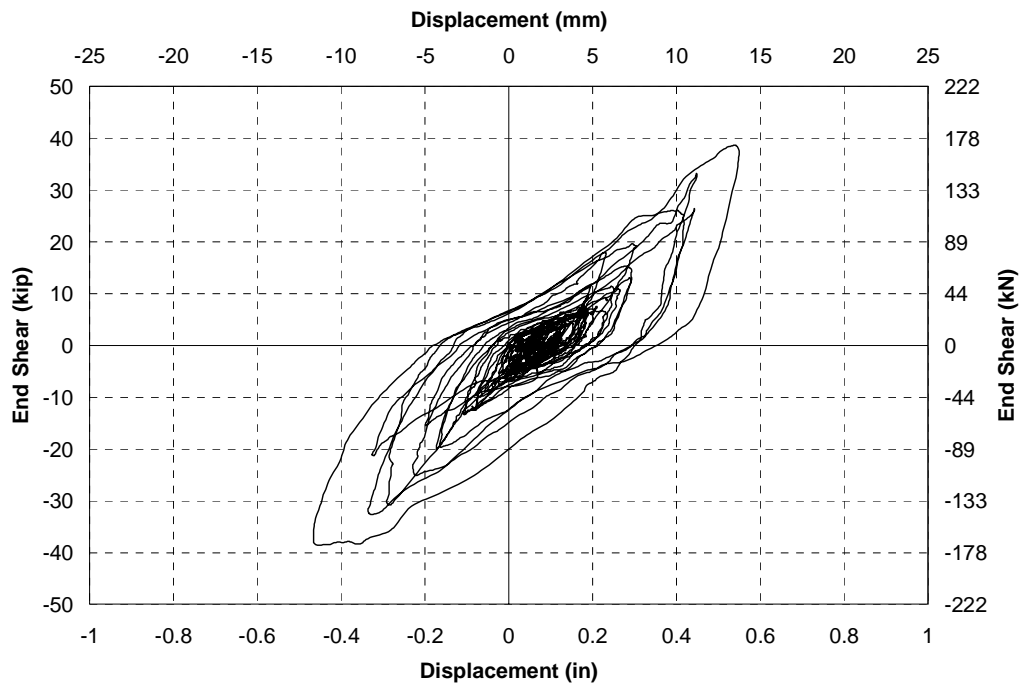


FIGURE 4-48 STFUB - South end shear vs end deck slab displacement relative to the bearing displacement in response to 2.25 El Centro

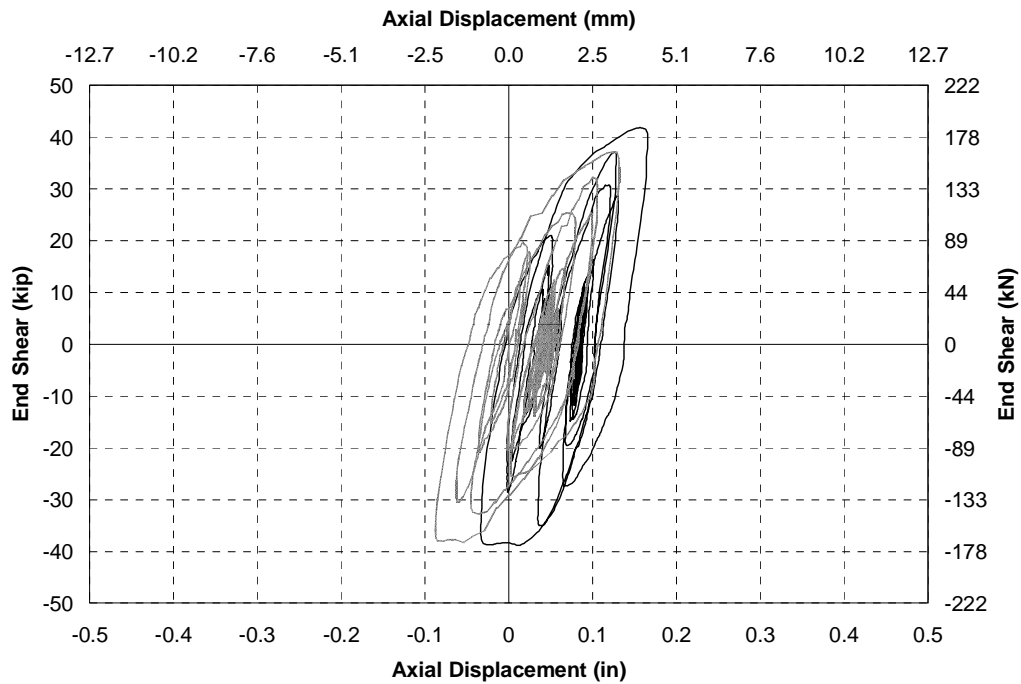


FIGURE 4-49 STFUB - End shear vs axial displacement for braces with fixed connections in response to 2.25 El Centro

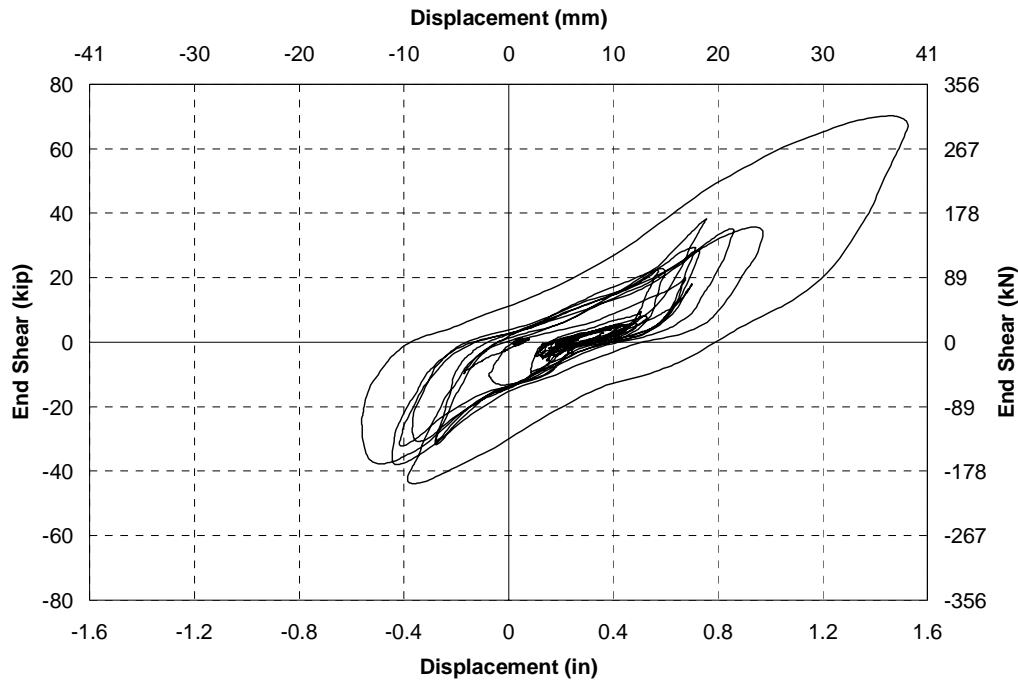


FIGURE 4-50 STFUB - North end shear vs end deck slab displacement relative to the bearing displacement in response to 1.0 Kobe

4.4.4.2 Maximum Forces

The maximum end shear forces for the bridge model with welded unbonded braces in response to 2.0 x El Centro were 159 and 152 kN respectively at the north and south ends. This was a slight increase compared to the pin ended braces. In response to 2.25 El Centro there was a further increase in end shear forces.

There were two likely sources for the increase in end shears observed in the bridge after welding of the connections. The first was because of larger axial displacements in the braces, which due to strain hardening, resulted in larger forces in the braces. The second was due to added stiffness in the cross frames from the flexural stiffness of the unbonded braces with fixed end connections. As the braces in the bridge model were much shorter than those in a typical building, they were flexurally more rigid and therefore bending in the brace contributed a greater level of lateral stiffness than typical in a building. While the increase in forces were relatively small in this case, in response to a larger earthquake the flexural stiffness may result in considerable post-yield overstrength as was observed in Figure 4-50, in response to Kobe. A post-yield to initial stiffness ratio of 0.125 is later found to model the post-yield behavior of the unbonded braces. This is notably higher than that for the pin ended connections. Not only is it higher, there is no way to predict it in braces with different sizes and properties. Therefore, it is recommended that the buckling restrained braces use, perhaps not ideal pin ended connections as in the bridge model, but effectively pin ended connections when designed as ductile end cross frames in bridges. In order to prevent excess slippage and provide good energy dissipation it is recommended that the connections be designed with tight tolerances.

4.4.4.3 *Maximum Displacements*

The maximum end displacements for the buckling restrained cross frames with welded connections in response to 2.0 x El Centro were equal to 14 and 12 mm at the north and south ends respectively when the braces were welded. These were almost the same as the bridge model with pin ended connections. The maximum displacements in the ends of the bridge in response to 2.25 x El Centro were 17 and 15 mm respectively, again similar to those with pin ended connections.

4.4.4.4 *Response to Sylmar and Kobe.*

In response to Sylmar the maximum end displacements were 18 and 15 mm respectively at the north and south ends. These displacements were slightly larger than the those measured in response to 2.0 x El Centro. In response to Kobe the maximum displacement was 39 mm at the north end and 24 mm at the south end. These correspond to drifts of 6.6% and 4.1%. The actual measured displacements in the braces were 11 and 9 mm, corresponding to a strains of 2.6% and 1.8% respectively at the two ends. At the north end this was in excess of the design limit of 2.0%, although no fracture was observed.

4.4.5 Experiment STFUB2S - Response of Two Span Bridge with Ductile End Cross Frames

After single span experiments the bridge model was supported at midspan to create a two span bridge. The response with ductile end cross frames was investigated using unbonded braces, with fixed ended connections located at the two ends and midspan of the bridge model. The distribution of forces between the ends and midspan of the bridge was close to expected based on a static analysis. However, as the brace at the middle support had the same yield force as those at the ends, it yielded earlier resulting in disproportionately large displacements at midspan (Table 4-1). This analysis supports the need to design the bridge as a system with different strength braces at the different supports depending on the demand. Analysis of seismic demand at individual supports without consideration of the coupling may result in an inaccurate estimation of the seismic response.

The maximum drift measured at the midspan of the bridge, at deck slab level relative to the bearings, was 1.63 in. corresponding to 7.0% of the girder height. No damage was observed in the girders at this level of drift, and little damage was observed in the haunch of the deck slab as shown in Figure 4-51. Where some cracking was observed it was in areas where the deck slab had been weakened by coring around the shear studs. With no shear studs in this region little damage would have been expected. The “rocking” mechanism promoted to allow large transverse drifts in the girder was found to be effective with no resulting damage to the primary gravity load carrying members.

4.5 Comparisons and Design Parameters for Ductile End Cross Frames

The maximum response of the bridge at 1.0, 1.5 and 2.0 x El Centro was summarized in Table 4-2 for the heavy X-braces, light X-braces and unbonded braces. The displacements in this table are based on the end deck slab displacement relative to the appropriate bearing displacements. This table shows that, as expected, the bridge model had the largest end shear forces with the heavy cross frames. The end shear forces in the bridge model with the light X-braces and unbonded

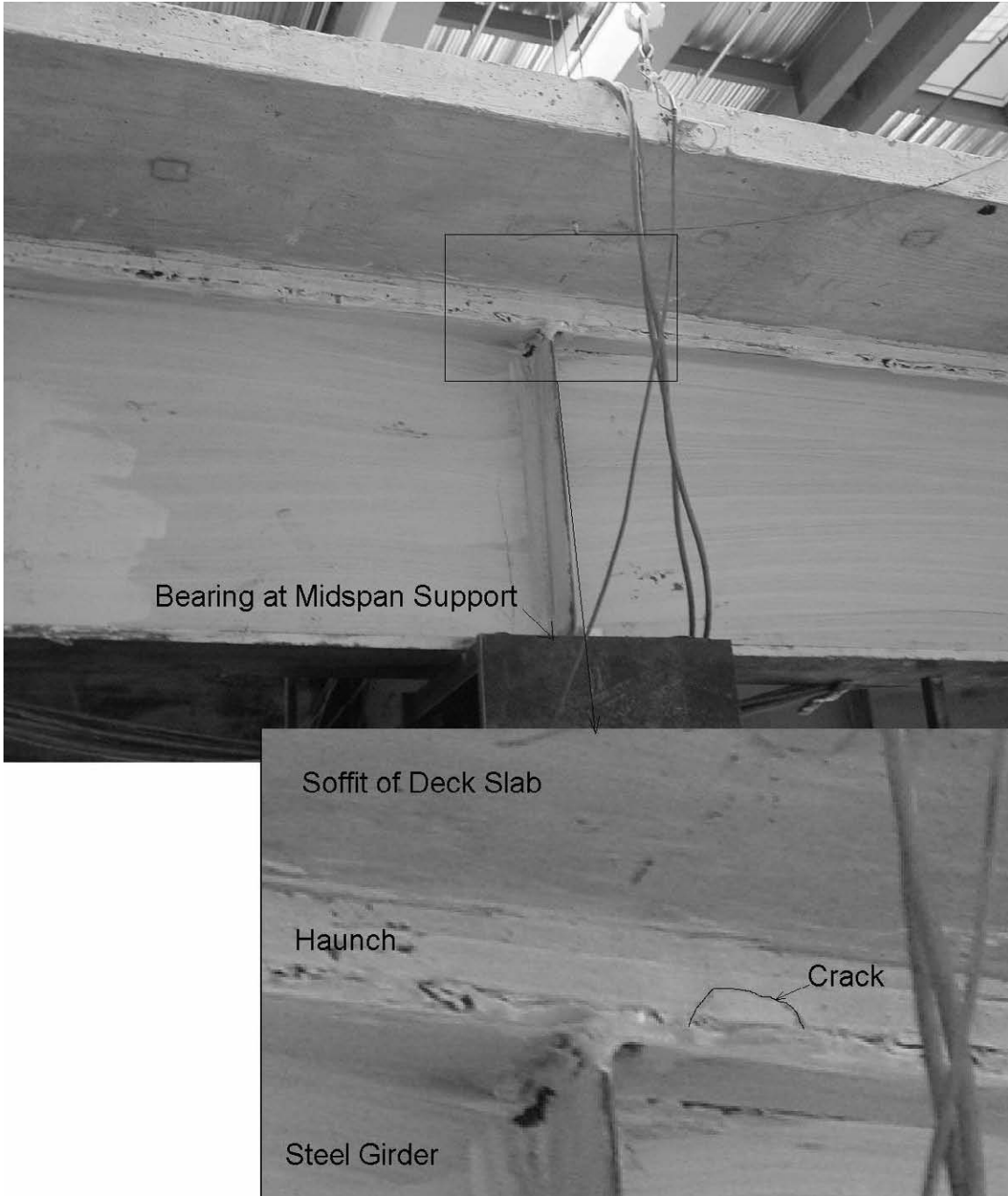


FIGURE 4-51 Haunch of deck slab and girder at midspan after maximum excitation at midspan resulting in 7% drift in the girders

braces were relatively similar at each earthquake level. However the drifts in the unbonded braces were notably less than the drifts in the X-braces as earthquake intensity increased. At 2.0 x El Centro the average end drift with the pinned unbonded brace was around 61% of that with X-braces at the north end and 75% of that at the south end. With fixed connections the drifts were

TABLE 4-1 Maximum Axial Brace Displacements at End and Midspan of 2 Span Bridge Model with Unbonded Braces in Response to Different Earthquake Excitations

Excitation	Units	Maximum Axial Brace Displacement		
		North End	Midspan	South End
0.5 El Centro	(mm)	0.1	0.4	0.1
	(% Comb. Disp.)	21	64	14
1.0 El Centro	(mm)	0.2	0.7	0.2
	(% Comb. Disp.)	18	65	17
1.5 El Centro	(mm)	0.3	2.2	0.4
	(% Comb. Disp.)	12	75	13
2.0 El Centro	(mm)	0.6	4.2	0.5
	(% Comb. Disp.)	11	79	10
2.5 El Centro	(mm)	1.0	5.6	1.0
	(% Comb. Disp.)	13	74	13
1.0 Sylmar	(mm)	1.1	4.5	1.1
	(% Comb. Disp.)	16	67	16
1.0 Kobe	(mm)	1.8	8.1	1.9
	(% Comb. Disp.)	15	69	16
1.5 Kobe	(mm)	3.7	11.9	3.4
	(% Comb. Disp.)	19	63	18

approximately the same as with the pin ended connections. Therefore at this level of earthquake motion the unbonded brace had an advantage over the X-braces in reducing the drifts in the girders. While the maximum forces in each system were similar, they were not identical, and the displacements are later shown to be quite sensitive to the level of force. The forces in the bridge model with unbonded braces were larger than the forces with ductile X-braces, therefore it was possible that some of the difference in displacements can be attributed to the difference in forces. Using a calibrated analytical model, a parametric study is performed in Chapter 6 to compare the forces and drifts for different ductile end cross frames of different strengths.

4.5.1 Post-Earthquake Evaluation

After an earthquake the buckling restrained cross frames have an advantage over the other ductile end cross frames in that the inelastic behavior is contained inside the brace eliminating damage after an earthquake. Assuming fracture has not occurred in the braces the transverse properties of the bridge should be similar to those before the earthquake. In contrast, the X-braces will exhibit immediate buckling with seismic demand which exceeds their yield strength and furthermore, degradation in the braces will mean that the bridge model has a lower transverse stiffness than before the earthquake. Therefore, while a bridge should remain open to traffic after a design level earthquake, X-braces will need replacing while buckling restrained cross frames should be able to remain in service for some period of time depending on the level of the event and the age of the braces in the bridge.

If necessary, repair of cross frames after an earthquake should be a relatively straight-forward exercise compared to the repair of a substructure. The damaged components between the different

TABLE 4-2 Comparisons of Bridge Model Response with X-braces and Unbonded Braces

System	End	1.0 El Centro		1.5 El Centro		2.0 El Centro	
		Max. Shear (kN)	Max. Displ. (mm)	Max. Shear (kN)	Max. Displ. (mm)	Max. Shear (kN)	Max. Displ. (mm)
"Heavy" X-Braces	North	112	2	174	4	228	6
	South	109	2	164	3	196	4
"Light" X-Braces	North	90	4	126	12	135	23
	South	84	3	111	12	124	17
Unbonded Braces	North - Pinned	75	4	110	11	148	16
	South - Pinned	80	5	142	8	147	13
	North - Fixed	-	-	-	-	166	14
	South - Fixed	-	-	-	-	150	12
Lead Rubber Bearings	North	26	16	32	22	36	33
	South	26	16	31	26	36	37

girders can be sequentially replaced without the need to close the bridge. If a permanent drift in the girders needs to be offset, this can be achieved by a simple jacking system in one of the bays while the components in the other bays are replaced, with stability maintained in the girders at all times.

SECTION 5

PERFORMANCE OF THE BRIDGE SUPERSTRUCTURE WITH SEISMIC ISOLATORS

5.1 Introduction

In order to compare the response of the bridge model with ductile end cross frames to that with seismic isolation, lead rubber isolation bearings were used to isolate the bridge. The properties of the bearings were described during design of the bridge model presented in Chapter 2. The lead rubber bearings (Fig. 2-16) were designed to isolate the bridge model and modify its seismic response. The properties and design response of these bearings are given in Appendix 1.

As the steel girder bridge superstructure is relatively lightweight compared to a corresponding concrete superstructure, in order to design for relatively low shear forces, compared to the weight of the bridge, the bearings required were relatively slender. The implication of this is demonstrated as the critical load was shown to dictate the displacement capacity in the bearings. The transverse, longitudinal and biaxial response of the bearings is discussed. A brief investigation into the response of the bridge with differential motions at the two ends is also considered.

5.2 Transverse Response of the Simply Supported Bridge Model

5.2.1 Hysteretic Response

As the bearings in the bridge model were much more flexible than the ductile end cross frames, it was expected that the bridge model would deform more like a rigid body with the lead rubber bearings. Time histories at the ends the bridge model and the midspan are shown in Figure 5-1 in response to 2.0 x El Centro. The deck slab was shown to have a 22% larger maximum displacement at the midspan than the ends, indicating some superstructure flexibility. There was also some rotation of the superstructure at midspan indicated by increased displacements in the bottom flange of the bridge model compared to that at the deck slab level. Figures 5-2 and 5-3 show that the displacements at the end of the deck slab were almost identical to the displacements in the corresponding bearings, indicating little deformation in the end cross frames. Therefore, the overall response of the bridge was dominated by deformation in the bearings, although the deformation in the flexible superstructure of the bridge model still needs to be considered in the response.

The hysteretic behavior in the bearings at the north and south ends of the bridge model subjected to increasing amplitude El Centro excitation in the transverse direction is shown in Figures 5-4 and 5-5. The backbone curve was shown to match the bi-linear model used for design, although the forces in the bearings were typically underestimated in the bi-linear model by around 10% at the maximum displacement.

5.2.2 Initial Stiffness

The initial stiffness of the bearings was estimated using the shear stiffness of the lead core and the shear stiffness of the rubber, as given in Appendix 1. The resulting calculated initial stiffness for

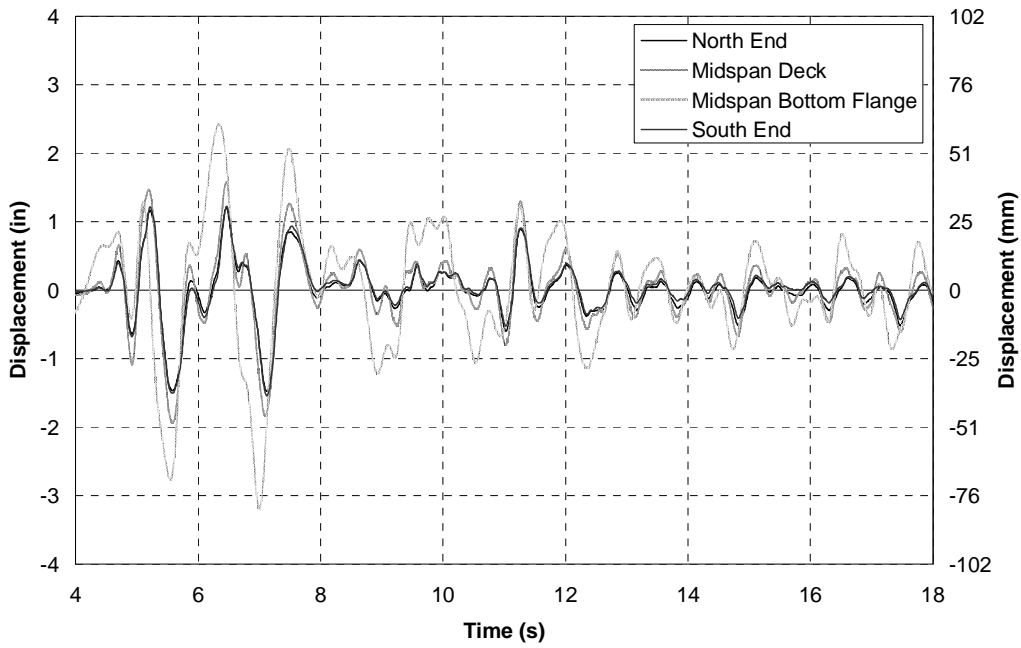


FIGURE 5-1 STLRB - Relative deck slab displacement in response to 2.0 El Centro

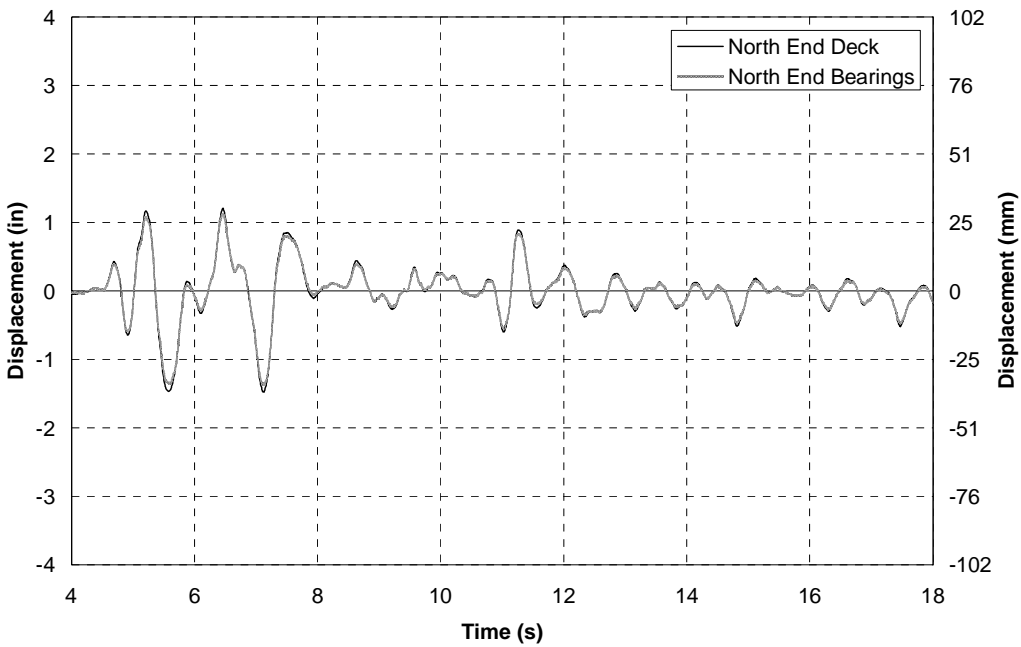


FIGURE 5-2 STLRB - Deck and bearing displacements at north end in response to 2.0 El Centro

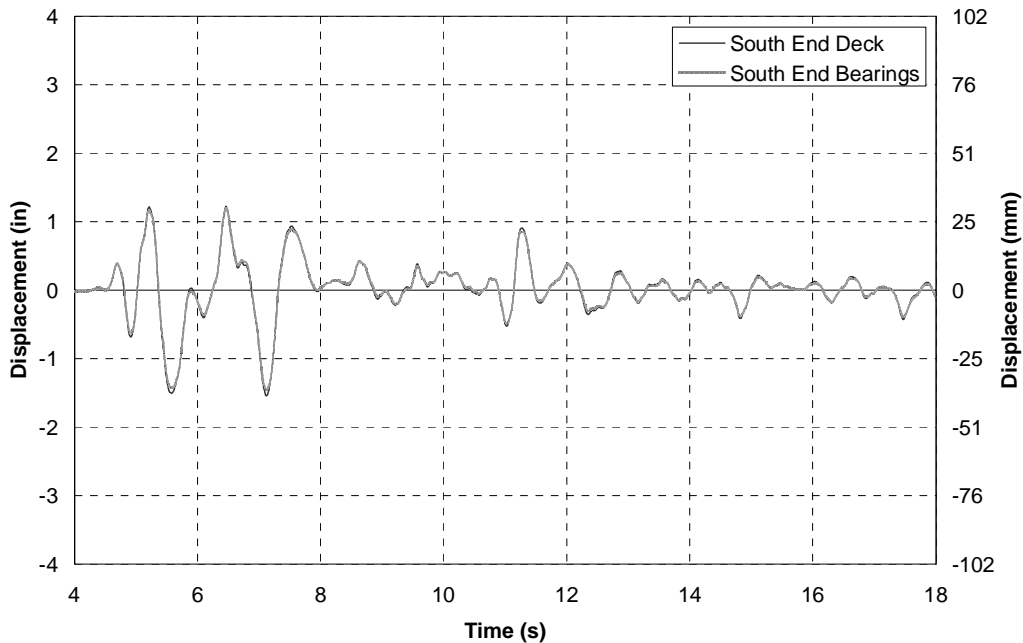


FIGURE 5-3 STLRB - Deck and bearing displacements at south end in response to 2.0 El Centro

the bearings was equal to 1.87 kN/mm. Therefore the initial stiffness at each end was equal to 3.75 kN/mm. When the end shear force was plotted against bearing displacement even for low amplitude motion such as 0.25 El Centro, as shown in Figure 5-6, some non-linear behavior was observed, although the estimated initial slope was close to the average slope of the measured force-displacement data. The response of the bearings was not particularly sensitive to the estimate of the initial slope as the ductility of the bearings was very large at the design displacement.

5.2.3 Characteristic Strength

The calculated characteristic strength in the lead rubber bearings, Q_d , was equal to 10.0 kN. From the component experiments in which the bearings were subjected to three cycles of loading at 100% shear strain in the bearings, after properties began to stabilize on the third cycle, the average measured Q_d was 9.29 kN, therefore matched the design data to within 7%.

The design Q_d for each end of the bridge model, with two bearings at each support, was equal to 20.0 kN. Shake table data shows that Q_d was dependent on the level of deformation in the bearings. For 2.0 x El Centro the average measured Q_d was 20.5 kN, close to the design Q_d . Although, with maximum displacements close to the design displacement of 53 mm, for example when the bridge was subjected to 1.5 El Centro Soil as shown in Figures 5-7 and 5-8, the average Q_d was equal to 23.4 kN. This was 16% larger than the expected characteristic strength. This indicates that the estimated Q_d was conservative. The increase in Q_d compared to the component

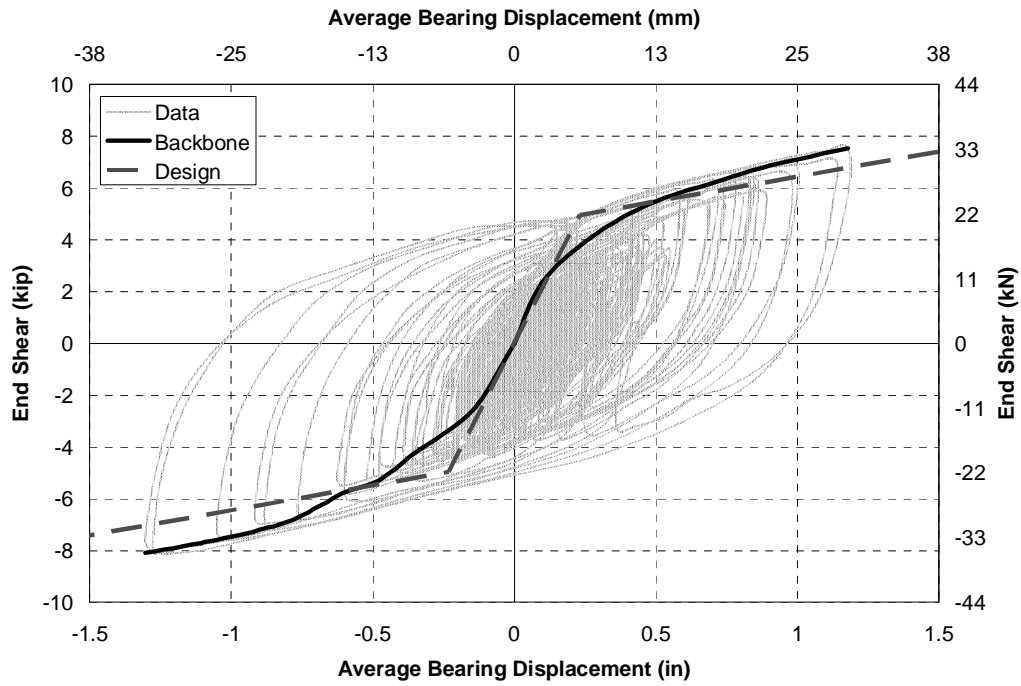


FIGURE 5-4 STLRB - Hysteretic response of bearings at north end for 0.25 - 2.0 El Centro compared to backbone and design curves

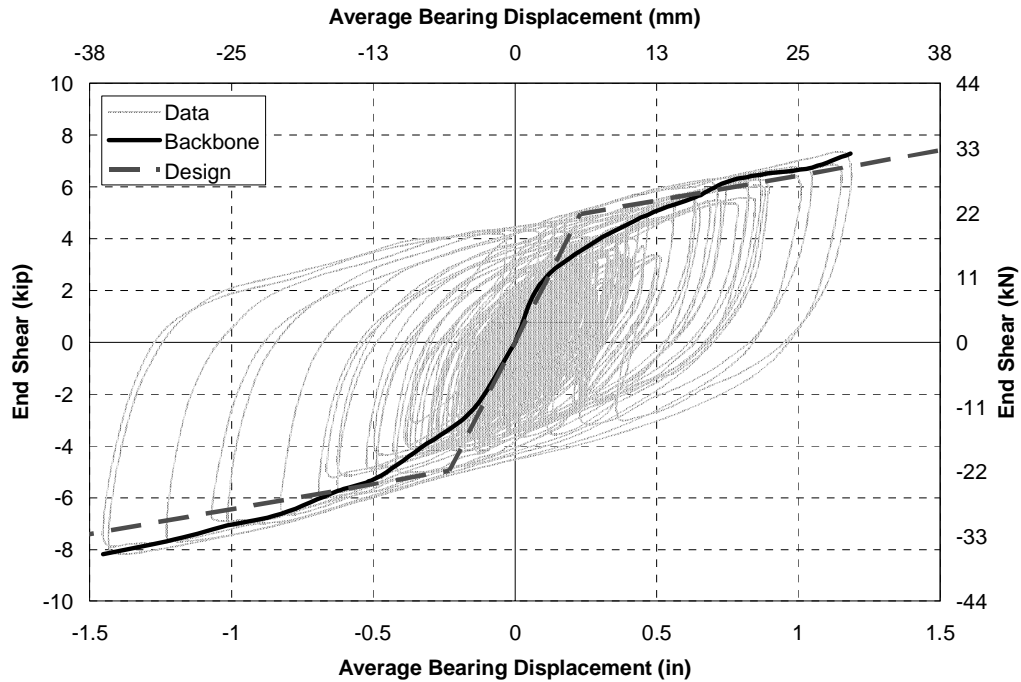


FIGURE 5-5 STLRB - Hysteretic response of bearings at south end for 0.25 - 2.0 El Centro compared to backbone and design curves

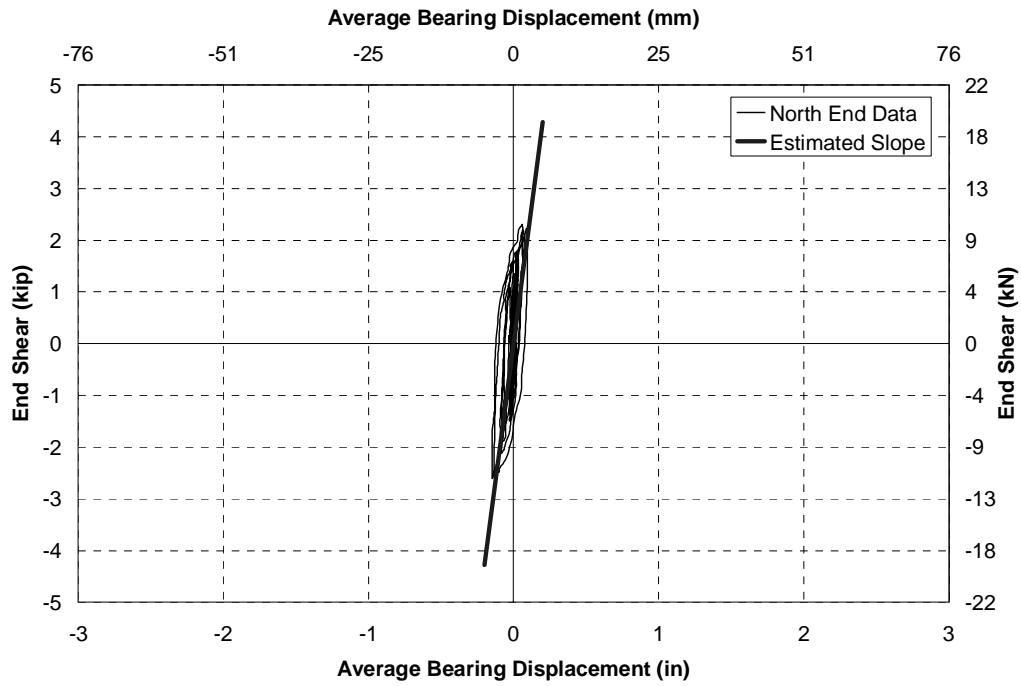


FIGURE 5-6 STLRB - Hysteresis loop at north end in response to 0.25 El Centro compared with calculated initial slope

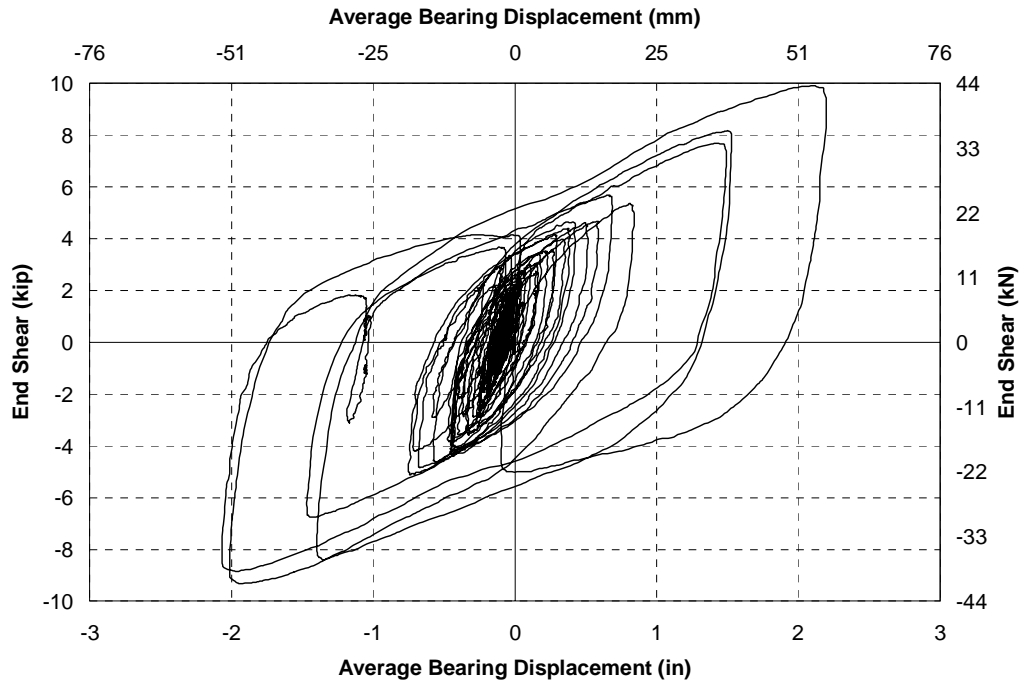


FIGURE 5-7 STLRB - Hysteresis loop at north end in response to 1.5 El Centro Soil

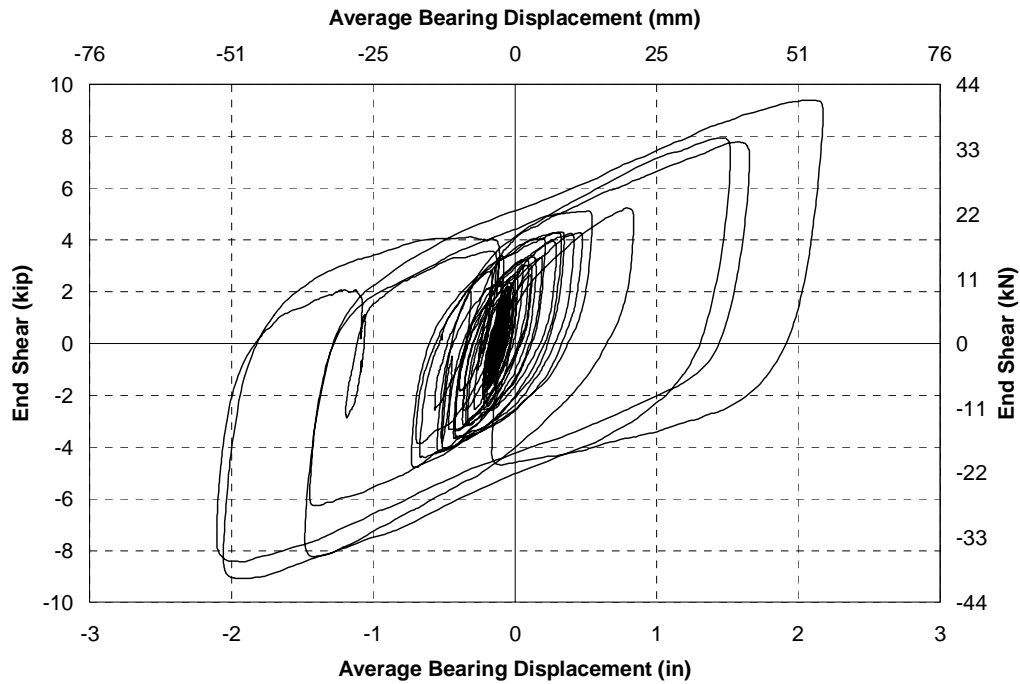


FIGURE 5-8 STLRB - Hysteresis loop at south end in response to 1.5 El Centro Soil

experiments may be partly due to dynamic strain rate effects similar to those seen in the unbonded braces. The properties of rubber have been shown to have negligible (2-3%) dependence on strain rate (MRPRA, 1979). Robinson (1982) suggested that at earthquake strain rates there was little rate dependence in a lead rubber bearing, however as rubber is known to creep some rate dependence is recognized. As a difference was apparent between the static component experiments and dynamic shake table experiments, a factor to account for the variability of characteristic strength of 15%, which can be used in design, was considered appropriate based on the relative strengths.

5.2.4 Post-yield Stiffness

The post yield stiffness for one bearing was expected to be equal to 0.17 kN/mm based on the shear stiffness and height of the rubber layers (Appendix 1). Therefore at each end the post-yield stiffness was expected to be 0.34 kN/mm. The average measured post yield stiffness from the component experiments was 0.28 kN/mm for each pair of bearings which was 18% lower than the design stiffness. However, during shake table experiments the post yield stiffness, as estimated from the hysteresis loops shown in Figures 5-4 and 5-5, resulted in a post yield stiffness close to the design stiffness. The average value of measured post yield stiffness was equal to 0.34 kN/mm, therefore was equal to the expected value. Each individual measurement was within 11% of the average value. Similar evaluations can be made for the other excitations of the bridge model. Results from the component experiments appeared to be conservative. As the measured stiffness was close to the design stiffness, no factor was considered necessary to modify the design stiffness for loading rate at large displacements.

5.2.5 Maximum Displacement and Critical Load

At the design displacement of the bearings the shear strain due to shear deformation was well below the allowable strain. However when combined with strain from axial loads the calculated strains were closer to the allowable strain. The displacement limit in the bearings was expected to be reached as a result of instabilities that occur due to the combined effect of axial loads and shear deformations. The displacement at which the critical load was calculated to be equal to the average axial load in the bearings was 82 mm, 54% above the design displacement. This was just above the limit for the design of the bearings which requires that the bearing be stable up to 1.5 times the design displacement.

A bearing is considered unstable when the slope of the hysteresis curve becomes negative. Static buckling of a system may be expected to cause collapse due to instabilities resulting in a member unable to carry its constantly applied loads. However dynamically, the load applied to a member changes with respect to time and if the loads on an unstable system are reversed before a member has time to collapse, it is possible for stability of the system to be restored. The combination of axial load and lateral displacement in a bearing at which stability is lost, albeit perhaps only temporarily, is considered the critical state. The critical combination of axial load and lateral displacement was reached in the bearings at the south end of the bridge during experiments on the bridge model, indicated by a flattening of the hysteresis loop followed by a negative stiffness in one of the cycles. Despite this observation, the structure did not collapse. This was attributed to dynamic inertia forces in the bridge model which were able to reverse the shear forces in the unstable bearings, causing the deformation to be reversed and the stability in the bearings to be restored. This is illustrated in Figure 5-9 in which large displacements well in excess of the design displacement of the bearings were observed at the south end of the bridge. Figure 5-9 shows that at the north end of the bridge the displacements were smaller as a result of different excitations at the two ends. Flattening and subsequent instability of the hysteresis loop was not observed at the north end due to the smaller levels of displacement, which also explains why the structure did not collapse, as overall stability of the structure was not lost. This is indicated by the total base shear plotted against bearing displacement averaged over both ends of the bridge, shown in Figure 5-10, which exhibits a significantly smaller maximum displacement averaged over both ends than the maximum south end displacement and a stiffness which is generally positive except at displacements very close to the maximum displacement.

Instability was first observed during an earlier excitation at a level of 2.0 x El Centro with differential ground motion at the two ends of the bridge. The response at each end for this excitation is shown in Figure 5-11. Flattening of the hysteresis loop was observed during this excitation, along with large displacements, as indicated in the figure. Figure 5-12 shows that the displacement averaged over both ends is smaller than the south end displacement and instability is not so apparent.

It was difficult to determine exactly when instability occurred in the bearings with a gradual transition in the slope of the hysteresis curves as the displacements increased, although the maximum shear force in Figure 5-11 was observed at a displacement of 93 mm, which is 13% greater than the estimated critical displacement of 82 mm. Thus the estimated critical displacement is reasonably accurate yet conservative when compared to the measured displacement. The characteristic strength of the bearings also appeared to increase indicated by

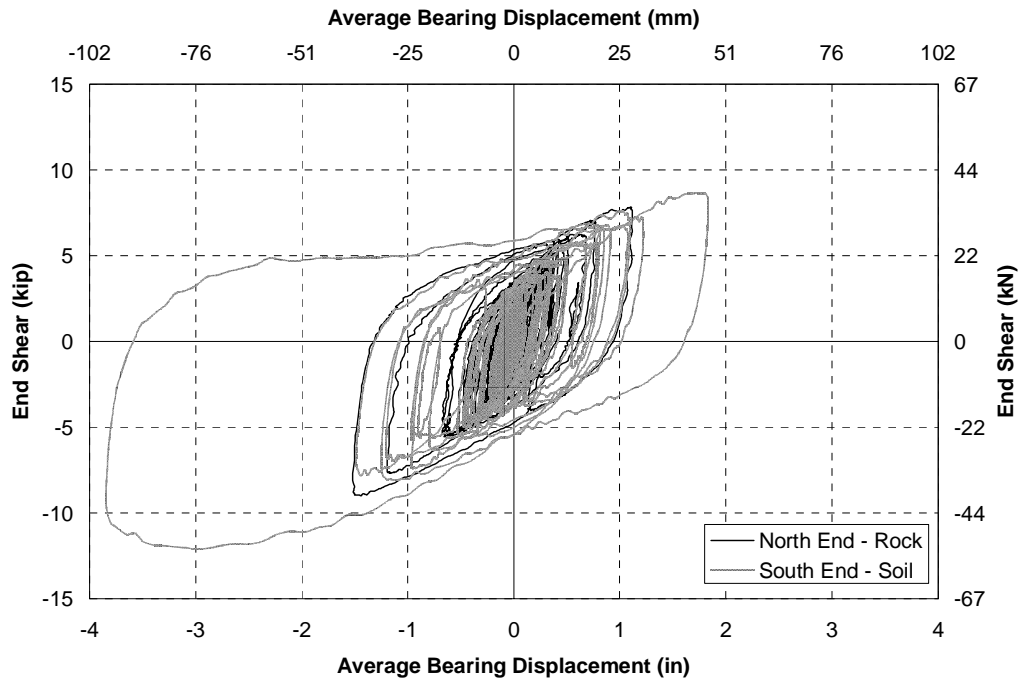


FIGURE 5-9 STLRB - Longitudinal bearing response at each end for 1.5 El Centro with rock excitation at north end and soil excitation at south end

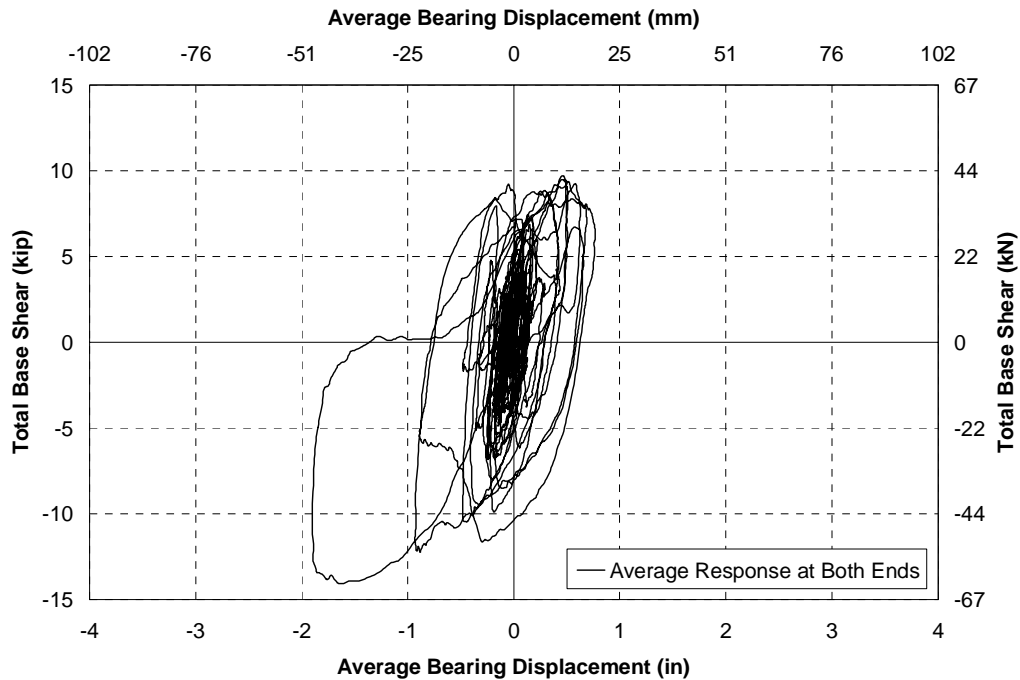


FIGURE 5-10 STLRB - Average longitudinal bearing displacement vs total base shear in response to 1.5 El Centro with rock excitation at north end and soil excitation at south end

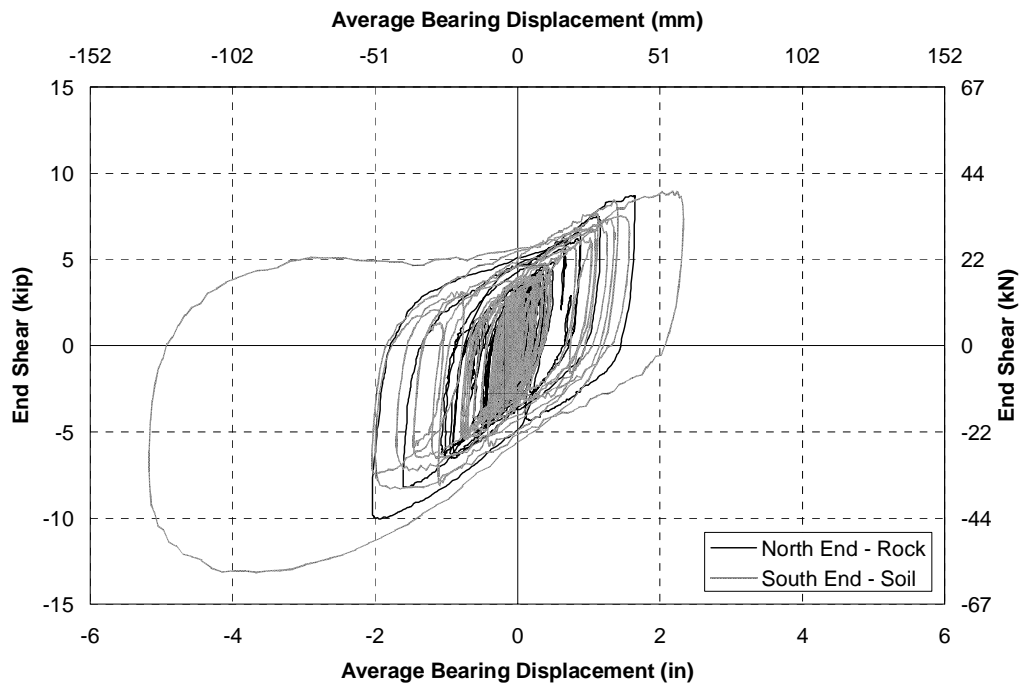


FIGURE 5-11 STLRB - Longitudinal bearing response at each end for 2.0 El Centro with rock excitation at north end and soil excitation at south end

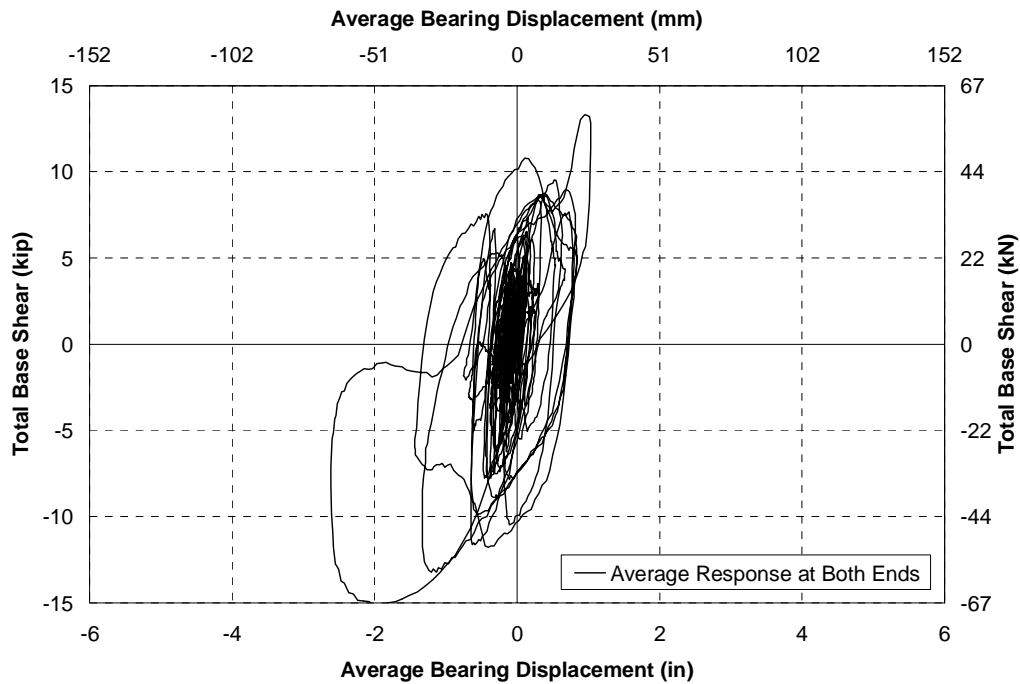


FIGURE 5-12 STLRB - Average longitudinal bearing displacement vs total base shear in response to 2.0 El Centro with rock excitation at north end and soil excitation at south end

“bulging” of the hysteresis loop during instability of the bearings. This was attributed to increased shear forces necessary in order to restore the stability of the bearings.

5.2.6 Longevity of Isolation Bearings

As the lead rubber bearings were subjected to an extremely large number of earthquake excitations, as given in Appendix 3, it was interesting to compare their properties near the beginning of experiments and end of experiments to determine whether they were notably different. There were two series of experiments performed with the lead rubbers bearings, the first series with light end X-braces, and the second with heavy X-braces. As previous analysis showed that the deformation in the end cross frames during isolation experiments was negligible, the response of the bridge model was expected to be the same in both cases. Figures 5-13 and 5-14 show the response of the bearings in the bridge model to 2.0 x El Centro during both series of experiments. The hysteretic response between the two series of experiments was shown to be very similar, with less than 10% difference between the maximum forces and displacements. The shape of the hysteresis loops was also very similar, indicating little apparent degradation in the bearings, despite having been subjected to a combination of loads and displacements beyond the critical in the bearings.

The cumulative plastic ductility demand through the bearings was estimated by calculating the cumulative plastic ductility in the bearings for a number of experiments and extrapolating data to estimate the total cumulative plastic ductility for all of the earthquake excitations. The cumulative plastic ductility observed in the bearings used in the single span and two span experiments was estimated between 6000 and 7000. This is an order of magnitude higher than the capacity of the unbonded braces, with little degradation observed in the bearings indicating that they could potentially undergo further deformations.

5.3 Biaxial Response of Simply Supported Bridge Model

In calculating the effects due to excitation in two or three orthogonal directions, for members such as columns or bridge bearings, there are two necessary considerations. The first is the combination of response quantity (such as bending moment, shear force or displacement) in a given direction due to excitations in the orthogonal directions. For example, there will be bearing displacements in the x-direction due to excitation in the x-direction, but also due to excitation in the y-direction resulting from any torsional response. The second consideration is the combination of biaxial actions, such as displacements in the x and y directions respectively.

In this study the effects of vertical excitation were not considered, therefore the analysis is limited to the two horizontal components of excitation. There are different methods prescribed by different building and bridge codes for combining actions in a given direction for the two horizontal components of earthquake excitation. These combination procedures are based on the assumption that the maximum response due to excitation in one direction will not coincide with the maximum response due to excitation in the orthogonal direction. The simplest and most common approach is to combine the actions due to excitation in one direction with a percentage, typically either 30 or 40%, of actions due to excitation in the orthogonal direction. The AASHTO Standard Specifications (AASHTO, 1996) and LRFD Specifications (AASHTO, 1998) prescribe that the actions from the maximum response in one direction shall be combined with 30% of the actions from the maximum orthogonal response. For an action in x-direction, Z_x , in terms of

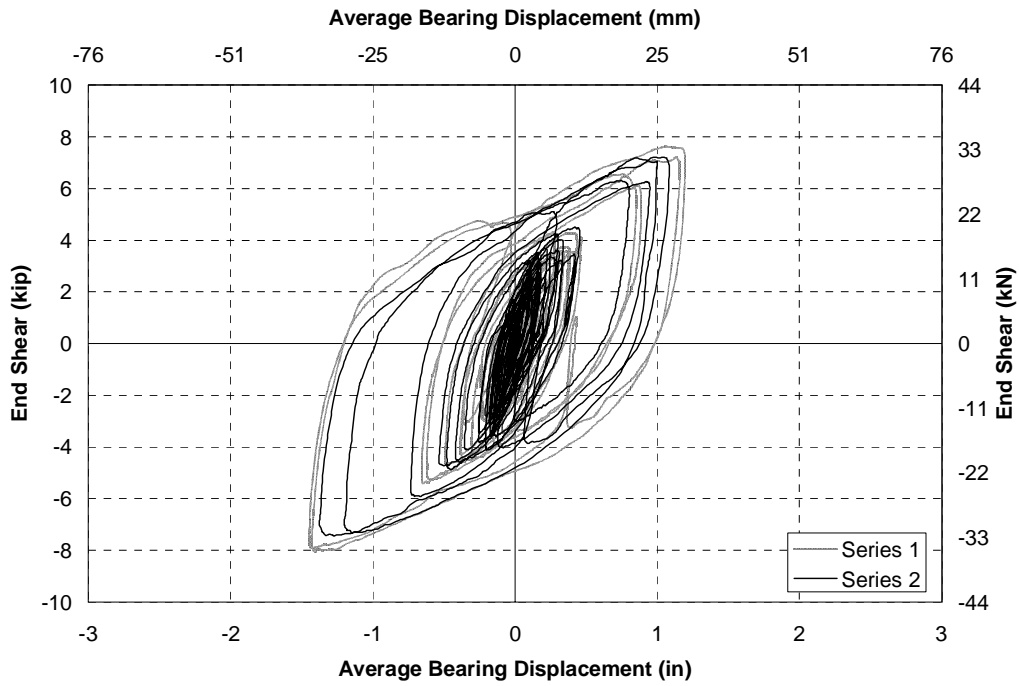


FIGURE 5-13 STLRB, STLRS2 - Hysteretic response of north end in response to 2.0 El Centro during two different series of shake table experiments

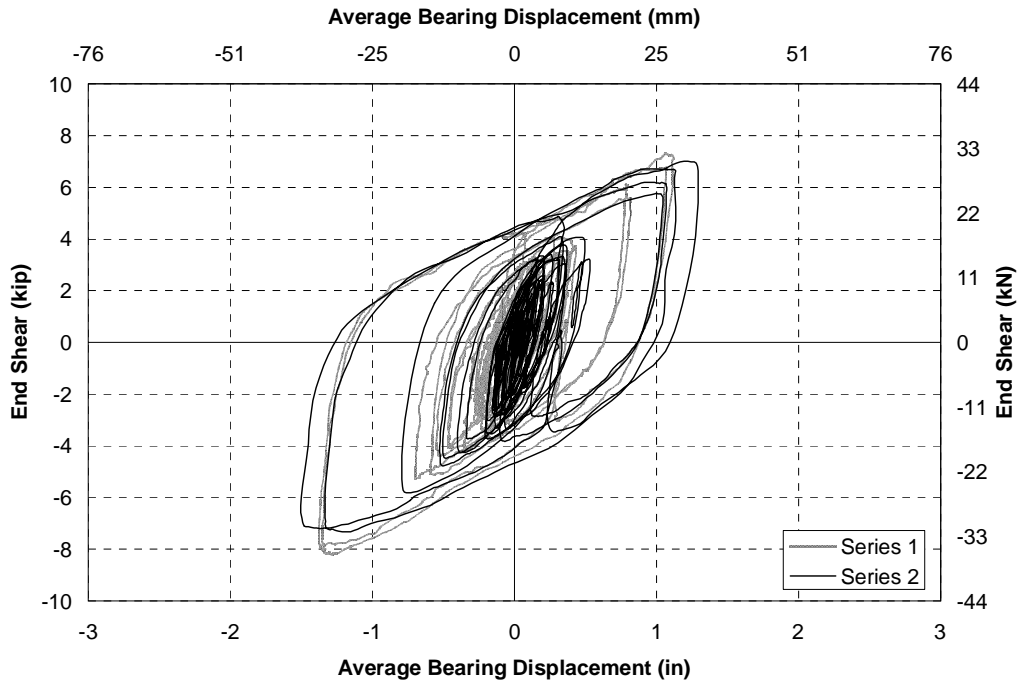


FIGURE 5-14 STLRB, STLRS2 - Hysteretic response of south end in response to 2.0 El Centro during two different series of shake table experiments

orthogonal excitations defined by the longitudinal and transverse axis of a bridge, this can be represented by:

$$Z_x = \max \begin{cases} Z_x^L + 0.3Z_x^T \\ 0.3Z_x^L + Z_x^T \end{cases} \quad \dots 5.1$$

where: Z_x^L is the action in the x-direction due to longitudinal earthquake excitation and Z_x^T is the action in the x-direction due to transverse earthquake excitation. A similar expression can be written for actions in the y-direction, Z_y . The ATC/MCEER recommendations (ATC/MCEER, 2003) suggest a 40% combination factor, thus the 0.3 in Equation 5.1 is replaced by 0.4. Another combination procedure commonly used or often proposed as an alternative to the 30% or 40% rules is the square root sum of the squares (SRSS) procedure (ATC, 1996; ATC/MCEER, 2003), which is given by:

$$Z_x = \sqrt{(Z_x^L)^2 + (Z_x^T)^2} \quad \dots 5.2$$

A common modal combination procedure is the Complete Quadratic Combination (CQC) procedure which is a more general combination procedure that accounts for coupling of modes which have similar natural frequencies. This has been applied to multi-axial excitation in the form of the CQC3 procedure (Smeby, 1985; Menum, 1998). It can be shown that the other rules described above are each special cases of the CQC3 rule when certain assumptions are made.

If a component of a structure such as a bearing or column needs to be designed for biaxial actions, different combination procedures can be used, depending on which combination procedure was used to combine the actions for excitation in the two directions, to find the resultant action. If the actions in each the x and y-directions of a bridge were calculated by combining the actions from orthogonal excitations using the 30% or 40% rules then the resultant action is typically found from the square root sum of the squares combination of the x and y components. The expression for the resultant, Z_r , is:

$$Z_r = \sqrt{Z_x^2 + Z_y^2} \quad \dots 5.3$$

While the AASHTO LRFD specifications (AASHTO, 1998) do not state this explicitly Equation 5.3 is implied, while in the ATC/MCEER guidelines (ATC/MCEER, 2003) it is explicitly stated. If the SRSS combination procedure is used to combine the actions resulting from orthogonal excitations, then a modification of the 30% rule or 40% rule has been proposed to find the resultant actions (ATC/MCEER, 2003), such that:

$$Z_r = \max \begin{cases} \sqrt{Z_x^2 + (0.4Z_y)^2} \\ \sqrt{(0.4Z_x)^2 + Z_y^2} \end{cases} \quad \dots 5.4$$

When the CQC3 rule was proposed to combine the actions in a given direction from orthogonal excitations rule (Smeby, 1985; Menum, 1998), no combination procedure was mentioned to account for the resultant of biaxial actions.

The critical actions in the design of an isolation system are the isolator displacements. The AASHTO Isolation Specifications state that forces should be combined due to different components of ground motion. However, in calculating the forces, the effective stiffness of the isolators should be taken at the design displacement, therefore the implication is that the maximum displacements can be combined in the same manner. Experiments were performed on the bridge model, seismically isolated with lead rubber bearings, to determine which combination rule is most appropriate for the bearing displacements.

The maximum displacements in response to the El Centro, Northridge and Kobe earthquake records described in Chapter 2 were calculated during excitation of the bridge model in order to compare the measured response with that calculated using the above formulations. Combinations of the uniaxial responses were compared to the measured biaxial response of the bridge model, in order to evaluate the different combination procedures. Table 5-1 gives the average maximum

TABLE 5-1 Combined Maximum Displacements from Uniaxial Excitation of the Bridge Model

Excitation	Maximum Displ. due to Long. Excitation (mm)		Maximum Displ. due to Trans. Excitation (mm)		Combined Displacement Components (mm)					
	Long.	Trans.	Long.	Trans.	SRSS		30% Rule		40% Rule	
					Long.	Trans.	Long.	Trans.	Long.	Trans.
Single Span Bridge										
1.0 El Centro	18	3	2	17	18	18	19	18	19	18
2.0 El Centro	45	4	3	35	45	35	46	36	46	37
Two Span Bridge										
1.0 El Centro	15	1	3	15	16	15	16	16	16	16
2.0 El Centro	44	2	5	36	44	36	44	37	44	38
0.5 Kobe	33	2	5	35	34	35	34	37	34	37
1.0 Kobe	68	2	4	54	68	54	68	56	68	56
0.5 Sylmar	30	4	9	31	32	32	32	34	32	35
1.0 Sylmar	85	3	10	77	85	77	86	80	86	81

TABLE 5-2 Measured and Calculated Maximum Displacements from Biaxial Excitation of the Bridge Model

Excitation	North-South Earthquake Component	Measured Displacements from Biaxial Excitation (mm)			Calculated Biaxial Displacement (mm)			
		Long.	Trans.	Biaxial	SRSS ¹	SRSS ²	30% Rule ³	40% Rule ³
Single Span Bridge								
1.0 El Centro	Longitudinal	19	16	22	26	27	19	20
	Transverse	21	18	22	26	27	19	20
2.0 El Centro	Longitudinal	53	48	61	59	59	46	48
	Transverse	46	49	55	59	59	46	48
Two Span Bridge								
1.0 El Centro	Longitudinal	17	19	20	22	22	16	17
	Transverse	17	15	18	22	22	16	17
2.0 El Centro	Longitudinal	43	40	47	58	58	45	47
0.5 Kobe	Longitudinal	35	24	40	50	50	37	38
1.0 Kobe	Longitudinal	66	48	72	88	89	70	72
0.5 Sylmar	Longitudinal	37	24	38	47	47	33	34
1.0 Sylmar	Longitudinal	97	63	101	117	118	88	91

Notes: 1. Displacement components taken from combined actions calculated from 30% rule

2. Displacement components taken from combined actions calculated from 40% rule

3. Displacement components taken from combined actions calculated from SRSS rule

bearings displacements in both the longitudinal and transverse directions due to uniaxial excitation in the longitudinal and transverse directions respectively for different earthquakes and levels of excitation. The earthquake component with the maximum peak ground acceleration (north-south component in each case) was used for each of the uniaxial excitations. The displacement components perpendicular to the direction of excitation were small at typically around 10% of the parallel component, with one isolated exception of up to 29% measured. This small level of cross-coupling was expected as symmetry of the bridge model should result in negligible accidental torsion. The displacements due to the two orthogonal excitations were combined in the longitudinal and transverse directions using the SRSS, 30% and 40% rules described by Equations 5-1 and 5-2. However, with minimal cross-coupling between the excitations the transverse response was barely affected by the longitudinal excitation, and vice versa, using any of the combination procedures. The 40% rule resulted in the largest difference between the combined response and uniaxial response, although, the maximum difference was only 12%.

The maximum biaxial displacements in the isolation bearings, averaged between each of the bearings, are outlined in Table 5.2. Both components of recorded earthquake excitation were applied to the bridge model in measuring the biaxial response, with the dominant north-south component noted for each case in the table. Table 5-2 shows that the maximum responses vary depending on the type of ground motion, magnitude of ground motion and direction of the major axis. It is generally assumed that the response to the minor horizontal earthquake component is

around 85% of the response to the major earthquake component (Clough, 1993). Comparison of the longitudinal and transverse responses in Table 5-1 show that on average the minor axis response is 81% of the major axis response, therefore close to that assumed, although there is some fluctuation depending on whether the dominant component is in the longitudinal or transverse direction, or depending on the earthquake. In general the longitudinal response is slightly larger than the transverse response, particularly for the single span bridge where superstructure flexibility has a larger impact on the transverse response. The near fault excitations of Sylmar and Kobe appear to have a larger difference between the major and minor response than El Centro.

The maximum measured biaxial displacement was calculated from the maximum vectorial combination of longitudinal and transverse displacements at each time increment, corrected for the angle of the displacement transducer cables. This can be compared to the expected maximum biaxial displacement calculated using the SRSS, 30% and 40% rules in Equations 5.3 and 5.4. In calculating the SRSS biaxial combination, the maximum longitudinal and transverse displacement components were calculated using the 30% and 40% combinations respectively to combine the effects of the two orthogonal excitations, as given by the corresponding excitations listed in Table 5-1. In calculating the 30% and 40% biaxial combinations, the SRSS combination of displacements from the two orthogonal excitations was used to calculate each displacement component. When compared to the measured biaxial responses, the SRSS combinations were typically conservative (by on average 16%), while the 30% and 40% combinations were both unconservative (by on average 13% and 10% respectively). Thus, the displacements calculated using the SRSS biaxial combination is most appropriate. Even if the effects of cross-coupling in the responses is ignored, the SRSS combination to calculate the maximum biaxial displacement is conservative, therefore the accidental torsional effects (for a symmetric bridge) could be ignored in calculating the maximum biaxial response.

5.4 Differential Support Excitation

As each support in the bridge model was located on different shake tables, it was possible to excite the different supports with different excitations. Differential excitations are primarily due to three effects, namely (Wang, 2003):

- Wave passage effect where the different supports are subjected to different motions due to a time lag between the seismic waves hitting the first support and subsequent supports.
- Incoherence due to seismic waves taking different travel paths through the ground and thus resulting in different excitations at different supports of a bridge.
- Soil effects if the different supports are founded on different soil types and depths.

For long bridges with many spans wave passage and incoherence effects are shown to affect the longitudinal response of a bridge (Wang, 2003; Wang, 2004). However, for relatively short bridges wave passage effects and incoherence effects can be considered to be minimal as the seismic waves follow effectively the same travel path to each of the supports and the time lag between them is negligible. However differential motion due to different soil conditions under the foundations at each support are a realistic source of differential ground motion in a relatively short bridge such as the bridge model. Therefore, this type of differential excitation was studied.

The isolated bridge model was excited with differential ground motion in the longitudinal direction, the direction considered most critical for differential ground motion because the bridge was effectively rigid between the two ends. The shake table displacements due to excitations of 1.5 x El Centro as recorded (rock) and 1.5 x El Centro after passing through a soil layer, applied in the longitudinal direction of the bridge, are shown in Figure 5-15. The soil motion was shown to have larger amplitude displacements due to lower frequency content and slightly larger accelerations. The soil motion can also be seen to begin approximately 1 second later than the rock motion due to the time taken to pass through the soil layer.

The hysteretic response of the bearings at the north and south ends due to the 1.5 x El Centro rock excitation applied at both ends of the bridge is shown in Figure 5-16. This figure shows the response of the two ends was very similar with relatively small displacements at a maximum of 27 mm. The response of the bearings for the bridge model subjected to the 1.5 x El Centro soil motion at both ends is shown in Figure 5-17. This figure shows that the displacements in the bearings increased to a maximum of 66 mm. The response of the bearings with differential excitation at the ends of the bridge model are shown in Figure 5-9. This figure shows that there was an extremely large displacement at the south end with a maximum displacement of 98 mm. The large displacement was attributed to reaching the critical state in the bearings at this end, which was discussed previously.

The experimental data shows that differential ground motion at the two ends of the bridge resulted in a worse response than the two motions applied uniformly through the bridge. Therefore, despite not being a central focus of this report, the topic of differential ground motion justifies further study.

5.5 Response of the Two Span Bridge Model

Bearings, theoretically identical to those at the ends of the bridge model, were placed at the midspan of the bridge model converting it into a two span bridge. If the superstructure of the bridge model was assumed to be infinitely rigid in the transverse direction and there was no torsional deformation, then the response of each bearing would be expected to be identical for a single mode of deformation. In contrast if the bridge model was assumed to be infinitely flexible then the response of the bearings at each support would be independent of each other and proportional to the tributary weight at each set of bearings. In reality the bridge model was in between these two limiting cases. As the support at midspan was expected to carry 62% of the bridge shear compared to 19% at each of the end supports then the midspan bearings could be expected to have larger deformations than the bearings at the ends of the bridge. Figure 5-18 shows that the displacements at the midspan of the bridge model were 10 - 20% higher than the displacements at the ends of the bridge model. Therefore, while the displacements were larger they were not proportional to the tributary weight and the bridge deformed almost rigidly, with similar shears in each bearing. This was quite different to the response with unbonded braces as the relative stiffness of the unbonded braces compared to the lead rubber bearings was much higher. As stated with analysis of the unbonded braces, a multi-span bridge should be analyzed as a system in order to determine the effect of superstructure stiffness relative to the ductile components.

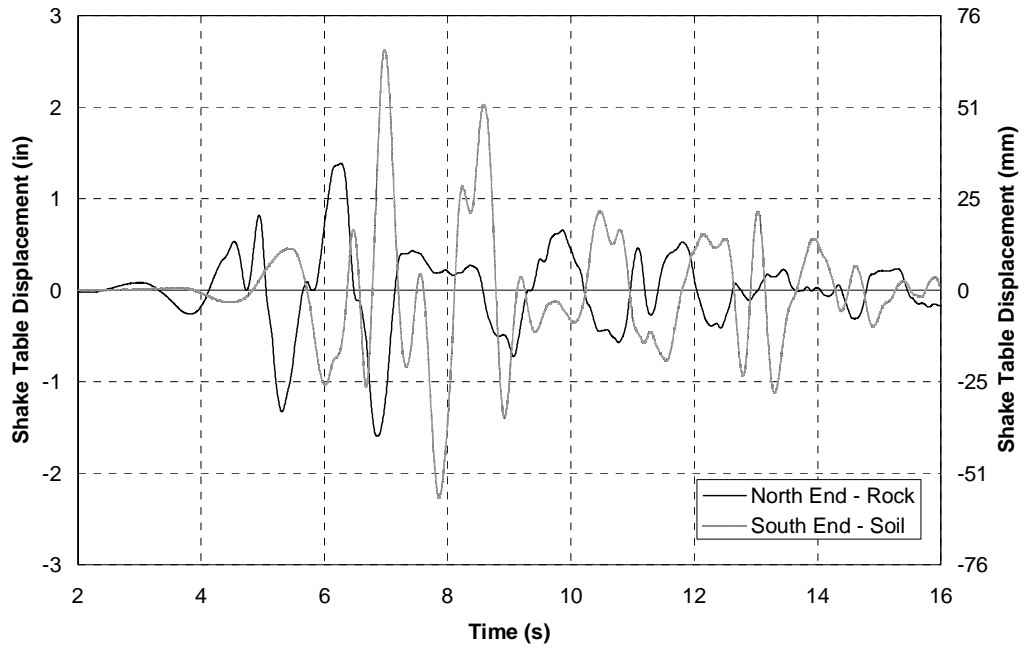


FIGURE 5-15 STLRB - Longitudinal shake table displacements in response to 1.5 El Centro with rock excitation at north end and soil excitation at south end

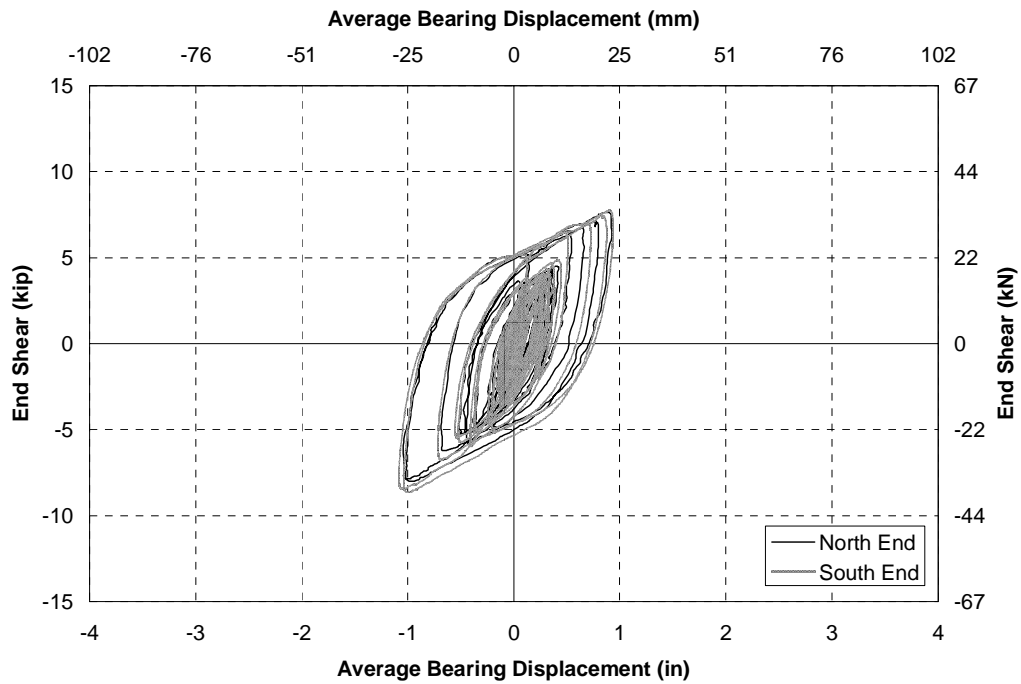


FIGURE 5-16 STLRB - Longitudinal bearing response to 1.5 El Centro with rock excitation at both ends

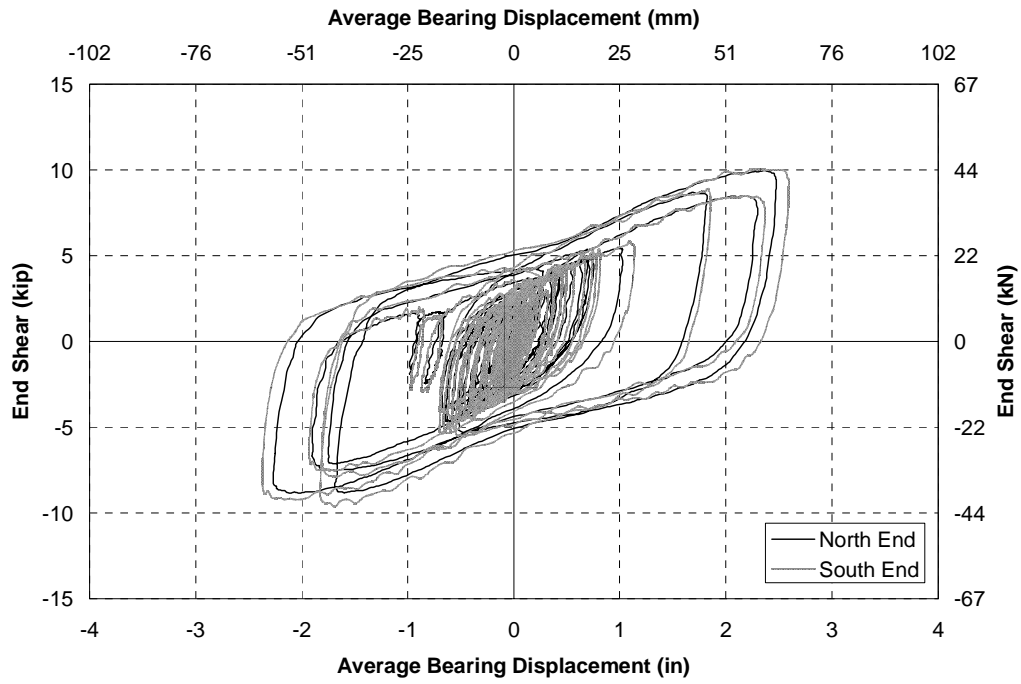


FIGURE 5-17 STLRB - Longitudinal bearing response to 1.5 El Centro with soil excitation at both ends

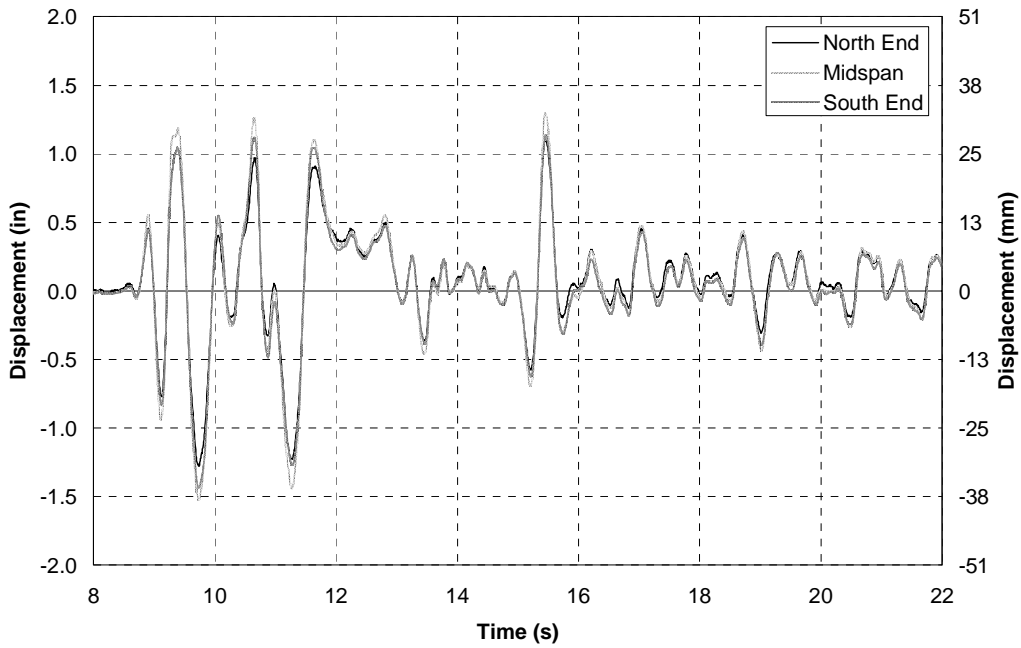


FIGURE 5-18 STLRB2S - Bearing displacements in response to 2.0 El Centro

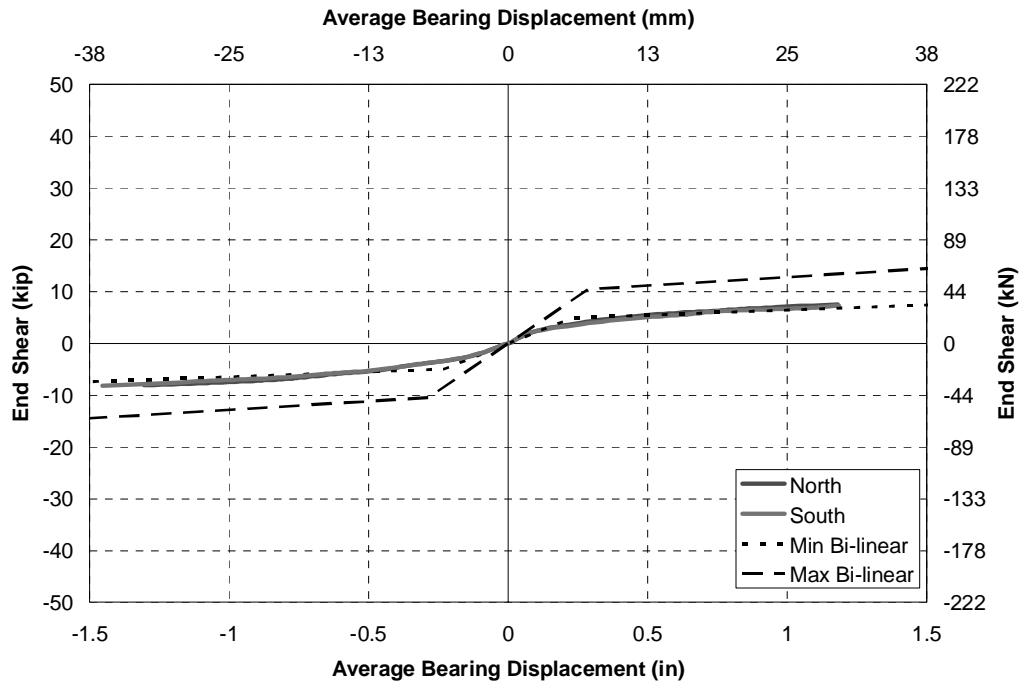


FIGURE 5-19 STLRB - Envelopes for horizontal bearing displacements and corresponding maximum and minimum design bi-linear models

5.6 Comparisons with Ductile End Cross Frames and Design Parameters for Seismic Isolation Bearings

The response of the bridge at 1.0, 1.5 and 2.0 x El Centro with the lead rubber bearings is summarized in Table 4-2 along with the response of the ductile end cross frames. The end shears for the bridge model with the isolation bearings were considerably less than with the ductile end cross frames at 15 to 18% of the shears with the heavy X-braces. This was largely due to the increased displacements possible in the bearings compared to the elastic and ductile end cross frames. If the displacements in the ductile end cross frames could be increased through lower strength ductile elements then their performance could be brought closer to that for the isolated bridge, although the displacement capacity of the LRBs cannot be matched by the ductile end cross frames. This is further discussed in the following section.

SECTION 6
PARAMETRIC STUDIES AND COMPARISONS OF THE NON-LINEAR
TRANSVERSE RESPONSE OF THE BRIDGE MODEL WITH DUCTILE END
CROSS FRAMES AND SEISMIC ISOLATORS

6.1 Introduction

The properties of the superstructure including the girders, deck slab and shear studs were studied in the preceding report (Carden, 2005) with an analytical model developed to capture the properties of the bridge model. Non-linear elements to model the X-braces, buckling restrained braces and lead rubber bearings were described in Chapter 5. As part of the bridge superstructure they were studied in Chapters 6 and 7. This chapter describes the combination of each of these elements and the development of a non-linear analytical model in order to compare the modeled behavior of the bridge model with experimental results using non-linear time history analysis. The model was developed so that it could be later generalized for the design and analysis of any bridge. The analytical model was also used to make further comparisons between the bridge response with ductile end cross frames and seismic isolators.

6.2 Non-Linear Modeling of the Bridge Model

6.2.1 Modeling of the Ductile X-braces, Unbonded Braces and Lead Rubber Bearings

The analytical model shown in Figure 6-1 was used to perform non-linear time-history analyses on the bridge model using SAP2000 v8.30 (Computers and Structures, 2004). More details for the analytical model are available in Carden et al. (2005).

Ductile components were added to the end regions in order to model the X-braces, buckling restrained braces and lead rubber bearings. Three configurations of end cross frames were considered. The heavy X-brace configuration was based on the configuration in the shake table experiments with welded connections. This configuration was similar to that in the reversed static experiments with bolted connections except that in the reversed static experiments slippage in the connections influenced the response. The geometry of the end region in the analytical model with the heavy X-braces is shown in Figure 6-2. Rigid links were used to connect the bearing stiffeners to the ends of the diagonal members. The diagonals were modeled using NLLink elements, although in the case of the heavy X-braces, the properties were linear. The diagonals were assumed to be purely axial elements as the effect of bending in the elements was shown to be relatively small.

The configuration of the model with light X-braces is shown in Figure 6-3. Each diagonal element for the light X-braces was modeled with two NLLink elements, one primarily to model the tension properties and a second for the compression properties. These elements had properties as described in Chapter 5 based on the single angle component experiments. The forces for the angle properties calculated in Chapter 5 were multiplied by 1.1 in order to allow for dynamic loading in the shake table experiments.

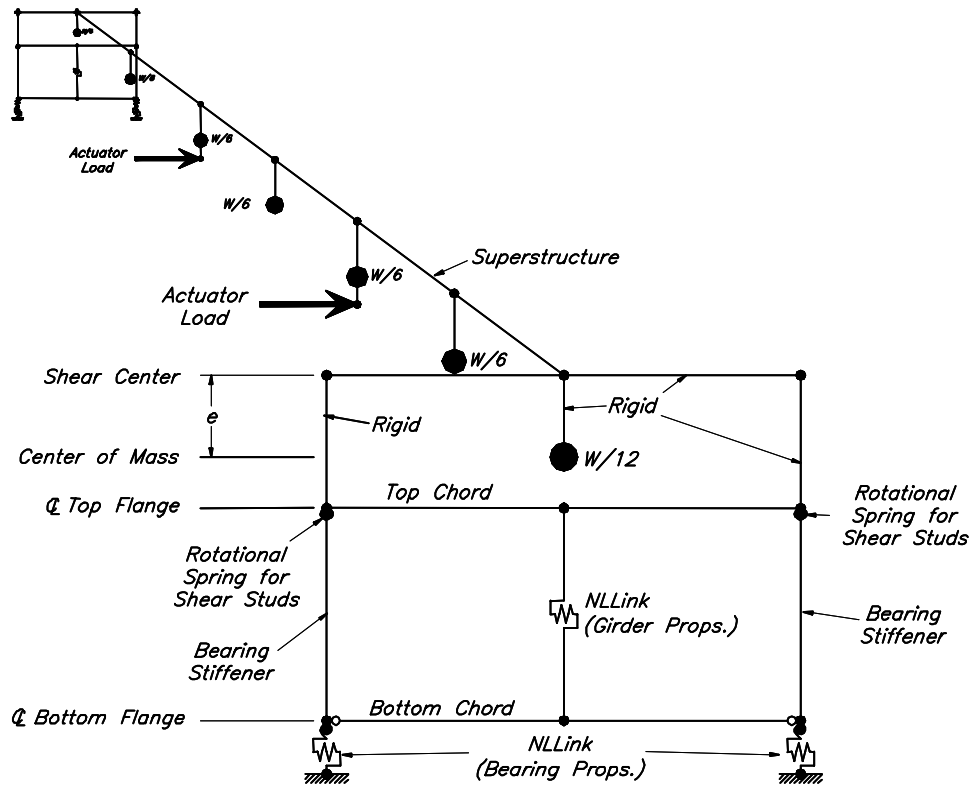


FIGURE 6-1 Illustration of simplified non-linear analytical model of bridge

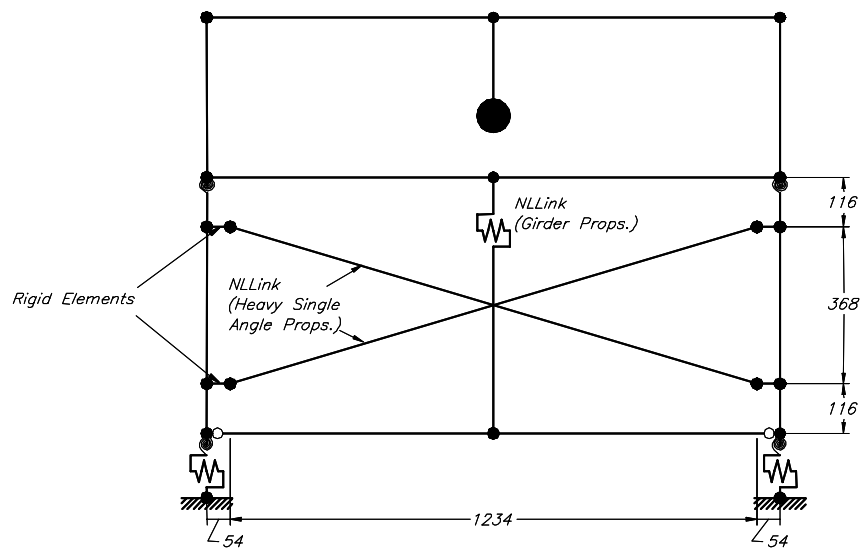


FIGURE 6-2 End region of analytical model with heavy X-braces

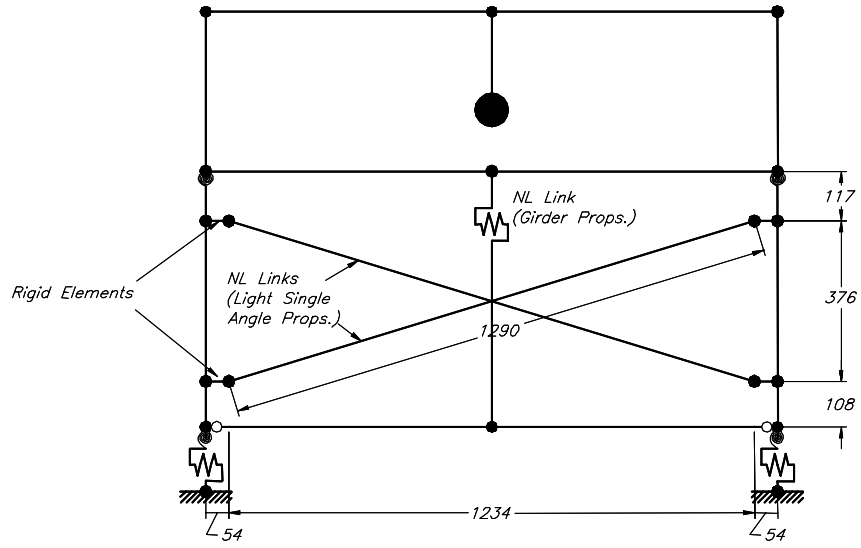


FIGURE 6-3 End region of analytical model with light X-braces

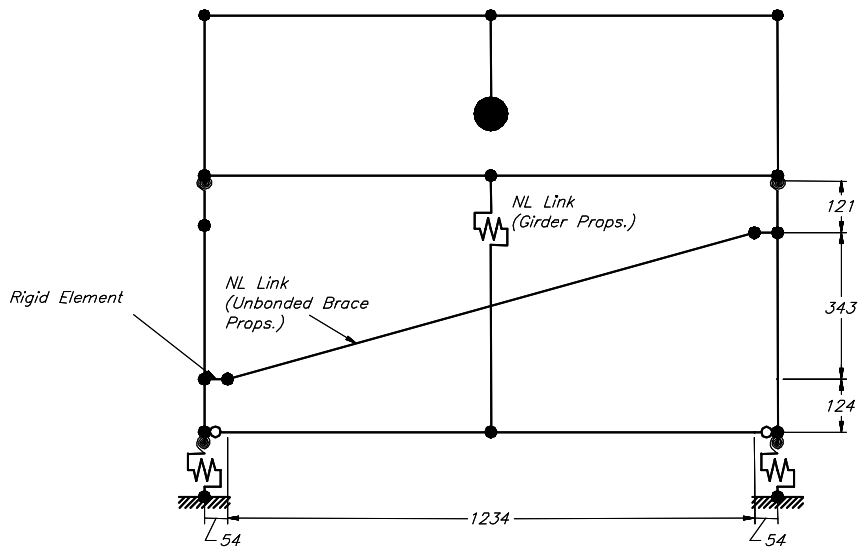


FIGURE 6-4 End region of analytical model with buckling restrained brace

The buckling restrained braces were modeled with a single NL Link element at each end of the bridge model (Fig. 6-4), incorporating the non-linear axial tension and compression properties of the brace using those properties described from the component experiments in Chapter 5. As the measured post-yield stiffness of the end region did not correspond to that calculated for the post-yield stiffness in the buckling restrained brace from component experiments, additional post-yield stiffness was assumed in the braces. For the pinned connections the effect of slippage was also investigated using another non-linear element connected between the rigid link and the buckling restrained brace element, modeling a slippage of 3mm in both directions.

Analytical models were considered for four of the bridge configurations with reversed static loading. These included the configuration with no end cross frames (RSNECF), with pinned top and bottom chords but no diagonals in the end cross frames (RSPC), with heavy X-braces (RSHXB2) and with light X-braces (RSLXB). Loading was applied to the analytical model in a cyclic fashion with increasing amplitudes of loads, similar to the loads measured during the corresponding experiments.

Six simply supported bridge configurations were considered when subjected to dynamic loads. These included the configuration with no end cross frame (STNECF), with heavy X-braces (STHXB), light X-braces (STLXB), unbonded braces with pin ended connections (STPUB), unbonded braces with fixed ended connections (STFUB) and the model with lead rubber isolation bearings (STLRB). Each model was compared in response to 2.0 x El Centro, with input for the analytical model taken directly from the recorded accelerations averaged between the shake tables at the two ends of the bridge model for each corresponding experiment. The exception to this was experiment STNECF as the bridge model was only excited up to 1.0 x El Centro in this configuration. Other ground motions were also considered for comparison as appropriate for selected experiments in different configurations of the bridge model.

6.2.2 Response during Reversed Static Experiments

With no end cross frames, the analytical model was assumed to respond elastically. Figures 6-5 and 6-6 show the response of the north and south ends respectively for the analytical model compared to the experimental data. The minimal hysteretic behavior observed in the experimental data indicates the elastic model was appropriate. At the north end the elastic slope was shown to fit the backbone for the response well. At the south end the backbone curve appears to slope upwards in the positive excursions, attributed to activation of the shear studs which were slightly damaged during previous experiments but not to the extent as those at the north end. Despite this the stiffness appeared to be reasonably represented by the analytical model. The transverse displacement was measured between the top and bottom chords of the girders. The maximum end shear forces, measured by the load cells in the bridge model, were shown to correspond well to the analytical model, as expected because the loading history was effectively force controlled. There was a little difference between the displacements with the maximum displacements being underestimated by the models except at the south end where stiffening was observed. Figure 6-7 shows the total applied force in the bridge model measured in the load cells compared to the midspan deck slab displacement. The analytical model is shown to correlate closely with the backbone curve of the experimental data, with correlation between maximum forces and displacements.

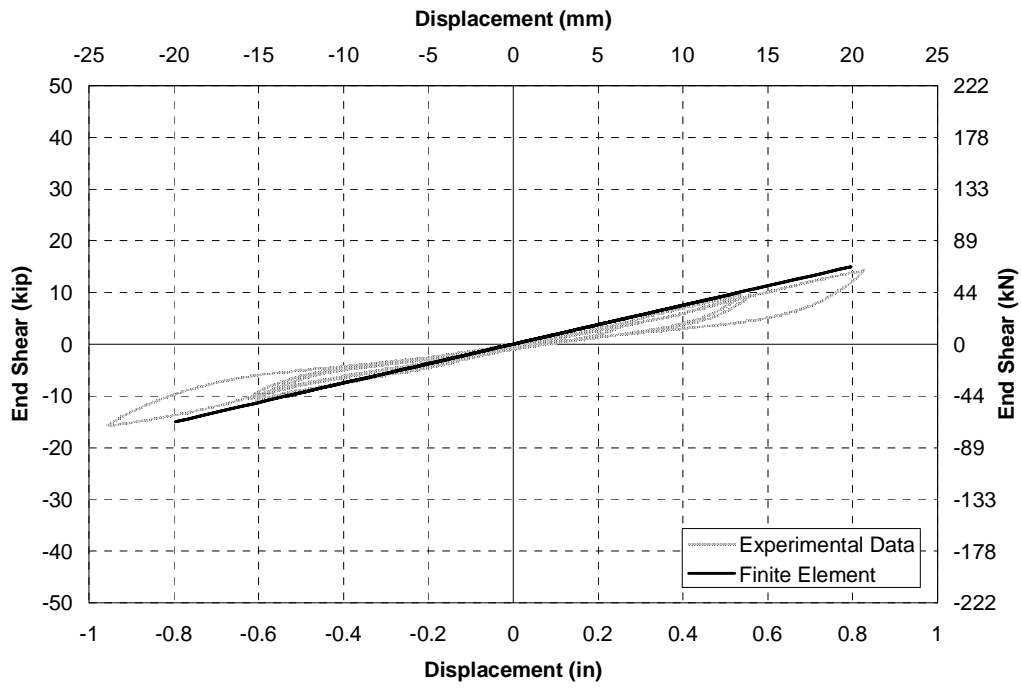


FIGURE 6-5 RSNECF - End shear vs end displacement at north end of analytical model compared to experimental data

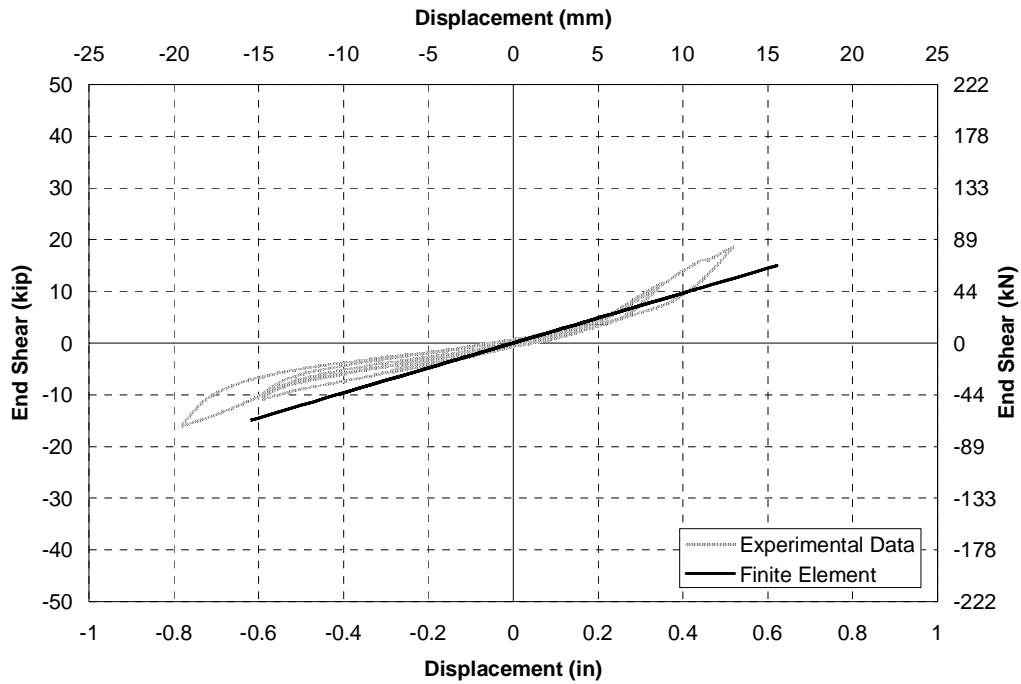


FIGURE 6-6 RSNECF - End shear vs end displacement at south end of analytical model compared to experimental data

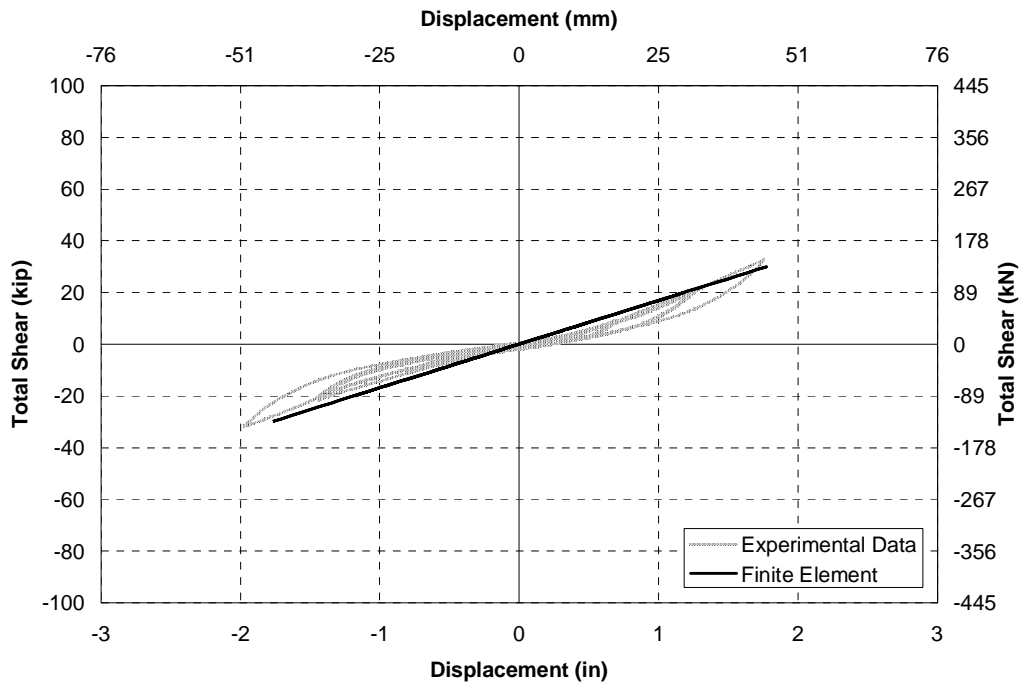


FIGURE 6-7 RSNECF - Total applied force vs midspan deck slab displacement of analytical model compared to experimental data

When the pin ended top and bottom chords were added to the bridge model it was previously shown that some hysteretic behavior was introduced into the ends due to friction in the connections. This behavior was modeled using an elasto-plastic element with a slip force, corresponding to an end shear at which slippage was observed, of 10 kN which was added to the elastic girder properties. The resulting analytical behavior at the north and south ends compared to the experimental data is given in Figures 6-8 and 6-9. These figures show good correlation between the analytical model and experimental model although the displacements for the positive excursions were overestimated by the analytical model while the displacements for the negative excursions were underestimated. Without friction being considered in the analysis the displacements were shown to be considerably overestimated by the analytical model. At the midspan the response of the analytical model shows a similar stiffness to the backbone curve in the experimental data (Fig. 6-10). The response exhibits less hysteretic behavior at midspan than at the ends showing that the hysteretic behavior at the ends has a reduced effect at the midspan of this relatively flexible superstructure.

The response at the ends of the bridge with the heavy X-braces, which used bolted connections in reversed static experiments, is shown in Figures 6-11 and 6-12. The analytical model for these cross frames did not attempt to model the slippage in the connections, the result of which is quite apparent in these figures. Although the displacements measured in the ends during the experiment are much larger than those calculated in the analytical model, the slope of the backbone curves neglecting an offset for slip, is comparable between the experimental data and analytical model. At the midspan, Figure 6-13 shows that stiffness is captured relatively well by the analytical model.

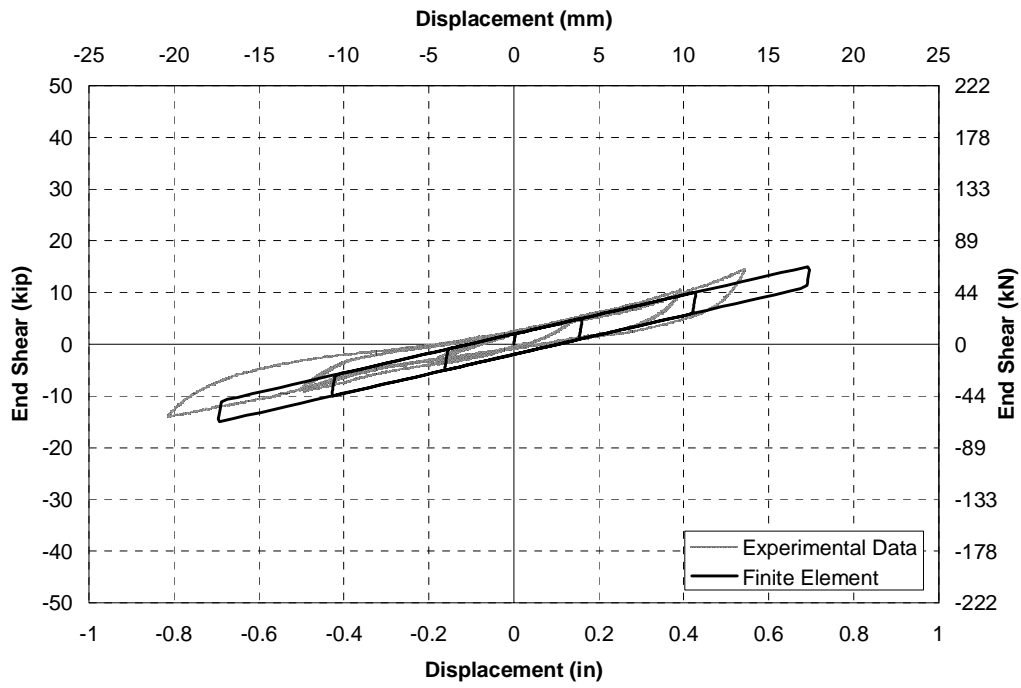


FIGURE 6-8 RSPC - End shear vs end displacement at north end of analytical model compared to experimental data

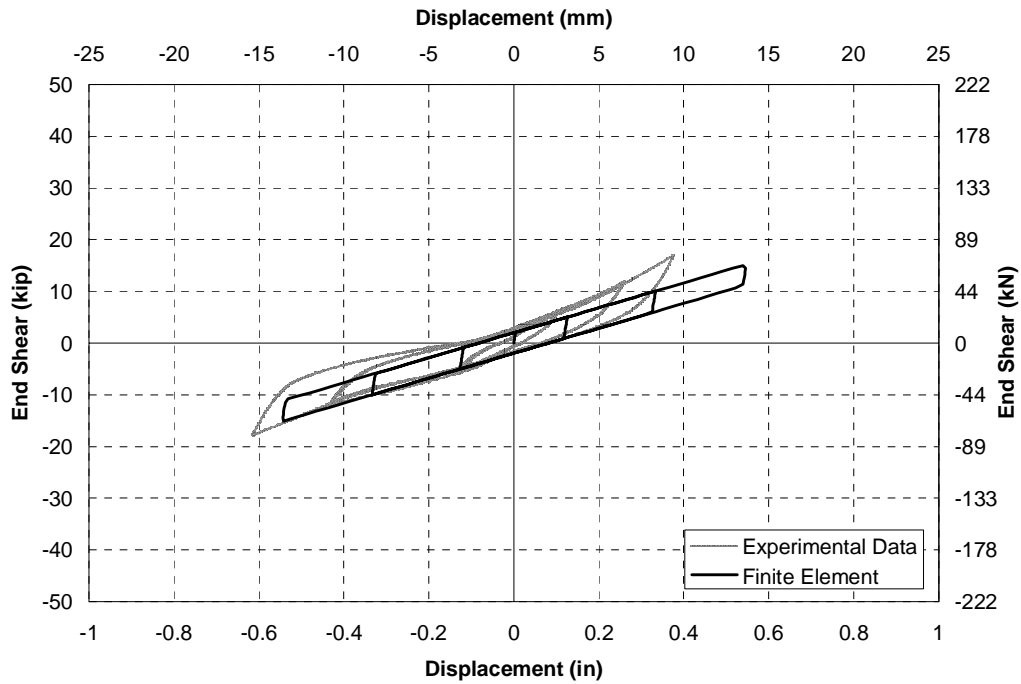


FIGURE 6-9 RSPC - End shear vs end displacement at south end of analytical model compared to experimental data

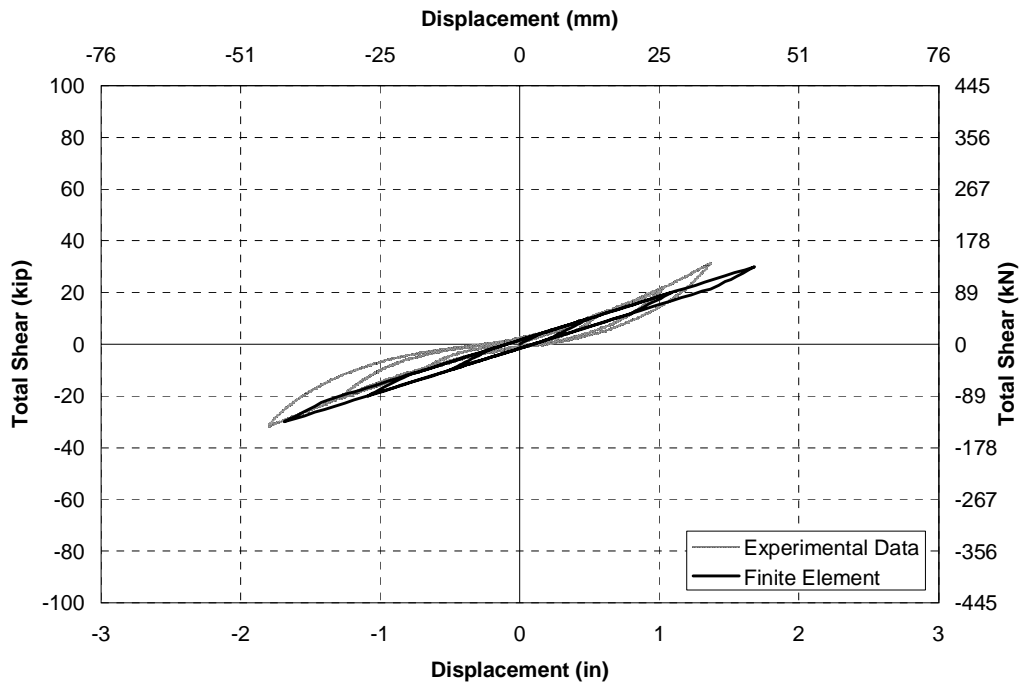


FIGURE 6-10 RSPC - Total applied force vs midspan displacement of analytical model compared to experimental data

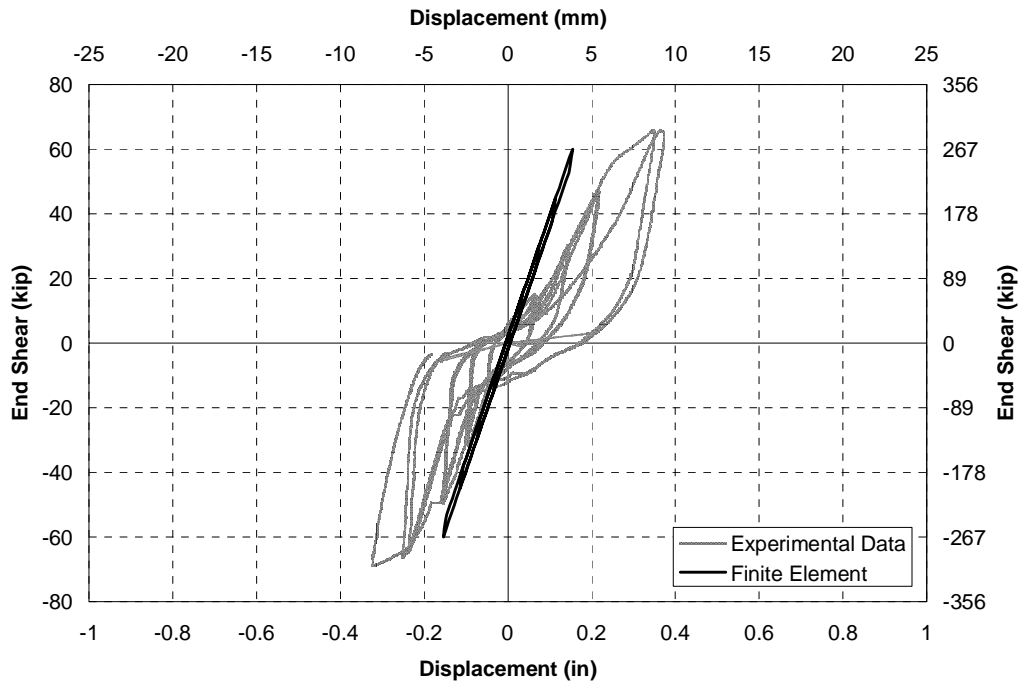


FIGURE 6-11 RSHXB2 - End shear vs end displacement at north end of analytical model compared to experimental data

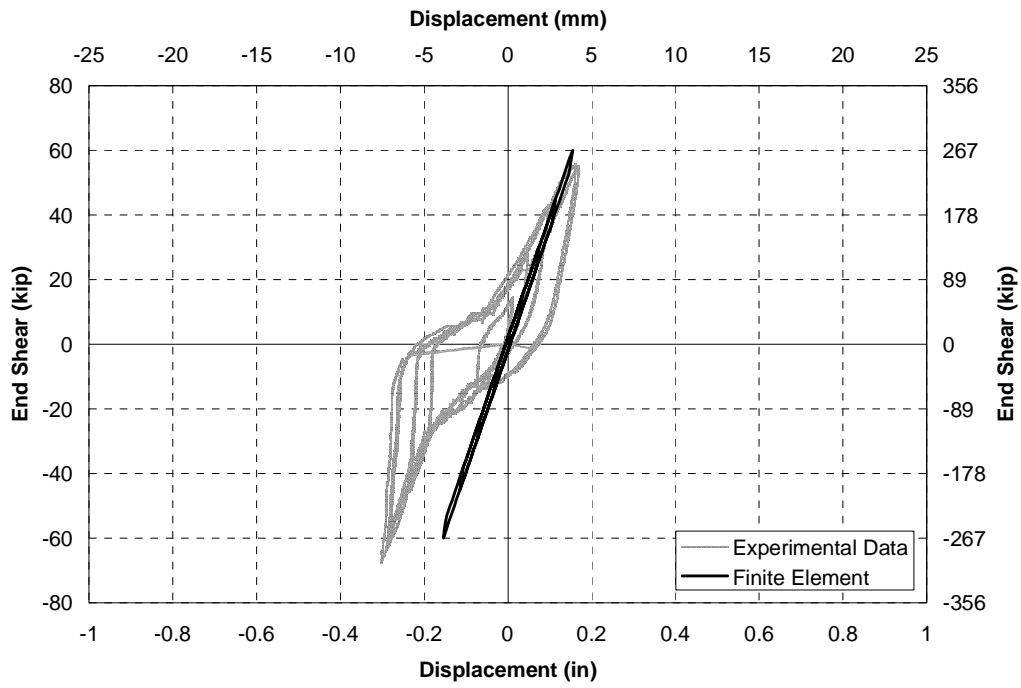


FIGURE 6-12 RSHXB2 - End shear vs end displacement at south end of analytical model compared to experimental data

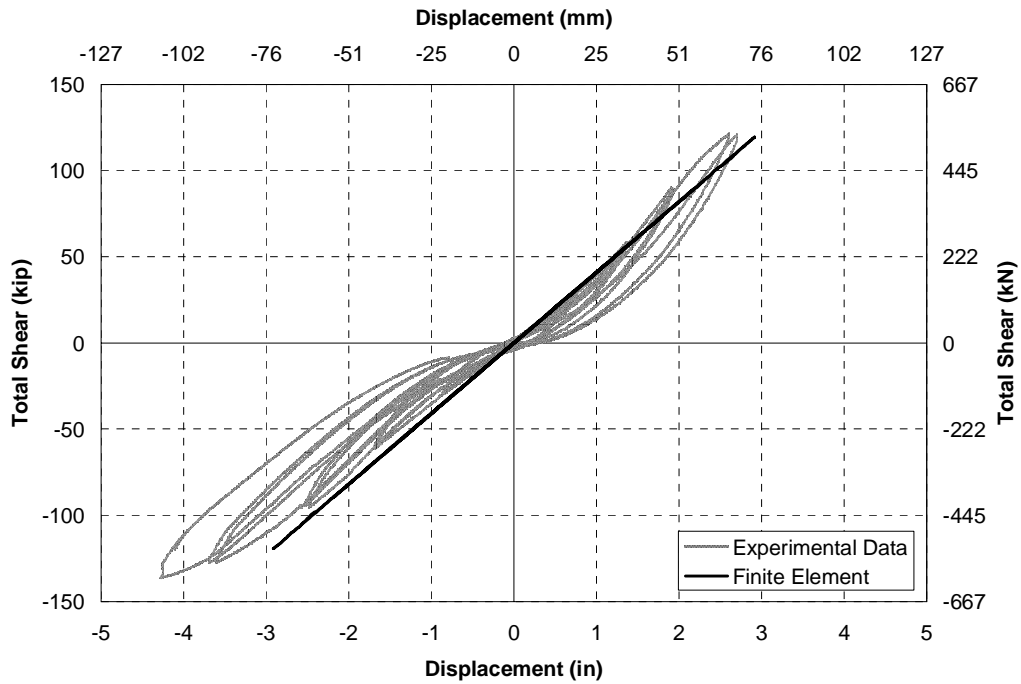


FIGURE 6-13 RSHXB2 - Total applied force vs midspan displacement of analytical model compared to experimental data

While the previously described models were largely elastic except for the friction modeled in the top and bottom chords, the non-linear behavior was prevalent in the analytical model with the light X-braces. The non-linear response of the cross frames at the north and south ends of the bridge model are shown in Figures 6-14 and 6-15. The model captures the buckling and yielding response of the cross frames well with the backbone of the force-displacement curve being captured, as well as the degradation in stiffness and strength for repeated cycles. The forces in the analytical model were close to the measured forces although the displacements were typically overestimated. At the north end the maximum displacement for the positive excursion from the analytical model is within 5% of the measured value. At the south end the effect of stiffening is again observed in the positive excursion resulting in a 12% difference in the maximum force but a 35% difference in the maximum displacement. At midspan it is again observed in Figure 6-16 that the apparent hysteretic area was reduced compared to a the ends, which it is consistent between the experimental data and analytical model. The maximum displacement at midspan also appears to be affected by stiffening which may result in crack closure and subsequent stiffening of the deck slab as displacements increased.

6.2.3 Response during Shake Table Experiments

The same analytical model was used to model the dynamic response with properties similar to those for the reversed static experiments, although different bearing properties and shear studs stiffnesses were assumed, consistent with those calculated previously (Carden, 2005). The displacement response at the ends was captured using the deck slab displacement relative to the bearing displacement.

The dynamic response at the ends of the analytical model with no end cross frames is shown in Figures 6-17 and 6-18. It was observed that there was greater hysteretic behavior in this response compared to the comparable response for the reversed static experiments. This was attributed to the lead rubber bearings which resulted in some hysteresis due to the properties of the lead core even when the bearings were only subjected to rotations as described by Carden (2005). For a normal reinforced elastomeric bearing this would not be expected and was not observed in the reversed static experiments. In order to account for the hysteretic behavior with the lead rubber bearings an additional 1.0 kip was added to the elasto-plastic model for the transverse stiffness of the girder. The analytical model response is shown in Figures 6-17 and 6-18 to compare very well with the measured response in the bridge model. The model captures the stiffness of the bridge model well which is most critical for modeling the girders as part of the ductile end cross frames. It also resulted in maximum displacements close to the measured maximum displacements at the ends of the bridge. At midspan the stiffness and displacements also compared well between the measured response and analytical model. The amplitude of the maximum displacement at midspan was not much higher than that at the ends indicating that with no end cross frames the response was dominated by the end regions despite the bridge model having a relatively flexible superstructure.

The responses of the ends of the bridge model with heavy end cross frames are shown in Figures 6-20 and 6-21. As the connections were welded during shake table experiments no slippage was observed like in the reversed static experiments. The stiffness of the ends were shown to be slightly higher in the analytical model than measured in the experiment. This was attributed to slippage between the deck slab and the girders which was not considered in the analytical model. This comparison shows that the displacement resulting from this slippage was small, although

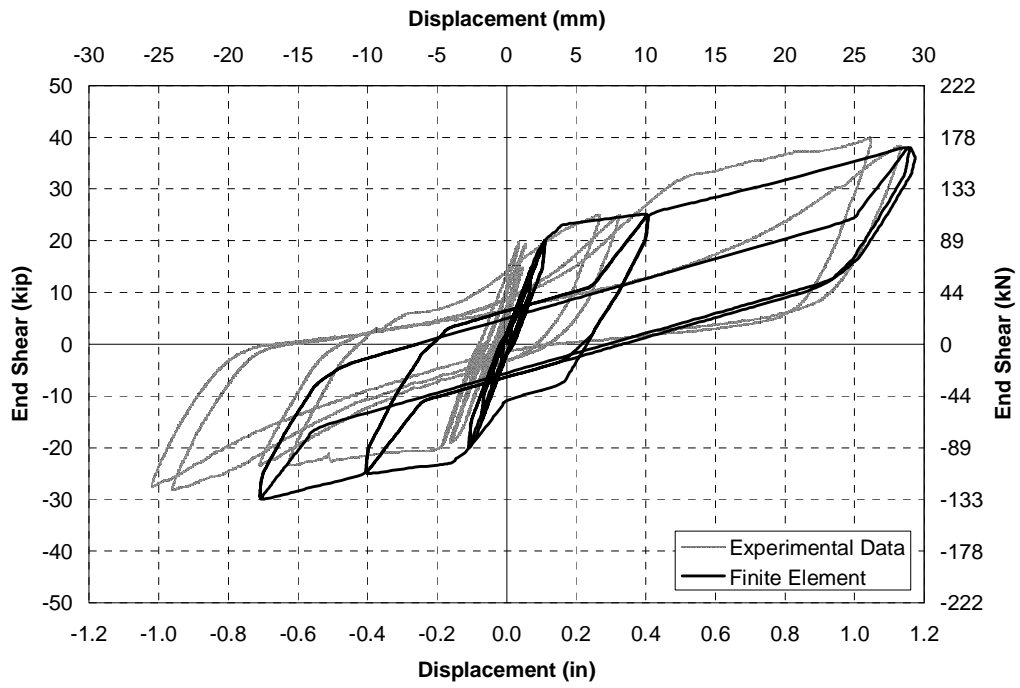


FIGURE 6-14 RSLXB - End shear vs end displacement at north end of analytical model compared to experimental data

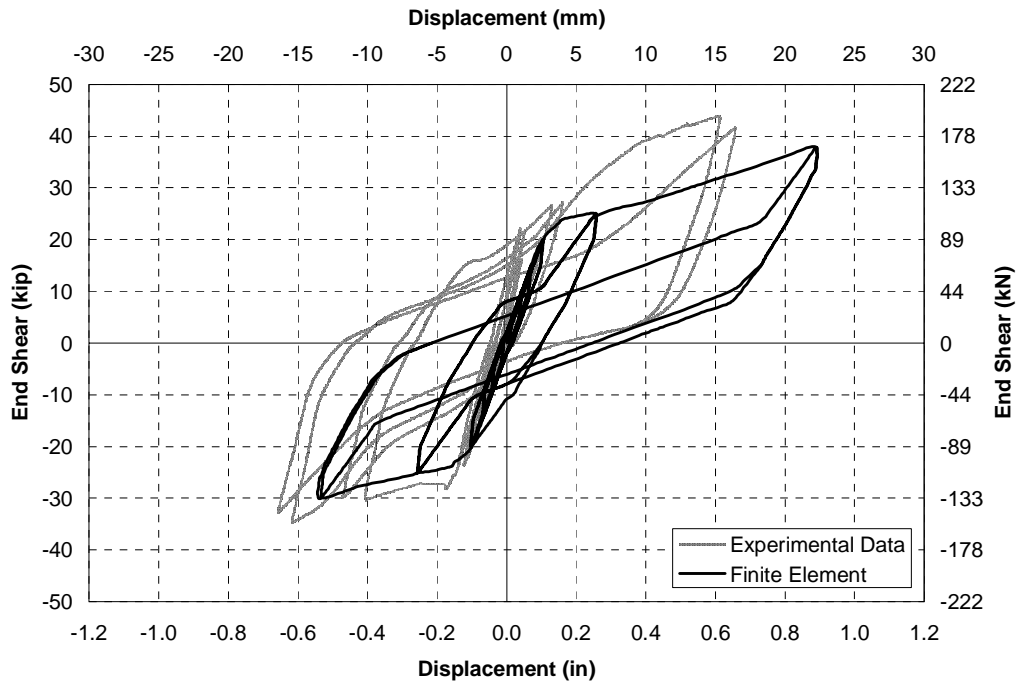


FIGURE 6-15 RSLXB - End shear vs end displacement at south end of analytical model compared to experimental data

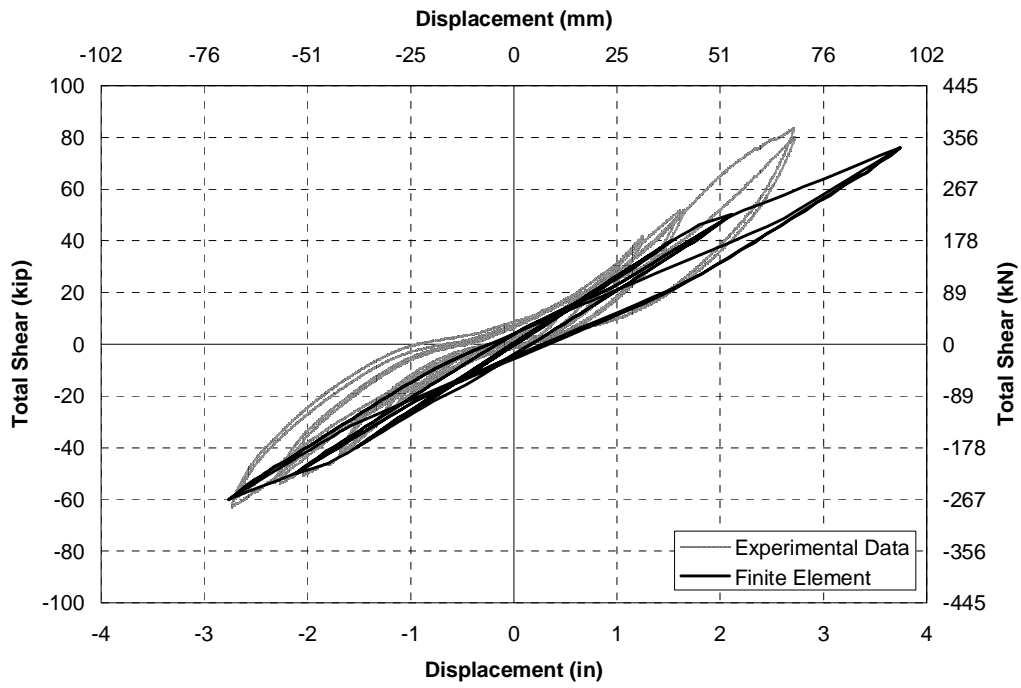


FIGURE 6-16 RSLXB - Total applied force vs midspan displacement of analytical model compared to experimental data

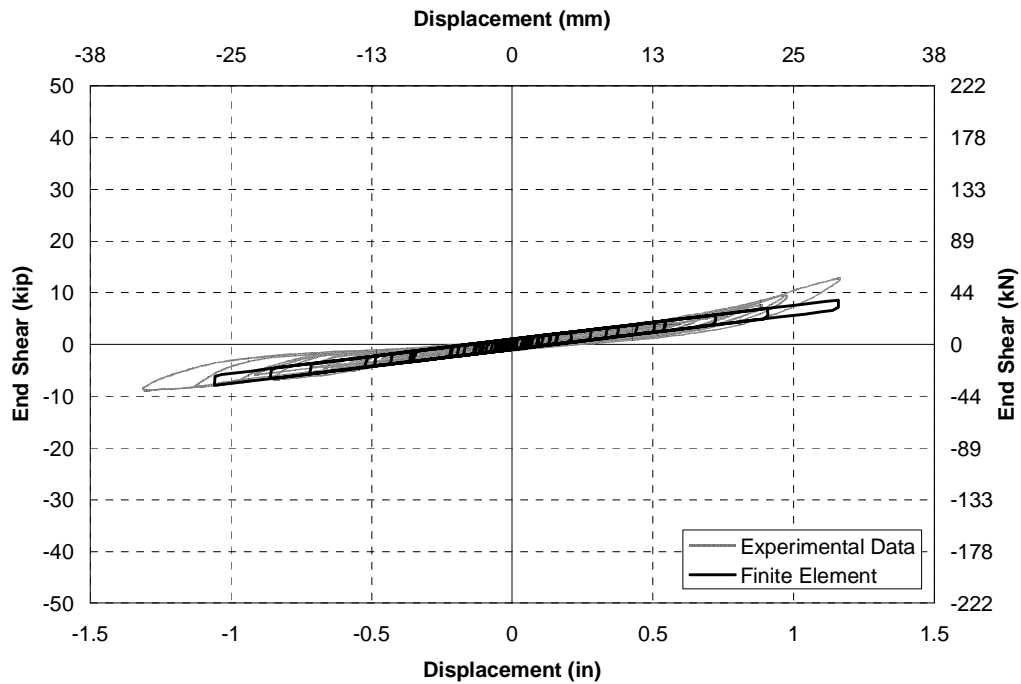


FIGURE 6-17 STNECF - End shear vs end displacement at north end of analytical model compared to experimental data in response to 1.0 El Centro

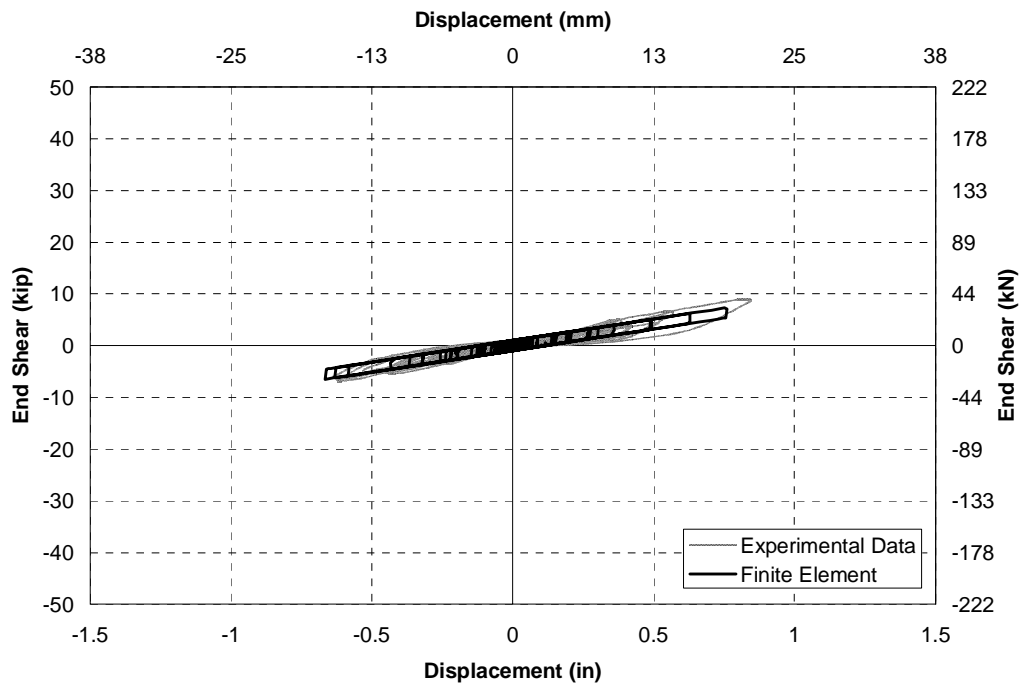


FIGURE 6-18 STNECF - End shear vs end displacement at south end of analytical model compared to experimental data in response to 1.0 El Centro

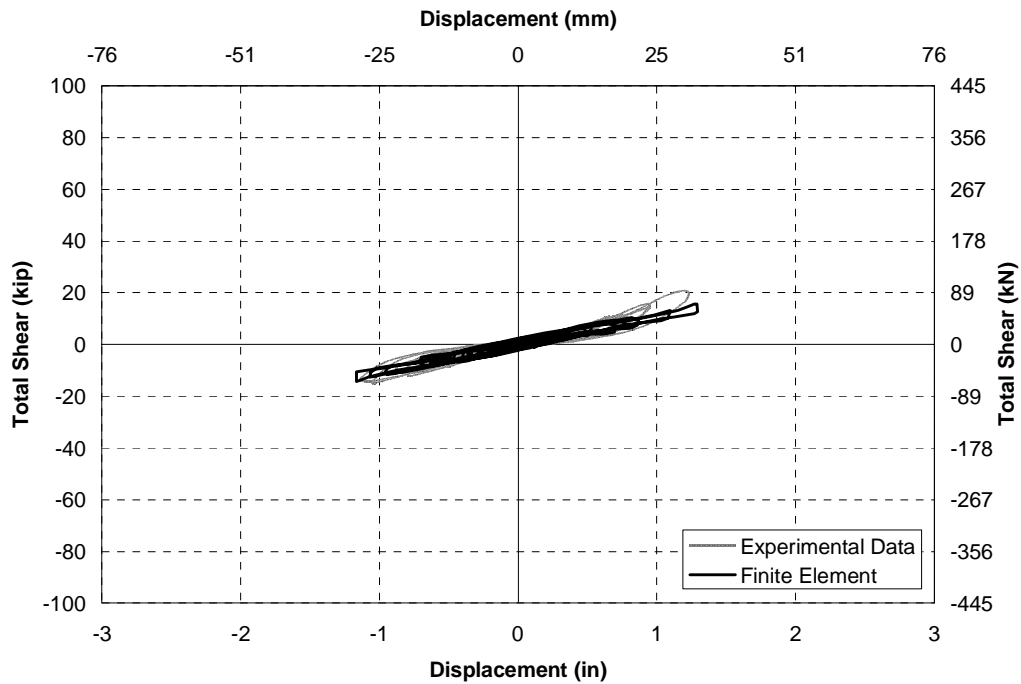


FIGURE 6-19 STNECF - Total shear vs midspan displacement of analytical model compared to experimental data in response to 1.0 El Centro

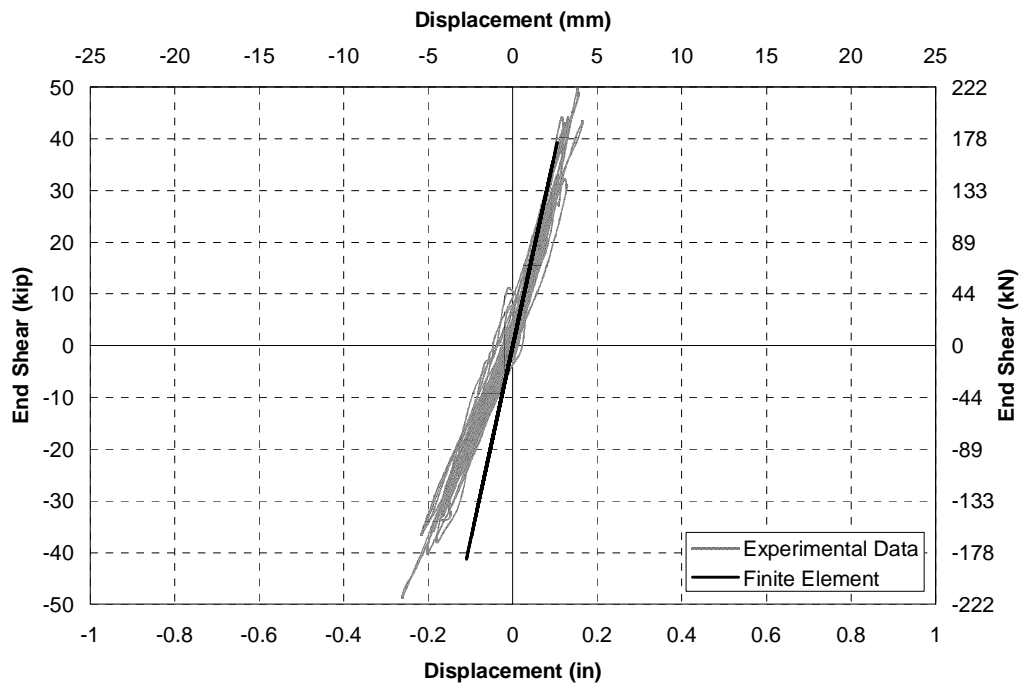


FIGURE 6-20 STHXB - End shear vs displacement at north end of analytical model compared to experimental data in response to 2.0 El Centro

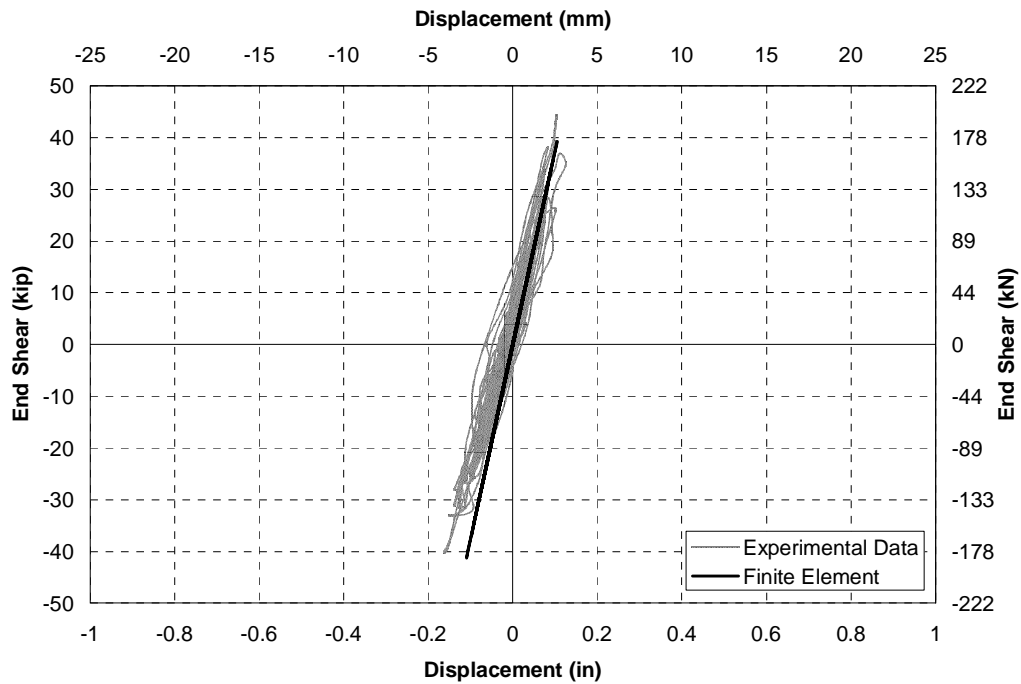


FIGURE 6-21 STHXB - End shear vs displacement at south end of analytical model compared to experimental data in response to 2.0 El Centro

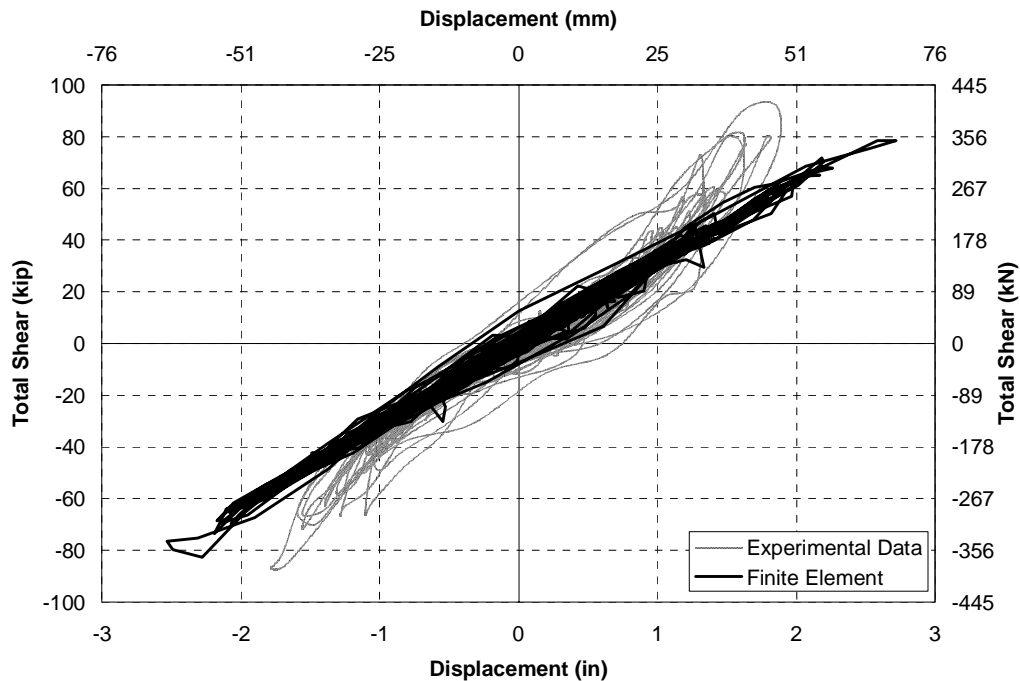


FIGURE 6-22 STHXB - Total shear vs midspan displacement of analytical model compared to experimental data in response to 1.0 El Centro

most noticeable with the heavy X-braces which resulted in small overall end displacements. At midspan (Fig. 6-22) the stiffness appeared to be underestimated by the analytical model due to stiffening in the bridge model at larger displacements. This resulted in displacements that were around 40% larger than measured although the maximum base shear was within 15%. Irregularities were observed in the hysteresis loops at midspan where the hysteresis loops double over themselves. This was observed in both the experimental and analytical responses. This irregularity was attributed to the forces being measured at the ends of the bridge while the displacements were measured at midspan, therefore deformations along the span not associated with the first mode resulted in displacements not directly proportional to forces. This was observed in each of the following hysteresis loops shown at midspan.

The response at the ends of the bridge with the light X-braces in response to 1.5 x El Centro, where first yielding was observed in the cross frames, is shown in Figures 6-23 and 6-24. As with the reversed static experiments the non-linear model of the X-braces appeared to capture the complex hysteretic behavior of the buckled cross frames well, although the maximum displacements at each end were overestimated by the analytical model by 45% at the north end and 15% at the south end. The end hysteresis loops in response to 2.0 x El Centro are shown in Figures 6-25 and 6-26. These show the degradation in strength and stiffness due to prior loading of 1.5 and 1.75 x El Centro. Again the measured response compared well to the calculated response from the analytical model, although the displacements were overestimated in the analytical model by 25% at the north end and 40% at the south end. The variability in the measured displacements and correlation with the analytical model reflects the nature of these types of braces. Despite the large variation in the response, the analytical model is conservatively higher than the measured displacements. At

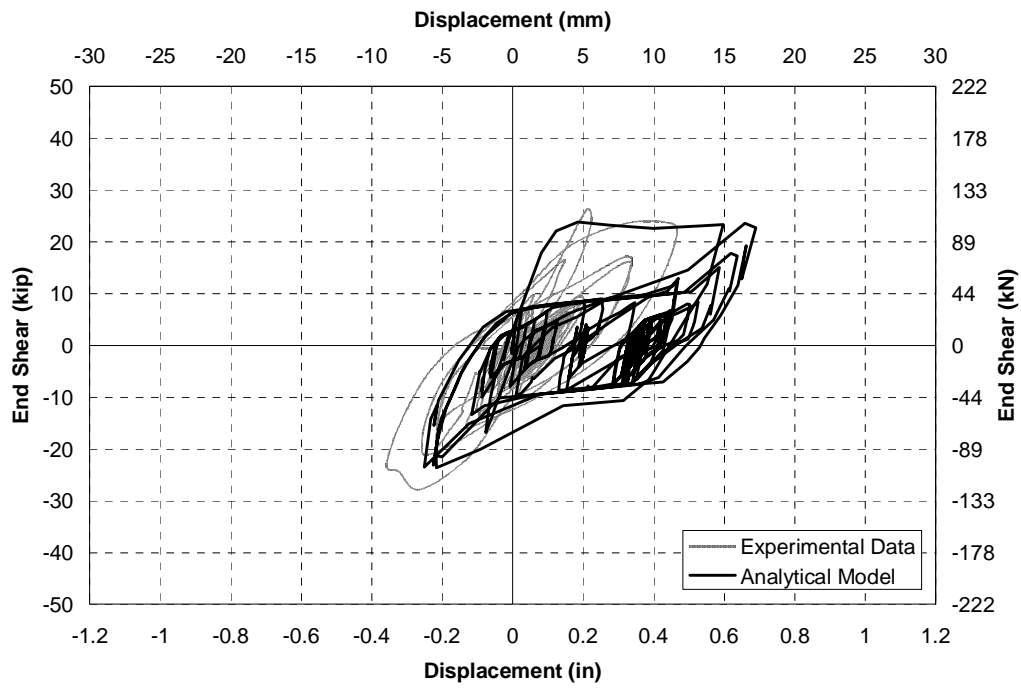


FIGURE 6-23 STLXB - End shear vs displacement at north end of analytical model compared to experimental data in response to 1.5 El Centro

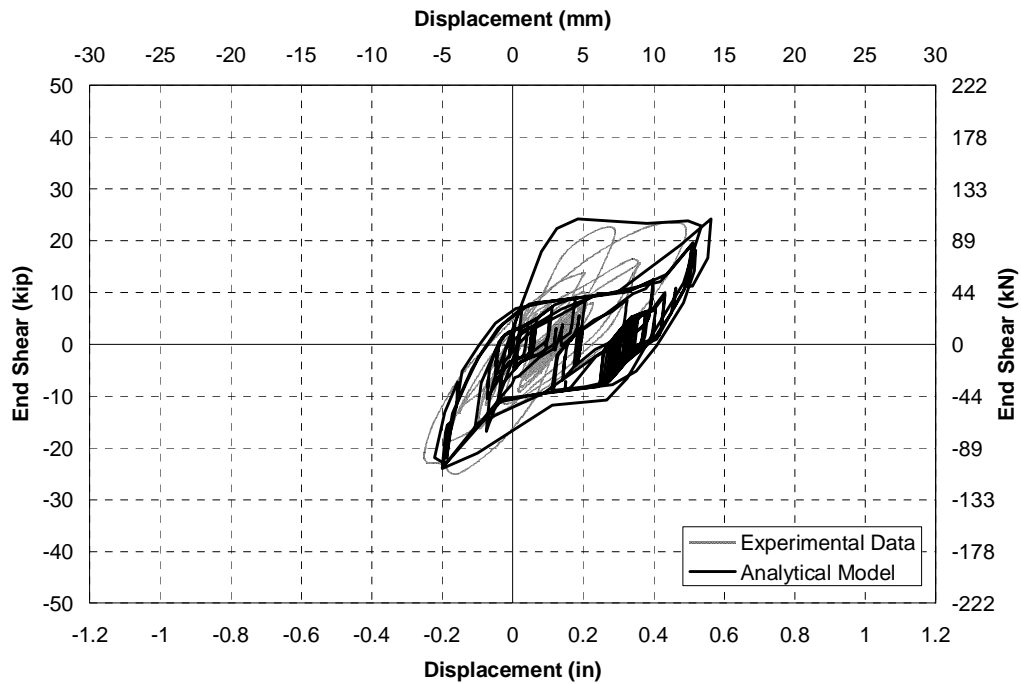


FIGURE 6-24 STLXB - End shear vs displacement at south end of analytical model compared to experimental data in response to 1.5 El Centro

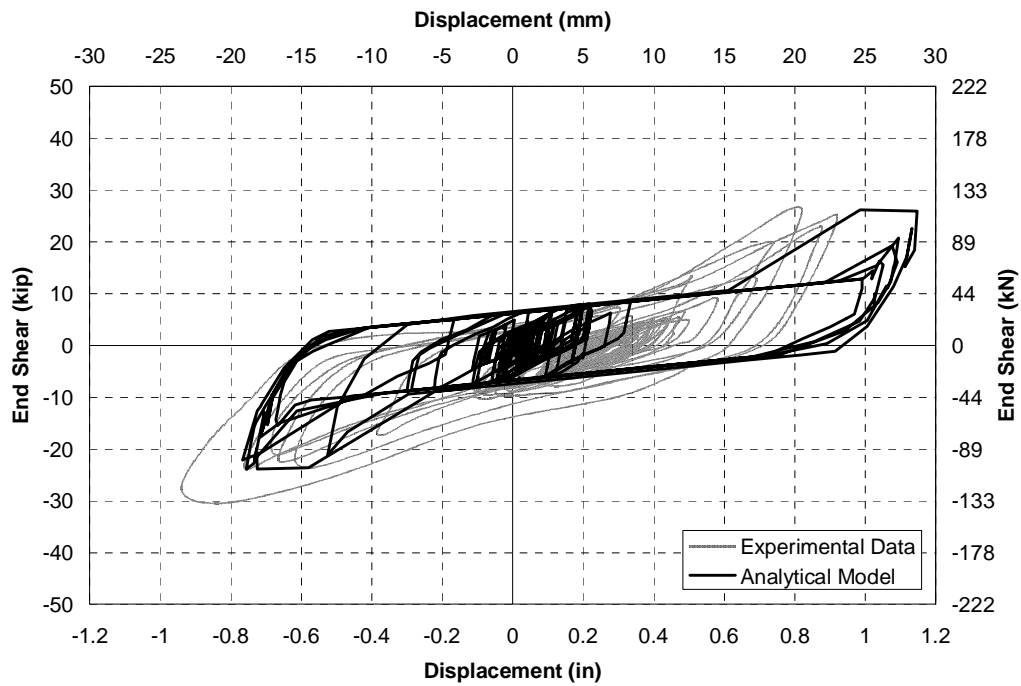


FIGURE 6-25 STLXB - End shear vs displacement at north end of analytical model compared to experimental data in response to 2.0 El Centro after previous excitation

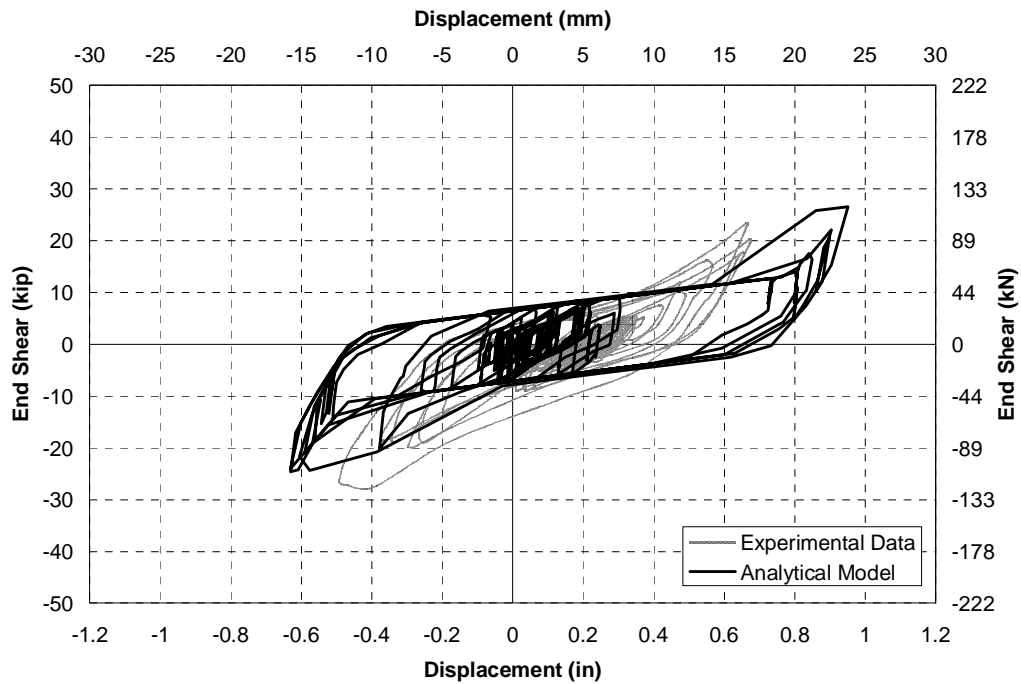


FIGURE 6-26 STLXB - End shear vs displacement at south end of analytical model compared to experimental data in response to 2.0 El Centro after previous excitation

midspan the stiffness and maximum displacement in analytical model were close to those from the measured response as shown in Figure 6-27.

It might be expected that if the bridge model had been subjected to 2.0 x El Centro immediately, instead of ramping up the level of excitation, the maximum displacement in the cross frames would be reduced due to less degradation in the angle members. Figures 6-28 and 6-29 show that the reverse is true for the case of 2.0 x El Centro applied without prior load, and in fact the displacements are larger than when the excitation was increased incrementally. This behavior was attributed to biased buckling of the cross frames and has been observed in past analyses of concentric braced framing systems in buildings (Sabelli, 2001). Such behavior is likely to be very dependent the loading history. This is a disadvantage of X-braces over the other ductile systems.

A model of the bridge with unbonded braces was first considered with fixed end connections. The responses to 2.0 x El Centro at each end of the bridge model are shown in Figures 6-30 and 6-31. These figures show that the braces have a relatively high post-yield slope with the fixed ended connections and the assumed post-yield stiffness of 0.125 times the initial stiffness was appropriate for modeling the post-yield slope of the hysteresis loops particularly at the north end, although it may have been conservative at the south end. The measured maximum displacements were within 10% of the calculated maximum displacements at the ends.

With the pin ended connections the post-yield stiffness of the end region was reduced to 0.075, as the effect of the flexural stiffness of the brace was reduced. However the post-yield stiffness was still higher than modeled for the component experiments (0.025). This was attributed to out-of-plane eccentricities in the brace and other factors that were apparent in the ductile cross frames in the bridge model but not apparent in axial experiments. The response of the end regions are shown in Figures 6-33 and 6-34. The modeled hysteresis loops were much “fuller” than those recorded in the bridge experiment, with the difference attributed to slippage in the connections between the unbonded braces and the bearing stiffeners. Despite the hysteretic energy dissipation being overestimated with the fuller hysteresis loops both the maximum force and maximum displacement were overestimated in the analytical model. The displacement was overestimated by 10% to 40% at the two ends while the forces were within around 10%. When a non-linear element to model the slippage was added in series to that used to model the unbonded brace the maximum displacement response did not change by more than 10%, therefore the slippage model was not considered necessary in calculating the response. The midspan response for the pin connected unbonded braces is shown in Figure 6-35. This was very similar to that from previous experiments with the stiffness of the model captured well, although the maximum displacement was overestimated in the analytical model by 20%.

The final bridge configuration considered was the model isolated with lead rubber bearings. The response of the ends of the isolated bridge are shown in Figures 6-36 and 6-37 with the same vertical scale as for the ductile end cross frames for comparison. The forces in the bridge model with lead rubber bearings are clearly lower than with the different ductile end cross frames systems with the displacements being typically 3 to 4 times larger. The analytical model, based solely on the design properties of the lead rubber bearings, captures the hysteretic behavior of bearings well, with maximum displacements 15% and 5% larger than the measured displacements at the north and south ends respectively. At midspan (Fig. 6-38) the hysteresis loops were similar to those at the ends and compared well to the measured response.

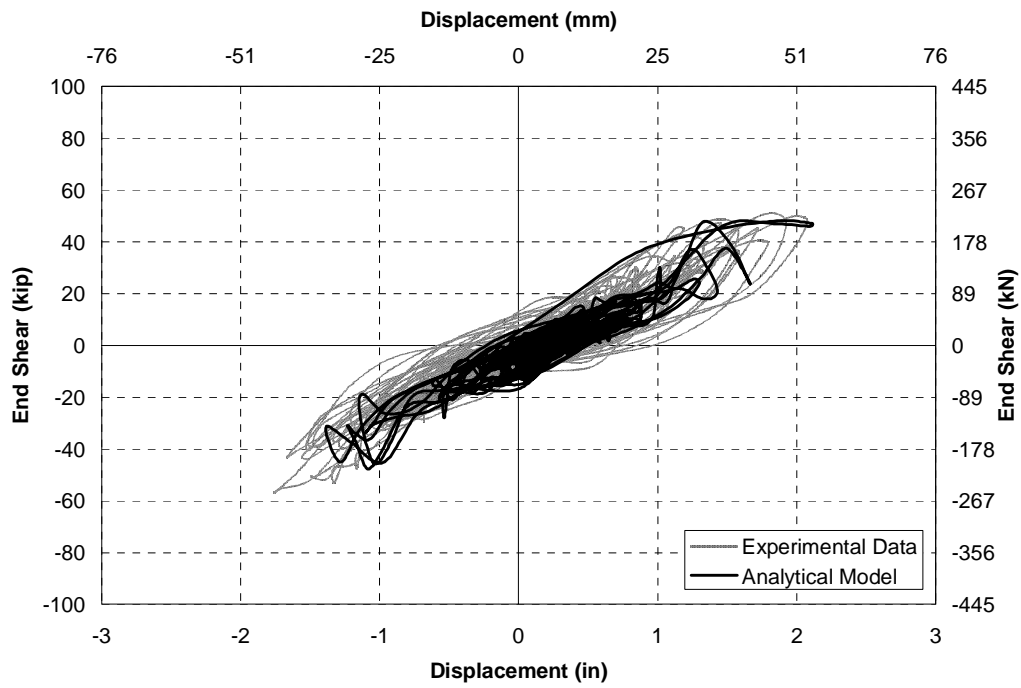


FIGURE 6-27 STLXB - Total shear vs midspan displacement of analytical model compared to experimental data in response to 2.0 El Centro

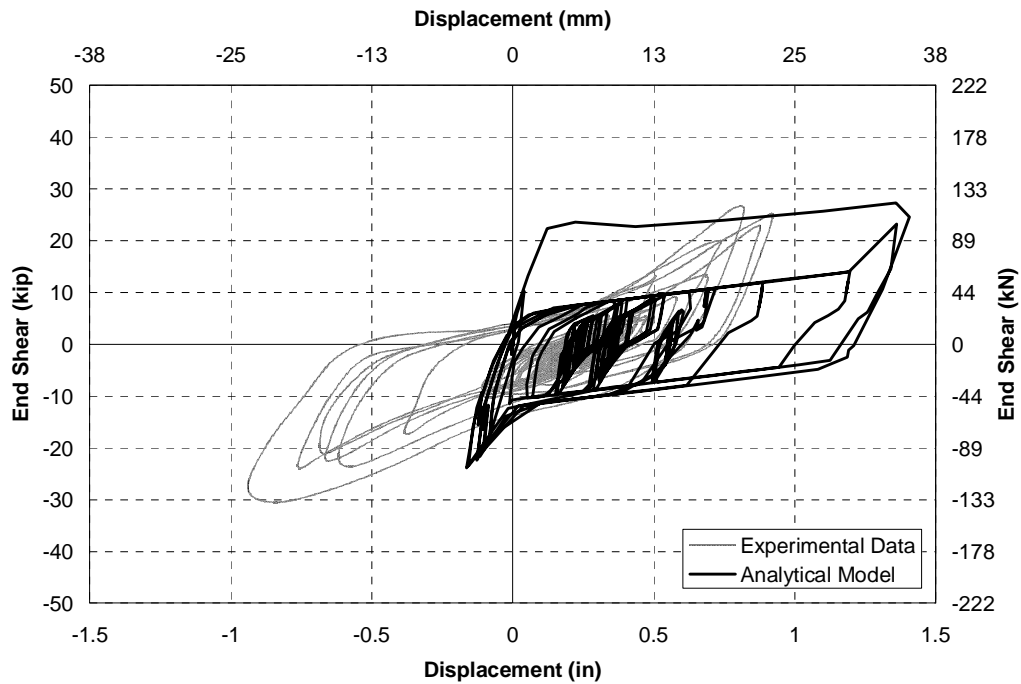


FIGURE 6-28 STLXB - End shear vs displacement at north end of analytical model compared to experimental data in response to 2.0 El Centro assuming no prior loading

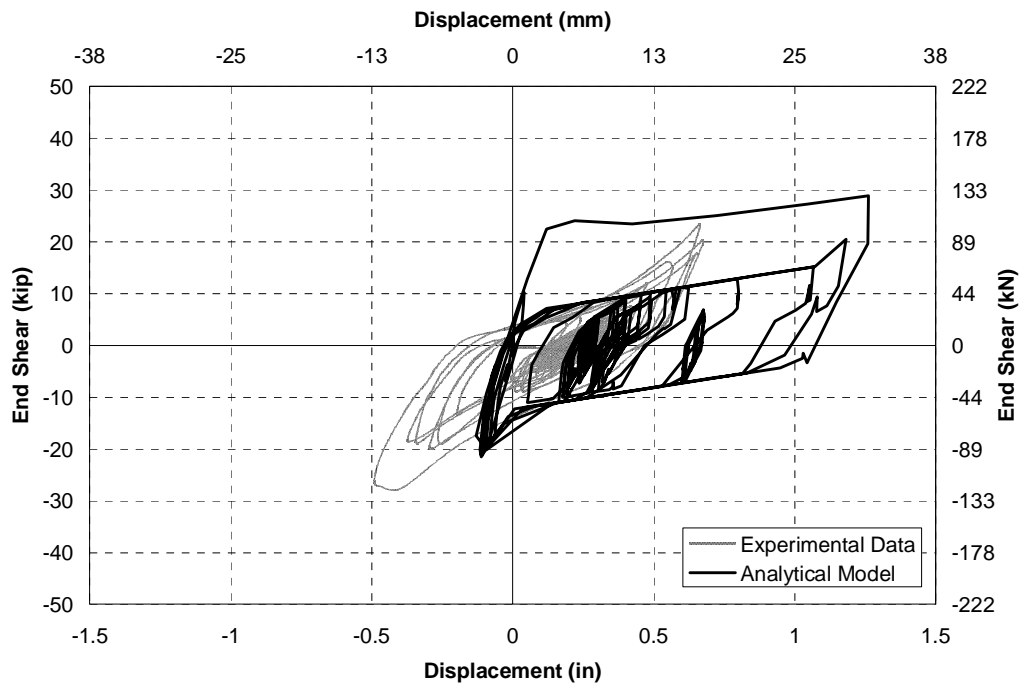


FIGURE 6-29 STLXB - End shear vs displacement at south end of analytical model compared to experimental data in response to 2.0 El Centro assuming no prior loading

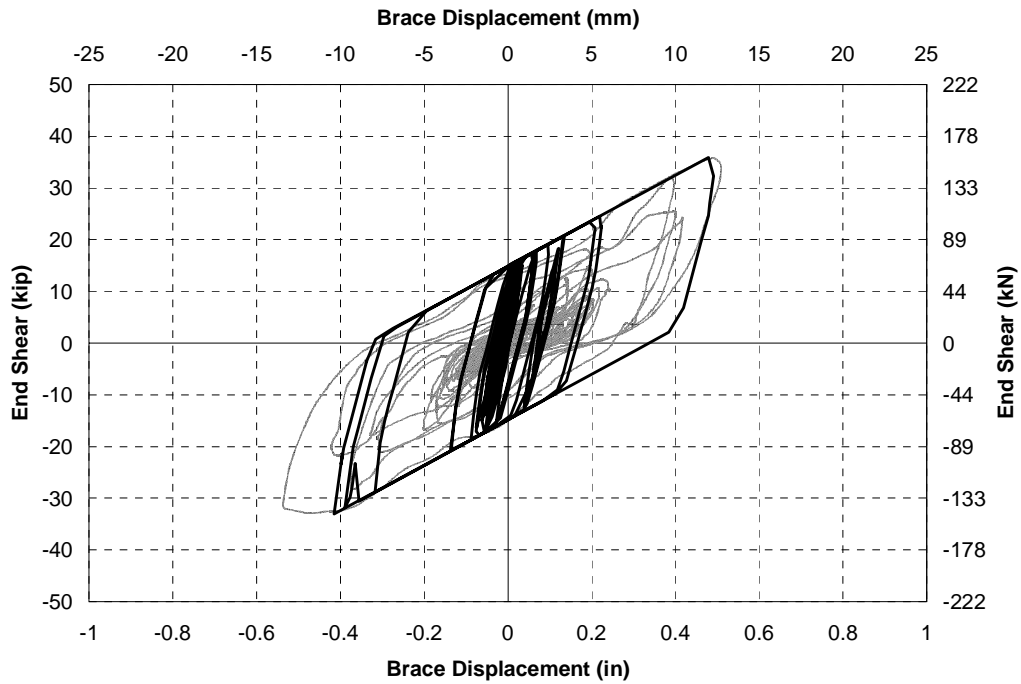


FIGURE 6-30 STFUB - End shear vs displacement at north end of analytical model compared to experimental data in response to 2.0 El Centro

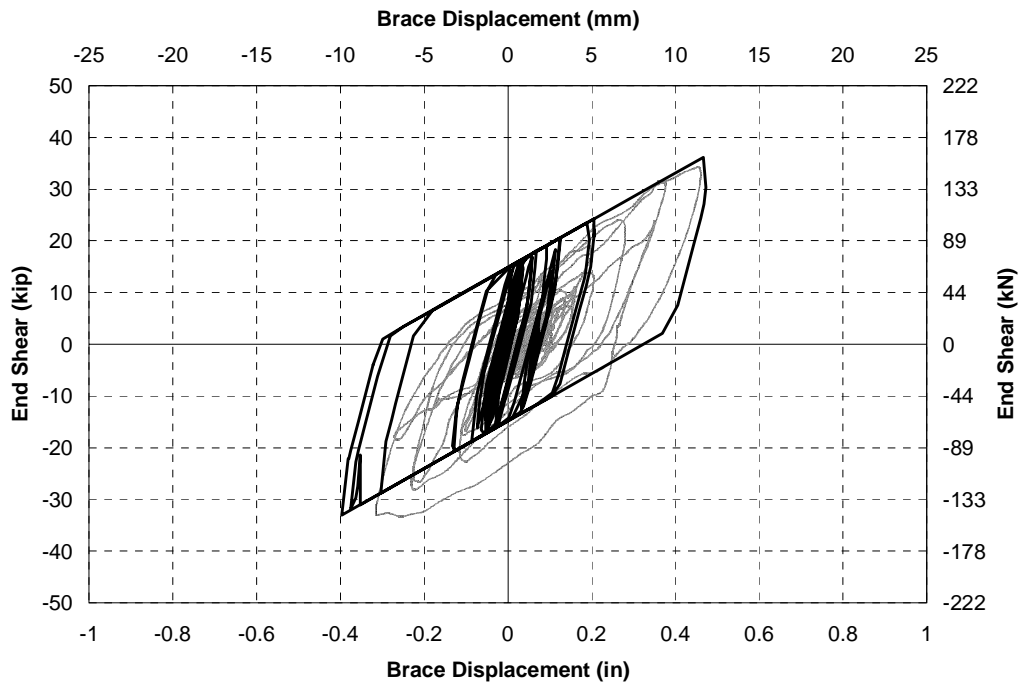


FIGURE 6-31 STFUB - End shear vs displacement at south end of analytical model compared to experimental data in response to 2.0 El Centro

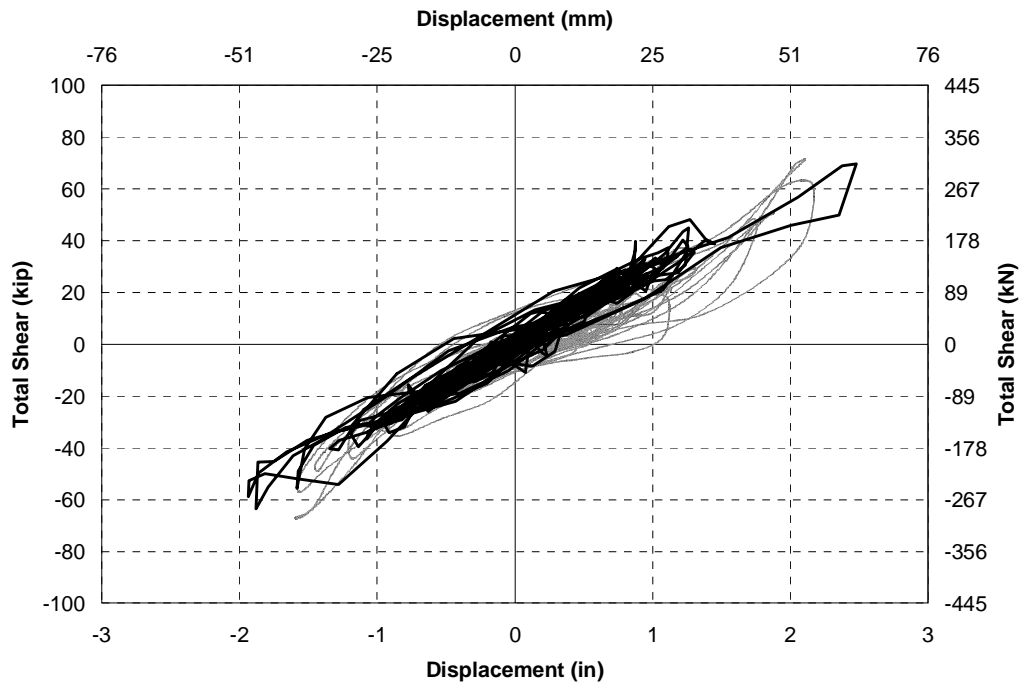


FIGURE 6-32 STFUB - Total shear vs midspan displacement of analytical model compared to experimental data in response to 2.0 El Centro

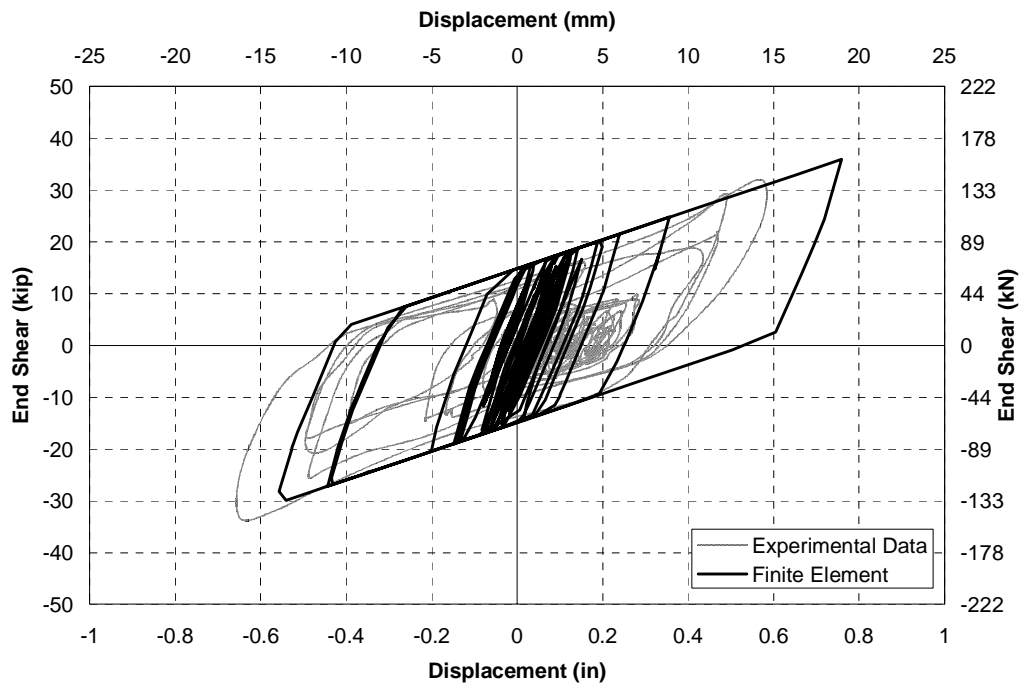


FIGURE 6-33 STPUB - End shear vs displacement at north end of analytical model compared to experimental data in response to 2.0 El Centro neglecting slippage

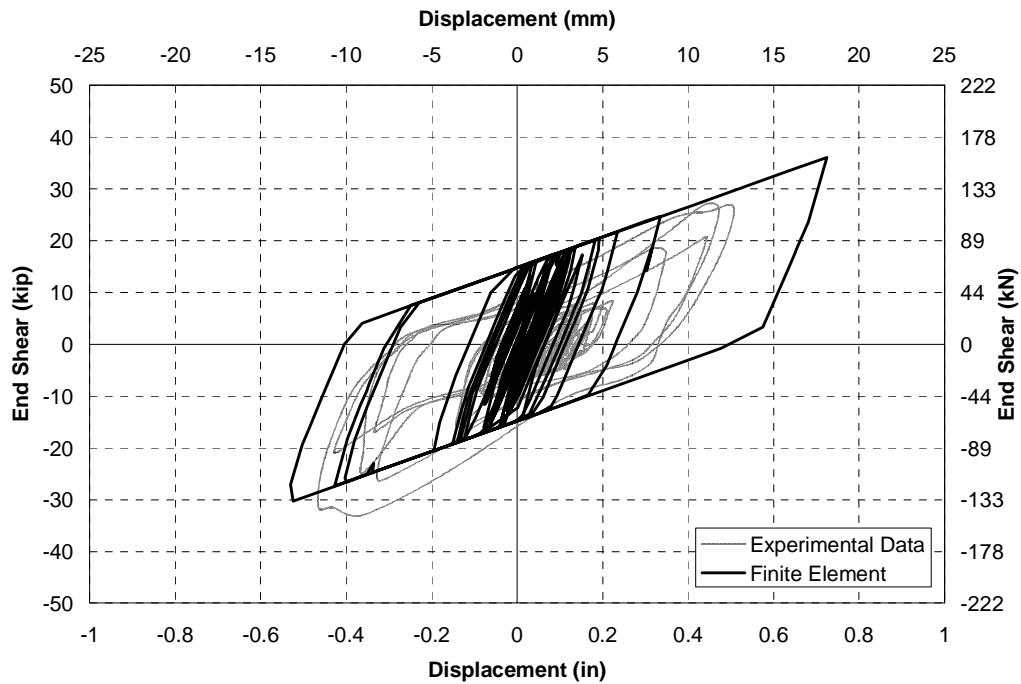


FIGURE 6-34 STPUB - End shear vs displacement at south end of analytical model compared to experimental data in response to 2.0 El Centro neglecting slippage

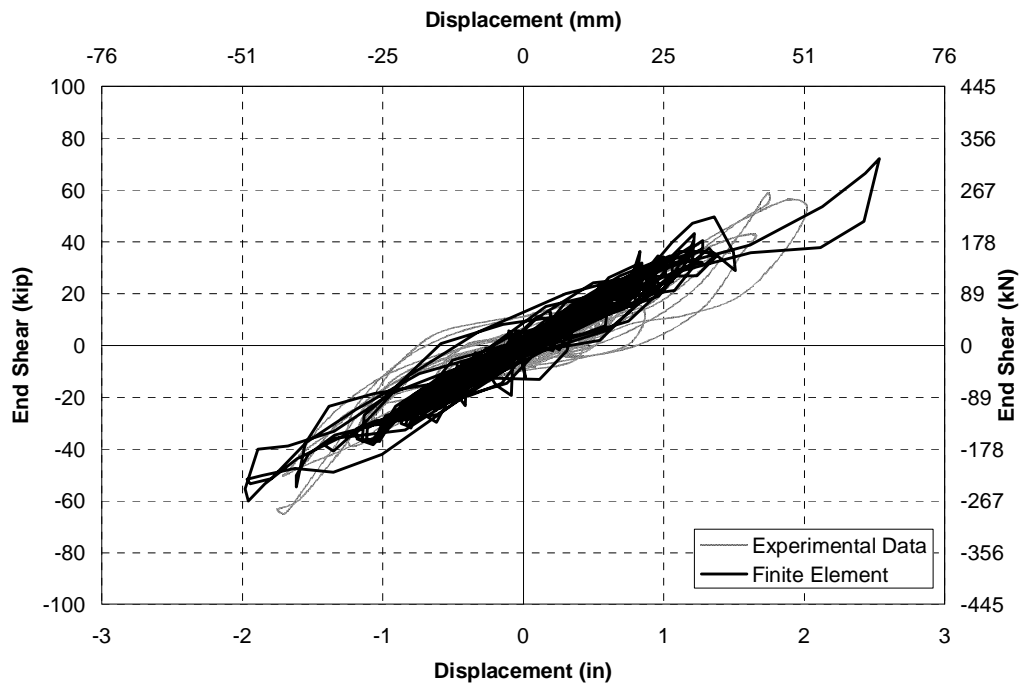


FIGURE 6-35 STPUB - Total shear vs midspan displacement of analytical model compared to experimental data in response to 2.0 El Centro neglecting slippage

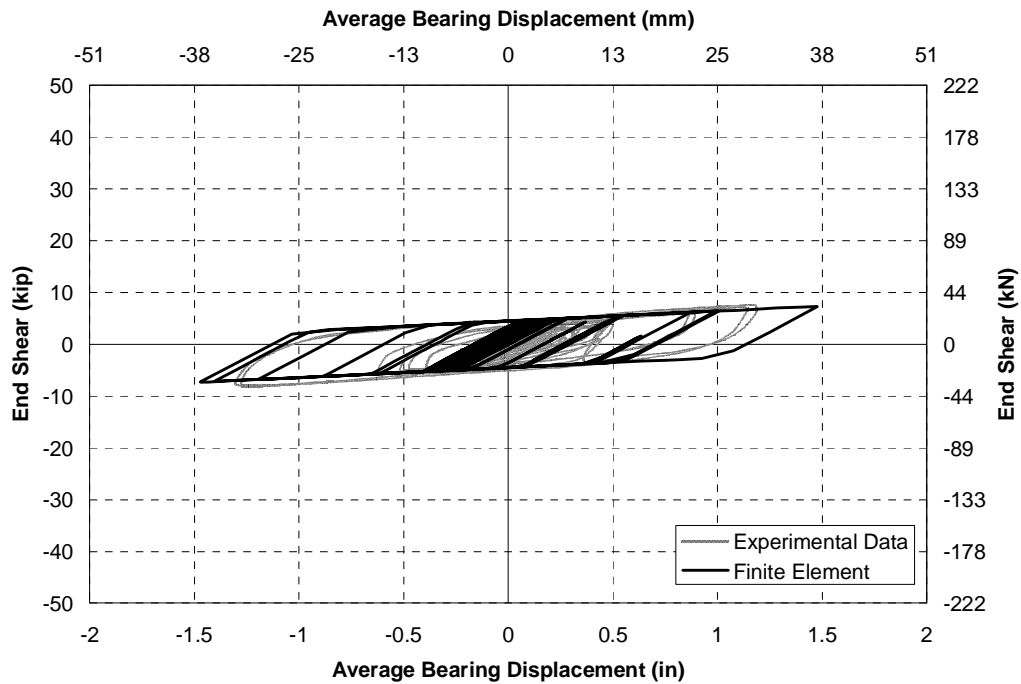


FIGURE 6-36 STLRB - End shear vs bearing displacement at north end of analytical model compared to experimental data in response to 2.0 El Centro

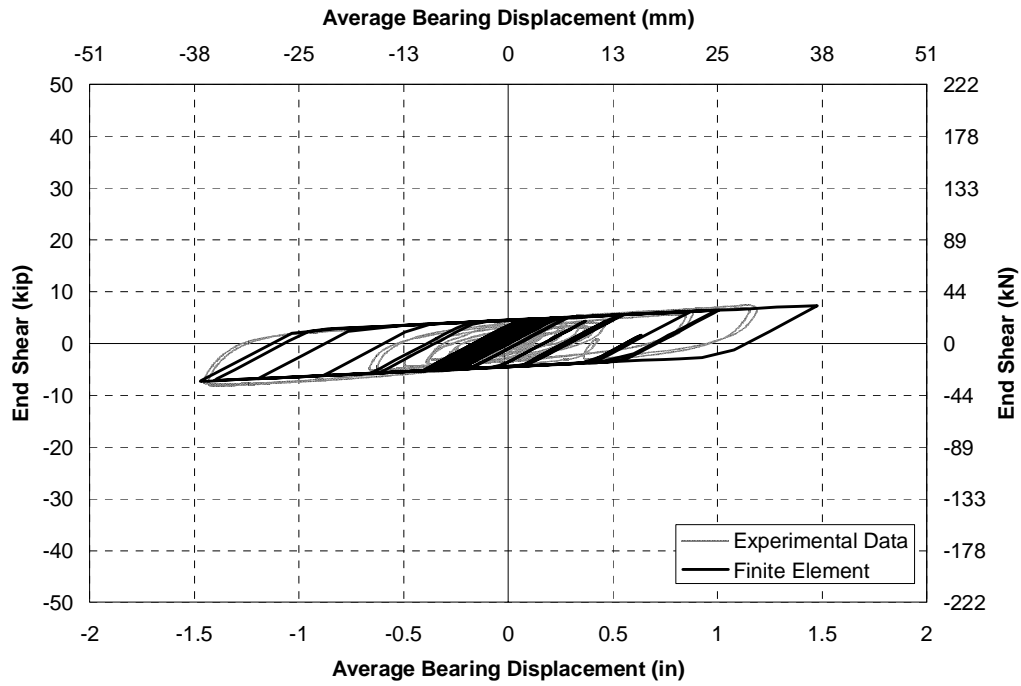


FIGURE 6-37 STLRB - End shear vs bearing displacement at north end of analytical model compared to experimental data in response to 2.0 El Centro

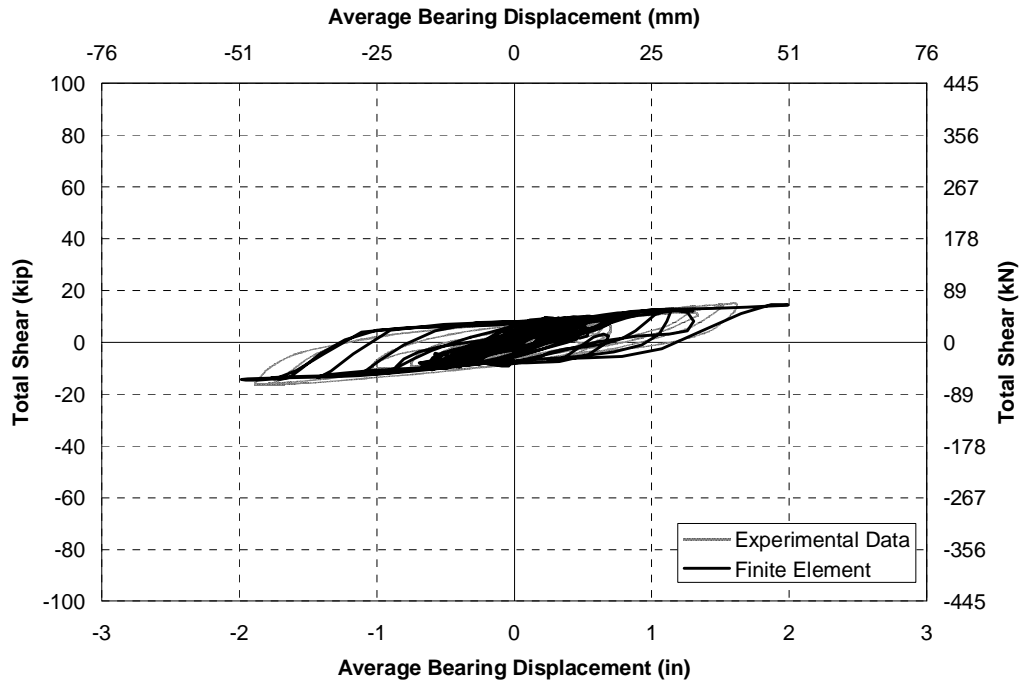


FIGURE 6-38 STLRB - End shear vs bearing displacement at north end of analytical model compared to experimental data in response to 2.0 El Centro

6.2.4 Summary and Comparison of Maximum Response for Ductile Systems

The response of the bridge from the experiments and corresponding analytical model is summarized in response to 2.0 x El Centro for the different configurations in Table 6-1. This table shows that the maximum forces and displacements from the analytical model were typically within 15% of the corresponding measured values during bridge experiments, although there are some exceptions. Generally the forces compared well, however the displacements were more variable, which may be partly attributed to the very small displacement values measured, and also the nature of the bridge response. The maximum shear at the north end of the model with heavy X-braces was 20% less in the analytical model. The measured displacements for this model were larger than those calculated due to slippage between the top of the girder and the deck, which was not considered in the analytical model, although the magnitude of these displacements were small. There are also differences in the displacements for the model with ductile end cross frames, although the calculated displacements are generally conservative.

6.3 Cumulative Plastic Strain Demand

Using the calibrated finite element models described in the previous section, the cumulative plastic strain (CPS) can be calculated in the bridge model for a series of different earthquakes. It is important that the braces do not fracture for earthquakes that excite the structure up to the maximum considered earthquake, therefore analytical models of the bridge were subjected to a series of ten earthquakes scaled such that the maximum strain in the braces reached 1.5 times the design level strain. For the X-braces this corresponded to a 6% average axial strain in the single angles, while for the unbonded braces this corresponded to a 3% axial strain in the core of the braces. The resulting CPS and CPD for each earthquake is given in Table 6-2 for the model with single angle X-braces. The average cumulative plastic strain was 70% with the mean plus one standard deviation CPS of 110%. This is close to the minimum calculated cumulative plastic strain in the single angles from component experiments of 113% (Table 3-5), for those members

TABLE 6-1 Comparisons of Bridge Model to Analytical Model Response with X-braces,

System	End	Experimental		Finite Element	
		Maximum Force (kip)	Maximum Disp (in)	Maximum Force (kip)	Maximum Disp (in)
"Heavy" X-Braces	North	228	6	184	3
	South	196	4	184	3
"Light" X-Braces	North	135	23	116	29
	South	124	17	118	24
Unbonded Braces	North - Pinned	148	16	160	19
	South - Pinned	147	13	161	18
	North - Fixed	166	14	159	12
	South - Fixed	150	12	161	12
Lead Rubber Bearings	North	36	33	33	39
	South	36	37	33	39

TABLE 6-2 Cumulative Plastic Strains and Ductilities in Analytical Model with Single Angle X-Braces for Different Earthquakes Subjected Braces to 3.0% Strain

Earthquake	Station	Amplitude Scale Factor	Max. Brace Strain (%)	Cumulative Plastic Strain	Cumul. Plastic Ductility
1940 Imperial Valley	El Centro Array#9 NS	5.10	5.98	136.2	633
1966 Parkfield	California Array#2 NS	3.20	6.01	80.0	372
1971 San Fernando	Pacoima Dam NS	2.00	5.86	52.9	246
1977 Bucharest	Building Res. Inst. NS	3.80	5.88	32.3	150
1979 Imperial Valley	Array #7 230°	3.00	5.95	68.0	316
1992 Landers	Lucerne EW	3.00	5.84	28.2	131
1994 Northridge	Sylmar Hospital NS	2.40	6.08	49.7	231
	Rinaldi S49W	1.25	5.89	44.3	206
1995 Kobe	KJMA NS	1.65	5.98	67.3	313
1999 Taiwan Chi-Chi	TCU084 EW	0.90	6.22	143.0	665
Average			5.97	70.2	326
Average + 1 Standard Deviation			6.08	110.1	512

TABLE 6-3 Cumulative Plastic Strains and Ductilities in Analytical Model with Unbonded Braces for Different Earthquakes Subjected Braces to 3.0% Strain

Earthquake	Station	Amplitude Scale Factor	Max. Brace Strain (%)	Cumulative Plastic Strain	Cumul. Plastic Ductility
1940 Imperial Valley	El Centro Array#9 NS	2.80	3.04	37.1	286
1966 Parkfield	California Array#2 NS	1.50	3.05	20.1	155
1971 San Fernando	Pacoima Dam NS	1.75	2.94	28.4	219
1977 Bucharest	Building Res. Inst. NS	3.70	3.00	18.3	141
1979 Imperial Valley	Array #7 230°	1.60	3.12	21.8	168
1992 Landers	Lucerne EW	2.50	2.93	13.7	106
1994 Northridge	Sylmar Hospital NS	1.30	3.00	11.8	91
	Rinaldi S49W	0.80	2.95	13.1	101
1995 Kobe	KJMA NS	1.10	2.94	46.3	357
1999 Taiwan Chi-Chi	TCU084 EW	0.85	3.13	49.2	380
Average			3.01	26.0	200
Average + 1 Standard Deviation			3.08	39.7	307

with connections designed to prevent premature fracture. Therefore 4% is an appropriate level of average axial strain for design of the single angles in ductile end cross frames using X-braces.

The resulting CPS and CPD for the model with unbonded braces are given in Table 6-3. The average cumulative plastic strain was 26% with the mean plus one standard deviation CPS of 40%. This is approximately equal to the minimum CPS measured in the unbonded braces during

component experiments (38% as given in Table 3-8). Therefore the design level strain of 2% is considered an appropriate level for unbonded braces in ductile end cross frames of bridges.

6.4 Parametric Studies

6.4.1 Ductile End Cross Frames and Seismic Isolation Systems of Different Strengths

As the analytical model was shown to effectively capture the response of the bridge model it was used to vary the properties of the model and determine the effect of different variations on the seismic response. Modifications were made to the properties of the end cross frames and isolation bearings in the analytical model in order to investigate the response of the model designed at different levels of yield force and stiffness.

The properties of the light X-braces were varied by varying the forces in the envelopes used to define the non-linear properties in the tension and compression elements, with different levels of 2.0, 1.5, 1.0, 0.75, 0.5, and 0.25 times the original levels in the bridge model. Both the strength and stiffness of the X-braces were changed by the same amount as a result of varying the forces in the envelopes. The stiffness properties associated with the stiffness of the girders, bearings and shear studs were assumed to remain constant therefore only the ductile components of the end cross frames were modified. Consequently, for the lowest strength X-braces the effect of the girders became very influential in the response.

The properties of the buckling restrained braces were also varied using the same scale factors for strength and stiffness as considered for the X-braces. The different properties were obtained by changing the axial yield force, initial and post-yield stiffness of the non-linear buckling restrained brace element. The buckling restrained braces were assumed to be pin connected.

The yield strength and stiffness of the lead rubber bearings in the isolated bridge model were also varied by factors of 4.0, 2.0, 1.5, 1.0, 0.75 and 0.5 times the original design values for the bearings in the bridge model. The axial, shear and rotational properties were all modified by the same factor.

6.4.2 Response to Artificial Design Level Earthquakes

In order to obtain a response consistent with a typical design spectrum three artificial earthquakes were generated, one using the RSCTH (SUNY, 2002) computer program and two using SIMQKE (Gasparini, 1976). These earthquakes were designed to be compatible with the design spectrum from the AASHTO Isolation Guidelines (1999) with an acceleration coefficient of 0.4 and site coefficient of 1.5. The periods used to define the design spectrum were reduced by a scale factor of $\sqrt{0.4}$ for the bridge model. The resulting design spectrum and 5% damped acceleration response spectra for the simulated earthquakes are shown in Figure 6-39. The response spectra are shown to generally capture the design spectrum well. The time histories for the artificial earthquakes are shown in Figures 6-40 to 6-42. In the two SIMQKE records large short duration spikes are observed in the time histories to match the spectrum at very short periods. As the duration of these spikes was very short they had little impact on the response.

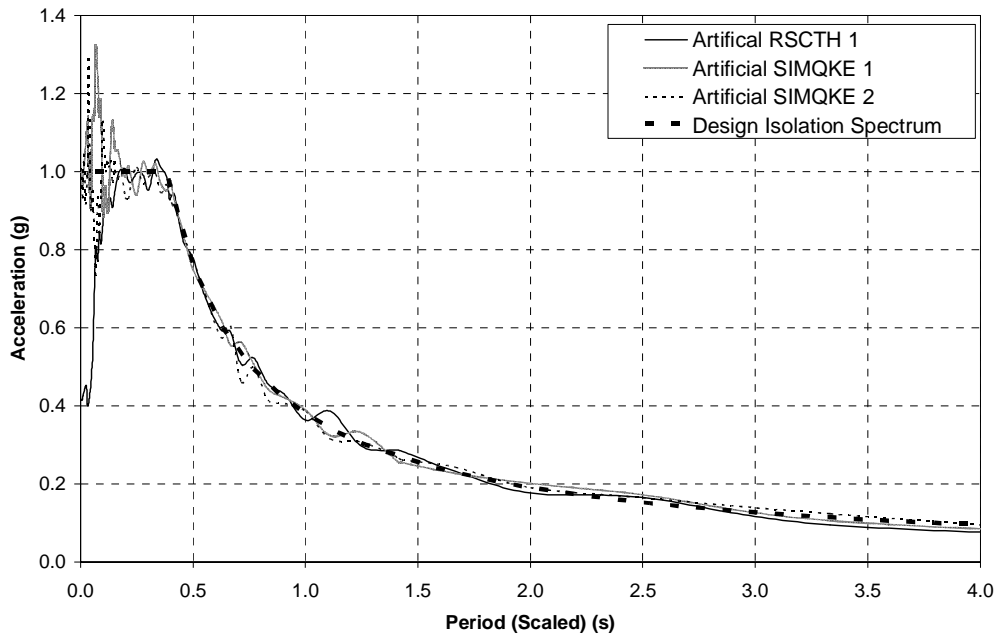


FIGURE 6-39 Acceleration response spectrum for simulated earthquake to match the time scaled AASHTO isolation design spectrum, site II.

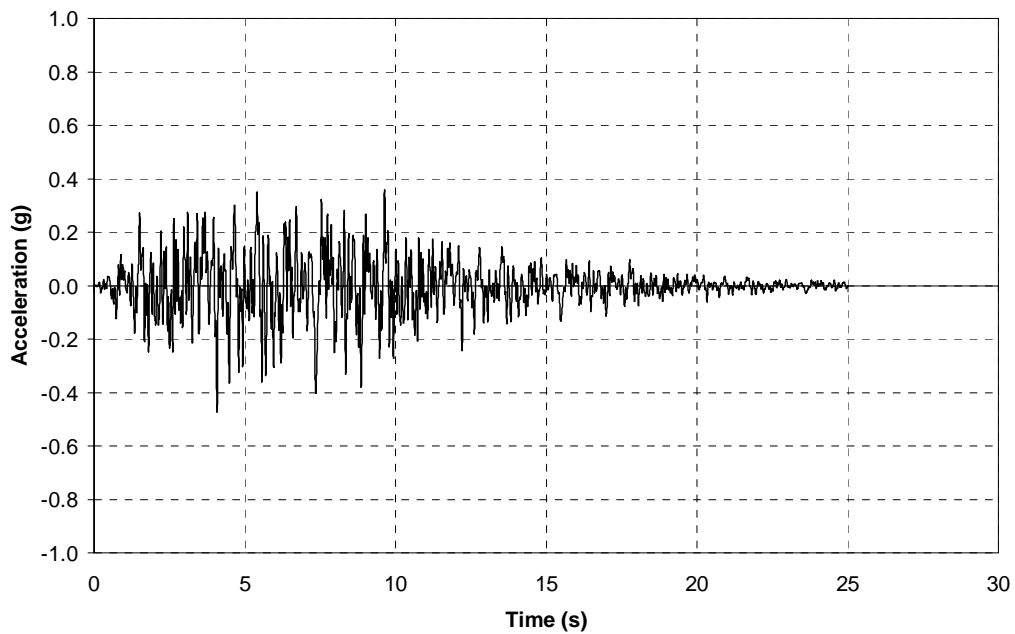


FIGURE 6-40 Acceleration time history for simulated earthquake using RSCTH (SUNY, 2002) to match the time scaled AASHTO isolation design spectrum, site II.

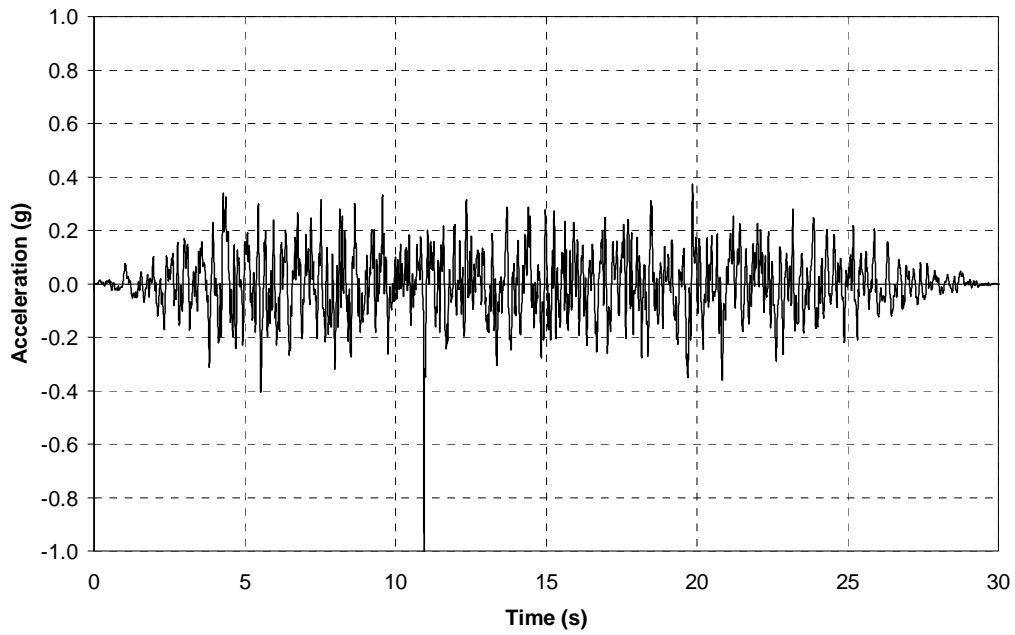


FIGURE 6-41 Acceleration time history for first simulated earthquake using SIMQKE (Gasparini, 1976) to match the time scaled AASHTO isolation design spectrum, site II.

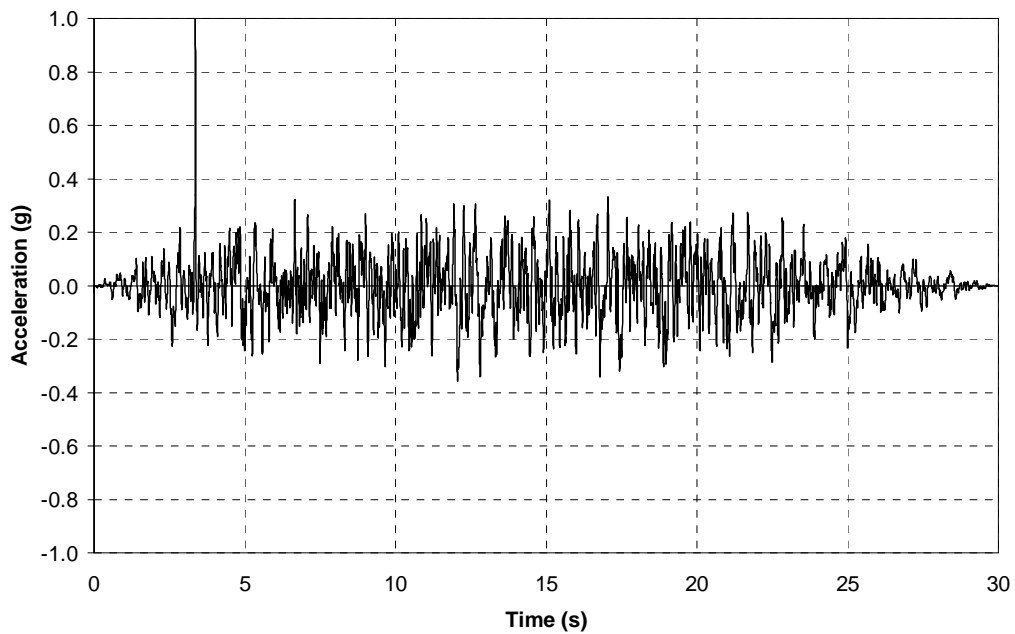


FIGURE 6-42 Acceleration time history for second simulated earthquake using SIMQKE (Gasparini, 1976) to match the time scaled AASHTO isolation design spectrum, site II.

The analytical models were simplified slightly from those calibrated to the experimental data for calculating the response to the artificial earthquakes, in that: nominal damping in the structure was assumed to be equal to zero with effective damping resulting from the hysteretic behavior of the non-linear elements alone; both ends were assumed to have the same properties with an average of those calculated for the two ends of the bridge model, and; the torsional stiffness was also assumed to be large and therefore superstructure flexibility was due to flexural behavior alone.

The resulting maximum displacement at the ends of the girders, averaged between the three artificial earthquakes, is plotted in Figure 6-43 against the maximum total base shear in the bridge for the ductile cross frames and isolation systems. Different points on the curves in Figure 6-43 represent the different strengths and stiffnesses of the cross frames or isolation bearings, with the decreasing strengths resulting in decreasing base shears and increasing displacements. Comparing the X-braces and buckling restrained braces shows that the buckling restrained braces resulted in typically 20 to 30% smaller displacements at a given level of base shear than the X-braces. The models with lead rubber bearings resulted in larger displacements, although, the bearings also have a larger displacement capacity and must be considered.

The maximum girder drift observed in the bridge model of 7%, corresponding to a displacement of 41 mm., can be used as one limit for design of the ductile end cross frames. Based on the responses calculated in Figure 6-43, the displacement limit will not be exceeded with even the lowest strength X-brace or buckling restrained brace members considered. For the modified buckling restrained brace a 4.6% (27mm) drift limit was calculated. Even this would not be exceeded for the weakest of members. In contrast, if the design displacement limit is between 2.0 and 2.5% (12 and 15 mm) as for the SPS, EBF and TADAS systems (Zahrai, 1998b) discussed in Chapter 4, and the curve for the buckling restrained brace in Figure 6-43 is assumed, then the end cross frames would need to be designed for a higher level of base shear.

The design displacement for the isolation bearings will change with the strength and stiffness properties of the bearings, due to a change in the geometry of the bearings. This is unlike the braces for which the design displacement was assumed to be fixed regardless of their strength. The allowable design displacement for the lead rubber bearings in the bridge model was 53 mm, 54% less than calculated buckling limit. An isolation system designed to this level will have a base shear equal to around 16% of the weight of the structure. This is less than the base shear for the cross frames considered which is limited to around 40% of the superstructure weight. Compared to the ductile end cross frames, the lead rubber bearings can be considered to perform in a different performance category with much lower shears allowed due to a large displacement capacity in the bearings. The displacement capacity is not limited by the limitations of the girders and the stiffness of the girders as for the ductile end cross frames.

6.4.3 Parametric Studies on Superstructure Stiffness

As described previously, the bridge model had a relatively flexible superstructure compared to a typical steel plate girder bridge superstructure with a larger number girders and a fully composite section. The effect of different superstructure stiffnesses was investigated in the response of a bridge model with the ductile end cross frames and seismic isolation. The strengths of the ductile end cross frames were assumed to be scaled by 0.36 for the X-braces and 0.27 for the buckling restrained braces for a similar level of displacement response in the two systems. The isolation system was assumed to have properties equal to those for the isolation system in the bridge model.

Three different superstructure stiffnesses were considered; 1, 10 and 100 times the actual stiffness of the superstructure in the bridge model with the transverse flexural properties modified by the above factors.

Figure 6-44 shows the effect of superstructure stiffness on the base shear in the bridge model for the average response to the three artificial earthquakes. A marginal reduction in the base shear was observed as the stiffness of the superstructure increased, which is most noticeable with the buckling restrained braces. The drifts in the ductile end cross frames or isolation system of the bridge model with different superstructure stiffnesses, are shown in Figure 6-45. As the end shears are proportional to the displacements in the cross frames or isolation system a reduction in drifts is also observed as the stiffness of the superstructure increased. These figures show that ductile end cross frames are slightly more effective when used in a bridge with a relatively rigid superstructure. In this respect the bridge model did not have the optimal properties to demonstrate the effects of ductile end cross frames. A typical four or five girder bridge may have a stiffness 10 - 20 times that of a two girder bridge like the bridge model. The reduction in base shear and displacements with increasing superstructure stiffness was largely attributed to an increase in damping in the structure. With a more rigid superstructure the end deformations accounted for a large proportion of the overall deformation in the structure. Therefore increasing the damping at the ends had a notable effect throughout the structure. In contrast with a flexible superstructure much of the deformation occurred along the span therefore the relatively small deformation at the ends had a less significant effect than for a rigid superstructure.

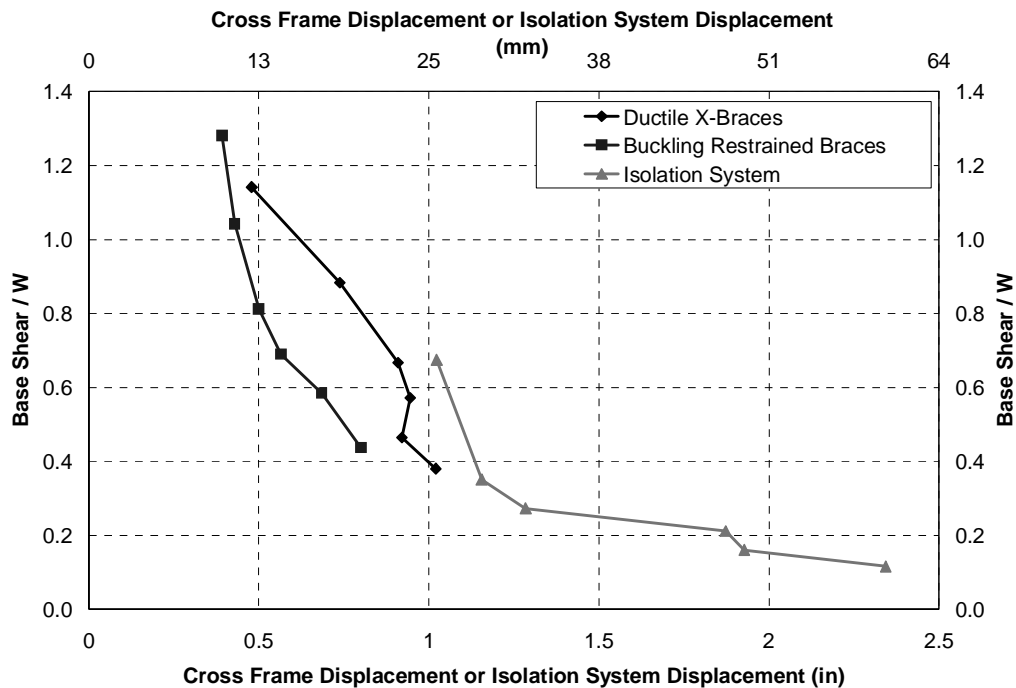


FIGURE 6-43 Maximum total base shear versus maximum north end drift in response to artificial design level earthquake

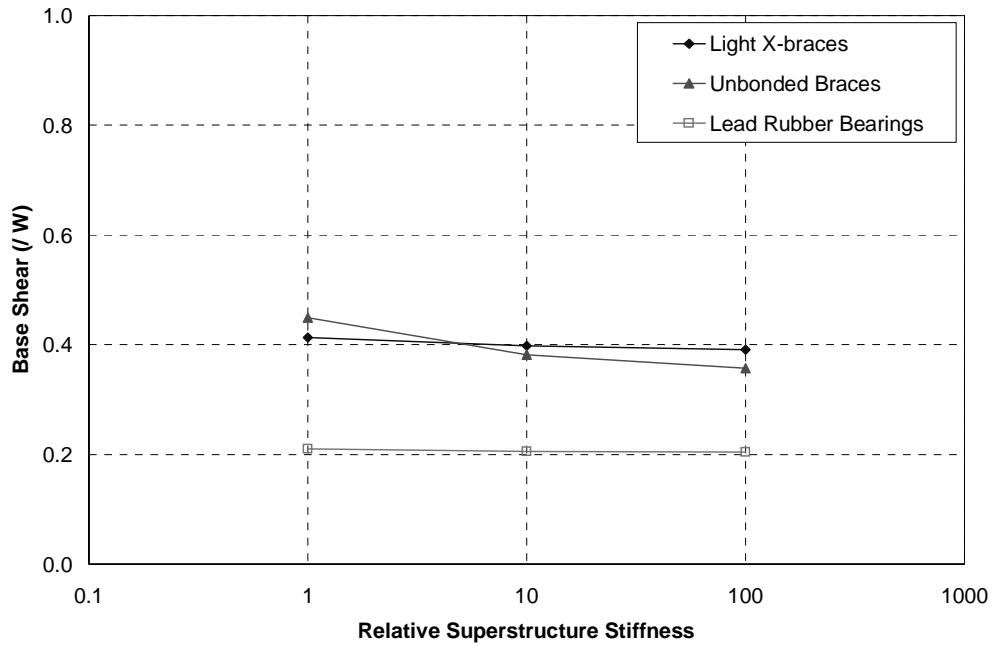


FIGURE 6-44 Maximum base shear for bridge model with different superstructure stiffnesses in response to artificial design level earthquakes

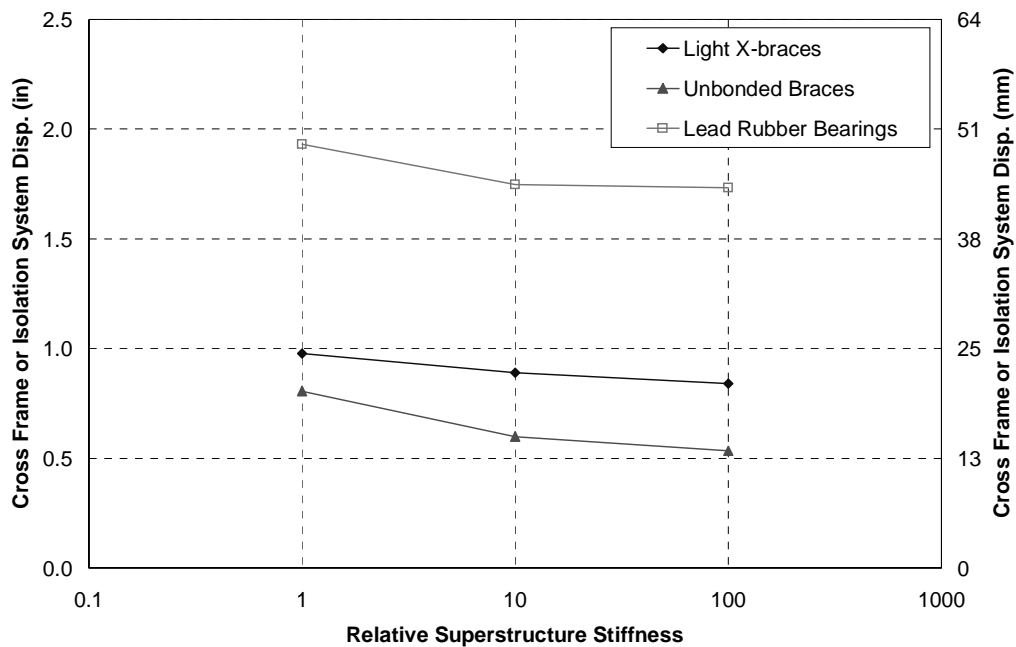


FIGURE 6-45 Maximum end drift for bridge model with different superstructure stiffnesses in response to artificial design level earthquakes

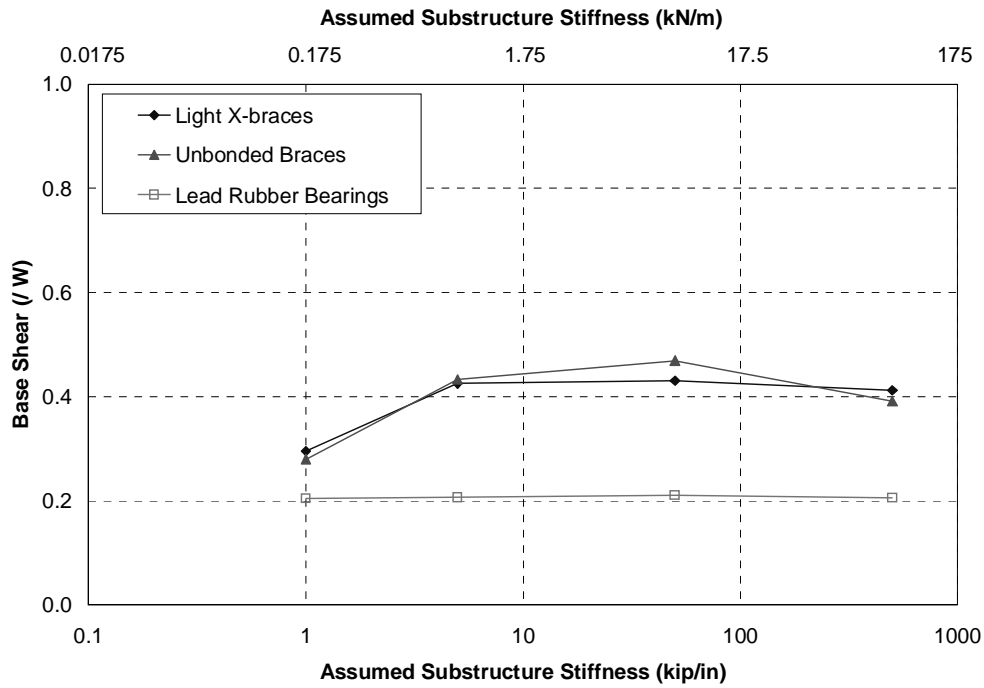


FIGURE 6-46 Maximum base shear for bridge model with different substructure stiffnesses in response to artificial design level earthquakes

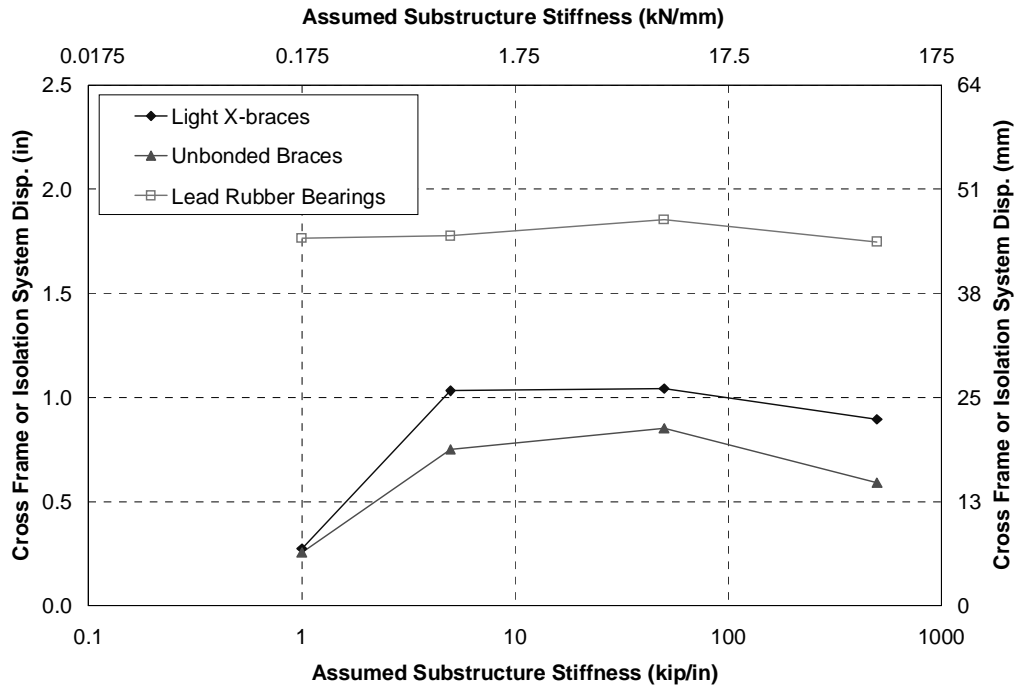


FIGURE 6-47 Maximum end drift for bridge model with different substructure stiffnesses in response to artificial design level earthquakes

The modification in superstructure stiffness also had an effect on the natural period for the dominant transverse mode of the bridge model. With an increase in superstructure stiffness it might be expected that the shorter period structure would have a larger base shear in response to an earthquake with a typically shaped response spectrum. However for this structure, the effect of variation in the damping was more pronounced than variations in the natural period.

6.4.4 Parametric Studies on Substructure Stiffness

The bridge model was assumed to have a relative rigid superstructure (100 times the calculated stiffness for the bridge model) while the effect of a flexible substructure was studied. A range of substructure stiffnesses were considered of 0.2 (corresponding to a relatively very flexible substructure with tall columns), 1, 10 and 100 kN/m (corresponding to a structure with rigid pier supports). The lateral column stiffness calculated from the prototype bridge for the scale model was in the midrange of substructure stiffnesses considered.

A more flexible substructure is shown to have a considerable impact on the response of the bridge model and effectiveness of ductile systems. Unlike the variations in the superstructure stiffness, the variation in the substructure stiffness had a notable effect on the natural period of the structure. Figure 6-46 shows the base shear of the bridge with different substructure stiffnesses with responses averaged between the three artificial earthquakes. The base shear was smallest with the most flexible substructure as the period of the structure was longest. With intermediate stiffnesses the largest base shears were observed, while the base shear was reduced for the most rigid of substructures. This can be explained because for the most flexible substructure the period of the bridge is sufficiently long that the seismic demand on the structure is lowest, despite the end cross frames becoming ineffective and providing little damping to the structure. For the larger stiffness substructures the period of the structure is sufficiently short that the response is insensitive to the period, and the level of damping becomes more critical. While the substructure is most rigid the cross frames are most effective and provide the most damping to the structure. The intermediate stiffness substructure represents a transition between these two conditions.

The above observations are more apparent when investigating the maximum displacements in the ductile end cross frames or isolation system, as shown in Figure 6-47. This figure shows that substructures with moderate flexibility resulted in the largest drifts in the ductile end cross frames. For flexible substructure the displacements in the ductile end cross frames were small since most of the total displacement was concentrated in the substructure. Thus for flexible substructures, while ductile end cross frames are not detrimental to the response of the bridge, they are not effective at reducing the base shear. For bridges with flexible substructures the base shear is reduced compared to a bridge with a rigid substructure due to the long period of the bridge alone. Ductile end cross frames are most effective for a bridge with a relatively rigid substructure. The same can be shown for an isolated bridge, although, as the isolation system is more flexible, the isolation system is less sensitive to substructure stiffness.

SECTION 7 CONCLUSIONS AND RECOMMENDATIONS

7.1 Summary

In this report three different systems are investigated for improving the ductile response of the superstructure of a steel plate girder bridge model for transverse earthquake excitation. Two of these systems used ductile end cross frames, one with single angle X-braces and the other with buckling restrained braces and a third system using isolation bearings. Comparative performance of the three systems is described.

Chapter 3 describes the properties of the different ductile members used in the bridge model in a series of component experiments. These included the single angles, buckling restrained (unbonded) braces and the lead rubber bearings. The tension and compression capacity of the single angles were shown to compare well with the theoretical values from AASHTO (1998). The cyclic performance of the different single angles was shown to be greatly affected by their connection details, and using a detail which ensured failure of the angles outside the connection region greatly enhanced their performance. With appropriate connection details the angles were able to withstand average cyclic axial strains in excess of 6%, with 4% recommended as a design limit, allowing an ultimate capacity 50% above the design capacity of the angles. This is a relatively large displacement capacity compared to other systems and compensates for sub-optimal energy dissipation characteristics due to buckling of the angles. A model was developed using a combination of kinematic non-linear elements in SAP2000 to model the single angles. The buckling restrained braces were shown to have predictable properties with improved hysteretic behavior compared to the single angles. Their properties were studied in relation to different loading histories, with some increase in force observed during dynamic loading compared to static loading. A bi-linear model was used to characterize the properties of the braces for use in modeling of the bridge model. The lead rubber bearings were shown to have properties similar to their design properties. The bearing properties were modeled effectively using a bi-linear model.

Chapter 4 describes the performance of the bridge model with ductile end cross frames during reversed static and shake table experiments. During the reversed static experiments the heavy X-braces remained essentially elastic with some non-linear behavior largely attributed to slippage. Large inelastic displacements were observed in the bridge model with the light X-braces. The end cross frames exhibited an essentially elasto-plastic envelope although strength and stiffness degradation were observed in the hysteresis loops after buckling of the diagonal members. During reversed static experiments the bridge model was able to achieve a maximum drift of around 5.0%, although some damage was observed in the shear studs at the end of the bridge model due to rotations of the top flange relative to the deck slab.

During shake table experiments the heavy X-braces remained elastic. The light X-braces yielded with a similar elasto-plastic envelope as observed during reversed static experiments. The maximum drift in the light X-braces was 4.0% during 2.0 x El Centro excitation applied in the transverse direction. The maximum base shear was 62% of the base shear with heavy X-braces for the same motion. In contrast, with pin ended, buckling restrained braces in the ductile end cross frames, the bridge model was shown to have better energy dissipation and resulted in smaller drifts with a maximum drift in the end cross frames of 2.5% during the 2.0 x El Centro motion, 62% of the drift with the X-braces. However, the maximum base shear was higher, with a value of 69% of

the base shear in the heavy X-braces. With the fixed connections the displacements were reduced slightly but the base shear was increased due to an increased post-yield stiffness. This was attributed to bending in the braces which was significant due to their relative short length compared to those used in building applications. As it is difficult to quantify the effect of flexure in the braces, pin ended connections are recommended for buckling restrained braces used in ductile end cross frames. Permanent drifts of around 10 to 25% of the maximum drifts were recorded in the cross frames with similar levels observed using the X-braces and buckling restrained braces.

Chapter 5 summarizes the response of the bridge model when seismically isolated with lead rubber bearings. The isolation bearings largely performed as expected with the characteristic strength and stiffness of the bearings close to design values. The resulting base shear in the bridge with lead rubber bearings was 17% of the shear in the bridge model with heavy cross frames in response to 2.0 x El Centro. This is significantly less than with the ductile X-braces and buckling restrained braces. The critical state was observed in the bearings at displacements 13% higher than the calculated critical displacement at which instability was expected for the given gravity loads, indicating that the theoretical estimate of the critical load and displacement combination was reasonably accurate and conservative. Despite instability at one end of the bridge, deformations in the bearings were reversed with minimal residual displacement and collapse was prevented due to reversing inertia forces in the bridge model and a smaller displacement response at the other end of the bridge. The bearings were shown to be remarkably resilient when subjected to a cumulative plastic displacement demand many times greater than that observed in any of the bracing systems with little change in properties. The biaxial displacement response of the isolated bearings was most accurately and conservatively captured by the SRSS rule to combine the uniaxial responses. Differential displacements due to soil at one support and rock at another support can result in larger displacements in the isolators than the same ground excitations at each support in turn.

An analytical model was generated with non-linear components included to model the ductile end cross frames and seismic isolation bearings. The non-linear components were based on the properties from the component experiments described in Chapter 3, although some modifications were necessary. The response of the bridge model with the different configurations of ductile end cross frames was compared to that of the analytical model in Chapter 6. The response generally compared well for the X-braces, although the analytical model had a tendency to overestimate the displacements at the ends. Post-yield stiffness at the ends observed during bridge experiments with unbonded braces was shown to be higher than that initially predicted based on the component experiments. The ratio of post-yield stiffness to initial stiffness of the buckling restrained braces was increased to 0.075 for the braces with pin ended connections and to 0.125 for braces with fixed end connections. The response of the analytical model with lead rubber bearings was found to match the measured response well.

After using the model to vary the strength of the ductile end cross frames and isolation systems, the buckling restrained braces exhibited typically 30% smaller displacements than the X-braces at the same level of base shear. However, the forces in the bridge with both ductile end cross frame systems could not be reduced to levels as low as those in a seismically isolated bridge. Isolation therefore represents a higher level of seismic protection than is possible with ductile end cross frames.

7.2 Conclusions

The conclusions from component experiments on single angles like those used in concentric cross frames, buckling restrained braces and lead rubber isolation bearings are:

- Using Kl/r ratios and b/t ratios according to AISC (2002) and AASHTO (1998) and connections designed to prevent fracture in the connection regions, single angles can achieve large cyclic inelastic strains. The stiffness and tensile strength degrades after repeated loading.
- The tensile and compression capacity of the single angle members can be calculated using AASHTO (1998) with reasonable accuracy.
- The ultimate axial displacement capacity of single angles subjected to increasing cyclic loads is greater than that for buckling restrained braces, however the energy dissipation of buckling restrained braces is better than that of single angle concentric braces.
- The properties of the lead rubber bearings are close to their design properties after the third cycle of loading.

The conclusions from the experimental and analytical study on bridges with ductile end cross frames and seismic isolation subjected to transverse seismic loading are:

- Ductile cross frames using X-braces and buckling restrained braces are both effective in reducing transverse seismic shear in a steel plate girder bridge. The buckling restrained braces resulted in smaller drifts in the ends of the girders for the same level of base shear.
- Drifts of up to 7% were observed in the I-girders at the supports with no damage to the girders and minimal damage to the deck slab. A “rocking” mechanism, which allows the girders twist about their longitudinal axis is effective in allowing these drift levels. Such a mechanism may comprise of rotationally flexible bearings and no shear studs between the girder flange and deck slab near the supports.
- The X-braces and cross frames with buckling restrained braces are capable of large drift capacities compared to other ductile end cross frame systems, with the X-braces having the largest capacity.
- It is possible to reduce the base shear in a bridge using seismic isolators using period shift and capacity for large displacements. This reduction is greater than possible with ductile end cross frames.
- For lightweight steel girder bridges stability of the lead rubber bearings can control the ultimate displacement of the bearings, but the ultimate limit states is conservatively estimated using existing theory. Bearings which buckle dynamically do not necessarily result in complete failure as reversing inertia forces can restore stability.
- The square root sum of the square procedure for combining the maximum orthogonal displacement components is the most appropriate and conservative. Cross-coupling due to

accidental torsion is negligible in calculating the maximum biaxial response and can be ignored for a symmetric bridge superstructure.

- Isolation bearing displacements can be considerably larger in response to differential ground motion at supports, when a bridge is subjected to longitudinal excitation, than for the same motions applied uniformly to at each support in turn.
- Ductile end cross frames and isolation become less effective with a flexible superstructure or substructure.

7.3 Recommendations

From this study the following recommendations are made for design of steel girder bridges with ductile end cross frames and seismic isolation:

- Single angle X-braces can be used as ductile cross frames with a maximum recommended design axial strain in the angles of 4.0%. The members should be designed to governing Kl/r ratios and b/t ratios according to AISC (2002) for concentric braced frames and bracing members in AASHTO (1998). The members should also be designed for a slenderness $\lambda < 2.25$. To prevent fracture in the connection regions, bolted connections for ductile angle members should be reinforced around the bolt holes. In this project such connections were achieved by welding thickening plates to the angles in the connection regions. For welded connections balanced welds with end returns are most effective at promoting optimal cyclic behavior. In calculating the buckling strength of the angles, the effective length is calculated between the centroid of the connections. An effective length factor of 0.7 is appropriate when the gusset plates are restrained from bending during buckling of the angles. A factor of 0.85 is appropriate when the gusset plates are not restrained.
- Buckling restrained braces provide a higher level of performance than X-braces as they result in lower girder drifts at a given level of base shear and their need for post earthquake repair is reduced. Their improved performance needs to be balanced against the cost premium. The buckling restrained braces can be designed for an axial strain of 2.5%.
- The maximum relative displacement in the girders when using ductile end cross frames, should be no more than 7% of their height, as P-delta moments and other effects have not been considered past this level of drift. The forces in the girders should be checked at the design drift using the formulations discussed by Carden et al. (2005). The strains in the ductile members should also be considered in calculating the allowable drift in the end cross frames. A displacement based design procedure is recommended for design of a bridge with ductile end cross frames
- Seismic isolation using lead rubber bearings can be used in steel girders bridges to achieve a high level of seismic performance. Lead rubber elastomeric bearings are effective isolators. However, possible instability of the slender elastomeric bearings, which may be necessary for optimal performance of a relatively lightweight steel bridge superstructure, should be considered at the design stage as it may limit the displacement capacity of the isolators.

- Isolation can be used for reducing both longitudinal and transverse seismic response. Where there are different foundation and soil conditions at the different supports of a bridge, differential support excitation should be considered since this can result in most severe demand on the isolation system, particularly in the longitudinal direction.

More detailed seismic design guidelines for straight steel I-girder bridges will be provided in the future.

SECTION 8 REFERENCES

Alfawakhiri, F. and Bruneau, M., (2000). Flexibility of Superstructures and Supports in Seismic Analysis of Simple Bridges. *Earthquake Engrg. and Struct. Dyn.* 29(5), 771-729.

Alfawakhiri, F. and Bruneau, M., (2001). Local versus Global Ductility Demands in Simple Bridges. *J. Struct. Engrg.* 127(5), 554-560.

American Association of State Highway and Transportation Officials (AASHTO), (1996). *Standard Specifications for Highway Bridges - Division I-A*. AASHTO, Washington, DC.

American Association of State Highway and Transportation Officials (AASHTO), (1998). *AASHTO LRFD Bridge Design Specifications (Customary U.S. Units Second Ed.)*. AASHTO, Washington, DC.

American Association of State Highway and Transportation Officials (AASHTO), (1999). *Guide Specifications for Seismic Isolation Design, (Second Edition including 2000 Interim Revisions)*. AASHTO, Washington, DC.

American Iron and Steel Institute (AISI), (1996). *Steel Bridge Bearing Selection and Design Guide - Highway Structures Design Handbook - Vol. II, Chap. 4*. AISI, Washington, DC.

American Institute of Steel Construction (AISC), (1997). *Manual of Steel Construction - Load Factor and Resistance Design, 2nd Edition*. AISC, Chicago, IL.

American Institute of Steel Construction (AISC), (1998). *Seismic Provisions for Structural Steel Buildings*. AISC. Chicago, IL.

American Institute of Steel Construction (AISC), (2002). *Seismic Provisions for Structural Steel Buildings*. AISC. Chicago, IL.

Applied Technology Council (ATC), (1992). *ATC 24 - Guidelines for Cyclic Seismic Testing of Components of Steel Structures*. ATC, Redwood City, CA.

Applied Technology Council (ATC) / Multidisciplinary Center for Earthquake Engineering Research (MCEER), (2003). *Recommended LRFD Guidelines for Seismic Design of Highway Bridges (2 Volumes)*. Report ATC/MCEER 49 (joint venture) , Redwood City, CA.

Astaneh-Asl, A., (1996). *Notes on the Cyclic Behavior and Design of Steel Bridges - Volume I - Response Modification Factor Based Design*. Report, American Iron and Steel Institute, Washington DC, November.

Astaneh-Asl, A., (1982). *Cyclic Behavior of Double Angle Bracing Members with End Gusset Plates*. Ph.D. Dissertation, University of Michigan, Ann Arbor, MI.

Astaneh-Asl, A., Bolt, B., McMullin, K.M., Donikian, R.R., Modjtahedi, D., and Cho, S., (1994). *Seismic Performance of Steel Bridges During the 1994 Northridge Earthquake*. Report UCB/CE-

STEEL-94/01. Department of Civil and Environmental Engineering, University of California, Berkeley, CA.

Beaulie, D. and A. Picard, (1989). *The Design of Diagonal Cross-Bracing*. 1989 Steel Structures-Structures Congress'89, ASCE, San Francisco, CA, May 1-5.

Black, C., Makris, N., and Aiken, I., (2002). *Component Testing, Stability Analysis and Characterization of Buckling Restrained Unbonded Braces*TM. PEER Report 2002/08, Berkeley, CA, September.

Bruneau, M., Wilson, J.W., and Tremblay, R., (1996). Performance of Steel Bridges during the 1995 Hyogoken-Nanbu (Kobe, Japan) Earthquake, *Canadian J. of Civil Engrg*, 23(3), 678-713.

Buckle, I.G., Mayes, R.L., and Button, M.R., (1986). *Seismic Design and Retrofit Manual for Highway Bridge*, Report FHWA-IP-87-6, U.S. Department of Transportation, Federal Highway Administration, Washington, DC.

Buckle, I.G., Nagarajaiah, S., and Ferrell, K., (2002). Stability of Elastomeric Isolation Bearings: Experimental Study. *J. of Struct. Engrg*. 128(1), 3-11.

Buckle, I.G. (1978). Factors Affecting the Performance of Lead Rubber Energy Dissipators. *Road and Research Unit Bulletin 73*, Transit New Zealand, Wellington, New Zealand.

Carden, L.P., Itani, A.M., and Buckle, I.G., (2005). *Seismic Performance of Steel Girder Bridge Superstructures with Conventional Cross Frames*. Report CCEER 05-03, Center for Civil Engineering Earthquake Research, University of Nevada - Reno, Reno, NV.

Chung, R. (Editor). (1996). *The January 17, 1995 Hyogoken-Nanbu (Kobe) Earthquake – Performance of Structures, Lifelines, and Fire Protection Systems*. NIST Special Publication 901. Building and Fire Research Laboratory, National Institute of Standards and Technology, Gaithersburg, MD.

Clark, P.W., Aiken, I.D., Tajirian, F.F., Kasai, K., Ko, E., Kimura, I., (1999). Design Procedures for Buildings Incorporating Hysteretic Damping Devices. *International Post-SMiRT Conference Seminar on Seismic Isolation, Passive Energy Dissipation and Active Control of Vibrations of Structures*, Cheju, Korea, August 23-25.

Clough, R.W., and Penzien, J., (1993). *Dynamics of Structures (2nd Ed.)*. McGraw Hill, Inc., Singapore.

Computers and Structures, Inc., (2003). *SAP2000 Nonlinear (Version 8.3.0): Structural Analysis Program*. Computers and Structures, Inc. Berkeley, CA.

El-Tayem, A. and S.C. Goel, (1986). Effective Length Factor for the Design of X-Bracing Systems. *AISC Engrg Journal*, 23, 41-45.

EduPro Civil Systems, (1999). *EduShake (Version 1.10)*. EduPro Civil Systems, Inc., Redmond, WA. <http://www.proshake.com>.

Gasparini, D.A., and Vanmarcke, E.H., (1976). *SIMQKE - A Program for Artificial Motion Generation - Users Manual and Documentation*. Massachusetts Institute of Technology - Department of Civil Engineering, Cambridge, MA, November.

Goel, S.C. and Itani, A.M., (1994). Seismic Resistant Special Truss Moment Frames. *J. of Struct. Engrg*, 126(6), 1781-1797.

Jain, K.A., Goel, S.C., and Hanson, R.D., (1978). *Hysteresis Behavior of Bracing Members and Seismic Response of Braced Frames With Different Proportions*. Report No. UMEE-78R3. University of Michigan, Ann Arbor, MN.

Kanada, M., and Astaneh-Asl, A., (1996). *Seismic Performance of Steel Bridges during the 1995 Kobe Earthquake*. Report No. UCB/CEE-Steel- 96/01, Department of Civil and Environmental Engineering, University of California, Berkeley, CA, December.

Kunde, M.C., and Jangid, R.S., (2003). Seismic Behavior of Isolated Bridges: A State-of-the-Art Review. *Electronic J. of Struct. Engrg.*, 3, 140-170.

Lee, G.C., Kitane, Y., and Buckle, I.G., (2001). *Literature Review of the Observed Performance of Seismically Isolated Bridges*. Multidisciplinary Center for Earthquake Engineering Research (MCEER) - Research Progress and Accomplishments 2000-2001. Buffalo, NY. Website: <http://mceer.buffalo.edu/publications/resaccom/0001/>.

Malaysian Rubber Producers' Research Association (MRPRA), (1979). *Natural Rubber Engineering Data Sheet (EDS 23)*. Malaysian Rubber Research and Development Board Organization, England.

Menem, C., and Der Kiureghian, A., (1998). A Replacement for the 30%, 40% and SRSS Rules for Multicomponent Seismic Analysis. *Earthquake Spectra*, 14(1), 153-163.

Maleki, S., (2002). Effect of Deck and Support Stiffness on Seismic Response of Slab-Girder Bridges. *Engineering Structures*, 24, 219-226.

Nippon Steel Corporation, (2002). *Seismic Behavior of Typical Steel (Unbonded Brace) - Tensile Test Report for Steel Material of LYP-225*. Nippon Steel Corporation, Japan. October.

Pacific Center for Earthquake Engineering Research (PEER) Strong Motion Database, (2002). Website: <http://peer.berkeley.edu/smcat/>

Reinhorn, A.M., Bracci, J. and Pekhan, G., (2001). *Design of Six Axis Load Cell*. Personal Communication.

Robinson, W.H., (1982). Lead-Rubber Hysteretic Bearings Suitable for Protecting Structures during Earthquakes. *Earthquake Eng. and Str. Dyn*, 10, 293-604.

Robinson, W.H., (1993). Seismic Isolation of Bridges in New Zealand. *Proc. of the Second US-Japan Workshop on Earthquake Protective Systems for Bridges*, Japan, 185-194.

- Sabelli, R., (2001). *Research on Improving the Design and Analysis of Earthquake-resistant Steel-braced Frames*. Report PF2000-9 - FEMA/EERI 2000 Professional Fellowship. October.
- Sabelli, R., and Aiken, I., (2003a). Development of Building Code Provisions for Buckling-Restrained Braced Frames. *Proc. of the 2003 SEAOC Convention*, Squaw Creek, CA, August.
- Sabelli, R., Mahin, S., and Chang, C., (2003b). Seismic Demands on Steel Braced Frame Buildings with Buckling-Restrained Braces. *Engineering Structures*, 25(5), 655-666.
- Saiidi, M., Maragakis, E., and Griffin, G., (1999). Effect of Base Isolation on the Seismic Response of Multi-column Bridges. *Struct. Engrg. and Mech.*, 8(4), 411-419.
- Seismic Isolation Engineering (SIE), (1999). *Tests of Nippon Steel Corporation Unbonded Braces - UC Davis Plant & Environmental Sciences Bldg*. Report by Nippon Steel Corporation, Tokyo, Japan.
- Shinozuka, M.(ed), Ballantyne, D., Borchardt, R., Buckle, I., O'Rourke, T., and Schiff, A., (1995). *The Hanshin-Awaji Earthquake of January 17, 1995 Performance of Lifelines*. Technical Report NCEER-95-0015, National Center for Earthquake Engineering Research, Buffalo, New York.
- Skinner, R.I., Robinson, W.H., and McVerry, G.H., (1993). *An Introduction to Seismic Isolation*. John Wiley & Sons Ltd, England.
- Smeby, W., and Der Kiureghian, A. (1985). Modal Combination Rules for Multicomponent Earthquakes, *Journal of the Mechanics Division*, 103, 895-911.
- Structural Engineering Association of Northern California (SEAONC) BRBF ad-hoc Committee (2003). *Recommended Provisions for Buckling-Restrained Brace Frames*. SEAOC, Sacramento, CA, July.
- State University of New York (SUNY) Buffalo - Engineering Seismological Laboratory, (2002). *Response Spectrum Compatible Time Histories (RSCTH) (Program for Generation of Artificial Acceleration Time Histories)*, <http://civil.eng.buffalo.edu/engseislab/products.htm>
- TRW Nelson Division, (1977). *Embedment Properties of Headed Studs*. TRW Nelson Division, Elyria, Ohio.
- TRW Nelson Division, (1988). *Nelson – Standard In-Shock Studs Brochure*. TRW Nelson Division, Elyria, Ohio.
- Wada, A., Saeki, E., Takeuchi, T., and Watanabe, A., (1989). Development of Unbonded Brace. *Column* (A Nippon Steel Publication), No 115, 12.
- Wang, J., Carr, A., Cooke, N., and Moss, P., (2004). Effects of Spatial Variation of Seismic Inputs on Bridge Longitudinal Response. *Proc. of 2003 Pacific Conference on Earthquake Engineering*, Christchurch, New Zealand.

Wang, J., Carr, A., Cooke, N., and Moss, P., (2003). Wave-Passage Effect on the Seismic Response of Long Bridges. *Proc. of 13th World Conference on Earthquake Engineering*, Vancouver, Canada, August 1-6.

Washington State Department of Transportation (WSDOT), (2001). Photos of Damage During the 2001 Nisqually Earthquake. *Personal communication*.

Wen, Y-K., (1976). Method for Random Vibration of Hysteretic Systems. *J. of Engrg Mech.* 102(EM2), 249-263.

Yamaguchi, T., Nakata, Y., Takeuchi, T., Ikebe, T., Nagao, T., Minami, A., Suzuki, T., (1998). *Seismic Control Devices using Low-Yield Point Steel*. Nippon Steel Technical Report, No. 77, July. Tokyo, Japan.

Zahrai, S. M., and Bruneau, M., (1998a). Impact of Diaphragms on Seismic Response of Straight Slab-on-Girder Steel Bridges, *J. of Struct. Engrg.*, 124(8), 938-947.

Zahrai, S. M., and Bruneau, M., (1998b). *Seismic Retrofit of Slab-on-Girder Steel Bridges using Ductile End Diaphragms*, Report OCEERC 98-20, University of Ottawa, Ottawa, Ontario.

Zahrai, S. M., and Bruneau, M., (1999a). Ductile End-Diaphragms for Seismic Retrofit of Slab-on-Girder Steel Bridges, *J. of Struct. Engrg.*, 125(1), 71-80.

Zahrai, S. M., and Bruneau, M., (1999b). Cyclic Testing of Ductile End-Diaphragms for Slab-on-Girder Steel Bridges, *J. of Struct. Engrg.*, 125(9), 987-996.

APPENDIX A. PROPERTIES OF LEAD RUBBER BEARINGS

Bearing Properties

A summary of the bearing properties are described below. Symbols follow those from the AASHTO Guide Specification for Seismic Isolation Design (1999) where possible.

Rubber properties:

$$G = 430 \quad \text{kPa} \quad \text{From manufacturer}$$

$$E = 4 \cdot G$$

$$E = 1720 \quad \text{kPa} \quad \text{Typical (AASHTO 1999)}$$

$$k_{\text{bar}} = 0.86 \quad \text{From Natural Rubber Bulletin (Malaysian 1979)}$$

Rubber layers:

$$t_i = 6.0 \quad \text{mm}$$

$$n_r = 10$$

$$T_r = t_i \cdot n_r$$

$$T_r = 60 \quad \text{mm}$$

Shims and top and bottom embedded plates:

$$t_s = 3.0 \quad \text{mm}$$

$$T_s = (n_r - 1) \cdot t_s$$

$$T_s = 27 \quad \text{mm}$$

$$t_p = 13 \quad \text{mm}$$

Total height:

$$H = T_r + (n_r - 1) \cdot t_s + 2 \cdot t_p \quad H = 113 \quad \text{mm}$$

Total rubber diameter including cover:

$$B_t = 178 \quad \text{mm}$$

Thickness of cover:

$$t_c = 13 \quad \text{mm}$$

Bonded width:

$$B_b = B_t - 2 \cdot t_c \quad B_b = 152 \quad \text{mm}$$

Total and bonded areas:

$$A_t = \frac{\pi \cdot B_t^2}{4} \quad A_t = 24885 \quad \text{mm}^2$$

$$A_b = \frac{\pi \cdot B_b^2}{4} \quad A_b = 18146 \quad \text{mm}^2$$

Lead core diameter:

$$B_c = 38 \quad \text{mm}$$

Check limits on diameter:

$$B_c > \frac{B_t}{6} \quad B_c < \frac{B_t}{3} \quad \text{Limits OK}$$

Core area:

$$A_c = \frac{\pi \cdot B_c^2}{4} \quad A_c = 1134 \quad \text{mm}^2$$

Total bearing area excluding the core:

$$A_i = A_t - A_c \quad A_i = 23750 \quad \text{mm}^2$$

Shear modulus of lead:

$$G_l = 130 \cdot 10^3 \quad \text{kPa}$$

Yield strength of lead:

$$\tau_y = 9.7 \cdot 10^3 \quad \text{kPa (Buckle 1978)}$$

Seismic Response

The seismic response of the bearings is calculated for the following seismic demand.

Acceleration and site coefficients:

$$S = 1.5 \quad (\text{AASHTO 1999})$$

$$A = 0.4$$

Average axial load on bearing:

$$W_i = 89 \quad \text{kN/bearing}$$

Calculated bi-linear properties:

$$k_s = \frac{G \cdot A_i}{T_r} \cdot 10^{-6} \quad k_s = 0.170 \quad \text{kN/mm}$$

$$k_l = \frac{G_l \cdot A_c}{(T_r + T_s)} \cdot 10^{-6} \quad k_l = 1.695 \quad \text{kN/mm}$$

$$k_{di} = k_s \quad k_{di} = 0.17 \quad \text{kN/mm}$$

$$k_u = k_l + k_s \quad k_u = 1.86 \quad \text{kN/mm}$$

$$F_y = \tau_y \cdot A_c \cdot 10^{-6} \quad F_y = 11.0 \quad \text{kN}$$

$$Q_{di} = F_y \cdot \left(1 - \frac{k_{di}}{k_u} \right) \quad Q_{di} = 10.0 \quad \text{kN}$$

Response of isolation system:

$$\text{Estimate} \quad d_i = 53 \quad \text{mm}$$

$$F_d = Q_{di} + k_{di} \cdot d_i \quad F_d = 19.0 \quad \text{kN}$$

$$k_{effi} = \frac{F_d}{d_i} \quad k_{effi} = 0.359 \quad \text{kN/mm}$$

$$g = 9.81 \quad \text{m/s}^2$$

$$T_{eff} = 2 \cdot \pi \cdot \sqrt{\frac{W_i}{g \cdot k_{effi} \cdot 10^3}} \quad T_{eff} = 1.00 \quad \text{s}$$

$$\beta_i = \frac{2 \cdot Q_{di}}{\pi \cdot F_d} \quad \beta_i = 0.335$$

$$B = 1.77$$

$$d_i = \frac{157 \cdot A \cdot S \cdot T_{eff}}{B} \quad d_i = 53 \quad \text{mm}$$

Final calculated displacement matches the initial displacement estimate for final iteration. The effect of torsion in the bridge is not considered.

Buckling and Rollover

The calculated critical load, following the procedure by Buckle (2002), is:

$$S = \frac{A_b}{\pi \cdot B_b \cdot t_i} \quad S = 6.33$$

$$R = k_s \cdot H \quad R = 19.2 \quad \text{kN}$$

$$f_b = 1 + 0.67 \cdot S^2 \quad f_b = 27.87$$

$$E_b = E \cdot f_b \quad E_b = 4.79 \times 10^4 \quad \text{kPa}$$

$$I_b = \frac{\pi \cdot B_t^4}{64} \quad I_b = 4.9 \times 10^7 \quad \text{mm}^4$$

assuming the total bearing width.

$$k_{\theta b} = \frac{E_b \cdot I_b}{T_r} \cdot 10^{-9} \quad k_{\theta b} = 39.4 \quad \text{kNm} \quad 3 \cdot k_{\theta b} = 118 \quad \text{kNm}$$

$$T = k_{\theta b} \cdot H \cdot 10^{-3} \quad T = 4.45 \quad \text{kN/m}^2$$

$$P_e = \frac{\pi^2 \cdot T}{H^2} \cdot 10^6 \quad P_e = 3439 \quad \text{kN}$$

$$P_{cro} = \sqrt{R \cdot P_e} \quad P_{cro} = 257 \quad \text{kN}$$

This is the critical load for an undisplaced bearing.

Check critical load at 1.5 x design displacement:

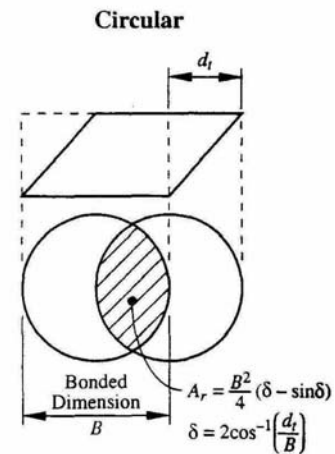
$$d_{i,max} = 1.5d_i \quad d_{i,max} = 80 \quad \text{mm}$$

$$\delta = 2 \cdot \arccos\left(\frac{d_{i,max}}{B_b}\right) \quad \delta = 2.037$$

$$A_r = \frac{B_b^2}{4} \cdot (\delta - \sin(\delta)) \quad A_r = 6605 \quad \text{mm}^2$$

$$\frac{A_r}{A_b} = 0.364$$

$$P_{cr} = \frac{A_r}{A_b} \cdot P_{cro} \quad P_{cr} = 93.6 \quad \text{kN}$$



(AASHTO 1999)

This is the critical load for at 1.5 times the design displacement. The average axial load applied to the bearings is:

$$P_{b,ave} = W_i \quad P_{b,ave} = 89 \quad \text{kip}$$

Therefore applied axial load is just less than calculated critical load and the bearing is OK.

The bearing should be OK for rollover as the plates are fully vulcanised to the rubber.

Bearing Rubber Strains

Shear strain due to shear deformation at design displacement (AASHTO 1999):

$$\gamma_{s.eq} = \frac{d_i}{T_r} \quad \gamma_{s.eq} = 0.886$$

Shear strain due to axial load at zero displacement:

$$A_r = A_b \quad A_r = 18146 \quad \text{mm}^2$$

$$\gamma_{c1} = \frac{3 \cdot S \cdot P_{b.ave} \cdot 10^6}{2 \cdot A_r \cdot G \cdot (1 + 2 \cdot k_{bar} \cdot S^2)} \quad \gamma_{c1} = 1.55$$

Axial strain at design displacement:

$$h_{eff} = 33.5 \quad h_{eff} = 33.5 \quad \text{mm}$$

$$s_g = 52.83 \quad s_g = 52.8 \quad \text{mm}$$

$$P_{b.max} = W_i + 2 \cdot F_d \cdot \frac{h_{eff}}{s_g} \quad P_{b.max} = 113 \quad \text{kN}$$

$$\delta = 2 \cdot \arccos\left(\frac{d_i}{B_b}\right) \quad \delta = 2.43$$

$$A_r = \frac{B_b^2}{4} \cdot (\delta - \sin(\delta)) \quad A_r = 10232 \quad \text{mm}^2$$

$$\gamma_{c2} = \frac{3 \cdot S \cdot P_{b.max} \cdot 10^6}{2 \cdot A_r \cdot G \cdot (1 + 2 \cdot k_{bar} \cdot S^2)} \quad \gamma_{c2} = 3.49$$

Rotational strain:

$$\gamma_r = 0$$

Strain limits:

$\gamma_c < 2.5$	$\gamma_{c1} = 1.55$	OK for zero displacement
	$\gamma_{c2} = 3.49$	Violated

Note that this limit is violated by the axial strain at the design transverse displacement. This suggests that instability is possible. However, the previous critical load analysis shows that the bearing was stable in excess of 1.5 times the design displacement, therefore the strain limit appears conservative when a lateral displacement is considered.

$$\gamma_c + \gamma_{s.eq} + 0.5\gamma_r < 5.5 \quad \gamma_{c2} + \gamma_{s.eq} + 0.5\gamma_r = 4.376 \quad \text{OK}$$

MCEER Technical Reports

MCEER publishes technical reports on a variety of subjects written by authors funded through MCEER. These reports are available from both MCEER Publications and the National Technical Information Service (NTIS). Requests for reports should be directed to MCEER Publications, MCEER, University at Buffalo, State University of New York, Red Jacket Quadrangle, Buffalo, New York 14261. Reports can also be requested through NTIS, 5285 Port Royal Road, Springfield, Virginia 22161. NTIS accession numbers are shown in parenthesis, if available.

- NCEER-87-0001 "First-Year Program in Research, Education and Technology Transfer," 3/5/87, (PB88-134275, A04, MF-A01).
- NCEER-87-0002 "Experimental Evaluation of Instantaneous Optimal Algorithms for Structural Control," by R.C. Lin, T.T. Soong and A.M. Reinhorn, 4/20/87, (PB88-134341, A04, MF-A01).
- NCEER-87-0003 "Experimentation Using the Earthquake Simulation Facilities at University at Buffalo," by A.M. Reinhorn and R.L. Ketter, to be published.
- NCEER-87-0004 "The System Characteristics and Performance of a Shaking Table," by J.S. Hwang, K.C. Chang and G.C. Lee, 6/1/87, (PB88-134259, A03, MF-A01). This report is available only through NTIS (see address given above).
- NCEER-87-0005 "A Finite Element Formulation for Nonlinear Viscoplastic Material Using a Q Model," by O. Gyebe and G. Dasgupta, 11/2/87, (PB88-213764, A08, MF-A01).
- NCEER-87-0006 "Symbolic Manipulation Program (SMP) - Algebraic Codes for Two and Three Dimensional Finite Element Formulations," by X. Lee and G. Dasgupta, 11/9/87, (PB88-218522, A05, MF-A01).
- NCEER-87-0007 "Instantaneous Optimal Control Laws for Tall Buildings Under Seismic Excitations," by J.N. Yang, A. Akbarpour and P. Ghaemmaghami, 6/10/87, (PB88-134333, A06, MF-A01). This report is only available through NTIS (see address given above).
- NCEER-87-0008 "IDARC: Inelastic Damage Analysis of Reinforced Concrete Frame - Shear-Wall Structures," by Y.J. Park, A.M. Reinhorn and S.K. Kunnath, 7/20/87, (PB88-134325, A09, MF-A01). This report is only available through NTIS (see address given above).
- NCEER-87-0009 "Liquefaction Potential for New York State: A Preliminary Report on Sites in Manhattan and Buffalo," by M. Budhu, V. Vijayakumar, R.F. Giese and L. Baumgras, 8/31/87, (PB88-163704, A03, MF-A01). This report is available only through NTIS (see address given above).
- NCEER-87-0010 "Vertical and Torsional Vibration of Foundations in Inhomogeneous Media," by A.S. Veletsos and K.W. Dotson, 6/1/87, (PB88-134291, A03, MF-A01). This report is only available through NTIS (see address given above).
- NCEER-87-0011 "Seismic Probabilistic Risk Assessment and Seismic Margins Studies for Nuclear Power Plants," by Howard H.M. Hwang, 6/15/87, (PB88-134267, A03, MF-A01). This report is only available through NTIS (see address given above).
- NCEER-87-0012 "Parametric Studies of Frequency Response of Secondary Systems Under Ground-Acceleration Excitations," by Y. Yong and Y.K. Lin, 6/10/87, (PB88-134309, A03, MF-A01). This report is only available through NTIS (see address given above).
- NCEER-87-0013 "Frequency Response of Secondary Systems Under Seismic Excitation," by J.A. HoLung, J. Cai and Y.K. Lin, 7/31/87, (PB88-134317, A05, MF-A01). This report is only available through NTIS (see address given above).
- NCEER-87-0014 "Modelling Earthquake Ground Motions in Seismically Active Regions Using Parametric Time Series Methods," by G.W. Ellis and A.S. Cakmak, 8/25/87, (PB88-134283, A08, MF-A01). This report is only available through NTIS (see address given above).
- NCEER-87-0015 "Detection and Assessment of Seismic Structural Damage," by E. DiPasquale and A.S. Cakmak, 8/25/87, (PB88-163712, A05, MF-A01). This report is only available through NTIS (see address given above).

- NCEER-87-0016 "Pipeline Experiment at Parkfield, California," by J. Isenberg and E. Richardson, 9/15/87, (PB88-163720, A03, MF-A01). This report is available only through NTIS (see address given above).
- NCEER-87-0017 "Digital Simulation of Seismic Ground Motion," by M. Shinozuka, G. Deodatis and T. Harada, 8/31/87, (PB88-155197, A04, MF-A01). This report is available only through NTIS (see address given above).
- NCEER-87-0018 "Practical Considerations for Structural Control: System Uncertainty, System Time Delay and Truncation of Small Control Forces," J.N. Yang and A. Akbarpour, 8/10/87, (PB88-163738, A08, MF-A01). This report is only available through NTIS (see address given above).
- NCEER-87-0019 "Modal Analysis of Nonclassically Damped Structural Systems Using Canonical Transformation," by J.N. Yang, S. Sarkani and F.X. Long, 9/27/87, (PB88-187851, A04, MF-A01).
- NCEER-87-0020 "A Nonstationary Solution in Random Vibration Theory," by J.R. Red-Horse and P.D. Spanos, 11/3/87, (PB88-163746, A03, MF-A01).
- NCEER-87-0021 "Horizontal Impedances for Radially Inhomogeneous Viscoelastic Soil Layers," by A.S. Veletsos and K.W. Dotson, 10/15/87, (PB88-150859, A04, MF-A01).
- NCEER-87-0022 "Seismic Damage Assessment of Reinforced Concrete Members," by Y.S. Chung, C. Meyer and M. Shinozuka, 10/9/87, (PB88-150867, A05, MF-A01). This report is available only through NTIS (see address given above).
- NCEER-87-0023 "Active Structural Control in Civil Engineering," by T.T. Soong, 11/11/87, (PB88-187778, A03, MF-A01).
- NCEER-87-0024 "Vertical and Torsional Impedances for Radially Inhomogeneous Viscoelastic Soil Layers," by K.W. Dotson and A.S. Veletsos, 12/87, (PB88-187786, A03, MF-A01).
- NCEER-87-0025 "Proceedings from the Symposium on Seismic Hazards, Ground Motions, Soil-Liquefaction and Engineering Practice in Eastern North America," October 20-22, 1987, edited by K.H. Jacob, 12/87, (PB88-188115, A23, MF-A01). This report is available only through NTIS (see address given above).
- NCEER-87-0026 "Report on the Whittier-Narrows, California, Earthquake of October 1, 1987," by J. Pantelic and A. Reinhorn, 11/87, (PB88-187752, A03, MF-A01). This report is available only through NTIS (see address given above).
- NCEER-87-0027 "Design of a Modular Program for Transient Nonlinear Analysis of Large 3-D Building Structures," by S. Srivastav and J.F. Abel, 12/30/87, (PB88-187950, A05, MF-A01). This report is only available through NTIS (see address given above).
- NCEER-87-0028 "Second-Year Program in Research, Education and Technology Transfer," 3/8/88, (PB88-219480, A04, MF-A01).
- NCEER-88-0001 "Workshop on Seismic Computer Analysis and Design of Buildings With Interactive Graphics," by W. McGuire, J.F. Abel and C.H. Conley, 1/18/88, (PB88-187760, A03, MF-A01). This report is only available through NTIS (see address given above).
- NCEER-88-0002 "Optimal Control of Nonlinear Flexible Structures," by J.N. Yang, F.X. Long and D. Wong, 1/22/88, (PB88-213772, A06, MF-A01).
- NCEER-88-0003 "Substructuring Techniques in the Time Domain for Primary-Secondary Structural Systems," by G.D. Manolis and G. Juhn, 2/10/88, (PB88-213780, A04, MF-A01).
- NCEER-88-0004 "Iterative Seismic Analysis of Primary-Secondary Systems," by A. Singhal, L.D. Lutes and P.D. Spanos, 2/23/88, (PB88-213798, A04, MF-A01).
- NCEER-88-0005 "Stochastic Finite Element Expansion for Random Media," by P.D. Spanos and R. Ghanem, 3/14/88, (PB88-213806, A03, MF-A01).

- NCEER-88-0006 "Combining Structural Optimization and Structural Control," by F.Y. Cheng and C.P. Pantelides, 1/10/88, (PB88-213814, A05, MF-A01).
- NCEER-88-0007 "Seismic Performance Assessment of Code-Designed Structures," by H.H-M. Hwang, J-W. Jaw and H-J. Shau, 3/20/88, (PB88-219423, A04, MF-A01). This report is only available through NTIS (see address given above).
- NCEER-88-0008 "Reliability Analysis of Code-Designed Structures Under Natural Hazards," by H.H-M. Hwang, H. Ushiba and M. Shinozuka, 2/29/88, (PB88-229471, A07, MF-A01). This report is only available through NTIS (see address given above).
- NCEER-88-0009 "Seismic Fragility Analysis of Shear Wall Structures," by J-W Jaw and H.H-M. Hwang, 4/30/88, (PB89-102867, A04, MF-A01).
- NCEER-88-0010 "Base Isolation of a Multi-Story Building Under a Harmonic Ground Motion - A Comparison of Performances of Various Systems," by F-G Fan, G. Ahmadi and I.G. Tadjbakhsh, 5/18/88, (PB89-122238, A06, MF-A01). This report is only available through NTIS (see address given above).
- NCEER-88-0011 "Seismic Floor Response Spectra for a Combined System by Green's Functions," by F.M. Lavelle, L.A. Bergman and P.D. Spanos, 5/1/88, (PB89-102875, A03, MF-A01).
- NCEER-88-0012 "A New Solution Technique for Randomly Excited Hysteretic Structures," by G.Q. Cai and Y.K. Lin, 5/16/88, (PB89-102883, A03, MF-A01).
- NCEER-88-0013 "A Study of Radiation Damping and Soil-Structure Interaction Effects in the Centrifuge," by K. Weissman, supervised by J.H. Prevost, 5/24/88, (PB89-144703, A06, MF-A01).
- NCEER-88-0014 "Parameter Identification and Implementation of a Kinematic Plasticity Model for Frictional Soils," by J.H. Prevost and D.V. Griffiths, to be published.
- NCEER-88-0015 "Two- and Three- Dimensional Dynamic Finite Element Analyses of the Long Valley Dam," by D.V. Griffiths and J.H. Prevost, 6/17/88, (PB89-144711, A04, MF-A01).
- NCEER-88-0016 "Damage Assessment of Reinforced Concrete Structures in Eastern United States," by A.M. Reinhorn, M.J. Seidel, S.K. Kunnath and Y.J. Park, 6/15/88, (PB89-122220, A04, MF-A01). This report is only available through NTIS (see address given above).
- NCEER-88-0017 "Dynamic Compliance of Vertically Loaded Strip Foundations in Multilayered Viscoelastic Soils," by S. Ahmad and A.S.M. Israil, 6/17/88, (PB89-102891, A04, MF-A01).
- NCEER-88-0018 "An Experimental Study of Seismic Structural Response With Added Viscoelastic Dampers," by R.C. Lin, Z. Liang, T.T. Soong and R.H. Zhang, 6/30/88, (PB89-122212, A05, MF-A01). This report is available only through NTIS (see address given above).
- NCEER-88-0019 "Experimental Investigation of Primary - Secondary System Interaction," by G.D. Manolis, G. Juhn and A.M. Reinhorn, 5/27/88, (PB89-122204, A04, MF-A01).
- NCEER-88-0020 "A Response Spectrum Approach For Analysis of Nonclassically Damped Structures," by J.N. Yang, S. Sarkani and F.X. Long, 4/22/88, (PB89-102909, A04, MF-A01).
- NCEER-88-0021 "Seismic Interaction of Structures and Soils: Stochastic Approach," by A.S. Veletsos and A.M. Prasad, 7/21/88, (PB89-122196, A04, MF-A01). This report is only available through NTIS (see address given above).
- NCEER-88-0022 "Identification of the Serviceability Limit State and Detection of Seismic Structural Damage," by E. DiPasquale and A.S. Cakmak, 6/15/88, (PB89-122188, A05, MF-A01). This report is available only through NTIS (see address given above).
- NCEER-88-0023 "Multi-Hazard Risk Analysis: Case of a Simple Offshore Structure," by B.K. Bhartia and E.H. Vanmarcke, 7/21/88, (PB89-145213, A05, MF-A01).

- NCEER-88-0024 "Automated Seismic Design of Reinforced Concrete Buildings," by Y.S. Chung, C. Meyer and M. Shinozuka, 7/5/88, (PB89-122170, A06, MF-A01). This report is available only through NTIS (see address given above).
- NCEER-88-0025 "Experimental Study of Active Control of MDOF Structures Under Seismic Excitations," by L.L. Chung, R.C. Lin, T.T. Soong and A.M. Reinhorn, 7/10/88, (PB89-122600, A04, MF-A01).
- NCEER-88-0026 "Earthquake Simulation Tests of a Low-Rise Metal Structure," by J.S. Hwang, K.C. Chang, G.C. Lee and R.L. Ketter, 8/1/88, (PB89-102917, A04, MF-A01).
- NCEER-88-0027 "Systems Study of Urban Response and Reconstruction Due to Catastrophic Earthquakes," by F. Kozin and H.K. Zhou, 9/22/88, (PB90-162348, A04, MF-A01).
- NCEER-88-0028 "Seismic Fragility Analysis of Plane Frame Structures," by H.H-M. Hwang and Y.K. Low, 7/31/88, (PB89-131445, A06, MF-A01).
- NCEER-88-0029 "Response Analysis of Stochastic Structures," by A. Kardara, C. Bucher and M. Shinozuka, 9/22/88, (PB89-174429, A04, MF-A01).
- NCEER-88-0030 "Nonnormal Accelerations Due to Yielding in a Primary Structure," by D.C.K. Chen and L.D. Lutes, 9/19/88, (PB89-131437, A04, MF-A01).
- NCEER-88-0031 "Design Approaches for Soil-Structure Interaction," by A.S. Veletsos, A.M. Prasad and Y. Tang, 12/30/88, (PB89-174437, A03, MF-A01). This report is available only through NTIS (see address given above).
- NCEER-88-0032 "A Re-evaluation of Design Spectra for Seismic Damage Control," by C.J. Turkstra and A.G. Tallin, 11/7/88, (PB89-145221, A05, MF-A01).
- NCEER-88-0033 "The Behavior and Design of Noncontact Lap Splices Subjected to Repeated Inelastic Tensile Loading," by V.E. Sagan, P. Gergely and R.N. White, 12/8/88, (PB89-163737, A08, MF-A01).
- NCEER-88-0034 "Seismic Response of Pile Foundations," by S.M. Mamoon, P.K. Banerjee and S. Ahmad, 11/1/88, (PB89-145239, A04, MF-A01).
- NCEER-88-0035 "Modeling of R/C Building Structures With Flexible Floor Diaphragms (IDARC2)," by A.M. Reinhorn, S.K. Kunnath and N. Panahshahi, 9/7/88, (PB89-207153, A07, MF-A01).
- NCEER-88-0036 "Solution of the Dam-Reservoir Interaction Problem Using a Combination of FEM, BEM with Particular Integrals, Modal Analysis, and Substructuring," by C-S. Tsai, G.C. Lee and R.L. Ketter, 12/31/88, (PB89-207146, A04, MF-A01).
- NCEER-88-0037 "Optimal Placement of Actuators for Structural Control," by F.Y. Cheng and C.P. Pantelides, 8/15/88, (PB89-162846, A05, MF-A01).
- NCEER-88-0038 "Teflon Bearings in Aseismic Base Isolation: Experimental Studies and Mathematical Modeling," by A. Mokha, M.C. Constantinou and A.M. Reinhorn, 12/5/88, (PB89-218457, A10, MF-A01). This report is available only through NTIS (see address given above).
- NCEER-88-0039 "Seismic Behavior of Flat Slab High-Rise Buildings in the New York City Area," by P. Weidlinger and M. Ettouney, 10/15/88, (PB90-145681, A04, MF-A01).
- NCEER-88-0040 "Evaluation of the Earthquake Resistance of Existing Buildings in New York City," by P. Weidlinger and M. Ettouney, 10/15/88, to be published.
- NCEER-88-0041 "Small-Scale Modeling Techniques for Reinforced Concrete Structures Subjected to Seismic Loads," by W. Kim, A. El-Attar and R.N. White, 11/22/88, (PB89-189625, A05, MF-A01).
- NCEER-88-0042 "Modeling Strong Ground Motion from Multiple Event Earthquakes," by G.W. Ellis and A.S. Cakmak, 10/15/88, (PB89-174445, A03, MF-A01).

- NCEER-88-0043 "Nonstationary Models of Seismic Ground Acceleration," by M. Grigoriu, S.E. Ruiz and E. Rosenblueth, 7/15/88, (PB89-189617, A04, MF-A01).
- NCEER-88-0044 "SARCF User's Guide: Seismic Analysis of Reinforced Concrete Frames," by Y.S. Chung, C. Meyer and M. Shinozuka, 11/9/88, (PB89-174452, A08, MF-A01).
- NCEER-88-0045 "First Expert Panel Meeting on Disaster Research and Planning," edited by J. Pantelic and J. Stoyke, 9/15/88, (PB89-174460, A05, MF-A01).
- NCEER-88-0046 "Preliminary Studies of the Effect of Degrading Infill Walls on the Nonlinear Seismic Response of Steel Frames," by C.Z. Chrysostomou, P. Gergely and J.F. Abel, 12/19/88, (PB89-208383, A05, MF-A01).
- NCEER-88-0047 "Reinforced Concrete Frame Component Testing Facility - Design, Construction, Instrumentation and Operation," by S.P. Pessiki, C. Conley, T. Bond, P. Gergely and R.N. White, 12/16/88, (PB89-174478, A04, MF-A01).
- NCEER-89-0001 "Effects of Protective Cushion and Soil Compliancy on the Response of Equipment Within a Seismically Excited Building," by J.A. HoLung, 2/16/89, (PB89-207179, A04, MF-A01).
- NCEER-89-0002 "Statistical Evaluation of Response Modification Factors for Reinforced Concrete Structures," by H.H-M. Hwang and J-W. Jaw, 2/17/89, (PB89-207187, A05, MF-A01).
- NCEER-89-0003 "Hysteretic Columns Under Random Excitation," by G-Q. Cai and Y.K. Lin, 1/9/89, (PB89-196513, A03, MF-A01).
- NCEER-89-0004 "Experimental Study of 'Elephant Foot Bulge' Instability of Thin-Walled Metal Tanks," by Z-H. Jia and R.L. Ketter, 2/22/89, (PB89-207195, A03, MF-A01).
- NCEER-89-0005 "Experiment on Performance of Buried Pipelines Across San Andreas Fault," by J. Isenberg, E. Richardson and T.D. O'Rourke, 3/10/89, (PB89-218440, A04, MF-A01). This report is available only through NTIS (see address given above).
- NCEER-89-0006 "A Knowledge-Based Approach to Structural Design of Earthquake-Resistant Buildings," by M. Subramani, P. Gergely, C.H. Conley, J.F. Abel and A.H. Zaghaw, 1/15/89, (PB89-218465, A06, MF-A01).
- NCEER-89-0007 "Liquefaction Hazards and Their Effects on Buried Pipelines," by T.D. O'Rourke and P.A. Lane, 2/1/89, (PB89-218481, A09, MF-A01).
- NCEER-89-0008 "Fundamentals of System Identification in Structural Dynamics," by H. Imai, C-B. Yun, O. Maruyama and M. Shinozuka, 1/26/89, (PB89-207211, A04, MF-A01).
- NCEER-89-0009 "Effects of the 1985 Michoacan Earthquake on Water Systems and Other Buried Lifelines in Mexico," by A.G. Ayala and M.J. O'Rourke, 3/8/89, (PB89-207229, A06, MF-A01).
- NCEER-89-R010 "NCEER Bibliography of Earthquake Education Materials," by K.E.K. Ross, Second Revision, 9/1/89, (PB90-125352, A05, MF-A01). This report is replaced by NCEER-92-0018.
- NCEER-89-0011 "Inelastic Three-Dimensional Response Analysis of Reinforced Concrete Building Structures (IDARC-3D), Part I - Modeling," by S.K. Kunnath and A.M. Reinhorn, 4/17/89, (PB90-114612, A07, MF-A01). This report is available only through NTIS (see address given above).
- NCEER-89-0012 "Recommended Modifications to ATC-14," by C.D. Poland and J.O. Malley, 4/12/89, (PB90-108648, A15, MF-A01).
- NCEER-89-0013 "Repair and Strengthening of Beam-to-Column Connections Subjected to Earthquake Loading," by M. Corazao and A.J. Durrani, 2/28/89, (PB90-109885, A06, MF-A01).
- NCEER-89-0014 "Program EXKAL2 for Identification of Structural Dynamic Systems," by O. Maruyama, C-B. Yun, M. Hoshiya and M. Shinozuka, 5/19/89, (PB90-109877, A09, MF-A01).

- NCEER-89-0015 "Response of Frames With Bolted Semi-Rigid Connections, Part I - Experimental Study and Analytical Predictions," by P.J. DiCorso, A.M. Reinhorn, J.R. Dickerson, J.B. Radzinski and W.L. Harper, 6/1/89, to be published.
- NCEER-89-0016 "ARMA Monte Carlo Simulation in Probabilistic Structural Analysis," by P.D. Spanos and M.P. Mignolet, 7/10/89, (PB90-109893, A03, MF-A01).
- NCEER-89-P017 "Preliminary Proceedings from the Conference on Disaster Preparedness - The Place of Earthquake Education in Our Schools," Edited by K.E.K. Ross, 6/23/89, (PB90-108606, A03, MF-A01).
- NCEER-89-0017 "Proceedings from the Conference on Disaster Preparedness - The Place of Earthquake Education in Our Schools," Edited by K.E.K. Ross, 12/31/89, (PB90-207895, A012, MF-A02). This report is available only through NTIS (see address given above).
- NCEER-89-0018 "Multidimensional Models of Hysteretic Material Behavior for Vibration Analysis of Shape Memory Energy Absorbing Devices, by E.J. Graesser and F.A. Cozzarelli, 6/7/89, (PB90-164146, A04, MF-A01).
- NCEER-89-0019 "Nonlinear Dynamic Analysis of Three-Dimensional Base Isolated Structures (3D-BASIS)," by S. Nagarajaiah, A.M. Reinhorn and M.C. Constantinou, 8/3/89, (PB90-161936, A06, MF-A01). This report has been replaced by NCEER-93-0011.
- NCEER-89-0020 "Structural Control Considering Time-Rate of Control Forces and Control Rate Constraints," by F.Y. Cheng and C.P. Pantelides, 8/3/89, (PB90-120445, A04, MF-A01).
- NCEER-89-0021 "Subsurface Conditions of Memphis and Shelby County," by K.W. Ng, T-S. Chang and H-H.M. Hwang, 7/26/89, (PB90-120437, A03, MF-A01).
- NCEER-89-0022 "Seismic Wave Propagation Effects on Straight Jointed Buried Pipelines," by K. Elhadi and M.J. O'Rourke, 8/24/89, (PB90-162322, A10, MF-A02).
- NCEER-89-0023 "Workshop on Serviceability Analysis of Water Delivery Systems," edited by M. Grigoriu, 3/6/89, (PB90-127424, A03, MF-A01).
- NCEER-89-0024 "Shaking Table Study of a 1/5 Scale Steel Frame Composed of Tapered Members," by K.C. Chang, J.S. Hwang and G.C. Lee, 9/18/89, (PB90-160169, A04, MF-A01).
- NCEER-89-0025 "DYNA1D: A Computer Program for Nonlinear Seismic Site Response Analysis - Technical Documentation," by Jean H. Prevost, 9/14/89, (PB90-161944, A07, MF-A01). This report is available only through NTIS (see address given above).
- NCEER-89-0026 "1:4 Scale Model Studies of Active Tendon Systems and Active Mass Dampers for Aseismic Protection," by A.M. Reinhorn, T.T. Soong, R.C. Lin, Y.P. Yang, Y. Fukao, H. Abe and M. Nakai, 9/15/89, (PB90-173246, A10, MF-A02). This report is available only through NTIS (see address given above).
- NCEER-89-0027 "Scattering of Waves by Inclusions in a Nonhomogeneous Elastic Half Space Solved by Boundary Element Methods," by P.K. Hadley, A. Askar and A.S. Cakmak, 6/15/89, (PB90-145699, A07, MF-A01).
- NCEER-89-0028 "Statistical Evaluation of Deflection Amplification Factors for Reinforced Concrete Structures," by H.H.M. Hwang, J-W. Jaw and A.L. Ch'ng, 8/31/89, (PB90-164633, A05, MF-A01).
- NCEER-89-0029 "Bedrock Accelerations in Memphis Area Due to Large New Madrid Earthquakes," by H.H.M. Hwang, C.H.S. Chen and G. Yu, 11/7/89, (PB90-162330, A04, MF-A01).
- NCEER-89-0030 "Seismic Behavior and Response Sensitivity of Secondary Structural Systems," by Y.Q. Chen and T.T. Soong, 10/23/89, (PB90-164658, A08, MF-A01).
- NCEER-89-0031 "Random Vibration and Reliability Analysis of Primary-Secondary Structural Systems," by Y. Ibrahim, M. Grigoriu and T.T. Soong, 11/10/89, (PB90-161951, A04, MF-A01).

- NCEER-89-0032 "Proceedings from the Second U.S. - Japan Workshop on Liquefaction, Large Ground Deformation and Their Effects on Lifelines, September 26-29, 1989," Edited by T.D. O'Rourke and M. Hamada, 12/1/89, (PB90-209388, A22, MF-A03).
- NCEER-89-0033 "Deterministic Model for Seismic Damage Evaluation of Reinforced Concrete Structures," by J.M. Bracci, A.M. Reinhorn, J.B. Mander and S.K. Kunnath, 9/27/89, (PB91-108803, A06, MF-A01).
- NCEER-89-0034 "On the Relation Between Local and Global Damage Indices," by E. DiPasquale and A.S. Cakmak, 8/15/89, (PB90-173865, A05, MF-A01).
- NCEER-89-0035 "Cyclic Undrained Behavior of Nonplastic and Low Plasticity Silts," by A.J. Walker and H.E. Stewart, 7/26/89, (PB90-183518, A10, MF-A01).
- NCEER-89-0036 "Liquefaction Potential of Surficial Deposits in the City of Buffalo, New York," by M. Budhu, R. Giese and L. Baumgrass, 1/17/89, (PB90-208455, A04, MF-A01).
- NCEER-89-0037 "A Deterministic Assessment of Effects of Ground Motion Incoherence," by A.S. Veletsos and Y. Tang, 7/15/89, (PB90-164294, A03, MF-A01).
- NCEER-89-0038 "Workshop on Ground Motion Parameters for Seismic Hazard Mapping," July 17-18, 1989, edited by R.V. Whitman, 12/1/89, (PB90-173923, A04, MF-A01).
- NCEER-89-0039 "Seismic Effects on Elevated Transit Lines of the New York City Transit Authority," by C.J. Costantino, C.A. Miller and E. Heymsfield, 12/26/89, (PB90-207887, A06, MF-A01).
- NCEER-89-0040 "Centrifugal Modeling of Dynamic Soil-Structure Interaction," by K. Weissman, Supervised by J.H. Prevost, 5/10/89, (PB90-207879, A07, MF-A01).
- NCEER-89-0041 "Linearized Identification of Buildings With Cores for Seismic Vulnerability Assessment," by I-K. Ho and A.E. Aktan, 11/1/89, (PB90-251943, A07, MF-A01).
- NCEER-90-0001 "Geotechnical and Lifeline Aspects of the October 17, 1989 Loma Prieta Earthquake in San Francisco," by T.D. O'Rourke, H.E. Stewart, F.T. Blackburn and T.S. Dickerman, 1/90, (PB90-208596, A05, MF-A01).
- NCEER-90-0002 "Nonnormal Secondary Response Due to Yielding in a Primary Structure," by D.C.K. Chen and L.D. Lutes, 2/28/90, (PB90-251976, A07, MF-A01).
- NCEER-90-0003 "Earthquake Education Materials for Grades K-12," by K.E.K. Ross, 4/16/90, (PB91-251984, A05, MF-A05). This report has been replaced by NCEER-92-0018.
- NCEER-90-0004 "Catalog of Strong Motion Stations in Eastern North America," by R.W. Busby, 4/3/90, (PB90-251984, A05, MF-A01).
- NCEER-90-0005 "NCEER Strong-Motion Data Base: A User Manual for the GeoBase Release (Version 1.0 for the Sun3)," by P. Friberg and K. Jacob, 3/31/90 (PB90-258062, A04, MF-A01).
- NCEER-90-0006 "Seismic Hazard Along a Crude Oil Pipeline in the Event of an 1811-1812 Type New Madrid Earthquake," by H.H.M. Hwang and C-H.S. Chen, 4/16/90, (PB90-258054, A04, MF-A01).
- NCEER-90-0007 "Site-Specific Response Spectra for Memphis Sheahan Pumping Station," by H.H.M. Hwang and C.S. Lee, 5/15/90, (PB91-108811, A05, MF-A01).
- NCEER-90-0008 "Pilot Study on Seismic Vulnerability of Crude Oil Transmission Systems," by T. Ariman, R. Dobry, M. Grigoriu, F. Kozin, M. O'Rourke, T. O'Rourke and M. Shinozuka, 5/25/90, (PB91-108837, A06, MF-A01).
- NCEER-90-0009 "A Program to Generate Site Dependent Time Histories: EQGEN," by G.W. Ellis, M. Srinivasan and A.S. Cakmak, 1/30/90, (PB91-108829, A04, MF-A01).
- NCEER-90-0010 "Active Isolation for Seismic Protection of Operating Rooms," by M.E. Talbott, Supervised by M. Shinozuka, 6/8/9, (PB91-110205, A05, MF-A01).

- NCEER-90-0011 "Program LINEARID for Identification of Linear Structural Dynamic Systems," by C-B. Yun and M. Shinozuka, 6/25/90, (PB91-110312, A08, MF-A01).
- NCEER-90-0012 "Two-Dimensional Two-Phase Elasto-Plastic Seismic Response of Earth Dams," by A.N. Yiagos, Supervised by J.H. Prevost, 6/20/90, (PB91-110197, A13, MF-A02).
- NCEER-90-0013 "Secondary Systems in Base-Isolated Structures: Experimental Investigation, Stochastic Response and Stochastic Sensitivity," by G.D. Manolis, G. Juhn, M.C. Constantinou and A.M. Reinhorn, 7/1/90, (PB91-110320, A08, MF-A01).
- NCEER-90-0014 "Seismic Behavior of Lightly-Reinforced Concrete Column and Beam-Column Joint Details," by S.P. Pessiki, C.H. Conley, P. Gergely and R.N. White, 8/22/90, (PB91-108795, A11, MF-A02).
- NCEER-90-0015 "Two Hybrid Control Systems for Building Structures Under Strong Earthquakes," by J.N. Yang and A. Daniellians, 6/29/90, (PB91-125393, A04, MF-A01).
- NCEER-90-0016 "Instantaneous Optimal Control with Acceleration and Velocity Feedback," by J.N. Yang and Z. Li, 6/29/90, (PB91-125401, A03, MF-A01).
- NCEER-90-0017 "Reconnaissance Report on the Northern Iran Earthquake of June 21, 1990," by M. Mehrain, 10/4/90, (PB91-125377, A03, MF-A01).
- NCEER-90-0018 "Evaluation of Liquefaction Potential in Memphis and Shelby County," by T.S. Chang, P.S. Tang, C.S. Lee and H. Hwang, 8/10/90, (PB91-125427, A09, MF-A01).
- NCEER-90-0019 "Experimental and Analytical Study of a Combined Sliding Disc Bearing and Helical Steel Spring Isolation System," by M.C. Constantinou, A.S. Mokha and A.M. Reinhorn, 10/4/90, (PB91-125385, A06, MF-A01). This report is available only through NTIS (see address given above).
- NCEER-90-0020 "Experimental Study and Analytical Prediction of Earthquake Response of a Sliding Isolation System with a Spherical Surface," by A.S. Mokha, M.C. Constantinou and A.M. Reinhorn, 10/11/90, (PB91-125419, A05, MF-A01).
- NCEER-90-0021 "Dynamic Interaction Factors for Floating Pile Groups," by G. Gazetas, K. Fan, A. Kaynia and E. Kausel, 9/10/90, (PB91-170381, A05, MF-A01).
- NCEER-90-0022 "Evaluation of Seismic Damage Indices for Reinforced Concrete Structures," by S. Rodriguez-Gomez and A.S. Cakmak, 9/30/90, PB91-171322, A06, MF-A01).
- NCEER-90-0023 "Study of Site Response at a Selected Memphis Site," by H. Desai, S. Ahmad, E.S. Gazetas and M.R. Oh, 10/11/90, (PB91-196857, A03, MF-A01).
- NCEER-90-0024 "A User's Guide to Strongmo: Version 1.0 of NCEER's Strong-Motion Data Access Tool for PCs and Terminals," by P.A. Friberg and C.A.T. Susch, 11/15/90, (PB91-171272, A03, MF-A01).
- NCEER-90-0025 "A Three-Dimensional Analytical Study of Spatial Variability of Seismic Ground Motions," by L-L. Hong and A.H.-S. Ang, 10/30/90, (PB91-170399, A09, MF-A01).
- NCEER-90-0026 "MUMOID User's Guide - A Program for the Identification of Modal Parameters," by S. Rodriguez-Gomez and E. DiPasquale, 9/30/90, (PB91-171298, A04, MF-A01).
- NCEER-90-0027 "SARCF-II User's Guide - Seismic Analysis of Reinforced Concrete Frames," by S. Rodriguez-Gomez, Y.S. Chung and C. Meyer, 9/30/90, (PB91-171280, A05, MF-A01).
- NCEER-90-0028 "Viscous Dampers: Testing, Modeling and Application in Vibration and Seismic Isolation," by N. Makris and M.C. Constantinou, 12/20/90 (PB91-190561, A06, MF-A01).
- NCEER-90-0029 "Soil Effects on Earthquake Ground Motions in the Memphis Area," by H. Hwang, C.S. Lee, K.W. Ng and T.S. Chang, 8/2/90, (PB91-190751, A05, MF-A01).

- NCEER-91-0001 "Proceedings from the Third Japan-U.S. Workshop on Earthquake Resistant Design of Lifeline Facilities and Countermeasures for Soil Liquefaction, December 17-19, 1990," edited by T.D. O'Rourke and M. Hamada, 2/1/91, (PB91-179259, A99, MF-A04).
- NCEER-91-0002 "Physical Space Solutions of Non-Proportionally Damped Systems," by M. Tong, Z. Liang and G.C. Lee, 1/15/91, (PB91-179242, A04, MF-A01).
- NCEER-91-0003 "Seismic Response of Single Piles and Pile Groups," by K. Fan and G. Gazetas, 1/10/91, (PB92-174994, A04, MF-A01).
- NCEER-91-0004 "Damping of Structures: Part 1 - Theory of Complex Damping," by Z. Liang and G. Lee, 10/10/91, (PB92-197235, A12, MF-A03).
- NCEER-91-0005 "3D-BASIS - Nonlinear Dynamic Analysis of Three Dimensional Base Isolated Structures: Part II," by S. Nagarajaiah, A.M. Reinhorn and M.C. Constantinou, 2/28/91, (PB91-190553, A07, MF-A01). This report has been replaced by NCEER-93-0011.
- NCEER-91-0006 "A Multidimensional Hysteretic Model for Plasticity Deforming Metals in Energy Absorbing Devices," by E.J. Graesser and F.A. Cozzarelli, 4/9/91, (PB92-108364, A04, MF-A01).
- NCEER-91-0007 "A Framework for Customizable Knowledge-Based Expert Systems with an Application to a KBES for Evaluating the Seismic Resistance of Existing Buildings," by E.G. Ibarra-Anaya and S.J. Fenves, 4/9/91, (PB91-210930, A08, MF-A01).
- NCEER-91-0008 "Nonlinear Analysis of Steel Frames with Semi-Rigid Connections Using the Capacity Spectrum Method," by G.G. Deierlein, S-H. Hsieh, Y-J. Shen and J.F. Abel, 7/2/91, (PB92-113828, A05, MF-A01).
- NCEER-91-0009 "Earthquake Education Materials for Grades K-12," by K.E.K. Ross, 4/30/91, (PB91-212142, A06, MF-A01). This report has been replaced by NCEER-92-0018.
- NCEER-91-0010 "Phase Wave Velocities and Displacement Phase Differences in a Harmonically Oscillating Pile," by N. Makris and G. Gazetas, 7/8/91, (PB92-108356, A04, MF-A01).
- NCEER-91-0011 "Dynamic Characteristics of a Full-Size Five-Story Steel Structure and a 2/5 Scale Model," by K.C. Chang, G.C. Yao, G.C. Lee, D.S. Hao and Y.C. Yeh," 7/2/91, (PB93-116648, A06, MF-A02).
- NCEER-91-0012 "Seismic Response of a 2/5 Scale Steel Structure with Added Viscoelastic Dampers," by K.C. Chang, T.T. Soong, S-T. Oh and M.L. Lai, 5/17/91, (PB92-110816, A05, MF-A01).
- NCEER-91-0013 "Earthquake Response of Retaining Walls; Full-Scale Testing and Computational Modeling," by S. Alampalli and A-W.M. Elgamel, 6/20/91, to be published.
- NCEER-91-0014 "3D-BASIS-M: Nonlinear Dynamic Analysis of Multiple Building Base Isolated Structures," by P.C. Tsopelas, S. Nagarajaiah, M.C. Constantinou and A.M. Reinhorn, 5/28/91, (PB92-113885, A09, MF-A02).
- NCEER-91-0015 "Evaluation of SEAOC Design Requirements for Sliding Isolated Structures," by D. Theodossiou and M.C. Constantinou, 6/10/91, (PB92-114602, A11, MF-A03).
- NCEER-91-0016 "Closed-Loop Modal Testing of a 27-Story Reinforced Concrete Flat Plate-Core Building," by H.R. Somaprasad, T. Toksoy, H. Yoshiyuki and A.E. Aktan, 7/15/91, (PB92-129980, A07, MF-A02).
- NCEER-91-0017 "Shake Table Test of a 1/6 Scale Two-Story Lightly Reinforced Concrete Building," by A.G. El-Attar, R.N. White and P. Gergely, 2/28/91, (PB92-222447, A06, MF-A02).
- NCEER-91-0018 "Shake Table Test of a 1/8 Scale Three-Story Lightly Reinforced Concrete Building," by A.G. El-Attar, R.N. White and P. Gergely, 2/28/91, (PB93-116630, A08, MF-A02).
- NCEER-91-0019 "Transfer Functions for Rigid Rectangular Foundations," by A.S. Veletsos, A.M. Prasad and W.H. Wu, 7/31/91, to be published.

- NCEER-91-0020 "Hybrid Control of Seismic-Excited Nonlinear and Inelastic Structural Systems," by J.N. Yang, Z. Li and A. Daniellians, 8/1/91, (PB92-143171, A06, MF-A02).
- NCEER-91-0021 "The NCEER-91 Earthquake Catalog: Improved Intensity-Based Magnitudes and Recurrence Relations for U.S. Earthquakes East of New Madrid," by L. Seeber and J.G. Armbruster, 8/28/91, (PB92-176742, A06, MF-A02).
- NCEER-91-0022 "Proceedings from the Implementation of Earthquake Planning and Education in Schools: The Need for Change - The Roles of the Changemakers," by K.E.K. Ross and F. Winslow, 7/23/91, (PB92-129998, A12, MF-A03).
- NCEER-91-0023 "A Study of Reliability-Based Criteria for Seismic Design of Reinforced Concrete Frame Buildings," by H.H.M. Hwang and H-M. Hsu, 8/10/91, (PB92-140235, A09, MF-A02).
- NCEER-91-0024 "Experimental Verification of a Number of Structural System Identification Algorithms," by R.G. Ghanem, H. Gavin and M. Shinozuka, 9/18/91, (PB92-176577, A18, MF-A04).
- NCEER-91-0025 "Probabilistic Evaluation of Liquefaction Potential," by H.H.M. Hwang and C.S. Lee," 11/25/91, (PB92-143429, A05, MF-A01).
- NCEER-91-0026 "Instantaneous Optimal Control for Linear, Nonlinear and Hysteretic Structures - Stable Controllers," by J.N. Yang and Z. Li, 11/15/91, (PB92-163807, A04, MF-A01).
- NCEER-91-0027 "Experimental and Theoretical Study of a Sliding Isolation System for Bridges," by M.C. Constantinou, A. Kartoum, A.M. Reinhorn and P. Bradford, 11/15/91, (PB92-176973, A10, MF-A03).
- NCEER-92-0001 "Case Studies of Liquefaction and Lifeline Performance During Past Earthquakes, Volume 1: Japanese Case Studies," Edited by M. Hamada and T. O'Rourke, 2/17/92, (PB92-197243, A18, MF-A04).
- NCEER-92-0002 "Case Studies of Liquefaction and Lifeline Performance During Past Earthquakes, Volume 2: United States Case Studies," Edited by T. O'Rourke and M. Hamada, 2/17/92, (PB92-197250, A20, MF-A04).
- NCEER-92-0003 "Issues in Earthquake Education," Edited by K. Ross, 2/3/92, (PB92-222389, A07, MF-A02).
- NCEER-92-0004 "Proceedings from the First U.S. - Japan Workshop on Earthquake Protective Systems for Bridges," Edited by I.G. Buckle, 2/4/92, (PB94-142239, A99, MF-A06).
- NCEER-92-0005 "Seismic Ground Motion from a Haskell-Type Source in a Multiple-Layered Half-Space," A.P. Theoharis, G. Deodatis and M. Shinozuka, 1/2/92, to be published.
- NCEER-92-0006 "Proceedings from the Site Effects Workshop," Edited by R. Whitman, 2/29/92, (PB92-197201, A04, MF-A01).
- NCEER-92-0007 "Engineering Evaluation of Permanent Ground Deformations Due to Seismically-Induced Liquefaction," by M.H. Baziar, R. Dobry and A-W.M. Elgamal, 3/24/92, (PB92-222421, A13, MF-A03).
- NCEER-92-0008 "A Procedure for the Seismic Evaluation of Buildings in the Central and Eastern United States," by C.D. Poland and J.O. Malley, 4/2/92, (PB92-222439, A20, MF-A04).
- NCEER-92-0009 "Experimental and Analytical Study of a Hybrid Isolation System Using Friction Controllable Sliding Bearings," by M.Q. Feng, S. Fujii and M. Shinozuka, 5/15/92, (PB93-150282, A06, MF-A02).
- NCEER-92-0010 "Seismic Resistance of Slab-Column Connections in Existing Non-Ductile Flat-Plate Buildings," by A.J. Durrani and Y. Du, 5/18/92, (PB93-116812, A06, MF-A02).
- NCEER-92-0011 "The Hysteretic and Dynamic Behavior of Brick Masonry Walls Upgraded by Ferrocement Coatings Under Cyclic Loading and Strong Simulated Ground Motion," by H. Lee and S.P. Prawl, 5/11/92, to be published.
- NCEER-92-0012 "Study of Wire Rope Systems for Seismic Protection of Equipment in Buildings," by G.F. Demetriades, M.C. Constantinou and A.M. Reinhorn, 5/20/92, (PB93-116655, A08, MF-A02).

- NCEER-92-0013 "Shape Memory Structural Dampers: Material Properties, Design and Seismic Testing," by P.R. Witting and F.A. Cozzarelli, 5/26/92, (PB93-116663, A05, MF-A01).
- NCEER-92-0014 "Longitudinal Permanent Ground Deformation Effects on Buried Continuous Pipelines," by M.J. O'Rourke, and C. Nordberg, 6/15/92, (PB93-116671, A08, MF-A02).
- NCEER-92-0015 "A Simulation Method for Stationary Gaussian Random Functions Based on the Sampling Theorem," by M. Grigoriu and S. Balopoulou, 6/11/92, (PB93-127496, A05, MF-A01).
- NCEER-92-0016 "Gravity-Load-Designed Reinforced Concrete Buildings: Seismic Evaluation of Existing Construction and Detailing Strategies for Improved Seismic Resistance," by G.W. Hoffmann, S.K. Kunnath, A.M. Reinhorn and J.B. Mander, 7/15/92, (PB94-142007, A08, MF-A02).
- NCEER-92-0017 "Observations on Water System and Pipeline Performance in the Limón Area of Costa Rica Due to the April 22, 1991 Earthquake," by M. O'Rourke and D. Ballantyne, 6/30/92, (PB93-126811, A06, MF-A02).
- NCEER-92-0018 "Fourth Edition of Earthquake Education Materials for Grades K-12," Edited by K.E.K. Ross, 8/10/92, (PB93-114023, A07, MF-A02).
- NCEER-92-0019 "Proceedings from the Fourth Japan-U.S. Workshop on Earthquake Resistant Design of Lifeline Facilities and Countermeasures for Soil Liquefaction," Edited by M. Hamada and T.D. O'Rourke, 8/12/92, (PB93-163939, A99, MF-E11).
- NCEER-92-0020 "Active Bracing System: A Full Scale Implementation of Active Control," by A.M. Reinhorn, T.T. Soong, R.C. Lin, M.A. Riley, Y.P. Wang, S. Aizawa and M. Higashino, 8/14/92, (PB93-127512, A06, MF-A02).
- NCEER-92-0021 "Empirical Analysis of Horizontal Ground Displacement Generated by Liquefaction-Induced Lateral Spreads," by S.F. Bartlett and T.L. Youd, 8/17/92, (PB93-188241, A06, MF-A02).
- NCEER-92-0022 "IDARC Version 3.0: Inelastic Damage Analysis of Reinforced Concrete Structures," by S.K. Kunnath, A.M. Reinhorn and R.F. Lobo, 8/31/92, (PB93-227502, A07, MF-A02).
- NCEER-92-0023 "A Semi-Empirical Analysis of Strong-Motion Peaks in Terms of Seismic Source, Propagation Path and Local Site Conditions, by M. Kamiyama, M.J. O'Rourke and R. Flores-Berrones, 9/9/92, (PB93-150266, A08, MF-A02).
- NCEER-92-0024 "Seismic Behavior of Reinforced Concrete Frame Structures with Nonductile Details, Part I: Summary of Experimental Findings of Full Scale Beam-Column Joint Tests," by A. Beres, R.N. White and P. Gergely, 9/30/92, (PB93-227783, A05, MF-A01).
- NCEER-92-0025 "Experimental Results of Repaired and Retrofitted Beam-Column Joint Tests in Lightly Reinforced Concrete Frame Buildings," by A. Beres, S. El-Borgi, R.N. White and P. Gergely, 10/29/92, (PB93-227791, A05, MF-A01).
- NCEER-92-0026 "A Generalization of Optimal Control Theory: Linear and Nonlinear Structures," by J.N. Yang, Z. Li and S. Vongchavalitkul, 11/2/92, (PB93-188621, A05, MF-A01).
- NCEER-92-0027 "Seismic Resistance of Reinforced Concrete Frame Structures Designed Only for Gravity Loads: Part I - Design and Properties of a One-Third Scale Model Structure," by J.M. Bracci, A.M. Reinhorn and J.B. Mander, 12/1/92, (PB94-104502, A08, MF-A02).
- NCEER-92-0028 "Seismic Resistance of Reinforced Concrete Frame Structures Designed Only for Gravity Loads: Part II - Experimental Performance of Subassemblages," by L.E. Aycaardi, J.B. Mander and A.M. Reinhorn, 12/1/92, (PB94-104510, A08, MF-A02).
- NCEER-92-0029 "Seismic Resistance of Reinforced Concrete Frame Structures Designed Only for Gravity Loads: Part III - Experimental Performance and Analytical Study of a Structural Model," by J.M. Bracci, A.M. Reinhorn and J.B. Mander, 12/1/92, (PB93-227528, A09, MF-A01).

- NCEER-92-0030 "Evaluation of Seismic Retrofit of Reinforced Concrete Frame Structures: Part I - Experimental Performance of Retrofitted Subassemblages," by D. Choudhuri, J.B. Mander and A.M. Reinhorn, 12/8/92, (PB93-198307, A07, MF-A02).
- NCEER-92-0031 "Evaluation of Seismic Retrofit of Reinforced Concrete Frame Structures: Part II - Experimental Performance and Analytical Study of a Retrofitted Structural Model," by J.M. Bracci, A.M. Reinhorn and J.B. Mander, 12/8/92, (PB93-198315, A09, MF-A03).
- NCEER-92-0032 "Experimental and Analytical Investigation of Seismic Response of Structures with Supplemental Fluid Viscous Dampers," by M.C. Constantinou and M.D. Symans, 12/21/92, (PB93-191435, A10, MF-A03). This report is available only through NTIS (see address given above).
- NCEER-92-0033 "Reconnaissance Report on the Cairo, Egypt Earthquake of October 12, 1992," by M. Khater, 12/23/92, (PB93-188621, A03, MF-A01).
- NCEER-92-0034 "Low-Level Dynamic Characteristics of Four Tall Flat-Plate Buildings in New York City," by H. Gavin, S. Yuan, J. Grossman, E. Pekelis and K. Jacob, 12/28/92, (PB93-188217, A07, MF-A02).
- NCEER-93-0001 "An Experimental Study on the Seismic Performance of Brick-Infilled Steel Frames With and Without Retrofit," by J.B. Mander, B. Nair, K. Wojtkowski and J. Ma, 1/29/93, (PB93-227510, A07, MF-A02).
- NCEER-93-0002 "Social Accounting for Disaster Preparedness and Recovery Planning," by S. Cole, E. Pantoja and V. Razak, 2/22/93, (PB94-142114, A12, MF-A03).
- NCEER-93-0003 "Assessment of 1991 NEHRP Provisions for Nonstructural Components and Recommended Revisions," by T.T. Soong, G. Chen, Z. Wu, R-H. Zhang and M. Grigoriu, 3/1/93, (PB93-188639, A06, MF-A02).
- NCEER-93-0004 "Evaluation of Static and Response Spectrum Analysis Procedures of SEAOC/UBC for Seismic Isolated Structures," by C.W. Winters and M.C. Constantinou, 3/23/93, (PB93-198299, A10, MF-A03).
- NCEER-93-0005 "Earthquakes in the Northeast - Are We Ignoring the Hazard? A Workshop on Earthquake Science and Safety for Educators," edited by K.E.K. Ross, 4/2/93, (PB94-103066, A09, MF-A02).
- NCEER-93-0006 "Inelastic Response of Reinforced Concrete Structures with Viscoelastic Braces," by R.F. Lobo, J.M. Bracci, K.L. Shen, A.M. Reinhorn and T.T. Soong, 4/5/93, (PB93-227486, A05, MF-A02).
- NCEER-93-0007 "Seismic Testing of Installation Methods for Computers and Data Processing Equipment," by K. Kosar, T.T. Soong, K.L. Shen, J.A. HoLung and Y.K. Lin, 4/12/93, (PB93-198299, A07, MF-A02).
- NCEER-93-0008 "Retrofit of Reinforced Concrete Frames Using Added Dampers," by A. Reinhorn, M. Constantinou and C. Li, to be published.
- NCEER-93-0009 "Seismic Behavior and Design Guidelines for Steel Frame Structures with Added Viscoelastic Dampers," by K.C. Chang, M.L. Lai, T.T. Soong, D.S. Hao and Y.C. Yeh, 5/1/93, (PB94-141959, A07, MF-A02).
- NCEER-93-0010 "Seismic Performance of Shear-Critical Reinforced Concrete Bridge Piers," by J.B. Mander, S.M. Waheed, M.T.A. Chaudhary and S.S. Chen, 5/12/93, (PB93-227494, A08, MF-A02).
- NCEER-93-0011 "3D-BASIS-TABS: Computer Program for Nonlinear Dynamic Analysis of Three Dimensional Base Isolated Structures," by S. Nagarajaiah, C. Li, A.M. Reinhorn and M.C. Constantinou, 8/2/93, (PB94-141819, A09, MF-A02).
- NCEER-93-0012 "Effects of Hydrocarbon Spills from an Oil Pipeline Break on Ground Water," by O.J. Helweg and H.H.M. Hwang, 8/3/93, (PB94-141942, A06, MF-A02).
- NCEER-93-0013 "Simplified Procedures for Seismic Design of Nonstructural Components and Assessment of Current Code Provisions," by M.P. Singh, L.E. Suarez, E.E. Matheu and G.O. Maldonado, 8/4/93, (PB94-141827, A09, MF-A02).
- NCEER-93-0014 "An Energy Approach to Seismic Analysis and Design of Secondary Systems," by G. Chen and T.T. Soong, 8/6/93, (PB94-142767, A11, MF-A03).

- NCEER-93-0015 "Proceedings from School Sites: Becoming Prepared for Earthquakes - Commemorating the Third Anniversary of the Loma Prieta Earthquake," Edited by F.E. Winslow and K.E.K. Ross, 8/16/93, (PB94-154275, A16, MF-A02).
- NCEER-93-0016 "Reconnaissance Report of Damage to Historic Monuments in Cairo, Egypt Following the October 12, 1992 Dahshur Earthquake," by D. Sykora, D. Look, G. Croci, E. Karaesmen and E. Karaesmen, 8/19/93, (PB94-142221, A08, MF-A02).
- NCEER-93-0017 "The Island of Guam Earthquake of August 8, 1993," by S.W. Swan and S.K. Harris, 9/30/93, (PB94-141843, A04, MF-A01).
- NCEER-93-0018 "Engineering Aspects of the October 12, 1992 Egyptian Earthquake," by A.W. Elgamal, M. Amer, K. Adalier and A. Abul-Fadl, 10/7/93, (PB94-141983, A05, MF-A01).
- NCEER-93-0019 "Development of an Earthquake Motion Simulator and its Application in Dynamic Centrifuge Testing," by I. Krstelj, Supervised by J.H. Prevost, 10/23/93, (PB94-181773, A-10, MF-A03).
- NCEER-93-0020 "NCEER-Taisei Corporation Research Program on Sliding Seismic Isolation Systems for Bridges: Experimental and Analytical Study of a Friction Pendulum System (FPS)," by M.C. Constantinou, P. Tsopelas, Y-S. Kim and S. Okamoto, 11/1/93, (PB94-142775, A08, MF-A02).
- NCEER-93-0021 "Finite Element Modeling of Elastomeric Seismic Isolation Bearings," by L.J. Billings, Supervised by R. Shepherd, 11/8/93, to be published.
- NCEER-93-0022 "Seismic Vulnerability of Equipment in Critical Facilities: Life-Safety and Operational Consequences," by K. Porter, G.S. Johnson, M.M. Zadeh, C. Scawthorn and S. Eder, 11/24/93, (PB94-181765, A16, MF-A03).
- NCEER-93-0023 "Hokkaido Nansei-oki, Japan Earthquake of July 12, 1993, by P.I. Yanev and C.R. Scawthorn, 12/23/93, (PB94-181500, A07, MF-A01).
- NCEER-94-0001 "An Evaluation of Seismic Serviceability of Water Supply Networks with Application to the San Francisco Auxiliary Water Supply System," by I. Markov, Supervised by M. Grigoriu and T. O'Rourke, 1/21/94, (PB94-204013, A07, MF-A02).
- NCEER-94-0002 "NCEER-Taisei Corporation Research Program on Sliding Seismic Isolation Systems for Bridges: Experimental and Analytical Study of Systems Consisting of Sliding Bearings, Rubber Restoring Force Devices and Fluid Dampers," Volumes I and II, by P. Tsopelas, S. Okamoto, M.C. Constantinou, D. Ozaki and S. Fujii, 2/4/94, (PB94-181740, A09, MF-A02 and PB94-181757, A12, MF-A03).
- NCEER-94-0003 "A Markov Model for Local and Global Damage Indices in Seismic Analysis," by S. Rahman and M. Grigoriu, 2/18/94, (PB94-206000, A12, MF-A03).
- NCEER-94-0004 "Proceedings from the NCEER Workshop on Seismic Response of Masonry Infills," edited by D.P. Abrams, 3/1/94, (PB94-180783, A07, MF-A02).
- NCEER-94-0005 "The Northridge, California Earthquake of January 17, 1994: General Reconnaissance Report," edited by J.D. Goltz, 3/11/94, (PB94-193943, A10, MF-A03).
- NCEER-94-0006 "Seismic Energy Based Fatigue Damage Analysis of Bridge Columns: Part I - Evaluation of Seismic Capacity," by G.A. Chang and J.B. Mander, 3/14/94, (PB94-219185, A11, MF-A03).
- NCEER-94-0007 "Seismic Isolation of Multi-Story Frame Structures Using Spherical Sliding Isolation Systems," by T.M. Al-Hussaini, V.A. Zayas and M.C. Constantinou, 3/17/94, (PB94-193745, A09, MF-A02).
- NCEER-94-0008 "The Northridge, California Earthquake of January 17, 1994: Performance of Highway Bridges," edited by I.G. Buckle, 3/24/94, (PB94-193851, A06, MF-A02).
- NCEER-94-0009 "Proceedings of the Third U.S.-Japan Workshop on Earthquake Protective Systems for Bridges," edited by I.G. Buckle and I. Friedland, 3/31/94, (PB94-195815, A99, MF-A06).

- NCEER-94-0010 "3D-BASIS-ME: Computer Program for Nonlinear Dynamic Analysis of Seismically Isolated Single and Multiple Structures and Liquid Storage Tanks," by P.C. Tsopelas, M.C. Constantinou and A.M. Reinhorn, 4/12/94, (PB94-204922, A09, MF-A02).
- NCEER-94-0011 "The Northridge, California Earthquake of January 17, 1994: Performance of Gas Transmission Pipelines," by T.D. O'Rourke and M.C. Palmer, 5/16/94, (PB94-204989, A05, MF-A01).
- NCEER-94-0012 "Feasibility Study of Replacement Procedures and Earthquake Performance Related to Gas Transmission Pipelines," by T.D. O'Rourke and M.C. Palmer, 5/25/94, (PB94-206638, A09, MF-A02).
- NCEER-94-0013 "Seismic Energy Based Fatigue Damage Analysis of Bridge Columns: Part II - Evaluation of Seismic Demand," by G.A. Chang and J.B. Mander, 6/1/94, (PB95-18106, A08, MF-A02).
- NCEER-94-0014 "NCEER-Taisei Corporation Research Program on Sliding Seismic Isolation Systems for Bridges: Experimental and Analytical Study of a System Consisting of Sliding Bearings and Fluid Restoring Force/Damping Devices," by P. Tsopelas and M.C. Constantinou, 6/13/94, (PB94-219144, A10, MF-A03).
- NCEER-94-0015 "Generation of Hazard-Consistent Fragility Curves for Seismic Loss Estimation Studies," by H. Hwang and J-R. Huo, 6/14/94, (PB95-181996, A09, MF-A02).
- NCEER-94-0016 "Seismic Study of Building Frames with Added Energy-Absorbing Devices," by W.S. Pong, C.S. Tsai and G.C. Lee, 6/20/94, (PB94-219136, A10, A03).
- NCEER-94-0017 "Sliding Mode Control for Seismic-Excited Linear and Nonlinear Civil Engineering Structures," by J. Yang, J. Wu, A. Agrawal and Z. Li, 6/21/94, (PB95-138483, A06, MF-A02).
- NCEER-94-0018 "3D-BASIS-TABS Version 2.0: Computer Program for Nonlinear Dynamic Analysis of Three Dimensional Base Isolated Structures," by A.M. Reinhorn, S. Nagarajaiah, M.C. Constantinou, P. Tsopelas and R. Li, 6/22/94, (PB95-182176, A08, MF-A02).
- NCEER-94-0019 "Proceedings of the International Workshop on Civil Infrastructure Systems: Application of Intelligent Systems and Advanced Materials on Bridge Systems," Edited by G.C. Lee and K.C. Chang, 7/18/94, (PB95-252474, A20, MF-A04).
- NCEER-94-0020 "Study of Seismic Isolation Systems for Computer Floors," by V. Lambrou and M.C. Constantinou, 7/19/94, (PB95-138533, A10, MF-A03).
- NCEER-94-0021 "Proceedings of the U.S.-Italian Workshop on Guidelines for Seismic Evaluation and Rehabilitation of Unreinforced Masonry Buildings," Edited by D.P. Abrams and G.M. Calvi, 7/20/94, (PB95-138749, A13, MF-A03).
- NCEER-94-0022 "NCEER-Taisei Corporation Research Program on Sliding Seismic Isolation Systems for Bridges: Experimental and Analytical Study of a System Consisting of Lubricated PTFE Sliding Bearings and Mild Steel Dampers," by P. Tsopelas and M.C. Constantinou, 7/22/94, (PB95-182184, A08, MF-A02).
- NCEER-94-0023 "Development of Reliability-Based Design Criteria for Buildings Under Seismic Load," by Y.K. Wen, H. Hwang and M. Shinozuka, 8/1/94, (PB95-211934, A08, MF-A02).
- NCEER-94-0024 "Experimental Verification of Acceleration Feedback Control Strategies for an Active Tendon System," by S.J. Dyke, B.F. Spencer, Jr., P. Quast, M.K. Sain, D.C. Kaspari, Jr. and T.T. Soong, 8/29/94, (PB95-212320, A05, MF-A01).
- NCEER-94-0025 "Seismic Retrofitting Manual for Highway Bridges," Edited by I.G. Buckle and I.F. Friedland, published by the Federal Highway Administration (PB95-212676, A15, MF-A03).
- NCEER-94-0026 "Proceedings from the Fifth U.S.-Japan Workshop on Earthquake Resistant Design of Lifeline Facilities and Countermeasures Against Soil Liquefaction," Edited by T.D. O'Rourke and M. Hamada, 11/7/94, (PB95-220802, A99, MF-E08).

- NCEER-95-0001 “Experimental and Analytical Investigation of Seismic Retrofit of Structures with Supplemental Damping: Part 1 - Fluid Viscous Damping Devices,” by A.M. Reinhorn, C. Li and M.C. Constantinou, 1/3/95, (PB95-266599, A09, MF-A02).
- NCEER-95-0002 “Experimental and Analytical Study of Low-Cycle Fatigue Behavior of Semi-Rigid Top-And-Seat Angle Connections,” by G. Pekcan, J.B. Mander and S.S. Chen, 1/5/95, (PB95-220042, A07, MF-A02).
- NCEER-95-0003 “NCEER-ATC Joint Study on Fragility of Buildings,” by T. Anagnos, C. Rojahn and A.S. Kiremidjian, 1/20/95, (PB95-220026, A06, MF-A02).
- NCEER-95-0004 “Nonlinear Control Algorithms for Peak Response Reduction,” by Z. Wu, T.T. Soong, V. Gattulli and R.C. Lin, 2/16/95, (PB95-220349, A05, MF-A01).
- NCEER-95-0005 “Pipeline Replacement Feasibility Study: A Methodology for Minimizing Seismic and Corrosion Risks to Underground Natural Gas Pipelines,” by R.T. Eguchi, H.A. Seligson and D.G. Honegger, 3/2/95, (PB95-252326, A06, MF-A02).
- NCEER-95-0006 “Evaluation of Seismic Performance of an 11-Story Frame Building During the 1994 Northridge Earthquake,” by F. Naeim, R. DiSulio, K. Benuska, A. Reinhorn and C. Li, to be published.
- NCEER-95-0007 “Prioritization of Bridges for Seismic Retrofitting,” by N. Basöz and A.S. Kiremidjian, 4/24/95, (PB95-252300, A08, MF-A02).
- NCEER-95-0008 “Method for Developing Motion Damage Relationships for Reinforced Concrete Frames,” by A. Singhal and A.S. Kiremidjian, 5/11/95, (PB95-266607, A06, MF-A02).
- NCEER-95-0009 “Experimental and Analytical Investigation of Seismic Retrofit of Structures with Supplemental Damping: Part II - Friction Devices,” by C. Li and A.M. Reinhorn, 7/6/95, (PB96-128087, A11, MF-A03).
- NCEER-95-0010 “Experimental Performance and Analytical Study of a Non-Ductile Reinforced Concrete Frame Structure Retrofitted with Elastomeric Spring Dampers,” by G. Pekcan, J.B. Mander and S.S. Chen, 7/14/95, (PB96-137161, A08, MF-A02).
- NCEER-95-0011 “Development and Experimental Study of Semi-Active Fluid Damping Devices for Seismic Protection of Structures,” by M.D. Symans and M.C. Constantinou, 8/3/95, (PB96-136940, A23, MF-A04).
- NCEER-95-0012 “Real-Time Structural Parameter Modification (RSPM): Development of Innervated Structures,” by Z. Liang, M. Tong and G.C. Lee, 4/11/95, (PB96-137153, A06, MF-A01).
- NCEER-95-0013 “Experimental and Analytical Investigation of Seismic Retrofit of Structures with Supplemental Damping: Part III - Viscous Damping Walls,” by A.M. Reinhorn and C. Li, 10/1/95, (PB96-176409, A11, MF-A03).
- NCEER-95-0014 “Seismic Fragility Analysis of Equipment and Structures in a Memphis Electric Substation,” by J-R. Huo and H.H.M. Hwang, 8/10/95, (PB96-128087, A09, MF-A02).
- NCEER-95-0015 “The Hanshin-Awaji Earthquake of January 17, 1995: Performance of Lifelines,” Edited by M. Shinozuka, 11/3/95, (PB96-176383, A15, MF-A03).
- NCEER-95-0016 “Highway Culvert Performance During Earthquakes,” by T.L. Youd and C.J. Beckman, available as NCEER-96-0015.
- NCEER-95-0017 “The Hanshin-Awaji Earthquake of January 17, 1995: Performance of Highway Bridges,” Edited by I.G. Buckle, 12/1/95, to be published.
- NCEER-95-0018 “Modeling of Masonry Infill Panels for Structural Analysis,” by A.M. Reinhorn, A. Madan, R.E. Valles, Y. Reichmann and J.B. Mander, 12/8/95, (PB97-110886, MF-A01, A06).
- NCEER-95-0019 “Optimal Polynomial Control for Linear and Nonlinear Structures,” by A.K. Agrawal and J.N. Yang, 12/11/95, (PB96-168737, A07, MF-A02).

- NCEER-95-0020 "Retrofit of Non-Ductile Reinforced Concrete Frames Using Friction Dampers," by R.S. Rao, P. Gergely and R.N. White, 12/22/95, (PB97-133508, A10, MF-A02).
- NCEER-95-0021 "Parametric Results for Seismic Response of Pile-Supported Bridge Bents," by G. Mylonakis, A. Nikolaou and G. Gazetas, 12/22/95, (PB97-100242, A12, MF-A03).
- NCEER-95-0022 "Kinematic Bending Moments in Seismically Stressed Piles," by A. Nikolaou, G. Mylonakis and G. Gazetas, 12/23/95, (PB97-113914, MF-A03, A13).
- NCEER-96-0001 "Dynamic Response of Unreinforced Masonry Buildings with Flexible Diaphragms," by A.C. Costley and D.P. Abrams, 10/10/96, (PB97-133573, MF-A03, A15).
- NCEER-96-0002 "State of the Art Review: Foundations and Retaining Structures," by I. Po Lam, to be published.
- NCEER-96-0003 "Ductility of Rectangular Reinforced Concrete Bridge Columns with Moderate Confinement," by N. Wehbe, M. Saiidi, D. Sanders and B. Douglas, 11/7/96, (PB97-133557, A06, MF-A02).
- NCEER-96-0004 "Proceedings of the Long-Span Bridge Seismic Research Workshop," edited by I.G. Buckle and I.M. Friedland, to be published.
- NCEER-96-0005 "Establish Representative Pier Types for Comprehensive Study: Eastern United States," by J. Kulicki and Z. Prucz, 5/28/96, (PB98-119217, A07, MF-A02).
- NCEER-96-0006 "Establish Representative Pier Types for Comprehensive Study: Western United States," by R. Imbsen, R.A. Schamber and T.A. Osterkamp, 5/28/96, (PB98-118607, A07, MF-A02).
- NCEER-96-0007 "Nonlinear Control Techniques for Dynamical Systems with Uncertain Parameters," by R.G. Ghanem and M.I. Bujakov, 5/27/96, (PB97-100259, A17, MF-A03).
- NCEER-96-0008 "Seismic Evaluation of a 30-Year Old Non-Ductile Highway Bridge Pier and Its Retrofit," by J.B. Mander, B. Mahmoodzadegan, S. Bhadra and S.S. Chen, 5/31/96, (PB97-110902, MF-A03, A10).
- NCEER-96-0009 "Seismic Performance of a Model Reinforced Concrete Bridge Pier Before and After Retrofit," by J.B. Mander, J.H. Kim and C.A. Ligozio, 5/31/96, (PB97-110910, MF-A02, A10).
- NCEER-96-0010 "IDARC2D Version 4.0: A Computer Program for the Inelastic Damage Analysis of Buildings," by R.E. Valles, A.M. Reinhorn, S.K. Kunnath, C. Li and A. Madan, 6/3/96, (PB97-100234, A17, MF-A03).
- NCEER-96-0011 "Estimation of the Economic Impact of Multiple Lifeline Disruption: Memphis Light, Gas and Water Division Case Study," by S.E. Chang, H.A. Seligson and R.T. Eguchi, 8/16/96, (PB97-133490, A11, MF-A03).
- NCEER-96-0012 "Proceedings from the Sixth Japan-U.S. Workshop on Earthquake Resistant Design of Lifeline Facilities and Countermeasures Against Soil Liquefaction, Edited by M. Hamada and T. O'Rourke, 9/11/96, (PB97-133581, A99, MF-A06).
- NCEER-96-0013 "Chemical Hazards, Mitigation and Preparedness in Areas of High Seismic Risk: A Methodology for Estimating the Risk of Post-Earthquake Hazardous Materials Release," by H.A. Seligson, R.T. Eguchi, K.J. Tierney and K. Richmond, 11/7/96, (PB97-133565, MF-A02, A08).
- NCEER-96-0014 "Response of Steel Bridge Bearings to Reversed Cyclic Loading," by J.B. Mander, D-K. Kim, S.S. Chen and G.J. Premus, 11/13/96, (PB97-140735, A12, MF-A03).
- NCEER-96-0015 "Highway Culvert Performance During Past Earthquakes," by T.L. Youd and C.J. Beckman, 11/25/96, (PB97-133532, A06, MF-A01).
- NCEER-97-0001 "Evaluation, Prevention and Mitigation of Pounding Effects in Building Structures," by R.E. Valles and A.M. Reinhorn, 2/20/97, (PB97-159552, A14, MF-A03).
- NCEER-97-0002 "Seismic Design Criteria for Bridges and Other Highway Structures," by C. Rojahn, R. Mayes, D.G. Anderson, J. Clark, J.H. Hom, R.V. Nutt and M.J. O'Rourke, 4/30/97, (PB97-194658, A06, MF-A03).

- NCEER-97-0003 "Proceedings of the U.S.-Italian Workshop on Seismic Evaluation and Retrofit," Edited by D.P. Abrams and G.M. Calvi, 3/19/97, (PB97-194666, A13, MF-A03).
- NCEER-97-0004 "Investigation of Seismic Response of Buildings with Linear and Nonlinear Fluid Viscous Dampers," by A.A. Seleemah and M.C. Constantinou, 5/21/97, (PB98-109002, A15, MF-A03).
- NCEER-97-0005 "Proceedings of the Workshop on Earthquake Engineering Frontiers in Transportation Facilities," edited by G.C. Lee and I.M. Friedland, 8/29/97, (PB98-128911, A25, MR-A04).
- NCEER-97-0006 "Cumulative Seismic Damage of Reinforced Concrete Bridge Piers," by S.K. Kunnath, A. El-Bahy, A. Taylor and W. Stone, 9/2/97, (PB98-108814, A11, MF-A03).
- NCEER-97-0007 "Structural Details to Accommodate Seismic Movements of Highway Bridges and Retaining Walls," by R.A. Imbsen, R.A. Schamber, E. Thorkildsen, A. Kartoum, B.T. Martin, T.N. Rosser and J.M. Kulicki, 9/3/97, (PB98-108996, A09, MF-A02).
- NCEER-97-0008 "A Method for Earthquake Motion-Damage Relationships with Application to Reinforced Concrete Frames," by A. Singhal and A.S. Kiremidjian, 9/10/97, (PB98-108988, A13, MF-A03).
- NCEER-97-0009 "Seismic Analysis and Design of Bridge Abutments Considering Sliding and Rotation," by K. Fishman and R. Richards, Jr., 9/15/97, (PB98-108897, A06, MF-A02).
- NCEER-97-0010 "Proceedings of the FHWA/NCEER Workshop on the National Representation of Seismic Ground Motion for New and Existing Highway Facilities," edited by I.M. Friedland, M.S. Power and R.L. Mayes, 9/22/97, (PB98-128903, A21, MF-A04).
- NCEER-97-0011 "Seismic Analysis for Design or Retrofit of Gravity Bridge Abutments," by K.L. Fishman, R. Richards, Jr. and R.C. Divito, 10/2/97, (PB98-128937, A08, MF-A02).
- NCEER-97-0012 "Evaluation of Simplified Methods of Analysis for Yielding Structures," by P. Tsopelas, M.C. Constantinou, C.A. Kircher and A.S. Whittaker, 10/31/97, (PB98-128929, A10, MF-A03).
- NCEER-97-0013 "Seismic Design of Bridge Columns Based on Control and Repairability of Damage," by C-T. Cheng and J.B. Mander, 12/8/97, (PB98-144249, A11, MF-A03).
- NCEER-97-0014 "Seismic Resistance of Bridge Piers Based on Damage Avoidance Design," by J.B. Mander and C-T. Cheng, 12/10/97, (PB98-144223, A09, MF-A02).
- NCEER-97-0015 "Seismic Response of Nominally Symmetric Systems with Strength Uncertainty," by S. Balopoulou and M. Grigoriu, 12/23/97, (PB98-153422, A11, MF-A03).
- NCEER-97-0016 "Evaluation of Seismic Retrofit Methods for Reinforced Concrete Bridge Columns," by T.J. Wipf, F.W. Klaiber and F.M. Russo, 12/28/97, (PB98-144215, A12, MF-A03).
- NCEER-97-0017 "Seismic Fragility of Existing Conventional Reinforced Concrete Highway Bridges," by C.L. Mullen and A.S. Cakmak, 12/30/97, (PB98-153406, A08, MF-A02).
- NCEER-97-0018 "Loss Assessment of Memphis Buildings," edited by D.P. Abrams and M. Shinozuka, 12/31/97, (PB98-144231, A13, MF-A03).
- NCEER-97-0019 "Seismic Evaluation of Frames with Infill Walls Using Quasi-static Experiments," by K.M. Mosalam, R.N. White and P. Gergely, 12/31/97, (PB98-153455, A07, MF-A02).
- NCEER-97-0020 "Seismic Evaluation of Frames with Infill Walls Using Pseudo-dynamic Experiments," by K.M. Mosalam, R.N. White and P. Gergely, 12/31/97, (PB98-153430, A07, MF-A02).
- NCEER-97-0021 "Computational Strategies for Frames with Infill Walls: Discrete and Smeared Crack Analyses and Seismic Fragility," by K.M. Mosalam, R.N. White and P. Gergely, 12/31/97, (PB98-153414, A10, MF-A02).

- NCEER-97-0022 "Proceedings of the NCEER Workshop on Evaluation of Liquefaction Resistance of Soils," edited by T.L. Youd and I.M. Idriss, 12/31/97, (PB98-155617, A15, MF-A03).
- MCEER-98-0001 "Extraction of Nonlinear Hysteretic Properties of Seismically Isolated Bridges from Quick-Release Field Tests," by Q. Chen, B.M. Douglas, E.M. Maragakis and I.G. Buckle, 5/26/98, (PB99-118838, A06, MF-A01).
- MCEER-98-0002 "Methodologies for Evaluating the Importance of Highway Bridges," by A. Thomas, S. Eshenaur and J. Kulicki, 5/29/98, (PB99-118846, A10, MF-A02).
- MCEER-98-0003 "Capacity Design of Bridge Piers and the Analysis of Overstrength," by J.B. Mander, A. Dutta and P. Goel, 6/1/98, (PB99-118853, A09, MF-A02).
- MCEER-98-0004 "Evaluation of Bridge Damage Data from the Loma Prieta and Northridge, California Earthquakes," by N. Basoz and A. Kiremidjian, 6/2/98, (PB99-118861, A15, MF-A03).
- MCEER-98-0005 "Screening Guide for Rapid Assessment of Liquefaction Hazard at Highway Bridge Sites," by T. L. Youd, 6/16/98, (PB99-118879, A06, not available on microfiche).
- MCEER-98-0006 "Structural Steel and Steel/Concrete Interface Details for Bridges," by P. Ritchie, N. Kauh and J. Kulicki, 7/13/98, (PB99-118945, A06, MF-A01).
- MCEER-98-0007 "Capacity Design and Fatigue Analysis of Confined Concrete Columns," by A. Dutta and J.B. Mander, 7/14/98, (PB99-118960, A14, MF-A03).
- MCEER-98-0008 "Proceedings of the Workshop on Performance Criteria for Telecommunication Services Under Earthquake Conditions," edited by A.J. Schiff, 7/15/98, (PB99-118952, A08, MF-A02).
- MCEER-98-0009 "Fatigue Analysis of Unconfined Concrete Columns," by J.B. Mander, A. Dutta and J.H. Kim, 9/12/98, (PB99-123655, A10, MF-A02).
- MCEER-98-0010 "Centrifuge Modeling of Cyclic Lateral Response of Pile-Cap Systems and Seat-Type Abutments in Dry Sands," by A.D. Gadre and R. Dobry, 10/2/98, (PB99-123606, A13, MF-A03).
- MCEER-98-0011 "IDARC-BRIDGE: A Computational Platform for Seismic Damage Assessment of Bridge Structures," by A.M. Reinhorn, V. Simeonov, G. Mylonakis and Y. Reichman, 10/2/98, (PB99-162919, A15, MF-A03).
- MCEER-98-0012 "Experimental Investigation of the Dynamic Response of Two Bridges Before and After Retrofitting with Elastomeric Bearings," by D.A. Wendichansky, S.S. Chen and J.B. Mander, 10/2/98, (PB99-162927, A15, MF-A03).
- MCEER-98-0013 "Design Procedures for Hinge Restrainers and Hinge Sear Width for Multiple-Frame Bridges," by R. Des Roches and G.L. Fenves, 11/3/98, (PB99-140477, A13, MF-A03).
- MCEER-98-0014 "Response Modification Factors for Seismically Isolated Bridges," by M.C. Constantinou and J.K. Quarshie, 11/3/98, (PB99-140485, A14, MF-A03).
- MCEER-98-0015 "Proceedings of the U.S.-Italy Workshop on Seismic Protective Systems for Bridges," edited by I.M. Friedland and M.C. Constantinou, 11/3/98, (PB2000-101711, A22, MF-A04).
- MCEER-98-0016 "Appropriate Seismic Reliability for Critical Equipment Systems: Recommendations Based on Regional Analysis of Financial and Life Loss," by K. Porter, C. Scawthorn, C. Taylor and N. Blais, 11/10/98, (PB99-157265, A08, MF-A02).
- MCEER-98-0017 "Proceedings of the U.S. Japan Joint Seminar on Civil Infrastructure Systems Research," edited by M. Shinozuka and A. Rose, 11/12/98, (PB99-156713, A16, MF-A03).
- MCEER-98-0018 "Modeling of Pile Footings and Drilled Shafts for Seismic Design," by I. PoLam, M. Kapuskar and D. Chaudhuri, 12/21/98, (PB99-157257, A09, MF-A02).

- MCEER-99-0001 "Seismic Evaluation of a Masonry Infilled Reinforced Concrete Frame by Pseudodynamic Testing," by S.G. Buonopane and R.N. White, 2/16/99, (PB99-162851, A09, MF-A02).
- MCEER-99-0002 "Response History Analysis of Structures with Seismic Isolation and Energy Dissipation Systems: Verification Examples for Program SAP2000," by J. Scheller and M.C. Constantinou, 2/22/99, (PB99-162869, A08, MF-A02).
- MCEER-99-0003 "Experimental Study on the Seismic Design and Retrofit of Bridge Columns Including Axial Load Effects," by A. Dutta, T. Kokorina and J.B. Mander, 2/22/99, (PB99-162877, A09, MF-A02).
- MCEER-99-0004 "Experimental Study of Bridge Elastomeric and Other Isolation and Energy Dissipation Systems with Emphasis on Uplift Prevention and High Velocity Near-source Seismic Excitation," by A. Kasalanati and M. C. Constantinou, 2/26/99, (PB99-162885, A12, MF-A03).
- MCEER-99-0005 "Truss Modeling of Reinforced Concrete Shear-flexure Behavior," by J.H. Kim and J.B. Mander, 3/8/99, (PB99-163693, A12, MF-A03).
- MCEER-99-0006 "Experimental Investigation and Computational Modeling of Seismic Response of a 1:4 Scale Model Steel Structure with a Load Balancing Supplemental Damping System," by G. Pekcan, J.B. Mander and S.S. Chen, 4/2/99, (PB99-162893, A11, MF-A03).
- MCEER-99-0007 "Effect of Vertical Ground Motions on the Structural Response of Highway Bridges," by M.R. Button, C.J. Cronin and R.L. Mayes, 4/10/99, (PB2000-101411, A10, MF-A03).
- MCEER-99-0008 "Seismic Reliability Assessment of Critical Facilities: A Handbook, Supporting Documentation, and Model Code Provisions," by G.S. Johnson, R.E. Sheppard, M.D. Quilici, S.J. Eder and C.R. Scawthorn, 4/12/99, (PB2000-101701, A18, MF-A04).
- MCEER-99-0009 "Impact Assessment of Selected MCEER Highway Project Research on the Seismic Design of Highway Structures," by C. Rojahn, R. Mayes, D.G. Anderson, J.H. Clark, D'Appolonia Engineering, S. Gloyd and R.V. Nutt, 4/14/99, (PB99-162901, A10, MF-A02).
- MCEER-99-0010 "Site Factors and Site Categories in Seismic Codes," by R. Dobry, R. Ramos and M.S. Power, 7/19/99, (PB2000-101705, A08, MF-A02).
- MCEER-99-0011 "Restrainer Design Procedures for Multi-Span Simply-Supported Bridges," by M.J. Randall, M. Saiidi, E. Maragakis and T. Isakovic, 7/20/99, (PB2000-101702, A10, MF-A02).
- MCEER-99-0012 "Property Modification Factors for Seismic Isolation Bearings," by M.C. Constantinou, P. Tsopelas, A. Kasalanati and E. Wolff, 7/20/99, (PB2000-103387, A11, MF-A03).
- MCEER-99-0013 "Critical Seismic Issues for Existing Steel Bridges," by P. Ritchie, N. Kauh and J. Kulicki, 7/20/99, (PB2000-101697, A09, MF-A02).
- MCEER-99-0014 "Nonstructural Damage Database," by A. Kao, T.T. Soong and A. Vender, 7/24/99, (PB2000-101407, A06, MF-A01).
- MCEER-99-0015 "Guide to Remedial Measures for Liquefaction Mitigation at Existing Highway Bridge Sites," by H.G. Cooke and J. K. Mitchell, 7/26/99, (PB2000-101703, A11, MF-A03).
- MCEER-99-0016 "Proceedings of the MCEER Workshop on Ground Motion Methodologies for the Eastern United States," edited by N. Abrahamson and A. Becker, 8/11/99, (PB2000-103385, A07, MF-A02).
- MCEER-99-0017 "Quindío, Colombia Earthquake of January 25, 1999: Reconnaissance Report," by A.P. Asfura and P.J. Flores, 10/4/99, (PB2000-106893, A06, MF-A01).
- MCEER-99-0018 "Hysteretic Models for Cyclic Behavior of Deteriorating Inelastic Structures," by M.V. Sivaselvan and A.M. Reinhorn, 11/5/99, (PB2000-103386, A08, MF-A02).

- MCEER-99-0019 "Proceedings of the 7th U.S.- Japan Workshop on Earthquake Resistant Design of Lifeline Facilities and Countermeasures Against Soil Liquefaction," edited by T.D. O'Rourke, J.P. Bardet and M. Hamada, 11/19/99, (PB2000-103354, A99, MF-A06).
- MCEER-99-0020 "Development of Measurement Capability for Micro-Vibration Evaluations with Application to Chip Fabrication Facilities," by G.C. Lee, Z. Liang, J.W. Song, J.D. Shen and W.C. Liu, 12/1/99, (PB2000-105993, A08, MF-A02).
- MCEER-99-0021 "Design and Retrofit Methodology for Building Structures with Supplemental Energy Dissipating Systems," by G. Pekcan, J.B. Mander and S.S. Chen, 12/31/99, (PB2000-105994, A11, MF-A03).
- MCEER-00-0001 "The Marmara, Turkey Earthquake of August 17, 1999: Reconnaissance Report," edited by C. Scawthorn; with major contributions by M. Bruneau, R. Eguchi, T. Holzer, G. Johnson, J. Mander, J. Mitchell, W. Mitchell, A. Papageorgiou, C. Scaethorn, and G. Webb, 3/23/00, (PB2000-106200, A11, MF-A03).
- MCEER-00-0002 "Proceedings of the MCEER Workshop for Seismic Hazard Mitigation of Health Care Facilities," edited by G.C. Lee, M. Ettouney, M. Grigoriu, J. Hauer and J. Nigg, 3/29/00, (PB2000-106892, A08, MF-A02).
- MCEER-00-0003 "The Chi-Chi, Taiwan Earthquake of September 21, 1999: Reconnaissance Report," edited by G.C. Lee and C.H. Loh, with major contributions by G.C. Lee, M. Bruneau, I.G. Buckle, S.E. Chang, P.J. Flores, T.D. O'Rourke, M. Shinozuka, T.T. Soong, C-H. Loh, K-C. Chang, Z-J. Chen, J-S. Hwang, M-L. Lin, G-Y. Liu, K-C. Tsai, G.C. Yao and C-L. Yen, 4/30/00, (PB2001-100980, A10, MF-A02).
- MCEER-00-0004 "Seismic Retrofit of End-Sway Frames of Steel Deck-Truss Bridges with a Supplemental Tendon System: Experimental and Analytical Investigation," by G. Pekcan, J.B. Mander and S.S. Chen, 7/1/00, (PB2001-100982, A10, MF-A02).
- MCEER-00-0005 "Sliding Fragility of Unrestrained Equipment in Critical Facilities," by W.H. Chong and T.T. Soong, 7/5/00, (PB2001-100983, A08, MF-A02).
- MCEER-00-0006 "Seismic Response of Reinforced Concrete Bridge Pier Walls in the Weak Direction," by N. Abo-Shadi, M. Saiidi and D. Sanders, 7/17/00, (PB2001-100981, A17, MF-A03).
- MCEER-00-0007 "Low-Cycle Fatigue Behavior of Longitudinal Reinforcement in Reinforced Concrete Bridge Columns," by J. Brown and S.K. Kunnath, 7/23/00, (PB2001-104392, A08, MF-A02).
- MCEER-00-0008 "Soil Structure Interaction of Bridges for Seismic Analysis," I. PoLam and H. Law, 9/25/00, (PB2001-105397, A08, MF-A02).
- MCEER-00-0009 "Proceedings of the First MCEER Workshop on Mitigation of Earthquake Disaster by Advanced Technologies (MEDAT-1), edited by M. Shinozuka, D.J. Inman and T.D. O'Rourke, 11/10/00, (PB2001-105399, A14, MF-A03).
- MCEER-00-0010 "Development and Evaluation of Simplified Procedures for Analysis and Design of Buildings with Passive Energy Dissipation Systems, Revision 01," by O.M. Ramirez, M.C. Constantinou, C.A. Kircher, A.S. Whittaker, M.W. Johnson, J.D. Gomez and C. Chrysostomou, 11/16/01, (PB2001-105523, A23, MF-A04).
- MCEER-00-0011 "Dynamic Soil-Foundation-Structure Interaction Analyses of Large Caissons," by C-Y. Chang, C-M. Mok, Z-L. Wang, R. Settgast, F. Waggoner, M.A. Ketchum, H.M. Gonnermann and C-C. Chin, 12/30/00, (PB2001-104373, A07, MF-A02).
- MCEER-00-0012 "Experimental Evaluation of Seismic Performance of Bridge Restrainers," by A.G. Vlassis, E.M. Maragakis and M. Saiid Saiidi, 12/30/00, (PB2001-104354, A09, MF-A02).
- MCEER-00-0013 "Effect of Spatial Variation of Ground Motion on Highway Structures," by M. Shinozuka, V. Saxena and G. Deodatis, 12/31/00, (PB2001-108755, A13, MF-A03).
- MCEER-00-0014 "A Risk-Based Methodology for Assessing the Seismic Performance of Highway Systems," by S.D. Werner, C.E. Taylor, J.E. Moore, II, J.S. Walton and S. Cho, 12/31/00, (PB2001-108756, A14, MF-A03).

- MCEER-01-0001 “Experimental Investigation of P-Delta Effects to Collapse During Earthquakes,” by D. Vian and M. Bruneau, 6/25/01, (PB2002-100534, A17, MF-A03).
- MCEER-01-0002 “Proceedings of the Second MCEER Workshop on Mitigation of Earthquake Disaster by Advanced Technologies (MEDAT-2),” edited by M. Bruneau and D.J. Inman, 7/23/01, (PB2002-100434, A16, MF-A03).
- MCEER-01-0003 “Sensitivity Analysis of Dynamic Systems Subjected to Seismic Loads,” by C. Roth and M. Grigoriu, 9/18/01, (PB2003-100884, A12, MF-A03).
- MCEER-01-0004 “Overcoming Obstacles to Implementing Earthquake Hazard Mitigation Policies: Stage 1 Report,” by D.J. Alesch and W.J. Petak, 12/17/01, (PB2002-107949, A07, MF-A02).
- MCEER-01-0005 “Updating Real-Time Earthquake Loss Estimates: Methods, Problems and Insights,” by C.E. Taylor, S.E. Chang and R.T. Eguchi, 12/17/01, (PB2002-107948, A05, MF-A01).
- MCEER-01-0006 “Experimental Investigation and Retrofit of Steel Pile Foundations and Pile Bents Under Cyclic Lateral Loadings,” by A. Shama, J. Mander, B. Blabac and S. Chen, 12/31/01, (PB2002-107950, A13, MF-A03).
- MCEER-02-0001 “Assessment of Performance of Bolu Viaduct in the 1999 Duzce Earthquake in Turkey” by P.C. Roussis, M.C. Constantinou, M. Erdik, E. Durukal and M. Dicleli, 5/8/02, (PB2003-100883, A08, MF-A02).
- MCEER-02-0002 “Seismic Behavior of Rail Counterweight Systems of Elevators in Buildings,” by M.P. Singh, Rildova and L.E. Suarez, 5/27/02. (PB2003-100882, A11, MF-A03).
- MCEER-02-0003 “Development of Analysis and Design Procedures for Spread Footings,” by G. Mylonakis, G. Gazetas, S. Nikolaou and A. Chauncey, 10/02/02, (PB2004-101636, A13, MF-A03, CD-A13).
- MCEER-02-0004 “Bare-Earth Algorithms for Use with SAR and LIDAR Digital Elevation Models,” by C.K. Huyck, R.T. Eguchi and B. Houshmand, 10/16/02, (PB2004-101637, A07, CD-A07).
- MCEER-02-0005 “Review of Energy Dissipation of Compression Members in Concentrically Braced Frames,” by K.Lee and M. Bruneau, 10/18/02, (PB2004-101638, A10, CD-A10).
- MCEER-03-0001 “Experimental Investigation of Light-Gauge Steel Plate Shear Walls for the Seismic Retrofit of Buildings” by J. Berman and M. Bruneau, 5/2/03, (PB2004-101622, A10, MF-A03, CD-A10).
- MCEER-03-0002 “Statistical Analysis of Fragility Curves,” by M. Shinozuka, M.Q. Feng, H. Kim, T. Uzawa and T. Ueda, 6/16/03, (PB2004-101849, A09, CD-A09).
- MCEER-03-0003 “Proceedings of the Eighth U.S.-Japan Workshop on Earthquake Resistant Design of Lifeline Facilities and Countermeasures Against Liquefaction,” edited by M. Hamada, J.P. Bardet and T.D. O’Rourke, 6/30/03, (PB2004-104386, A99, CD-A99).
- MCEER-03-0004 “Proceedings of the PRC-US Workshop on Seismic Analysis and Design of Special Bridges,” edited by L.C. Fan and G.C. Lee, 7/15/03, (PB2004-104387, A14, CD-A14).
- MCEER-03-0005 “Urban Disaster Recovery: A Framework and Simulation Model,” by S.B. Miles and S.E. Chang, 7/25/03, (PB2004-104388, A07, CD-A07).
- MCEER-03-0006 “Behavior of Underground Piping Joints Due to Static and Dynamic Loading,” by R.D. Meis, M. Maragakis and R. Siddharthan, 11/17/03, (PB2005-102194, A13, MF-A03, CD-A00).
- MCEER-03-0007 “Seismic Vulnerability of Timber Bridges and Timber Substructures,” by A.A. Shama, J.B. Mander, I.M. Friedland and D.R. Allicock, 12/15/03.
- MCEER-04-0001 “Experimental Study of Seismic Isolation Systems with Emphasis on Secondary System Response and Verification of Accuracy of Dynamic Response History Analysis Methods,” by E. Wolff and M. Constantinou, 1/16/04 (PB2005-102195, A99, MF-E08, CD-A00).

- MCEER-04-0002 “Tension, Compression and Cyclic Testing of Engineered Cementitious Composite Materials,” by K. Kesner and S.L. Billington, 3/1/04, (PB2005-102196, A08, CD-A08).
- MCEER-04-0003 “Cyclic Testing of Braces Laterally Restrained by Steel Studs to Enhance Performance During Earthquakes,” by O.C. Celik, J.W. Berman and M. Bruneau, 3/16/04, (PB2005-102197, A13, MF-A03, CD-A00).
- MCEER-04-0004 “Methodologies for Post Earthquake Building Damage Detection Using SAR and Optical Remote Sensing: Application to the August 17, 1999 Marmara, Turkey Earthquake,” by C.K. Huyck, B.J. Adams, S. Cho, R.T. Eguchi, B. Mansouri and B. Houshmand, 6/15/04, (PB2005-104888, A10, CD-A00).
- MCEER-04-0005 “Nonlinear Structural Analysis Towards Collapse Simulation: A Dynamical Systems Approach,” by M.V. Sivaselvan and A.M. Reinhorn, 6/16/04, (PB2005-104889, A11, MF-A03, CD-A00).
- MCEER-04-0006 “Proceedings of the Second PRC-US Workshop on Seismic Analysis and Design of Special Bridges,” edited by G.C. Lee and L.C. Fan, 6/25/04, (PB2005-104890, A16, CD-A00).
- MCEER-04-0007 “Seismic Vulnerability Evaluation of Axially Loaded Steel Built-up Laced Members,” by K. Lee and M. Bruneau, 6/30/04, (PB2005-104891, A16, CD-A00).
- MCEER-04-0008 “Evaluation of Accuracy of Simplified Methods of Analysis and Design of Buildings with Damping Systems for Near-Fault and for Soft-Soil Seismic Motions,” by E.A. Pavlou and M.C. Constantinou, 8/16/04, (PB2005-104892, A08, MF-A02, CD-A00).
- MCEER-04-0009 “Assessment of Geotechnical Issues in Acute Care Facilities in California,” by M. Lew, T.D. O’Rourke, R. Dobry and M. Koch, 9/15/04, (PB2005-104893, A08, CD-A00).
- MCEER-04-0010 “Scissor-Jack-Damper Energy Dissipation System,” by A.N. Sigaher-Boyle and M.C. Constantinou, 12/1/04 (PB2005-108221).
- MCEER-04-0011 “Seismic Retrofit of Bridge Steel Truss Piers Using a Controlled Rocking Approach,” by M. Pollino and M. Bruneau, 12/20/04 (PB2006-105795).
- MCEER-05-0001 “Experimental and Analytical Studies of Structures Seismically Isolated with an Uplift-Restraint Isolation System,” by P.C. Roussis and M.C. Constantinou, 1/10/05 (PB2005-108222).
- MCEER-05-0002 “A Versatile Experimentation Model for Study of Structures Near Collapse Applied to Seismic Evaluation of Irregular Structures,” by D. Kusumastuti, A.M. Reinhorn and A. Rutenberg, 3/31/05 (PB2006-101523).
- MCEER-05-0003 “Proceedings of the Third PRC-US Workshop on Seismic Analysis and Design of Special Bridges,” edited by L.C. Fan and G.C. Lee, 4/20/05, (PB2006-105796).
- MCEER-05-0004 “Approaches for the Seismic Retrofit of Braced Steel Bridge Piers and Proof-of-Concept Testing of an Eccentrically Braced Frame with Tubular Link,” by J.W. Berman and M. Bruneau, 4/21/05 (PB2006-101524).
- MCEER-05-0005 “Simulation of Strong Ground Motions for Seismic Fragility Evaluation of Nonstructural Components in Hospitals,” by A. Wanitkorkul and A. Filiatrault, 5/26/05 (PB2006-500027).
- MCEER-05-0006 “Seismic Safety in California Hospitals: Assessing an Attempt to Accelerate the Replacement or Seismic Retrofit of Older Hospital Facilities,” by D.J. Alesch, L.A. Arendt and W.J. Petak, 6/6/05 (PB2006-105794).
- MCEER-05-0007 “Development of Seismic Strengthening and Retrofit Strategies for Critical Facilities Using Engineered Cementitious Composite Materials,” by K. Kesner and S.L. Billington, 8/29/05 (PB2006-111701).
- MCEER-05-0008 “Experimental and Analytical Studies of Base Isolation Systems for Seismic Protection of Power Transformers,” by N. Murota, M.Q. Feng and G-Y. Liu, 9/30/05 (PB2006-111702).
- MCEER-05-0009 “3D-BASIS-ME-MB: Computer Program for Nonlinear Dynamic Analysis of Seismically Isolated Structures,” by P.C. Tsopelas, P.C. Roussis, M.C. Constantinou, R. Buchanan and A.M. Reinhorn, 10/3/05 (PB2006-111703).


- MCEER-05-0010 "Steel Plate Shear Walls for Seismic Design and Retrofit of Building Structures," by D. Vian and M. Bruneau, 12/15/05 (PB2006-111704).
- MCEER-05-0011 "The Performance-Based Design Paradigm," by M.J. Astrella and A. Whittaker, 12/15/05 (PB2006-111705).
- MCEER-06-0001 "Seismic Fragility of Suspended Ceiling Systems," H. Badillo-Almaraz, A.S. Whittaker, A.M. Reinhorn and G.P. Cimellaro, 2/4/06 (PB2006-111706).
- MCEER-06-0002 "Multi-Dimensional Fragility of Structures," by G.P. Cimellaro, A.M. Reinhorn and M. Bruneau, 3/1/06 (PB2007-106974, A09, MF-A02, CD A00).
- MCEER-06-0003 "Built-Up Shear Links as Energy Dissipators for Seismic Protection of Bridges," by P. Dusicka, A.M. Itani and I.G. Buckle, 3/15/06 (PB2006-111708).
- MCEER-06-0004 "Analytical Investigation of the Structural Fuse Concept," by R.E. Vargas and M. Bruneau, 3/16/06 (PB2006-111709).
- MCEER-06-0005 "Experimental Investigation of the Structural Fuse Concept," by R.E. Vargas and M. Bruneau, 3/17/06 (PB2006-111710).
- MCEER-06-0006 "Further Development of Tubular Eccentrically Braced Frame Links for the Seismic Retrofit of Braced Steel Truss Bridge Piers," by J.W. Berman and M. Bruneau, 3/27/06 (PB2007-105147).
- MCEER-06-0007 "REDARS Validation Report," by S. Cho, C.K. Huyck, S. Ghosh and R.T. Eguchi, 8/8/06 (PB2007-106983).
- MCEER-06-0008 "Review of Current NDE Technologies for Post-Earthquake Assessment of Retrofitted Bridge Columns," by J.W. Song, Z. Liang and G.C. Lee, 8/21/06 06 (PB2007-106984).
- MCEER-06-0009 "Liquefaction Remediation in Silty Soils Using Dynamic Compaction and Stone Columns," by S. Thevanayagam, G.R. Martin, R. Nashed, T. Shenthan, T. Kanagalingam and N. Ecemis, 8/28/06 06 (PB2007-106985).
- MCEER-06-0010 "Conceptual Design and Experimental Investigation of Polymer Matrix Composite Infill Panels for Seismic Retrofitting," by W. Jung, M. Chiewanichakorn and A.J. Aref, 9/21/06 (PB2007-106986).
- MCEER-06-0011 "A Study of the Coupled Horizontal-Vertical Behavior of Elastomeric and Lead-Rubber Seismic Isolation Bearings," by G.P. Warn and A.S. Whittaker, 9/22/06 (PB2007-108679).
- MCEER-06-0012 "Proceedings of the Fourth PRC-US Workshop on Seismic Analysis and Design of Special Bridges: Advancing Bridge Technologies in Research, Design, Construction and Preservation," Edited by L.C. Fan, G.C. Lee and L. Ziang, 10/12/06 (PB2007-109042).
- MCEER-06-0013 "Cyclic Response and Low Cycle Fatigue Characteristics of Plate Steels," by P. Dusicka, A.M. Itani and I.G. Buckle, 11/1/06 06 (PB2007-106987).
- MCEER-06-0014 "Proceedings of the Second US-Taiwan Bridge Engineering Workshop," edited by W.P. Yen, J. Shen, J-Y. Chen and M. Wang, 11/15/06.
- MCEER-06-0015 "User Manual and Technical Documentation for the REDARSTM Import Wizard," by S. Cho, S. Ghosh, C.K. Huyck and S.D. Werner, 11/30/06 (PB2007-114766).
- MCEER-06-0016 "Hazard Mitigation Strategy and Monitoring Technologies for Urban and Infrastructure Public Buildings: Proceedings of the China-US Workshops," edited by X.Y. Zhou, A.L. Zhang, G.C. Lee and M. Tong, 12/12/06 (PB2008-500018).
- MCEER-07-0001 "Static and Kinetic Coefficients of Friction for Rigid Blocks," by C. Kafali, S. Fathali, M. Grigoriu and A.S. Whittaker, 3/20/07 (PB2007-114767).
- MCEER-07-0002 "Hazard Mitigation Investment Decision Making: Organizational Response to Legislative Mandate," by L.A. Arendt, D.J. Alesch and W.J. Petak, 4/9/07 (PB2007-114768).

- MCEER-07-0003 “Seismic Behavior of Bidirectional-Resistant Ductile End Diaphragms with Unbonded Braces in Straight or Skewed Steel Bridges,” by O. Celik and M. Bruneau, 4/11/07 (PB2008-105141).
- MCEER-07-0004 “Modeling Pile Behavior in Large Pile Groups Under Lateral Loading,” by A.M. Dodds and G.R. Martin, 4/16/07(PB2008-105142).
- MCEER-07-0005 “Experimental Investigation of Blast Performance of Seismically Resistant Concrete-Filled Steel Tube Bridge Piers,” by S. Fujikura, M. Bruneau and D. Lopez-Garcia, 4/20/07 (PB2008-105143).
- MCEER-07-0006 “Seismic Analysis of Conventional and Isolated Liquefied Natural Gas Tanks Using Mechanical Analogs,” by I.P. Christovasilis and A.S. Whittaker, 5/1/07.
- MCEER-07-0007 “Experimental Seismic Performance Evaluation of Isolation/Restraint Systems for Mechanical Equipment – Part 1: Heavy Equipment Study,” by S. Fathali and A. Filiatrault, 6/6/07 (PB2008-105144).
- MCEER-07-0008 “Seismic Vulnerability of Timber Bridges and Timber Substructures,” by A.A. Sharma, J.B. Mander, I.M. Friedland and D.R. Allicock, 6/7/07 (PB2008-105145).
- MCEER-07-0009 “Experimental and Analytical Study of the XY-Friction Pendulum (XY-FP) Bearing for Bridge Applications,” by C.C. Marin-Artieda, A.S. Whittaker and M.C. Constantinou, 6/7/07.
- MCEER-07-0010 “Proceedings of the PRC-US Earthquake Engineering Forum for Young Researchers,” Edited by G.C. Lee and X.Z. Qi, 6/8/07.
- MCEER-07-0011 “Design Recommendations for Perforated Steel Plate Shear Walls,” by R. Purba and M. Bruneau, 6/18/07.
- MCEER-07-0012 “Performance of Seismic Isolation Hardware Under Service and Seismic Loading,” by M.C. Constantinou, A.S. Whittaker, Y. Kalpakidis, D.M. Fenz and G.P. Warn, 8/27/07.
- MCEER-07-0013 “Experimental Evaluation of the Seismic Performance of Hospital Piping Subassemblies,” by E.R. Goodwin, E. Maragakis and A.M. Itani, 9/4/07.
- MCEER-07-0014 “A Simulation Model of Urban Disaster Recovery and Resilience: Implementation for the 1994 Northridge Earthquake,” by S. Miles and S.E. Chang, 9/7/07.
- MCEER-07-0015 “Statistical and Mechanistic Fragility Analysis of Concrete Bridges,” by M. Shinozuka, S. Banerjee and S-H. Kim, 9/10/07.
- MCEER-07-0016 “Three-Dimensional Modeling of Inelastic Buckling in Frame Structures,” by M. Schachter and AM. Reinhorn, 9/13/07.
- MCEER-07-0017 “Modeling of Seismic Wave Scattering on Pile Groups and Caissons,” by I. Po Lam, H. Law and C.T. Yang, 9/17/07.
- MCEER-07-0018 “Bridge Foundations: Modeling Large Pile Groups and Caissons for Seismic Design,” by I. Po Lam, H. Law and G.R. Martin (Coordinating Author), 12/1/07.
- MCEER-07-0019 “Principles and Performance of Roller Seismic Isolation Bearings for Highway Bridges,” by G.C. Lee, Y.C. Ou, Z. Liang, T.C. Niu and J. Song, 12/10/07.
- MCEER-07-0020 “Centrifuge Modeling of Permeability and Pinning Reinforcement Effects on Pile Response to Lateral Spreading,” by L.L. Gonzalez-Lagos, T. Abdoun and R. Dobry, 12/10/07.
- MCEER-07-0021 “Damage to the Highway System from the Pisco, Perú Earthquake of August 15, 2007,” by J.S. O’Connor, L. Mesa and M. Nykamp, 12/10/07.
- MCEER-07-0022 “Experimental Seismic Performance Evaluation of Isolation/Restraint Systems for Mechanical Equipment – Part 2: Light Equipment Study,” by S. Fathali and A. Filiatrault, 12/13/07.
- MCEER-07-0023 “Fragility Considerations in Highway Bridge Design,” by M. Shinozuka, S. Banerjee and S.H. Kim, 12/14/07.

MCEER-07-0024 "Performance Estimates for Seismically Isolated Bridges," by G.P. Warn and A.S. Whittaker, 12/30/07.


MCEER-08-0001 "Seismic Performance of Steel Girder Bridge Superstructures with Conventional Cross Frames," by L.P. Carden, A.M. Itani and I.G. Buckle, 1/7/08.

MCEER-08-0002 ""Seismic Performance of Steel Girder Bridge Superstructures with Ductile End Cross Frames with Seismic Isolators," by L.P. Carden, A.M. Itani and I.G. Buckle, 1/7/08.



EARTHQUAKE ENGINEERING TO EXTREME EVENTS

University at Buffalo, The State University of New York
Red Jacket Quadrangle ▪ Buffalo, New York 14261
Phone: (716) 645-3391 ▪ Fax: (716) 645-3399
E-mail: mceer@buffalo.edu ▪ WWW Site <http://mceer.buffalo.edu>



University at Buffalo *The State University of New York*

ISSN 1520-295X